

BULGARIAN CHEMICAL COMMUNICATIONS

2017 Volume 49 / Number 4

*Journal of the Chemical Institutes
of the Bulgarian Academy of Sciences
and of the Union of Chemists in Bulgaria*

Catalytic oxidation of Rhodamine B in aqueous solutions with sulphate radicals over $\text{Co}_3\text{O}_4/\text{MgO}$ and $\text{CoFe}_2\text{O}_4/\text{MgO}$

I. A. Slavova, St. G. Christoskova, M. K. Stoyanova*

Department of Physical Chemistry, University of Plovdiv, 24 Tzar Asen Str, Plovdiv, 4000, Bulgaria

Received April 11, 2016; Accepted October 25, 2016

The oxidative degradation of Rhodamine B (RhB) in aqueous solutions with peroxyomonosulphate (PMS) was studied using $\text{Co}_3\text{O}_4/\text{MgO}$ and $\text{CoFe}_2\text{O}_4/\text{MgO}$ as catalysts. The as-prepared samples demonstrated strong PMS-activating ability despite low active phase loading percentage (5 wt%) and very low catalysts concentration (0.15 g dm^{-3}). The performance of the supported catalysts was found much better than that of their bulk analogues and mechanical mixtures of corresponding bulk oxide and bare MgO due to the crucial role of basic support for facilitating decomposition of PMS into highly reactive radicals. RhB degradation was found to follow the first order kinetics. The effect of catalyst dosage, PMS concentration, and pH on the rate of RhB oxidation was investigated. The radical species generated from the catalytic decomposition of PMS were identified by quenching studies.

Keywords: Rhodamine B degradation; Sulphate radicals; $\text{Co}_3\text{O}_4/\text{MgO}$; $\text{CoFe}_2\text{O}_4/\text{MgO}$; Peroxyomonosulphate activation.

INTRODUCTION

Dyestuffs represent one of the largest groups of organic pollutants in wastewaters, generally released from textile finishing, dye manufacturing, leather dyeing, pulp and paper production, Kraft bleaching and tannery industries [1]. Dyes are considered hazardous to the environment and could cause significant health concerns due to their non-biodegradability, toxicity, potential carcinogenic and mutagenic nature [2]. Therefore, the removal of dyes from industrial effluents prior to their discharge into natural water bodies has attracted much interest and is an important practical problem.

Advanced oxidation processes (AOPs) based on the activation of environmental friendly oxidants to generate highly reactive radicals are recognized as effective technologies for degradation of refractory organic pollutants in water at ambient conditions [3-5]. Over the past few years, sulphate radical based-AOPs are attracting considerable attention in the area of wastewater treatment because, compared to hydroxyl radicals, sulphate radicals ($\text{SO}_4^{\bullet-}$) have higher oxidizing strength, longer half-life and are more selective for the oxidation of contaminants in industrial effluents, thus overcoming some limitations of the conventional Fenton processes [5,6]. An efficient route for production of $\text{SO}_4^{\bullet-}$ is the homogeneous activation of peroxy-monosulphate (PMS) with transition metal ions, cobalt ions being the best activator [7]. However, cobalt is recognized as a priority pollutant in water and the adverse effect of dissolved cobalt ions on

animals and human beings might result in environmental concern [8]. Several researchers have found that heterogeneous cobalt-based catalysts - bulk and immobilized on various supports such as TiO_2 , Al_2O_3 , SiO_2 , activated carbon, etc., coupled with PMS exhibited a good performance on the degradation of 2,4-dichlorophenol and phenol [8-10]. However, few studies have been conducted on cobalt oxides and supported Co oxides for degradation of organic dyes using PMS as oxidant [11-13]. Considering the environmentally friendly nature, relative low cost and abundance of iron, Su *et al.* [14] have investigated the catalytic activity of a series of $\text{Co}_x\text{Fe}_{3-x}\text{O}_4$ nanoparticles for activation of PMS for heterogeneous degradation of RhB dye and found that the increase in cobalt content in the catalyst resulted in higher degradation efficiency. In our previous study cobalt and mixed iron-cobalt oxides immobilized on MgO were synthesized and were proven to be very effective heterogeneous catalysts for Acid Orange 7 oxidation in aqueous solution by using PMS as oxidant [15]. To date, few studies have reported the heterogeneous degradation of RhB in aqueous solution through sulphate radical approach [13, 14, 16].

This study reports the oxidative degradation of the refractory dye Rhodamine B in aqueous solutions using Co_3O_4 and CoFe_2O_4 supported on MgO as catalysts for heterogeneous activation of PMS. The kinetics of the oxidation process and the effect of some important factors such as catalyst dosage, PMS concentration, and initial solution pH on the RhB degradation efficiency were investigated. Furthermore, quenching experiments were conducted for identifying the dominating reactive

* To whom all correspondence should be sent:

E-mail: marianas@uni-plovdiv.bg

radicals generated from the catalyst-mediated decomposition of PMS.

EXPERIMENTAL

MgO supported catalysts with 5 wt. % Co_3O_4 or CoFe_2O_4 loading were prepared by incipient wetness impregnation [15]. Bulk Co_3O_4 and CoFe_2O_4 were prepared by a precipitation/co-precipitation method.

XRD patterns of the samples were obtained on a TUR M62 powder X-ray diffractometer (XRD) using Co-K α radiation ($\lambda=1.789 \text{ \AA}$) at 40 kV and 20 mA. The morphology of the catalysts was characterized on a JEOL JEM 2100 high resolution transmission electron microscope (TEM) using an accelerating voltage of 60 kV. Two basic regimes of microscope mode were used – bright field transmission microscopy (TEM) and selected area electron diffraction (SAED). The pH of the point of zero charge (pH_{PZC}) of the catalysts was determined by the pH drift method [17]. The amount of cobalt and iron in the prepared samples, as well as the concentrations of leached Co and Fe in the solution were measured by atomic absorption spectrometry (AAS, Perkin-Elmer).

Catalytic oxidation of RhB with PMS was carried out in a 400 cm³ glass reactor at 293 K with constant stirring at around 400 rpm. In a typical experimental procedure, a fixed amount of catalyst was added to a 200 cm³ solution containing 50 mg dm⁻³ of RhB and the suspension was stirred for 30 min to achieve adsorption-desorption equilibrium. The reaction was initiated by addition of oxidant to attain the predefined PMS/RhB molar ratio. Aliquots of 4.0 cm³ withdrawn from the mixture at given time intervals were immediately mixed with 1 mL of methanol to quench the reaction. The RhB concentration in the aqueous solution was determined by means of UV–Vis spectrophotometry (Cintra 101, GBS) at 554 nm. All tests were conducted in triplicate to ensure the reproducibility of experimental results.

RESULTS AND DISCUSSION

The crystal structure of the synthesized supported catalysts was investigated by XRD and compared with those of the MgO support and bulk cobalt and iron-cobalt oxides (Fig. 1). The spectra of unsupported samples showed distinct peaks, which match well with cubic spinel-type Co_3O_4 (JCPDS 42-1467, lattice parameter $a=8.08 \text{ \AA}$) and CoFe_2O_4 (JCPDS 22-1086, lattice parameter $a=8.37 \text{ \AA}$), respectively. The average crystallite size of bulk Co_3O_4 and CoFe_2O_4 , calculated according to the Debye-Scherrer equation, was found to be 34.7 and 11.3 nm, respectively. As seen in Fig.1, the XRD

patterns of $\text{Co}_3\text{O}_4/\text{MgO}$ and $\text{CoFe}_2\text{O}_4/\text{MgO}$ are similar to that of bare MgO and no obvious reflections typical of the corresponding spinel oxide phases could be observed. This suggests a high dispersion of cobalt and iron particles on MgO because the Fe and/or Co levels on supported catalysts were close to preparation settings as revealed from the AAS analysis.

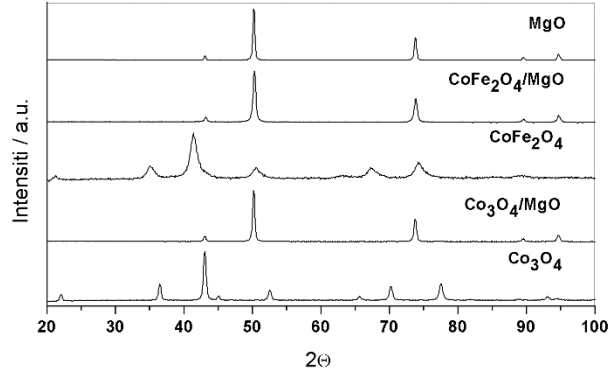


Fig. 1. XRD patterns of bulk and MgO supported Co_3O_4 and CoFe_2O_4

The presence of spinel structured oxide phases on MgO was evidenced by using TEM (Fig. 2). The bright field TEM images (Fig. 2a) show that the immobilized spinel oxide nanoparticles (the small dark spots) are well dispersed on the surface of the MgO support and their size is in the range of about 10-20 nm. The diffraction patterns (SAED) obtained from the TEM (Fig. 2b) show spinel phases Co_3O_4 and CoFe_2O_4 , respectively, with the diffraction rings corresponding to reflections from the crystal planes of the expected phases marked on the figure.

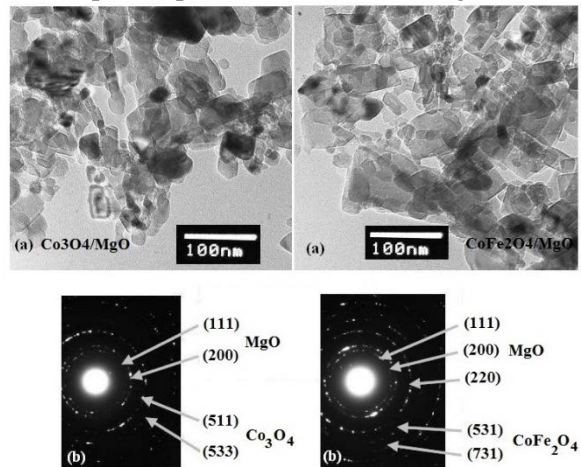


Fig. 2. (a) Bright field TEM (60 kX) and (b) SAED patterns of the synthesized supported catalysts.

The temporal spectral changes of RhB in solution during oxidative degradation on the $\text{Co}_3\text{O}_4/\text{MgO}$ sample are depicted in Fig. 3. It is seen that the characteristic RhB absorption peak at 554 nm rapidly decreases throughout the reaction and finally disappears, indicating the facile break-up of the

conjugated xanthene structure. Meanwhile, no hypsochromic shift in the maximum absorption band of RhB was observed during oxidation, implying that no N-de-ethylation of the dye takes place in competition with the degradation of the RhB chromophore ring. Furthermore, a simultaneous reduction in the absorption peak at 259 nm attributed to the $\pi-\pi^*$ transition in the aromatic ring group was also registered, indicating concomitant degradation of the aromatic part of the RhB dye. Since there are no additional peaks appearing in the UV–Vis spectra in the course of the experiment, it could be speculated that no other products detectable by UV–Vis spectroscopy are left in the reaction mixture.

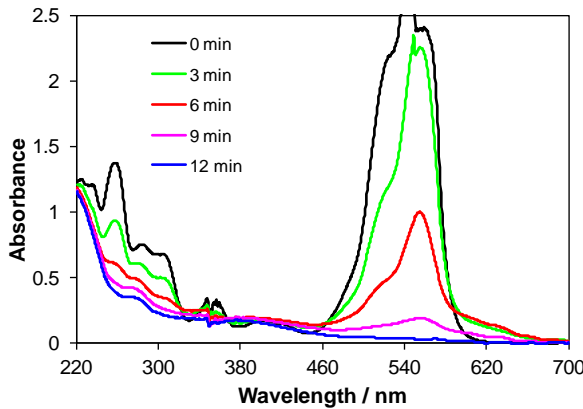


Fig. 3. UV-vis spectral changes of RhB in the $\text{Co}_3\text{O}_4/\text{MgO}$ -PMS process.

The representative data for degradation of RhB in different systems are presented in Fig. 4.

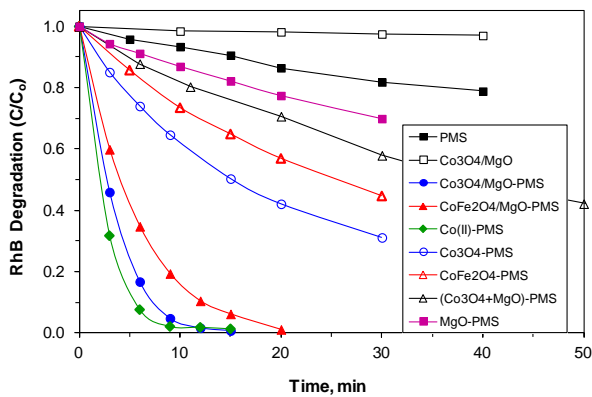
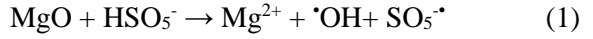


Fig. 4. RhB degradation with time in different systems. Reaction conditions: $[\text{RhB}]_0 = 50 \text{ mg dm}^{-3}$, catalyst loading = 0.15 g dm^{-3} , PMS/RhB=20:1.

In the control experiment without PMS a negligible decay of nearly 2.5% in RhB concentration was noticed within 30 min, which could be attributed to physical adsorption of dye molecules on the surface of the supported catalysts. PMS alone brought about only 22% RhB removal after 30 min, indicating that the oxidant itself could not induce significant RhB oxidation. A limited RhB degradation was also observed in the presence of

bare MgO coupled with PMS. After 30 min, the RhB reduction was less than 30%, implying that PMS could be activated by MgO to produce peroxyomonosulphate radicals ($\text{SO}_5^{\cdot-}$) probably due to the following reaction,



However, the RhB oxidation over bare MgO slightly differs from that of PMS self-oxidation, suggesting that generation of radical species in the given case takes place at a very low rate. Besides, the observed linear RhB removal profile in the MgO–PMS mixture further evidences that activation of oxidant is the rate-limiting step of the oxidation process rather than the destruction of the dye molecules by radicals formed.

The catalytic performance of unsupported Co_3O_4 and CoFe_2O_4 oxides was also explored. The results reported in Fig. 4 revealed that the RhB degradation rate has reached less than 60% and 43 % within 20 min in the Co_3O_4 -PMS and CoFe_2O_4 -PMS systems, respectively. However, when Co_3O_4 and CoFe_2O_4 nanoparticles immobilized on MgO were used as catalysts for PMS activation, RhB underwent rapid and almost complete degradation. More than 99% of RhB was eliminated in 12 min using $\text{Co}_3\text{O}_4/\text{MgO}$, whereas $\text{CoFe}_2\text{O}_4/\text{MgO}$ displayed lower activity, with complete dye removal after 20 min. Moreover, the performance of the supported catalyst was found only slightly inferior to that of the homogeneous $\text{Co}(\text{II})/\text{PMS}$ reagent. A very low extent of cobalt and iron leaching from $\text{Co}_3\text{O}_4/\text{MgO}$, and $\text{CoFe}_2\text{O}_4/\text{MgO}$ catalysts (less than 3%) during the reaction suggests that the RhB degradation is not influenced by the homogeneous reaction taking place due to the leached metal ions. These results strongly suggested that the spinel structured oxide supported on MgO has strong PMS activation functionalities. The relatively slower RhB degradation kinetics assisted by supported cobalt ferrite could be attributed to the lower cobalt content in this catalyst. Moreover, our previous Mössbauer studies showed that Fe ions in the synthesized $\text{CoFe}_2\text{O}_4/\text{MgO}$ are in 3+ oxidation state and occupy both tetrahedral and octahedral sites in a face-centered cubic crystalline structure [15]. Unlike Co (II), Fe (III) is an electron acceptor and decomposes PMS by generating $\text{SO}_5^{\cdot-}$. These radicals are much less reactive than sulphate radicals and hence their contribution to the oxidative destruction of the dye is insignificant.

Meanwhile, Co species in Co_3O_4 are also a mixture of Co(II) and Co(III) with Co(III) being predominant (the molar ratio of Co(III)/Co(II) is 2 as it is the Fe(III)/Co(II) ratio in CoFe_2O_4). It could be

speculated that the better catalytic activity of $\text{Co}_3\text{O}_4/\text{MgO}$ resulted from the more intimate interactions between Co(III) and Co(II) at the molecular level (i.e. Co–Co linkages) than Fe–Co interactions in $\text{CoFe}_2\text{O}_4/\text{MgO}$. As a result, the cobalt redox cycling in Co_3O_4 could take place faster thus facilitating the radical generation. Although the $\text{Co}_3\text{O}_4/\text{MgO}$ catalyst exhibited higher catalytic effect on RhB degradation than supported cobalt ferrite, the latter is a more relevant catalyst considering environmental and practical aspects (non-toxicity and abundance of iron).

The observed enhancement in the catalytic activity of MgO loaded Co_3O_4 and CoFe_2O_4 could be attributed to two factors: (i) the hydroxyl groups on the surface of MgO facilitate the formation of functional Co(II)–OH complexes through direct interaction of surface cobalt species with the nearby surface OH groups on the support, which are crucial for radical generation in the subsequent step of PMS activation [18]; (ii) the basic surface of MgO ensures good dispersion of the active phase, leading to more intimate interaction of cobalt species with the surface hydroxyl groups of the support. Hence, more active sites for PMS activation were produced on $\text{Co}_3\text{O}_4/\text{MgO}$ and $\text{CoFe}_2\text{O}_4/\text{MgO}$ compared to their bulk analogues, which led to the accelerated generation of active radicals and thus to the higher RhB degradation efficiency. The much weaker catalytic performance exhibited by the mechanical mixture of Co_3O_4 and MgO confirms the crucial role of the close contact between the support and the active oxide phase for the efficient PMS activation.

Experimental data revealed that RhB oxidation over bulk and MgO supported catalysts follows the first order kinetics. The reaction rate constants (k) and regression coefficients (R^2) of the model fitting are given in Table 1.

Table 1. Kinetic parameters of RhB degradation in different catalyst – PMS systems

Catalyst	Rate constant (min^{-1})	R^2
Co_3O_4	0.0428	0.992
CoFe_2O_4	0.0274	0.994
$\text{Co}_3\text{O}_4/\text{MgO}$	0.3243	0.994
$\text{CoFe}_2\text{O}_4/\text{MgO}$	0.2212	0.991

Further assessment of the efficiency of the as-prepared supported catalysts for RhB degradation was done by studying the influence of several operating parameters, including catalyst dosage, PMS concentration, and initial solution pH.

The RhB degradation efficiency was enhanced with the increase in catalyst dosage regardless the nature of the supported active phase (Fig. 5). The increased reaction rate with catalyst loading is

evidently due to the availability of more active sites on the catalyst surface for activation of PMS, resulting in faster generation of more reactive radicals. In fact, complete RhB removal could be reached within 12 min at $\text{Co}_3\text{O}_4/\text{MgO}$ loading of 0.15 g dm^{-3} , whereas catalyst concentration at 0.5 g dm^{-3} resulted in 100% dye degradation within very short duration of 3 min. Accordingly, upon the same increase in the amount of $\text{CoFe}_2\text{O}_4/\text{MgO}$ catalyst, the time required for full discoloration of dye solution was reduced 2.5 times.

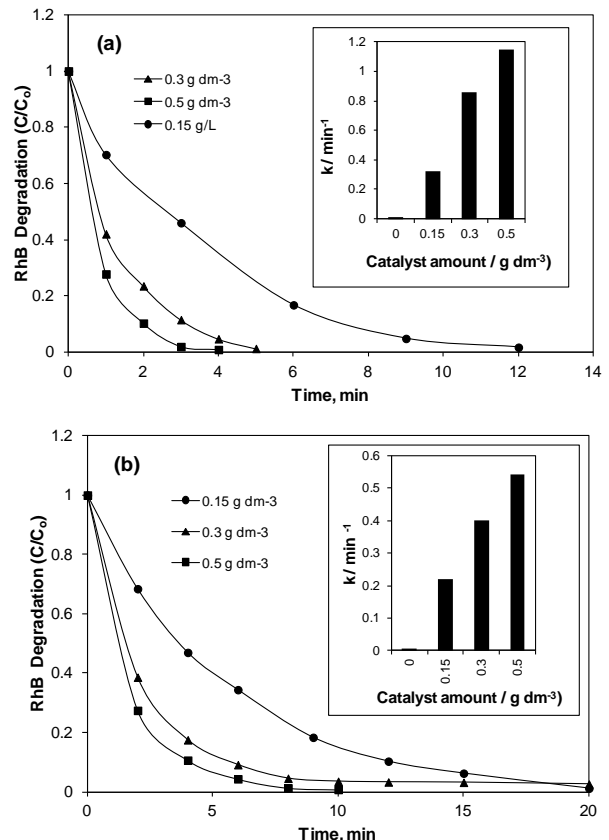


Fig. 5. Effect of catalyst amount on the RhB degradation rate. (a) $\text{Co}_3\text{O}_4/\text{MgO}$; (b) $\text{CoFe}_2\text{O}_4/\text{MgO}$ (0.15 g dm^{-3}). Reaction conditions: $[\text{RhB}]^0 = 50 \text{ mg dm}^{-3}$, $\text{PMS/RhB}=20:1$.

However, a less pronounced increase of the rate constants with catalyst amount increasing from 0.3 to 0.5 g dm^{-3} was found (inset of Fig. 5), which could be due to the self-quenching of a rapidly generated large amount of radicals by PMS instead of reacting with target molecules. Another reason could be the formation of aggregates between catalyst particles which resulted in a reduced number of available sites for PMS activation. It should be emphasized that although a difference in the degradation rate of RhB was observed, the final removal efficiencies were similar due to the same concentration of oxidant.

Fig. 6 presents RhB degradation kinetics in the presence of $\text{Co}_3\text{O}_4/\text{MgO}$ at different PMS concentrations (in terms of molar ratio of

PMS/RhB). As can be seen, faster RhB decay rate and higher removal efficiency are achieved by increasing the PMS/RhB molar ratio due to the production of more radicals to degrade RhB dye. At a molar ratio of 2/1, RhB was slowly and not completely degraded with a final removal of 51.8 % after 20 min, while for the same duration at a five-fold higher PMS concentration, the removal efficiency was near 100%. Incomplete degradation of the dye was also registered using a molar ratio of 6/1, attributed to the depletion of oxidant, which dosage was much less than the required stoichiometric dosage for complete RhB mineralization [13].

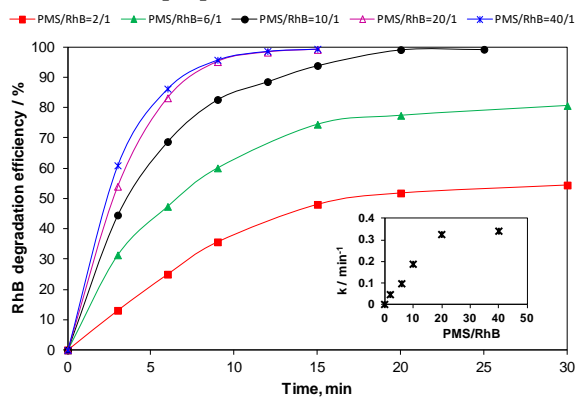


Fig. 6. RhB degradation over $\text{Co}_3\text{O}_4/\text{MgO}$ at different PMS concentrations. Reaction conditions: $[\text{RhB}]^0 = 50 \text{ mg dm}^{-3}$, catalyst loading = 0.15 g dm^{-3} .

The RhB removal rate, as characterized by the pseudo-first order rate constant, increased almost linearly with increasing PMS/RhB ratio up to 20/1, implying that the active sites on the catalyst surface were still not totally occupied by PMS, but no significant change in the removal efficiency was observed at further increasing the PMS dosage (inset of Fig. 6). The observed trend might be attributed to the fixed number of surface active sites, which gradually became the limiting factor controlling the yield of radicals at high PMS concentration, so that the radical yield was almost independent of PMS. Less pronounced enhancement of the RhB removal efficiency when the molar ratio of PMS/RhB was higher than 20/1 could also be explained by the increased competition of the higher number of PMS molecules for absorption and consequent activation on the finite number of surface sites.

Since the dye-containing effluents are discharged at various pH, the ability of a heterogeneous catalyst to operate efficiently under different pH conditions is highly desirable. The effect of initial pH on the RhB degradation over supported catalysts was studied at pH 4.1, 6.98 and 9.2 and the results are presented in Fig. 7. It is obvious that acidic medium is more suitable for the catalytic degradation reaction

and an evident decrease in the RhB degradation efficiency can be observed in neutral-alkaline conditions. At the initial pH of 6.98, 100% RhB removal was achieved after 40 min using the $\text{CoFe}_2\text{O}_4/\text{MgO}$ catalyst, while the dye was fully degraded for a twice shorter period when pH was decreased to 4.1. It is worthy to note that even under alkaline conditions, a complete discoloration of the RhB solution could be achieved in about one hour, implying that the catalysts prepared still exhibited a good catalytic activity at high pH values.

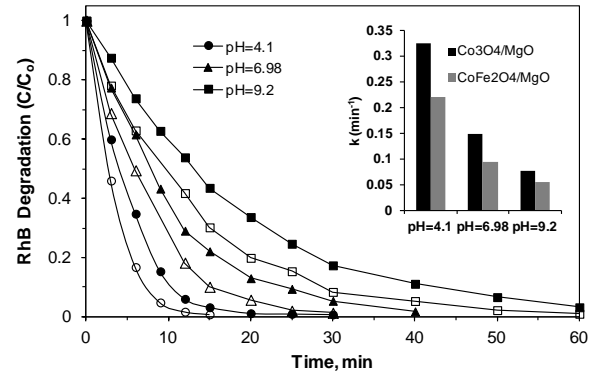


Fig. 7. Effect of pH on RhB degradation over $\text{Co}_3\text{O}_4/\text{MgO}$ (open symbols) and $\text{CoFe}_2\text{O}_4/\text{MgO}$ (closed symbols). Reaction conditions: $[\text{RhB}]^0 = 50 \text{ mg dm}^{-3}$, catalyst loading = 0.15 g dm^{-3} , PMS/RhB=20:1.

The decrease in dye removal rate with increasing pH (inset of Fig. 7) might be explained considering that the solution pH significantly affects the surface charge of the catalysts and the speciation of RhB and PMS in solution. Hence, the adsorption of dye molecules and the effectiveness of oxidant activation on the catalyst surfaces could change at different pH and thus influence the degradation efficiency. Since the pH_{PZC} of the MgO supported catalysts was found about 9.8 – 10.1, the surface of the catalyst particles was positively charged in the entire pH range studied. On the other hand, at pH values higher than pK_a of RhB (3.7), the carboxyl group of the cationic form of the dye is deprotonated and the zwitterionic form of RhB is formed [19]. Accordingly, due to the electrostatic interaction, RhB species tend to adsorb on the positively charged surface sites of the catalyst via the negatively charged carboxyl group. However, the positively charged surface sites decrease with increasing pH, while the fraction of zwitterionic form increases. The latter would favor the aggregation of RhB by forming dimers due to the electrostatic interactions between the xanthenes and the carboxyl groups of the RhB monomers. The adsorption of large dimers is hindered and under such conditions the RhB removal might be inhibited. Furthermore, the observed decreasing trend could also be due to the radical scavenging effect of bicarbonate anions used to adjust pH, as well as to

the inefficient self-decomposition of PMS through a non-radical pathway at high pH values [20]. Thus, these could be possible reasons for the lower RhB degradation rates observed at neutral-alkaline conditions.

The activation of PMS by heat, UV, metal ions or metal oxides usually generates two major kinds of radicals, *viz.*, hydroxyl radicals ($\cdot\text{OH}$) and sulphate radicals ($\text{SO}_4^{\cdot-}$) [3, 9, 21]. To confirm that RhB degradation resulted from radical attack and to identify the dominant radical species generated by catalyst/PMS couples, quenching tests were conducted with the addition of EtOH and TBA as radical scavengers. Ethanol acts as a scavenger of both $\cdot\text{OH}$ and $\text{SO}_4^{\cdot-}$, while TBA is often used as an effective $\cdot\text{OH}$ quenching agent because the rate constant of TBA with $\cdot\text{OH}$ is approximately 1000 times greater than that with $\text{SO}_4^{\cdot-}$ [3]. The effect of both quenching agents on the rate and efficiency of RhB catalytic oxidation over $\text{Co}_3\text{O}_4/\text{MgO}$ is shown in Fig. 8.

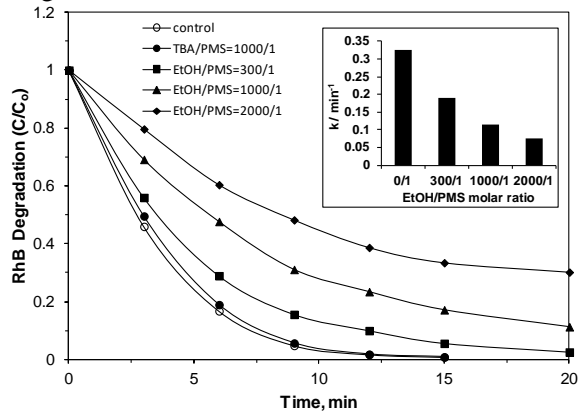


Fig. 8. Effect of different radical scavengers on RhB degradation in the $\text{Co}_3\text{O}_4/\text{MgO}$ - PMS system. Reaction conditions: $[\text{RhB}]_0 = 50 \text{ mg dm}^{-3}$, catalyst loading = 0.15 g dm^{-3} , PMS/RhB=20:1.

Results showed that there was no distinct difference in the rate and efficiency of RhB removal when TBA was added to the reaction mixture even at very high dosage. However, addition of ethanol suppressed the oxidation process and the inhibition was enhanced with increasing EtOH concentration (inset of Fig. 8). In fact, only 10% drop in RhB degradation efficiency with rate constant decreasing from 0.3243 min^{-1} at lower EtOH/PMS molar ratio (300/1) was observed despite the fact that ethanol is a strong quencher of both sulphate and hydroxyl radicals. The RhB degradation was more significantly inhibited on further increase in the ethanol dosage (EtOH/PMS =2000/1), attaining only 70.6% oxidation upon exhaustion of the oxidant. The

same effect of both scavenging agents was also observed in the PMS- $\text{CoFe}_2\text{O}_4/\text{MgO}$ oxidation system. The results provided evidence that sulphate radicals appeared to be the major radical species generated during the activation of PMS by the catalysts prepared in this work and controlling the oxidation reaction.

CONCLUSIONS

In this study, sulphate radical-based degradation of RhB in aqueous solutions was studied. Reactive radicals were produced through heterogeneous activation of PMS mediated by Co_3O_4 and CoFe_2O_4 supported on MgO. Deposition of Co_3O_4 and CoFe_2O_4 nanoparticles on a basic MgO support led to considerable enhancement of their PMS activation functionality. MgO-supported catalysts produced fast and complete degradation of RhB (50 mg dm^{-3}) the apparent rate constants being almost eight-fold of that over corresponding bulk analogues. More than 99% of RhB was degraded in 12 min using $\text{Co}_3\text{O}_4/\text{MgO}$, while a slightly inferior catalytic performance was presented by the $\text{CoFe}_2\text{O}_4/\text{MgO}$ catalyst with complete dye removal after 20 min. The higher catalytic activity of supported catalysts compared to bulk oxides is attributed to the increased basicity of the catalyst surfaces, which facilitates decomposition of oxidant and thus favors radical generation. Increasing the catalyst amount and PMS concentration enhanced the RhB degradation rate, while removal efficiency decreased as solution pH rose. Quenching studies showed that the destruction of RhB is due to the generated sulphate radicals.

Acknowledgements: Authors gratefully acknowledge financial support by the National Science Fund (Project DFNI-T02/4) and by the University of Plovdiv Research Fund (Project NI HF-2017).

REFERENCES

- D. J. Ju, I.G. Byun, J.J. Park, C.-H. Lee, G.H. Ahn, T.J. Park, *Bioresour. Technol.*, **99**, 7971 (2008).
- A. Babuponnusami, K. Muthukumar, *JECE* **2** (1), 557 (2014).
- G.P. Anipsitakis, D.D. Dionysiou, *Environ. Sci. Technol.* **37**, 4790.
- A.D. Bokare, W. Choi, *J. Hazard. Mater.* **275**, 121 (2014).
- M.V Bagal, P.R. Gogate, *Ultrason. Sonochem.* **21**, 1(2014).
- Q. Yang, H. Choi, Y. Chen, D.D. Dionysiou, *Appl. Catal. B- Environ.*, **77**, 300 (2008).
- S. Yang, P. Wang, X. Yang, L. Shan, W. Zhang, X. Shao, R. Niu, *J. Hazard. Mater.*, **179** (2010) 552–558.

8. P. Shukla, H.Q. Sun, S.B. Wang, H.M. Ang, M.O. Tade, *Catal. Today*, **175**, 380 (2011).
9. Q. Yang, H. Choi, Y. Chen, D.D. Dionysiou, *Appl. Catal. B- Environ.*, **77**, 300 (2008).
10. E. Saputra, S. Muhammad, H. Sun, H.M. Ang, M.O. Tade, S. Wang, *J. Colloid Interface Sci.*, **407**, 467 (2013).
11. W. Zhang, H.L. Tay, S.S. Lim, Y. Wang, Z. Zhong, R. Xu, *Appl. Catal. B- Environ.*, **95**, 93 (2010).
12. P. Shi, R. Su, S. Zhu, M. Zhu, D. Li, S. Xu, *J. Hazard. Mater.*, **229-230**, 331 (2012).
13. L. Hu, F. Yang, W. Lu, Y. Hao, H. Yuan, *Appl. Catal. B- Environ.*, **134-135**, 7 (2013).
14. S. Su, W. Guo, Y. Leng, C. Yi, Z. Ma, *J. Hazard. Mater.*, **224-245**, 736 (2013).
15. M. Stoyanova, I. Slavova, St. Christoskova, V. Ivanova, *Appl. Catal., A-Gen.*, **476**, 121 (2014).
16. F. Ji, C. Li, Y. Liu, P. Liu, *Sep. Purif. Technol.*, **135**, 1 (2014).
17. P.C.C. Faria, J.J.M. Órfão, M.F.R. Pereira, *Water Res.*, **38**, 2043 (2004).
18. Q. Yang, H. Choi, and D.D. Dionysiou, *Appl. Catal. B- Environ.*, **74**, 170 (2007).
19. S. Merouani, O. Hamdaoui, F. Saoudi, M. Chiha, *Chem. Eng. J.*, **158**, 550 (2010).
20. A. Rastogi, S.R. Al-Abed, D.D. Dionysiou, *Appl. Catal. B- Environ.*, **85**, 71 (2009).

КАТАЛИТИЧНО ОКИСЛЕНИЕ НА РОДАМИН В ВЪВ ВОДНИ РАЗТВОРИ СЪС СУЛФАТНИ РАДИКАЛИ ВЪРХУ Co₃O₄/MgO И CoFe₂O₄/MgO

И. А. Славова, Ст. Г. Христоскова, М. К. Стоянова*

Катедра "Физикохимия", Пловдивски университет "Паисий Хилендарски", ул. „Цар Асен“, № 24, 1000
Пловдив, България

Получена на 11 април, 2016 г.; коригирана на 25 октомври 2016 г.

(Резюме)

Изследвано е окислителното разграждане на Родамин B във водни разтвори с пероксимоносулфат (PMS) с използване на Co₃O₄/MgO и CoFe₂O₄/MgO като катализатори. Синтезираните образци показват висока PMS-активационна способност, независимо от ниското съдържание на нанесената активна фаза (5wt%) и много ниската концентрация на катализатора (0.15 g dm⁻³). Активността на нанесените катализатори е значително по-висока от тази на масивните им аналоги и на физични смеси на шпинелните оксиди и MgO, дължащо се на определящата роля на базичния носител за подпомагане разлагането на PMS до силно реактивоспособни радикали. Разграждането на RhB се подчинява на кинетичните закономерности на реакции от първи порядък. Изследвано е влиянието на количеството на катализатора, концентрацията на PMS и pH върху скоростта на окислителния процес. Чрез експерименти с добавяне на радикал-улавящи агенти са идентифицирани радикаловите частици, образувани при катализитичното разлагане на окислителя.

Modeling of the relationship between biological activity of delta-selective enkephalin analogues and docking results by polynomials

F.I. Sapundzhi^{1*}, T.A. Dzimbova², N.S. Pencheva¹, P.B. Milanov^{1,3}

¹South-West University "Neofit Rilski", Bulgaria, 2700 Blagoevgrad

²Institute of Molecular Biology, Bulgarian Academy of Sciences, Bulgaria, 1113 Sofia

³Institute of Mathematics and Informatics, Bulgarian Academy of Sciences, Bulgaria, 1113 Sofia

Received November 30, 2016; Accepted February 10, 2017

One of the areas of bioinformatics is the development of fast and reliable methods for predicting the biological activity of compounds. This will facilitate the design of new compounds and reduce costs. The process of creating selective ligands of a delta opioid receptor (DOR) was directed towards the synthesis of enkephalin analogues. Their biological activity was determined by using *in vivo* and *in vitro* methods, which allows establishing the relationship between structure and biological activity. The relationship between the values of the ChemScore scoring function from the docking procedure in GOLD 5.2 and the values of the total energy of the ligand-receptor complex in MolleGro was modeled with first- to third-degree polynomials and a surface fitted method. The polynomial surface of third degree displayed the best fit, assessed by the least squares method. In our previous study with the theoretical model of DOR (PDBid:1ozc) the relationship between the values of efficacy of the compound, the values of the GoldScore scoring function from the docking procedure in GOLD 5.2 and the values of the total energy of the ligand-receptor complex in MolleGro was established. This relationship was modeled with a third-degree polynomial in software MATLAB. The aim of the present work was to find an optimal fitting polynomial function modeling the relationship between the quantitative parameters of *in vitro* bioassay and the values of the scoring functions from molecular docking with crystal structure of DOR (PDBid:4ej4) and delta-opioid ligands using the least squares method. The third-degree polynomial was successfully used for modeling the relationship between the efficacy of delta-selective enkephalin analogues and docking results. It was described by a polynomial surface of third degree.

Keywords: Computer modelling, QSAR, Surface fitting, Scoring functions, Molecular docking, Delta opioid receptor.

INTRODUCTION

Morphine produces a large diversity of pharmacological responses by interacting with the opioid receptors in the nervous system. It is an agonist ligand for μ -, δ - and κ -opioid receptors and that is why most of its effects are due to particular ligand-receptor interactions. The delta-opioid receptor (DOR) is part of the G-protein-coupled receptors (GPCR) and plays an important role in the perception of pain.

The design of selective and effective ligands for DOR is related with a lot of experiments with different enkephalin analogues. These analogues were synthesized and biologically tested in previous *in vitro* studies [1, 2]. According to the *in vitro* results and the mathematical model of a partial agonism [3], the potency (concentration which produces 50 % of the maximal response of the tissue, IC_{50}), could be calculated with the explicit formulas of the affinity (reciprocal of the dissociation constant, K_A) of the respective analogues, and the relative efficacy (e_{rel}).

In silico experiments are very helpful in drug design, because of their major role in reducing the time and the costs of the studies and they can be used as viable alternatives to animal trials. The structure-based drug design methods which include three-dimensional structural information from biological targets are an important component of modern medicinal chemistry [4]. Molecular docking and structure-based virtual screening are often used in structure-based drug design because of their applications in the analysis of molecular recognition such as binding, energetic, molecular interactions and conformational changes [5]. The molecular docking of ligands with a protein structure (in our case DOR with crystal structure) aims to predict the ligand-protein complex structure by exploring the conformational space of the ligands within the binding site of the protein. The scoring functions are then used to approximate the free energy of binding between the protein and the ligand in each docking pose.

The aim of the present study was to investigate the relationship between the values of the quantitative parameters of *in vitro* tests e_{rel} , K_A , IC_{50} and the results of the molecular docking - the minimum energy conformation for each ligand-receptor complex, the scoring functions to calculate

* To whom all correspondence should be sent:
E-mail: sapundzhi@swu.bg

binding affinities of protein-ligand complexes based on experimental structure and the data from *in vitro* bioassay.

To this purpose the following tasks should be solved: 1) implementation of the molecular docking calculations of the model of DOR with crystal structure (PDBid:4ej4) and the delta-selective enkephalin analogues, and calculation of the total energies of the formed ligand-receptor complex after the docking procedure and 2) finding a function $z = f(x, y)$ from some class of polynomials, that fits given n distinct data points $\{(x_i, y_i, z_i)\}_{i=1}^n$ in R^3 by the least squares method.

MATERIALS AND METHODS

Receptor – DOR (PDBid:4ej4)

The model of the delta-opioid receptor with crystal structure published in the RCSB Protein Data Base (PDBid: 4ej4) was used (<http://www.rcsb.org>). This protein is long 461 amino acids [6].

Ligand - delta-selective enkephalin analogues and related compounds

The ligands used in this study were tested for their values of IC_{50} , K_A , e_{rel} in an *in vitro* test in previous research [1-3]. The results from the *in vitro* bioassay of Cys²-containing and related analogues of enkephalins on their inhibitory effects of the mouse *vas deferens* tissue are presented in Table 1.

Docking procedure and scoring functions

The docking procedure was performed with the software GOLD 5.2 and all four scoring functions available in the program: GoldScore, ChemScore, ChemPLP, ASP scoring functions [7- 10]. In this paper we examined the ChemScore function as a scoring function for the protein-ligand docking program GOLD 5.2 and its benefits to carry out

accurate docking, to predict the binding energies, and to realise the biological effects of the tested compounds.

The ChemScore scoring function is an empirical function which contains angular terms for hydrogen bond interactions and emphasizes these directed interactions more strongly. It was trained by regression against measured affinity data. The ChemScore function estimates the total free energy change that occurs on ligand binding [7].

The binding site of DOR is known from the literature [11]: it comprises the residues within 10 Å around an aspartic acid residue, Asp128.

The total energies of binding of the formed ligand-receptor complexes were calculated by the Ligand Energy Inspector Tool and MolDock scoring function in software Molegro Molecular Viewer (<http://molegromolecular-viewer.software.xinformer.com>), (MMV Version 2.5) [12,13]. This tool allows getting detailed information about the energy interactions for the protein-ligand complex.

Fitting methods

The fitting of the experimental data for DOR (PDBid: 4ej4) is performed by the polynomial function (Eqn.1), where z is a dependent variable, x and y are independent variables. The values of z_1, z_2, \dots, z_n represent the values of the *in vitro* parameters IC_{50}, K_A or e_{rel} ; the values of x_1, x_2, \dots, x_n represent the results from the docking procedure, i.e. the values of GoldScore, ChemScore, ChemPLP, and ASP scoring functions; the values of y_1, y_2, \dots, y_n represent the total energies for the formed ligand-receptor complex; a_{ij} are the parameters of the model; n is the degree of the polynomial ($0 \leq i + j \leq n$). The coefficients of Eqn.1 were determined by the least squares method (Eqn.2), where m is the number of ligand-receptor complexes (data points).

Table 1. The eleven ligands used in this study

Primary structure	Ligand	Mouse <i>vas deferens</i>		
		IC_{50} (nM)	K_A (nM)	e_{rel}
Tyr-D-Pen-Gly-Phe-D-Pen	DPDPE	6.18±1.17	180±35	30.2±10.0
Tyr-Gly-Gly-Phe-Leu	[Leu ⁵]-enk	11.45±2.06	54.9±13.1	5.8±1.0
Tyr-Gly-Gly-Phe-Met	[Met ⁵]-enk	18.91±2.15	48.4±7.5	3.6±0.3
Tyr-Cys(Bzl)-Gly-Phe-Leu	[Cys(Bzl) ² , Leu ⁵]-enk	8.30±1.40	68.5±29.7	9.3±3.2
Tyr-Cys(Bzl)-Gly-Phe-Met	[Cys(Bzl) ² , Met ⁵]-enk	9.53±1.20	23.8±3.0	3.5±0.3
Tyr-Cys(O ₂ NH ₂)-Gly-Phe-Leu	[Cys(O ₂ NH ₂) ² , Leu ⁵]-enk	1.29±0.31	36.4±16.4	29.2±9.5
Tyr-Cys(O ₂ NH ₂)-Gly-Phe-Met	[Cys(O ₂ NH ₂) ² , Met ⁵]-enk	2.22±0.45	14.1±5.4	7.3±2.0
Tyr-D-Cys(O ₂ NH ₂)-Gly-Phe-Leu	[DCys(O ₂ NH ₂) ² , Leu ⁵]-enk	11.40±2.01	73.4±12.7	7.4±1.9
Tyr-D-Cys(O ₂ NH ₂)-Gly-Phe-Met	[DCys(O ₂ NH ₂) ² , Met ⁵]-enk	75.96±11.67	463±161	7.1±1.8
Tyr-HCys(O ₂ NH ₂)-Gly-Phe-Leu	[HCys(O ₂ NH ₂) ² , Leu ⁵]-enk	31.92±5.10	76.4±7.1	3.4±0.2
Tyr-HCys(O ₂ NH ₂)-Gly-Phe-Met	[HCys(O ₂ NH ₂) ² , Met ⁵]-enk	16.09±1.90	55.7±6.1	4.5±0.3

$$(1) \quad z = f(x, y) = \sum_{0 \leq i+j \leq k} a_{ij} x^i y^j$$

$$(2) \quad \underset{(a_{00}, \dots, a_{0k})}{\text{minimize}} F(a_{00}, \dots, a_{0k}) = \sum_{s=1}^t \left(z_s - \sum_{0 \leq i+j \leq k} a_{ij} x_s^i y_s^j \right)^2$$

In order to explore the fitting behavior of some polynomial degree functions, a series of fittings was carried out by a polynomial with two variables from a first to a third order. The Surface Fitting Tool of MATLAB (<http://www.mathworks.com/products/matlab>) [14] was applied and the individual model could be interpreted as a surface fitting function of the experimental data by the least squares method. This tool provides descriptive statistics, including: *R-square* (R^2), *adjusted R²* (*adj R²*), *sum of squares due to errors* (SSE), *root mean squared error* (RMSE), etc. The goodness of fit of a statistical model describes how well it fits into a set of observations: 1) SSE is a quantity used in describing how well a model represents the data being modeled, where the values of SSE near to 0 show that the model has a smaller random error component and then the fit will be useful for prediction; 2) R^2 measures how successful the fit is in explaining the variation of the data and it is defined as the ratio of the sum of squares of the regression and the total sum of squares about the mean, where the values of R^2 closer to 1 indicate that a greater proportion of variance is accounted for by the model; 3) *Adj R²* is a modified version of R^2 for the number of predictors in a model and it gives the percentage of variation explained by those independent variables only that in reality affect the dependent variable. It can take on any value less than or equal to 1, with a value closer to 1 indicating a better fit; 4) RMSE is a measure of the difference between values predicted by a model and the values actually observed from the environment that is being modeled. The values of RMSE closer to 0 indicate a fit that is more useful for prediction.

RESULTS AND DISCUSSION

The molecular docking calculations with the model of DOR with crystal structure (PDBid:4ej4) and the 11 ligands from Table 1 were carried out with software GOLD 5.2. The program for docking generated several probable ligand binding conformations at the active site around the protein target - DOR (PDBid: 4ej4). The active site of the DOR (PDBid: 4ej4) includes the residues within 10 Å around an Asp128 [19]. All four scoring functions embedded in the program in GOLD 5.2 (GoldScore,

ChemScore, ChemPLP and ASP scoring functions) were used to rank the conformations of the opioid ligands by evaluating the binding density of each of the probable complexes.

An example of the ligand-receptor interaction between DOR (PDBid:4ej4) and an endogenous ligand [Leu^5]-enkephalin around the active site - Asp128 residue - is presented in Fig. 1.

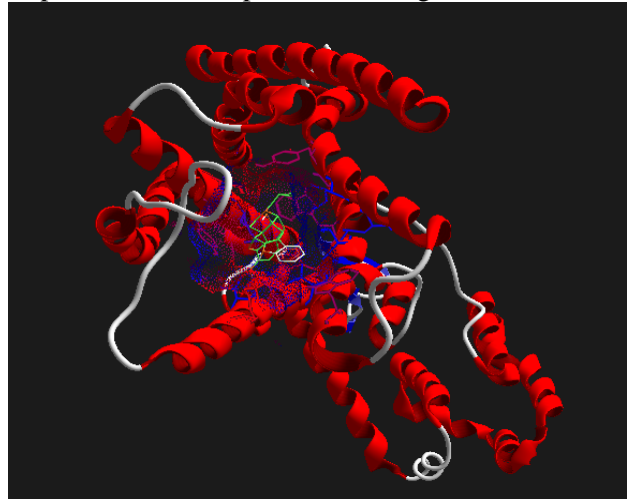


Fig. 1. Diagram of the ligand-receptor complex between DOR (PDBid:4ej4) and an endogenous ligand [Leu^5]-enkephalin. The receptor is presented in ribbons and helices. The ligand is presented in yellow circles (picture generated by Molegro Molecular Viewer).

In order to assess the suitable relationship between biological activity of the delta opioid ligands and the docking results (the values of the scoring functions in GOLD 5.2) the Surface Curve Fitting Toolbox in the software MATLAB was applied [14].

The total energies of the ligand-receptor complexes formed after molecular docking in GOLD 5.2 with the model of the DOR (PDBid: 4ej4) and the best pose of the ligands were calculated in software MMV 2.5 [12,13].

The aim of the curve fitting was to find the parameters of a mathematical model that describes the data by minimizing the difference between the model and the set of data. By using polynomial least squares surface fitting methods, polynomials of a first to a third order were used for fitting of the experimental data in both X-axis and Y-axis. These data can be represented as follows: 1) the values of z

represent the values of the *in vitro* parameters e_{rel} , K_A or IC_{50} [2]; 2) the values of x represent the docking results (the values of scoring functions GoldScore, ChemScore, ASP and ChemPLP calculated by GOLD 5.2); 3) the values of y represent the total energies for the ligand-receptor complex formed after docking with the corresponding scoring functions (the values of MolDock scoring function calculated by MMV).

The best results of the parameters used for surface fitting in MATLAB for DOR (PDBid:4ej4) can be presented as follows: the values of z represent the values of e_{rel} from *in vitro* parameters [1-3], the values of x represent the values of the ChemScore function and the values of y represent the values of the total energies for the ligand-receptor complexes. The modeling of the relationship between efficacies of enkephalin analogues, total energies calculated by MMV and ChemScore scoring function calculated by GOLD 5.3 was carried out with methods described in Section 2. The results are presented in Table 2.

The polynomial models from the first to the third degree were estimated with the statistical criteria of goodness of fit – SSE, R^2 , adjusted R^2 , RMSE. The obtained results for the statistic parameters are presented in Table 3. The goodness of fit statistics shows that the obtained model for fitting the experimental data for DOR (PDBid: 4ej4) with the third degree for x and the third degree for y is a good one.

As it can be seen from Table 3 the model of third degree is with the highest values of R^2 and the values closer to 1 show that a greater proportion of variance is explained by the model. The values of SSE for the

cubic polynomial are close to 0, which indicates that the model of third degree has a smaller random error component and the fit will be more useful for prediction. The values of $Adj\ R^2$ for the cubic polynomial are less than 1. It is a good indicator of the fit quality when two models are compared and a value closer to 1 shows a better fit. The values of RMSE for the third degree of polynomial for DOR are closer to 0 and demonstrate a fit that is more useful for prediction.

After analysing the results from Table 3 we found that the polynomial model of third degree for the surface fitting data is a good model which explains a high proportion of the variability in experimental data, and it is able to predict new observations with high certainty [21]. This model is represented as the following Eqn.(3) and the coefficients are given in Table 4.

$$(3) f(x,y) = a_{00} + a_{10} * x + a_{01} * y + a_{20} * x^2 + a_{11} * x * y + a_{02} * y^2 + a_{30} * x^3 + a_{21} * x^2 * y + a_{12} * x * y^2 + a_{03} * y^3$$

The surface fitting by the first to the third degree of the polynomial of the experimental data from Table 2 for the DOR (PDBid:4ej4) is presented in Fig. 2 (A,B,C). A graphic representation of the relationship between the three numeric variables in 2D is presented in Fig. 3 (A, B, C). The values of the ChemScore function and the values of total energy are for X and Y axes, and the values of the potency – IC_{50} are for contour levels. Fig. 4 (A, B, C) represents the residual plot for the polynomial models from the first to the third degree. These diagrams provide visual displays for assessing how well the model fits the data. They are used to evaluate the distribution of the residuals and identify influential observations [14].

Table 2. Values of the parameters used for surface fitting: ChemScore scoring function calculated by GOLD 5.2, total energy calculated by MMV and e_{rel} obtained by *in vitro* bioassay

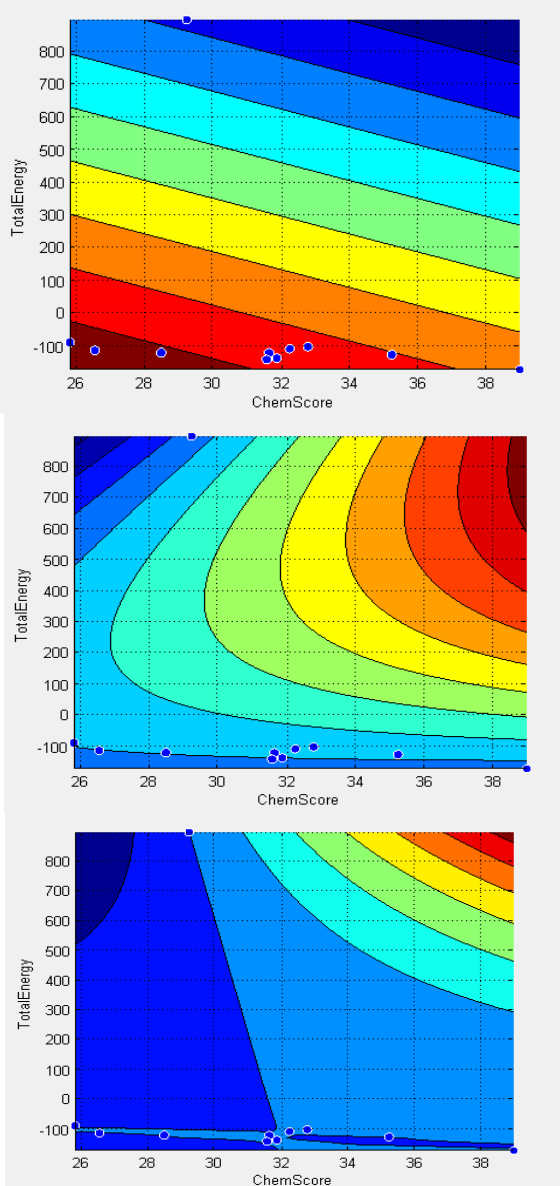
Ligand	ChemScore	Total energy	e_{rel}
[Cys(Bzl) ² , Leu ⁵]-enk	38.91	-170.657	9.3
[Cys(Bzl) ² , Met ⁵]-enk	35.19	-125.108	3.5
[Cys(O ₂ NH ₂) ² , Leu ⁵]-enk	28.48	-118.805	29.2
[Cys(O ₂ NH ₂) ² , Met ⁵]-enk	25.82	-87.343	7.3
[DCys(O ₂ NH ₂) ² , Leu ⁵]-enk	31.84	-136.187	7.4
[DCys(O ₂ NH ₂) ² , Met ⁵]-enk	31.55	-139.449	7.1
[HCys(O ₂ NH ₂) ² , Leu ⁵]-enk	32.75	-100.702	30.2
[HCys(O ₂ NH ₂) ² , Met ⁵]-enk	26.55	-112.164	3.4
DPDPE	29.23	896.877	4.5
[Leu ⁵]-enk	31.62	-119.009	5.8
[Met ⁵]-enk	32.22	-106.792	3.6

Table 3. Assessing the goodness of fit for the polynomial models obtained by the least squares method

Degree	SSE	R^2	$Adj\ R^2$	RMSE	Coefficient
First	443.5817	0.5446	0.4308	7.4463	3
Second	167.1000	0.8285	0.6569	5.7810	6
Third	0.0092	1.0000	0.9999	0.0960	10

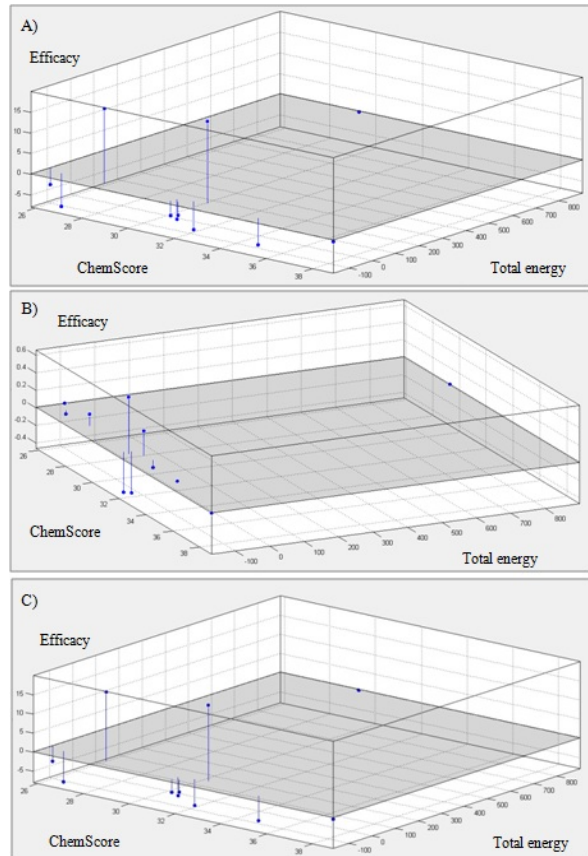
Table 4. Mean values (confidence bounds) of the coefficients of the third-order polynomial model.

Coefficients	Mean (with 95% confidence bounds)
a ₀₀	-188.4 (-705.4; 373.7)
a ₁₀	1855 (-17.99; 3279)
a ₀₁	-828.1 (-4019; 2363)
a ₂₀	740.8 (48.93; 1433)
a ₁₁	1.3 (-397.5; 2.639)
a ₀₂	839.8 (-1929; 3609)
a ₃₀	83.1 (29.72; -136.5)
a ₂₁	2506 (119.9, 4892)
a ₁₂	2.3 (-1630; 4.563)
a ₀₃	4556 (-1526; 1.065)

**Fig.3.** 2D contour plot of the 3D surface in Fig. 2 for the model of DOR (PDBid:4ej4). The first degree polynomial fitting is presented in (A); the second degree in (B); the third degree in (C). The diagrams were generated with MATLAB.

The top plot of the residual plot presented in Fig. 4 (A, B, C) shows that the residuals are calculated as

the vertical distance from the data point to the fitted curve [14]. The bottom plot presented in Fig. 4 (A, B, C) displays the residuals relative to the fit which is the zero line.

**Fig. 4.** The residuals plot for the obtained polynomial models of the first degree is presented in (A); the second degree in (B); the third degree in (C). The diagrams were generated with MATLAB.

Several studies were performed in this direction with other two models of DOR: 1) a theoretical model of DOR (PDBid:1ozc) and 2) a model of DOR obtained by homology modeling, named *Model B* [15-26].

A relationship between the values of the efficacy e_{rel} from *in vitro* parameters [1,2,3] and the values of GoldScore scoring function from docking procedure in GOLD 5.2 and the values of total energies of formed ligand-receptor complexes was established for the theoretical model of DOR (PDBid:1ozc). The polynomial surface of the 3rd order has the best fit, assessed by the method of least squares ($R^2 = 1.0$, $SSE = 0.009207$, $adjusted R^2 = 0.9999$, $RMSE = 0.096$) [15].

A relationship between the values of the potency IC_{50} from *in vitro* parameters [1,2,3] and the values of ASP scoring function from docking procedure in GOLD 5.2 and the values of total energies of formed ligand-receptor complexes was found for the *Model*

B of DOR, obtained by homology modeling [16-18]. The best fitting of experimental data for the *Model B* of DOR was obtained for a polynomial surface of the 3rd order again ($R^2 = 1.0$, $SSE = 0.2460$, *adjusted R*² = 0.9999, RMSE = 0.1568).

According to the established relationships for the three models of DOR we suggest that the polynomial surface of the 3rd order has the best fit, assessed by the least squares method [21]. This polynomial order could be successfully used for modeling of the relationship between the efficacy of delta-selective enkephalin analogues and the results from the docking procedure. Furthermore, the ligand-based and the structure-based approaches of virtual screening are a hopeful and effective search of effective δ -selective enkephalin candidates.

The number of these parameters is determined exactly from the degree of the found “optimal” polynomial.

Usually we solve the fitting problem by the least squares method for polynomials of second, third, fourth, etc. degree and choose the best.

CONCLUSIONS

Analysis of the data from *in vitro* bioassay and *in silico* docking studies may help to better understand the relationship between *in vitro* biological effects and molecular docking results; the docking studies are in good agreement with the *in vitro* studies.

Acknowledgements. This work is partially supported by the project of the Bulgarian National Science Fund, entitled: Bioinformatics research: protein folding, docking and prediction of biological activity, NSF I02/16, 2014.

REFERENCES

1. N. Pencheva, P. Milanov, L. Vezenvkov, T. Pajpanova, E. Naydenova, *Eur. J. Pharmacol.*, **498**, 249 (2004).
2. N. Pencheva, A. Bocheva, E. Dimitrov, C. Ivancheva, *Eur. J. Pharmacol.*, **304**, 99 (1996).
3. P. Milanov, N. Pencheva, *Serdica Journal of Computing*, **5**, 333 (2011).
4. L. Salum, I. Polikarpov, A. Andricopulo, *J. Chem. Inf. Model.*, **48**, 2243 (2008).
5. L. Ferreira, R. Santos, G. Oliva, A. Andricopulo, *Molecules*, **20**, 13384 (2015).
6. S. Vellankar, Y. Alhroub, C. Best, et al., *Nucleic Acids Res.*, **40**, 445 (2012).
7. GOLD, version 5.2 UserGuide; CCDC Software Ltd.: Cambridge, UK, (2010),(<http://www.ccdc.cam.ac.uk/Lists/DocumentationList/gold.pdf>).
8. M. Verdonk, J. Cole, M. Hartshorn, C. Murray, R. Taylor, *Proteins*, **52**, 609 (2003).
9. M. Eldridge, C. Murray, T. Auton, G. Paolini, R. Mee, *J. Comput. Aided Mol. Des.*, **11**, 425 (1997).
10. C. Braxte, C. Murray, D. Clark, D. Westhead, M. Eldridge, *Proteins*, **33**, 367 (1998).
11. K. Befort, L. Tabbara, S. Bausch, C. Chavkin, C. Evans, B. Kieffer, *J. Mol. Pharmacol.*, **49**, 216 (1996).
12. (http://www.clcbio.com/files/usermanuals/MMV_Manual.pdf).
13. R. Thomsen, M. Christensen, *J. Med. Chem.*, **49**, 3315 (2006).
14. (http://www.mathworks.com/help/curvefit/evaluating_goodness-of-fit.html)
15. F. Sapundzhi, T. Dzimbova, N. Pencheva, P. Milanov, *J. Comput. Methods Molec. Design*, **5**, 98 (2015).
16. F. Sapundzhi. *Proceedings of the Fifth International Scientific Conference - FMNS 2013, 12– 16 June 2013, Blagoevgrad, Bulgaria*. **2013**: 193-201.
17. F. Sapundzhi, T. Dzimbova, N. Pencheva, P. Milanov, *Proceedings of the Sixth International Scientific Conference - FMNS 2015, 10 – 14 June 2015, Blagoevgrad, Bulgaria*, **6**, 104-112, (2015).
18. F. Sapundzhi, T. Dzimbova, N. Pencheva, P. Milanov, *Bulg. Chem. Commun.*, **47**, 613 (2015).
19. T. Dzimbova, F. Sapundzhi, N. Pencheva, P. Milanov, *Int. J. Bioautomation*, **17**, 5, (2013).
20. F. Sapundzhi, T. Dzimbova, N. Pencheva, P. Milanov, *Journal of Peptide Science*, **20**, 294 (2014).
21. F. Sapundzhi, T. Dzimbova, N. Pencheva, P. Milanov. *Biomath. Commun.*, **2**, 47 (2015).
22. F. Sapundzhi, T. Dzimbova, N. Pencheva, P. Milanov, *Biomath. Commun.*, **1**, 84 (2014).
23. F. Sapundzhi, T. Dzimbova, N. Pencheva, P. Milanov, *Proceedings of 7th Bulgarian Peptide Symposium, Emilia Naydenova, Tamara Pajpanova, Dancho Danalev (Eds). 10-12 June 2016, Blagoevgrad, Bulgaria*, p.89 (2016).
24. P. Milanov, N. Pencheva, F. Sapundzhi. *Biomath. Commun.*, **3**, 47 (2016).
25. F. Sapundzhi, T. Dzimbova, N. Pencheva, P. Milanov, *Jurnal of Bulgarian Chemical Communication*. **49**, Special issue E, 23-30 (2017).
26. F. Sapundzhi, T. Dzimbova, N. Pencheva, P. Milanov, *Jurnal Biomath Communications Supplement*, **4 (1)** (2017).

МОДЕЛИРАНЕ НА ВРЪЗКАТА МЕЖДУ БИОЛОГИЧНАТА АКТИВНОСТ НА ДЕЛТА-СЕЛЕКТИВНИ ЕНКЕФАЛИНОВИ АНАЛОЗИ И РЕЗУЛТАТИ ОТ МОЛЕКУЛЕН ДОКИНГ С ПОЛИНОМИ

Ф.И. Сапунджи^{1*}, Т.А. Дзимбова², Н.С. Пенчева¹, П.Б. Миланов^{1,3}

¹Югозападен университет "Неофит Рилски", България, 2700 Благоевград

²Институт по молекуларна биология, Българска Академия на Науките, България, 1113 София

³Институт по Математика и Информатика, Българска Академия на Науките, България, 1113 София

Получена: 30 Ноември 2016; Приета: 10 Февруари 2017

(Резюме)

Една от областите на биоинформатиката е разработването на бързи и надеждни методи за предсказване на биологична активност на съединения. Това ще улесни дизайнът на нови съединения и ще намали разходите по експерименталната дейност. Процесът на създаване на селективни лиганди на делта опиоиден рецептор (ДОР) е насочен към синтезата на енкефалинови аналоги. Тяхната биологична активност се определя чрез използване на *in vivo* и *in vitro* методи, които позволяват да се установи връзка между структурата и биологичната активност на съединенията.

Целта на представеното изследване е да се намери функция, която да моделира връзката между стойностите на количествените параметри от *in vitro* изследванията и стойностите на скоринг функциите от молекулния докинг, проведен с делта-опиоидни лиганди и ДОР (PDBid: 4ej4) с кристална структура.

Връзката между стойностите на ефикасността на изследваните съединения, стойностите на скоринг функцията - ChemScore от молекулния докинг проведен в GOLD 5.2 и стойностите на общата енергия на лигандрецепторните комплекси, изчислена в Molegro беше моделирана с полиноми от първа до трета степен в тримерното пространство в Matlab. Най-доброто фитване на данните беше установено за полином от трета степен, оценено по метода на най-малките квадрати.

Получените резултати показват, че полиномът от трета степен в тримерното пространство може да се прилага успешно за моделиране на връзката между ефикасността на делта-селективните енкефалинови аналоги и резултати от молекулен докинг.

Shear on particles exposed to backswept mixing flow with a view to stress-sensitive cell response

S.D. Vlaev^{1*}, D. Georgiev²

¹Institute of Chemical Engineering, Bulgarian Academy of Sciences, Acad. G. Bonchev Str., Bl. 103, 1113, Sofia, Bulgaria.

²Chemical Engineering Department, Bourgas University “Prof. Dr. A. Zlatarov”, 1 Boul. Prof. Yakimov, 8010 Bourgas, Bulgaria

Received April 3, 2017; Accepted May 23, 2017

The flow impact over a spherical particle immersed in a biofluid at the impeller plane of a stirred laboratory bioreactor is examined. Based on the entire particle surface, the system mimics the flow effect upon living cells at growth being affected by hydrodynamic stress. Backswept (BS) circulation flow showed weak shear effect and was expected to stand as prospective operational means for growth in suspension cultures. A dual modified backswept impeller was selected to generate the flow circulation around the particle. Computational fluid dynamics (CFD) methodology was used. The shear distribution was obtained in the reactor inner volume as well as on the surface of the immersed body. The maximum wall-shear rate values were determined to be in the range from 1200 to 4000 s⁻¹. Evidence is given for areas of critical performance that imply cell damage in practical culture.

Keywords: mixing, backswept impeller, colloidal dispersions, wall shear, CFD

INTRODUCTION

The flow shear conditions near immersed particles in agitated bioreactors are important in biotechnology. Rapid deformations occur in many industrial systems, including cell and mycelia cultures in bioreactors for production of proteins, antibiotics, and other value added products. Cell fragmentations have been reported to be caused by such complications. Therefore, works devoted to hydrodynamic stress in mixing reactors and process strategies in relation to rotational speed and gassing present continuous interest [1]. Among these, the problem of cell negative response by the flow impact at shear conditions near immersed living particles in sparged cultures of agitated bioreactors prevails [2–7]. Shear has been identified as the cause of decreasing cell viability and morphology changes are frequently observed [8, 9]. Gas bubbles have been also reported to increase the shear stress around floating micro-objects [9]. In case of growth in micro-carrier cultures, loss of viable cells has been reported even at laminar stresses in the range of 0.5 to 10 Pa [10]. Referring to the overview of Nienow and coworkers [1], one finds that potential risks of cell damage lie within the specific flow field generated by the impeller and the performance of the gas flow related to bubble formation in the sparger zone, impeller discharge area and bubble bursting at the air-medium interface. In some cases, liquid jets (up to 5 m/s) are produced at gas cavities that may increase shear stress up to 100–300 Pa [11].

Considering the regions of potential risk for cell fragmentation in agitated reactors, namely, the sparger, the impeller discharge area, the vessel bulk bubble rise, it is of potential interest to reveal the value of shear force per unit surface acting on a particle in these zones.

In general, referring to the properties of impeller mixing of cell suspensions, one should avoid intensive high-shear conventional impellers. Recommendations for effective operation of sparged agitated bioreactors have been given [11]. Exemplifying animal cells, in order to avoid cell damage the impeller should be of a type that does not produce excessively high local rates of energy dissipation. Relatively large fluid-foil impellers, such as Elephant ear impeller [12] have been studied. Data on particle wall shear rates generated by radial flow conventional Rushton (RT) impellers [12, 13] and fluid-foil Narcissus [12] have been reported. RT showed high wall-shear rates critical for cells. In contrast, recent comparison of radial flow (RT) and backswept flow (BSF) impellers [14] has shown mild operating conditions in terms of shear in favor of the latter. It is expected that backswept impellers could be appropriate operational means for mixing and growth of stress-sensitive suspension culture. However, data on wall shear generated by backswept impellers on particles in bioreactors are lacking. In most cases, aeration of culture takes place and the effect of gassing in cases of BSF is also unknown.

In view of responding to engineering interest on a new BSF impeller, the aim of the study is to uncover the shear conditions in the flow over a

* To whom all correspondence should be sent:
E-mail: mixreac@gmail.com

particle exposed to the impact of BS impeller discharge and to compare these conditions with reference critical values in order to assess the flow properties of a relevant bioreactor operation.

The flow is a highly non-uniform one due to the impeller induced generic wide-spectrum velocity variation in stirred tanks, as well as due to the non-linearity of shear stress vs. shear deformation rate in agitated complex fluids. For that reason, the visualization technique based on CFD methodology was implemented as the most appropriate one for the analysis.

EXPERIMENTAL

Focusing on the physical model, the experimental reactor schematic is shown in Fig. 1. Addressing standard conditions in biological reactors, a dual impeller stirred Biostat vessel with tank diameter of 0.165 m and impeller diameter of 0.066 m (*Sartorius Biostat Aplus*) [15] was simulated (Fig.1). The working volume was 4.5 dm³. Impellers with modified curved arc-shaped blades [16] were used to generate the vessel backswept hydrodynamics. In cases, air was fed through a ring sparger with 12 one-mm openings. Further details on the system geometry have been reported elsewhere [14].

Interaction between flow and particles was included by assuming a single stagnant particle exposed to flow discharge driven by the rotating impeller, thus developing the strain corresponding to the maximum (i.e. relative between the fluid and the particle surface) velocity at the immersed body. For that purpose, a model sphere 5 mm in diameter was positioned in the impeller plane at a distance of 2 cm off the impeller tip opposing the discharge flow direction (Fig. 1). The shear parameters around and upon this probe were targeted.

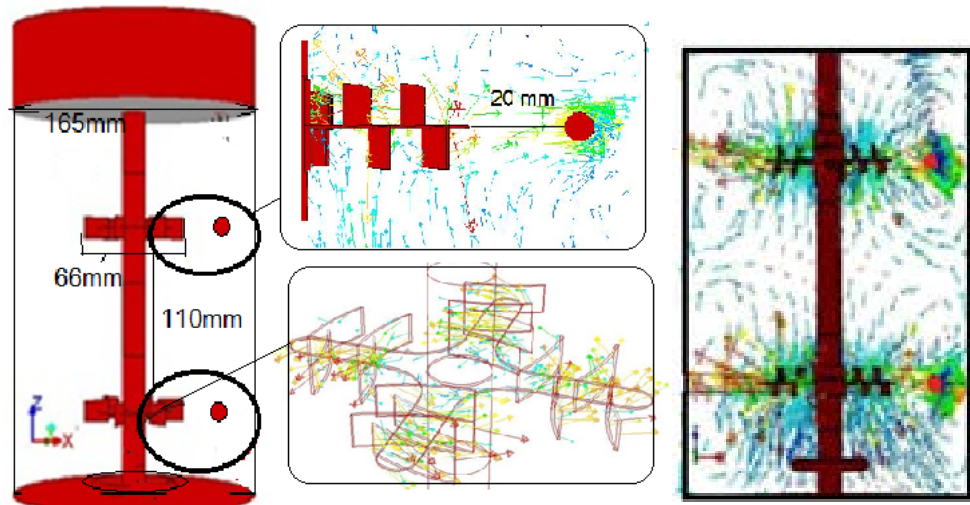


Fig.1. Reactor, impeller and spherical probe schematic and flow patterns observed.

The significance of fluid friction property for the fragmentation analysis was recognized and fluids of non-Newtonian flow properties frequent in practice were studied. The reference practical range of S for mixing of cell culture $\sim 10 \text{ s}^{-1}$ through 10 ks^{-1} was met by various rotational speeds N . Four prototype fluids corresponding to different states of the experimental biofluid [15] were simulated, the flow index n and consistency coefficient K varying as follows: $n=0.78$, $K=0.02 \text{ Pa.s}^n$, $n=0.78$, $K=0.1 \text{ Pa.s}^n$, $n=0.38$, $K=0.26 \text{ Pa.s}^n$ and $n=0.34$, $K=0.55 \text{ Pa.s}^n$.

The Metzner constant required to calculate the average shear rate for curved blades was 7.1, as reported determined by Taniyama and Sato [17] and reported in [18].

The study covers an apparent viscosity range less than 50 m Pa.s and relative aeration flow rate of 1 vvm that applies to a wide range of bioprocess technical scale conditions [15]. The flow pattern in small vessels is an intensive one and the corresponding Reynolds numbers for rotational flow of $0.5\text{--}1.10^4$ obtained assumed turbulent conditions.

Shear rate was determined by a numerical procedure using CFD model and solution methodology. The following details were worked out.

The flow field was simulated by the RANS standard k- ϵ (SKE) model and the Eu-Eu formulation of two-phase gas-liquid flow. For the moving volume the multiple reference frame approach [19] was used.

The hydrodynamic stress was determined from the shear rate (\dot{S}) and the constitutive equation of the fluid (non-Newtonian power law one):

$$\dot{S} = \frac{\partial V_j}{\partial x_i} + \frac{\partial V_i}{\partial x_j} \quad (1)$$

$$\tau = K \dot{S}^n \quad (2)$$

$$\mu_a = K \left(\frac{\partial V_j}{\partial x_i} + \frac{\partial V_i}{\partial x_j} \right)^{n-1} \quad (3)$$

In equations (1-3) V indicates local velocity, τ is shear stress, μ_a is apparent viscosity.

The governing equations [19] were solved numerically by Fluent (*ANSYS FLUENT Release 13.0, ANSYS, Inc., 2010*). The computational grid was generated by using Gambit (version 2.1). Unstructured mesh for complex shape with approx. 10^5 cells tetrahedral mesh for the volumes next to the impeller blades and the probe and hexahedral mesh for the rest of the tank was used. The grid interface between the inner rotating cylindrical volume and the outer stationary volume was a conformal one. Mesh refinement degrees down to <0.05 mm linear dimension were generated in order to achieve near-surface velocity gradients.

The boundary conditions for the single phase case were symmetry for the bed top and no-slip for wall boundaries in single phase flow and air velocity inlet and pressure outlet for the gas phase in cases of two-phase gas-liquid flow. A steady solution was performed for the single phase cases and a transient one for the presence of gas. The convergence criterion was set for the velocities and turbulence values equal to 1×10^{-6} . Reasonable convergence was achieved. Validation was carried out by basic parameters, momentum, power number, as well as by comparing values of experimental and predicted wall shear rates. The simulation in this format has been experienced formerly for radial flow and its validation related to non-Newtonian flow has been reported [12].

RESULTS AND DISCUSSION

Assuming that cell fragmentation is proportional to the slip velocity of fluid-particle interaction, shear rate on particle \dot{S}_p was selected as the representative parameter of interest. However, overall shear rate (\dot{S}) distribution, including bulk fluid shear \dot{S}_f was also examined. Answers of three basic issues were sought: (1) How much is the extent of inner fluid shear rate \dot{S}_f and the corresponding particle wall shear rate \dot{S}_p generated by the BS impeller-imposed

flow; (2) Is the effect of gas presence a significant one; (3) Within the practical range of input power, could the flow produce shear stress values τ_p critical for processing of mycelia or animal cells?

The flow pattern caused by backswept flow is a small loop radial one, as illustrated in **Fig. 1**. Thus, the impeller zone facing the particles was of major interest.

Both fluid shear rate and particle wall shear were target values and the vessel bulk and particle surface were examined. Accordingly, tank-scale and particle-scale data are illustrated, the first ones showing the flow field and its zones of spread in 2-D vertical plane ($x=y$) passing through the particle (Fig. 2) and in radial $X-Y$ plots along a tangent and a central line adhering and passing through the particle, respectively (Figs. 3, 4); The second scale visualized the near-wall shear distribution directly as a solid body representation of particle surface (Fig. 5). Figs. 2-5 and Tables 1-2 contain the results.

Fig. 2 illustrates the typical flow field for the case of backswept flow in both 2-D zones of spread and average zone shear rate (in s^{-1}) at the two degrees of a non-Newtonian flow, i.e. low consistency ($K=0.02 \text{ Pa.s}^n$) and high consistency ($K=0.1 \text{ Pa.s}^n$) one. Impeller speed $N=750 \text{ rpm}$ was selected as the most representative for the configuration of the dual arc-shaped impeller employed. The choice was based on previous comparative analysis with conventional BIOSTAT showing equal reaction effectiveness of the conventional Rushton (RT) radial flow impeller at 400 rpm and the present one at 750 rpm relevant to a biological system producing exopolysaccharides [15]. The contour plots in the figure correspond to increasing deviation from Newtonian flow properties at no gas and gassed conditions. As illustrated, the bulk fluid shear rate \dot{S}_f , generated by the backswept impeller, is of the order of magnitude reported for conventional impellers, namely $<2.10^2 \text{ s}^{-1}$ [20, 21]. As estimated by the spread of zone ($\dot{S}_f \sim 10 \text{ s}^{-1}$), \dot{S}_f is getting damped successively by rising consistency and gas introduction.

Shear distribution along selected lines, i.e. a central one and a tangent one, is shown in Figs. 3 and 4. Both upper and lower impeller zone were examined and showed similar patterns; the results in the figures represent the upper impeller and particle zone. Fig. 3 shows the effect of mixing intensity controlled by rpm and consistency at no gas conditions. Point values of maximum shear \dot{S}

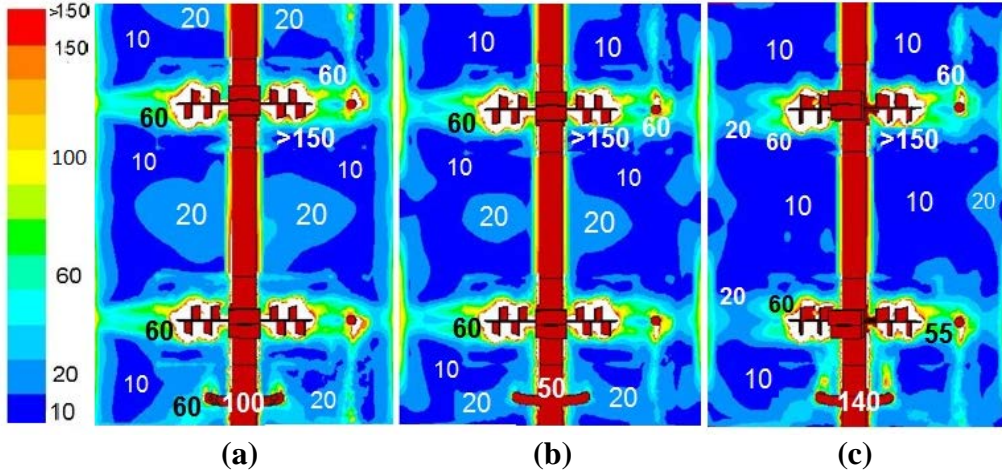


Fig. 2. Typical 2-D image of the vessel bulk fluid shear rates (s^{-1}) at $N=750$ rpm and increasing deviation from Newtonian properties at no gas and gassed conditions: (a) fluid $n=0.78/K=0.02$ Pa.s n , no gas, (b) fluid $n=0.78/K=0.1$ Pa.s n , no gas, (c) fluid $n=0.78/K=0.1$ Pa.s n , gassed.

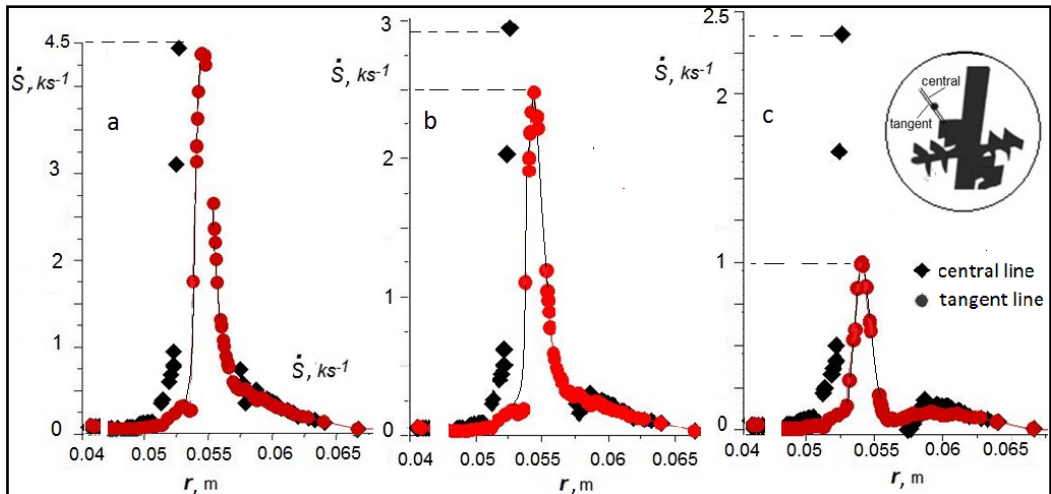


Fig. 3. Effect of rpm and consistency on shear rates (\dot{S}) generated by backswept flow at no gas conditions: \dot{S} versus radial position along the central (◆) and tangent (●) lines (a) $N=1080$ rpm, $n=0.78$, $K=0.02$ Pa.s n (b) $N=750$ rpm, $n=0.78$, $K=0.02$ Pa.s n , and (c) $N=750$ rpm, $n=0.78$, $K=0.1$ Pa.s n

corresponding to the radial locations near particle surface, e.g. frontal and tangent ones, are seen; only the radial interval around the particle ($0.04 < r < 0.068$, $0.053 < r_p < 0.058$) is shown. Fig. 3(a) *versus* 3(b) shows the rpm effect, while Fig. 3(b) *versus* Fig. 3(c) shows the effect of fluid consistency. One estimates that the maximum particle wall shear rate imposed by BS flow is of the order of 1000 to 4500 s^{-1} . In parallel, mixing intensity shows strong impact on shear, i.e. 30 % speed deviation (18 rps to 12.5 rps) might cause a 2-fold particle shear decrease (between 4.5 and 2 ks^{-1}). Comparing the \dot{S} -profiles of a moderately viscous fluid (~ 7 mPa.s, $K=0.02$ Pa.s n) and a highly viscous fluid (~ 37 mPa.s, $K=0.1$ Pa.s n) at similar mixing intensity ($N=750$ rpm), the shear deformation rate decrease is obvious.

Fig. 4 shows the effect of gas presence at low ($K=0.02$ Pa.s n) and high consistency ($K=0.1$ Pa.s n).

The case of low consistency corresponding to low apparent viscosity (~ 7 mPa.s) at 900 rpm indicates sharp decrease of shear rate more than 30 % in gas presence. In contrast, (Fig. 3c and Fig. 4c compared), shear rate at high consistency corresponding to 5-fold viscosity rise is only slightly affected by gas presence and shows no shear increase or only slight increase, e.g. 7%, possibly due to the increase of fluid mobility in parallel to the intensified motion caused by the gas bubbles.

In Figs. 5(a) and 5(b) shear rate zonal spread on the particle surface is revealed. In both figures particle wall-shear \dot{S}_p (in ks^{-1}) is illustrated. Extreme non-uniformity of shear, as well as zones of maximum shear showing different spread over particle side and rear are registered. Inferring on the effects seen in the figure, the high stress zone is expected by the side stream, while the lowest stress

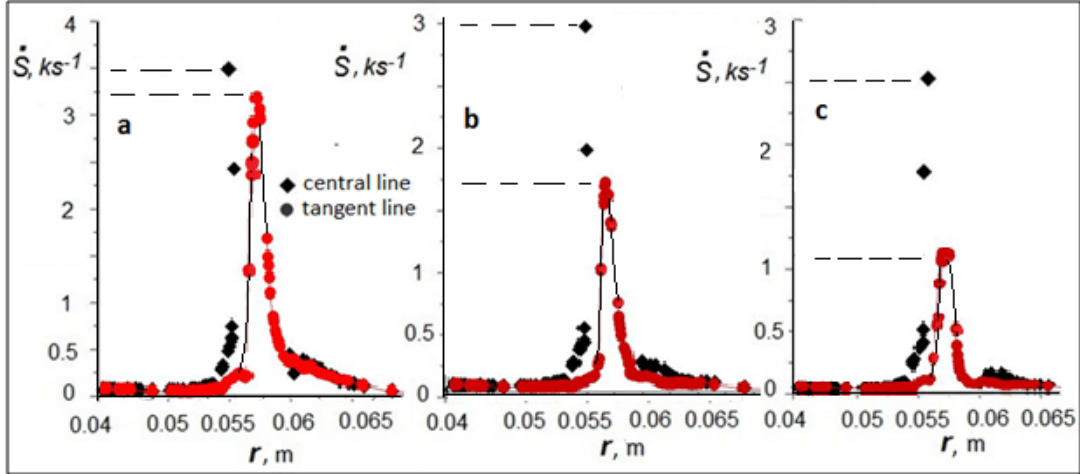


Fig. 4. Effect of gas on shear rate (ks^{-1}) generated by backswept flow at low and high consistency: \dot{S} versus radial position along the central (◆) and tangent (●) lines at: no gas, $N=900 \text{ rpm}$, $K=0.02 \text{ Pa.s}^n$, $n=0.78$, (b) with gas, $N=900 \text{ rpm}$, $n=0.78$, $K=0.02 \text{ Pa.s}^n$, (c) with gas, $N=750 \text{ rpm}$, $n=0.78$, $K=0.1 \text{ Pa.s}^n$,

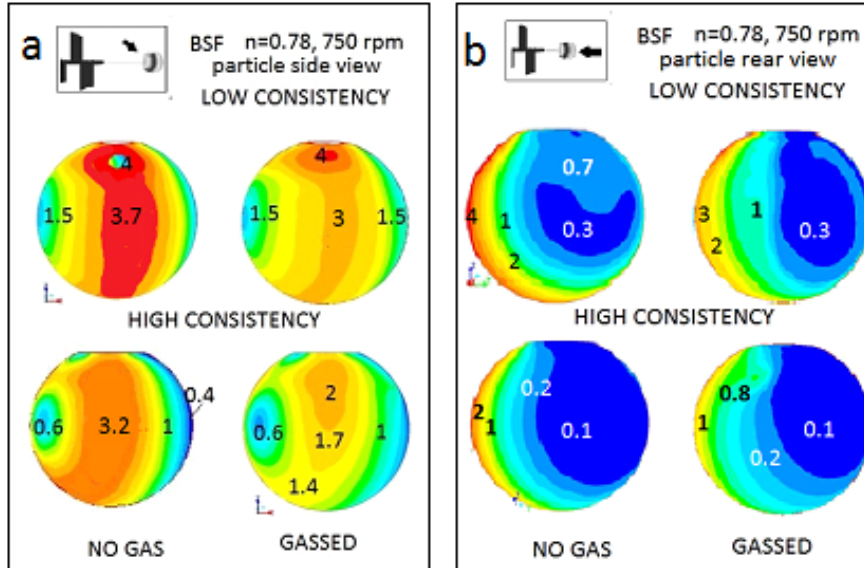


Fig. 5. Solid body image of \dot{S} - zonal spread ($\dot{S}_p \cdot 10^3 \text{ s}^{-1}$) at backswept flow (BSF): \dot{S} - distribution at 750 rpm corresponding to low ($K=0.02 \text{ Pa.s}^n / n=0.78$) and high ($K=0.1 \text{ Pa.s}^n / n=0.78$) consistency, gas absence and presence in (a) particle side view, and (b) particle rear view

zone in gas presence coincides with the low pressure gas filled zone at the particle rear. This is valid strongly for the case of low consistency ($K=0.02 \text{ Pa.s}^n$).

Figs. 3-5 present local \dot{S} - values. Based on the cross-sectional area of the plane ($x=y$) and the particle considered, surface-area averaged values corresponding to the various performance variables were determined. Table 1 contains the summary of results. In the Table, the values of shear stress are determined and the opposite effect of gas on shear at low and high consistency is registered. The data allow comparison between cases of backswept flow (BSF) and other flow types, e.g. generated by radial flow by Rushton (RT) impeller. Table 2 compares

the cases' parameters including data for flat-blade (RT) impeller mixing [12] based on specific input power, i.e. power P per unit fluid volume V_r . Referring to a similar range of input power, e.g. 1-6 W/dm³, particle wall shear imposed by a conventional flat-blade impeller RT is about 3-fold higher than the one determined for the backswept impeller studied.

While showing the magnitude and the effects, it is the practical outcome of the result that is important: what are the ranges of shear stress imposed on a stagnant particle in configuration of backswept flow and how they conform to reported criteria for cell damage? The results in Tables 1 and 2 suggest the answer.

Table 1 Average wall shear stress: the effect of gassing

Fluid	N [rpm]	Gas U/G	μ_a [mPa s]	Re_m [-]	\dot{S}_f [s ⁻¹]	\dot{S}_p [s ⁻¹]	τ_p [Pa]
$n=0.78$ $K=0.02 \text{ Pas}^n$	600	U*	7.8	5680	43.9	1680	6.6
		G			41.5	1530	6.1
	750	U	7.5	7700	56.6	2360	8.55
		G			50.7	1950	7.4
	900	U	7.3	9200	67.3	3000	10.3
		G			54.6	1940	7.3
	1080	U	6.9	11600	75.6	3900	12.6
		G			67.7	2720	9.6
$N=0.78$ $K=0.1 \text{ Pas}^n$	750	U	37.4	1600	47.2	1220	25.5
		G			48.5	1330	27.3

*Conditions: U ungassed, G gassed

Table 2 Comparison of shear imposed by the backswept (BS) and Rushton (RT) impellers

Flow Pattern	N [rps]	P/V_r [Wdm ⁻³]	\dot{S}_f [s ⁻¹]	\dot{S}_p [ks ⁻¹]	τ_p [Pa]
BSF	10	1.7	43.9	1.68	6.1
	12.5	3.3	56.6	2.36	8.5
	15	5.7	67.3	3.0	10.3
RT [12]	6.7	1.4	24.5	9.57	25.4
	10	4.6	36.7	9.64	25.6

Recalling critical values of shear stress likely to cause damage to animal cells or mycelia reported in the literature, the relevant flow conditions could be classified in terms of shear inducing properties as appropriate or non-appropriate for the specific operation.

Critical values for cell damage have been reported in the literature [1-9]. Animal cell damage was found to start in the range of shear stress from 0.2-200 Pa [2]. Recent studies pointed at threshold values of hydrodynamic stress of ~25-30 Pa [6]. Studies related to the performance of *Carthamus tinctorius* L. by Liu *et al.* [7] showed that changing shear stress between 10 and 50 Pa, the specific death rate of the plant cells increased 5-fold. They confirmed the previous result [3] that significant cell damage of plant cells occurred when the maximum shear stress exceeded 70 Pa. In case of growth in microcarrier cultures, loss of viable cells has been reported even at laminar stresses in the range 0.5 to 10 Pa [10]. Referring to living microobjects, studying the effect of hydrodynamic stress on the growth of *Xanthomonas campestris* cells, Garcia-Ochoa *et al.* [8] reported morphology changes yet at 9 Pa and a 40 % decrease of cell viability at shear stress of 35 Pa.

Based on these data, one could realize that a vessel could operate at a mixing regime generating particle shear stress exceeding 70 Pa at an increased degree of risk for damage in case of shear-sensitive

biomass. Nevertheless, to avoid detrimental effects shear deformation rate should not exceed ~3 ks⁻¹ and shear stress ~10 Pa. Referring to the typical range of mixing variables in Table 2, the backswept induced circulation studied is well within the limits for bioprocessing. The analysis based on the results points at the range of moderate rotational motion generated by the backswept unit at lower rotational speed, e.g. less than 900 rpm to be the most appropriate one for feasible operation involving cell culture. Operational modes exceeding 10 Pa could be acceptable for bioreactors processing mycelia biomass with a danger of some loss of activity.

CONCLUSIONS

In conclusion, the study presents a CFD-based assessment of an important flow parameter - an image of shear imposed on particles immersed in a complex non-Newtonian fluid with a view to engineering application to suspension culture of stress-sensitive cells in stirred bioreactors. It reveals the maximum flow impact at the wall of a stagnant particle in colloidal dispersion circulated by means of a backswept impeller. The rates of shear generated by the radial velocity-dominated circulation flow, as well as the hydrodynamic shear stress on particles at no gas conditions and in gas presence are determined. Evidence is given for areas of critical performance in a case of primary circulation that imply changes in cell physiological response in

practical cases of culture bioprocessing. Referring to reported critical shear stress values in the literature, the data for backswept flow allow extension of classification of practically occurring operational regimes in terms of potential risks for cell damage.

Acknowledgement: This article is based upon work from European Cooperation in Science and Technology (COST) Action MP1305, supported by COST.

REFERENCES

- 1.A. Amanullah, B.C. Buckland, A. W. Nienow, in: Handook of Industrial Mixing. E.L Paul, V.A. Atiemo-Obeng, S.M. Kresta (eds), Wiley, New Jersey, 2004, Ch. 18.
- 2.L.Van der Pol, J. Tramper, *Trends Biotechnol.*, **16**, 323, 1998.
- 3.D.D. Sowana, D.R.G. Williams, E.H. Dunlop, B.B. Dally, B.K. O'Neill, D.F. Fletcher, *Trans. Inst. Chem. Eng.*, **79A**, 867 (2001).
- 4.E.V. Guseva, N.V. Menshutina, J. Boudrant, J., in: Proc. 15th Eur. Conf. on Mixing, R. Abiev (ed.), S. Petersburg State Inst. Technol., S. Petersburg, 2015, p. 134.
- 5.Th. T. Tran, W.R. Hwang, in: Proc. 15th Eur. Conf. on Mixing, Abiev, R. (ed.), S. Petersburg State Inst. Technol., S. Petersburg, 2015, p. 345.
- 6.B. Neunstoecklin, M. Stettler, Th. Solacroup, H. Broly, M. Morbidelli, M. Soos, *J. Biotechnol.*, **194**, 100 (2015).
- 7.Yu Liu, Z.J. Wang, J. Xia, C. Haringa, Y.Liu, J. Chu, Y.P. Zhuang, S.L. Zhang, *Biochem. Eng. J.*, **14**, 209 (2016).
- 8.F. Garcia-Ochoa, E. Gomez, A. Alcon, V.F. Santos, *Bioprocess Biosyst. Eng.*, **36**, 911 (2013).
- 9.S.J. Meier, T.A. Hatton, D.I.C. Wang, *Biotechnol. Bioeng.*, **62**, 468 (1999).
- 10.J.G. Aunins, H.J. Henzler, in: Biotechnology 2nd Edn, (Vol. 3, Bioprocessing), H.J. Rehm, G. Reed (eds.), VCH, Weinheim, 1993.
- 11.Y. Chisti, *Trends Biotechnol.*, **18**, 420, 2006.
- 12.S.D. Vlaev, I. Nikov, M. Martinov, *Chem. Eng Sci.*, **61**, 5455 (2006).
- 13.C.C. Bustamante, W.O. Cerri, A.C. Badino, *Chem. Eng. Sci.*, **90**, 82 (2013).
- 14.S.D. Vlaev, D. Georgiev, in: Scientific Works of University of Food Technologies vol. 61, University of Food Technologies, Plovdiv, 2014, 745.
- 15.S.D. Vlaev, S. Rusinova-Videva, K. Pavlova, M. Kuncheva, I. Panchev, S. Dobreva, *Appl. Microbiol. Biotechnol.*, **97**, 5303 (2013).
- 16.S. Kraitschev, S.D. Vlaev, V. Lossev, P. Staykov, *Biotechnol. Biotechnol. Eq.*, **15**, 128 (2000).
- 17.I. Taniyama, T. Sato, *Kagaku Kogaku*, **29**, 709 (1965).
- 18.S. Nagata, Mixing Principles and Applications, Wiley, New York, 1975.
- 19.V.V. Ranade, Computational flow modeling for chemical reactor engineering, Academic Press, London, 2002.
- 20.R. R. Hemrajani, G. B. Tatterson, in: Handook of Industrial Mixing (Eds. E.L. Paul, V.A. Atiemo-Obeng, S.M. Kresta), Wiley, New Jersey, 2004, Ch. 6.
- 21.K. Van't Riet, J.M. Smith, *Chem. Eng. Sci.*, **30**, 1093 (1975).

СКОРОСТИ НА СРЯЗВАНЕ ВЪРХУ ЧАСТИЦИ ПРИ РАЗБЪРКВАНЕ С ДЪГООБРАЗНИ ЛОПАТКИ СЪС ЗНАЧЕНИЕ ЗА ФИЗИОЛОГИЯТА НА МИКРООРГАНИЗМИ ЧУВСТВИТЕЛНИ КЪМ МЕХАНИЧНО НАПРЕЖЕНИЕ

С.Д. Влаев Д. Георгиев

Институт по инженерна химия, БАН, ул. Акад. Г. Бонев бл. 103, София 1113, България
Бургаски университет „Проф. Асен Златаров“, кат. „Инженерна химия“, бул. Проф. Якимов, 1, Бургас 8010,
България

Получена на 3 април, 2017 г.; приета на 23 май, 2017 г.

(Резюме)

Изследвано е влиянието на хидродинамиката на разбъркване върху сферична частица, потопена във флуид в равнината на импелер с реактивни дъгообразни лопатки. Системата наподобява влияние на поток върху живи клетки на микроорганизми в биореактори с разбъркване. Импелерът с реактивни лопатки осигурява понижено механично напрежение и е перспективен за приложение във ферментатори със суспендирали микроорганизми. Приложена е методика на компютърна изчислителна хидродинамика. Получени са 2-D и 3-D разпределения на скоростта на срязване в обема на флуида и върху повърхността на потопеното тяло. Установени са максимални стойности на повърхностната скорост на срязване в интервала 1200–4000 сек⁻¹. Показани са зони на тангенциална деформация, които могат да се окажат критични за физиологията на клетки на микроорганизми, чувствителни към механично въздействие.

Evaluation of chemical composition, energy and biological value of typical Bulgarian traditional foods

D.S. Hristov¹, S.K. Velikov², V.E. Vodenicharov¹, S.P. Tsanova-Savov², F.T. Ribarova^{2*}

¹ Medical University – Sofia, Faculty of Hygiene, 15, Iv. Ev. Geshov Blvd., Sofia 1531

² Medical College “J. Filaretova”, Medical University – Sofia, 3, J. Filaretova Str., Sofia 1606.

Received May 22, 2017; Accepted June 2, 2017

A great number of recent scientific studies provide data characterizing the chemical composition of traditional foods from different geographical regions and describe their essentiality for healthy nutrition. The information concerning Bulgarian traditional foods is scarce. The aim of the current study is to assess the energy and biological value of Bulgarian traditional foods by implementing modern scientific approaches to food chemical composition data. The study covers a total of 15 products typical of the traditional Bulgarian diet. The original data are obtained by application of routine methods for the determination of total protein and fat, and classical chromatographic analysis of amino acids (AA) composition. New advanced approaches to assess the proteins biological value and energy content of the studied traditional Bulgarian foods were applied. New information is presented about the composition of amino acids and their proteins biological value in the examined Bulgarian traditional foods. Their energy content was determined in compliance with current scientific requirements. The content of saturated fats is also listed and their necessity and essentiality for health is clarified. The new data for the chemical composition of traditional foods in Bulgarian diet will play an important role in the assessment of nutritional intake, supporting human health and contributing to the revitalization of Bulgarian food chemistry, nutrition and technology.

Keywords: food chemistry, Bulgarian traditional foods, energy, saturated fats, biological value

INTRODUCTION

Numerous scientific studies in the recent years have been focused on studying the chemical composition of traditional foods using up to date analytical equipment and presenting correct data about their role and importance for healthy nutrition [1-5]. The global diet diversity and geographic specificity in the prevalence of different diseases are some of the reasons to search for an explanation of the mechanisms by which food affects health and longevity.

The role of traditional foods in the healthy diet of Bulgarian population identifies a number of controversial issues. For example, traditional foods for Bulgarians in the past as pork, bacon, butter and whole fat dairy products had constituted a high percentage rate of their diet, and despite the high consumption of saturated fats, Bulgaria was known with a high number of centenarians. Today, after more than a century, during which mainly fat-free animal food products have been consumed, with almost total oblivion of fat, grease and oil, the average life expectancy is extended, unfortunately along with many diseases. It is clear that the recommendations for healthy nutrition have had an

impact on food production, consumption and consumer preferences but regardless of this fact, not only the lack of reduction of cardiovascular diseases, but also the significant incidence rate of overweight and obesity among our population could hardly be explained.

The view that animal fats mainly consist of saturated fatty acids has already been revised since in their composition except for saturated fatty acids, numerous monounsaturated and some polyunsaturated ones have also been identified, determining the specificity of the products [6].

In response to the scientific advice for healthy nutrition, the food technology was driven to production of new products in which animal fats were replaced with saturated vegetable fats or were defatted. Creating new assortments required additional finances, shifting the old traditional food, but the problems still continued to exist.

Startled by the invasion of various foreign cuisines, and taking into consideration the free movement of food in the global market, the researchers began looking for risk factors suspected in this invasion and came to the conclusion to rediscover the power of traditional foods [7]. The present study addresses those aspects through chemical composition data of Bulgarian traditional foods.

* To whom all correspondence should be sent:
E-mail: fanny.r@mail.bg

The aim of the study was to assess the energy and biological value of Bulgarian traditional foods, implementing modern scientific approaches to food chemical composition data.

MATERIALS AND METHODS

The study covers a total of 15 products typical of the traditional Bulgarian diet: milk and dairy products (4 different products), pork, legumes (beans and lentils), fruits and vegetables (a total of 8 different species). The original data were obtained as results of a random selection of analytical samples from the food market, with subsequent use of classical routine methods for the determination of total protein and fat (Kjeldahl and Folch). Carbohydrates were calculated through the difference. The data for macronutrients were based on our own studies and on published data in the Tables on the composition of Bulgarian food and European food composition database [8-10]. The amino acid (AA) composition of proteins was determined after acid and alkaline hydrolysis, applying the classical ion-exchange chromatography method with post-column ninhydrin derivatization, and UV-detection at 570 nm for amino and 440 nm for imino acids, using amino acid analyser – Hitachi, KLA-5 and HPLC-Perkin Elmer, series-2 [11].

New, advanced approaches to assess the proteins biological value and energy content, based on the chemical composition of the studied traditional Bulgarian food were also applied [12,13].

RESULTS AND DISCUSSION

The results of the study of traditional Bulgarian foods will be presented in the following order: determination of the biological value of the protein components; evaluation of the energy content; biological interpretation of the content of saturated fats.

Quality of food proteins

Currently, the main criteria for assessing the quality of dietary proteins according to current scientific concepts are the amino acid composition and the extent of bioavailability in the body. Therefore, we would like to provide data on the biological value of proteins in some traditional Bulgarian foods, calculated by recommended new scientific approaches, based on their amino acids composition.

Over the past 50 years many analytical methods and computational approaches used to assess the

quality of the protein have been modified. The amino acid score calculated from its limiting amino acid in comparison with the reference amino acid pattern, adopted in the past century, appears to be not fully correct. The efficiencies of proteins utilization including their digestibility and metabolic availability of amino acids are also important [12,14]. Therefore, expert advice by FAO and WHO after numerous studies reached the opinion to modify the amino acid score that could take into consideration the level of availability. Therefore, the Expert Advice Committee of FAO/WHO, after extensive research, agreed on modifying the amino acid score, also including the level of digestibility [15]. The application of this new protein digestibility-corrected amino acid score to evaluate the quality of dietary protein requires knowledge of the formula for old *Amino Acid Score* and the formula for the new *Corrected Amino Acid Score*, as follows:

1. *Amino Acid Score* = mg essential amino acids in g of studied protein / mg of essential amino acids in g of reference protein × 100;

2. *Corrected Amino Acid Score* = first limiting amino acid content in the test product / the same amino acid content in egg white × 100;

It has been found that egg white had a high bioavailability.

Table 1 presents the results for the new, *Corrected AA scores* of the studied traditional Bulgarian food, having higher protein content.

Fruits and vegetables were excluded, since they were considered as sources mainly of carbohydrates, vitamins, trace elements and biologically active compounds and not as sources of proteins. The data presented above show the probable digestibility of amino acids included in the overall evaluation of biological value. The amino acids data, calculated with respect to protein content were preferred, as the variation of the results produced by that method was lower. The results in Table 1 provide new, much more correct data regarding the qualitative assessment of dietary proteins. The higher biological value of dairy foods, followed by the results for meat is clearly shown. A positive characteristic of beans is the rich content of the nonessential amino acid arginine which in its metabolic course is a source of nitric oxide - a potent vasodilator and neurotransmitter factor. In this aspect, a number of studies support the importance of arginine as a powerful factor in preventive cardiology and immunology.

Table 1. Corrected amino acids score for quality of proteins in traditional foods

Product	Name	First limiting amino-acid			New Corrected Score %
		Protein %	g/100g product	g/100g protein	
Pork	Methionine and Cystine	12.49%	0.39	3.13	6.41
Cow's milk - fresh	Methionine and Cystine	3.21%	0.10	3.15	6.41
Cow's milk - yoghurt	Methionine and Cystine	3.24%	0.10	3.09	6.41
Cow's cheese	Methionine and Cystine	16.41%	0.49	4.03	6.41
Balkan yellow cheese	Methionine and Cystine	24.02%	0.72	3.97	6.41
Bread wheat	Lysine	7.11%	0.17	2.33	7.18
Beans	Methionine and Cystine	19.14%	0.35	1.79	6.41
Lentil	Methionine and Cystine	23.33%	0.36	1.53	6.41
					23.87

The traditional combination made by Bulgarians consisting of bean meals and bread provides the necessary amount of all essential amino acids. It is recommended that future research focused on assessment of proteins biological value in food and in nutritional intake would implement the new approach - "*Corrected amino acid score*", providing more precise evaluation of food quality.

The determination of the energy content of the diet depends on the quantitative presence of individual nutrients. In the evolution of knowledge on the energy value of food, three different systems with different conversion factors for estimation of the amount of nutrients converted into energy were implemented. The first and oldest system is that of Atwater and Woods, 1896, known as the "*Main factor system*", including the energy from proteins, lipids and carbs [11].

The energy content of Bulgarian foods in the Tables for chemical composition of food products, as well as in a number of scientific studies was determined according to this oldest factor system that is nowadays no longer in use in respected analytical laboratories [8]. The carbohydrates in this system were determined by weight, expressed as the difference between the total weight and the sum of the weights of the other ingredients in the food (proteins, fats) without them being individually analysed. Thus, the content of total carbohydrates includes fibers which are, however, not fully utilized and thus the calculated energy is higher in comparison to its real values, resulting in incorrect data, not only for energy, but also for nutrients density as well.

The second system is "*Expanded Factor System of Atwater*", wherein the factors are increased (for monosaccharides, organic acids, polyols and fibers).

The most accurate third system for calculating energy, applied today in scientific studies, is the "*Specific Factor System of Atwater*" with a wider range of factors related to the different and specific

building blocks of protein, fat and carbohydrates [13].

Based on those scientific facts and our efforts to provide correct results, we made a comparative evaluation of the energy content of traditional foods studied in the first and second system, presented in Table 2.

There are differences in the figures presented in the last two columns. Logically, in products from 1 to 6 there was no difference in energy content, because they do not contain fibers. In products with higher carbohydrate content and fibers, respectively, higher energy differences were established. The application of this approach to calculate food energy level results in more correct data, particularly important in the construction of various dietary regimes and achieving low energy levels for each product is a desirable feature for both consumers and manufacturers.

The interpretation of the content of saturated fats has undergone significant development in the international scientific publications from a total ban in the past, to recommendations for their inclusion in healthy diets nowadays [6]. The selected traditional Bulgarian food will be assessed in this aspect by the present study.

One popular but already outdated myth that saturated fats are a major risk factor for development of cardiovascular disease begins to retreat positions, albeit new scientific evidence suggests their biological importance in human nutrition and health [6].

The view that animal fats were constituted mainly of saturated fats has already been revised, since in their composition except for saturated fatty acids, monounsaturated and polyunsaturated ones are also present, which determines the specificity of the product. The task of this study was focused on this aspect, in order to provide data for saturated fats content in traditional Bulgarian food and evaluation of their biological importance, based on current scientific understandings and achievements.

Table 2. Energy content of traditional Bulgarian foods, calculated by two different factor systems

Product	Water	Proteins	Fat	Carbo-hydrates Total	Dietary Fibers	Ash	E1 kJ	E2 kJ
Cow's milk 3%	88	3.2	3	5.2	0	0.7	254	n/a
Cow's cheese	55	16.8	19.7	6	0	4.5	1123	n/a
Sheep's milk	81	5.5	7.7	5.5	0	1	474	n/a
Sheep's cheese	51	15.9	26.5	4.6	0	4	1341	n/a
Balkan yellow cheese	41	24.6	30.7	1.84	0	4.3	1599	n/a
Pork	71	20.4	8	0	0	0.99	642	n/a
Bread wheat	38.8	7.6	1	52	4.0	1.35	1035	1002
Onion old	86	1.72	0.3	9.6	1.9	0.61	201	185
Garlic old	64	6.5	0.1	29.2	2.1	1.33	601	584
Red tomatoes	94.8	1	0.2	3.74	1.4	0.5	87	75
Paprika	92.4	1.22	0.51	5.4	1.7	0.61	130	116
Beans	12	24.9	1.6	59.2	18.4	4.3	1468	1314
Lentil	9.7	26.2	2.6	59.3	11.2	2.4	1529	1435
Apples	84	0.3	0.3	14.9	2.2	0.3	266	242
Pears	84.4	0.3	0.4	14.7	3.2	0.3	266	239

Popular, though without in-depth understanding is the widespread opinion that saturated fats content in contemporary diet in different regions or countries is richer than in traditional diets. The explanation is related to the following two false statements: (i) animal fats are mostly saturated and plant fats - mostly unsaturated; (ii) the modern diet is rich in saturated fats (view of historical value), assuming an inert wrong opinion about the nature of animal fats. Fats and oils with least saturated fats level are of plant origin, but those containing the most saturated fats are also of plant origin, while animal fats have a moderate amount, which is seen very clearly on Figure 1. Table 3 presents data on the content of saturated fatty acids in selected traditional foods. The high total fat content in pork was clearly outlined, followed by yellow and white sheep's cheese. The saturated fat content, expressed in g/100 g product was highest again in pork meat, as

logically the pattern for total fat content was repeated. To a certain extent differences were found in the ratio of saturated fat/total fat content, as the leading place belonged to yellow cheese, followed by cow's and sheep's cheese. These data emphasize that the ratios between saturated and mono- and polyunsaturated fats are specific characteristics of the different food products. The highest total fat content in pork meat can be explained with the hidden fat and the meat structure, when the measurement is based on 100 g fresh weight. The determination of saturated-to- total fat ratio gives more stable results, which in our study gave advantage to pork bacon. Moreover, this pork product contains high quantity of arachidonic polyunsaturated fatty acid (about 2%), with already confirmed physiological role as a precursor of eicosanoids, classified by many authors as essential fatty acids.

Table 3. Total fats and saturated fatty acids content in traditional Bulgarian foods

Product	Total Fats (GF) g/100g	Saturated Fatty Acids (SFA) g/100g	SFA/GF %
Cow's milk 3 %	3	1.94	65
Cow's cheese	19.7	11.2	59
Sheep's milk	7.7	4.62	60
Sheep's cheese	26.5	11.1	42
Balkan yellow cheese	30.7	22.8	74.3
Pork	52	26.7	51.3
Bread wheat	1	0.25	25
Onion old	0.3	0.06	20
Garlic old	0.1	0.02	20
Red tomatoes	0.2	0.09	45
Paprika	0.51	0	0
Beans	1.6	0.54	34.6
Lentil	1.03	0.27	26.2
Apples	0.3	0.081	27
Pears	0.4	0.04	10

CONCLUSIONS

Traditional foods have established over the centuries a comprehensive food culture. The knowledge of their chemical composition is a basic requirement towards the assessment of their nutritional and biological value. Some of the Bulgarian traditional foods are on the verge of being lost, therefore more efforts are needed to improve them using modern knowledge and technology, to explore and preserve them. Including traditional foods in the Bulgarian diet will play an important role in supporting human health and will contribute to the revitalization of Bulgarian agriculture.

REFERENCES

- 1.A. Trichopoulou, E. Vasilopoulou, K. Georga, S. Soukara, V. Dilis, in Food Science and Technology, Traditional foods: why and how to sustain them, *Trends*, **17**, 498-504, (2006).
2. H.S. Costa, E. Vasilopoulou, A. Trichopoulou, P. Finglas, *Journal of Clinical Nutrition*, **64**, Suppl. 3, S73 (2010).
3. C. Jeppesen, P. Bjerregaard, *Scandinavian Journal of Public Health*, **40** (5), 475- (2012).
4. V. Dilis, E. Vasilopoulou, I. Alexieva, N. Boyko, A. Bondrea, S. Fedosov, O. Hayran, M. Jorjadze, D. Karpenko, H.S. Costa, P. Finglas, A. Trichopoulou *Journal of the Science of Food & Agriculture*, **93** (14), 3473 (2013).
5. V. Afari-Sefa, S. Rajendran, R.F. Kessy, D.K. Karanja, R. Musebe, S. Samali, M. Makaranga, *Experimental Agriculture*, **52**(2) 300 (2016).
6. IOI Group Loders Croklaan, North America. Recent Development in Saturated Fat Nutrition, 1-35, (2010).
7. P.A. Kroon, L.F. D'Antuono, *Journal of the Science of Food & Agriculture*, **93** (14), 3403 (2013).
8. T. Tashev, G. Shichkov, in: Tables of Bulgarian foods composition. Medicina i Fiskultura Publ., Sofia (1975).
9. F. Ribarova, E. Vazelov, S. Shichkov, in: Nutrition and Chronic Renal Failure. Composition of food products, IPK "Rodina" Publ., 59-71, (2003).
10. Danish Food Composition Databank, version 7.0, 2008. <http://www.foodcomp.dk/>
11. F. Ribarova F., S. Shichkov, I. Baklova, in: Amino acids composition of Bulgarian food products, Zemizdat Publ., Sofia, 26-45 (1978).
12. C.L. Levesque, R. Elango, R. O. Ball, in: Metabolic availability of amino acids in food proteins: New methodology (Book Chapter), Amino acids in human nutrition and health, 256-266, (2011).
13. FAO, Food and Nutrition Paper. Food energy - methods of analysis and conversion factors, Rome, **77** (2003).
14. D. J. Millward, *British Journal of Nutrition*, **108**, S2, S3 (2012).
D.J. Millward, *British Journal of Nutrition*, **108**, S2, S31 (2012).

ОЦЕНКА НА ХИМИЧНИЯ СЪСТАВ, ЕНЕРГИЯТА И БИОЛОГИЧНАТА СТОЙНОСТ НА ТИПИЧНИ ТРАДИЦИОННИ БЪЛГАРСКИ ХРАНИ

Д.С. Христов¹, С.К. Великов², В.Е. Воденичаров¹, С.П. Цанова-Савова², Ф.Т. Рибарова^{2*}

¹ Медицински Университет – София, Факултет по Хигиена, 15, Ив. Ев. Гешов бль., София 1531

² Медицински Колеж „Й. Филаретова”, Медицински Университет – София, 3, Й. Филаретова ул., София 1606.

Получена на 22 май, 2017 г.; приета на 2 юни, 2017 г.

(Резюме)

Голям брой съвременни научни изследвания предоставят данни за химичния състав на традиционни храни от различни географски региони на света, описвайки тяхната есенциалност за здравословното хранене. Информацията относно българските традиционни храни е много осъкъдна. Целта на настоящото проучване е да оцени енергийното съдържание и биологичната стойност на български традиционни храни, прилагайки съвременни научни подходи при анализа на данните за химичния им състав. Проучването обхваща общо 15 хранителни продукта, типични за традиционната българска диета. Използвани са рутинни методи за определяне на общ белтък и мазнини, а аминокиселинният състав е определен чрез приложение на хроматографски анализ. Оценката на енергийното съдържание и биологичната стойност на изследваните традиционни продукти е постигната чрез нови съвременни научни подходи. Предоставена е нова информация за аминокиселинното съдържание и съответно за биологичната стойност на белтъка в изследваните продукти. Нова е и информацията за енергийното им съдържание, определено в съответствие със съвременните научни изисквания. Предоставени са данни за наситените мазнини и е изяснена тяхната есенциалност за здравето. Новите данни за химическия състав на традиционни храни, типични за българската диета, са от значение за оценка на хранителния прием, за поддържане на здравословно хранене и допринасят за възстановяване на виталността на химията на храните в България, на хранителните технологии и общественото хранене.

Spectrophotometric investigations on liquid-liquid extraction systems containing cobalt and tetrazolium salts. Application of the developed method for analysis of the cobalt content of biological samples (mushrooms and tobaccos)

L. Dospatliev^{1*}, M. Ivanova²

¹Department of Pharmacology, Animal Physiology and Physiological Chemistry, Trakia University, Stara Zagora, Bulgaria.

²Department of Informatics and Mathematics, Faculty of Economics, Trakia University, Stara Zagora, Bulgaria;

Received April 5, 2016; Accepted June 19, 2017

The study presents a newly-developed method for extraction-spectrophotometric determination of Co (II) in samples by means of iodnitrotetrazolium chloride (INT). According to our studies, the electronic spectrum of the cobalt ion associate has a peak at 630 nm. The INT:[Co(SCN)₄] ratio in the triple ion-associate complex was 2:1, and due to the good solubility of the Co(II) ion associate and INT in 1,2-dichloroethane, maximum extraction into the organic phase was achieved for 30 s. The molar absorptivity of the studied ion associate INT₂[Co(SCN)₄] was $\epsilon_{630} = 0.6 \times 10^3$ L/mol cm. Sandell's sensitivity of the method was 9.8×10^{-2} µg/cm². The maximum quantity of Co was extracted with INT at pH 2-7. Maximum absorption of the extracts was registered at thiocyanate ions concentration (≥ 1 M) in the aqueous phase. The ion associate displayed the highest absorption at INT concentration $\geq 6 \times 10^{-4}$ M. The relationship between Co (II) concentration and absorption was linear in the range of 6 – 125 µg Co(II) in 10 ml aqueous solutions. The content of Co in *Amanita calsarea* was 1.543 ± 0.158 mg/kg dry weight, in *Boletus pinophilus* - 0.257 ± 0.042 mg/kg dry weight and in *Burley tobacco* - 1.967 ± 0.229 mg/kg dry weight. The extraction-spectrophotometric method for cobalt determination in biological samples with iodnitrotetrazolium chloride, developed in the present study, is characterized with high speed, selectivity and satisfactory accuracy.

Keywords: Co, INT, spectrophotometry, application, mushrooms and tobaccos.

INTRODUCTION

It is known that long-term cobalt deficiency can result in demyelination of large nerve trunks and spinal cord, reduced white blood cells, pernicious anemia and reduced resistance to parasite and microbial infections. On the other hand, cobalt can be toxic in high doses, causing polycythemia, bone marrow hyperplasia, pancreatic failure, congestive heart failure and cardiomyopathy [1, 2]. That is why its content in various systems should be monitored [3–5].

It is widely known that Co content in agrochemical objects is insignificant [3–8]. The scientific literature presents many methods for separation, preconcentration and determination of cobalt in samples [2–20]. The widely applied methods for determination of the element content are photocolorimetric, polarographic and spectral. Extraction-photometric methods are applied for determination of ultra-small Co quantities in agrochemical objects. Their major advantages are simplicity, rapidity and accessibility. In the analytical practice, the reaction between Co (II) and nitroso-R-salt is widely used. One of the base factors that reduce the precision of the photometric determination of Co microquantities in soil samples

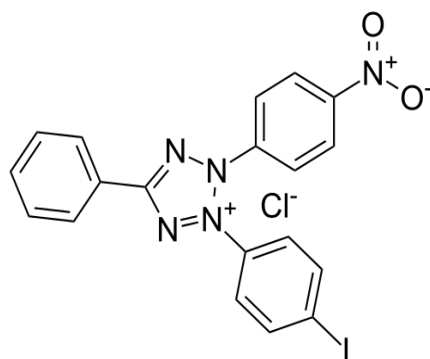
is the presence of colored organic compounds, as well as of Fe, Ni and Cu salts.

Till now the literature presents only a few methods for Co determination in soil and plants. The following reagents are used: 1,10-phenanthroline, eosin, thiodibenzoylmethane, picraminazo-4-cyclohexylresorcinol, diantipyril-methane, and 2-(2-benzthiazolylazo)-5-dimethyl-aminobenzoic acid. Some of these methods require exact working pH and preliminary stay of the samples before Co determination. Other methods are characterized with low sensitivity and selectivity. Another method for quantitative determination of Co includes heating to 80° C. However, the complex formed is stable for only 20 min [14–26].

The aim of the present study was to develop an extraction-spectrophotometric method for Co (II) determination in biological samples (mushrooms and tobaccos), with selectivity and speed exceeding those of most up-to-date applied methods. The structure formula of INT is presented in Fig. 1.

IUPAC name: 3-(4-iodophenyl)-2-(4-nitrophenyl)-5-phenyl-2H-tetrazol-3-ium chloride. Other names: 2-(4-Iodophenyl)-3-(4-nitrophenyl)-5-phenyl-tetrazolium chloride; Iodnitrotetrazolium chloride, INT.

* To whom all correspondence should be sent:
E-mail: lkd@abv.bg

**Fig. 1.** Structure formula of INT

The following objectives have to be studied:

- the solubility of the ion-associated thiocyanate complex of Co(II) with iodnitrotetrazolium chloride (INT) in different organic solvents and to select the most appropriate of them;
- the effect of pH;
- the time necessary for Co extraction, and to estimate the time necessary for complete metal extraction as an ionic associate in the organic phase;
- the effect of the concentrations of the reagents participating in the extraction equilibrium of the system. The optimal established quantity of each of them would guarantee the complete extraction of Co (II) using the investigated monotetrazolium salt;
- the effect of side ions on Co extraction and determination in order to assess the selectivity of the developed method.

EXPERIMENTAL

Reagents and apparatus

Apparatus

Absorbance measurements were made on a UV - Vis spectrophotometer, Germany, with a 1 cm quartz cuvette at 630 nm.

Reagents

The reagents used were of analytical grade (p.a., Merck and Fluka). All solutions were prepared with distilled demineralized water.

Extraction procedure

In a separating funnel of 100 ml the following solutions were added: 1 ml of 1×10^{-3} M Co (II), 1 ml of 4M potassium thiocyanate and 7 ml of 1.5×10^{-3} M iodnitrotetrazolium chloride (INT). Distilled water was added to the aqueous phase to 10 ml volume. The following step was extraction with 3 ml of 1,2-dichloroethane for 30 s. After phase separation, the organic phase was transferred through a paper filter

into a cuvette b = 1 cm and subjected to photometric analysis at 630 nm on a UV - Vis spectrophotometer.

RESULTS AND DISCUSSION

Optimal Conditions

Solvent

The extraction of the Co ion associate in different organic solvents: methyl ethyl ketone, 1,2-dichloroethane, chloroform, benzene, toluene, tetrachloromethane and diethyl ether, was studied.

1,2-dichloroethane was found as the most suitable solvent. The electronic spectrum of the cobalt ion associate has a maximum at 630 nm. The maximum absorption was detected at this wavelength.

The bond in the molecule of the obtained ion associate, formed between $[\text{Co}(\text{SCN})_4]^{2-}$ and the tetrazolium salt was electrostatic.

Composition of the triple ion-associated complex

The composition of the triple ion-associated complex was determined by the Ostromislensky - Job method [26]. It was found that the ratio INT:[Co(SCN)₄] was 2:1.

Extraction time

The effect of time as a factor for achieving extraction equilibrium between the two phases was studied. Due to the good solubility of the ion-associated complex of cobalt (II) and INT in 1,2-dichloroethane, maximum extraction of the organic phase was achieved for 30 s.

Determination of the molar absorbance of the ion triple associated thiocyanate complex of cobalt (II) and INT

Molar absorbance of the ion associate $\text{INT}_2[\text{Co}(\text{SCN})_4]$ was determined by the method of Komar-Tolmachov [26] by measuring the light absorbance of solutions with different concentration of the reagents at constant stoichiometry. The obtained results are presented in Table 1.

The molar absorbance of the studied ion associate $\text{INT}_2[\text{Co}(\text{SCN})_4]$ was $\epsilon_{630} = 0,6 \times 10^3 \text{ L/mol cm}$. The sensitivity of the method according to Sandell [4] was $9.8 \times 10^{-2} \mu\text{g}/\text{cm}^2$.

Table 1. Determination of the molar absorptivity of the ion-associated complex.

ml Co(II) 1.10 ⁻³ M	C _{Co(II)}	A	$\frac{C \cdot l}{A} = \frac{1}{\epsilon} \cdot 10^{-3}$	$1/\sqrt[n+1]{A}$
0.1	0.00001	0.020	0.0005	0.50
0.2	0.00002	0.030	0.0007	0.76
0.8	0.00008	0.080	0.001	1.00
2	0.0002	0.160	0.00125	1.25
				2.67

Study of the medium acidity

The acidity of the medium is a factor that affects the amount of cobalt uptake by the organic phase. There is a very large pH range in which it has constant values. Experimental data showed that light absorption in neutral and acidic medium to pH 2 has a constant (maximum) value. At pH < 2, it begins to decrease and the determination becomes impossible. Maximum Co(II) uptake was achieved at pH 2-7. The wide pH range makes it possible to work without precisely controlling the pH, or using buffer solution. This makes the method less pretentious.

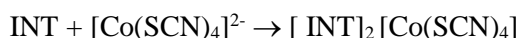
Reagents quantity

To find out the optimal conditions for the extraction of the thiocyanate complex of Co (II) with INT the influence of tetrazole salt and thiocyanate ions was examined. The formation of the ion associate significantly depends on the concentration of the thiocyanate ions. In order to shift the equilibrium to the formation of the thiocyanate complex of Co (II) an excess of thiocyanate ions was required. This excess had no effect on the extraction equilibrium and facilitated the quantitative extraction of cobalt in the organic phase. By varying the amount of thiocyanate ions in the aqueous phase the highest light absorbance of the extracts was found at a concentration of ≥ 1 M.

An important factor in the photometric determination of cobalt is the concentration of the tetrazole salt. In order to maximize the recovery of the metal from the aqueous phase, the influence of different INT concentrations was investigated. The light absorption of the ion associate has a maximum value at a concentration of 6×10^{-4} M INT. With increasing concentrations of the tetrazole salt, the light absorption of the associate remains constant.

Effect of Co(II) concentration on the light absorption

When INT was added to the thiocyanate solution of cobalt (II) a pale green precipitate soluble in the organic solvent was obtained.



The intensity of the precipitate color increased with increasing cobalt (II) concentration. The relationship between cobalt (II) concentration and light absorption is linear in the range from 6 mg to 125 mg Co (II) in 10 ml aqueous phase.

Effect of side ions

To get a more complete picture of cobalt (II) extraction and to characterize the selectivity of the extraction, the influence of some ions, which would probably be present in the analyzed samples, was studied. Experimental data are given in Table 2. The results qualify the tetrazolium salt used as a selective reagent for the determination of cobalt. Among all examined ions, only Fe (III) interferes with the determination. The interference is removed by the addition of ascorbic acid as a masking agent which has pronounced reduction properties.

Table 2. Effect of some ions on Co(II) extraction with INT: $C_{\text{Co(II)}} = 0.5 \times 10^{-4}$ M, $C_{\text{INT}} = 4.5 \times 10^{-4}$ M, $C_{\text{SCN}} = 0.8$ M

Side ion	Concentration limit of the side ion, mg	Limit ratio $C_x/C_{\text{Co(II)}}, \text{mg}$
K^+	300	10204:1
Na^+	100	3401:1
$\text{Sr}^{2+}; \text{S}_2\text{O}_3^{2-}$	50	1700:1
$\text{C}_2\text{O}_4^{2-}$	20	680:1
Hg^{2+}	15	510:1
$\text{Al}^{3+}; \text{Ca}^{2+}; \text{Ni}^{2+}; \text{BO}_3^{3-}$	10	340:1
Pb^{2+}	8	272:1
W^{6+}	7.4	251:1
Cd^{2+}	5	170:1
V^{5+}	0.5	17:1
Cr^{6+}	0.3	10:1
Br^-	0.2	6.8:1
$\text{EDTA}; \text{NO}_3^-; \text{J}^-; \text{SO}_4^{2-}$	0.1	3.4:1
ClO_4^-	0.05	1.7:1
Fe^{3+}	0.01	interferes

Application of the developed method for analysis of the cobalt content in biological samples (mushrooms and tobaccos).

Accuracy and precision

In order to check the accuracy of the method a reference material CTA-VTL-2 (Virginia tobacco leaves) was used. For evaluation of the accuracy of the digestion and measuring procedures, we have used the R criterion showing the percent extraction of the element from the certified value. When the measured value X is within the limits of $X_{\text{CRM}} \pm U_{\text{CRM}}$, where U_{CRM} is the indefiniteness of the certified value, we accept the extent of extraction to be 100%. In all remaining cases, the extent of extraction is equal to $X / X_{\text{CRM}} \cdot 100$. As can be seen from Table 3, the results obtained for the certified material yield a 100% recovery of Co.

Mineralization of the samples

Mushroom samples (*Amanita calsarea* and *Boletus pinophilus*) were collected in Batak-Shiroka Poliana, Bulgaria, in 2015 and dried at 105 °C for 24 h.

Tobacco samples (*Burley*) were collected in Stara Zagora, Bulgaria in 2015. They were dried at 650 °C in a fan oven and stored in dark polyethylene bottles.

The mineralization of the samples was carried out according to EPA Method 3052 [27]. 0.5 g of air-dry sample was weighed to the nearest 0.001 g in PTFE vessels. HNO₃, HF, HCl and H₂O₂ were added using a microwave system Multiwave 3000. The maximum power was 1400 W, and the maximum pressure in the Teflon vessels - 40 bar.

The concentrations of cobalt were determined in an air-acetylene flame by the Perkin–Elmer Aanalyst 800 model atomic absorption spectrometer.

Cobalt extraction

A 5 ml sample, several drops of 1 M NaOH (for adjustment of pH 9.0-10.0) and 5 ml of 0.02% dithizone in chloroform were consecutively added in a 100 ml separating funnel. The system was left to extract for 1 min. Adequate quantity of HCl (1:1) (for adjustment of pH 1.0-2.0) and 2 ml of 4 M thiocyanate solution were added to the organic phase. Re-extraction was carried out for 1 min. The organic phase was discharged, then 1 M NaOH (for pH 3.0-4.0), 0.6 ml of 1.5×10⁻² M INT and 2 ml of a saturated solution of ascorbic acid (for masking of the interfering ions) were added to the aqueous phase. Distilled water was supplemented to a volume of 20 ml. Extraction with 3 ml 1,2-dichloroethane was carried out for 30 s. After phase separation the organic was filtered through a paper filter, placed in a cuvette, b = 1 cm, and measured at λ = 630 nm.

A blank, not containing a sample, was also analyzed for reliability of the experimental results.

The experimental data are shown in Tables 3 and 4. A good correlation of our results with data for the certified Virginia Tobacco Leaves (CTA – VTL – 2) samples was established.

Table 3. Co content in Virginia Tobacco-CTA-VTA-2 certified reference material (n = 3).

	Co CTA-VTA-2 $X \pm \sigma$ mg/kg	R %
Certified value	0.429 ± 1.4	100
AAS	0.420 ± 0.027	98
INT	0.415 ± 0.015	97

Table 4. Co content in mushroom samples (*Amanita calsarea* and *Boletus pinophilus*) (n = 15) and Burley tobacco (n = 15).

Sample	Co X±σ mg/kg	Co INT X±σ mg/kg
<i>Amanita calsarea</i>	1.543 ± 0.158	1.532 ± 0.154
<i>Boletus pinophilus</i>	0.257 ± 0.042	0.246 ± 0.041
<i>Burley</i>	1.967 ± 0.229	1.896 ± 0.251
Tobacco		

CONCLUSIONS

The extraction-spectrophotometric method for cobalt determination in biological samples with iodnitrotetrazole chloride (INT) developed in the present study is characterized with high speed, high selectivity and satisfactory accuracy. According to these indices, this method excels some of the currently applied techniques for cobalt determination in biological samples.

Acknowledgement: This work was financially supported by the project: ref. no. NP 05/14, 2014/2015, Trakia University.

REFERENCES

- D. G. Barceloux, D. Barceloux, *Clin. Toxicol.*, **37**, 201 (1999).
- B. B. Tewari, *Rev. Bol. Quim.*, **26**, 30 (2009).
- R. A. Meyers (ed.), Encyclopedia of Analytical Chemistry: Applications, Theory and Instrumentation, Wiley, Chichester (2000).
- E. Sandell, Colorimetric methods for determining traces of metals, (Moscow) 1964.
- M. Jakubowski, M. Trzcinka-Ochocka, *J. Occup. Health*, **47**, 22 (2005).
- A. Tsuyoshi, H. Hoshino, T. Yotsuyanagi, *Chem. Lett.*, **30**, 302 (2001).
- I. V. Pyatnitskii (ed.), Analytical Chemistry of Cobalt, Nauka, Moscow (1965) (in Russian).
- G. Ram, R. S. C hauhan, A. K. Goswami, *Rev. Anal. Chem.*, **22**, 255 (2003).
- N. Makarova, E. Kulapina, *Electroanalysis*, **27**, 621 (2015).
- B. Tewari, *Rev. Bol. Quim.*, **26**, 30 (2009).
- Z. Marczenko, M. Balcerzak, UV-Vis Spectrophotometric Methods in Inorganic Analysis, (BINOM Laboratoriya znanij, Moscow) 2007.
- S. Tokalioglu, S. Kartal, *Bull. Korean Chem. Soc.*, **27**, 1293 (2006).
- V. Cucinotta, R. Caruso, A. Giuffrida, M. Messina, G. Maccarrone, J. A. Torrisi, *Chromatogr. A*, **1179**, 17 (2008).
- Z. Jiang, J. Yu, H. Liu, *Anal. Sci.*, **21**, 851 (2005).
- P. Berton, R. Wuilloud, *Anal. Methods*, **3**, 664 (2011).
- H. Ciftci, A. Olçucu, A. Ozkaya, T. Ciftci, *Asian J. Chem.*, **21**, 2643 (2009).
- C. Sabel, J. Shepherd, S. Siemann, *Anal. Biochem.*, **391**, 74 (2009).
- H. Pouretedal, P. Sononi, M. Keshavarz, A. Semnani, *Chemistry*, **18**, 22 (2009).

19. L. Dospatliev, M. Ivanova, *Chemistry: Bulgarian Journal of Science Education*, **26**, 377 (2017).
20. K. Gavazov, A. Dimitrov, V. Lekova, *Usp. Khim.*, **76**, 187 (2007).
21. K. Gavazov, K. Stojnova, T. Stefanova, G. Toncheva, V. Lekova, A. Dimitrov, *Chemija*, **23**, 278 (2012).
22. T. Stefanova, K. Gavazov, *Cent. Eur. J. Chem.*, **11**, 280 (2013).
23. M. Boggs, L. Gribat, C. Boele, N. Wall, *J. Radioanal. Nucl. Chem.*, **293**, 843 (2012).
24. K. Gavazov, *Chemistry: Bulgarian Journal of Science Education*, **22**, 222 (2013).
25. V. Divarova, P. Racheva, V. Lekova, K. Gavazov, A. Dimitrov, *Journal of Chemical Technology and Metallurgy*, **48**, 623 (2013).
26. I. Bulatova, I. Kalinkin, *Chemistry*, (Leningrad) 1972.
27. Method EPA 3052, *US EPA*, (Washington, DC, USA) 1996.

СПЕКТРОФОТОМЕТРИЧНО ИЗСЛЕДВАНЕ НА СИСТЕМИ ЗА ТЕЧНО-ТЕЧНА ЕКСТРАКЦИЯ, СЪДЪРЖАЩИ КОБАЛТ И ТЕТРАЗОЛИЕВИ СОЛИ. ПРИЛАГАНЕ НА РАЗРАБОТЕНИЯ МЕТОД ЗА ОПРЕДЕЛЯНЕ СЪДЪРЖАНИЕТО НА КОБАЛТ В БИОЛОГИЧНИ ПРОБИ (ГЪБИ И ТЮТЮН)

Л. Доспатлиев^{1*}, М. Иванова²

¹Катедра "Фармакология, физиология на животните и физиологична химия", Ветеринарно-медицински факултет, Тракийски университет, Стара Загора

²Катедра "Информатика и математика", Стопански факултет, Тракийски университет, Стара Загора

Получена на 5 април, 2016 г.; приета на 19 юни, 2017 г.

(Резюме)

Разработена е методика за екстракционно-спектрофотометрично определяне на кобалт в проби чрез използване на йоднитротетразолов хлорид. Нашите изследвания показваха, че електронният спектър на кобалтовия йонен асоциат има един максимум при 630 nm. При тази дължина на вълната поглъщането е максимално. Съставът на тройния йонно-асоцииран комплекс е с отношение INT: [Co(SCN)₄] = 2:1, а поради добрата разтворимост на йонно-асоциирания комплекс на кобалт(II) и INT в 1,2-дихлороетан, максимално извличане в органичната фаза се постига при 30 s екстракция. Моларната абсорбируемост на изследвания йонен асоциат INT₂[Co(SCN)₄] е $\epsilon_{630} = 0,6 \times 10^3$ L/mol.cm. Чувствителността на метода по Сендел е $9,8 \times 10^{-2}$ $\mu\text{g}/\text{cm}^2$. Установено е, че максимално извличане на кобалт(II) с INT се постига в pH интервала от 2 до 7. Също така е установено, че чрез вариране количеството на тиоцианатните йони, при концентрация ≥ 1 M във водната фаза, светлинната абсорбция на екстрактиите е максимална. Светлинната абсорбция на йонния асоциат има максимална стойност при концентрация на INT $\geq 6 \times 10^{-4}$ M. Определена е зависимостта между концентрацията на кобалт(II) и светлинната абсорбция, която е линейна в интервала от 6 μg до 125 μg Co(II) в 10 ml водна фаза. Концентрацията на Co в гъби Булка (*Amanita calsarea*) е $1,543 \pm 0,158$ mg/kg, в гъби Манатарка (*Boletus pinophilus*) - $0,257 \pm 0,042$ mg/kg и в проби от тютюн (*Burley*) - $1,967 \pm 0,229$ mg/kg. Разработеният екстракционно-спектрофотометричен метод за определяне на кобалт в биологични преби с йоднитротетразолов хлорид (INT) е прост, евтин, експресен, селективен и се характеризира със задоволителна точност.

Novel dextran/β-cyclodextrin and dextran macroporous cryogels for topical delivery of curcumin in the treatment of cutaneous T-cell lymphoma

M. Iv. Slavkova¹, D. B. Momekova¹, B. D. Kostova¹, G. Tz. Momekov¹, P. D. Petrov^{2*}

¹Faculty of Pharmacy, Medical University-Sofia; 2 Dunav St., 1000 Sofia, Bulgaria

²Institute of Polymers, Bulgarian Academy of Sciences, Akad. Georgi Bonchev St. 103A, 1113 Sofia, Bulgaria

Received March 31, 2017; Accepted May 5, 2017

Cutaneous T-cell lymphoma (CTCL) is a rare disease affecting middle-aged as well as paediatric patients. The early stages might be successfully treated with local medications. As a phytochemical with pleiotropic pharmacological activity including anti-inflammatory and anti-cancer activity curcumin presents a safe alternative to the current state for the early therapy of CTCL, albeit its low water solubility and chemical instability. In this study, original sponge-like cryogels based on dextran/β-cyclodextrin mixture and pure dextran were prepared and assessed as platforms for topical controlled delivery of curcumin. Cryogel carriers with macroporous structure were synthesized by photochemical crosslinking in frozen state and subsequent thawing. Curcumin was successfully loaded into the cryogels by physical adsorption and satisfactory encapsulation efficiency was achieved, especially in the case of dextran/β-cyclodextrin systems (57.8%). The *in vitro* dissolution tests showed sustained release of the API within 72 h and when dextran/β-cyclodextrin was used as a carrier no burst effect was noticed. In addition, cytotoxicity assessment on both tumour and non-malignant cells was performed whereby comparable activity and selectivity with the free drug were evident. The proposed novel macroporous cryogel systems with curcumin show aptitude for application as controlled dermal drug delivery systems for the treatment of CTCL.

Keywords: Curcumin; CTCL local therapy; cryogel; macroporous sponges; dextran; β-cyclodextrin.

INTRODUCTION

The primary lymphoproliferative disorders are divided into the groups of B-cell and T-cell lymphomas. Although the T-cell lymphomas are not very common a tendency is observed regarding the increase of new patients per year [1]. Cutaneous T-cell lymphomas (CTCL) in particular are characterized with heterogeneous manifestations, mycosis fungoides and Sézary syndrome being the two main forms. They predominantly affect middle-aged or older people (average onset 50-60 years of age) but also children in the first decade of their life can be affected [2]. The disease is considered a rare one according to the European Medicine Agency (EMA) criteria, the prevalence varies between 3 and 6 cases per million [3] and is a life-threatening condition. The early stage CTCL are mainly topically treated while in advanced stages the topical therapy is adjuvant [4] but there are no established protocols neither for adults nor for paediatric patients [2]. The main issues related to the disease are its early and correct diagnosis, as well as the complex and usually chronic therapy [2].

Curcumin is a natural yellow pigment isolated from the plant *Curcuma longa*. It is practically a polyphenol not soluble in water (about 11 ng/ml) with pleiotropic pharmacological activities

including anti-inflammatory, anti-cancer, antioxidant, hypoglycaemic and other effects [5, 6]. Curcumin's mechanism of action is based mainly on the inhibition of the NF-κB signalling pathway related to both inflammation and tumour biology [7]. Other pharmacological targets of this phytochemical include growth factors, protein kinases and other enzymes such as cyclooxygenase 2 and 5 lipoxygenase [8]. The oral application of curcumin, albeit very attractive, has major drawbacks as it is characterized by chemical instability, low water solubility, low intestinal absorption, rapid metabolism and rapid elimination of the drug, leading together to a disappointingly low bioavailability [9]. Considering these issues and the cutaneous manifestation of CTCL, curcumin can be successfully applied topically, thus bypassing the pharmacokinetic barriers and attaining pharmacologically active levels at the targeted neoplastic lesions. Moreover, an anticipated advantage of topical curcumin *versus* the available conventional local treatments in CTCL, such as retinoids, corticosteroids, photosensitizers and especially cytotoxic agents such as mechlorethamine is the excellent safety profile of this natural compound.

The literature survey shows several approaches for topical delivery of curcumin employing hydrogels [10], foams [11], sponges [12, 13] nanosized delivery systems [14] and others in which

* To whom all correspondence should be sent:
E-mail: ppetrov@polymer.bas.bg

it is used as wound healing [11, 12, 14], antipsoriatic [15], anti-inflammatory [10] or anticancer agent [13]. In particular, the macroporous sponges represent a promising system for tissue engineering, wound dressings and local drug delivery [16]. Controlling the release of the API by loading macroporous sponges can result in an enhanced bioavailability and better efficacy of hydrophobic drugs such as curcumin [13].

The present study aims at developing original sponge-like cryogels based on the natural polymer dextran and β-cyclodextrin and to assess their applicability as controlled drug delivery system for curcumin intended to be used in the treatment of CTCL.

MATERIALS AND METHODS

Materials

Dextran (DEX) from Leuconostoc spp. with molar mass ~ 2 000 000 g/mol, β-cyclodextrin (β-CD), acryloyl chloride, trimethylamine (TEA), (4-benzoylbenzyl) trimethylammonium chloride (BBTMAC), N,N'-methylenebisacrylamide (BAAm), acetic acid (analytical grade), sodium acetate, acetone, N,N-dimethylformamide (DMF, anhydrous, 99.8 %), ethanol 95 % (analytical grade), L-glutamine, RPMI-1640 cell medium and foetal calf serum (FCS) were purchased from Sigma-Aldrich (USA).

Methods

Synthesis of β-CD-acrylate

β-CD (4.0 g, 3.52 mmol) was added to 10 mL of toluene and dried by azeotropic distillation. Then, the dry β-CD was dissolved in 30 mL of freshly distilled DMF and TEA (2 mL, 24.64 mmol) was added via syringe. The solution was cooled down to 0 °C by dint of an ice bath and acryloyl chloride (3.43 mL, 24.64 mmol) was added dropwise. The reaction mixture was stirred at 700 rpm for 20 h at 20 °C. Thereafter, the reaction mixture was filtered off to remove the insoluble white salt. The residual solution of β-CD-acrylate (β-CD-Ac) in DMF was concentrated by rotary evaporation prior to precipitation into a 10-fold excess of cold acetone (-20 °C) and recovered by filtration. Yield 60%.

Synthesis of cryogels

Dextran (1 g) was dissolved in deionized water (8 mL) under stirring to obtain a homogeneous solution. Then, the photoinitiator BBTMAC (0.05 g, 5 wt.% with respect to dextran) and crosslinking agent, β-CD-Ac (0.25 g) or BAAm (0.05 g, 5 wt.% with respect to dextran), dissolved in 2 mL water were added under stirring at room temperature. The

solution was poured into 8 Teflon dishes (2 cm diameter) forming layers with a thickness of 2.5 mm. Then, the solution was frozen at -20 °C for 2 h. After that the frozen system was irradiated with full spectrum UV-vis light with "Dymax 5000-EC" UV equipment with 400 W metal halide flood lamp for 5 min (dose rate = 5.7 J/cm².min).

Calculation of gel fraction yield and swelling degree

Gel fraction (GF) yield and swelling degree (SD) of cryogels were determined gravimetrically. Prior to calculation all samples were extracted in distilled water for 6 days at room temperature, freeze-dried and weighed. GF yield was calculated by the relationship:

$$GF (\%) = \frac{\text{weight of freeze-dried sample}}{\text{initial weight of polymer and crosslinking agent}} * 100$$

SD was determined as follow:

$$SD = \frac{\text{weight of swollen sample}}{\text{weight of freeze-dried sample}}$$

The experimental errors of GF yields and SD calculations are in the range of 2 – 3 %.

Drug loading and encapsulation efficiency

Curcumin was loaded onto the prepared cryogels by physical adsorption. The cryogels based on dextran and dextran/β-cyclodextrin were immersed into a solution of curcumin (0.5 mg/ml in anhydrous ethanol:water 7:3 v/v mixture) and left in the dark at 36 °C for 6 h to allow loading of the API. Afterwards, ethanol was removed by immersing the cryogels in water for 15 min. Finally, the cryogels loaded with curcumin were lyophilized.

The encapsulation efficiency of the model systems based on dextran and dextran/β-cyclodextrin was calculated according to the equation:

$$EE\% = \frac{\text{Curcumin (mg) in polymer disk}}{\text{Total Curcumin (mg) in loading solution}} * 100$$

The amount of curcumin loaded into the systems was determined spectrophotometrically at 427 nm

after incubation of the cryogel disks for 24 h in 95% ethanol at 36 °C.

Release profiles

The curcumin release from DEX and DEX/β-CD macroporous cryogels was investigated as a function of time at 35 °C. As a dissolution medium 50 ml acetate buffer (pH 5.5) with 10 % anhydrous ethanol under constant stirring at 50 rpm was used. Samples from the acceptor phase were withdrawn at predetermined time intervals and the amount of released curcumin was evaluated spectrophotometrically at 427 nm on the UV-vis

spectrophotometer Evolution EVOT063002 (Thermo Fisher Scientific, Germany). All samples were measured in triplicate and the mean cumulative percentage of drug release was calculated based on a calibration curve of curcumin in the dissolution medium in the concentration range from 0,0005 to 0,01 mg/ml ($y=69.826x-0.0033$; $R^2=0.994$).

¹H-NMR analysis of β-CD-Ac

The ¹H-NMR spectrum of β-CD-Ac was recorded in D₂O using a 600 MHz Bruker AC-spectrometer.

Scanning electron microscopy (SEM)

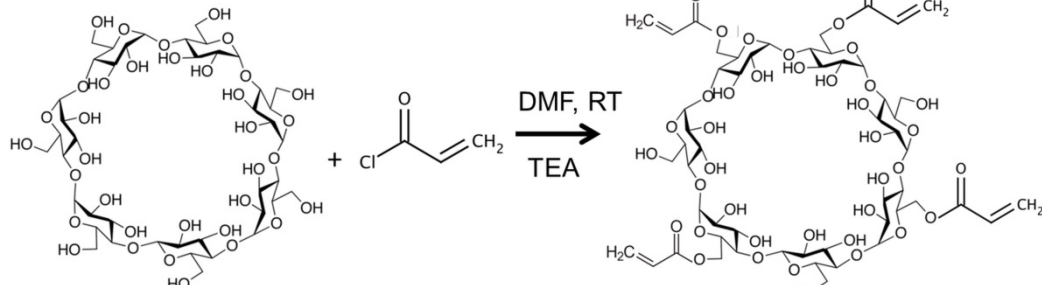
The morphology of the fractured surface of cryogels was examined on a scanning electron microscope (JSM-5510, JEOL, Japan) operating at 10 kV. The samples were coated with gold for 30 s using a sputter-coater (JSC 1200, JEOL, Japan) in an inert argon atmosphere prior to imaging.

Differential scanning calorimetry (DSC)

DSC was performed on a DSC apparatus Q200, TA instruments, USA. The temperature calibration was performed with a sapphire disc supplied by TA instruments in Standard aluminium pans (TA instruments) in the desired temperature interval. Samples with room humidity were tested in the same type of pans from 20 to 250 °C with 10 °C/min heating rate under nitrogen flow (50 ml/min).

Cell lines and culture conditions

The cytotoxic activity of free drug and curcumin loaded on macroporous cryogels was assessed against the skin T-cell lymphoma derived cell line Hut-78 and non-malignant human embryonal kidney cells (HEK-293). The cell lines were purchased from the German Collection of Microorganisms and Cell Cultures (DSMZ GmbH, Braunschweig, Germany). The cells were grown in controlled environment – cell culture flasks at 37 °C in an incubator 'BB 16-Function Line' Heraeus (Kendro, Hanau, Germany) with humidified atmosphere and 5 % CO₂. The growth medium was 90 % RPMI-1640 + 10 % FBS.



Scheme 1. Synthesis of crosslinking agent based on β-CD.

Cytotoxicity assessment (MTT-dye reduction assay)

The cellular viability after exposure to free curcumin or its formulations was assessed using the standard MTT-dye reduction assay as previously described [17] with slight modifications [18]. The method is based on the reduction of the yellow tetrazolium salt MTT to a violet MTT-formazan via the mitochondrial succinate dehydrogenase in viable cells. In brief, exponentially proliferating cells were seeded in 6-well flat-bottomed microplates (3 ml/well) at a density of 1×10^5 cells per ml and after 24 h incubation at 37 °C, they were exposed to various concentrations of the tested curcumin formulations (see below) or free drug, used as a reference antineoplastic agent for 72 h. For each concentration a set of 3 wells was used. After the exposure period, 100 µl MTT solution (10 mg/ml in PBS) aliquots were added to each well. Thereafter, the microplates were incubated for 4 h at 37 °C and the MTT-formazan crystals formed were dissolved through addition of 100 µl per well of 5 % formic acid-acidified 2-propanol. The MTT-formazan absorption was recorded using a LabeximLMR-1 microplate reader at 580 nm. Cell survival fractions were calculated as a percentage of the untreated control. In addition, IC₅₀ values were derived from the concentration-response curves using non-linear regression analysis (GraphPad Prism Software for PC).

RESULTS AND DISCUSSION

Macroporous dextran cryogels with incorporated β-CD moieties (DEX/β-CD) were synthesized by photochemical crosslinking of high molar mass dextran and β-CD-Ac in frozen aqueous solution and subsequent thawing. Firstly, β-CD-Ac was synthesized by reacting β-CD with acryloyl chloride in DMF in the presence of triethylamine (Scheme 1).

An excess of acryloyl chloride (7 mol eq. with respect to β-CD) was used to achieve attachment of several acryloyl groups to one β-CD molecule. The reaction product was purified, isolated and analysed by ¹H-NMR (Fig. 1).

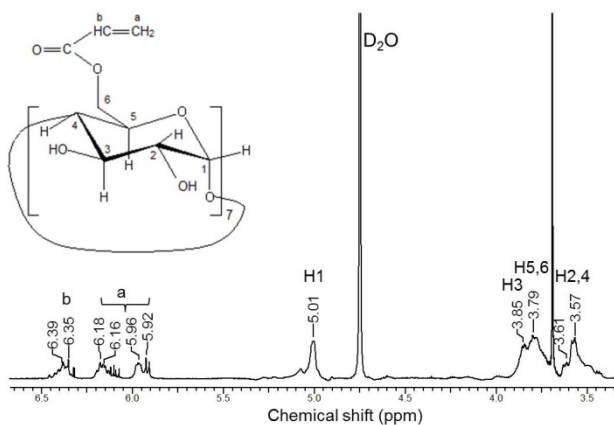


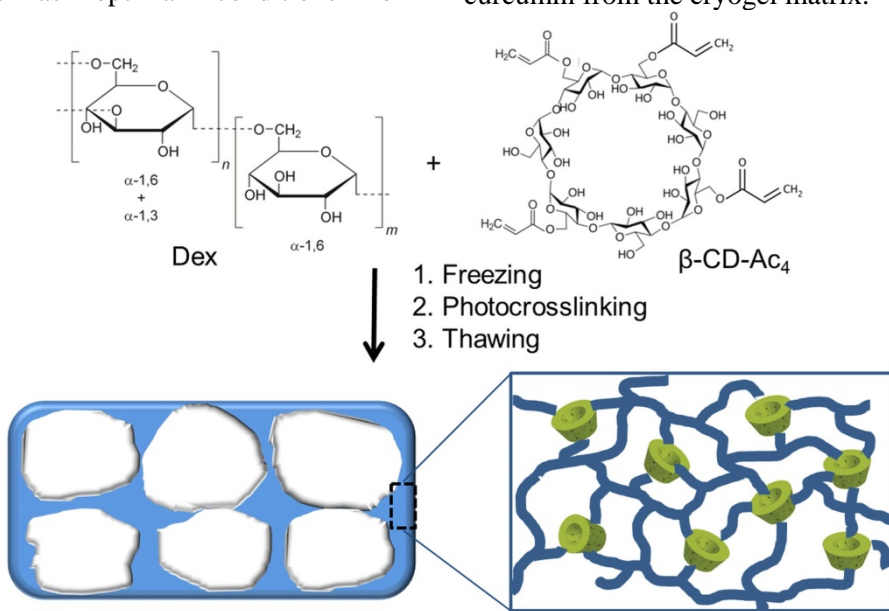
Fig. 1. Proton-NMR spectrum of β-CD-Ac in D₂O.

Based on peak integrals assigned to the β-CD protons at 5.01 ppm to the vinyl protons at 5.8 – 6.4 ppm a degree of substitution equal to four was calculated. Thus, a crosslinking agent (denoted as β-CD-Ac₄), containing four reactive vinyl groups per molecule, was synthesized and used for preparation of cryogels. Macroporous dextran cryogels with incorporated β-CD moieties were prepared by freezing an aqueous solution of reagents at – 20 °C for 2 h, irradiation with UV light for 5 min with an irradiation dose rate of 5.7 J/cm².min and subsequent thawing to room temperature (Scheme 2). These experimental conditions have been established in our previous studies as optimal conditions for

preparation of cryogels from high molar mass polysaccharides with fairly high gel fraction yield and good mechanical properties [19, 20].

The freezing of the aqueous solution led to formation of a solid phase (ice crystals) and a liquid microphase, where non-frozen water, dextran, photoinitiator and cross-linking agent were located. The reaction of crosslinking took place in the liquid microphase by recombination of (macro)radicals generated in dextran and β-CD-Ac molecules by UV light. In fact, the liquid microphase acted as a template for the formation of cryogel walls, while ice crystals acted as a porogen. As expected, the combination of cryogenic treatment and photochemical crosslinking resulted in formation of sponge-like cryogels comprising large interconnected pores surrounded by thin walls (Fig. 2a).

In addition, dextran cryogels without β-CD were synthesized following the same synthesis procedure by using BAAM as a crosslinking agent instead of β-CD-Ac₄. The use of a small amount of BAAM was essential to obtain gels of good strength since dextran cryogels synthesized without crosslinking agent were weak and fell to pieces on handling. Importantly, DEX/β-CD cryogels exhibited similar morphology and swelling properties as compared to DEX cryogels. Actually, the calculated GF yield (73 ± 3 %) and SD (34 ± 3) of DEX/β-CD cryogels were comparable to the GF yield (82 ± 3 %) and SD (28 ± 3) of pure dextran cryogels. This fact allowed us to compare the two cryogels as carriers of curcumin and to emphasize the role of β-CD on the release of curcumin from the cryogel matrix.



Scheme 2. Preparation of sponge-like cryogels by photochemical crosslinking of DEX and β-CD-Ac₄ in a frozen aqueous solution and thawing.

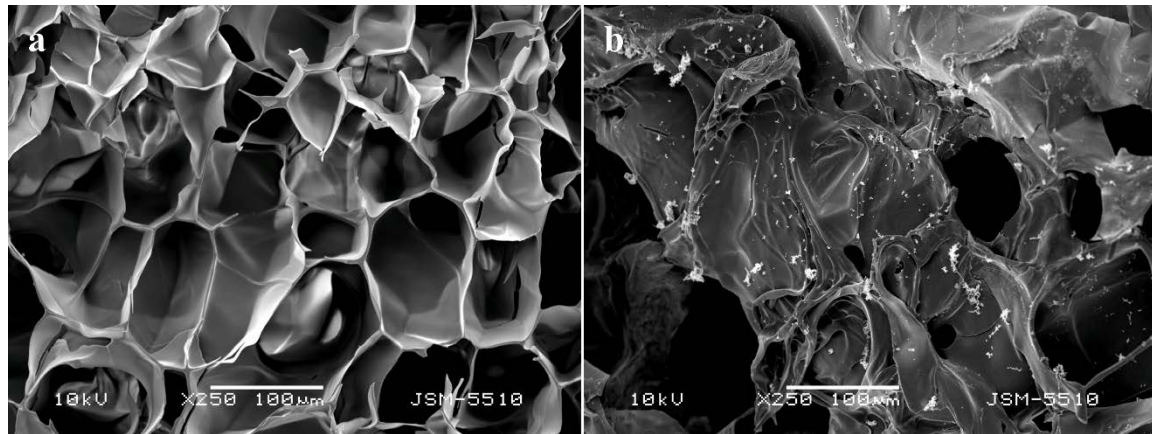


Fig. 2. SEM micrograph of freeze dried DEX/β-CD cryogel (a) and curcumin loaded DEX/β-CD cryogel (b).

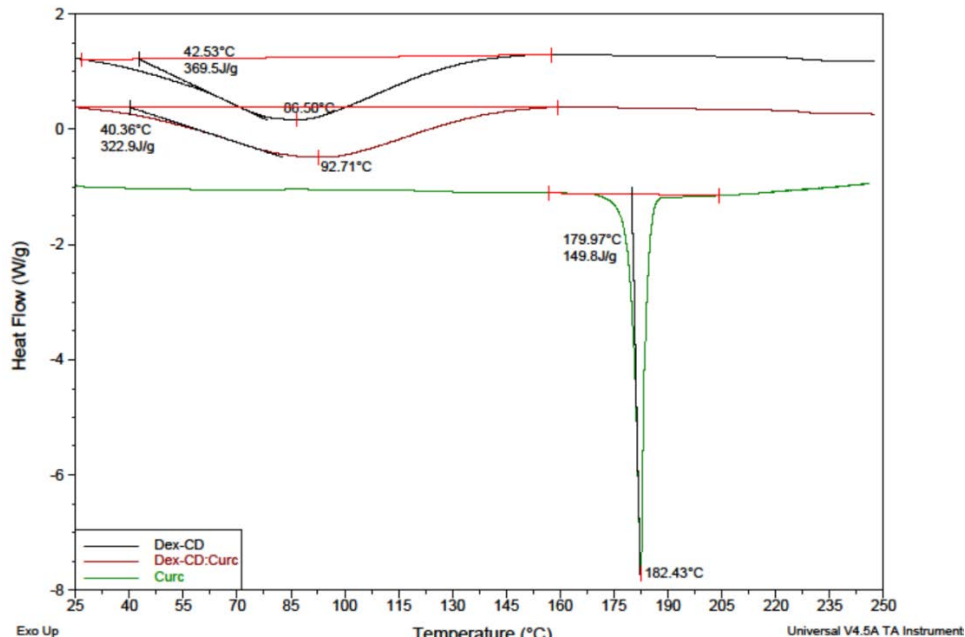


Fig. 3. DSC thermograms of Dex/β-CD cryogel, curcumin loaded Dex/β-CD cryogel and pure curcumin.

Both cryogels were loaded with curcumin by the physical adsorption method. Freeze dried disks were immersed in a solution of curcumin in ethanol/water (7:3 v/v) and allowed to absorb the drug for 6 h at 36 °C. Since curcumin is a hydrophobic substance, one may expect that in the case of DEX/β-CD cryogels a portion of the drug will be located into the cavity of β-CD molecules. In the next step, the curcumin solution filling the cryogel pores (free volume) was replaced by pure water to minimize the content of drug molecules which are not embedded into polymer matrix. Finally, the carriers were freeze dried and utilized for further experiments.

The calculated encapsulation efficiencies of DEX and DEX/β-CD cryogels were 36.2 % and 57.8 %, respectively. This significant difference could be attributed to the presence of cyclic oligosaccharides in the polymer matrix. Being very hydrophobic ($\log P=2.3$) [21] curcumin has higher affinity towards the hydrophobic cavities of β-CD and, therefore, larger

amount of the drug were loaded into the DEX/β-CD systems.

DEX/β-CD cryogels loaded with curcumin were further analysed by SEM (Fig. 2b). In this case, unlike the smooth surface of pure DEX/β-CD cryogels (Fig. 2a), small particles regularly distributed on the inner cryogel surface were observed. Undoubtedly, this result confirms that curcumin is loaded into the cryogel carrier. However, the surface analysis by SEM cannot provide information whether and what amount of curcumin is embedded inside the polymer matrix. Additional information about the phase state of curcumin loaded in the polymer carriers was obtained from DSC analysis. DCS curves of pure curcumin and DEX/β-CD cryogel with and without curcumin are shown in Fig. 3.

Curcumin is a crystalline solid and DSC analysis of pure powder showed a narrow melting peak at 182 °C. However, the melting peak ascribed to curcumin

disappeared in the drug-loaded DEX/β-CD cryogel. This fact implies that curcumin is in amorphous state probably due to some specific interaction with the polymer carrier. The broad exothermic peaks in the 40–120 °C temperature range are attributed to some remaining bound water in the cryogel matrix. At first glance DSC results seem contradictory to SEM observation. Here, one should point out that DSC is a quantitative analysis unlike SEM. On this ground, one may suggest that the main portion of curcumin is homogeneously entrapped into the polymer matrix where the formation of typical crystalline structure of curcumin (Fig. 4) inside the polymer network is hindered. Most probably, the drug particles observed by SEM on the cryogel inner surface are crystalline, however, their portion is very small and cannot be detected by DSC.

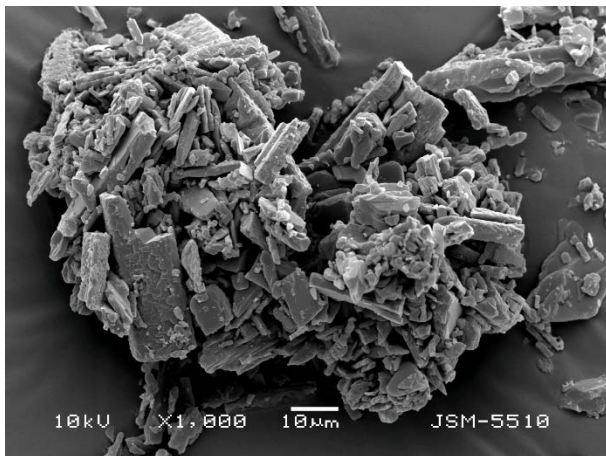


Fig. 4. SEM micrograph of pure curcumin.

The evaluation of the dissolution test shows sustained release from both model formulations (Fig. 5). After 72 h the amount of API released from DEX cryogels was about 36.9 % while the released amount from DEX/β-CD was almost twice as low (14.98 %).

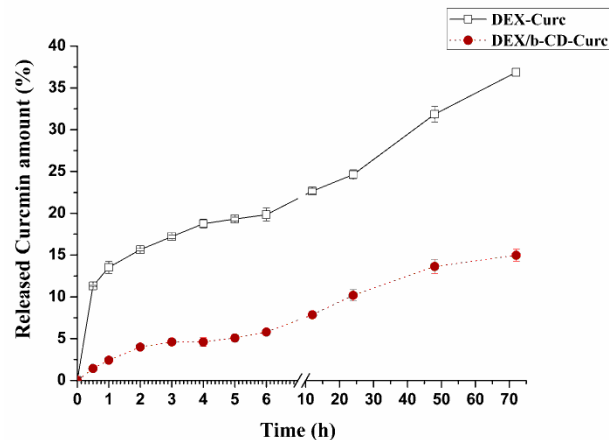


Fig. 5. Cumulative dissolution profiles of curcumin from the model formulations in acetate buffer (pH 5.5) and 10% ethanol; mean \pm SD, n=3.

DEX cryogels showed burst release in the first hour of the dissolution. This fact can be due to the presence of some amount of curcumin on the inner surface of the sponge, resulting in fast diffusion and release into the dissolution medium in the beginning of the process. In the case of DEX/β-CD systems no burst effect was registered. Here, more pronounced sustained release was observed. Although the difference of the released curcumin in % is almost double the actual amount released from DEX cryogels is 0.331 ± 0.007 mg/ml, while in the case of DEX/β-CD it is 0.217 ± 0.004 . The difference in the release behaviour is most probably due to the location of some portion of hydrophobic curcumin into the β-CD cavities as an inclusion complex, which slows down the release of the drug to the polar dissolution medium.

An integral element of the presented study was the comparative bioassay of cell growth-inhibitory effects of DEX and DEX/β-CD based systems vs. free drug (DMSO solution). The pharmacological study was conducted using the MTT-dye reduction assay in the skin T-cell lymphoma derived cell line Hut-78 and non-malignant human embryonal kidney cells (HEK-293).

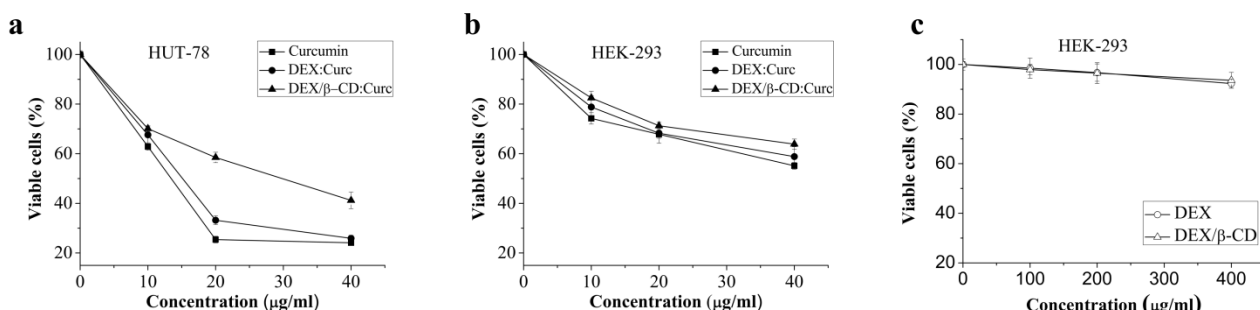


Fig. 6. Growth inhibitory concentration-response curves of loaded cryogels and free drug (a, b) and cytotoxicity of non-loaded systems (c) determined by the MTT-dye reduction assay after 72 h of continuous exposure. Each bar represents cell survival fractions (as percentage of the untreated control) from 3 independent experiments.

Evident from the concentration-response curves depicted in Figure 6 (a), the free drug in DMSO solution caused strong, concentration-dependent inhibition of malignant cell (HUT-78) growth ($IC_{50}=13.35\text{ }\mu\text{g/ml}$), which was practically paralleled by the cytotoxicity pattern of curcumin, loaded in the dextran-based system ($IC_{50}=15.11\text{ }\mu\text{g/ml}$). The slower and less steeper release pattern of curcumin from the DEX/β-CD-system as compared to the dextran carrier was consistent with the less pronounced tumour cell growth inhibition at all data points, which is undoubtedly conditioned by the less intensive exposure to the free antineoplastic natural compound. The IC_{50} of DEX/β-CD-loaded curcumin was $29.71\text{ }\mu\text{g/ml}$. Compared to the malignant cells the tested formulations showed far less cytotoxicity against non-malignant cell line (HEK-293) (Fig. 6 b), whereby they failed to induce 50 % inhibition of cellular viability. This finding could be explained with the pronounced selectivity of curcumin against tumour cells.

In order to determine whether the cytotoxic effect of the prepared formulation is caused only by the cytotoxic potential of curcumin rather than the toxic effect of the cryogel carriers, we sought to determine the intrinsic inhibitory potential of the non-loaded DEX and DEX/β-CD sponges. As is evident from the results presented the non-loaded cryogels are practically devoid from cytotoxic activity against the cell line under investigation. Even at the highest tested concentrations on empty sponges ($200\text{ }\mu\text{g/ml}$) the cell viability was only slightly affected and over 90 % of treated cells retained their vitality as compared to the untreated control (Fig. 6c).

CONCLUSIONS

Novel dextran/β-cyclodextrin and dextran macroporous cryogels were synthesized as potential platforms for dermal controlled delivery of curcumin for topical treatment of CTCL. The elaborated sponges were characterized with high drug loading efficiency (up to 57.8 %). DSC analysis showed that the encapsulation of curcumin into macroporous sponges is associated with transition from crystalline to amorphous state of the drug. This is a prerequisite for improved aqueous solubility of curcumin. Both model formulations demonstrated sustained release profiles of API within 72 h and in the case of DEX/β-CD no burst effect was evident. The cytotoxicity assessment of curcumin loaded DEX and DEX/β-

CD showed comparable activity with the free drug while maintaining pronounced selectivity against tumour cells. Consequently, the novel macroporous cryogel systems based on dextran/β-cyclodextrin can be considered as an advantageous alternative to the current CTCL local treatment options.

REFERENCES

1. Olsen EA., *Dermatol. Clin.*, **33**(4), 643 (2015).
2. K. Ferenczi, H. Makkar, *Clin. Dermatol.* **34**, 749 (2016).
3. Wilson LD., Hinds GA., and Yu JB. *Clin Lymphoma Myeloma Leukemia* **12**(5), 291 (2012).
4. Nguyen CV., and Bohjanen KA. *Dermatol. Clinics* **33**(4), 683 (2015).
5. Prasad S., Gupta SC., Tyagi AK. and Aggarwal BB. *Biotech. Adv.* **32**(6), 1053 (2014).
6. Rezaee R., Momtazi AA., Monemi A. and Sahebkar A. *Pharmacol. Res.* **117**, 218 (2017).
7. Panahi Y., Darvishi B., Ghanei M., Jowzi N., Beiraghdar F. and Varnamkhasti BS. *Cytokine & Growth Factor Rev.* **28**, 29 (2016).
8. Zhou H., Beevers CS. and Huand S. *Curr. Drug Targets* **12**(3), 332 (2011).
9. Lelli D., Sahebkr A., Johnston TP. and Pedone C. *Pharmacol. Res.* **115**, 133 (2017).
10. Koop HS., de Freitas RA., de Souza MM., Savi-Jr R. and Silveira JLM. *Carbohydr. Polym.* **113**, 229 (2015).
11. Hegge AB., Andersen T., Melvik JE., Kristensen S. and Tonnesen HH. *J. Pharm. Sci.* **99**(8), 3499 (2010).
12. Dai M., Zheng X., Xu X., Kong X., Li X., Gou G., Luo F., Zhao X., Wie YQ. and Qian Z. *J. Biomed. Biotech.*, 1 (2009).
13. Lerdchai K., Kitsongsermthon J., Ratanavaraporn J., Kanokpanont S. and Damrongsakkul S. *J. Pharm. Sci.* **105**(1), 221 (2016).
14. Hussain Z., Thu HE., Ng S., Khan S. and Katas, H. *Colloids Surf. B: Biointerfaces* **150**, 223 (2017).
15. Jain, A., Doppalapudi, S., Domb, AJ., Khan, W. *J. Contr. Rel.* **243**, 132 (2016).
16. Josef E. and Bianco-Peled H. *Int. J. Pharm.* **458**(1), 208 (2008).
17. Mosmann T. *J. Immunol. Methods* **65**(1-2), 55 (1983).
18. Konstantinov SM., Eibl H. and Berger MR. *Br. J. Haematol.* **107**(2), 365 (1999).
19. Petrov P., Petrova E. Stamenova R., Tsvetanov ChB. and Riess G. *Polymer*, **47**(19), 6481 (2006).
20. Petrov P., Petrova P., Tchorbanov B. and Tsvetanov CB. *Polymer*, **48**(17), 4943 (2007).
21. Jankun J., Aleem AM., Malgorzewicz S., Szkudlarek M., Zavodsky MI., Dewitt DL., Feig M., Selman SH. and Skrzypczak-Jankun E. *Mol. Cancer Ther.* **5**, 1371 (2006).

НОВИ МАКРОПОРЕСТИ КРИОГЕЛОВЕ ОТ ДЕКСТРАН/β-ЦИКЛДЕКСТРИН И ДЕКСТРАН ЗА ДЕРМАЛНО ДОСТАВЯНЕ НА КУРКУМИН ПРИ ЛЕЧЕНИЕ НА КОЖЕН Т-КЛЕТЪЧЕН ЛИМФОМ

М. Ив. Славкова¹, Д. Б. Момекова¹, Б. Д. Костова¹, Г. Цв. Момеков¹, П. Д. Петров^{2*}

¹Фармацевтичен факултет, Медицински университет-София, ул. Дунав №2, София 1000, България

²Институт по полимери, Българска академия на науките, ул. акад. Георги Бончев №103А, София 1113,
България

Получена на 31 март, 2017 г.; приета на 5 май 2017 г.

(Резюме)

Кожната форма на Т-клетъчен лимфом (CTCL) представлява рядко заболяване, което засяга както пациенти на средна възраст, така и деца. Началните стадии могат успешно да бъдат лекувани с локална лекарствена терапия. Куркуминът – природно, фитохимично вещество с доказана плейотропна противовъзпалителна и противотуморна активност, предоставя безопасна алтернатива на настоящата терапия, независимо от ниската си водна разтворимост и химична нестабилност. В настоящото изследване оригинални криогелове на основата на смес от декстран и β-цикодекстрин и чист декстран бяха пролучени и оценени като платформи за дермално доставяне на куркумин. Криогелове с макропореста структура бяха синтезирани чрез фотохимично омрежване в замразено състояние с последващо размразяване. Куркумин беше натоварен чрез физична адсорбция при задоволителна ефикасност на енкапулиране, особено в случая на криогелове от декстран/β-цикодекстрин (57.8%). *In vitro* тестовете за освобождаване показваха забавено лекарствено освобождаване в рамките на 72 ч, като за носителите от декстран/β-цикодекстрин, освобождаването на куркумин е плавно без първоначален ефект на бързо освобождаване. Цитотоксичният потенциал на натоварен в макропорестите носители куркумин бе оценен в сравнителен аспект със свободното вещество върху туморни клетки с произход от Т-клетъчен лимфом и върху немалгинени клетки. Получените резултати показваха съизмерима цитотоксична активност и селективност със свободното лекарствено вещество. Предложените нови макропорести криогелове показват потенциал за приложение като системи за контролирано дермално доставяне на куркумин при лечение на CTCL.

Synthesis of 5-nitrosalicylaldehyde based hydrazones and DFT-calculations of their structure and reactivity

B. I. Nikolova-Mladenova^{1*}, S. E. Angelova²

¹Department of Chemistry, Faculty of Pharmacy, Medical University of Sofia, 2, Dunav Street, 1000 Sofia, Bulgaria

²Institute of Organic Chemistry with Centre of Phytochemistry, Bulgarian Academy of Sciences, Sofia 1113, Bulgaria

Received November 14, 2016; Accepted May 5, 2017

New arylhydrazones derived from 5-nitrosalicylaldehyde, namely 5-nitrosalicylaldehyde benzoylhydrazone, 5-nitrosalicylaldehyde-4-hydroxybenzoylhydrazone and 5-nitrosalicylaldehyde isonicotinoylhydrazone were designed and synthesized. The compounds were characterized by elemental and thermogravimetric analyses, IR, ¹H and ¹³C NMR spectroscopy. Geometry optimization of the neutral hydrazones were carried out using density functional theory with Becke's three-parameter hybrid method and correlation functional of Lee, Yang and Parr with 6-31+G (d,p) basis set. The calculated bond lengths and angles of the new hydrazones are in good agreement with the experimental electron diffraction data. Molecular electrostatic potential calculations showed that the most preferred sites for iron chelation are the carbonyl oxygen atom, the imine nitrogen atom and the hydroxyl oxygen atom.

Keywords: 5-nitrosalicylaldehyde; arylhydrazones; iron chelators; DFT calculations; molecular electrostatic potential.

INTRODUCTION

Development and synthesis of novel hydrazone derivatives continuously attracts the attention of organic and medicinal chemists due to interesting biological properties and coordinative capability of these compounds. Hydrazones demonstrate many pharmacological activities, such as anti-inflammatory [1, 2], analgesic [2], antituberculosis [3, 4], antibacterial [5], antimicrobial [6], anti-HIV [6, 7] and anticancer [6, 8–9] activity. Moreover, hydrazones are some of the most widely used ligands as they easily form stable complexes with many transition metals. Hydrazone derivatives have been intensively studied for their potential as chelating agents in medical treatment for reducing the toxic effects of metals.

Iron overload is a common clinical problem, arising as a consequence of continued blood transfusions for various blood disorders. Iron is essential for life as it plays an important role in many cellular processes. Excessive amounts of iron, however, may become very toxic to the human body. Iron ions can catalyze the generation of damaging oxygen radicals, leading to oxidative damage and subsequent cell death. Therefore, it is important to eliminate the unnecessary iron before damage can occur. The medicinal iron reduction is accomplished with chelation therapy, i.e. pharmacological removal of iron with iron-chelating agents. Only two iron chelator drugs are currently approved for administration - desferrioxamine and deferasirox. Regrettably, these medicines possess many side

effects and can affect individual people in different ways. This fact inspires the development of novel chemotherapeutic agents with potent chelating activities and reduced side effects. Very promising iron chelators are hydrazones derived from 3-hydroxy-5-(hydroxymethyl)-2-methylpyridine-4-carbaldehyde (pyridoxal) and salicylaldehyde [10–12]. Iron chelators are capable of binding the toxic metal ions to form complex structures which are easily excreted from the body.

Salicylaldehyde benzoylhydrazone (SBH) belongs to a series of iron chelators effective in chemotherapy of iron overload diseases such as β-thalassemia [13–16]. Many derivatives of SBH and their metal complexes have been synthesized to obtain new pharmacologically active compounds [17–20]. Hydrazones obtained from 3-methoxysalicylaldehyde exerted a potent antiproliferative effect on a wide spectrum of human tumor cell lines [20]. This activity may be due to the high ability of the hydrazones to chelate Fe(III) from the cells thus inhibiting the proliferation of the neoplastic cells [19]. In this paper, we describe the synthesis of new potential iron chelating agents derived from 5-nitrosalicylaldehyde and three acid hydrazides. The structures of the new arylhydrazones are shown on Fig.1. These compounds possess several potential donor sites and can chelate metal ions in versatile manners. To predict the coordination ability and the preferred sites for binding during chelation with iron and other metal ions, the molecular electrostatic potential values were calculated and the reaction properties of the novel 5-nitrosalicylaldehyde hydrazone derivatives were evaluated.

* To whom all correspondence should be sent:
E-mail: boriananik@abv.bg

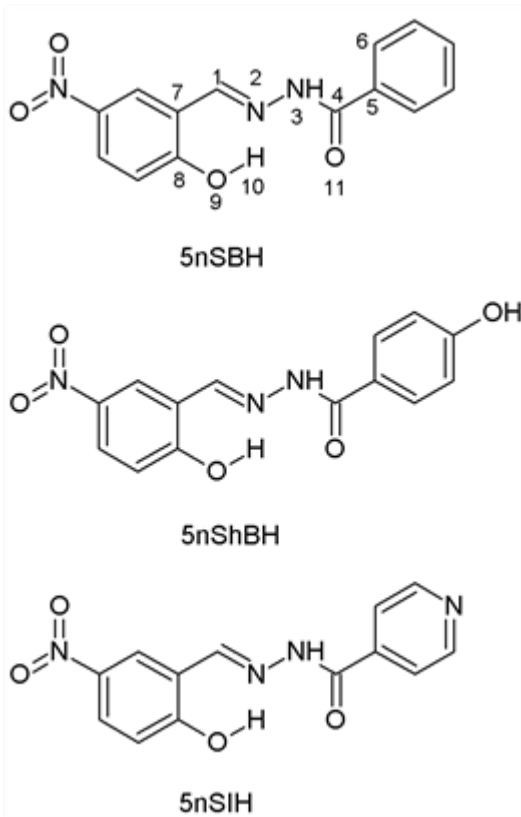


Fig. 1. Chemical structures of the synthesized hydrazones: 5-nitrosalicylaldehyde benzoylhydrazone (**5nSBH**), 5-nitrosalicylaldehyde-4-hydroxybenzoylhydrazone (**5nShBH**) and 5-nitrosalicylaldehyde isonicotinoylhydrazone (**5nSIH**).

EXPERIMENTAL

Materials and Measurements

All chemicals used for the synthesis of the compounds: 5-nitrosalicylaldehyde, benzhydrazide, 4-hydroxybenzhydrazide, isonicotinoyl hydrazide and 96% ethanol, were purchased from commercial sources (Merck, Sigma-Aldrich) and were used without any further purification. The carbon, nitrogen and hydrogen contents of the compounds were determined by elemental analyses on a "Euro Vector SpA" apparatus. The melting points were determined in open capillary tubes using a Büchi B-540 apparatus. The IR-spectra were recorded in solid state (in KBr pallets) on a Bruker Tensor 27 spectrophotometer in the range of 4000-400 cm⁻¹. The ¹H NMR and ¹³C NMR spectra were recorded on a Bruker Avance DRX 250 instrument in DMSO-d₆ as a solvent. Chemical shifts (δ) were reported in parts per million (ppm), *J* values were given in Hz. Thermal decomposition studies were carried out on a Setaram Setsys TG-DSC 15 apparatus in air atmosphere by using a corundum crucible with a sample weight of 10 mg in the temperature range of 20 - 600 °C.

Synthesis of the hydrazones

A solution of 5-nitrosalicylaldehyde (1.671 g, 10 mmol) in 96% ethanol (30 mL) was slowly dropwise added to the solutions of the respective benzhydrazides (10 mmol) in 50% aqueous ethanol (100 mL) and immediately precipitates were formed. The mixtures were stirred for 30 min and then were left to stay for 24 h at room temperature. During this time the products fully precipitated as dark-yellow solids. The crude solids were filtered off and washed with 96% ethanol. The solid hydrazones were dried for 2 days in a vacuum desiccator.

5-nitrosalicylaldehyde benzoylhydrazone (5nSBH**) (1):** Yield: 79%; m.p. 303-304 °C; Color: Yellow; Anal. Calcd. for C₁₄H₁₁N₃O₄: C 58.95, H 3.89, N 14.73, O 22.43. Found: C 58.92, H 3.88, N 14.80, O, 22.40. IR (KBr, cm⁻¹): 3440 (Ar-OH), 3303 (N-H), 1632 (C=O), 1602 (C=N), 1576 (C-NH), 1242 (C-O). ¹H NMR (250 MHz, DMSO-d₆) δ 7.12 (d, *J* 9 Hz, 1H, ArH_{aldehyde}), 8.17 (d, *J* 9 Hz, 1H, ArH_{aldehyde}), 8.59 (s, 1H, ArH_{aldehyde}), 7.59 (m, 3H, ArH_{hydrazone}), 7.95 (d, *J* 7 Hz, 2H, ArH_{hydrazone}), 8.75 (s, 1H, N=CH), 12.26 (s, 1H, N-H), 12.26 (br s, 1H, O-H). ¹³C NMR (250 MHz, DMSO-d₆) δ 117.09, 119.95, 123.80, 126.51, 127.67, 127.67, 128.04, 128.04, 132.04, 132.65, 139.91 (C-NO₂), 144.39 (CH=N), 162.55 (C=O), 163.00.

5-nitrosalicylaldehyde-4-hydroxybenzoylhydrazone (5nShBH**) (2):** Yield: 93%; m.p. 338-339 °C; Color: Yellow; Anal. Calcd. for C₁₄H₁₁N₃O₅: C 55.82, H 3.68, N 13.95, O 26.55. Found: C 55.98, H 3.85, N 14.05, O 26.12. IR (KBr, cm⁻¹): 3440, 3400 (Ar-OH), 3300 (N-H), 1654 (C=O), 1603 (C=N), 1592 (C-NH), 1236 (C-O). ¹H NMR (250 MHz, DMSO-d₆) δ 7.10 (d, *J* 9 Hz, 1H, ArH_{aldehyde}), 8.15 (d, *J* 9 Hz, 1H, ArH_{aldehyde}), 8.54 (s, 1H, ArH_{aldehyde}), 6.88 (d, *J* 8.75 Hz, 2H, ArH_{hydrazone}), 7.84 (d, *J* 8.75 Hz, 2H, ArH_{hydrazone}), 8.69 (s, 1H, N=CH), 12.08 (s, 1H, N-H), 10.17 (s, 1H, O-H_{hydrazone}), 12.43 (br s, 1H, O-H_{aldehyde}). ¹³C NMR (250 MHz, DMSO-d₆) δ 115.09, 115.09, 117.09, 119.91, 123.04, 124.02, 126.28, 129.85, 129.85, 139.89 (C-NO₂), 143.80 (CH=N), 161.00, 162.57 (C=O), 163.00.

5-nitrosalicylaldehyde isonicotinoylhydrazone (5nSIH**) (3):** Yield: 97 %; m.p. 318-319 °C; Color: Yellow; Anal. Calcd. for C₁₃H₁₀N₄O₄: C 54.55, H 3.52, N 19.57, O 22.36. Found: C, 54.42, H 3.50, N 19.24, O 22.84. IR (KBr): 3350 (Ar-OH), 3301 (N-H), 1664 (C=O), 1609 (C=N), 1582 (C-NH), 1243 (C-O). ¹H NMR (250 MHz, DMSO-d₆) δ 7.10 (d, *J* 9 Hz, 1H, ArH_{aldehyde}), 8.16 (d, *J* 9 Hz, 1H, ArH_{aldehyde}), 8.59 (s, 1H, ArH_{aldehyde}), 7.84 (d, *J* 6 Hz, 2H, ArH_{hydrazone}), 8.79 (d, *J* 6 Hz 2H, ArH_{hydrazone}), 8.75 (s, 1H, N=CH), 12.16 (s, 1H, N-H), 12.34 (br s,

1H, O-H). ^{13}C NMR (250 MHz, DMSO-d₆) δ 117.07, 119.94, 121.48, 121.48, 123.45, 126.77, 139.81, 139.93 (C-NO₂), 145.07 (CH=N), 150.34, 150.34, 161.58, 162.55 (C=O).

Theoretical studies

The geometry optimizations of the neutral hydrazones were carried out using density functional theory (DFT) calculations with Becke's three-parameter hybrid functional [21] combined with the Lee-Yang-Parr [22] correlation functional - B3LYP with 6-31+G (d,p) basis set. The calculations of the studied hydrazones were performed using the Gaussian 09 program suite [23]. A tight SCF convergence criterion (10^{-8} Hartree) was employed in all calculations. Frequency calculations were carried out to examine the stationary points in the optimization procedure and no imaginary frequencies were found.

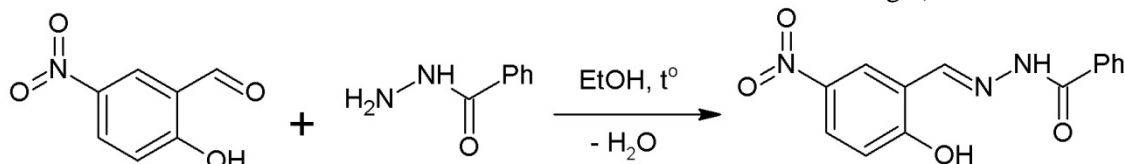
Further, the molecular electrostatic potential (MEP) was calculated. The electrostatic potential created by the nuclei and electrons of a molecule in the surrounding space is well established as a guide to the interpretation and prediction of the chemical reactivity of a number of biological systems which take part in both electrophilic and nucleophilic reactions [24–28]. The electrostatic potential study also explains the electronic distribution and structure formation in a molecule. The MEP of a molecule is a real physical property that can be experimentally determined by diffraction methods, as well as computationally. At present, however, computational approaches are more often used as a practical alternative. The calculated values were used to predict the reactive behavior and the potential donor sites of the new hydrazones as ligands for iron chelation.

RESULTS AND DISCUSSION

Chemistry

5-Nitrosubstituted hydrazones were synthesized by condensation of 5-nitrosalicylaldehyde with three benzhydrazides as previously described [20, 29] according to Scheme 1.

The structures of the isolated products were confirmed on the basis of their respective analytical



Ph = C₆H₅, 4-hydroxy-C₆H₄, 4-Pyr

Scheme 1. Synthesis of the hydrazones.

and spectral data. The water content was determined thermogravimetrically. The DTA and TGA data showed that the three hydrazones are anhydrous. The structures of the new compounds were characterized using IR, ^1H NMR and ^{13}C NMR spectral analyses and by comparison with the available literature data.

The IR spectra of all compounds show a medium intensity band at 3350-3440 cm⁻¹ due to v(O-H) of the phenolic groups. The stretching vibration of the NH group appears as a weak broad band at 3300-3303 cm⁻¹. The above band, accompanied by a C=N absorption band between 1602-1609 cm⁻¹, is a good evidence for the presence of an azomethine linkage. The strong band in the region 1632-1664 cm⁻¹ was assigned to stretching vibration of the carbonyl group of amide v(C=O). Another important band at 1576-1592 cm⁻¹ was attributed to v(C-NH).

The hydrazones were further studied by their ^1H NMR and ^{13}C NMR spectra in deuterated dimethyl sulfoxide. ^1H NMR spectra revealed the presence of the aromatic protons in the region of δ from 6.88 to 8.79. Signals for the protons of the azomethine group HC=N- (characteristic for hydrazones) were observed between δ 8.69 and 8.75. The broad singlets around δ 12.26-12.43 were assigned to the protons of the hydroxyl group from the aldehyde ring. ^{13}C NMR spectra demonstrated signals corresponding to the carbon atoms of azomethine group between δ 143.80 and 150.34. The peaks at δ 162.55-162.57 were assigned to the C=O group.

Computational study

The molecular structures of the new compounds were studied theoretically and quantum-chemical calculations were carried out. The structural parameters were computed at B3LYP level of theory using a 6-31+G (d, p) basis set. This level of calculations was tested in our previous study on 3-methoxysalicylaldehyde hydrazones and the results obtained showed a very good agreement with the experimental structural parameters available [20]. The calculated bond lengths and angles of the new hydrazones were compared with the experimental crystallographic data for SBH and 5nSBH. The experimental data and the calculated structural parameters are presented in Table 1 (the atomic numbers are shown in Fig.1).

Table 1. Selected bond lengths (\AA) and angles ($^\circ$) for SBH and 5-nitro derivatives.

Selected geometric parameters (\AA , $^\circ$)	SBH Meas.	SBH calc.	5nSBH Meas.	5nSBH calc.	5nShBH calc.	5nSIH calc.
C1-N2	1.291	1.291	1.266	1.288	1.289	1.289
N2-N3	1.365	1.360	1.382	1.355	1.354	1.357
N3-C4	1.332	1.388	1.338	1.392	1.394	1.388
C4-C5	1.502	1.501	1.489	1.498	1.492	1.503
C1-C7	1.432	1.452	1.464	1.455	1.455	1.454
C4-O11	1.221	1.222	1.233	1.221	1.222	1.220
C8-O9	1.356	1.346	1.339	1.336	1.336	1.336
O9-H10	-	1.291	0.850	0.990	0.990	0.989
C1-N2-N3	118.2	118.7	115.2	119.5	119.6	119.3
N2-N3-C4	118.9	120.1	119.9	119.6	119.5	119.6
N3-C4-O11	123.1	122.3	122.3	121.8	121.4	122.5
N3-C4-C5	116.9	114.8	116.8	114.9	115.2	114.7
C5-C4-O11	119.9	122.9	120.9	123.2	123.3	122.7
C1-C7-C8	122.6	121.9	119.8	121.9	121.9	121.9

The average calculated bond length C1-N2 in the three 5-nitro-compounds is 1.289 \AA , very close to the experimentally measured one for SBH (1.291 \AA) and perfectly matches the length of the double bond C = N equal to 1.29 \AA . The calculated length of the bond N3-C4 is slightly above that experimentally determined for 5nSBH and SBH, whereas the average calculated distance N2-N3 (1.355 \AA) is slightly shorter than the experimental one in 5nSBH (1.382 \AA). An excellent match exists between the experimentally measured and calculated distances of the carbonyl group C4-O11 for the three compounds (1.221 \AA) and the typical length of a double bond C = O (1.22 \AA).

The values of the calculated angles are very close to the experimentally measured ones and reveal that all carbon atoms are in sp^2 hybridization. Minor differences of about $\pm 3^\circ$ were observed in the calculated angles C1-N2-N3, N3-C4-C5 and C5-C4-O11.

Despite the small differences obtained, the optimized geometries of nitro-hydrazone are in good agreement with the experimental electron diffraction data. The substituents at the 4th position in the hydrazide ring insignificantly affect the bond lengths and angles and all 5-nitrosalicylaldehyde hydrazone derivatives have similar geometry. The optimized structures of the 5-nitro derivatives are presented in Fig.2.

Aroylhydrazones can act as polydentate ligands depending on the reaction conditions, the nature of metal ion and hydrazone ligand, and the pH of the medium. Salicylaldehyde benzoylhydrazone and its substituted derivatives have four donor atoms N2, N3, O9 and O11 which allow binding to a central metal ion in a versatile manner. However, in most of their complex compounds, they react as tridentate ligands in mono-anionic form after deprotonation of

the phenolic hydroxyl group [32–35]. Deprotonation equilibrium between the neutral and the deprotonated form occurs in weak basic medium (Scheme 2) and the phenolic hydroxyl group loses its proton [36].

In general, the most negative value of the electrostatic potential in the neutral molecules LH is focused on the carbonyl oxygen O11, whereas the other donor atoms have a higher, even positive value of the electrostatic potential. So it is practically impossible to realize a complex compound with the neutral forms of the hydrazones. Deprotonation of O9 brings about considerably negative values of the electrostatic potential for it, as well as the appearance of such over N2. Appearance of a NO₂-group in the salicylaldehyde moiety slightly increases the value of the electrostatic potential, probably due to its negative inductive effect.

In view of these observations it can be concluded that the hydroxyl oxygen atom O9, the imine nitrogen atom N2 and the carbonyl oxygen atom O11 will be the preferred sites for complex formation with metal ions. Compounds 5nSBH and 5nSIH will have similar activity like SBH, 5nShBH being the most potent chelating agent among the new compounds.

The nitro-group withdraws electron density from the aldehyde ring, thus the replacement of the hydrogen in SBH with a nitro group in nitro-derivatives will result in partially positive charges at *ortho*- and *para*-positions. Additionally, this will increase the polarity of the phenolic group on *para*-position and will influence and facilitate its deprotonation during complexation.

To predict the reactivity of the new hydrazones as iron-chelators, MEP was calculated. The negative regions in the molecules with negative values of electrostatic potential were related to the

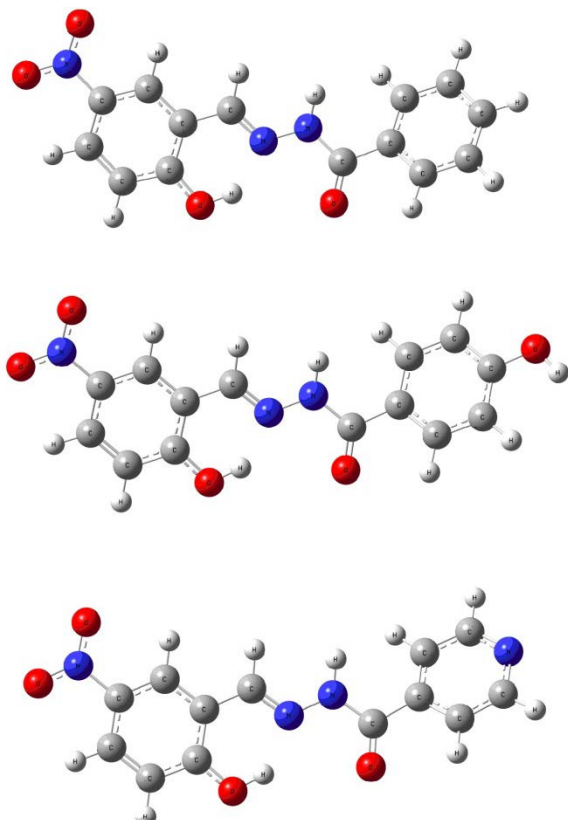
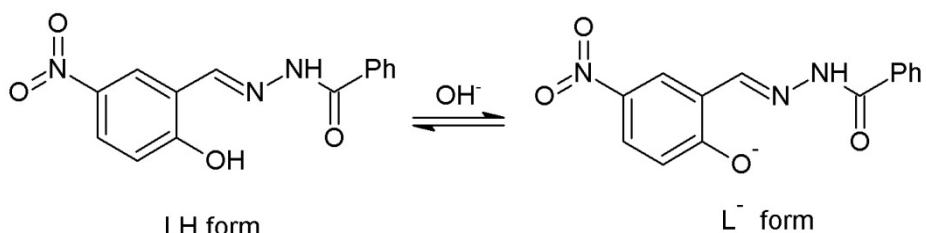


Fig. 2. B3LYP/6-31+G (d,p) optimized structures of 5nSBH, 5nShBH and 5nSIH.

electrophilic reactivity and were found as the reactive sites where the metal ion will prefer to coordinate. An approaching iron ion will be attracted to the region of the molecule with the most negative values, i.e., where the effects of the electrons are dominant [24]. Table 2 presents recently calculated minima of the molecular electrostatic potentials V_{min} for the nitro-derivatives, compared with these of SBH [37]. Both of the oxygen atoms - O9 and O11 have two values of the electrostatic potential due to the presence of two electron pairs around them. The values for O9 in the neutral form LH are identical and only one is shown.

CONCLUSIONS

In conclusion, three hydrazones, 5-nitroderivatives of salicylaldehyde benzoyl hydrazone were synthesized. The molecular formulas of the substances were confirmed by elemental, thermogravimetric and spectral analyses such as IR, ^1H NMR and ^{13}C NMR. Computational studies were carried out in order to evaluate the molecular structure. The substitutions in the aromatic nuclei insignificantly influenced the geometries and all derivatives have similar structure. The DFT-calculated molecular electrostatic potentials for all molecules indicate the favorable sites for iron chelation - hydroxyl oxygen atom, imine nitrogen atom and carbonyl oxygen atom.



Scheme 2. Equilibrium of 5-nitrohydrazones in basic media.

Table 2. Calculated minima of the molecular electrostatic potentials V_{min} / kcal mol⁻¹ for selected atoms in the neutral molecules LH and deprotonated molecules L⁻.

Molecule	LH				L ⁻			
	V_{min} O9	V_{min} N2	V_{min} N3	V_{min} O11	V_{min} O9	V_{min} N2	V_{min} N3	V_{min} O11
SBH	-44.43	-21.27	-5.65	-53.02 -50.32	-179.0 -157.6	-175.7	-87.7	-145.0 -119.9
5nSBH	-31.75	-13.55	+1.76	-37.96 -37.96	-158.6 -138.3	-150.7	-80.2	-125.8 -100.4
5nShBH	-31.69	-10.67	+7.53	-45.81 -44.18	-208.6 -177.0	-200.9	-138.7	-194.8 -177.0
5nSIH	-25.98	+1.88	+18.45	-38.84 -37.90	-155.4 -133.1	-144.6	-76.1	-125.8 -101.0

REFERENCES

1. Z. A. Kaplancikli, M. D. Altintop, A. Ozdemir, G. Turan-Zitouni, S. I. Khan, N. Tabanca, *Lett. Drug Des. Discovery*, **9**, 310 (2012).
2. W. B. Júnior, M. S. Alexandre-Moreira, M. A. Alves, A. Perez-Rebolledo, G. L. Parrilha, E. E. Castellano, O. E. Piro, E. J. Barreiro, L. M. Lima, H. Beraldo, *Molecules* **16**, 6902 (2011).
3. A. Ozdemir, G. Turan-Zitouni, Z. A. Kaplancikli, G. Revial, *Marm. Pharm. J.*, **14**, 79 (2010).
4. B. Koçyiğit-Kaymakçıoğlu, E. E. Oruç-Emre, S. Unsalan, S. Rollas, *Med. Chem. Res.*, **18**, 277 (2009).
5. T. Govindasami, A. Pandey, N. Palanivelu, A. Pandey, *Int. J. Org. Chem.*, **1**, 71 (2011).
6. L. Savini, P. Massarelli, V. Travagli, C. Pellerano, E. Novellino, S. Cosentino, M. B. Pisano, *Eur. J. Med. Chem.*, **39**, 113 (2004).
7. P. Vicini, M. Incerti, P.L. Colla, R.E. Loddo, *Eur. J. Med. Chem.*, **44**, 1801 (2009).
8. T. B. Chaston, R. N. Watts, J. Yuan, D. R. Richardson, *Clin. Cancer Res.*, **10**, 7365 (2004).
9. D. K. Johnson, T. B. Murphy, N. J. Rose, W. H. Goodwin, L. Pickart, *Inorg. Chim. Acta*, **67**, 159 (1982).
10. J.T. Edward, *BioMetals*, **11**, 203 (1998).
11. J.T. Edward, P. Ponka, D.R. Richardson, *BioMetals*, **8**, 209 (1995).
12. E.M. Becker, D.R. Richardson, *J. Lab. Clin. Med.*, **134**, 510 (1999).
13. P. Ponka, D. Richardson, E. Baker, H. M. Schulman, J. T. Edward, *Biochim. Biophys. Acta*, **967**, 122 (1988).
14. E. Baker, D. R. Richardson, S. Gross, P. Ponka, *Hepatology*, **15**, 492 (1992).
15. D. R. Richardson, P. Ponka, *J. Lab. Clin. Med.*, **131**, 306 (1998).
16. J. L. Buss, E. Arduini, P. Ponka, *Biochem. Pharmacol.*, **64**, 1689 (2002).
17. D. B. Lovejoy, D. R. Richardson, *Blood*, **100**, 666 (2002).
18. D. R. Richardson, K. Milnes, *Blood*, **89**, 3025 (1997).
19. D.R. Richardson, *Antimicrob. Agents Chemother.*, **41**, 2061 (1997).
20. B. Nikolova-Mladenova, N. Halachev, R. Iankova, G. Momekov, D. Ivanov, *Arzneim.-Forsch.*, **61(12)**, 714 (2011).
21. A. D. Becke, *J. Chem. Phys.*, **98**, 5648 (1993).
22. C. Lee, W. Yang, R. G. Parr, *Phys. Rev. B*, **37**, 785 (1998).
23. M. Frisch, G. W. Trucks, H. B. Schlegel, G. E. Scuseria, M. A. Robb, J. R. Cheeseman, G. Scalmani, V. Barone, B. Mennucci, G. A. Petersson, H. Nakatsuji, Gaussian 09, revision A. 02; Gaussian, Inc. Wallingford, CT, **19**, p. 227 (2009).
24. P. Politzer, J. S. Murray, in: K. B. Lipkowitz, D. B. Boyd (Eds.): *Reviews in Computational Chemistry*, vol. 2, VCH Publishers, New York, 1991, p. 273.
25. P Politzer, J. S. Murray, *Theor. Chem. Acc.*, **108**, 134 (2002).
26. C. Munoz-Caro, A. Nino, M. L. Senent, J. M. Leal, S. Ibeas, *J. Org. Chem.*, **65**, 405 (2000).
27. N. Okulik, A. H. Jubert, *Internet Electron. J. Mol. Des.*, **4**, 17 (2005).
28. R. Soliva, F. J. Luque, M. Orozco, *Theor. Chem. Acc.*, **98**, 42 (1997).
29. J.T. Edward, M. Gauthier, F.L. Chubb, P. Ponka, *J. Chem. Eng. Data*, **33**, 538 (1988).
30. A. Lyubchova, A. Cossé-Barbi, J.P. Doucet, *Acta Cryst. C***51**, 1893 (1995).
31. H. M. Ali, S. Puvaneswary, S. W. Ng, *Acta Cryst. E***61**, 3464 (2005).
32. R. M. El-Bahnasawy, S. E. El-Meleigy, A. El-Tawansi, *Trans. Met. Chem.*, **19**, 270 (1994).
33. B. Mladenova, D. S. Ivanov, M. H. Umbreit, J. Klos, S. Konstantinov, M. Karaivanova, *Pharmacy*, **3-4**, 3 (2003).
34. B. Nikolova-Mladenova, D. Ivanov, *Pharmacia*, **61(4)**, 7 (2014).
35. S. A. Yasrebi, H. Mobasher, I. Sheikhshoaei, M. Rahban, *Inorg. Chim. Acta*, **400**, 222 (2013).
36. Yi-H. Lu, Yu-W. Lu, C.-Li Wu, Q. Shao, X.-L. Chen, R. Bimbong, *Spectrochim. Acta Mol. Biomol. Spectrosc.*, **65**, 695 (2006).
37. N. Halachev, R. Iankova, St. Manolov, B. Nikolova-Mladenova, D. S. Ivanov, *Annual Assen Zlatarov University*, **XXXVI (1)**, 44 (2007).

СИНТЕЗ НА ХИДРАЗОНИ, ПОЛУЧЕНИ ОТ 5-НИТРОСАЛИЦИЛАЛДЕХИД И DFT-ИЗЧИСЛЕНИЯ ЗА ТЯХНАТА СТРУКТУРА И РЕАКЦИОННА СПОСОБНОСТ

Б. И. Николова-Младенова^{1*}, С. Е. Ангелова²

¹ Фармацевтичен факултет, Медицински университет София, София 1000, България

² Институт по органична химия с Център по фитохимия, Българска Академия на Науките, София 1113, България

Получена на 14 ноември, 2016 г.; приета на 5 май, 2017 г.

(Резюме)

Синтезирани са нови ароилхидразони чрез кондензацията на 5-нитросалицилалдехид и три ароматни хидразида –ベンзхидразид, 4-хидроксibenзхидразид и изоникотиноил хидразид. Съединенията са охарактеризирани с елементен и термогравиметричен анализ, ИЧ, ¹H и ¹³C ЯМР спектроскопия. Геометриите на неутралните хидразони са оптимизирани с методите на теория на функционала на пълността (density functional theory, DFT), като са използвани функционал B3LYP и базисен набор 6-31+G (d, p). Изчислените дължини на връзки и ъгли на новите хидразони са в добро съгласие с експерименталните данни от рентгеноструктурен анализ. Изчислените стойности на електростатичния потенциал показват, че най-предпочитаните места за хелатотерапия са кислородният атом от карбонилната група, азотният атом от имино групата и кислородният атом от хидроксилната група.

Optimal energy management in brewing

D. S. Nikolova¹, B. B. Ivanov², D. G. Dobruzhaliev¹

¹Prof. Dr. Assen Zlatarov University Bourgas, Prof. Yakimov Str. 1, 8000 Bourgas, Bulgaria

²Process Systems Engineering Laboratory, Institute of Chemical Engineering, Bulgarian Academy of Sciences
Acad. St. Angelov Str.Bl. 103, Sofia 1113, Bulgaria

Received March 8, 2016; Accepted February 3, 2017

The energy performance is one very important parameter in evaluating the resilience of industrial processes. The optimal usage of the energy is a key task today, because it determines the state of the environment and the final product's price. In this paper is described a method for minimizing energy consumption by heat integration in conventional brewing. A scheme for heat integration with usage of separated heat tanks is proposed, their aim is to save heat energy. A mathematical model that describes the heat transfer processes is developed. Based on this model is proposed a strategy for optimal management of energy resources with separate heat tanks. The optimization task is formulated in accordance with the mathematical nonlinear programming MNLP and is solved with the program package GAMS. The proposed method was tested with data from a real working production.

Keywords: heat integration, batch reactors, heat tanks, brewing

INTRODUCTION

Energy saving is cited as one of the global problems to be solved in the contemporary world. Sources of energy constantly decrease which has a negative effect on the environment. This fact provokes work in two main directions - searching for alternative energy sources and developing approaches for optimal utilization of energy resources.

In industrial production systems, the optimal use of energy sources is one of the main problems [1]. The use of energy and raw materials in different industrial productions requires improving of the efficiency in process management and waste minimization to meet the environmental specifications [2, 3]. The contemporary tendencies indicate that the industry is working towards waste reduction and improving the sustainability of the processes. This is because the effective usage of the sources is admitted as a key element of sustainable development and a successful strategy for reducing negative environmental impacts and production costs. One of the approaches used in solving the problems related to the optimal use of energy, is the integration approach. It can be described as a systematically oriented method that is used during the design and reconstruction of industrial production systems for optimal use of resources (energy or raw materials) and/or reduction of the emissions of harmful gases. The method of heat integration of the processes is focused on optimizing the consumption of heat, power and fuel [4, 5].

In most batch productions, there is a large number of processes requiring heating and cooling from external sources. Utilization of heat energy in batch processes is limited in terms of temperature levels and time intervals [6, 7]. Such is the production of dairy products, beer, biochemical substances. They require large amounts of water and energy [8]. In particular, upto 8% of the total production costs of beer are estimated as energy costs [9]. There are various scientific studies, which present approaches for improving energy efficiency of the breweries. In [10-11] it is presents guide layout of monitoring and measuring energy, the consumption of utilities and target setting for brewing in Canada and in London. It is provided information on the relationship between the use of energy and the generation of greenhouse gases in the brewing industry. The guide attention is directed to potential opportunities to improve energy efficiency in brewery processes. The research [12] provides information on potential energy efficiency opportunities for breweries. In [13], it is suggested includes cogeneration systems with different prime movers (steam turbine and gas turbine), and a generation system with a back-pressure steam turbine. The paper [14] gives an overview over the state of the art in the brewing industry commonly realized in large breweries and presents important barriers to efficiency in smaller companies. It is proposed [15] a brewery modeling tool, who can predict industrial thermal energy demand variables to satisfactory extent.

Due to growing concerns about the increased emissions of CO_2 and the need to implement more sustainable solutions are offered measures, such as those presented by [16] and [17].

* To whom all correspondence should be sent:

E-mail: bivanov1946@gmail.com

© 2017 Bulgarian Academy of Sciences, Union of Chemists in Bulgaria 807

Numerous studies in this area indicate the ongoing interest of the authors, caused by the untapped potential of batch production of the food industry, eg. beer production. Most of the proposed solutions are based only on theoretical assumptions and do not take into account data from existing industries. Because of this, the question for optimal management aiming to reduce energy dependence on real production processes, still remains.

The aim of this work is to propose a practical method for energy saving through process heat integration in a batch system by conventional brewing.

PROCESS DESCRIPTION

It is studying a beer production process, which corresponds to the conventional brewing and includes the following main stages (Figure 1):

Stage 1: Milling - Before the mashing process, the malt/barley must be milled in a wet or dry process. It is done for easier malt degradation to sugars, amino acids and other substances;

Stage 2: Mashing - Mashing is carried out after mixing of the malt with water 45 °C. This process forms a so-called malt mash. A special feature here is that the temperature during the mashing is raised in steps and then kept constant for a while at different mashing rests;

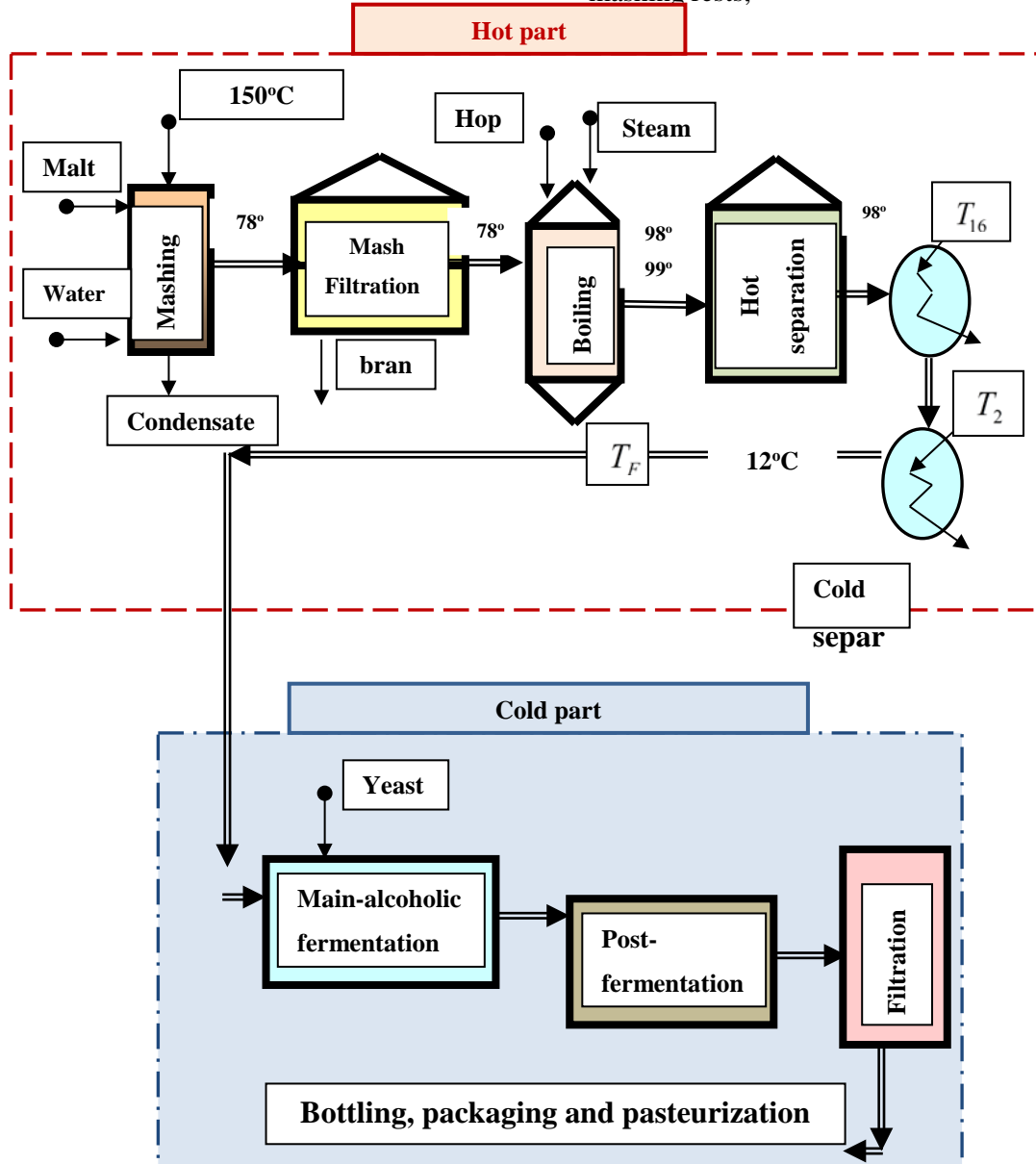


Fig.1. Scheme of conventional beer production without heat integration

Stage 3: Mash Filtration - During mash filtration, the wort is separated from the spent grains with filter bags. The wort is with temperature of 78°C . From wort subsequently is obtained beer.;

Stage 4: Boiling - After mash filtration, the wort is boiled together with hops to add bitterness to the taste of the beer. The boiling takes roughly an hour and the boiler is heated with steam. After the brewing the wort's temperature is 98°C ;

Stage 5: Hot separation of hops and malt residues - During this stage, is formed a sludge as a boiling result. The process is carried out by temperature $98-99^{\circ}\text{C}$;

Stage 6: Cold separation - Cold sludge is formed after cooling the hopped wort. Cooling is carried out in two sections. In the first section, wort is cooled with water with a temperature of 16°C . The second section cools with water with a temperature of 2°C . At the end of the process, the wort is with temperature 12°C .

Stage 7: Adding of yeast

Main-alcoholic fermentation performed by yeast;

Post-fermentation and maturation - two interrelated processes that naturally follow the main alcoholic fermentation;

Stage 8: Filtration of beer;

Stage 9: Bottling, packaging and pasteurization

The so called "Calming" of beer is mandatory operation that occurs immediately after its filtration. Then beer is fed for bottling.

The production process of beer is presented as composed of two parts - hot (production of wort Stage 2 - Stage 6) and cold (fermentation, maturing and beer processing Stage 6 - Stage 9). Figure 1 presents the scheme of conventional beer production without heat integration.

PROBLEM DESCRIPTION

The focus in this work is the conventional brewing process, presented in two parts - hot (wort production) and cold (fermentation, maturation and beer treatment). For the purposes of heat integration, we are interested in the hot part of brewing. This is so because there could be seen the basic processes of "Heating" and "Cooling." Generally, after wort boiling with hops and the following separation of hops and malt waste, the mixture with temperature 98°C is cooled to 12°C . For the cooling purposes is used water with temperature 16°C and water with temperature 2°C . The idea for the reduction of energy consumption is to integrate processes "Heating" and "Cooling" by using thermal tanks.

These reservoirs act as separate heat reservoirs. The purpose of this operation is that the heated water, stored in the heat storage tanks is used for carrying out the processes of mash production and mash filtration and for vessels washing.

In this case, it is not necessary to stick to a work schedule of the devices in industrial unit. This leads to reducing the amount of wastewater and steam.

This idea can be realized through the creation of an appropriate scheme, along which we need to define the set of independent variables to ensure minimum means spent for carrying out of processes. Figure 2 presents the proposed scheme for process management.

Heat integration using heat tanks

From the presented technology can be seen that there are processes "Heating" and "Cooling", which demand usage of energy from outside. The reduction of energy used from outside can be achieved by certain scheme of heat integration. Due to process constraints it is not possible to use the scheme for direct heat integration. For this it is proposed the usage of segregated heat tanks serving for storing thermal energy for its use in another time interval (Fig. 2).

The characteristic feature of the proposed scheme shown in Figure 2 is the block for cooling and heat integration. Wort with temperature T_0^P and debit m_n^P enters for cooling in heat exchangers A_1, A_2, A_3, A_4 . The waste water after the heat exchangers is stored in four tanks $V_{80}^*, V_{45}^*, V_{Washing}^*, V_{Waste}^*$.

The task of process management is limited to the determination of multitude independent variables which to minimize the money spent to conduct processes. The task restrictions are related to the technological requirements for carrying out the processes, and also with the demands to the technical equipment for performing cooling.

Mathematical model of the motivation example

The proposed method for heat integration can be applied to traditional brewing. The technological process includes 9 main stages. The data about the parameters of the "heating-cooling" process are presented in Table 1.

It is assumed that the process of cooling and heat integration is carried out in N successive time intervals. For each time interval the cooling is carried out with a constant debit of streams.

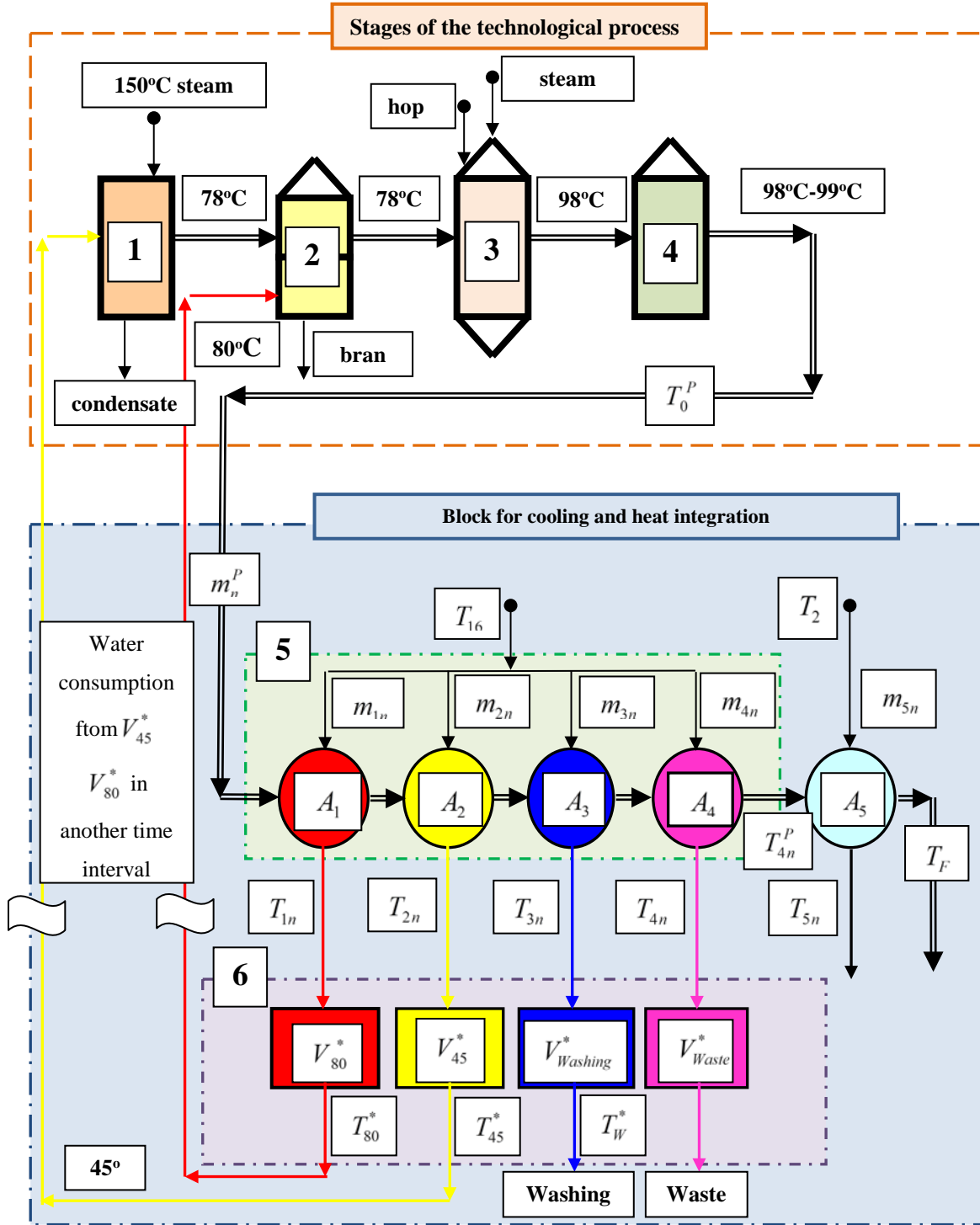


Fig. 2. Scheme of the system for heat integration with separated heat tanks

The mathematical model describing the temperature levels (for n -th time interval) that are achieved in each of the heat exchangers is given by the following relationships:

For heat exchanger A_1 that performs wort cooling from starting temperature T_0^P to temperature T_{1n}^P , the

water temperature after the heat exchanger A_1 will be T_{1n} :

$$T_{1n}^P = T_0^P - (T_0^P - T_{16}) \Phi e_{1n} \quad (1)$$

$$T_{1n} = T_{16} + (T_0^P - T_{16}) k_{1n} \Phi e_{1n}$$

where

$$k_{1n} = \left| \frac{T_{16} - T_{1n}}{T_{1n}^P - T_0^P} \right| = \frac{m_n^P Cp_P}{m_{1n} Cp_{16}},$$

$$w_{1n} = \frac{1}{m_n^P Cp_P} - \frac{1}{m_{1n} Cp_{16}},$$

$$\Phi e_{1n} = \frac{T_{1n}^P - T_0^P}{T_{1n}^P - T_{16}^P} = \frac{1 - \exp(-w_{1n} U_1 A_1)}{1 - k_{1n} \exp(-w_{1n} U_1 A_1)}$$

Table 1. Parameters of the processes in a brewery

Parameters	Value	Dimension
Cp_P	3970	[kJm ⁻³ K ⁻¹]
Cp_{H_2O}	4190	[kJkm ⁻³ K ⁻¹]
m_n^P	0.0139	[m ³ /sec]
m_{1n}	0.025	[m ³ /sec]
T_0^P	98	[°C]
T_{16}	16	[°C]
T_2	2	[°C]
V_{80}	≤ 35	[m ³]
V_{45}	≤ 34	[m ³]
$V_{Washing}$	≤ 35	[m ³]
V_{Waste}	≤ 35	[m ³]
$Cost_{16}$	2,184	[lw/m ³]
C_{Steam}	0.075510 ⁻³	[lw/kJ]
C_{W2}	0.16210 ⁻³	[lw/kJ]

For heat exchanger A_2 that performs wort cooling from starting temperature T_{1n}^P to temperature T_{2n}^P , the water temperature after the heat exchanger A_2 will be T_{2n} :

$$T_{2n}^P = T_{1n}^P - (T_{1n}^P - T_{16}) \Phi e_{2n}$$

$$T_{2n} = T_{16} + (T_{1n}^P - T_{16}) k_{2n} \Phi e_{2n} \quad (2)$$

where

$$k_{2n} = \left| \frac{T_{16} - T_{2n}}{T_{2n}^P - T_{1n}^P} \right| = \frac{m_n^P Cp_P}{m_{2n} Cp_{16}},$$

$$w_{2n} = \frac{1}{m_n^P Cp_P} - \frac{1}{m_{2n} Cp_{16}},$$

$$\Phi e_{2n} = \frac{T_{2n}^P - T_{1n}^P}{T_{2n}^P - T_{16}^P} = \frac{1 - \exp(-w_{2n} U_2 A_2)}{1 - k_{2n} \exp(-w_{2n} U_2 A_2)}$$

For heat exchanger A_3 that performs wort cooling from starting temperature T_{2n}^P to temperature T_{3n}^P , the water temperature after the heat exchanger A_3 will be T_{3n} :

$$T_{3n}^P = T_{2n}^P - (T_{2n}^P - T_{16}) \Phi e_{3n} \quad (3)$$

$$T_{3n} = T_{16} + (T_{2n}^P - T_{16}) k_{3n} \Phi e_{3n}$$

where

$$k_{3n} = \left| \frac{T_{16} - T_{3n}}{T_{3n}^P - T_{2n}^P} \right| = \frac{m_n^P Cp_P}{m_{3n} Cp_{16}},$$

$$w_{3n} = \frac{1}{m_n^P Cp_P} - \frac{1}{m_{3n} Cp_{16}},$$

$$\Phi e_{3n} = \frac{T_{3n}^P - T_{2n}^P}{T_{3n}^P - T_{16}^P} = \frac{1 - \exp(-w_{3n} U_3 A_3)}{1 - k_{3n} \exp(-w_{3n} U_3 A_3)}$$

For heat exchanger A_4 that performs wort cooling from starting temperature T_{3n}^P to temperature T_{4n}^P , the water temperature after the heat exchanger A_4 will be T_{4n} :

$$T_{4n}^P = T_{3n}^P - (T_{3n}^P - T_{16}) \Phi e_{4n} \quad (4)$$

$$T_{4n} = T_{16} + (T_{3n}^P - T_{16}) k_{4n} \Phi e_{4n}$$

where

$$k_{4n} = \left| \frac{T_{16} - T_{4n}}{T_{4n}^P - T_{3n}^P} \right| = \frac{m_n^P Cp_P}{m_{4n} Cp_{16}},$$

$$w_{4n} = \frac{1}{m_n^P Cp_P} - \frac{1}{m_{4n} Cp_{16}},$$

$$\Phi e_{4n} = \frac{T_{4n}^P - T_{3n}^P}{T_{4n}^P - T_{16}^P} = \frac{1 - \exp(-w_{4n} U_4 A_4)}{1 - k_{4n} \exp(-w_{4n} U_4 A_4)}$$

For heat exchanger A_5 that performs wort cooling from starting temperature T_{4n}^P to temperature T_{5n}^P , the water temperature after the heat exchanger A_5 will be T_{5n} :

$$T_{5n}^P = T_{4n}^P - (T_{4n}^P - T_2) \Phi e_{5n} \quad \left. \right\} \quad (5)$$

$$T_{5n} = T_2 + (T_{4n}^P - T_2) k_{5n} \Phi e_{5n}$$

where

$$k_{5n} = \left| \frac{T_2 - T_{5n}}{T_{5n}^P - T_{4n}^P} \right| = \frac{m_n^P Cp_P}{m_{5n} Cp_2},$$

$$w_{5n} = \frac{1}{m_n^P Cp_P} - \frac{1}{m_{5n} Cp_2}$$

$$T_{5n}^P = T_F^*,$$

$$\Phi e_{5n} = \frac{T_{5n}^P - T_{4n}^P}{T_{5n}^P - T_2} = \frac{1 - \exp(-w_{5n} U_5 A_5)}{1 - k_{5n} \exp(-w_{5n} U_5 A_5)}$$

The mathematical model describing the working temperature and volume, which are reached as a result of the heat exchange for each heat tank is given in the following way:

For heat tank V_{80} the volume V_{80}^* and the temperature T_{80}^* are reached as a result of heat exchange:

$$V_{80}^* = \sum_{n=1}^5 (m_{1n} t_n) \quad (6)$$

$$T_{80}^* = \frac{\sum_{n=1}^5 (T_{1n} m_{1n} t_n)}{\sum_{n=1}^5 (m_{1n} t_n)} \quad (7)$$

For heat tank V_{45} the volume V_{45}^* and the temperature T_{45}^* is reached as a result of heat exchange:

$$V_{45}^* = \sum_{n=1}^5 (m_{2n} t_n) \quad (8)$$

$$T_{45}^* = \frac{\sum_{n=1}^5 (T_{2n} m_{2n} t_n)}{\sum_{n=1}^5 (m_{2n} t_n)} \quad (9)$$

For heat tank $V_{Washing}$ the volume $V_{Washing}^*$ and the temperature $T_{Washing}^*$ is reached as result of heat exchange:

$$V_{Washing}^* = \sum_{n=1}^5 (m_{3n} t_n) \quad (10)$$

$$T_{Washing}^* = \frac{\sum_{n=1}^5 (T_{3n} m_{3n} t_n)}{\sum_{n=1}^5 (m_{3n} t_n)} \quad (11)$$

For heat tank V_{Waste} the volume V_{Waste}^* and the temperature T_{Waste}^* is reached as a result of heat exchange:

$$V_{Waste}^* = \sum_{n=1}^5 (m_{4n} t_n) \quad (12)$$

$$T_{Waste}^* = \frac{\sum_{n=1}^5 (T_{4n} m_{4n} t_n)}{\sum_{n=1}^5 (m_{4n} t_n)} \quad (13)$$

The energy that is necessary to carry out the processes can be presented by the following mathematical relationships:

$$E_{45} = (T_{45} - T_{45}^*) V_{45}^* Cp_{16} + (T_{45} - T_{16}) (V_{45} - V_{45}^*) Cp_{16} \quad (14)$$

$$E_{80} = (T_{80} - T_{80}^*) V_{80}^* Cp_{16} + (T_{80} - T_{16}) (V_{80} - V_{80}^*) Cp_{16} \quad (15)$$

$$E_{Washing} = (T_{Washing} - T_{Washing}^*) V_{Washing}^* Cp_{16} + (T_{Washing} - T_{16}) (V_{Washing} - V_{Washing}^*) Cp_{16} \quad (16)$$

$$E_2 = \sum_{n=1}^{n=5} (Cp_2 m_{5n} t_n (T_{5n} - T_2)) \quad (17)$$

The cost of the energy that is necessary to ensure the technological processes is calculated according to the relation:

$$Cost = (E_{45} + E_{80} + E_{Washing}) Cost_{16} + E_2 Cost_2 \quad (18)$$

Variables

The essence of the management process is to determine the set of independent variables to ensure the fulfillment of the objective function or in other words to minimize the money spent on conducting the processes.

These independent variables are:

$$X = \{m_{in}, A_n, m_n^P, t_n\}, \forall i, n$$

where

$$\left. \begin{array}{l} m_{in}, \quad \forall n \in (1, N), \forall i \in (1, 5) \\ A_n, m_n^P, t_n, \quad \forall n \in (1, N) \end{array} \right\} \quad (19)$$

Restrictions

Task restrictions are related to the technological requirements for carrying out the processes, and also with requirements to the technical equipment carrying out the cooling. In this case, the plurality of task restrictions are:

$$\left. \begin{array}{l} T_{45}^* \leq T_{45} \\ V_{45}^* = V_{45} \end{array} \right\} \quad (20)$$

$$\left. \begin{array}{l} T_{80}^* \leq T_{80} \\ V_{80}^* = V_{80} \end{array} \right\} \quad (21)$$

$$\left. \begin{array}{l} T_{Washing}^* \leq T_{Washing} \\ V_{Washing}^* \leq V_{Washing} \end{array} \right\} \quad (22)$$

$$V_{Beer}^P = \sum_{n=1}^{n=5} (t_n m_n^P) \quad (23)$$

$$A_i \leq A_i^{MAX}, \quad \forall i \in (1,5) \quad (24)$$

$$\sum_{n=1}^{n=5} t_n \leq t_{cold} \quad (25)$$

$$T_{5n}^P \leq T_F \quad (26)$$

Aim of heat integration

The aim of heat integration is to minimize the amount of used energy resources for carrying out the processes. This can be achieved by providing a possibility of maximum utilization of the heat from the cooling of the wort.

The objective function of the heat integration is:

$$\text{MINIMIZE } \{Cost(X)\} \quad (27)$$

The presented task is formulated in terms of the mathematical nonlinear programming MNLP and it is solved with programming package GAMS.

RESULTS

As a result of applying the method of heat integration using heat tanks in the process of brewing were achieved results presented in the following tables:

In Table 2 the optimal temperature levels of the wort are shown that are reached at the output of the heat exchangers.

Table 2 shows that by the proposed scheme with heat integration (Fig.2) the temperature of the wort gradually decreases after leaving each of the heat exchangers, which results in reducing the energy usage required for the cooling process.

Table 2. Optimal temperature of the wort at the output of the heat exchangers

Heat exchangers	Temperature by scheme without heat integration [°C]	Temperature by scheme with one heat tank [°C]	Temperature by scheme with separate heat tanks [°C]
A_1	22	22	55.016
A_2	12	12	36.095
A_3	-	-	23.308
A_4	-	-	18.560
A_5	-	-	12.000

Table 3 presents the optimal parameters (temperature and volume) in the used additional heat tanks.

Table 3. Optimal temperature and volume in the heat tanks

Hot tank	Scheme without heat integration		Scheme with one heat tank		Scheme with separate heat tanks	
	V [m³]	T [°C]	V [m³]	T [°C]	V [m³]	T [°C]
V_{80}	-	-	-	-	35	80
V_{45}	-	-	140	45.57	34	45
V_{Wash}	-	-	-	-	35	35.039
V_{waste}	-	-	-	-	36	22.872

The energy required to carry out the processes in the execution of various schemes is presented in Table 4. It follows from Table 4 that by the implementation of the heat integration scheme with usage of separate heat tanks (Fig.2) the energy needed to obtain water with a temperature of 45°C and water with a temperature of 80°C is minimized. The total amount of energy required to carry out the processes by using separate heat tanks (Fig.2) is by about 45% lower than that according to the scheme realized in the practice (scheme with one heat tank).

Table 4. Energy needed for carrying out the processes

Resource	Energy needed to carry out processes without heat integration [kJ]	Energy needed to carry out processes with one heat tank [kJ]	Energy needed to carry out processes with separate heat tanks [kJ]
E_2	1432469.724	1432469.724	1432469.724
E_{45}	4131340.000	81171.729	1.944
E_{80}	9385600.000	5049190.867	2.145
E_{Wash}	5719350.000	1382940.867	2927238.395
Total	20668759.72	7945773.187	4359712.208

From Table 5 is clear that the optimal process control leads to significant cost reductions for obtaining water with temperature of 45°C and 80°C.

Table 5. Cost of energy sources without heat integration and with heat integration processes

Resource	Cost of energy by scheme	Cost of energy by scheme	Cost of energy by scheme
	without heat integration	with one heat tank	with separate heat tanks
	[lv.]	[lv.]	[lv.]
$Cost_2$	232.060	232.060	232.060
$Cost_{45}$	311.916	-6.128	1.467841E-4
$Cost_{80}$	708.613	381.214	1.619686E-4
$Cost_{Wash}$	431.811	104.412	221.006
Total	1684.400	711.558	453.067

The installation of one heat tank, as is often the case in practice, leads to a reduction in energy consumption by about 57% compared to the case without heat integration. When specialized segregated tanks are used, as shown in Fig.2, the cost of energy is by 36% lower compared to the case realized in practice.

It can be noted that by optimal process management no special devices that provide optimal change of the coolant flow are necessary.

CONCLUSIONS

In this study, it was described a conventional brewing. The production process was presented as composed of two parts - hot and cold. In presented paper, it was proposed strategy for optimal management of processes "Heating" and "Cooling". It was designed a new structure for heat integration with separated heat tanks and the suitable mathematical model describing the process of wort production.

Optimization task was formulated in accordance with the mathematical nonlinear programming MNLP, aiming to minimize the cost of reusing energy resources, and was solved with the software package GAMS. The proposed method was tested with data from a real working production. The results were indicated in a few summary tables. As a strategy result (when specialized segregated tanks are used), it is possible the energy cost to be a 36% lower compared to the case realized in practice.

NOTATIONS

C_p	Heat capacity, $[kJm^{-3}K^{-1}]$
ρ	Density, $[kg / m^3]$
T	Flow temperature, $[^\circ C]$
V	Volume of apparatus, $[m^3]$

t	Time intervals, $[s]$
C_{Steam}	Cost of steam, $[lw / kJ]$
C_{W5}	Cost of water with temperature $5^\circ C$, $[lw / kJ]$
F^{MAX}	Maximum flow rate, $[m^3 / s]$
A	Heat exchange surface, $[m^2]$
U	Coefficient of heat transfer, $[kJ \sec^{-1} m^{-2} K^{-1}]$
m	Flow rate, $[m^3 / sec]$
E	Energy needed to carry out the processes, $[kJ]$
V^*	Volume, which is reached as a result of heat exchange, $[m^3]$
V_{Beer}	Volume of cooling wort, $[m^3]$
A_i^{MAX}	Maximum heat exchange surface, $[m^2]$
T_F	Temperature of the cooled wort, $[^\circ C]$
V_{45}	Volume of water with temperature $45^\circ C$, $[m^3]$
V_{80}	Volume of water with temperature $80^\circ C$, $[m^3]$
$V_{Washing}$	Volume of water for washing, $[m^3]$
T_{45}	Water temperature $45^\circ C$
T_{80}	Water temperature $80^\circ C$
\dots	Water temperature $16^\circ C$
$T_{Washing}$	Temperature of washing water, $[^\circ C]$
T_2	Water temperature
$Cost_{16}$	Cost per unit of energy consumed to heat water $16^\circ C$ for technological needs, $[lv]$
$Cost_2$	Cost per unit of energy by cooling the beer with water $2^\circ C$, $[lv.]$
$lv.$	Bulgarian levs

REFERENCES

- J. A. Vaselenak, Grossmann I. E., A. W. Westerberg, *Ind. Eng. Chem. Process Des. Dev.*, **25**, 357, (1986)
- S. Thevendiraraj, J. Klemes, D. Paz, G. Aso, G. Cardenas, *Resour. Conserv. Recycl.*, **37**, 227–250, (2003)
- J. K. Kim, R. Smith, *Trans. Chem. E*, **82**, 3, 238–248, (2004)
- D. K. Sum, D. C. Y. Foo, R. R. Tan, C. H. Pau, Y. L. Tan, *Chem. Eng. J.*, **149**, 87, (2009)
- M. M. El-Halwagi, I. M. Glasgow, X. Qin, M. R. Eden, *AIChEJ*, **50**, 854, (2004)
- K. Halim, R. Srinivasan, *Ind. Eng. Chem. Res.*, **48**, 8551, (2009)

- 7.S. Morrison, M. R. Walmsley, J. R. Neale, C. P. Burrell, P. J. Kamp,*Asia-Pac. J. Chem. Eng.*,**2**, 380, (2007)
- 8.L. Puigjaner,*Chem. Prod. Process. Modell.*,**2**, 1934, (2007)
- 9.BLRA, Utilities & Environmental Survey Report, Technical Circular 344, Brewers & Licensed Retailers Association, London, (1999)
- 10.Natural Resources Canada and Brewers Association of Canada, Guide to Energy Efficiency Opportunities in the Canadian Brewing Industry, Canadian Industry Program for Energy Conservation, Ottawa, Canada, (2012).
- 11.Industrial Energy Efficiency Accelerator – Guide to the Brewing Sector, The Carbon Trust, London, (2011)
- 12.C. Galitsky, N. Martin, E. Worrell, B. Lehrman, LBNL, (2003)
- 13.H. Tokos, Z.N. Pintarić, P. Glavić, *Appl. Therm. Eng.*,**30**, 36, (2012)
- 14.B. Sturm, S. Hugenschmidt, Sh.Joyce, W. Hofacker, A. Roskilly, *Appl. Therm. Eng.*,**53**, 397, (2013)
- 15.B. Muster-Slawitsca, M. Hubmann, M. Murkovic, *Chemical Engineering and Processing*,**84**, 98, (2014)
- 16.B. Muster-Slawitsch, W. Weiss, H. Schnitzer, C. Brunner, *Applied Thermal Engineering*,**31**, 2123, (2011)
- 17.B. Sturm, M. Butcher, Y.D. Wang, Y. Huang, T. Roskilly, *Applied Thermal Engineering*,**39**, 45, (2011)

ОПТИМАЛНО УПРАВЛЕНИЕ НА ЕНЕРГИЯТА В ПИВОВАРСТВОТО

Д. Ст. Николова¹, Б. Б. Иванов², Д. Г. Добруджалиев¹

¹Университет „Проф. д-р Асен Златаров“ гр.Бургас8000, бул Яким Якимов 1

²Институт по инженерна химия, БАН гр София1113, ул Акад. Ст. Ангелов, бл 103

Постъпила на 8 Март, 2016; Коригирана на 3 Февруари 2017

(Резюме)

Енергийната ефективност е един много важен показател при оценка устойчивостта на промишлените процеси. Оптималното използване на енергията е основна задача и днес, тъй като определя състоянието на околната среда и крайната цена на продукта. Настоящата разработка описва метод за минимизиране консумацията на енергия чрез топлинна интеграция на процесите при конвенционално пивопроизводство. Предложена е схема за топлинна интеграция с използване на разделни топлинни резервоари, служещи за съхранение на топлинна енергия. Разработен е математичен модел, който описва топлопреносните процеси. На база на модела е предложена стратегия за оптимално управление на енергоресурсите с използване на разделни топлинни резервоари. Оптимизационната задача е формулирана в термините на математичното нелинейно програмиране MNLP и е решена с програмния пакет GAMS. Предложеният метод е тестван с използване на данни от реално работещо производство.

Diamond green dye adsorptive removal from water by carrot pulpy waste and potato peels

R. Rehman¹, S. Alam¹, L. Mitu^{2*}

¹Institute of Chemistry, University of the Punjab, Lahore-54590, Pakistan

²Department of Chemistry, University of Pitesti, Pitesti-110040, Romania

Received June 1, 2016; Accepted May 25, 2017

Diamond green dye is an example of textile dye. In this study, *Daucus carota* (carrot) waste and *Solanum tuberosum* (potato) peels were used for dye removal from water. These are low-cost and commonly available materials. Their adsorption capacity for Diamond green dye was tested for the first time in this study for possible application on industrial scale water treatment. Optimum conditions for the removal of 25 ppm of Diamond green dye from 100 mL of synthetic wastewater by carrot pulpy waste were: 0.6 g adsorbent dose, pH 2.0, 40 min contact time, 30°C temperature and 150 rpm agitation speed. Using potato peels, the optimum conditions were: 0.4 g adsorbent dose, pH 1.0, 15 min contact time, 30°C temperature and 50 rpm agitation speed. Various conditions affecting the sorption of Diamond green dye from water were optimized by carrying out isothermal and kinetic studies. Isothermal studies indicated that chemisorptive mode is predominant over physio-sorption with maximum removal capacities for carrot waste and potato peels of 4.14 and 3.13 mg/g, respectively. Kinetic studies pointed to a pseudo-second order model. Both materials are suitable for bulk-scale removal of Diamond green dye from waste water streams.

Keywords: Diamond green dye; Carrot pulpy waste; Potato peels, Isotherm; Kinetic models.

INTRODUCTION

Rapid growth in population in recent years resulted in higher development of industrialization to support people economically and to offer them better living standards. But this leads to environmental pollution which may be lethal for living creatures. It acts as a slow poison, e.g., toxic metals or excessive organic pollutants discharged into water bodies. Mainly dyes, colorants, synthetic drugs, pesticides, herbicides, germicides, and detergents are the common examples of organic pollutants found in industrial waste water streams. Organic pollutants are sometimes biodegradable, but synthetic dye stuff is resistible to biodegradation. So, its removal from waste streams is necessary.

Dyes removal by adsorption process is getting more important nowadays. Different researchers are working with various types of waste materials from indigenous sources to remove toxic matter from water by adsorption.

Agricultural waste, like leaves, peels, seeds, pulp, etc., is more popular among them due to its easy handling, availability and non-toxic nature [1-8].

In this work, the removal of Diamond green dye from water by carrot waste and potato peels was studied. Its λ_{max} is 625 nm and the formula is given in Fig. 1. It is a textile dye with synonyms used in various texts: Brilliant green, Astradiamant green

GX, Basic green 1, Emerald green, Ethyl green, Malachite green G and Solid green JO.

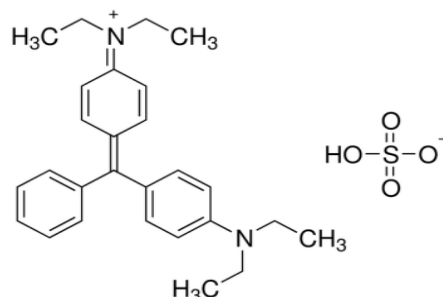


Fig. 1. Structure of Diamond green.

It is injurious to health if comes in skin or eye contact or orally ingested. Burning of items coated with this dye results in NO_x and SO_x fumes, causing air pollution, leading to eye infection and skin ulcer [9-11].

Various adsorbents were used for its removal from aqueous medium, e.g., saklikent mud, cactus fruit peels, saw dust, rice husks, fly ash, eucalyptus wood, bottom ash, de-oiled soya, palm kernels, sunflower, rubber wood, babassu coconut epicarp, etc. [12-32].

Potato (*Solanum tuberosum*) peels and carrot (*Daucus carota*) pulpy waste were used for adsorption of Diamond green dye. Carrots and potatoes are extensively used as food. They are not only used in homemade food items, but also extensively employed in industrial level-processed food like chips, French fries, carrot juice, muraba,

* To whom all correspondence should be sent:
E-mail: ktm7ro@yahoo.com

pickles, desserts, cakes and soups [33-41]. Both of them are nutritionally rich and economical food. They are easily available all over the world. Their adsorption capacity for removing Diamond green dye was tested for the first time in this study for possible application on industrial scale water treatment. Their use on a large scale can significantly increase the organic matter in water due to leaching, but that organic matter is decomposable; moreover, it usually contains different chelating agents that can reduce toxic metallic ions concentration in waste water streams. So their usage as adsorbents is preferable as compared to synthetic adsorbents.

EXPERIMENTAL

Materials and instrumentation

Diamond green dye ($\lambda_{\text{max}} = 625$ nm), HCl (Merck), NaOH (Merck), Vis spectrophotometer 721, grinder (Philips), digital balance, FT-IR spectrometer (Perkin Elmer), oven (Haier).

Sorbent matter preparation

Potato peels and carrot pulpy waste were collected from cafeteria of home institutes making potato chips and carrot juice. They were washed, strained, dried in sunlight and ground to fine powder. The ground material was sieved through 60 mesh and stored in plastic jars. Potato peels were labeled as S.T.P and carrot waste - as D.C.W. Their FT-IR spectra were recorded on a Perkin Elmer spectrometer (ATR supported) and are given in Figs. 2 and 3, respectively. Their physical characterization was carried out using standard methods and is reported in Table 1.

Adsorption studies

Adsorption studies were carried out with synthetic Diamond green dye solutions. The effect of various parameters on the rate of the biosorption process was investigated by varying biosorbent amount (0.2-2.0 g), contact time, (5-60 min), initial pH of the solution (1-10), agitation speed (0-200 rpm) and temperature (20-70 °C) using potato peels and carrot waste. The solution volume (V) was kept constant (50 mL). 25 ppm dye solution was used and photometric measurement was done at $\lambda_{\text{max}} = 625$ nm. Diamond green (B.G) dye adsorption was calculated by the following equation:

$$\% \text{ adsorption of B.G dye} = (C_0 - C_e)/C_0 \times 100 \quad (1)$$

After completion of the adsorption process, the adsorbents were separated from water by vacuum filtration using a Büchner funnel.

Isothermal modeling

Optimized operational conditions were applied on dye solutions of various concentrations (from 15 to 80 ppm) for isothermal modeling of equilibrium data. Langmuir model equation is [35]:

$$\frac{1}{q} = \frac{1}{bq_m C_e} + \frac{1}{q_m} \quad (2)$$

where q is the adsorption capacity (mg/g) [33-35].

The value of b was used to calculate the separation factor R_L and ΔG° .

Separation factor is determined by:

$$R_L = 1/(1+bC_0) \quad (3)$$

When its value is greater than 1, the adsorption process is unfavorable using that specific adsorbent.

$$\Delta G^\circ = -RT \ln K \quad (4)$$

Here K = 1/b and Gibbs free energy is given in KJ/mol [7-12].

Freundlich isotherm is [12]:

$$\log q = \log K_F + \frac{1}{n} \log C_e \quad (5)$$

Kinetic modeling

Optimized operational conditions were applied on a 50 ppm dye solution for different time periods ranging from 5 to 120 min for kinetic modeling of the equilibrium data. Kinetic modeling was done using equation 6 and equation 7 [12]:

$$\log(q_e - q_t) = \log q_e - \frac{k_1}{2.303} t \quad (6)$$

$$\frac{t}{q_t} = \frac{1}{k_2 q_e} + \frac{t}{q_e} \quad (7)$$

Here t corresponds to the time interval of contact between sorbent and dye solution in min, k_1 is a first-order constant and k_2 is a second-order constant.

RESULTS AND DISCUSSION

Characterization of adsorbent samples

Different functional groups were identified by FT-IR studies on the biosorbent samples that can interact with dye molecules and ionized species in aqueous medium (see Fig. 2 for *Solanum tuberosum*). -OH, C-H, C=O, N-H bonds at peaks 3300.20, 2924.09, 1244.09, 1149.57 and 1639.49, 1537.27 cm⁻¹ were found in the spectrum of potato peels. The FT-IR spectrum of carrot waste (Fig. 3) shows the same trend.

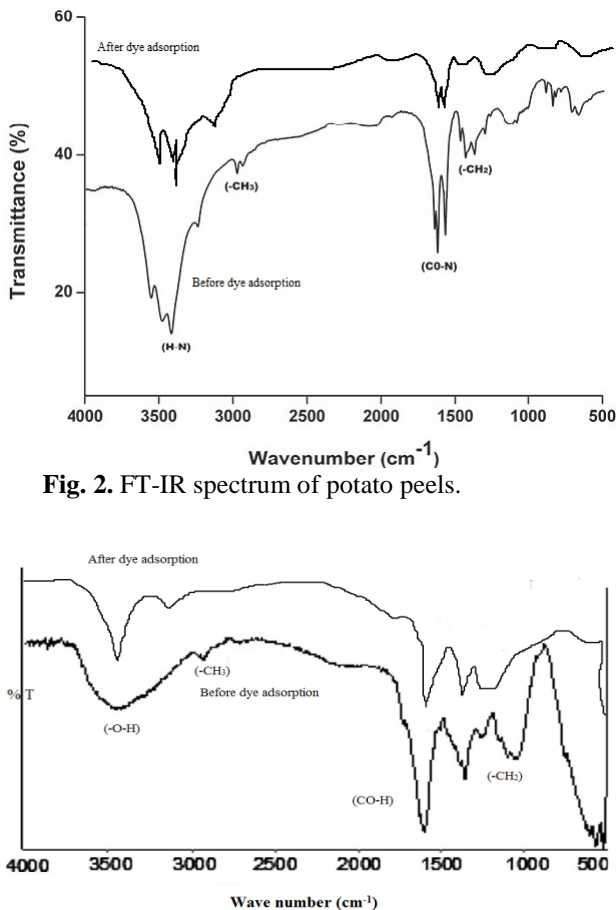


Fig. 2. FT-IR spectrum of potato peels.

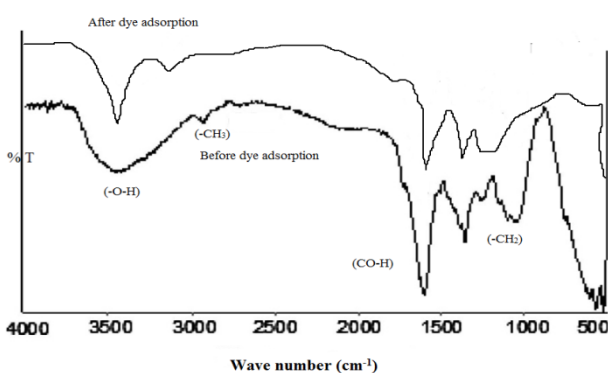


Fig. 3. FT-IR spectrum of carrot pulpy waste.

After dye adsorption, the samples were again analysed for observing if changes took place. After comparing with the original adsorbent before adsorption, it was observed that the wavenumber values shifted towards lower numbers, indicating that chemisorption mode is predominant.

Table 1 indicates that potato peels have a more acidic nature which will help to adsorb cationic dye more efficiently.

Table 1. Physical characteristics of adsorbents

Physical properties	Carrot pulpy waste	Potato peels
pH	7	6
Moisture content (%)	7.4	8.6
Ash (%)	3.51	3.93
Volatile matter (%)	18.8	21.4

The moisture, ash and volatile matter contents were higher in potato peels than in carrot waste. This is an evidence for the easy decomposition of potato peels after usage, which will help in dumping of waste after adsorption of dye. Higher ash content indicates that the physisorption capacity of potato peels for dye removal is higher as compared to carrot waste. This was further confirmed by isothermal modeling of equilibrium data.

Results of optimized operational conditions

Adsorbent dose

The effect of adsorbent dose is shown in Fig. 4 which indicates that the maximum removal of Diamond green dye by D.C.W occurred at 0.4 g and by S.T.P at 0.6 g. The use of a lower quantity with maximum removal of dye within 20 min revealed that carrot waste contains a larger number of binding sites for chemisorption of Diamond green dye. So, it is better than potato peels for adsorption of Diamond green on bulk scale removal of dye.

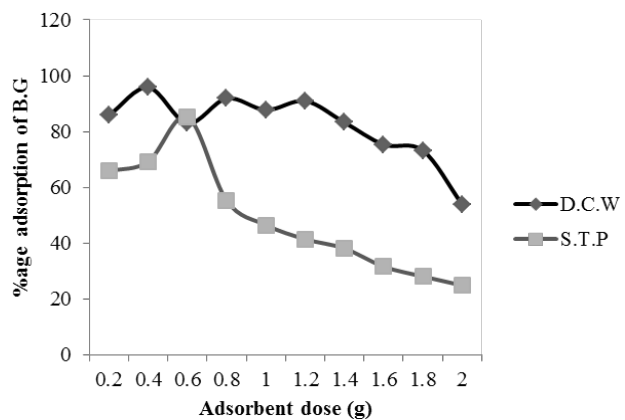


Fig. 4. Adsorbent dose effect on the removal of Diamond green dye.

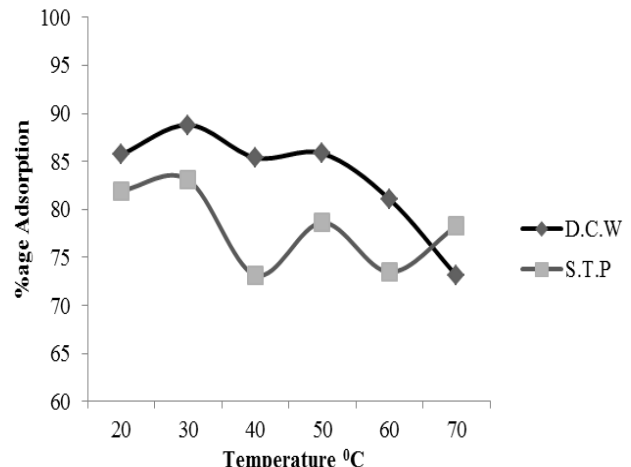


Fig. 5. Temperature effect on the removal of Diamond green dye.

Temperature

The effect of temperature on the adsorption of Diamond green dye by potato peels and carrot pulpy waste is presented in Fig. 5 which indicates that the maximum removal occurs at 30°C using both adsorbing materials, carrot pulpy waste providing a higher percent removal.

This means that higher temperature does not favour the removal of Diamond green dye, because it is an exothermic process. Additional movement of molecules surges with rise in temperature; therefore

depression in adsorption occurred at higher temperatures [28].

Dye solution pH

Dye solution pH alters the various ionized species present in solution that can interact with biosorbent surface. So its effect was monitored and is shown in Fig. 6.

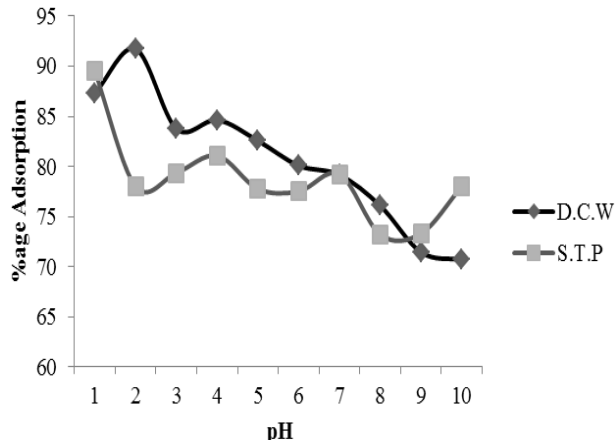
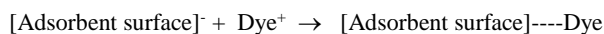
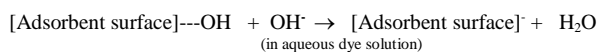


Fig. 6. Dye solution pH effect on the removal of Diamond green dye.

It indicates that the maximum removal of Diamond green dye takes place at pH of the dye solution of 2 and 1 for carrot pulpy waste and potato peels, respectively. Depression in adsorption occurs at higher pH of Diamond green dye solution. Alteration in the molecular structure of Diamond green dye due to ionization and protonation in acidic medium along with changes in functional groups of the carrot pulpy waste and potato peels are responsible for this effect. In basic conditions, the higher concentration of hydroxide ions leads to polarization of the adsorbent surface that in turn can easily remove a cationic dye like Diamond green by stronger electrostatic attraction. This can be pictured by the following equations [16, 25]:



Contact time

The effect of contact time is shown in Fig. 7 which indicates that the maximum removal of Diamond Green dye occurs in 40 min using carrot waste and in 15 min using potato peels. This trend is

due to the fact that carrot waste is more porous and contains a larger number of binding sites as compared to potato peels, so it needs more time for attaining adsorption equilibrium with Diamond green dye molecules. Also, the adsorbed amount is larger than with potato peels. At the initial stage of the process, the removal of Diamond green dye is rapid, but with passage of time, the process slows down because now the surface binding sites are covered by dye molecules. Further removal of dye can only occur, if the dye molecules penetrate into deeper layers of the sorbent. So after the saturation point of the sorbent, further adsorption was suppressed [30].

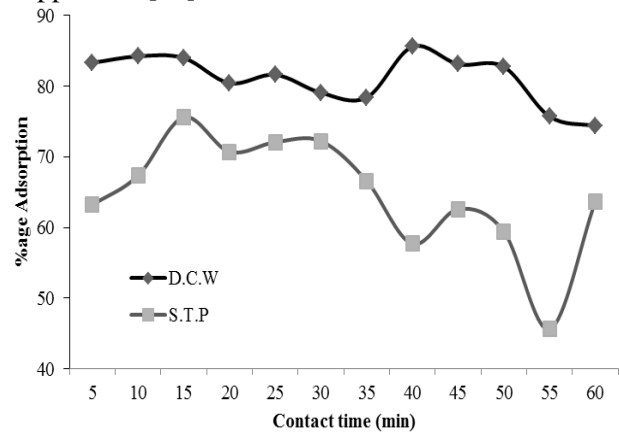


Fig. 7. Contact time effect on the removal of Diamond green dye.

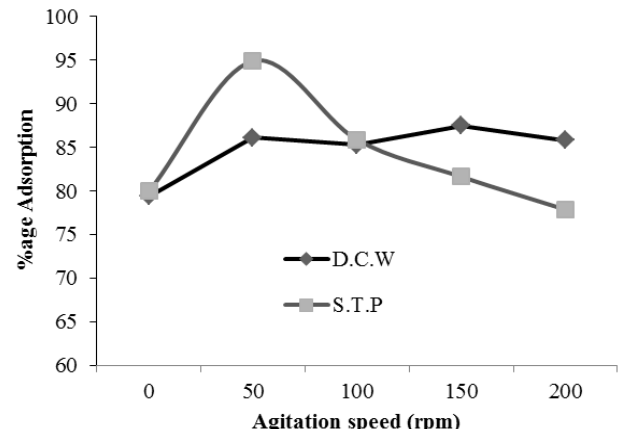


Fig. 8. Agitation speed effect on the removal of Diamond green dye.

Agitation speed

Agitation of the dye solution helps the penetration of dye molecules into deeper layers of the sorbent, which enhances the contact with.

Table 2. Langmuir isothermal parameters for the adsorption of Diamond green dye

Adsorbent	Slope	Intercept	R ²	q _{max} (mg/g)	b (L/mg)	ΔG ⁰ (KJ/mol)
Carrot pulpy waste	0.8856	0.2044	0.921	4.44	0.674	-9.772
Potato peels	6.754	-0.479	0.937	3.13	0.949	-0.13

Table 3. Freundlich isothermal parameters for the adsorption of Diamond green dye

Adsorbent	Slope	Intercept	R ²	K _F (mg ^{1-(1/n)} L ^{1/n} g ⁻¹)	n
Carrot pulpy waste	0.707	0.078	0.900	0.77	6.86
Potato peels	1.464	0.906	0.896	0.124	0.68

Table 4. Kinetic modeling parameters for the adsorption of Diamond green dye.

Adsorbent	Pseudo-first order			Pseudo-second order			q _{e(exp)} mg/g
	k ₁	q _{e(cal)} mg/g	R ²	k ₂	q _{e(cal)} mg/g	R ²	
Carrot pulpy waste	0.0311	0.758	0.938	0.0351	1.354	0.991	1.2
Potato peels	0.0223	0.203	0.929	0.0397	2.287	0.996	2.2

binding sites. However, very high agitation speeds have a negative effect on adsorption, because in that case less time is available to contact dye molecules with the active sites of the sorbent. It is clear from Fig. 8 that the maximum removal of Diamond green dye is achieved at 150 rpm for carrot pulpy waste and at 50 rpm for potato peels

Isothermal studies of adsorption data

Isothermal studies were carried out on the mechanism of removal of Diamond green dye by carrot pulpy waste and potato peels and the results are presented in Tables 2 and 3.

R² (regression coefficient) value is greater for Langmuir isotherm than for Freundlich model using both carrot pulpy waste and potato peels. This means that chemisorption occurred on homogenously distributed active binding sites rather than physisorption in multilayer fashion.

The greater value of q_{max} (4.44 mg/g) for carrot waste proves it a better adsorbent as compared to potato peels. In this study, the separation factor R_L value less than unity using both carrot pulpy waste and potato peels points to the favorable sorption of Diamond green dye on these sorbents [40, 41]. ΔG⁰ values are negative, indicating the spontaneous and exothermic nature of Diamond green dye removal process using carrot pulpy waste and potato peels.

The values of K_F and n for carrot pulpy waste and potato peels indicating that first one provides more removal of Diamond green dye.

Sorption kinetics

Generally, the pseudo-first order kinetic equation is not applicable for biosorption of dye systems. Same is the case here. Kinetic parameters are given in Table 4. The correlation coefficient of the pseudo-second order model was greater than that of the other model using carrot waste and potato peels for Diamond green dye removal from water. This indicated that the adsorption system is not a first-order reaction. Secondly, the q_{e(cal)} values of the

pseudo-second order kinetic model are closer to q_{e(exp)}. So both these parameters suggest that the pseudo-second order kinetic model is followed in Diamond green dye adsorption by carrot pulpy waste and potato peels.

CONCLUSIONS

It is found that Diamond green dye can be easily removed from water by employing carrot waste (D.C.W) and potato peels (S.T.P) as sorbents with maximum adsorption capacity of 4.44 mg/g for carrot pulpy waste and 3.13 mg/g for potato peels. Optimum conditions for the removal of 25 ppm of Diamond green dye from 100 mL of synthetic wastewater by carrot pulpy waste were: 0.6 g adsorbent dose, pH 2.0, 40 min contact time, 30°C temperature and 150 rpm agitation speed. Using potato peels, the optimum conditions were: 0.4 g adsorbent dose, pH 1.0, 15 min contact time, 30°C temperature and 50 rpm agitation speed. Kinetic modeling of equilibrium data indicated that pseudo-second order model was followed and thermodynamic studies revealed the spontaneous nature of this process. Both of these adsorbents, i.e., carrot pulpy waste and potato peels, can be easily employed for bulk-scale Diamond green dye removal from waste water streams.

REFERENCES

1. K.A. Adegoke and O.S. Bello, *Water Resources and Industry*, **12**, 8 (2015).
2. I. Anastopoulos and G.Z. Kyzas, *Journal of Molecular Liquids*, **200**, Part B, 381 (2014).
3. M. Asgher and H.N. Bhatti, *Ecological Engineering*, **38**, 79 (2012).
4. A. Bhatnagar, M. Sillanpää and A. Witek-Krowiak, *Chemical Engineering Journal*, **270**, 244 (2015).
5. A. Bhatnagar, V.J.P. Vilar, C.M.S. Botelho and R.A.R. Boaventura, *Advances in colloid and interface science*, **160**, 1 (2010).
6. K.G. Bhattacharyya and A. Sharma, *Journal of Environmental Management*, **71**, 217 (2004).
7. M. Feizi and M. Jalali, *Journal of the Taiwan Institute of Chemical Engineers*, **54**, 125 (2015).

- 8.E. Forgacs, T. Cserháti and G. Oros, *Environment International*, **30**, 953 (2004).
- 9.M. Ghaedi, H. Hossainian, M. Montazerozohori, A. Shokrollahi, F. Shojaipour, M. Soylak and M.K. Purkait, *Desalination*, **281**, 226 (2011).
- 10.Y. Kismir and A.Z. Aroguz, *Chemical Engineering Journal*, **172**, 199 (2011).
- 11.M. R. Kosseva, Processing of Food Wastes. In *Advances in Food and Nutrition Research*, Chapter 3, Academic Press; **58**, 57 (2009).
- 12.R. Kumar and M.A. Barakat, *Chemical Engineering Journal*, **226**, 377 (2013).
- 13.A.K. Kushwaha, N. Gupta and M.C. Chattopadhyaya, *Journal of Saudi Chemical Society*, **18**, 200 (2014).
- 14.V.S. Mane and P.V.V. Babu, *Desalination*, **273**, 321 (2011).
- 15.V.S. Mane, I. Deo Mall and V.C. Srivastava, *Journal of Environmental Management*, **84**, 390 (2007).
- 16.V.S. Mane, I.D. Mall and V.C. Srivastava, *Dyes and Pigments*, **73**, 269 (2007).
- 17.V.S. Mane and P.V. Vijay Babu, *Journal of the Taiwan Institute of Chemical Engineers*, **44**, 81 (2013).
- 18.A. Mittal, D. Kaur and J. Mittal, *Journal of Colloid and Interface Science*, **326**, 8 (2008).
- 19.B.K. Nandi, A. Goswami and M.K. Purkait, *Journal of Hazardous Materials*, **161**, 387 (2009).
- 20.T. Nharingo and M. Moyo, *Journal of Environmental Management*, **166**, 55 (2016).
- 21.A.E. Ofomaja and Y.S. Ho, *Dyes and Pigments*, **74**, 60 (2007).
- 22.G.B. Oguntiemein, *Journal of Environmental Chemical Engineering*, **3**, 2647 (2015).
- 23.V. Ponnusami, S. Vikram and S.N. Srivastava, *Journal of Hazardous Materials*, **152**, 276 (2008).
- 24.S. Rangabhashiyam, N. Anu and N. Selvaraju, *Journal of Environmental Chemical Engineering*, **1**, 629 (2013).
- 25.M.S.U. Rehman, M. Munir, M. Ashfaq, N. Rashid, M.F. Nazar, M. Danish and J.I. Han, *Chemical Engineering Journal*, **228**, 54 (2013).
- 26.M.A. Salem, R.G. Elsharkawy and M.F. Hablas, *European Polymer Journal*, **75**, 577 (2016).
- 27.A.T. Shah, M.I. Din, F.N. Kanwal and M.L. Mirza, *Arabian Journal of Chemistry*, **8**, 579 (2015).
- 28.M.P. Tavlieva, S.D. Genieva, V.G. Georgieva and L.T. Vlaev, *Journal of Colloid and Interface Science*, **409**, 112 (2013).
- 29.K. Vasanth Kumar and S. Sivanesan, *Dyes and Pigments*, **72**, 124 (2007).
- 30.A.P. Vieira, S.A.A. Santana, C.W.B. Bezerra, H.A.S. Silva, J.A. Chaves, J.C.P. Melo, E.C.S. Filho and C. Airolidi, *Chemical Engineering Journal*, **173**, 334 (2011).
- 31.W.S. Wan Ngah and M.A.K.M. Hanafiah, *Bioresource Technology*, **99**, 3935 (2008).
- 32.M.T. Yagub, T.K. Sen, S. Afroze and H.M. Ang, *Advances in Colloid and Interface Science*, **209**, 172 (2014).
- 33.H.N. Bhatti, A.W. Nasir and M.A. Hanif, *Desalination*, **253**, 78 (2010).
- 34.F. Güzel, H. Yakut and G. Topal, *Journal of Hazardous Materials*, **153**, 1275 (2008).
- 35.T. Aman, A.A. Kazi, M.U. Sabri and Q. Bano, *Colloids and Surfaces B: Biointerfaces*, **63**, 116 (2008).
- 36.A.C. Arampatzidou and E.A. Deliyanni, *Journal of Colloid and Interface Science*, **466**, 101 (2016).
- 37.G.Z. Kyzas and E.A. Deliyanni, *Chemical Engineering Research and Design*, **97**, 135 (2015).
- 38.G.Z. Kyzas, E.A. Deliyanni and K.A. Matis, *Colloids and Surfaces A: Physicochemical and Engineering Aspects*, **490**, 74 (2016).
- 39.Y. Li, Y. Deng and B. Chen, *Journal of Environmental Sciences*, **24**, 675 (2012).
- 40.J.C. Moreno-Piraján and L. Giraldo, *Journal of Analytical and Applied Pyrolysis*, **90**, 42 (2011).
- Z. Zhang, X. Luo, Y. Liu, P. Zhou, G. Ma, Z. Lei and L. Lei, *Journal of the Taiwan Institute of Chemical Engineers*, **49**, 206 (2015).

ОТСТРАНЯВАНЕ НА БАГРИЛОТО ДИАМАНТЕНО ЗЕЛЕНО ОТ ВОДИ ЧРЕЗ
АДСОРБЦИЯ ВЪРХУ ОТПАДЪЧНА МОРКОВЕНА ПУЛПА И КАРТОФЕНИ ОБЕЛКИ

Р. Рехман¹, С. Алам¹, Л. Миту^{2*}

¹Институт по химия, Университет на Пенджаб, Лахор-54590, Пакистан

²Департамент по химия, Университет на Питещи, Питещи-110040, Ромъния

Получена на 1 юни, 2016 г.; коригирана на 25 май 2017 г.

(Резюме)

Багрилото диамантено зелено е пример за текстилна боя. В това проучване е използвана отпадъчна пулпа от моркови (*Daucus carota*) и обелки от картофи (*Solanum tuberosum*) за отстраняване на багрилото от водата. Това са евтини и лесно достъпни материали. Техният адсорбционен капацитет за отстраняване на багрилото диамантено зелено е тестван за пръв път в това проучване с оглед възможно приложение за индустриално пречистване на водата. Оптималните условия за отстраняване на 25 ppm диамантено зелено багрило от 100 mL синтетична отпадна вода чрез отпадъци от моркови са: 0.6 g адсорбент, pH 2.0, 40 минути контактно време, 30 °C температура и 150 rpm скорост на разбъркване. Когато се използват обелки от картофи, оптималните условия са: 0.4 g адсорбент, pH 1.0, 15 минути контактно време, 30 °C температура и 50 rpm скорост на разбъркване. Различните условия, влияещи върху сорбцията на багрилото диамантено зелено от вода, са оптимизирани чрез изотермични и кинетични изследвания. Изотермичните проучвания показват, че хемисорбцията преобладава над физисорбцията, като максималният капацитет за отстраняване чрез отпадъци от моркови и обелки от картофи е съответно 4.14 и 3.13 mg/g. Кинетичните изследвания сочат модел от псевдо-втори порядък. И двата сорбента са подходящи за отстраняване на багрилото диамантено зелено от отпадни води.

Analysis of caffeine contents in commercial beverages and tea samples of Pakistan using UV/Visible spectrometry

R. Rehman*, S. Ashraf

Institute of Chemistry, University of the Punjab, Lahore-54590, Pakistan

Received April 13, 2016; Accepted May 26, 2017

In this study, caffeine contents in tea samples and beverages were determined photometrically using UV/Visible spectrometry which is a rapid, precise and accurate method. Calibration solutions were prepared in the concentration range of 1-25 ppm from a 100 ppm stock solution. Absorbance of all calibration solutions was measured at the absorption maximum at 274 nm. Caffeine was extracted from tea samples and beverages by chloroform and reading was performed against chloroform as a reference. The concentration of unknown samples was read from the calibration graph. Various concentrations of caffeine were present in the tea samples and beverages. Results showed that in case of tea samples the highest amount of caffeine (16.111 mg/g) was present in Tetley and the lowest amount (0.251 mg/g) - in Ghatnctr. In case of beverages the highest amount of caffeine (222.3 mg/L) was present in Boost and the lowest (0.101 mg/L) - in 7-up.

Keywords: Beverages, tea samples, UV/Vis spectrometry, caffeine.

INTRODUCTION

Caffeine is an alkaloid belonging to the methylxanthines family. pH of a 1% solution of caffeine in water is 6.9. It is a stimulant drug having bitter taste in its pure state and it is white crystalline xanthine [1]. 1,3,7-trimethylxanthine is the systematic name of caffeine. Other names of caffeine are trimethylxanthine, theine, mateine, guaranine and methyl theobromine. Formula of caffeine is given in Fig. 1 and molar mass is 194.19 g/mol. It is an odorless white powder or needles. Density of caffeine is 1.2 g/cm³. Caffeine solubility is very low in water, slight in ethyl acetate, pyrimidine, pyrrole, acetone, and very high in petroleum ether, ether, benzene and chloroform. The melting point of caffeine is 237 °C and the boiling point is 178 °C (sublimation) [2].

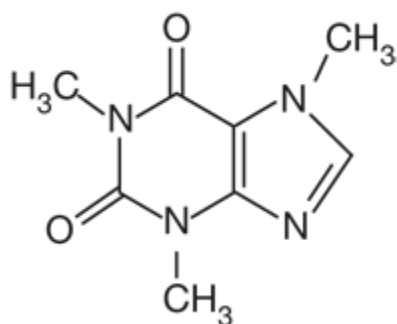


Fig. 1. Caffeine structure.

Acidity of caffeine is 10.4. At room temperature caffeine solubility in water is moderate (2 g/100 mL), but very high in boiling water (66 g/100 mL). It is also moderately soluble in ethanol (1.5 g/100

ml) [3]. Caffeine is weakly basic having a pK_a value of 0.6; a strong acid is required to protonate it. Caffeine is included in achiral molecule [4] because it contains no stereogenic centres. Methylation of theobromine forms caffeine. Caffeine and related compounds contain an imidazole ring fused to a pyrimidine ring [5]. The metabolic product of caffeine is divided into three primary metabolites (paraxanthine 84%, theobromine 12% and theophylline 4%) - metabolic products formed in the liver. Caffeine is an antagonist of adenosine. It possesses diuretic action (favors urination) [6].

There are many sources of caffeine including tea, coffee, soft drinks, energy drinks, chocolates, cocoa beans, etc. Tea is a common major source of caffeine. Certain types of tea such as black tea and oolong tea contain a higher concentration of caffeine, as compared to other types of tea, such as green tea. Small amounts of theobromine are present in tea. The latter also contains theophylline at a slightly higher level as compared to coffee. The colour of tea is not a good indicator of caffeine amount because the colour of caffeine is white [5].

Tea is included in aromatic beverages; preparation of tea is by pouring hot or boiling water over leaves of the tea plant. China is the origin of tea as a medicinal drink [7]. Tea is derived from a plant called *Camellia sinensis*, which is a shrub native to China and India (Asian countries) but its cultivation also occurs in tropical and subtropical areas. Tee contains unique antioxidants called flavonoids. During the seventeen century it became popular in British countries. The British are responsible for the introduction of tea in India. Anti-inflammatory and neuroprotective properties have been known in tea catechins, helping to regulate food consumption [1].

* To whom all correspondence should be sent:

E-mail: grinorganic@yahoo.com

The risk of diseases such as stroke, cognitive impairment, and osteoporosis is lower for elderly people consuming green tea. Many other nutrients including anti-oxidants, minerals, caffeine, vitamins, amino-acids, theobromine and theophylline which have strong beneficial effects on human health are also present in tea. The tea differences arise from geography, growing conditions, method of processing and time of vintage. White, green, black and oolong tea include herbal infusions, also called herbal tea. Each type of tea has specific characteristics including different taste and various benefits to health. There are five basic types of tea: black, oolong, green, white, and puer.

The purest form of tea includes white tea and has light flavor and color, the most delicate form of all teas is white tea. Green tea is the most favorite choice of beverage in Asia. It is made of steamed tea leaves having high amount of epigallocatechin Gallate (EGCG). Green tea has a subtle flavor. Non-fermented tea is green tea having catechins in a large amount as compared to black tea or oolong tea. Wu long tea is another name of Oolong tea, having a flavor full aroma. Oolong tea is undergoing partial oxidation. The taste and fragrance of fresh flowers are often compared to Oolongs. Oolong tea contains large amounts of antioxidants. Black tea has a robust flavor. Aged black tea is imported from China. It is incredibly deep and rich in flavor without bitterness. It is made of fermented tea leaves; black tea has the greatest caffeine content and a high quantity of polyphenols such as flavonoids. These flavonoids work against harmful agents [8]. Y The most common component of soft drinks is caffeine, such as Coca-Cola, which is derived from kola nuts. 10 to 50 mg of caffeine per serving are present in soft drinks but the energy drink Bull contains 80 mg of caffeine per serving [9].

There are many advantages of caffeine like: it is used to reduce physical fatigue due to its medicinal properties [6]. Caffeine can induce hair growth. Dopamine concentration increases in the brain by caffeine which helps to ease depression. Glutamate and dopamine concentrations enhance by caffeine in shell of nucleus accumbens [10]. Caffeine increases stamina, protects the person from eyelid spasms, cataracts, prevents skin cancer. Caffeine can decrease the risk of several types of cancer including liver and colorectal cancer. These cancer risks are reduced by drinking coffee. Caffeine reduces the risk of type 2 diabetes and Parkinson's disease. In type 2 diabetes, the ability to use insulin regulates blood sugar effectively in the body [11].

There are many disadvantages of caffeine, e.g., it can cause anxiety if high doses of 300 mg or higher

are taken [12], accelerates bone loss at the spine in elderly postmenopausal women and causes an increase in the likelihood of experiencing auditory hallucinations. The central and sympathetic nervous systems are stimulated by caffeine which results in an elevation of hormones which causes the body to enter in a state similar to that of the fight or flight response [11]. Excess or higher dosages of caffeine can cause several problems that include high blood pressure, restlessness, irritability, anxiety, heartburn, headache (sometimes severe), sleeplessness, increased heartbeat, nausea, enhanced urination, heart palpitations, gastrointestinal disturbance (diarrhea), dizziness, nervousness and jitters.

The absorbance of calcium, magnesium, zinc, chloride and sodium in the body is reduced by using caffeine. Osteoporosis is caused by caffeine. Iron present in blood is oxidized by caffeine as much as 75%. Sugar and fatty acid concentrations in blood and homocysteine level increase by caffeine. Melatonin formation is reduced by caffeine [13].

Beverages are drinks containing caffeine mainly for human use [14]. There are two types of beverages: alcoholic and non-alcoholic beverages. Non-alcoholic drinks include those beverages that have a small quantity of alcohol or alcohol may not be present. Examples of non-alcoholic beverages are non-alcoholic wine, energy drinks including Red Bull, Monster and Power House. Alcoholic beverages are those which contain alcohol in varying amounts. Examples of alcoholic drinks are cider, wine, etc.

There are many advantages of drinking tea. Antioxidants present in green tea affect the growth of bladder, breast, stomach, pancreatic, lungs and colorectal cancers. The antioxidant EGCG is present in green tea, which can treat various diseases. Green tea has health enhancing benefits as compared to black and oolong tea [15]. White tea can help you look younger, white tea helps to inhibit wrinkle production by strengthening the collagen and elastin. Antioxidants found in oolong tea decrease the bad cholesterol levels. Wuvi is a variety of oolong tea used as a weight loss diet; green tea also reduces the bad cholesterol amount and prevents platelet clumping [16].

There are many disadvantages of drinking tea. Fluoride is present in all tea leaves, mature leaves contain a higher amount of fluorides as compared to young leaves from the same plant [17]; overconsumption of tea can cause fluorosis in humans [18]. Tea leaves contain some amount of aluminium [19]. The levels are safe but sometime that level of aluminium becomes the cause of

Alzheimer's disease [20]. The symptoms of Alzheimer's disorder are lack of learning skills, loss of memory, lack of imagining power and reasoning skills in acute cases. Oxalates are also present in tea, kidney stone are formed by oxalates. Oxalates are accumulated in the kidney tissue [21]. Large amounts of black tea use by men, enhance risk of prostate cancer by 50% [22]. Uv/Vis spectrometry is used for the determination of caffeine in tea, coffee and beverages [23].

EXPERIMENTAL WORK

Chemicals

The chemicals used in this study include hydrochloric acid (HCl), chloroform (CHCl_3) obtained from Friend's laboratory chemical, sodium carbonate (Na_2CO_3) obtained from Riedel-de Haen and caffeine obtained from AppliChem.

Sample collection

Different samples of tea and beverages were purchased from different markets of Kasur (Pakistan). Different types of energy drinks and soft drinks including Coca-Cola, Pepsi, diet cola, mountain dew, Gourmet cola, Boost, Panda, Red bull, Sting, Mask, Pepsi diet, Power house were purchased from the local markets in Pakistan.

Instrument

The UV/vis spectrometer Labomed UVD-3500 was used for the analysis of caffeine in different samples of tea and beverages.

Calibration solutions preparation

Caffeine stock solution of 1000 ppm was prepared by dissolving 0.1 g of pure caffeine in 100 mL chloroform. It was analyzed by UV/Vis spectrometry for determining λ_{max} and the resulting spectrum is shown in Fig. 2. Further dilutions were prepared in the range of 1-25 ppm and their absorbances were measured at λ_{max} 274 nm as shown in Fig. 2. The resulting values are given in Table 1. They were used to draw the calibration line for caffeine analysis as shown in Fig. 3. Cuvettes of plastic were not used because chloroform dissolved plastic.

Extraction of caffeine from tea

All glass apparatus was rinsed with chromic acid and distilled water before use. 2 g of dried tea powder was taken in a beaker and 20 mL of distilled water was added to it and boiled. After boiling, 2 g of sodium carbonate was added for precipitating tannins, then filtered. The filtrate was heated and concentrated to 5 mL. Then 5 mL of chloroform was

added for extraction of caffeine using a separatory funnel. The extract was analyzed for caffeine contents and the average values are reported in Table 2.

Extraction of caffeine from beverages

A beverage portion was drawn by a 10 mL pipette and poured directly in a separatory funnel, then 1 mL of 20% (w/v) sodium carbonate solution and 5 mL of chloroform were added and shaken for few minutes. The lower (organic) layer containing caffeine was taken in a sample cell [6].

Preparation of a sample solution of tea

The best solvent used for the direct UV-Vis spectrophotometric determination of caffeine in tea and beverages was chloroform, as shown by Maidon [1]. He compared four solvents for caffeine analysis including chloroform, methanol, ethyl acetate and water. Among them, chloroform displayed the best ability to dissolve tea leaves [1]. Initially 0.1 mL of the extract of tea, present in the sample cell was taken to the test tube and 5 mL of chloroform was added to it. Then the absorbance of the solutions was measured at 274 nm. Three samples of each brand were used for caffeine analysis and the average values are given in Table 2.

Preparation of a sample solution of beverages

0.1 mL of the extract of beverages, present in the sample cell, was dissolved in 5 mL of chloroform to form the sample solution. Reading was performed at a wavelength of 274 nm. Three samples of each brand were used for caffeine analysis and the average values are given in Table 3.

RESULTS AND DISCUSSION

Calibration line preparation for caffeine analysis

In Fig. 2 the caffeine spectrum is given which indicates that its maximum absorption occurs at 274 nm. So further photometric analysis of all samples was carried out at 274 nm.

In Fig. 3 the calibration curve for caffeine was drawn by using calibration solutions of caffeine in the concentration range of 1-25 ppm and absorbance was measured on a UV/Vis spectrometer at wavelength 274 nm, as shown in Table 1.

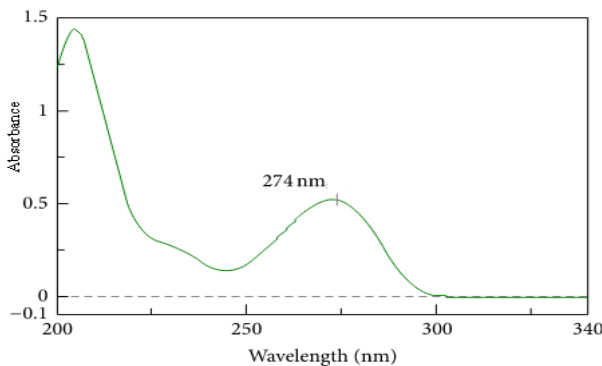


Fig. 2. Caffeine spectrum

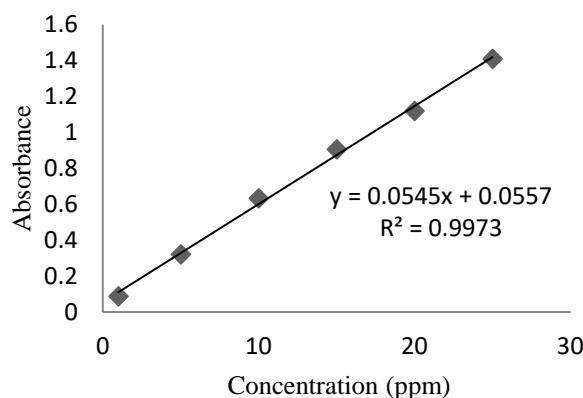


Fig. 3. Calibration curve of caffeine.

Table 1. Absorbance of the calibration solutions of caffeine

No.	Concentration (ppm)	Absorbance
1	1	0.088
2	5	0.322
3	10	0.633
4	15	0.906
5	20	1.12
6	25	1.411

Determination of caffeine in different tea samples

The UV/Vis spectrometric method was used for the quantitative analysis of caffeine in different samples of tea and beverages. This method is rapid, cheap, simple, reproducible, accurate and precise. The concentration of caffeine in the tea samples was determined in triplicate and the average values are given in Table 2. Some tea samples contain large amounts of caffeine, and others less. Thirty two different samples of tea were analyzed. The level of caffeine in Tetley, Lipton, Alkozoay, Doctor, Utility and Vital tea samples lies in the range of 16.111–11.371 mg/g, whereas in Tezdam, A1 Kark, Danadar, Supreme samples, it was in the range of 7.622–6.44 mg/g. In Khuli Kenya, Qamar, Bangladesh Kenya, Kenya, Islam Brand Kenya, Golden Kenya and Green leaf samples, the concentration of caffeine was in the range of 5.744–

3.262 mg/g. The lowest range was found in the tea samples of Sapna, Thomata, Malnya 8, Sea Shad 49, Kanya F1, Kagra, Kateve F1, Malnya F1, Kagway, Tameta, Manga, Sea shad 55 and Ghatnctr. The Tetley sample had the highest amount of caffeine and the Ghatnctr – the lowest one. Al Rasbi analyzed different tea samples and according to his result Lipton tea contained 22 mg/g of caffeine but in this analysis Lipton tea contained 13.672 mg/g of caffeine [24].

Table 2. Determination of caffeine in different tea samples available in Pakistan.

Sample	Caffeine Concentration (mg/g)	Sample	Caffeine Concentration (mg/g)
Ghatnctr	0.251	Green leaf	3.262
Kanya F1	0.312	Kenya Golden Kenya	3.421
Sea shad 55	0.363	Bangladesh Kenya	3.791
Malnya 8	0.422	Qamar	4.353
Kagway	0.421	Khuli	5.712
Seashad49	0.430	Kenya	5.744
Kagra	0.430	Supreme	6.442
Malnya F1	0.433	Danadar	6.821
Kateve F1	0.511	A1 kark	6.991
Thomata	0.582	Tezdam	7.622
Manga	0.591	Vital	11.371
Tameta	1.011	Doctor	11.532
Sapna	2.221	Utility	12.071
Lajpal	2.273	Alkozoay	12.892
Islam brand Kenya	2.952	Lipton	13.672
Alaicee tea	3.006	Tetley	16.111

Result obtained in these analyses were different from the reported one, maybe due to the different place, laboratory conditions and most importantly different tea brewing method. Tea brewing conditions and time are mainly responsible for caffeine contents determination by UV/Visible spectrometry.

Analysis of caffeine in different beverages

In beverages different concentrations of caffeine were found. Various analytical techniques are used for the analysis of caffeine in different beverages, like: high performance liquid chromatography, derivative spectrophotometry, ion chromatography, Fourier transform infrared spectrophotometry, partial least squares method, solid phase Fourier transform-Raman spectrometry, a novel auto analyzer method, continuous-flow solid-phase spectrophotometric sensing method, GC/MC method, sample pre-treatment method, solid phase

extraction method, multivariate method, reversed phase ultraviolet visible high performance liquid chromatography method, etc. In this study, UV/Vis spectrometric method was used. In table 3 the concentration of caffeine in different beverages is reported as an average of three replicates.

Fourteen different beverages were analyzed. The level of caffeine in Coca Cola, Pepsi, 7-up, Gourmet Cola, Mountain Dew, Big Apple, Diet Cola, and Pepsi Diet was found to be in the range of 0.101-96.1 mg/L. The concentration of caffeine in Boost, Power Horse, Panda, Red Bull, Sting, Mask was in the range of 130.2-222.3 mg/L. In all of these samples, Boost had the largest amount of caffeine (222.3mg/L), whereas the smallest amount (0.101 mg/L) was found in 7-up. Carbonated soft drinks contain lower amounts of caffeine as compared to energy drinks available in the commercial market.

Tauta *et al.* [6], also worked on carbonated soft drinks and energy drinks. Tauta used a UV-Vis spectrometric method for the determination of caffeine content in different beverages. The result obtained by this method was that carbonated Coca cola had small amount of caffeine and Red Bull had large amount of caffeine. Kalra also worked on beverages and showed that the highest concentration of caffeine was present in Power-ex (46 µg/mL) and the lowest concentration - in XXX (19.5 µg/mL) [25].

Musa Ali also worked on beverages. The result obtained was that energy drinks contained large amount of caffeine as compared to carbonated soft drinks [2]. Results obtained in these analyses were not similar, maybe due to the different place, seasonal changes and different laboratory conditions.

MgO supported catalysts with 5 wt. % Co₃O₄ or CoFe₂O₄ loading were prepared by incipient wetness impregnation [15]. Bulk Co₃O₄ and CoFe₂O₄ were prepared by the precipitation/co-precipitation method.

Table 3. Determination of caffeine in different beverages available in Pakistan.

Sample	Caffeine Concentration (mg/10mL)	Caffeine Concentration (mg/L)	Sample	Caffeine Concentration (mg/10mL)	Caffeine Concentration (mg/L)
7 up	0.001	0.101	Gourmet cola	0.381	38.1
Panda	0.091	9.1	Diet cola	0.812	81.2
Big Apple	0.102	10.2	Coca cola	0.961	96.1
Mountain dew	0.105	10.5	Power horse	1.302	130.2
Mask	0.17	17	Sting	1.643	164.3
Pepsi	0.199	19.9	Red bull	1.914	191.4
Pepsi diet	0.319	31.9	Boost	2.223	222.3

XRD patterns of the samples were obtained on a TUR M62 powder X-ray diffractometer (XRD) using Co-K α radiation ($\lambda = 1.789 \text{ \AA}$) at 40 kV and 20 mA. The morphology of the catalysts was characterized by a JEOL JEM 2100 high resolution transmission electron microscope (TEM) using an accelerating voltage of 200 kV. Two basic regimes of microscope mode were used – bright field transmission microscopy (TEM) and selected area electron diffraction (SAED). The pH of the point of zero charge (pH_{PZC}) of the catalysts was determined by the pH drift method [17]. The amount of cobalt and iron in the prepared samples as well as the concentrations of leached Co and Fe in the solution were measured by atomic absorption spectroscopy (AAS, Perkin-Elmer).

Catalytic oxidation of RhB with PMS was carried out in a 400 cm³ glass reactor at 293 K with constant stirring at around 400 rpm. In a typical experimental procedure, a fixed amount of catalyst was added to a 200 cm³ solution containing 50 mg dm⁻³ of RhB and the suspension was stirred for 30 min to achieve adsorption-desorption equilibrium. The reaction was initiated by addition of oxidant to attain the predefined PMS/RhB molar ratio. Aliquots of 4.0 cm³ withdrawn from the mixture at given time intervals were immediately mixed with 1 mL methanol to quench the reaction. The RhB concentration in aqueous solution was determined by means of UV/Vis spectrophotometry (Cintra 101, GBS) at 554 nm. All tests were conducted in triplicate to ensure reproducibility of experimental results.

CONCLUSIONS

UV/Vis spectrophotometry was used for the determination of caffeine in tea samples and beverages. Caffeine is the world's most widely consumed psychoactive drug. It is important to obtain information about the drinks because they

are widely consumed all over the world. Various analytical techniques are used for tea analysis like HPLC because these technique has high accuracy and precision but UV-Vis spectrophotometry is mostly used because it is cheap and easily available in laboratories. Results showed that in case of tea samples the largest amount of caffeine was present in Tetley and the smallest amount - in Ghatnctr. In case of beverages the largest amount of caffeine was present in Boost and the smallest amount - in 7-up.

REFERENCES

1. A. Maidon, A. O. Mansoer, H. Sulistyarti, *J. Appl. Sci. Res.*, **8**, 2439 (2012).
2. M.M. Ali, M. Eisa, M.I. Taha, B.A. Zakaria, A. A. Elbashir, *Pak. J. Nut.*, **11**, 336 (2012).
3. A. Mumin, K.F. Akhter, Z. Abedin, Z. Hossain, *Malaysian J. Chem.*, **8**, 45 (2006).
4. A. Ascherio, S.M. Zhang, M.A. Hernán, I. Kawachi, G.A. Colditz, F.E. Speizer, W.C. Willett, *Ann. Neurol.*, **50**, 56 (2001).
5. H. N. Wanyika, E. G. Gatebe, L. M. Gitu, E. K. Ngumba and C. W. Maritim, *Afri. J. Food Sci.*, **4**, 353 (2010).
6. A. Tautua, W.B. Martin, E.R.E. Diepreye, *Adv. J. Food Sci. Tech.*, **6**, 155 (2014).
7. T. Atomssa and A.V. Gholap, *Afr. J. Pure & Appl. Chem.*, **5**, 1 (2011).
8. A.B. Sharangi, *Food Res. Int.*, **42**, 529 (2009).
9. D. K. Bempong, P. J. Houghton, K. Steadman, *Pharma. Bio.*, **31**, 175 (1993).
10. D. Mejia, E. Gonzalez, R. Mares, *J. Brain, Behave. & Immune.*, **23**, 721 (2009).
11. D. Graham, *Nutr Rev.*, **36**, 97 (1978).
12. A. Smith, *Food Chem. Toxic.*, **40**, 1243 (2002).
13. Wiseman, S.A. Balentine, D. A. Frei, *Critical Rev. Food Sci. Nut.*, **37**, 705 (1997).
14. C.O. Ogah, O. Tobebe, *J. Innovative Res. Eng. Sci.*, **3**, 404 (2012).
15. I. A. Siddiqui, M.M. Mukhtar, V.M. Saleem, *J. Mol. Nut. Food Res.*, **50**, 130 (2006).
16. M.L. Bunker, M. McWilliams, *J. Am. Diet. Assoc.*, **74**, 28 (1979).
17. M. H. Wong, K. F. Fung and H.P. Carr, *Toxicology lett.*, **137**, 111 (2003).
18. K.F. Fung, M.H. Wong, *J. Sci. Food Agr.*, **84**, 1469 (2004).
19. R. Street, O.Drabek, J. Szakova, L. Mladkova, *J. Food Chem.*, **104**, 1662 (2007).
20. G. Schwalfenberg, Stephen. J. Genuis, I. Rodushkin, *J. Toxicology*, **2013**, 8 (2013).
21. M. Liebman, S. Murphy, *Nutrition Res.*, **27**, 273 (2007).
22. K. Shafique, H. Leung, C. Hart, D.S. Morrison, *Nutr Cancer*, **64**, 790 (2012).
23. S. Armenta, S. Garrigues, M. de la Guardia, *Anal Chim Acta.*, **547**, 197 (2005).
24. M.M. Al Rasbi, S. A. Khan, *Scholars Acad. J. Biosci.*, **1**, 67 (2013).
25. K. Kalra, S. Kumar and J. Maithani, *Int. J. Res. Dev. Pharm. L. Sci.*, **2**, 1214 (2011).

АНАЛИЗ НА СЪДЪРЖАНИЕТО НА КОФЕИН В ТЪРГОВСКИ НАПИТКИ И ПРОБИ ОТ ЧАЙ С ПОМОЩТА НА УВ-СПЕКТРОМЕТРИЯ

Р. Рехман*, С. Ашраф

Институт по химия, Университет в Пунджаб, Лахор-54590, Пакистан

Постъпила на 13 април, 2016 г.; приета на 26 май, 2017 г.

(Резюме)

В това изследване се определя фотометрично съдържанието на кофеин в чаени преби и в напитки с помощта UV/Vis-спектрофотометрия. Методът е бърз и точен. Калибровката е направена в интервал от концентрации 1-25 ppm от изходен разтвор от 100 ppm. Абсорбцията на всички калибрационни разтвори при абсорбционен максимум при 274 nm. Кофеинът се екстрагира от пробите с хлороформ, който се използва като фон при фотометрията. Резултатите показват, че в случая на чаени преби кофеинът е в по-голямо количество на кофеин (16.111 mg/g) в чая „Tetley“, а най-ниско – в Ghatnctr (0.251 mg/g). При напитките най-високо е съдържанието в Boost (222.3 mg/L), а най-ниско - 7-up (0.101 mg/L).

Experimental studies on a horn-shaped booster pellet

L.-Sh Hu^{1*}, B.-F. Sun²

¹School of Environment and Safety Engineering, North University of China, 030051, Taiyuan, Shanxi, P. R. China

²State Key Laboratory of Explosion Science and Technology, Beijing Institute of Technology, 10081, Beijing, P. R. China

Received September 26, 2016; Accepted July 17, 2017

All insensitive munitions contain explosive trains which need to meet insensitive munitions criteria but reliably initiate the main charge explosives. The traditional cylindrical booster pellets have insufficient energy output for reliably initiating the insensitive main charge explosives. To ensure that the requirement can be achieved, a horn-shaped booster pellet having high initiation capacity was designed and experimentally studied. The results show that the horn-shaped booster pellet has higher initiation capacity than the cylindrical booster pellet for the same mass and density of explosive. The convergence pressure of the horn-shaped booster pellet is 34 GPa, which is higher than the value of 27 GPa for the cylindrical booster pellet.

Keywords: booster pellet, insensitive main charge, pressure, initiation capacity.

INTRODUCTION

The first demonstration of the Munroe effect for high explosives was achieved by Munroe C. E. in 1885 [1]. In one of his experiments, Munroe observed that when a cavity was formed in a cylinder of explosive, opposite the point of initiation, the depth of the crater produced in the steel target was deeper compared with the cylindrical explosive without cavity. The increase in penetration resulted from the focusing of the detonation products by the hollow cavity. The history of shaped charges was discussed in reference [2].

Now, the shaped charge effect is widely applied in the following fields: the common term in military terminology for shaped charge warhead is high explosive anti-tank (HEAT). HEAT warheads are frequently used in anti-tank guided missiles, unguided rockets, rifle grenades, and various other weapons. In non-military applications, shaped charges are used in the explosive demolition of buildings and structures, in particular for cutting through metal piles, columns and beams [3]. Shaped charges are used most extensively in the petroleum and natural gas industries, in particular in the completion of oil and gas wells, in which they are detonated to perforate the metal casing of the well at intervals to admit the influx of oil and gas [4]. Shaped charge technique is also regarded aimed at the formation of hypervelocity fragments for the investigation of space debris effects on shielding screens [5, 6]. Smirnov [7] considered the problem of non-stationary formation of a cumulative jet in a medium that offers resistance to the motion of the jet and obtained an analytical solution of the non-

stationary problem. However, the number of studies using the shaped charge effect to initiate insensitive explosives is limited.

The insensitive main charge explosives are assuming a key role in the development of modern weapons. The exploitation of the insensitive munitions technology resulted in improved survivability from accidents, enemy actions, weapon systems and their associated platforms [8]. The munitions contain a number of explosive trains to provide reliable initiation and detonation transfer. The main charge explosives filled in the weapons are becoming increasingly insensitive to hazard stimuli. The traditional method of increasing the energy output for reliably initiating the insensitive main charge explosives is to increase the size and amount of the booster explosives [9]. This approach resulted in the explosive train becoming a significant factor in weapons vulnerability.

The developmental efforts in booster explosives have therefore been aimed at highly effective booster charge structures that reliably initiate insensitive main charge explosives in small size and quantity.

Dallman [10] investigated the initiation capacity of a hemispherical booster pellet and reported that its output is powerful even when it is small in size. Spahn [11, 12] conducted studies on an embedded can booster and also a booster explosive ring. The results showed that the initiation capacities of the embedded can booster and booster explosive ring are more powerful than the initiation capacity of a cylindrical booster pellet. In a recent work of the authors [13], the initiation capacities of the ring and conical ring booster pellets were studied. The results showed that the initiation capacities of the ring and conical ring booster pellets are higher than those of

* To whom all correspondence should be sent:

E-mail: hlsly1314@163.com

the cylindrical pellets. The energy output of the conical ring booster pellet was found to be higher than that of the ring booster pellet.

In this paper, a booster pellet with a horn-shaped cavity was experimentally studied. The initiation capacities of horn-shaped and cylindrical booster pellets were compared.

DESIGN THEORY

In order to produce a powerful convergence shock wave, the products moving to the focus from different points of the explosive surface should be simultaneously converged. The problem in two dimensions was studied and an “energy-convergence” curvilinear equation was deduced. The diagram of the energy-convergence surface is shown in Fig. 1.

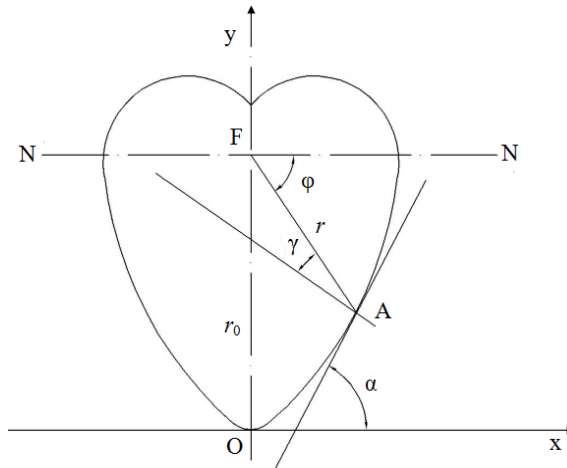


Fig. 1. Diagram of the energy-convergence surface

Origin of the coordinates is set on the focus of this curve. Suppose explosion starts from the point O. According to the Fermi principle, it can be got that

$$\frac{\widehat{OA}}{D} + \frac{AF}{\bar{u}} = \frac{OF}{\bar{u}} = \text{const} \quad (1)$$

where point A is any point along the charge surface, point F is the convergence focus of explosion products, arc OA is the propagation distance of detonation wave, lines AF and OF are the propagation distances of explosion products. D is the detonation velocity, \bar{u} is the velocity of explosion products. Then, the length expression of arc OA could be gained,

$$\widehat{OA} = \int_{\frac{\pi}{2}}^{\phi} \sqrt{r^2 + \left(\frac{dr}{d\phi}\right)^2} d\phi = (OF - AF) \frac{D}{\bar{u}} = \frac{D}{\bar{u}} (r_0 - r) \quad (2)$$

$$\frac{D}{\bar{u}} (r_0 - r)$$

where r is the length of line AF, r_0 is the length of line OF, ϕ is the angle between line FN and line FA. Through ϕ differential to Equation (2), it gets

$$\frac{dr}{r} = -\frac{d\phi}{\sqrt{\frac{D^2}{\bar{u}^2} - 1}} \quad (3)$$

solve it and then,

$$r = r_0 e^{\frac{\phi + \frac{\pi}{2}}{\sqrt{\frac{D^2}{\bar{u}^2} - 1}}} \quad (4)$$

This is the logarithmic spiral equation.

After the surface of revolution (rotation axis is line OF) is formed, the energy-convergence surface that forms the convergence shock wave could be calculated. As we know, the logarithmic spiral has the following property: the angle between the tangent line of any point A and the radius vector is a constant. It can be seen clearly from Fig. 1 that this angle is $90^\circ - \gamma$ (γ is the angle between the normal line of any point A and the radius vector), and $90^\circ - \gamma = 180^\circ - (\alpha + \phi)$ (α is the inclination angle of the tangent line).

Therefore,

$$\gamma = \alpha - 90^\circ + \phi \quad (5)$$

Since

$$\tan(90^\circ - \alpha) = \cot \alpha = \frac{\frac{r}{r'} - \tan \phi}{\frac{r}{r'} \tan \phi + 1} = \frac{\frac{r}{r'} - \tan \phi}{\frac{r}{r'} \tan \phi + 1} \quad (6)$$

$$\tan[\arctan \frac{r}{r'} - \phi] = \tan[-(\phi + \gamma)]$$

So,

$$\arctan \frac{r}{r'} = -\gamma \quad (7)$$

$$\frac{r}{r'} = -\tan \gamma \quad (8)$$

However, we have known that,

$$\frac{r}{r'} = -\frac{1}{\sqrt{\frac{D^2}{\bar{u}^2} - 1}} \quad (9)$$

Therefore,

$$\tan \gamma = \frac{1}{\sqrt{\frac{D^2}{u^2} - 1}} \quad (10)$$

$$\sin \gamma = \frac{u}{D} \quad (11)$$

So, the logarithmic spiral is the sole curve during focusing of explosion products, the logarithmic spiral not only has the property of Fermi principle, but also could guide the explosion products from every surface element to the focus at the same parameters and same angle.

The volume charge is formed by rotation of the logarithmic spiral centered as line OF. It could produce convergence shock wave of explosion products. If the volume charge is large enough in size, it could generate pressure of millions of atmospheric pressure at the focus. The average initial pressure of the explosion products is equal to 100000 atmospheric pressures.

The surface formed by rotation of the logarithmic spiral is the “energy-convergence” surface of the charge. Cut the charging part (e.g. along the plane N-N) that is formed by rotation of a logarithmic spiral, and the actual energy-convergence charge which could generate high pressure could be acquired.

According to that, the horn-shaped booster pellet was designed and it is shown in Fig. 2.

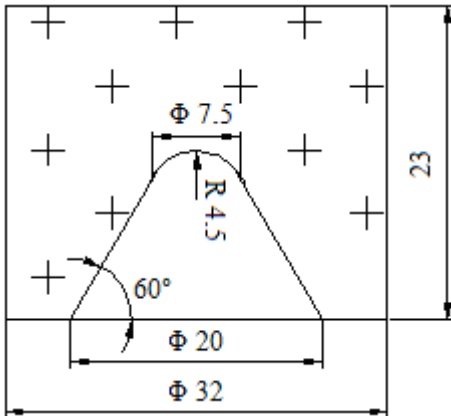


Fig. 2. Structure and size of the horn-shaped booster pellet

EXPERIMENTS

Experimental method

Four different methods were selected to comprehensively study the initiation capacity of the horn-shaped booster pellet [14, 15].

(1) Main charge detonation distance method. The main charge is initiated by the booster pellet. The

detonation distance of the main charge represents the initiation capacity of the booster pellet. The detonation distance of the main charge is affected by the initiation energy of the booster pellet. The more powerful the initiation energy is, the longer the detonation distance propagates.

(2) Main charge axial-steel-dent method. In this method, the main charge in contact with the steel witness plate is directly initiated by the booster pellet. The depth of the dent represents the initiation capacity of the booster pellet.

(3) Booster pellet axial-steel-dent method. The booster pellet is in direct contact with the steel witness plate. Initiated by the detonator, the booster pellet detonates and produces a steel dent. The depth of the dent represents the initiation capacity.

(4) Pressure test method. In the pressure test method, low-resistance manganin piezoresistors sensor was used for accurate measurement of the convergence pressure [16, 17].

The convergence pressure could be calculated by using the following relationship:

$$p = 0.9447 + 35.5887 \times \left(\frac{\Delta R}{R} \right) + 6.986 \times \left(\frac{\Delta R}{R} \right)^2 \quad (12)$$

where, R is the resistance of the manganin piezoresistors sensor, ΔR is the variation of resistance, p is the convergence pressure.

In the experiment, a constant current source was used to measure $\Delta U/U$ by an oscilloscope. $\Delta R/R$ was obtained from the following relationship:

$$\frac{\Delta R}{R} = \frac{\Delta RI}{RI} = \frac{\Delta U}{U} \quad (13)$$

where, U is the voltage, ΔU is the variation of voltage, I is the electric current.

Experimental conditions

The plastic-bonded booster explosive PBXN-5 was selected for the experiments. The density of the compacted booster pellet was 1.68 g/cm³. The density and diameter of the cylindrical pellet were 1.68 g/cm³ and 29.58 mm, respectively.

Nitroguanidine-based composite explosive was chosen as the main charge. The nitroguanidine-based composite explosive contains nitroguanidine (NQ), polytetrafluoroethylene (PTFE) and graphite (G).

The steel witness plate was an ordinary carbon steel of size Φ100×50 mm.

Experimental devices

The experimental device of the main charge axial-steel-dent method and the main charge detonation distance method is shown in Fig. 3. The booster pellet axial-steel-dent method is similar to

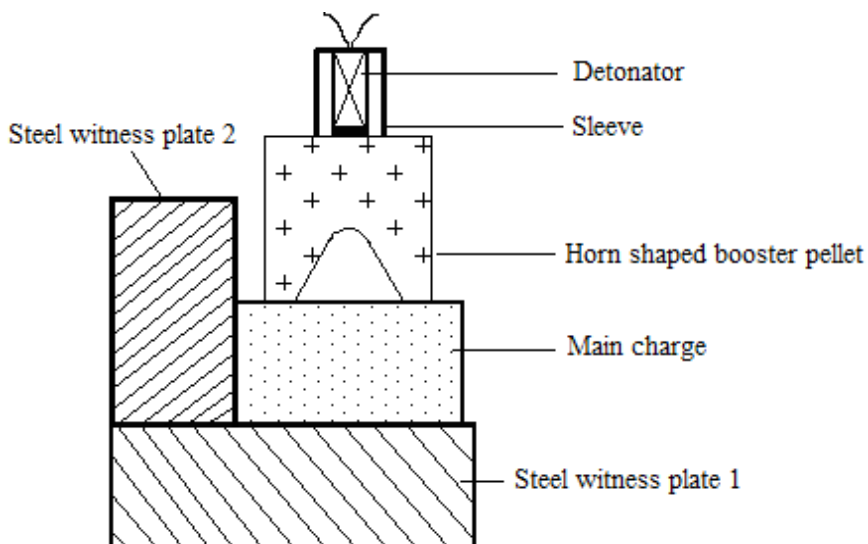


Fig. 3. Experimental device of the main charge axial-steel-dent method and the main charge detonation distance method

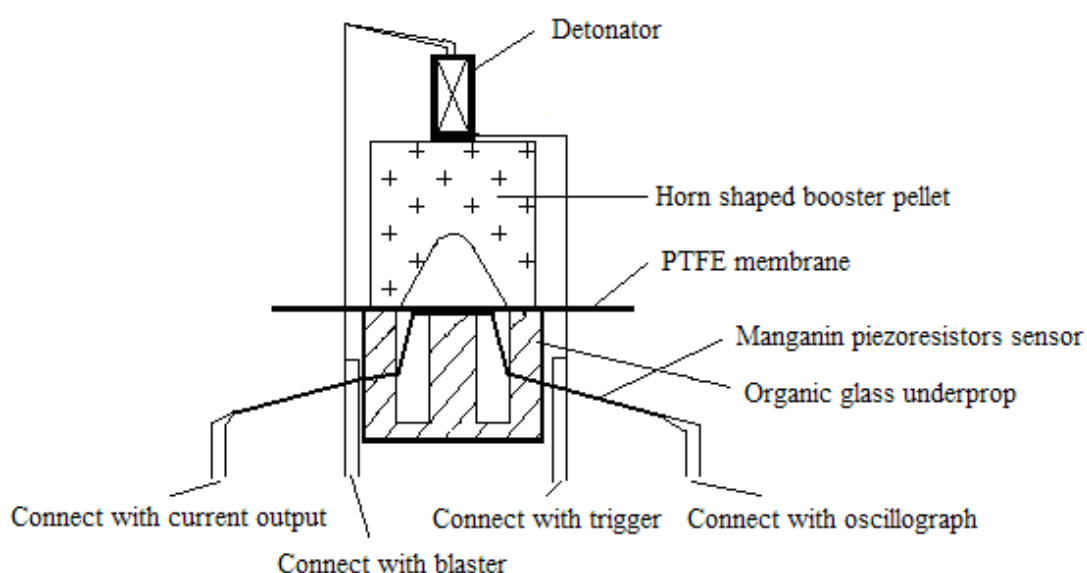


Fig. 4. Installation diagrammatic illustration of the pressure test method

the main charge axial-steel-dent method except that it excluded the main charge and the steel witness plate 2. The testing instrument used for measuring the convergence pressure is illustrated in Fig. 4.

EXPERIMENTAL RESULTS AND DISCUSSION

Comparison of initiation capacities of horn-shaped and cylindrical booster pellets

The initiation capacities of the horn-shaped and cylindrical booster pellets were measured using the main charge detonation distance method. The main charge explosive was an NQ-based composite explosive. The components of the main charge were in the following proportions: NQ/PTFE/G=46/53/1. The density, diameter and height of the NQ-based composite explosive were 1.17 g/cm³, 70.0 and 80.0

mm, respectively. The results obtained from the experiments are presented in Table 1.

The results in Table 1 show that when the main charges were initiated by the horn-shaped booster pellet and the cylindrical pellet at the same density of explosive, the average detonation distance of the main charge initiated by the cylindrical booster pellet is 55 mm. However, the one initiated by the horn shape booster pellet is 75 mm. Therefore, the horn shaped booster pellet has more initiation capacity than the cylindrical booster pellet for the same mass and density of explosive.

The data of the present work are the results of five parallel experiments. The detonation distances of the main charge initiated by the cylindrical booster pellets are 54.5, 54.8, 55.2, 56.2, 56.4 mm, respectively, the variance value of the data is 0.57. The detonation distances of the main charge

Table 1. Results of the initiation capacities of booster pellets for the detonation distance method

Shape	Booster pellet		Main charge		Time of Experiment
	Mass (g)	Height (mm)	Average Detonation Distance (mm)		
Horn-shaped booster pellet	19.6	80±0.2	75.04		5
Cylindrical booster pellet	19.6	80±0.2	55.42		5

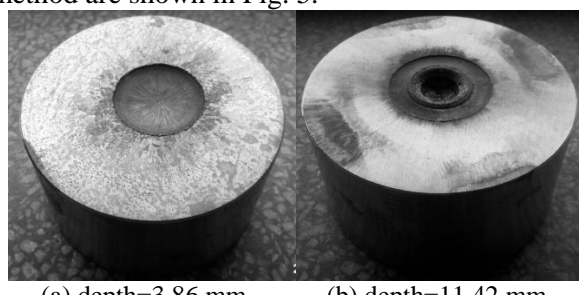
Table 2. Results of the initiation capacities of booster pellets for the axial-steel-dent method and pressure test method

Shape	Mass, (g)	Dent depth of method (2), (mm)	Dent depth of method (3), (mm)	Convergence pressure, (GPa)
Cylindrical	19.7	1.20	2.65	
Cylindrical	22.4	1.46	3.02	
Cylindrical	26.7	1.72	3.44	27
Cylindrical	33.1	1.90	3.86	
Horn-shaped	25.3	2.16	11.62	34

initiated by the horn shape booster pellets are 73.8, 74.1, 75.2, 75.3, 76.8 mm, respectively, the variance value of the data is 1.12. The variance values were small, therefore, it can be reasonably considered that the results are true and considerably credible.

Additional studies on the initiation capacity of horn-shaped booster pellet

Experiments using the main charge axial-steel-dent, booster pellet axial-steel-dent, and pressure test method were also conducted. The components of the main charge were in the following proportions: NQ/PTFE/G=70/29/1. The density, diameter and height of NQ-based composite explosive were 1.20 g/cm³, 42.6 and 40 mm, respectively. The results are shown in Table 2. The pictures of the steel witness plates employed in the booster pellet axial-steel-dent method are shown in Fig. 5.



(a) depth=3.86 mm

(b) depth=11.42 mm

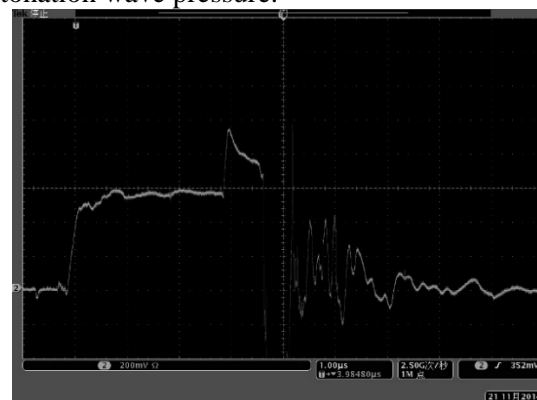
Fig. 5. Steel witness plates for the booster pellet axial-steel-dent method

The pressure waveforms of the cylindrical and horn shaped booster pellets are shown in Figs. 6 (a) and (b), respectively.

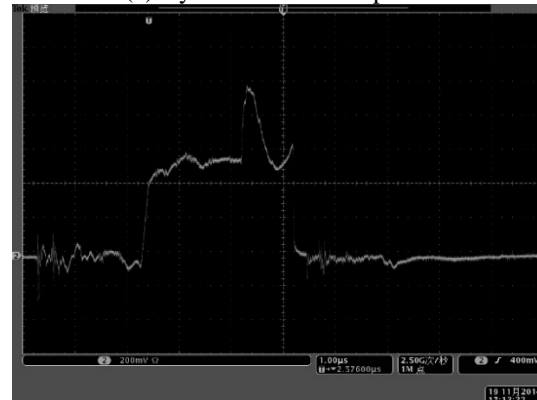
The steel dent depth of the horn-shaped booster pellet is higher than that of the cylindrical booster pellet for both main charge and booster axial-steel-dent methods. It can be seen that the convergence pressure of the new booster pellet is 34 GPa, which

is higher than the value of 27 GPa for the cylindrical booster pellet. The results from the three methods are in good agreement.

From Fig. 5 (b) it can be seen that the hole at the center of the steel witness plate is deep and the ring around the hole is shallow. The hole at the center is produced by the convergence pressure. The ring dent is created by the detonation wave pressure. It is also seen that the convergence pressure is higher than the detonation wave pressure.



(a) Cylindrical booster pellet



(b) Horn-shaped booster pellet

Fig. 6. Pressure waveform of the cylindrical and horn-shaped booster pellets

The dent depth h is expressed as [18, 19]:

$$h = M \frac{(p_0 - \sigma_s)^2}{p_0 \sqrt{p_0 \sigma_s}} r_e \quad (14)$$

where, h is the dent depth, M is a constant determined by the explosive and metal material, p_0 is the pressure of the shock wave, σ_s is the dynamic elastic limit of the metal material, r_e is the explosive radius. So, the higher the shock wave pressure is, the deeper becomes the dent depth. That is to say that the horn-shaped booster pellet has more powerful energy output than the cylindrical booster pellet.

Factors influencing the experimental results

There are two main factors affecting the experimental results.

(1) Effect of PTFE powder content. The main charge explosive contains PTFE powder as the inert material. But the PTFE powder is difficult to be press molded. The more PTFE powder is added, the looser is the main charge. So, the densities of the main charge explosives are variable. The experimental results are not in agreement with each other, but the difference is small.

(2) Effect of the manganin piezoresistors. When the horn-shaped booster pellet is initiated, the detonation wave propagates downward in the form of a spherical wave. When the detonation wave reaches the energy cavity surface, the detonation wave attenuates into the shock wave. The shock wave begins to converge towards the energy cavity center, and the output pressure of the bottom center area of the horn-shaped booster pellet is the largest. However, the test point of the manganin piezoresistors sensor is very small, the size of the sensitive area is 0.5×0.5 mm. It is difficult to align the test point of the manganin piezoresistors sensor with the bottom center point of the horn-shaped booster pellet. Therefore, the data of the output pressure are not in agreement with each other, and the maximum one was chosen.

CONCLUSIONS

The initiation capacity of the horn-shaped booster pellet was studied experimentally. Following are the conclusions.

The initiation capacity of the horn-shaped booster pellet is higher than that of the cylindrical booster pellet for the same mass and density of explosive.

The output pressure of the horn shaped booster pellet was studied experimentally. The valve is much

higher than that of the cylindrical booster pellet for the same density of explosive.

Acknowledgement: The project is supported by the Science foundation of North University of China (no. XJJ2016012).

REFERENCES

- 1.C. E. Munroe, *Popular Science Monthly*, **56**, 300 (1900).
- 2.W. Walters: A brief history of shaped charges. 24th International Symposium on Ballistics, New Orleans, LA, 2008, p. 3.
- 3.T. F. Grattan, T. X. Alvarado, *US Patent* 0310940 A1 (2014).
- 4.E. Galante, A. Haddad, N. Marques, *Int. J. Oil Gas Coal Eng.*, **1**, 16 (2013).
- 5.V. F. Minin, I. V. Minin, O. V. Minin, *Acta Astronautica*, **104**, 77 (2014).
- 6.B. V. Rumyantsev, A. I. Mikhaylin, *Acta Astronautica*, **109**, 166 (2015).
- 7.N. N. Smirnov, *Mosc. Univ. Mech. Bull.*, **40**, 1 (1985).
- 8.Department of Defense, Department of Defense Test Method Standard: Hazard Assessment Tests for Non-Nuclear Munitions, MIL-STD-2105B (1994).
- 9.G. T. Flegg, P. J. Frankl, T. T. Griffiths, Explosive train scale shock testing of new energetic materials. QinetiQ, Fort Halstead, Sevenoaks, Kent, TN14 7BP, UK (2010).
- 10.J. C. Dallman, Measurements of detonation-wave spreading and local particle velocity at the surface of 17-mm LX-07 hemispherical boosters. Report No. LA-11414-MS, Los Alamos National Laboratory (1988).
- 11.P. F. Spahn, *US Patent* 5 233 929 (1993).
- 12.P. F. Spahn, *US Patent* 5 221 810 (1993).
- 13.L. -S. Hu, S. -Q. Hu, X. Cao, *Cent. Eur. J. Energ. Mat.*, **9**, 261 (2012).
- 14.L. -S. Hu, Study on the structures of booster pellets having high initiation capacity. North University of China, China (2013).
- 15.China Military Standards, Test methods of initiating explosive devices-part 16: steel dent test. Standard number GJB 5309.16 (2004).
- 16.H. -X. Zhao, Study on characteristics of the detonation propagation for micro-diameter charge. North University of China, China (2008).
- 17.N. K. Bourne, A. M. Milne, R. A. Biers, *J. Phys. D: Appl. Phys.*, **38**, 1984 (2005).
- 18.Y. -C. Liu, Z. -S. Wang, C. -L. Lü, J. -H. Wang, *Journal of North China Institute of Technology*, **22**, 304 (2001).
- 19.J. Bauer, Detonation pressure, hardness of steel and dent depth. 8th Symposium on Explosives and Pyrotechnics, Los Angeles, CA, (1974).

ЕКСПЕРИМЕНТАЛНО ИЗСЛЕДВАНЕ НА РОГО-ОБРАЗНИ ВЗРИВНИ КАПСУЛИ

Л.Ш. Ху^{1*}, Б.Ф. Сун²

¹Училище по околната среда и техника на безопасност, Северен университет на Китай, 030051, Тайюан, Шанси, Китайска НР

²Държавна лаборатория по експлозивни науки и технологии, Пекински институт на технологиите, 10081, Пекин, Китайска НР

Получена на 26 септември, 2016 г.; Приета на 17 юли, 2017 г.

(Резюме)

Всички муниции съдържат детонатори, които трябва да отговарят на определени критерии, но най-вече да инициират взривяването на основния експлозив. Традиционните цилиндрични взриватели нямат достатъчно енергия за надеждното взривяване на основния експлозив. За повишаването на тази надеждност, се предлагат нови рого-образни взриватели, проектирани и изпитани експериментално. Резултатите показват, че новите взриватели имат по-голям иницииращ капацитет от цилиндричните при същата маса и плътност на експлозива. Конвергентното налягане на роговите капсули е 34 GPa, по-високо от налягането при цилиндричните капсули - higher than the value of 27 GPa.

Phytochemical composition and biological activity of *Echium italicum* L. plant extracts

I. D. Bošković^{1*}, D. A. Đukić², P. Z. Mašković², L. G. Mandić²

¹University of East Sarajevo, Faculty of Agriculture, Vuka Karadzica 30, 71 123 East Sarajevo, Bosnia and Herzegovina

²University of Kragujevac, Faculty of Agronomy, Cara Dusana 34, 32000 Čačak, Serbia

Received November 23, 2016; Accepted July 28, 2017

The aim of this study was to assess the biological activity of five different extracts of the plant *Echium italicum* L. and to determine their phytochemical composition. The chloroform, ethyl-acetate, ethanol, acetone and petroleum ether extracts of the plant were examined. The ethanol extract of the plant *E. italicum* had the highest content of total phenolics and flavonoids, while the chloroform and acetone extracts had the highest tannin content. Several different methods were used to determine the antioxidant activity of the tested extracts, and the ethanol and acetone extracts of the plant displayed the best antioxidant activity. HPLC analysis showed that the main phenolic compounds in the tested extracts were rosmarinic acid, chlorogenic acid, *p*-hydroxybenzoic acid and rutin. Evaluation of the antimicrobial activity of plant extracts was conducted by the microdilution method. The results of MIC ranged from 3.91 to 500 µg/ml. Determinations of cytotoxic activity were done according to the MTT assay on human rhabdomyosarcom cells (RD), a cell line derived from human cervix carcinoma (Hep2c) and a cell line derived from mouse fibroblast carcinoma (L2OB). This study suggests that the examined extracts of the plant *E. italicum* L. may serve as sources of antioxidants and antibiotic agents.

Keywords: *Echium italicum* L., phytochemical composition, biological activity.

INTRODUCTION

Throughout history and across the globe, the plant kingdom has provided a variety of medicines. From ancient times, traditional medicinal plants have been known to possess diverse biological activities as antimicrobial, analgetic, anticancer, antipyrexial, and antihypertensive activity and to be an important source of many biological active compounds [1]. Medicinal plants have been used extensively for their health care and remedy of diseases during 2000 years and a high degree of correlation between traditional medicinal plant uses and laboratory analysis has been revealed [2]. Today, using the most modern instrumental methods, detailed qualitative and quantitative analysis, isolation and testing of even traces of substances present in plant tissue is possible [3]. The most interesting area of application of medicinal plant extracts is the inhibition of growth and reduction in the number of serious pathogens [4, 5], and a great deal of efforts is focused on using available experimental techniques to identify natural antioxidants from plants. In the search for sources of natural antioxidants, in recent years some medicinal plants have been extensively studied for their antioxidant activity and radical-scavenging activity [6, 7]. Also, a number of clinical trials have shown that various secondary

metabolites of plants can be used in the treatment of different cancer types [8].

The family *Boraginaceae* is known as medicinal plants classified as dicotyledones. Many members of the *Boraginaceae* family produce secondary metabolites such as alkaloids, naphthoquinones, polyphenols, phytosterols and terpenoids [9, 10]. Polyphenols, including flavonoids and phenolic acids, produced by the family *Boraginaceae*, have a wide range of pharmaceutical activities, including antiinflammatory, antiviral and antibacterial activities [11, 12]. *Echium italicum* is a perennial, shrub-like plant, inhabiting thermophilic, sandy grounds of the submediterranean area [13]. Its leaves are used as seasoning; apiarists use the plant to make uniquely flavoured honey [14]; flowers are used as an „anti-stress“, tranquilizer, and energizer drink, fighting common cold and bronchitis. In Turkish folk medicine, roots of *Echium italicum* and *Echium vulgare* are used externally for healing wounds [15-18]. Phytochemical analysis of the *E. italicum* plant has shown that the contents of condensed tannins and gallotannins were 21.49 mg Ga/g and 28.85 mg GA/g, while the total antioxidant capacity of the plant extract was 112.92 µg AA/g [19]. Albreht [20] identified in the root of *E. italicum* L. nine shikonin pigments: shikonin, acetylshikonin, propionylshikonin, isobutylshikonin, tigla shikonin, 3,3-dimethylacrylshikonin, angelylshikonin, 2-methyl-*n*-butyrylshikonin and isovalerylshikonin. The *E. italicum* oil exhibited

* To whom all correspondence should be sent:
E-mail: ivana.boskovic@pof.ues.rs.ba

concentration-dependent antimicrobial activity on all microorganisms tested [21]. The aim of this study was to assess *in vitro* the biological activity of five different extracts of *Echium italicum* L. and to determine their phytochemical composition.

EXPERIMENTAL

Preparation of the plant extracts

The plant material was collected from Brdjanska gorge near Gornji Milanovac in June 2013, in the flowering stage. The above-ground parts of the plant were crushed using a cylindrical crusher. The plant material was extracted in a Soxhlet extractor. The plant material was degreased by extraction with petroleum ether (40°C), followed by extraction with a series of solvents. The resulting solutions were allowed to cool and after 24 h their pairing in a rotary vacuum evaporator at a temperature of 40°C was performed. Investigations were carried out in the chemical and microbiological laboratories of the Faculty of Agronomy in Čačak.

Determination of total phenolic content

Total phenols were estimated according to the Folin-Ciocalteu method [22]. The extracts were diluted to a concentration of 1 mg/ml, and aliquots of 0.5 ml were mixed with 2.5 ml of Folin-Ciocalteu reagent (previously diluted 10-fold with distilled water) and 2 ml of NaHCO₃ (7.5%). After 15 min of staying at 45°C, the absorbance was measured against a blank sample at 765 nm.

Determination of flavonoid content

Total flavonoids were determined according to Brightene *et al.* [23]. A total of 0.5 ml of 2% aluminium chloride (AlCl₃) in methanol was mixed with the same volume of methanol solution of plant extract. After 1 h of staying at room temperature, the absorbance was measured at 415 nm on a spectrophotometer against a blank sample.

Determination of tannin content

The method for determination of condensed tannins relies on the precipitation of proanthocyanidins with formaldehyde [24]. First, total phenolics were measured using the Folin-Ciocalteu reagent as described above. A 0.5 mol equivalent of phloroglucinol was added for every gallic acid equivalent in the extract. An aliquot of 2 ml of the extract dissolved in methanol was mixed with a calculated amount of phloroglucinol, followed by 1 ml of 2:5 HCl/H₂O solution and 1 ml of formaldehyde solution (13 ml of 37% formaldehyde diluted to 100 ml with water). After overnight incubation at room temperature,

unprecipitated phenols were determined in the supernatant by the Folin-Ciocalteu method.

Determination of total antioxidant activity

The total antioxidant activity of *E. italicum* extracts was evaluated using the phosphomolybdenum method [25]. This assay is based on the reduction of Mo (VI) to Mo (V) by antioxidant compounds and subsequent formation of a green phosphate/Mo (V) complex at acidic pH. A total of 0.3 ml of sample extract was combined with 3 ml of reagent solution (0.6 M sulfuric acid, 28 mM sodium phosphate and 4 mM ammonium molybdate). The tubes containing the reaction solutions were incubated at 95°C for 90 min. After staying at room temperature, the absorbance of the solutions was measured at 695 nm against a blank sample. Methanol (0.3 ml) was used as the blank.

Determination of DPPH free radical scavenging activity

The method used by Takao *et al.* [26] was adopted with suitable modifications from Kumarasamy *et al.* [27]. DPPH (8 mg) was dissolved in MeOH (100 ml) to obtain a concentration of 80 µg/ml. Serial dilutions were carried out with the stock solution (1 mg/ml) of the extract. Solutions (2 ml each) were then mixed with DPPH (2 ml) and allowed to stay for 30 min to allow any reaction to occur, and the absorbance was measured at 517 nm. Ascorbic acid (AA), gallic acid and BHT were used as reference standards and were dissolved in methanol to prepare stock solutions with the same concentrations (1 mg/ml). Control samples were prepared containing the same volume without test compounds or reference antioxidants.

Determination of inhibitory activity against lipid peroxidation

Antioxidant activity was determined by the thiocyanate method [28]. Serial dilutions were carried out with stock solutions (1 mg/ml) of the extracts, and 0.5 ml of each solution was added to a linoleic acid emulsion (2.5 ml, 40 mM, pH 7.0). The linoleic acid emulsion was prepared by mixing 0.2804 g of linoleic acid and 0.2804 g of Tween-20 as an emulsifier in 50 ml of 40 mM phosphate buffer and the mixture was homogenised. The final volume was adjusted to 5 ml with 40 mM phosphate buffer, pH 7.0. After incubation at 37°C in the dark for 72 h, 0.1 ml aliquot of the reaction solution was mixed with 4.7 ml of ethanol (75%), 0.1 ml of FeCl₂ (20 mM) and 0.1 ml of ammonium thiocyanate (30%). The mixture was stirred for 3

min and the absorbance was measured at 500 nm. Ascorbic acid, gallic acid, α -tocopherol and BHT were used as reference compounds.

Determination of hydroxyl radical scavenging activity

The ability of *E. italicum* extracts to inhibit non-sitespecific hydroxyl radical-mediated peroxidation was carried out according to Hinneburg *et al.* [29]. The reaction mixture contained 100 μ l of extract dissolved in water, 500 μ l of 5.6 mM 2-deoxy-D-ribose in KH₂PO₄– NaOH buffer (50 mM, pH 7.4), 200 μ l of premixed 100 μ M FeCl₃, 104 mM EDTA (1:1 v/v) solution, 100 μ l of 1.0 mM H₂O₂ and 100 μ l of 1.0 mM aqueous ascorbic acid. Tubes were vortexed and incubated at 50°C for 30 min. Thereafter, 1 ml of 2.8% TCA and 1 ml of 1.0% TBA were added to each tube. The samples were vortexed and then heated in a water bath at 50°C for 30 min. The extent of oxidation of 2-deoxyribose was estimated from the absorbance of the solution at 532 nm. The percentage inhibition was calculated from the absorbances of the controls (Ac) and the samples (As), where the controls contained all reaction reagents except the extract or positive control substance. The values are presented as the means of triplicate analyses. Spectrophotometric measurements were performed using a UV–Vis spectrophotometer MA9523-Spekol 211 (ISKRA, Horjul, Slovenia).

HPLC analysis of *E. italicum* plant extracts

Determination of polyphenol components in the tested extracts was done on the HPLC Agilent 1200 Series instrument (Agilent Technologies, USA) with UV-Vis DAD for multiwavelength detection. After injecting 5 μ l of sample, the separation was performed in an Agilent-Eclipse XDB C-18 4.6·150 mm column. The column was thermostated at 25 °C. Two solvents were used for the gradient elution: A - (H₂O+2% HCOOH) and B - (80% ACN+2% HCOOH+H₂O). The elution program used was as follows: from 0 to 10 min 0% B, from 10 to 28 min gradual increase 0-25% B, from 28 to 30 min 25% B, from 30 to 35 min gradual increase 25-50% B, from 35 to 40 min gradual increase 50-80% B, and finally for the last 5 min gradually decrease 80-0% B. All identifications of individual compounds were based on the retention times of the original standards, where available, and spectral data.

Measurement of minimum inhibitory concentration (MIC and MBC) of *E. italicum* extracts

MIC of the crude extracts was determined by the microdilution method using 96-multi-well

microtiter plates [30]. In the experiment were included pure cultures of the following bacteria: *Listeria ivanovii* ATCC 19119, *Listeria innocua* ATCC 33090, *Enterococcus faecalis* ATCC 29212, *Listeria monocytogenes* ATCC 19112, *Bacillus spiezenii* ATCC 6633, *Enterococcus faecium* ATCC 6057, *Staphylococcus aureus* ATCC 25923, *Staphylococcus saprophyticus* ATCC 15035, *Klebsiella pneumoniae* ATCC 13883, *Escherichia coli* ATCC 25922, *Proteus vulgaris* ATCC 13315, *Proteus mirabilis* ATCC 14153, *Salmonella enteritidis* ATCC 13076, *Enterobacter aerogenes* ATCC 13048, *Citrobacter freundii* ATCC 43864, *Salmonella Typhimurium* ATCC 14028, *Pseudomonas aeruginosa* ATCC 27853 and yeast *Candida albicans* ATCC 10231 and *Aspergillus niger* ATCC 16404, obtained from the Microbiological laboratory of the Faculty of Agronomy in Čačak. All tests of bacterial and yeast cultures were performed in Mueller–Hinton broth and Sabouraud dextrose broth, respectively. In the first row of the plate 100 μ l of a stock solution of *E. italicum* extracts (200 μ g/ml) and a solution of cirsimarin (2 mg/ml) in 10 % DMSO were applied. In the other wells 50 μ l of Mueller Hinton or Sabouraud dextrose broth containing Tween 80 to a total concentration of 0.5 % (v/v) was added for analysis of the extracts. From the first row test wells a volume of 50 μ l was transferred into the second row wells. Thereafter, from the second to the twelfth well a volume of 50 μ l of scalar dilution was transferred. Then, to each well 10 μ l of indicator solution (prepared by dissolving resazurin in sterile distilled water) and 30 μ l of nutrient broth was added. Finally, to each well 10 μ l of bacterial suspension (10⁶ CFU/ml) and yeast spore suspension (3×10⁴ CFU/ml) were added. Amracin (tetracycline hydrochloride) and ketoconazole were used as positive control for the test bacteria and yeast, respectively. The plates were wrapped loosely with cling film to ensure that bacteria did not become dehydrated. The plates were prepared in triplicate and incubated at 37 °C for 24 h for the bacteria and 48 h for the yeast. Mean MIC (n = 3) for the test extracts and standard drugs were taken. For the determination of MBC, a portion of liquid (5 μ l) from each plate well that exhibited no growth was taken and then incubated at 37 °C for 24 h. The lowest concentration that revealed no visible bacterial growth after subculturing was taken as MBC.

Measurement of cytotoxic activity by MTT assay

Determinations of cytotoxic activity were done according to the MTT assay (3-[4,5-

dimethylthiazol-2-yl-2,5-diphenyl tetrazolium bromide test). The following cell lines were used: Hep2c (cell line derived from human cervix carcinom), RD (cell line derived from human rhabdomyosarcom), and L2OB (cell line derived from mouse fibroblast carcinom). Using 96-well cell culture plates, the cells were seeded in nutrient medium (minimum essential medium—MEM) and grown at 37 °C in humidified atmosphere for 24 h. After completing 24 h of incubation the medium was replaced with 100 ml of medium with different concentrations of extracts of the test plant (25, 50, 100, 250, 500, 750 and 1000 µg/ml). Control cells were added to fresh medium without the extract. After incubation of the cell extracts MTT was added (to a final concentration of 5 mg/ml PBS) to each well, and the plate was incubated for 24 h at 37° C. Colored formazan crystals generated were dissolved with 150 ml of DMSO. The absorbance was measured at 570 nm on a microplate reader. The percentage of viable cells was determined as the ratio of absorbance of treated cells and control cells multiplied by 100. Experiments as those using MTT [3-(4,5-dimethylthiazol-2-yl)-2,5-diphenyltetrazolium bromide] are based on the ability of the viable cells to dissolve the tetrazolium salt. IC₅₀ concentration was defined as the concentration of an agent inhibiting cell survival by 50%, compared with a vehicle-treated control. The results of the measurements were expressed as the percentage of positive control growth taking the Cis-DDP used in positive control wells as 100 % growth [31-33]. All experiments were done in triplicate.

Statistical analysis

The results were subjected to a one-factor analysis of variance (extracts), and the significance of differences was computed by the LSD test. The results of antioxidant activity are presented as means ± standard deviations of three analytical determinations.

RESULTS

The results of total phenolics, flavonoids and tannin content of various extracts of the plant *E. italicum* are presented in Table 1. The phenolic contents in the ethanol (109.15±0.51 mg GA/g), chloroform (105.22±0.07 mg GA/g) and acetone extract (104.39±0.18 mg GA/g) were higher than the phenolic contents in the ethyl acetate and petroleum extract. Statistically significant differences in the concentrations of total phenolics are between chloroform and ethanol extracts in comparison to the ethyl acetate and petroleum ether

extracts. The highest flavonoid contents were in the ethanol (25.16±0.19 mg RU/g) and petroleum ether extracts (25.03±0.29 mg RU/g). Statistically significant differences in the concentrations of flavonoids were between petroleum ether and ethanol extracts in comparison to the chloroform extract. The tannin contents ranged from 75.44±0.26 to 79.60±0.18 mg GA/g in the chloroform extract (79.60±0.18 mg GA/g) and the acetone extract (79.43±0.20 mg GA/g) had the highest value of tannins. Statistically significant differences in the concentrations of tannins were between chloroform and acetone extracts in comparison to the other examined extracts.

Table 1. Total phenolics, flavonoids and tannins content in the various extracts of the plant *E. italicum*

Extracts of <i>E. italicum</i>	T. phenolics (mgGA/g)	Flavonoids (mgRU/g)	Tannins (mgGA/g)
Chloroform	105.22±0.07b	23.20±0.51b	79.60±0.18a
Et. acetate	97.10±0.25c	24.09±0.60ab	78.18±0.38b
Ethanol	109.15±0.51a	25.16±0.19a	75.97±0.34c
Acetone	104.39±0.18b	24.11±0.06ab	79.43±0.20a
Petr. ether	93.02±0.38d	25.03±0.29a	75.44±0.26c

Statistically significant difference for the level of 0.05% is shown by the letter next to the concentration value (compared to extract employed). With the same letters that difference is not significant. If the letters are different, the difference is significant. Several methods were used to determine the antioxidant activity of the tested extracts - Table 2. The values of total antioxidant capacity ranged from 86.09±1.40 µg AA/g to 97.31±0.69 µg AA/g, and ethanol extract (97.31±0.69 µg AA/g) and chloroform extract (95.22±0.78 µg AA/g) had the highest values of total antioxidant capacity. The acetone extract (42.54±1.13 µg/ml IC₅₀) and chloroform extract (43.29±1.20 µg/ml IC₅₀) displayed the highest lipid peroxidation inhibition. The ethanol extract (61.55±0.79 µg/ml IC₅₀) and the acetone extract (62.15±0.27 µg/ml IC₅₀) had the highest hydroxyl radical scavenging activity. The acetone extract had the highest DPPH scavenging activity (62.46±0.66 µg/ml IC₅₀).

HPLC analysis of the phenolic components from various extract of the plant *E. italicum* enabled the identification of 9 compounds (Table 3). The petroleum ether extract had the highest number of identified compounds, followed by the acetone extract, the ethanol extract, the ethyl acetate extract and the chloroform extract. Among the identified constituents, rosmarinic acid, chlorogenic acid, *p*-hydroxybenzoic acid and rutin were found as major components in the tested extracts.

Table 2. Total antioxidant capacity, inhibitory activity against lipid peroxidation, hydroxyl radical and DPPH scavenging activity of the plant *E. italicum*

Extracts of <i>E. italicum</i>	Total antioxidant capacity (µg AA/g)	Inhibition activity against lipid peroxidation (µg/ml)	Hydroxyl radical scavenging activity (µg/ml)	DPPH (µg/ml)
Chloroform	95.22±0.78	43.29±1.20	63.00±0.98	65.07±1.02
Et. acetate	93.12±0.55	47.26±1.12	65.37±0.68	66.00±0.92
Ethanol	97.31±0.69	44.56±1.29	61.55±0.79	63.59±0.48
Acetone	94.15±0.78	42.54±1.13	62.15±0.27	62.46±0.66
Petr. ether	86.09±1.40	49.36±1.10	70.16±0.78	71.79±0.89
Gallic acid	-	255.43±11.68	59.14±1.10	3.79±0.69
Ascorb.acid	-	> 1000	160.55±2.31	6.05±0.34
BHT	-	1.00±0.23	33.92±0.79	15.61±1.26
α-Tocopherol	-	0.48±0.05	-	-

Table 3. HPLC analysis of the plant *E. italicum*

Compound/ Sample	Petroleum ether (mg/g)	Chloroform (mg/g)	Acetone (mg/g)	Ethyl acetate (mg/g)	Ethanol (mg/g)
Protocatechuic acid					
p-Hydroxybenzoic acid	9.143	1.468	4.865		1.930
Caffeic acid					
Vanillic acid					
Chlorogenic acid	10.776		1.915		1.293
Syringic acid					
p-Coumaric acid					
Ferulic acid	0.928	0.408	0.519		0.346
Synapic acid					
Rutin	6.024	6.080	4.926	9.091	10.739
Luteolin-glycine	2.542		0.748		0.626
Apigenin-glycine					
Rosmarinic acid	44.134	1.632	12.131	2.494	8.452
Quercetin	0.887	0.581	1.006	0.879	0.902
Luteolin					
Naringenin		0.244	0.371		0.411
Caempherol	0.729	0.287	0.985	0.919	0.927
Apigenin					
Σ	75.163	10.700	27.466	13.383	25.626

Antimicrobial activity was tested using the broth dilution procedure for determination of minimum inhibitory concentration (MIC). MICs were determined against seventeen strains of bacteria, and the antifungal activity was tested against *Aspergillus niger* and *Candida albicans* - Table 4. The tested extracts showed strong antimicrobial activity against Gramm-positive, Gramm-negative bacteria and fungi. MIC of the ethyl acetate extract for *Escherichia coli* ATCC 8739, *Proteus vulgaris* ATCC 13315, *Citrobacter freundii* ATCC 43864 were 3.91 µg/ ml, and for *Listeria innocua* ATCC 33090, *Listeria monocytogenes* ATCC 19112, *Enterococcus faecium* ATCC 6057 and *Aspergillus niger* ATCC 16404 were 7.81 µg/ ml. MICs of the

petroleum ether extract were 3.91 µg/ ml for *Proteus mirabilis* ATCC 35659, *Enterobacter aerogenes* ATCC 13048 and *Aspergillus niger* ATCC 16404, and MIC for *Listeria ivanovii* ATCC 19119, *Enterococcus faecalis* ATCC 29212 and *Staphylococcus saprophyticus* ATCC 15035 were 7.81 µg/ml. MIC of the acetone extract were 3.91 µg/ml for *Salmonella enteritidis* ATCC 13076, and 7.81 µg/ml for *Escherichia coli* ATCC 8739, *Klebsiella pneumoniae* ATCC 13883, *Proteus vulgaris* ATCC 13315, *Enterococcus faecium* ATCC 6057 and *Candida albicans* ATCC 10231. MIC of ethanol extract were 3.91 µg/ml for *Salmonella Typhimurium* ATCC 14028 and *Staphylococcus aureus* ATCC 25923, and for

Table 4. MIC/MBC values ($\mu\text{g}/\text{ml}$) of *E. italicum* plant extracts

Bacteria	MIC/MBC ($\mu\text{g}/\text{ml}$)						Amracin	Ketoconazole
	Ethanol extract	Ethyl acetate extract	Chloroform extract	Petroleum ether extract	Acetone extract			
<i>Proteus mirabilis</i>	250.00/500.00	125.00/250.00	7.81/15.625	3.91/7.82	62.5/125.00	0.49	-	-
<i>Escherichia coli</i>	62.5/125.00	3.91/7.82	15.625/31.25	31.25/62.5	7.81/15.625	0.97	-	-
<i>Klebsiella pneumoniae</i>	125.00/250.00	31.25/62.5	3.91/7.82	62.5/125.00	7.81/15.625	0.49	-	-
<i>Proteus vulgaris</i>	250.00/500.00	3.91/7.82	125.00/250.00	62.5/125.00	7.81/15.625	0.49	-	-
<i>Salmonella enteritidis</i>	7.81//15.625	31.25/62.5	62.5/125.00	125.00/250.00	3.91/7.82	0.49	-	-
<i>Enterobacter aerogenes</i>	15.625/31.25	62.5/125.00	31.25/62.5	3.91/7.82	125.00/250.00	0.97	-	-
<i>Citrobacter freundii</i>	31.25/62.5	3.91/7.82	125.00/250.00	62.5/125.00	500.00/1000	0.49	-	-
<i>Salmonella Typhimurium</i>	3.91/7.82	125.00/250.00	7.81/15.625	31.25/62.5	125.00/250.00	0.49	-	-
<i>Pseudomonas aeruginosa</i>	7.81/15.625	62.5/125.00	3.91/7.82	125.00/250.00	250.00/500.00	0.97	-	-
<i>Listeria ivanovii</i>	125.00/250.00	31.25/62.5	250.00/500.00	7.81/15.625	62.5/125.00	0.97	-	-
<i>Listeria inocu</i>	31.25/62.5	7.81/15.625	125.00/250.00	500.00/1000	62.5/125.00	0.49	-	-
<i>Enterococcus faecalis</i>	125.00/250.00	31.25/62.5	250.00/500.00	7.81/15.625	62.5/125.00	0.97	-	-
<i>Listeria monocytogenes</i>	31.25/62.5	7.81/15.625	125.00/250.00	500.00/1000	62.5/125.00	0.97	-	-
<i>Bacillus spieizenii</i>	7.81/15.625	31.25/62.5	125.00/250.00	62.5/125.00	31.25/62.5	0.97	-	-
<i>Enterococcus faecium</i>	62.5/125.00	7.81/15.625	31.25/62.5	15.625/31.25	7.81/15.625	0.49	-	-
<i>Staphylococcus aureus</i>	3.91/7.82	62.5/125.00	7.81/15.625	125.00/250.00	15.625/31.25	0.97	-	-
<i>Staphylococcus saprophyticus</i>	62.5/125.00	125.00/250.00	31.25/62.5	7.81/15.625	31.25/62.5	0.97	-	-
<i>Aspergillus niger</i>	31.25/62.5	7.81/15.625	15.625/31.25	3.91/7.82	62.5/125.00	-	0.97	-
<i>Candida albicans</i>	15.625/31.25	31.25/62.5	500.00/1000	31.25/62.5	7.81/15.625	-	1.95	-

Salmonella enteritidis ATCC 13076, *Pseudomonas aeruginosa* ATCC 27853, *Bacillus spieizenii* ATCC 6633 MIC values were 7.81 $\mu\text{g}/\text{ml}$. MIC of chloroform extract were 3.91 $\mu\text{g}/\text{ml}$ for *Klebsiella pneumoniae* ATCC 13883 and *Pseudomonas aeruginosa* ATCC 27853, and 7.81 $\mu\text{g}/\text{ml}$ for *Proteus mirabilis* ATCC 35659, *Salmonella Typhimurium* ATCC 14028 and *Staphylococcus aureus* ATCC 25923. The results of MBC are shown in Table 4. The MBC values ranged from 7.82 $\mu\text{g}/\text{ml}$ to 1000 $\mu\text{g}/\text{ml}$. The lowest MBC values 7.82 $\mu\text{g}/\text{ml}$ had the ethyl acetate extract for *Escherichia coli* ATCC 8739, *Proteus vulgaris* ATCC 13315, *Citrobacter freundii* ATCC 43864, the petroleum ether extract for *Proteus mirabilis* ATCC 35659, *Enterobacter aerogenes* ATCC 13048 and *Aspergillus niger* ATCC 16404, the acetone extract for *Salmonella enteritidis* ATCC 13076, the ethanol extract for *Salmonella Typhimurium* ATCC 14028 and *Staphylococcus aureus* ATCC 25923, and chloroform extract for *Klebsiella pneumoniae* ATCC 13883 and *Pseudomonas aeruginosa* ATCC 27853.

Determinations of cytotoxic activity were done according to the MTT assay on the three cell lines: cell line derived from human rhabdomyosarcom

(RD), cell line derived from human cervix carcinom (Hep2c) and cell line from mouse fibroblast carcinom (L2OB) - Table 5. The IC₅₀ values of cytotoxic activity of the tested extracts ranged from 87.30 \pm 4.09 $\mu\text{g}/\text{ml}$ to 172.52 \pm 2.44 $\mu\text{g}/\text{ml}$. The chloroform (87.30 \pm 4.09 $\mu\text{g}/\text{ml}$) and acetone extracts of plant (91.56 \pm 2.31 $\mu\text{g}/\text{ml}$) showed the best cytotoxic activity on L2OB cells. The ethanol and acetone plant extracts significantly influenced Hep 2c, the petroleum ether extract significantly influenced RD cells and the chloroform and acetone extracts significantly influenced L2OB cells.

Table 5. Cytotoxic activities ($\mu\text{g}/\text{ml}$) of *Echium italicum* plant extracts

Extract	Hep 2c	RD	L2OB
Chloroform	129.70 \pm 2.04b	161.56 \pm 0.43b	87.30 \pm 4.09c
Et. acetate	158.42 \pm 0.36a	173.61 \pm 1.30a	137.36 \pm 0.53b
Ethanol	121.48 \pm 0.85c	172.52 \pm 2.44a	133.20 \pm 0.04b
Acetone	122.37 \pm 1.47c	162.35 \pm 0.28b	91.56 \pm 2.31c
Petr. ether	162.80 \pm 2.14a	106.59 \pm 1.21c	146.33 \pm 0.76a

DISCUSSION

Phenolic compounds are a major class of plant secondary metabolites. These compounds represent an important component of human diets and exhibit a wide range of biological effects, including antioxidant, antimutagenic, and anticarcinogenic effects. The phenolic contents in the ethanol, chloroform and acetone extracts were higher than in the ethyl acetate and petroleum extracts. The highest total phenolic contents of the plant *E. italicum* were found in the ethanol extract. The highest flavonoid content was in the ethanol extract and the highest tannin contents in the chloroform and acetone extracts. The study of total phenolic and flavonoid contents obtained from the ethanol extract of roots and herbs of *E. italicum* L. [34] showed a lower phenolics content and a higher flavonoid content than our study. This can be related to the type of solvent and the period of collecting the plants (in June), which is consistent with the results obtained by Meddini [35] that at the flowering stage the plant has a higher level of phenolic compounds than at the vegetative stage. Bano *et al.* [36] have shown that the amount of polyphenols in plants and their antioxidant activities depend on both biological factors (genotype, organ andontogeny) and edaphic and environmental (temperature, salinity, water stress and light intensity) conditions. The solubility of phenolic compounds is governed by the type of solvent (polarity) used, the degree of polymerization of phenols and their interaction [37]. The content of total phenolics is in positive correlation with the total antioxidant capacity. These results were consistent with the findings of various research groups, who reported positive correlations between total phenolic content and antioxidant activity [38, 39].

The acetone extract displayed the highest lipid peroxidation inhibition, followed by the chloroform and ethanol extracts. The results of hydroxyl radical scavenging activity of the various extracts of the plant *E. italicum* showed that the ethanol extract had the highest IC₅₀ value, followed by the acetone extract and the chloroform extract. The DPPH scavenging activity in the various extracts of the plant *E. italicum* showed that the acetone extract had the highest activity IC₅₀, followed by the ethanol extract and chloroform extract. Previous studies showed that concentration-response is related to the DPPH scavenging activity, and an increase in the concentration of extract is synonymous with an increase in scavenging capacity [34]. Many researchers reported an influence of different extraction techniques on the

content of natural antioxidants in the extracts [40, 41]. Efficiency of solvents and methods is strongly dependent on the plant matrix used [41-43]. Solvents such as methanol, ethanol, acetone, propanol and ethyl acetate have been commonly used for the extraction of phenolics from fresh products [42, 43].

HPLC analysis of the phenolic components from various extracts of the plant *E. italicum* enabled the identification of 9 compounds. Among the identified constituents, rosmarinic acid, chlorogenic acid, *p*-hydroxybenzoic acid and rutin were determined as major components in the tested extracts. Rosmarinic acid and rutin have been reported to have strong antioxidant properties and also antidiabetic, antithrombotic, antiinflammatory and anticarcinogenic activity [44, 45]. Bouayed *et al.* [46] have found that chlorogenic acid has anxiolytic and antioxidant activity.

The antibacterial activity of plants is continuously attracting global attention [47]. The antimicrobial activity may be due to the presence of antioxidants in the extracts that have the potential to prevent the activity of free radicals and reactive oxygen species thus helping in fighting diseases caused by bacteria and other pathogens [48, 49]. All extracts expressed a certain level of antimicrobial activity with MIC values in the range from 3.91 µg/ml to 500 µg/ml, which is considered to be very good compared to standard antibiotics amracin (for bacteria) and ketoconazole (for fungi). The ethyl acetate extract dieplayed the greatest antimicrobial activity against *Escherichia coli*, *Proteus vulgaris*, *Citrobacter freundii*, the petroleum ether extract - against *Proteus mirabilis*, *Enterobacter aerogenes* and *Aspergillus niger*, the acetone extract - against *Salmonella enteritidis*, the ethanol extract - against *Salmonella Typhimurium* and *Staphylococcus aureus*, the chloroform extract - against *Klebsiella pneumoniae* and *Pseudomonas aeruginosa*. Overall, the antibacterial activity of the tested samples was noticeably higher against the growth of Gram-negative bacteria strains compared to Gram-positive bacteria strains. The antimicrobial activity of the *E. italicum* oil was studied against *Bacillus subtilis*, *Staphylococcus aureus*, *Escherichia coli*, *Salmonella Typhimurium*, *Pseudomonas aeruginosa*, *Aspergillus niger* and *Candida albicans* and showed a pronounced concentration dependence on all microorganisms tested [21]. The MBC values ranged from 7.82 µg/ml to 1000 µg/ml. Antimicrobial activity of the plant extracts might be explained by the synergistic or additive effects of several phytochemicals rather than arising from a

single compound. Different bioactive compounds in a mixture can interact to provide a combined effect which is similar to the sum of the effects of the individual components (additive), or greater than the sum of the individual components (synergistic). The mechanisms of action of each phenolic compound against various bacteria are also very complicated [50, 51]. Therefore, it is necessary to further investigate and understand the relationship between antibacterial activity and chemical structure of each phenolic compound in the tested extracts.

Cancer development, a dynamic and long-term process, involves many complex factors with stepwise progression ultimately leading to an uncontrolled spreading and growth of cancerous cells throughout the body, called metastasis. Laboratory research has further demonstrated that a number of bioactive dietary components, collectively referred to as natural products, have the ability to prevent cancer [52] and other chronic diseases [53, 54]. Results obtained in the present study show that all examined samples exhibit *in vitro* cytotoxic activity against the target cells. Phytochemical analysis of plant extracts of *Echium italicum* showed the presence of a large number of bioactive phenolic components (chlorogenic acid, *p*-hydroxybenzoic acid, naringenin, kaempferol, lutein), and numerous literature data suggest their anticancer effect [55-63]. Biological activity of the plant extracts from the family *Boraginaceae* growing in Serbia has been confirmed by other authors [64, 65].

CONCLUSIONS

The results of this investigation which determined the phytochemical composition and biological activity of five different extracts of *E. italicum* L., demonstrate that these might be proposed as antioxidant dietary supplements for the prevention and/or treatment of conditions that occur due to oxidative damage and can protect DNA damage by hydroxyl radicals. The plant has got a broad spectrum of antimicrobial and biological activity and could be a potential alternative for treating various diseases.

REFERENCES

- 1.D. Webster, P. Taschereau, R. J. Belland, C. Sand, R. P. Rennie, *J Ethnopharmacol.*, **115**, 140 (2008).
- 2.M. Singh, N. Singh, P. B. Khare, A. K. S. Rawat, *J. Ethnopharmacol.*, **115**, 327 (2008).
- 3.A. L. Harvey, *Drug Discov. Today*, **13**, 894 (2008).
- 4.V. Kuete, J. R. Nguemeveing, V. P. Beng, A. G. B. Azebaze, F. X. Etoa, M. Meyer, B. Bodo, E. Nkengfack, *J. Ethnopharmacol.*, **109**, 372 (2007).
- 5.P. Kotzekidou, P. Giannakidis, A. Boulamatsis, *LWT*, **41**, 119 (2008).
- 6.G. R. Schinella, H. A. Tournier, J. M. Prieto, P. Mordujovich de Buschiazzo, J. L. Rios, *Life Sci.*, **70**, 1023 (2002).
- 7.T. J. VanderJagt, R. Ghattas, D. J. VanderJagt, M. Crossey, R. H. Glew, *Life Sci.*, **70**, 1035 (2002).
- 8.M. S. Butler, *J Nat Prod.*, **67**, 2141 (2004).
- 9.M. Gottschling, H. H. Hilger, M. Wolf M, N. Diane, *Plant Biology*, **3**, 629 (2001).
- 10.R. H. Zhou, J. A. Duan, Plant Chemotaxonomy 1028, Shanghai scientific & Technical Publishers, Shanghai, 2005.
- 11.K. Iqbal, S.A. Nawaz, A. Malik, N. Riaz, N. Mukhtar, P. Mohammad, M. I. Choudhary, *Chem. Biodivers.*, **2**, 104 (2005).
- 12.M. Y. Zeng, J. F. Zeng, Traditional Chinese medicine resources *Zhi Yao*, 7. *Science Press*, Beijing, 1994.
- 13.M. Josifović, Flora Srbije, SANU, Beograd, 1974.
- 14.C. A. Wright, Mediterranean vegetables, Harvard Common Press, Boston, 2001.
- 15.E. Yesilada, G. Honda, E. Sezik, M. Tabata, T. Fujita, T. Tanaka, Y. Takeda, Y. Takaishi, *J Ethnopharmacol.*, **46**, 133 (1995).
- 16.E. Sezik, M. Tabata, G. Honda, Y. Takashi, T. Fujita, T. Anaka, Y. Takeda, *Economy Botany*, **51**, (1997).
- 17.E. Altundag, M. Özer, *Procedia Social and Behavioral Sci.*, **19**, 756 (2011).
- 18.T. Fujita, M. Tabata, E. Yesilada, G. Honda, Y. Takeda, T. Tanaka, Y. Takaishi, *Econ. Bot.*, **49**, 406 (1995).
- 19.N. Nićiforović, M. Mihailović, S. Solujić, D. Pavlović- Murataspahić D, *Planta Med.*, **76**, 248 (2010).
- 20.A. Albreht, I. Vovk, B. Simonovska, M. Srbinoska, *J. Chromatogr. A*, **1216**, 3156 (2009).
- 21.K. Morteza-Semnani, M. Saeedi, M. Akbarzadek, *JEOP*, **12**, 557 (2009).
- 22.V. L. Singleton, R. Orthofer, R. M. Lamuela-Raventos, *Method. Enzymol.*, **299**, 152 (1999).
- 23.I. M. C. Brightene, M. Dias, L. G. Verdi, M. G.M. Pizzolatti, *Pharmac. Biol.*, **45**, 156 (2007).
- 24.W. Verrmeris, R. Nicholson, Phenolic compound Biochemistry, Dordrecht, The Netherlands, Springer, 2006.
- 25.P. Prieto, M. Pineda, M. Aguilar, *Anal. Biochem.*, **269**, 337 (1999).
- 26.T. Takao, F. Kitatani, N. Watanabe, A. Yagi, K. Sakata, *Biosc. Biotech. Biochem.*, **58**, 1780 (1994).
- 27.[Y. Kumarasamy, M. Byres, P. Y. Cox, M. Jaspars, L. Nahar, S. D. Sarker, *Phytother. Res.*, **21**, 615 (2007).
- 28.[C. K. Hsu, B. H. Chiang, Y. S. Chen, J. H. Yang, C. L. Liu, *Food Chem.*, **108**, 633 (2008).
- 29.I. Hinneburg, H. J. D. Dorman, R. Hiltunen, *Food Chem.*, **97**, 122 (2006).
- 30.NCCLS, Methods for dilution antimicrobial susceptibility tests for bacteria that grow aerobically;

- Approved standard NCCLS Publication M7/A2, Villanova, PA, USA (1990b).
31. T. Mosmann, *J. Immunol. Meth.*, **65**, 55, (1983).
32. R. D. Dighe, M. R. Shiradkara, S. Rohomb, P. D. Dighe, *Der Chem. Sin.*, **2**, 70 (2011).
33. B. A. Baviskar, S. S. Khadabadia, S. L. Deore, M. R. Shiradkar, *Der Pharm. Sin.*, **3**, 24 (2012).
34. N. Eruygur, G. Yilmaz, O. Ustun, *J. Pharm. Sci.*, **37**, 151 (2012).
35. F. Medini, H. Fellah, R. Ksouri, C. Abdelly, *JTUSCI*, **8**, 216 (2014).
36. M. J. Bano, J. Lorente, J. Casstillo, G. O. Benavente, J. AA. Rio, A. Ortuno, K. W. Quirin, D. Gerard, *J. Agric. Food Chem.*, **51**, 4247 (2003).
37. A. Djerdane, M. Yousfi, B. Nadjem, D. Boutassouna, P. Stocker, N. Vidal, *Food Chem.*, **97**, 654, (2006).
38. Y. Cai, Q. Luo, M. Sun, H. Corke, *Life Sci.*, **74**, 2157, (2004).
39. W. Zheng, S. Y. Wang, *J. Agric. Food Chem.*, **49**, 5165, (2001).
40. D. Grigonia, P. R. Venskutonis, B. Sivikb, M. Sandahlb, C. S. Eskilsson, *J. Supercrit. Fluids*, **33**, 223, (2005).
41. J. A. Michiels, C. Kevers, J. Pincemail, J. O. Defraigne, J. Dommes, *Food Chem.*, **130**, 986 (2012).
42. N. E. Durling, O. J. Catchpole, J. B. Grey, R. F. Webby, A. Kevin, L. Mitchell, N. Perry, *Food Chem.*, **101**, 1417 (2007).
43. M. Alothman, B. Rajeev, A. Karim *Food Chem.*, **115**, 785 (2009).
44. M. Petersen, M. S. J. Simmonds, *Phytochem.*, **62**, 121 (2003).
45. P. Lacopini, M. Baldi, P. Storchi, L. Sebastiani, *J. Food Compos. Anal.*, **21**, 589 (2008).
46. J. Bouayed, H. Rammal, A. Dicko, C. Yonos, R. Soloumani, *J. Neurol. Sci.*, **262**, 77 (2007).
47. Y. Rukayadi, K. Lee, S. Han, D. Yong, J-K. Hwang J-K, *Antimicrob. Agents Chemother.*, **53**, 4529 (2009).
48. A. Parray, A. N. Kamili, R. Hamid, B. A. Ganai, K. G. Mustafa, R. A. Qadri, *Pharm. Res.*, **4**, 2170 (2011).
49. M. Adamu, N. Vinny, J. N. Eloff, *BMC Vet. Res.*, **10:52**, 2 (2014).
50. D. Kalemba, A. Kunicka, Antibacterial and antifungal properties of essential oils, *Curr. Med. Chem.*, **10**, 813 (2003).
51. S. Burt, *Int. J. Food Microbiol.*, **94**, 223 (2004).
52. S. Sharma, J. D. Stutzman, G. J. Kelloff, V. E. Steele, *Cancer Res.*, **54**, 5848 (1994).
53. R. Doll, *Cancer Res.*, **52**, 2024s (1992).
54. A. E. Rogers, S. H. Zeisel, J. Groopman, *Carcinogenesis*, **14**, 2205 (1993),
55. Y. Jiang, K. Kusama, K. Satoh, E. Takayama, S. Watanabe, H. Sakagami, *Phytomed.*, **7**, 483 (2000).
56. F. Yin, A. E. Giuliano, R. E. Law, A. J. Van Herle, *Anticancer Res.*, **21**, 413 (2001),
57. T. D. Way, M. C. Kao, J. K. Lin, *FEBS Lett.*, **579**, 145 (2005).
58. B. B Aggarwal, S. Shishodia, *Biochem. Ph.*, **71**, 1397 (2006).
59. T.A. Bhat, R. P. Singh, *Food Chem. Toxicol.*, **46**, 1334 (2008).
60. S. Ramos, *Mol Nutr Food Res.*, **52**, 507 (2008).
61. E. J. Choi, G. H. Kim, *J. Clin. Biochem. Nutr.*, **44**, 260 (2009).
62. C. J. Weng, C. G. C. Yen, *Cancer Metastasis Rev.*, **31**, 323 (2012).
63. A. Y. Chen, Y. C. Chen, *Food Chem.*, **138**, 2099 (2013).
64. P. Mašković, J. Dragičić-Maksimović, V. Maksimović, J. Blagojević, M. Vujošević, N. T. Manojlović, M. Radojković, M. Cvijović, S. Solujić, *Cent. Eur. J. Biol.*, **7**, 327 (2012).
65. P. Z. Mašković, L. D. Diamanto, J. M. Vujić, A. D. Cvetanović, M. M. Radojković, S. B. Gadžurić, G. Zengin, *Onosma aucheriana: J. Funct. Food*, **19**, 479 (2015)

ФИТО-ХИМИЧЕН СЪСТАВ И БИОЛОГИЧНА АКТИВНОСТ НА ЕКСТРАКТИ ОТ *Echium italicum* L.

И.Д. Бошкович¹, Др.А. Ђжукич², П.З. Машкович², Л.Г. Мандич²

¹Университет в Източно Сараево, Земеделски факултет, 71 123 Източно Сараево, Босна и Херцеговина

²Университет в Крагуевац, Агрономически факултет, Чачак, Сърбия

Постъпила на 23 ноември, 2016 г.; приета на 28 юли, 2017 г.

(Резюме)

Целта на тази работа е да се оцени биологичната активност на пет различни екстракти от растението *Echium italicum* L. и да се определи тяхния фито-химичен състав. Изпитани са хлороформ, етилацетат, етанол, ацетон и петролев естер като разтворители. Спиртният екстракт от *E. italicum* е с най-високо съдържание на общи феноли и flavonoidи, докато екстрактите в хлороформ и ацетон имат най-много танинови вещества. Няколко различни метода са използвани за определянето на анти-оксидантна активност на изпитваните екстракти, като тези в етанол и ацетон показват най-висока активност. HPLC-анализът показва, че основните фенолни съединения в изпитваните екстракти са розмаринова, хлорогенова, p-хидроксибензоена киселини и рутин. Определянето на анти-микробната им активност е извършено по метода на микроразреждането. Резултатите от микроразреждането са в граници от 3.91 до 500 µg/ml. Определянето на цито-токсичната активност са извършено по метода MTT върху човешки клетки на рабдомиосаркома (RD), клетъчна линия от човешки карцином на маточната шийка (Нер2c) и клетъчна линия от карцином на миши фибропласти (L2OB). Изследването внушава, че изследваните екстракти от растението *E. italicum* L. Може да послужат като източници на антиоксиданти и антибиотични агенти.

Theoretical basis for the corrosion inhibition feature of Argan oil

G. Gece

Department of Chemistry, Faculty of Natural Sciences, Architecture and Engineering, Bursa Technical University,
Bursa, 16310 Turkey

Received April 3, 2017; Accepted May 2, 2017

Natural oils play a pivotal role in corrosion inhibition of various metals and alloys. However, their potential inhibition efficiency in acidic media has been barely investigated from a theoretical point of view. Despite a shared experimental justification, the corrosion inhibition feature of such oils resulted in a sustained debate on how the inhibition mechanism could be related to their ingredients. Given the need to better understand the protection behaviour of Argan oil on carbon steel in molar HCl solutions, the electronic properties of two unsaturated fatty acids, i.e., oleic and linoleic acids were studied by density functional theory (DFT) calculations. The protonated forms of oleic and linoleic acids yielded quantum chemical parameters that confirm linoleic acid to be the most stable unsaturated fatty acid, which seems to be responsible for the inhibition efficiency of Argan oil in acidic medium.

Keywords: Argan oil; Oleic acid; Linoleic acid; Corrosion inhibition; DFT.

INTRODUCTION

Despite its relatively limited corrosion resistance, carbon steel is more commonly used than any other metal, and has long been admired for its versatility and low cost. Generally, the application of corrosion inhibitors is one of the most common practices for the protection of steel structures and their alloys in industry [1]. In many cases, the role of inhibitors is to form a surface coating one or several molecular layers thick that serves as a barrier. This in turn depends on the chemical composition, the structure of the inhibitor, the nature of the metal surface, and the properties of the medium. Structural and electronic parameters such as type of the functional group, steric, and electronic effects, are broadly responsible for the inhibition efficiency of any inhibitor, that is, for the adsorption mechanism [2].

Environmental awareness has been gaining attention in recent years, along with growing emphasis on substitution of harmful inhibitors with effective non-hazardous alternatives [3]. Considerable success has been achieved in this regard through the use of some natural oils for corrosion inhibition of different metals [4].

A recent study by Afia *et al.* [5] found evidence that in the presence of Argan oil the corrosion of C38 steel in chloride solution was considerably slowed. Argan oil, obtained from the pit of *Argania spinosa*, is a vegetable oil rich in unsaturated fatty acids (~80%) mainly oleic and linoleic acids (46-48 and 31-35%, respectively) [6]. The experimental results showed that the inhibition efficiency of Argan oil reached about 85% at a concentration of 5 g/L. A

tentative explanation was offered that this inhibition effect may be due to physical adsorption resulting from the displacement of adsorbed water molecules by the inhibitor species, leading to specific adsorption on the metal surface.

It is clear that an evaluation of the protection property of Argan oil from a theoretical point of view would be needed before more definite conclusions about the underlying inhibition mechanism could be drawn. The present study, prompted by the successful application of theoretical calculations in corrosion inhibitor research [7-13], is offered as a further contribution to gain a better understanding of the inhibition effect of Argan oil, whose underlying mechanism is still far from explicit.

COMPUTATIONAL DETAILS

All quantum mechanical geometry optimizations and single-point energy computations were achieved using the Gaussian 09 package [14]. Geometries of all investigated systems were optimized at the density functional theory level using the 6-311G+(d,p) basis set and B3LYP functional. The bulk solvent effects were included through the Integral Equation Formalism version of the Polarizable Continuum Model (IEF-PCM). For the calculations of the interaction energies between oleic and linoleic acids and iron surface, two models were built based on the X-ray diffraction structures [15]. Each of them contained three individual oleic or linoleic acid molecules oriented vertically on the surface in lengthwise direction. A moderate spacing of 10 Å was inserted between these molecules which was seen to be sufficient to allow packing. The

* To whom all correspondence should be sent:
E-mail: gokhangc@gmail.com

carboxyclic oxygen atoms lie 3 Å above the Fe (110) surface. The Fe10 cluster with a lattice constant of 2.86 Å for body-centered-cubic Fe was used to represent the Fe(110) surface [16]. Single-point energy calculations were performed by using universal force field approach with the semiempirical quantum mechanical (QM/PM6) method to calculate the interaction energy due to the compromise between available computing power and the attempt to study the system as thoroughly as possible [17].

RESULTS AND DISCUSSION

Fatty acids are organic acids characterized by the presence of a carboxyl group at one end and a methyl group at the other end. Due to their variation in length and degree of saturation, they are classified either as saturated or unsaturated. The saturated ones are straight-chains and consist of a carbon chain with single bonds, while the unsaturated ones contain one or more double carbon-carbon bonds (C=C), which introduces fixed bends into the carbon chain. The results of gas chromatography analysis of Argan oil [5] revealed that the oil tested as corrosion inhibitor contained large amounts of unsaturated fatty acids. The most abundant was the mono-unsaturated oleic acid (45.1%) and the bi-unsaturated linoleic acid (34.5%). This is the gist of why our theoretical calculations particularly focus on those two molecules. As can be seen from Fig. 1, oleic acid, a C-18 fatty acid, consists of a long chain of carbon atoms with a central C=C bond introducing a slight kink and a monocarboxyl head. On the other hand, linoleic acid is an 18-carbon unsaturated fatty acid with two double bonds in positions 9 and 12, respectively, and both are in the *cis* configuration.

Evidence from earlier electrochemical measurements propounds that the monolayer characteristics of fatty acids are strictly dependent upon pH change [18]. At low pH (< 7), oleic acid is principally protonated and no added ion-dipole interaction exists between the ionized and unionized groups; at intermediate pHs (7-9) almost half of the acid groups are protonated; at high pHs (>9) oleic acid is mostly ionized, and ionic repulsion between the carboxylate ions keeps the molecules apart [19]. The experimental data resorted to were predicated on the results of electrochemical tests in 1 M HCl solution, and therefore, a rough-and-ready way to examine whether the criterion of protonation is satisfied here was to run DFT calculations for the protonated forms of these compounds (Fig. 1).

Thus, to validate whether the calculation method selected fulfils the requirements of accuracy for

geometry optimization, one would need to compare experimental geometric parameters with the theoretical predictions. We will focus particularly on the geometry of oleic acid (Fig. 1(a)) for which experimental data are available. Below its freezing point (13.3°C), three oleic acid solid state polymorphs (α , β , and γ) have been identified [20].

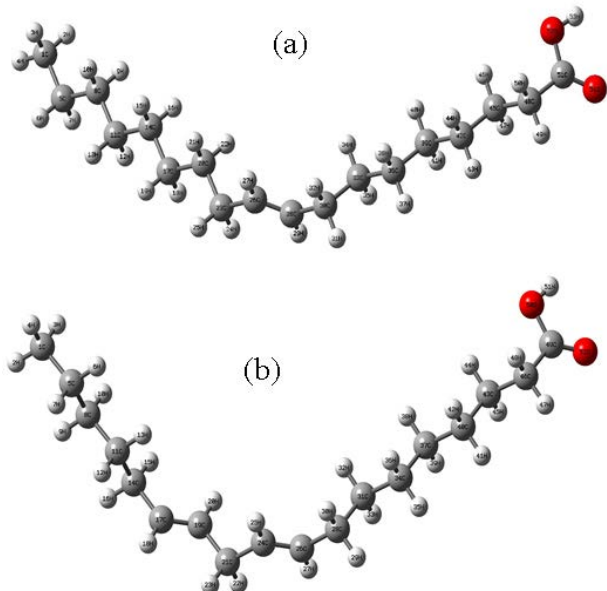


Fig. 1. Optimized structures using the B3LYP/6-311+G(d,p) level for the protonated forms of (a) oleic acid and (b) linoleic acid in the gas phase.

The β phase is unique in contrast to the α and γ phases due to its presence only in oleic acid and appears as two forms: stable $\beta 1$ and metastable $\beta 2$. Guided by known structures for the stable $\beta 1$ phase, configurations for two crystallographically different molecules, A and B were considered [21]. Some selected bond lengths, bond angles, and torsion angles of molecules A and B were compared with those calculated for oleic acid. Bond distances are largely unremarkable: C-C single and double-bond distances are virtually identical at ca. 1.51 Å and 1.31 Å, respectively. In addition, the C51-O52 single bonds and C51=O54 double bonds are also very similar for the structures. The carbon-carbon bonds between C20 and C1 show slight contractions from 1.533 Å to 1.509 (molecule A) and 1.502 Å (molecule B). This trend, although not pronounced, is likely a consequence of reduced steric interactions due to the increase in dihedral angles. There are no other obvious trends noted except for nearly uniformly larger bond distances for the optimized structure. However, this corresponds to only about 0.06 Å at its maximum and is not considered to be very significant. Also, the predicted oleic acid structure agrees rather closely with the experimentally determined conformations, given

that the calculated results are for a single isolated molecule. The sum of the angles around the carboxylic carbon atom C₅₁ does not differ much from planarity, and particularly for dihedral angles between adjacent chain atoms C₂₃-C₁, very close agreement with experimental data was obtained (differences are less than 1°). Larger difference was obtained for the carboxylic acid moiety. This indicates that the positions of C₅₁, O₅₂ and O₅₄ atoms are rather affected by the molecular packing. In general, the bond distances and angles obtained from the X-ray structure determinations compare favorably with those determined from the calculations, and can provide a starting point to calculate other parameters, such as the energies of the frontier molecular orbitals.

The chemical bond between the inhibitor and the surface can be considered a combination of double interactions of the highest occupied molecular orbitals (HOMO) and the lowest unoccupied molecular orbitals (LUMO). Certain quantum chemical parameters, i.e., frontier orbital energies such as E_{HOMO} , E_{LUMO} , and $\Delta E = E_{\text{LUMO}} - E_{\text{HOMO}}$, were used for the sake of comparison in Table 1. According to the results, the highest E_{HOMO} (-6.639 eV), the lowest E_{LUMO} (-0.309 eV) and ΔE (6.330 eV) values are found for linoleic acid. The results for E_{HOMO} , E_{LUMO} and ΔE yield that linoleic acid molecule could prevail for the inhibitory action of Argan oil as a constituent, compared to oleic acid. These results were also supported by the global reactivity parameters. In Table 1, global properties obtained by the frontier molecular orbital energies according to Koopmans theorem [22] are also listed. The ionization potential (I) and electron affinity (A)

are given by $I = -E_{\text{HOMO}}$ and $A = -E_{\text{LUMO}}$. In numerical applications, chemical potential μ and hardness η are expressed on the basis of finite difference approximations in terms of the ionization potential I and the electron affinity A ; $-\mu = \frac{1}{2}(I + A) = \chi$ and $\eta = \frac{1}{2}(I - A)$, where μ is the chemical potential and χ is the electronegativity. The electrophilicity is a descriptor of reactivity that allows a quantitative classification of the global electrophilic nature of a molecule within a relative scale and is effectively the power of a system to soak up electrons. The electrophilicity index ω can be expressed by $\omega = \mu^2/2\eta$ and the global softness is defined as $\sigma = 1/\eta$.

During the interaction of the inhibitor molecule with bulk metal, electrons flow from the lower electronegative molecule to the higher electronegative metal until the chemical potential becomes equalized. The fraction of the transferred electron, ΔN , was estimated according to Pearson [24], $\Delta N = \chi_m - \chi_i / 2(\eta_m + \eta_i)$, where the indices m and i refer to metal atom and inhibitor molecule, respectively. The fraction of transferred electrons given in the table is calculated for iron metal, the experimental work function of polycrystalline Fe (4.5 eV) [25] was employed for electronegativity, and a global hardness of zero was used due to the $I = A$ approximation for bulk iron. If $\Delta N < 3.6$, the inhibition efficiency increases by increasing the electron-donating ability of these molecules to donate electrons to the metal surface [7]. Linoleic acid has the largest fraction of transferred electrons to the iron metal, closely followed by oleic acid, in agreement with the above ordering supported by electronic parameters.

Table 1. Calculated quantum chemical descriptors at the B3LYP/6-311G+(d,p) basis set for oleic and linoleic acids in gas and aqueous phases.

Compound	Oleic acid		Linoleic acid	
	G	A	G	A
E_{HOMO} (eV)	-6.714	-6.726	-6.639	-6.676
E_{LUMO} (eV)	-0.303	-0.422	-0.309	-0.421
ΔE ($E_L - E_H$) (eV)	6.411	6.304	6.330	6.255
μ (D)	2.064	2.507 (2.47/2.63±0.05) ^b	2.072	2.529
ω	1.920	2.026	1.907	2.013
χ	3.509	3.574	3.474	3.549
η	3.206	3.152	3.165	3.128
σ	0.312	0.317	0.316	0.319
ΔN	0.155	0.147	0.162	0.152
E_T	-0.802	-0.788	-0.791	-0.782

^a G – gas phase ($\epsilon = 1.0$), A – aqueous phase ($\epsilon = 78.5$); ^b Ref. [26]

The dipole moment of oleic acid in the gaseous phase is not known, and as experimental moments only the calculated dipole moments were available for these molecules on the basis of Debye's and Kirkwood-Frölich's theories [26]. The fit of the calculated dipole moments with the experimental dipole moments is also of the same accuracy, considering the values for aqueous phase. The dipole moment of linoleic acid is found to be slightly higher than that of oleic acid, which probably increases its adsorption on the metal surface.

To understand the adsorption of Argan oil over an iron surface at a molecular level, two models were used for single-point energy calculations. For ease of presentation, each model was composed of two-directional oleic or linoleic acid molecules and two ranks of Fe clusters labeled OA, LA, F1, and F2, in which OA and LA represent individual oleic and linoleic acid molecules, and F1 and F2 represent the two ranks of Fe clusters (Fig. 2). To investigate the interactions between the iron clusters in the model, F1F2 and OAOA (or LALA) were considered to be two independent entities. The interaction energy (E) between the two ranks of iron clusters and the OA molecules (Model 1) can be expressed as follows:

$$E(\text{Model 1}) = E(\text{OAF1F2OA}) - E(\text{F1F2}) - E(\text{OAOA}) \quad (1)$$

A similar equation can be written to express the interaction energy (E) between the two ranks of iron clusters and the LA molecules (Model 2):

$$E(\text{Model 2}) = E(\text{LAF1F2LA}) - E(\text{F1F2}) - E(\text{LALA}) \quad (2)$$

According to the results derived from the calculations by the PM6 method, interaction energies were found to be $-5846.41 \text{ kcal mol}^{-1}$ and $-115.35 \text{ kcal mol}^{-1}$ for Models 1 and 2, respectively. The results indicate that the interaction energy for Model 2 is dominated by the main interaction between Fe and O atoms of linoleic acid molecules due to the hybridization. However, it should be noted here that structural and energetic factors cannot always be in direct correlation for a metal atom- π interaction because the strength of the interaction is grossly decided by the electrostatic interactions and the size of the π -system. Our calculated results indicate a preference for linoleic acid to be oriented towards the metal surface, and the hydrophobic component to be oriented away from the surface. In the light of the findings above, linoleic acid appears to be the predominant molecule which synergistically interacts with other active substances naturally present in the oil and enables Argan oil to be an effective corrosion inhibitor in acidic media.

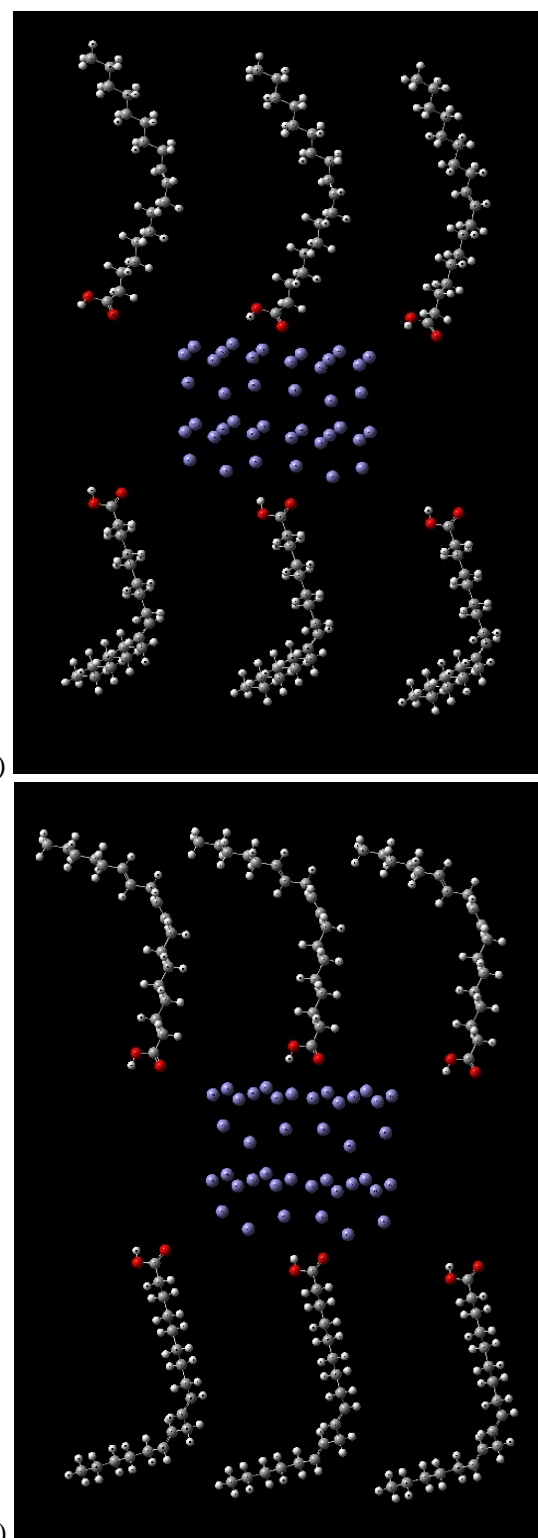


Fig. 2. Regularly spaced iron clusters (purple spheres) trapped in (a) Model 1 between OA molecules and (b) Model 2 between LA molecules.

CONCLUSIONS

Despite the vast literature on natural oils as corrosion inhibitors there was no unified explanation for all known examples. We have shown how an understanding of typical inhibition efficiency of such oils can arise from the use of density functional

theory calculations. Although a clear decomposition of the energetic contributions of individual interactions is, strictly speaking, impossible, approximate propensities can be derived. Noteworthy is the fact that the ground state of the protonated forms of the compounds yields the electronic and global reactivity parameters giving considerable credence for the identified structures in acidic medium. On the basis of the data obtained at the B3LYP/6-311+G(d,p) level, we can confirm that the most stable unsaturated fatty acid is linoleic acid, which seems to be responsible for the inhibition efficiency of Argan oil in chloride solutions.

REFERENCES

1. K. K. Anupama, K. Ramya, A. Joseph, *Measurement*, **95**, 297 (2017).
2. K. Cherrak, A. Dafali, A. Elyoussfi, Y. El Ouadi, N. K. Sebbar, M. El Azzouzi, H. Elmselleem, E. M. Essassi, A. Zarrouk, *JMES*, **8**, 636 (2017).
3. G. Gece, *Corros. Sci.*, **53**, 3873 (2011).
4. M. A. Dar, *Ind. Lubr. Tribol.*, **63**, 227 (2011).
5. L. Afia, R. Salghi, L. Bammou, E. Bazzi, B. Hammouti, L. Bazzi, A. Bouyanzer, *J. Saudi Chem. Soc.*, **18**, 19 (2014).
6. Z. Charrouf, D. Guillaume, *Eur. J. Lipid Sci. Technol.*, **110**, 632 (2008).
7. G. Gece, *Corros. Sci.*, **50**, 2981 (2008).
8. I. B. Obot, S. A. Umoren, Z. M. Gasem, R. Suleiman, B. El Ali, *J. Ind. Eng. Chem.*, **21**, 1328 (2015).
9. H. M. Abd El-Lateef, *Corros. Sci.*, **92**, 104 (2015).
10. G. Gece, *Corros. Rev.*, **33**, 195 (2015).
11. M. K. Awad, M. R. Mustafa, M. M. Abouelnga, *Prot. Met. Phys. Chem. Surf.*, **52**, 156 (2016).
12. A. Valbon, M. A. Neves, A. Echevarria, *Int. J. Electrochem. Sci.*, **12**, 3072 (2017).
13. M. E. Mashuga, L. O. Olasunkanmi, E. E. Ebenso, *J. Mol. Struct.*, **1136**, 127 (2017).
14. M. J. Frisch, G. W. Trucks, H. B. Schlegel, G. E. Scuseria, M. A. Robb, J. R. Cheeseman, G. Scalmani, V. Barone, B. Mennucci, G. A. Petersson, H. Nakatsuji, M. Caricato, X. Li, H. P. Hratchian, A. F. Izmaylov, J. Bloino, G. Zheng, J. L. Sonnenberg, M. Hada, M. Ehara, K. Toyota, R. Fukuda, J. Hasegawa, M. Ishida, T. Nakajima, Y. Honda, O. Kitao, H. Nakai, T. Vreven, J. A. Montgomery, Jr., J. E. Peralta, F. Ogliaro, M. Bearpark, J. J. Heyd, E. Brothers, K. N. Kudin, V. N. Staroverov, R. Kobayashi, J. Normand, K. Raghavachari, A. Rendell, J. C. Burant, S. S. Iyengar, J. Tomasi, M. Cossi, N. Rega, J. M. Millam, M. Klene, J. E. Knox, J. B. Cross, V. Bakken, C. Adamo, J. Jaramillo, R. Gomperts, R. E. Stratmann, O. Yazayev, A. J. Austin, R. Cammi, C. Pomelli, J. W. Ochterski, R. L. Martin, K. Morokuma, V. G. Zakrzewski, G. A. Voth, P. Salvador, J. J. Dannenberg, S. Dapprich, A. D. Daniels, Ö. Farkas, J. B. Foresman, J. V. Ortiz, J. Cioslowski, D. J. Fox, Gaussian 09, Revision C.01, Gaussian, Inc., Wallingford CT, 2010.
15. M. Iwahashi, Y. Kasahara, H. Matsuzawa, K. Yagi, K. Nomura, H. Terauchi, Y. Ozaki, M. Suzuki, *J. Phys. Chem. B*, **104**, 6186 (2000).
16. G. E. Doan, *The Principles of Physical Metallurgy*, McGraw-Hill, New York, 1953.
17. J. J. P. Stewart, *J. Mol. Model.*, **13**, 1173 (2007).
18. J. H. Schulman, A. H. Hughes, *Proc. R. Soc. London A*, **138**, 430 (1932).
19. J. R. Kanicky, D. O. Shah, *J. Colloid Interface Sci.*, **256**, 201 (2002).
20. M. Suzuki, T. Ogaki, K. Sato, *J. Am. Oil Chem. Soc.*, **62**, 1600 (1985).
21. F. Kaneko, K. Yamazaki, K. Kitagawa, T. Kikyo, M. Kobayashi, *J. Phys. Chem. B*, **101**, 1803 (1997).
22. T. Koopmans, *Physica*, **1**, 104 (1934).
23. B. Gómez, N. V. Likhanova, M. A. Dominguez-Aguilar, R. Martínez-Palou, A. Vela, J. L. Gazquez, *J. Phys. Chem. B*, **110**, 8928 (2006).
24. R. G. Pearson, *Inorg. Chem.*, **27**, 734 (1988).
25. H. Michaelson, *J. Appl. Phys.*, **48**, 4729 (1977).
26. F. F. De Sousa, S. G. C. Moreira, S. J. Dos Santos Da Silva, J. D. Nero, Jr. P. Alcantara, *J. Bionanosci.*, **3**, 139 (2009).

ТЕОРЕТИЧНА ОСНОВА ЗА ХАРАКТЕРИСТИКАТА НА ИНХИБИРАНЕ НА КОРОЗИЯТА НА АРГАНОВО МАСЛО

Г. Гедже

*Департамент по химия, Факултет по природни науки, архитектура и инженерство, Технически университет
на Бурса, Бурса, 16310 Турция*

Получена на 3 април, 2017 г.; коригирана на 2 май, 2016 г.

(Резюме)

Естествените масла играят централна роля при инхибиране на корозията на различни метали и сплави. Въпреки това, потенциалната им ефективност на инхибиране в киселинни среди е много слабо изследвана от теоретична гледна точка. Въпреки частичното експериментално потвърждение, характеристиката за инхибиране на корозията на такива масла води до продължителен дебат за това как механизъмът на инхибиране може да бъде свързан с техните съставки. Предвид необходимостта от по-добро разбиране на поведението на защитата на аргановото масло върху въглеродната стомана в моларни разтвори на НС1, електронните свойства на две ненаситени мастни киселини, т.е. молекули на олеинова и линоленова киселина, са изследвани чрез изчисления с теория на функционалната на плътността (DFT). Протонираните форми на олеиновите и линоленовите киселини дадоха квантови химични параметри, които потвърждават, че линоленовата киселина е най-стабилната ненаситена мастна киселина, която също изглежда е отговорна за ефективността на инхибиране на арганово масло в кисела среда.

Modeling of the physicochemical properties of aliphatic alcohols using topological indices and quantitative structure-property relationship

F. Arjmand¹, F. Shafiei^{2*}

¹Department of Chemistry, Science Faculty, Arak Branch, Islamic Azad University, Arak, Iran

²Department of Chemistry, University of Pitesti, Pitesti-110040, Romania

Received May 23, 2017; Accepted June 14, 2017

QSPR models are mathematical equations that attempt to correlate chemical structure with a wide variety of physical, chemical and biological properties. In this study, the relationships between the Randic' ($^1\chi$), Balaban (J), Wiener polarity (W_p), Hyper Wiener (WW), Szeged (Sz), Harary (H), and Wiener (W) indices to the entropy (S), thermal energy (E_{th}) and heat capacity (C_v) of alcohols are presented. Physicochemical properties are determined by the quantum mechanics methodology at the Hartree-Fock (HF) level using the *ab initio* 6-31G basic set. Multiple linear regressions (MLR) and backward methods were employed to obtain the QSPR models. After MLR analysis, we studied the validation of linearity between the molecular descriptors in the best models for the used properties. The satisfactory results obtained show that the combination of the three descriptors ($^1\chi$, J, W) is excellent to predict heat capacity and thermal energy while the three descriptors (J, W, W_p) are useful to predict the entropy of the 158 aliphatic alcohols.

Keywords: Topological indices; Aliphatic alcohols; QSPR; MLR method; Validation.

INTRODUCTION

Quantitative structure-activity/property relationships (QSAR/QSPR) represent an attempt to relate structural descriptors of molecules with their physicochemical properties and biological activities [1].

Topological indices (TIs), as molecular descriptors, are important tools in QSPR/QSAR studies [2]. A topological index is a graph invariant number calculated from a graph representing a molecule.

The basic strategy of QSPR is to find the optimum quantitative relationship which can then be used for the prediction of the properties of molecular structures including those unmeasured or even unknown [3].

The Xu index, the atomic index (AI) and the MLR method were used to predict some properties of alcohols [4].

The novel edge connectivity index (mF) is introduced for predicting some properties of alcohols. The results show that the MLR method can provide high-quality models for several representative properties of alcohols [5].

The QSPR analysis of 58 saturated alcohols for predicting some physicochemical properties such as boiling point (B_p), water solubility ($\log W$) and *n*-octanol-water partition coefficient ($\log Pow$) by using odd-even index (OEI) combined with the

novel molecular polarizability effect index (MPEI) was studied [6].

The novel atom-type indices (DAI) have been used to construct QSPR/ QSAR models for some physical properties and biological activities of alcohols by using MLR analysis [7].

Predictive methods for estimating physicochemical properties, such as the heat capacity of alcohols and aldehydes in liquid phase have been reported [8].

The semi-empirical electrotopological index (I_{SET}) has been developed to describe the gas chromatographic retention of aliphatic alcohols [9].

The minimal boiling point of simple saturated alcohols has been predicted by using the Wiener, first and second Zagreb indices [10].

QSPR models have been proposed for prediction of molecular properties such as molecular weight (mw), hardness (η), chemical potential (μ), total energy (E_{total}), and electrophilicity index (ω) of phenols [11].

The semi-empirical topological index has been calculated for predicting the relationship between structure and chromatographic retention for several data sets of alkanes, alkenes, esters, ketones, aldehydes and alcohols [6, 12].

In the present study, multiple linear regression (MLR) techniques and backward methods were used for modeling the thermal energy (E_{th} kcal/mol), heat capacity (C_v cal/molK) and entropy (S cal/molK) of 158 alcohols.

* To whom all correspondence should be sent:
E-mail: f-shafiei@iau-arak.ac.ir

MATERIALS AND MATHEMATICAL METHOD

The aliphatic alcohols are a homologous series of organic compounds containing one or more hydroxyl groups [-OH] attached to a single-bonded alkane.

Alcohols are important in organic chemistry because they can be converted to and from many other types of compounds. Alcohols are also technologically important materials and are used in the manufacture of a large number of products.

Quantum chemistry method

The entropy, thermal energy, and heat capacity of 158 saturated alcohols were obtained by the quantum mechanics methodology at HF level using the *ab initio* 6-31G basic set. To obtain a suitable model, QSPR used the linear multiple regression method, backward methods and the software SPSS Version 20. Microsoft Office 2010 programs were employed to chart results.

The molecules used in this collection include a variety of aliphatic alcohols that are classified into primary, secondary (*sec-*, *s-*), and tertiary (*tert-*, *t-*), based upon the number of carbon atoms connected to the carbon atom that bears the hydroxyl group. The quantum chemistry data of the 158 congeners are listed in Table 1.

Topological indices

Topological indices are numerical parameters of a graph that characterize its topology and are usually graph-invariant. Nowadays, in the literature, hundreds of topological indices, suitable to describe different properties, are reported.

The indicators used in this study are those with first-order molecular connectivity [13], such as Balaban [14], Randic' [15], Wiener [16], Hyper-Wiener [17], Wiener Polarity [18], Szeged [19], and Harary [20]. All used topological indices were calculated with the Chemicalize program [21].

Statistical analysis

Structure-property models were generated using the MLR procedure of SPSS Version 20. The entropy, thermal energy, and heat capacity as dependent variables and ($^1\chi$, J, H, W, W_p , WW, Sz) indices as independent variables were used.

The models were assessed with correlation coefficient (R), squared multiple correlation coefficient (R^2), adjusted correlation coefficient (R^2_{adj}), Fisher ratio (F), standard error of estimate (s), and Durbin-Watson value (D).

RESULTS

Several linear QSPR models were created that contain 3-7 descriptors. To develop a linear model for predicting the entropy, thermal energy and heat capacity topological description was used. The strongest correlation is based on multivariate step backwards, and was conducted using the SPSS software.

The distribution of dependent variable *versus* independent variable was used for 158 alcohols in the development of structure-property relationships.

QSPR models for the entropy

Table 2 shows the regression parameters and the relationships between the proposed models for the entropy of 158 alcohols.

The best linear model for the entropy includes four topological descriptors ($^1\chi$, J, W, W_p). The regression parameters of the best model of the four descriptors are collected in Eqn. (1):

$$S = 38.963 + 14.628 \chi + 3.217 J + 0.009 W - 0.809 W_p \quad (1)$$

where N=158, R=0.992, $R^2=0.984$, $R^2_{adj}=0.983$, s=3.276 cal mol⁻¹ K⁻¹, F=2297.445, D=1.988.

QSPR models for the thermal energy

Table 3 shows the regression parameters and the relationships between the proposed models for the thermal energy of 158 alcohols.

The best linear model for the thermal energy includes six topological descriptors ($^1\chi$, J, H, W, WW, W_p). The regression parameters of the best model of the six descriptors are collected in Eqn. (2):

$$Eth = 5.339 + 24.145 \chi + 4.227 J + 4.540 H - 0.151 W + 0.019 WW - 1.681 W_p \quad (2)$$

where N=158, R=0.999, $R^2=0.998$, $R^2_{adj}=0.998$, s=3.403 kcal mol⁻¹, F=10555.138, D=1.906.

QSPR models for the heat capacity

Table 4 shows the regression parameters and the relationships between the proposed models for the heat capacity of 158 alcohols.

The best linear model for the heat capacity includes six topological descriptors ($^1\chi$, J, H, W, WW, W_p). The regression parameters of the best model of the six descriptors are collected in Eqn. (3):

$$CV = 2.706 + 3.321 \chi + 1.615 J + 1.418 H - 0.037 W + 0.005 WW - 0.407 W_p \quad (3)$$

where N=158, R=0.998, $R^2=0.996$, $R^2_{adj}=0.995$, s=1.026 cal mol⁻¹.K⁻¹, F=5686.131, D=1.821

The results for the entropy, thermal energy, and heat capacity are very satisfactory.

Table 1. Alcohols used in the present study

Compound	No.	Compound	No.	Compound	No.
methanol	1	1-octanol	54	4-methyl-4-octanol	107
ethanol	2	6-methyl-1-heptanol	55	4-ethyl-4-heptanol	108
1-propanol	3	2-octanol	56	3-methyl-3-octanol	109
2-propanol	4	3-octanol	57	1-decanol	110
1-butanol	5	4-methyl-1-heptanol	58	8-methyl-1-nonanol	111
2-methyl-1-propanol	6	4-octanol	59	2-decanol	112
2-butanol	7	2-ethyl-1-hexanol	60	4-decanol	113
2-methyl-2-propanol	8	2-methyl-2-heptanol	61	3,7-dimethyl-1-octanol	114
1-pentanol	9	5-methyl-2-heptanol	62	2,7-dimethyl-3-octanol	115
3-methyl-1-butanol	10	6-methyl-3-heptanol	63	2,6-dimethyl-4-octanol	116
2-pentanol	11	3-methyl-2-heptanol	64	2,3-dimethyl-3-octanol	117
2-methyl-1-butanol	12	2-methyl-3-heptanol	65	5-methyl-5-nonanol	118
3-pentanol	13	2-methyl-4-heptanol	66	4-methyl-1-nonanol	119
2,2-dimethyl-1-propanol	14	5-methyl-3-heptanol	67	2-methyl-3-nonanol	120
2-methyl-2-butanol	15	3-methyl-3-heptanol	68	2,2,5,5-tetramethyl-3-hexanol	121
1-hexanol	16	4-methyl-3-heptanol	69	4-propyl-4-heptanol	122
4-methyl-1-pentanol	17	3-methyl-4-heptanol	70	2,4,6-trimethyl-4-heptanol	123
2-hexanol	18	3,4-dimethyl-2-hexanol	71	3-ethyl-3-octanol	124
3-methyl-1-pentanol	19	2,5-dimethyl-2-hexanol	72	3-ethyl-2-methyl-3-heptanol	125
2-methyl-1-pentanol	20	4-methyl-4-heptanol	73	1-undecanol	126
3-hexanol	21	3-ethyl-3-hexanol	74	2-undecanol	127
2-ethyl-1-butanol	22	2,3-dimethyl-2-hexanol	75	3-undecanol	128
4-methyl-2-pentanol	23	3,5-dimethyl-3-hexanol	76	4-undecanol	129
3,3-dimethyl-1-butanol	24	2,3-dimethyl-3-hexanol	77	5-undecanol	130
2,3-dimethyl-1-butanol	25	2-methyl-3-ethyl-2-pentanol	78	6-undecanol	131
2-methyl-2-pentanol	26	2,4,4-trimethyl-2-pentanol	79	1-dodecanol	132
3-methyl-2-pentanol	27	2,2,4-trimethyl-3-pentanol	80	2-dodecanol	133
2-methyl-3-pentanol	28	2,2-dimethyl-3-hexanol	81	3-dodecanol	134
2,2-dimethyl-1-butanol	29	2,5-dimethyl-3-hexanol	82	4-dodecanol	135
3-methyl-3-pentanol	30	4,4-dimethyl-3-hexanol	83	1-tridecanol	136
3,3-dimethyl-2-butanol	31	3,4-dimethyl-2-hexanol	84	2-tridecanol	137
2,3-dimethyl-2-butanol	32	6-methyl-2-heptanol	85	3-tridecanol	138
1-heptanol	33	3-methyl-1-heptanol	86	4-tridecanol	139
5-methyl-1-hexanol	34	2-methyl-3-ethyl-3-pentanol	87	1-tetradecanol	140
2-heptanol	35	2,3,4-trimethyl-3-pentanol	88	2-tetradecanol	141
4-methyl-1-hexanol	36	1-nonanol	89	3-tetradecanol	142
2-methyl-1-hexanol	37	7-methyl-1-octanol	90	4-tetradecanol	143
3-heptanol	38	2-nonanol	91	1-pentadecanol	144
3-methyl-1-hexanol	39	3-nonanol	92	2-pentadecanol	145
4-heptanol	40	4-nonanol	93	3-pentadecanol	146
5-methyl-2-hexanol	41	5-nonanol	94	4-pentadecanol	147
2-methyl-3-hexanol	42	2-methyl-2-octanol	95	1-hexadecanol	148
2-methyl-2-hexanol	43	2,6-dimethyl-2-heptanol	96	2-hexadecanol	149
2,4-dimethyl-1-pentanol	44	2,6-dimethyl-3-heptanol	97	3-hexadecanol	150
5-methyl-3-hexanol	45	2,6-dimethyl-4-heptanol	98	4-hexadecanol	151
3-methyl-3-hexanol	46	3,6-dimethyl-3-heptanol	99	1-heptadecanol	152
2,4-dimethyl-2-pentanol	47	2,2,3-trimethyl-3-hexanol	100	2-heptadecanol	153
2,4-dimethyl-3-pentanol	48	3,5-dimethyl-4-heptanol	101	3-heptadecanol	154
3-ethyl-3-pentanol	49	2,3-dimethyl-3-heptanol	102	4-heptadecanol	155
2,3-dimethyl-2-pentanol	50	2,4-dimethyl-4-heptanol	103	1-nonadecanol	156
2,3-dimethyl-3-pentanol	51	2-methyl-3-ethyl-3-heptanol	104	2-nonadecanol	157
2,3,3-trimethyl-2-butanol	52	2,4,4-trimethyl-3-hexanol	105	1-icosane	158
3-methyl-2-hexanol	53	3,4,4-trimethyl-3-hexanol	106		

Table 2. Statistical parameters of models calculated with SPSS software for S.

Model	Independent variable	R	R ²	R ² _{adj}	s	F
1	¹ χ, J, H, W, WW, W _p , Sz	0.992	0.984	0.983	3.305	1290.019
2	¹ χ, J, H, W, W _p , Sz	0.992	0.984	0.983	3.294	1515.037
3	¹ χ, J, H, W, W _p	0.992	0.984	0.983	3.283	1829.730
4	¹ χ, J, W, W _p	0.992	0.984	0.983	3.276	2297.445

Table 3. Statistical parameters of models calculated with SPSS software for E_{th}.

Model	Independent variable	R	R ²	R ² _{adj}	s	F
5	¹ χ, J, H, W, WW, W _p , Sz	0.999	0.998	0.998	3.413	8992.932
6	¹ χ, J, H, W, WW, W _p	0.999	0.998	0.998	3.403	10555.138

Table 4. Statistical parameters of models calculated with SPSS software for Cv.

Model	Independent variable	R	R ²	R ² _{adj}	s	F
7	¹ χ, J, H, W, WW, W _p , Sz	0.998	0.996	0.995	1.029	4848.430
8	¹ χ, J, H, W, WW, W _p	0.998	0.996	0.995	1.026	5686.131

Table 5. Correlation between the molecular descriptors for S (model 4).

Pearson correlations (model 4)				Collinearity statistical		Corrected model	
J	W _p	¹ χ	W	Tolerance	VIF	VIF	
J	1	-0.831	0.458	0.237	0.261	3.828	3.026
W _p		1	-0.725	-0.019	0.071	14.113	6.693
¹ χ			1	-0.636	0.052	19.184	-
W				1	0.108	9.272	5.521

Table 6. Correlation between the molecular descriptors for E_{th}, Cv (models 6, 8).

Pearson correlations (models 6, 8)				Collinearity statistical			Corrected model	
J	W _p	¹ χ	H	WW	W	Tolerance	VIF	VIF
J	1	-0.354	0.557	-0.744	-0.636	0.680	0.108	9.244
W _p		1	-0.044	-0.246	-0.064	0.086	0.065	15.342
¹ χ			1	-0.713	-0.074	0.127	0.010	105.182
H				1	0.678	-0.735	0.003	319.815
WW					1	-0.993	0.002	633.551
W						1	0.001	1289.381

DISCUSSION

In this study, we will use the following sections to find the best model for predicting the properties mentioned.

Multicollinearity

In regression analysis collinearity occurs when two predictor variables in a multiple regression have a non-zero correlation. Multicollinearity occurs when more than two predictor variables are inter-correlated. The multicollinearity is a basis of the variance inflation factor (VIF) value of multicollinearity tests using SPSS. If the VIF value lies between 1 and 10, there is no multicollinearity; if VIF<1 or >10, there is multicollinearity.

In all our final models there is multicollinearity, because the values of correlations between

independent variables are near to one and VIF values are not between 1 and 10.

Verification and validation

Verification and validation are the primary processes for quantifying and building confidence (or credibility) in numerical models [22].

In this section for verification and validation of the regression models, we will focus on the Durbin-Watson statistics and unstandardized predicted and residual values.

Durbin-Watson statistics

The Durbin-Watson statistics is a test statistic tool used to detect the presence of auto correlation in residuals from a regression analysis. The value of D always lies between 0 and 4. If the Durbin-Watson statistics is substantially below 2, this is an evidence of a positive serial correlation.

If the Durbin-Watson is below 1.0, there might be a cause for alarm. Small values of D indicate that the successive error terms are, on the average, close in value to one another, or positively correlated. If $D > 2$, it indicates that the successive error terms are, on the average, much different in value from one another, i.e., they are negatively correlated.

In addition, if the value is between 1.5 and 2.5, it indicates that there is no correlation. In all our models, the value of Durbin-Watson statistics is close to 2 (see eqns. 1-3) and hence the errors are uncorrelated.

For validation of the linearity between the molecular descriptors in the equations 1-3 we obtained the Pearson coefficient of correlation and collinearity statistics by SPSS as follows from Tables 5, 6.

For model 4, VIF values for two descriptors, W_p and $^1\chi$, are bigger than 10, therefore there is a linearity between these descriptors. After removing $^1\chi$ from this model, we corrected model 4 as follows:

$$S = 97.531 - 8.187 J + 3.496 WP + 0.051 W \quad (4)$$

where $N=158$, $R=0.965$, $R^2=0.931$, $R^2_{adj}=0.929$, $Q^2_{LOO}=0.937$, $s=6.726 \text{ cal mol}^{-1} \text{ K}^{-1}$, $F=687.413$, $D=0.971$.

Similar to model 4 we obtained the corrected models 6 and 8 as follows:

$$E_{th} = -9.881 + 37.254 1\chi + 12.466 J + 0.003 WW \quad (5)$$

where $N=158$, $R=0.998$, $R^2=0.996$, $R^2_{adj}=0.996$, $Q^2_{LOO}=0.997$, $s=4.475 \text{ kcal mol}^{-1}$, $F=12182.971$, $D=1.832$.

$$CV = -7.109 + 8.031 1\chi + 4.512 J + 0.001 WW \quad (6)$$

where $N=158$, $R=0.996$, $R^2=0.992$, $R^2_{adj}=0.992$, $Q^2_{LOO}=0.993$, $S=1.385 \text{ cal .mol}^{-1} \text{ K}^{-1}$, $F=6222.373$, $D=1.724$.

In eqns. 4, 5, and 6, Q^2_{LOO} are the squared cross-validation coefficients for leave-one-out, respectively. We have computed Q^2_{LOO} (Eqn. 7) by randomly taking 50% of the data that are positive and less than one.

$$Q^2 = 1 - \frac{\sum(Y_i - \hat{Y}_{i|i})^2}{\sum(Y_i - \bar{Y})^2} \quad Q^2 \leq 1 \quad (7)$$

In eqn. (7), the notation $i|i$ indicates predicted by a model estimated when the i -th sample was left out from the training set.

Regular residuals

The residual is the difference between the observed and predicted value. A residual plot is a graph that shows the residual values on the vertical

axis and the independent variables on the horizontal axis.

If the points in a residual plot are randomly dispersed around the horizontal axis, a linear regression model is appropriate for the data; otherwise, a non-linear model is more appropriate.

The residual values of the entropy, thermal energy, and heat capacity expressed by Eqns. (4-6) were calculated. The residual values show a relatively random pattern (see Figs. 1-3). This relatively random pattern shows that a linear model provides a decent fit to the data.

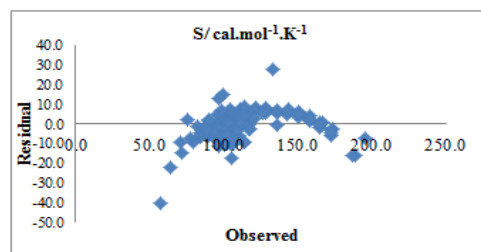


Fig. 1. Plot of residuals against observed values of the entropy.

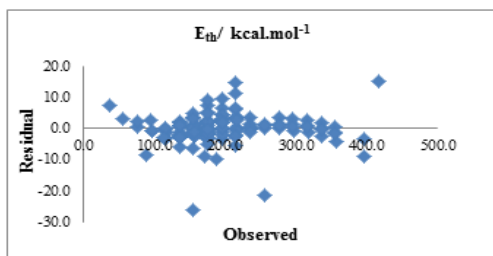


Fig. 2. Plot of residuals against observed values of the thermal energy.

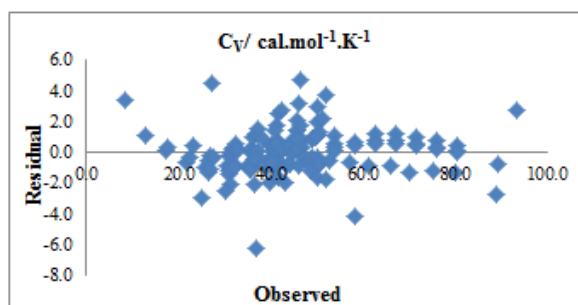


Fig. 3. Plot of residuals against observed values of the heat capacity.

Figs. 4-6 show the linear correlation between the observed and the predicted entropy, thermal energy, and heat capacity values obtained using eqns. (4-6), respectively.

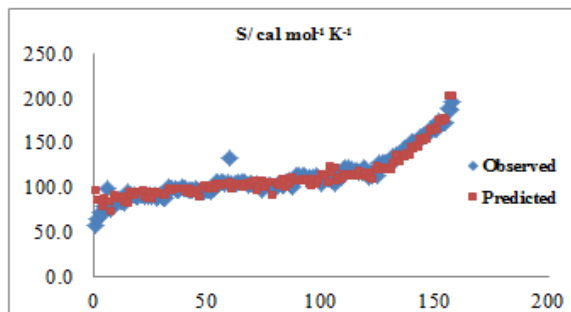


Fig. 4. Comparison between predicted and observed entropy by the MLR method.

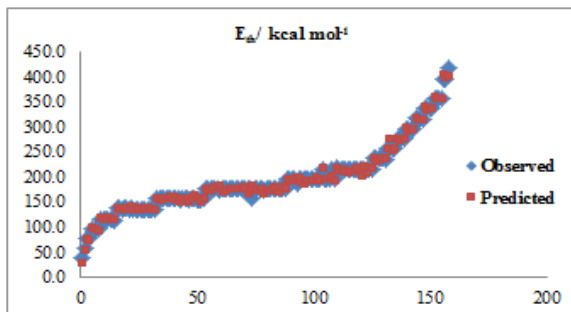


Fig. 5. Comparison between predicted and observed thermal energy by the MLR method.

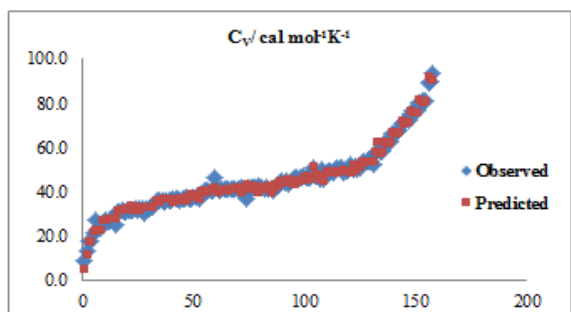


Fig. 6. Comparison between predicted and observed heat capacity by the MLR method.

CONCLUSIONS

The conception that there exists a close relationship between bulk properties and molecular structure is quite deeply rooted in chemistry. The basic tenet of chemistry is to identify these assumed relationships between molecular structure and physicochemical properties and to quantify them.

The QSPR approach, including multivariate data analysis in combination with statistical design, has been extensively employed.

In this study, QSPR mathematical models for the prediction of the entropy, thermal energy and heat capacity of alcohols by using methods based on topological descriptors calculated from molecular structure alone were developed. These QSPR models

showed high values of the multiple correlation coefficient ($R > 0.99$) and Fisher-ratio statistics.

The MLR model proved to be a useful tool in the prediction of S, E_{th} and the leave-one-out cross-validation, as the evaluation technique was designed to evaluate the quality and predictive ability of the MLR model. The obtained results showed that the three topological indices (J, W, W_P) are suitable for predicting S, and the three descriptors (¹ χ , J, W) are suitable for predicting E_{th} and C_v of 158 alcohols.

REFERENCES

1. A. Kumar, B. Narasimhanb, and D. Kumar, *Bioorg. Med. Chem.*, **15**, 4113 (2007).
2. F. Shafiei, H. Hosseini, *MATCH Commun. Math. Comput. Chem.*, **75**, 583 (2016).
3. M. Pashmforush, F. Shafiei, and F. Dialamehpour, *Iran. J. Math. Chem.*, **7**, 15 (2016).
4. B. Ren, *Comput. Chem.*, **26**, 223 (2002).
5. L. Mu, C. Feng, *MATCH Commun. Math. Comput. Chem.*, **56**, 217 (2006).
6. F. Liu, C. Cao, and B. Cheng, *Int. J. Mol. Sci.*, **12**, 2448 (2011).
7. C. Lu, W. Guo, Y. Wang, *J. Mol. Model.*, **12**, 749 (2006).
8. F. Ashrafi, R. Saadati, and A. Behboodi Amlashi, *Afr. J. Pure Appl. Chem.*, **2 (11)**, 116 (2008).
9. B. da Silva Junkes, R.D.D.M.C. Amboni, R.A. Yunes, and V.E.F. Heinzen, *Internet Electron. J. Mol. Des.*, **2**, 33 (2003).
10. M. Goubko, O. Miloserdov, *MATCH Commun. Math. Comput. Chem.*, **75**, 29, (2016).
11. F. A. Pasha, H. K. Srivastava, Y. Beg, and P. P. Singh, *Am. J. Immunology*, **2 (1)**, 23 (2006).
12. Z. Lin, J. Xu, X. Zheng, and Z. Li, *Acta Phys. Chem. Sin.*, **16**, 153 (2000).
13. M. Randić, *J. Math. Chem.*, **7**, 155 (1991).
14. A. T. Balaban, *Chem. Phys. Lett.*, **89**, 399 (1982).
15. M. Randić, *Acta. Chim. Slov.*, **49**, 483 (2002).
16. B. Zhou, I. Gutman, *Chem. Phys. Lett.*, **394**, 93 (2004).
17. D. J. Klein, W. Yan, and Y.N. Yeh, *Int. J. Quantum Chem.*, **106**, 1756 (2006).
18. M. Liu, B. Liu, *MATCH Commun. Math. Comput. Chem.*, **66**, 293 (2011).
19. P. V. Khadikar, N. V. Deshpande, P. P. Kale, A. Dobrynin, I. Gutman, and G. Dömötör, *J. Chem. Inf. Compt. Sci.*, **35**, 547(1995).
20. K. C. Das, B. Zhou, and N. Trinajstić, *J. Math. Chem.*, **46**, 1369 (2009).
21. Web search engine developed by ChemAxon; software available at <http://WWW.Chemicalize.Org>.
22. P.J. Roach, Verification and Validation in Computational Science and Engineering, Hermosa Publishers, Albuquerque, NM, 1998, p.446.

МОДЕЛИРАНЕ НА ФИЗИКОХИМИЧНИТЕ СВОЙСТВА НА АЛИФАТНИ АЛКОХОЛИ, ИЗПОЛЗВАЙКИ ТОПОЛОГИЧНИ ИНДЕКСИ И КОЛИЧЕСТВЕНА ВРЪЗКА СТРУКТУРА- СВОЙСТВА

Ф Арджманд¹, Ф. Шафиei^{2*}

¹Департамент по химия, Факултет по наука, Клон Арак, Исламски университет "Арак", Арак, Иран

²Департамент по химия, Университет на Питещи, Питещи-110040, Ромъния

Получена на 23 май, 2017 г.; коригирана на 14 юни 2017 г.

(Резюме)

QSPR моделите са математически уравнения, които целят да свържат химическата структура с голямо разнообразие от физични, химични и биологични свойства. В тази работа е изследвана връзката между Randic' (${}^1\chi$), Balaban (J), Wiener polarity (W_p), Hyper Wiener (WW), Szeged (Sz), Harary (H) и Wiener (W) индекси и ентропията (S), топлинната енергия (E_{th}) и топлинния капацитет (CV) на алкохоли. Физикохимичните свойства се пресмятат с метода на квантовата механика с нивото на Hartree-Fock (HF), като се използват базовите сетове ab initio 6-31G. Многобройните линейни регресии (MLR) и обратните методи са използвани за получаване на моделите QSPR. След MLR анализ ние проучихме валидирането на линейността между молекулните дескриптори в най-добрите модели за използваните свойства. Задоволителните резултати показват, че комбинирането на трите дескриптора (${}^1\chi$, J, W) е подходящо за предсказване на топлинен капацитет и топлинна енергия, докато трите дескриптора (J, W, WP) са полезни за предсказване ентропията на 158 алифатни алкохола.

Improvement of physical and optical properties of chitosan-rice starch films pre-treated with ultrasound

U. Vr. Brodnjak

University of Ljubljana, Faculty of Natural Sciences and Engineering, Department of Textiles, Graphic Arts and Design, Snežniška 5, SI-1000, Ljubljana, Slovenia

Transparent films of chitosan, rice starch and a blend of chitosan-rice starch were prepared using water, malic acid and glycerol as a plasticiser. Before casting, the film solutions were treated with ultrasound with a view to improve the physical, optical and surface properties of the films. The results showed that an ultrasonic treatment improved elasticity, moisture resistance and transparency of the films. For all ultrasound-treated films, elongation at break and tensile strength increased, especially for the blend films. Moreover, the moisture content decreased proportionally to the increase in thickness with decreasing film solubility for all treated samples. The surface of the untreated blend film was more uneven compared to chitosan and rice starch films, which improved after the treatment. The preparation of film solutions using ultrasound is an improved procedure to increase many properties of biodegradable films.

Keywords: ultrasonic treatment; biodegradable polymers; blend films; material testing.

INTRODUCTION

Packaging is a part of the goods, which causes a big environmental impact after its use. Producers of bio-based materials are keen on replacing oil-based packaging materials with green, sustainable materials which also have improved mechanical, antimicrobial and barrier properties [1, 2]. Therefore, every year, new biodegradable materials are produced. Some of the most nontoxic and widely used polymers are polysaccharides, chitosan being one of them. It is a natural polysaccharide derived from the deacetylation of chitin [3]. Chitosan has also attracted interest in packaging, especially in food packaging area as edible films and coatings [4]. From the research it is known that chitosan films have good mechanical properties, e.g., they are flexible, long lasting, of good strength and increase the storage life of fresh food [5]. They also have good barrier properties against grease due to the positive charge on the amino group under acidic conditions, where chitosan binds negatively charged molecules. Moreover, chitosan films exhibit excellent oxygen-barrier properties, due to their high crystallinity and hydrogen bonds between the molecular chains [6]. Some of the most important properties as regards food packaging are the moisture properties. Chitosan exhibits good moisture properties, however, not sufficient for food applications, as its hydrophilic nature attracts moisture [7]. In order to improve the moisture properties and functional properties of chitosan films, blending with other biopolymers and

hydrophobic substances has been proposed [8, 9]. In previous research, chitosan films and chitosan blends with other natural polymers have been made [9–11]. Due to the high amount of amylase, rice starch is attractive for food packaging as a film barrier [12]. It has also been used to replace plastic film barriers as it has good mechanical properties [12–14]. Rice is the most widely used basic food in the world. Due to different climates, soil characteristics and cultures, more than 240 000 registered varieties of rice and consequently, as many different types of rice starch exist in the world [6]. The ultrasonic technology is an environmentally friendly technology which is nowadays used in food, pharmaceutical, chemical, etc., industries. With this technology, improvements in materials can be achieved. Previous research has shown a positive effect of ultrasonic treatment on the gelatinisation of starch dispersions [15]. It is known that the application of ultrasonic treatment to starch films improved the moisture properties of the treated starch and provided stronger structures [16]. Bourtoom & Chinnan studied the effect of rice starch incorporated into a chitosan film. The composite film showed an increase in tensile strength, moisture, water vapor permeability, but a decrease in elongation at break [10].

This research describes the preparation, characterisation and ultrasonic treatment of the chitosan-rice starch blend films. The aim of the research was to improve the mechanical, moisture and optical properties of chitosan, rice starch and composite chitosan-rice starch film using ultrasonic treatment. Previously, no research has been

* To whom all correspondence should be sent:

E-mail: urska.vrabić@ntf.uni-lj.si

conducted on rice starch-chitosan blend films, and the improvement of their properties with ultrasound. Our research was focused on the effect of ultrasonic treatment on the solutions for the preparation of the mentioned films. Using ultrasound is an environmentally friendly process and it can be used for all solutions in order to improve biodegradable films. Such a treatment and materials could be used as a substitute for packaging films that are currently on the market.

MATERIALS AND METHODS

Materials

Rice starch was obtained from Farmalabor Srl (Italy), with 14% moisture content, 1% proteins and 0.6% ashes. Chitosan, with molecular weight 20kDa and deacetylation degree higher than 85%, was purchased from Sigma Aldrich (Austria). Chitosan solutions were prepared by dissolving 2 g of chitosan in 100 ml of malic acid. Malic acid (98%) was purchased from Sigma Aldrich (Austria). Glycerol (Sigma Aldrich, Austria), was used as a plasticiser.

Preparation of film-forming dispersions

Preparation of a dispersion for rice starch film

The rice starch dispersion was prepared by dissolving 2 g of rice starch in 100 ml of distilled water and glycerol (40% w/w) was added as a plasticiser. The solution was mixed until it gelatinised (85 °C for 20 min) and then cooled to room temperature.

Preparation of solution for chitosan film

The chitosan solution was prepared by dissolving 2 g of chitosan in 100 ml (2% w/w) malic acid and glycerol (40% w/w) was added as a plasticiser. The solution was stirred at 90 °C for 5 min until chitosan was dispersed. Then the solution was cooled to room temperature. Before cooling down, the film solution was filtered through a polyester screen (mesh no. 140 with mesh opening 160 µm) with aspiration to remove small lumps from the solution.

Preparation of a solution for a chitosan-rice starch blend film

The rice starch-chitosan film was prepared by mixing 100 ml of 2% rice starch solution with 100 ml of 2% chitosan solution. After that, 40% of glycerol (w/w of total solid weight in solution) was added as a plasticiser to the solution. The total solution for the blend film was stirred at 800 rpm for 5 min at room temperature and filtered through a polyester screen with the same mesh opening as for the chitosan solution. Aspiration was performed in order to remove small lumps from the solution.

Ultrasonic treatment of solutions

After the aspiration, the solutions (for chitosan film, rice starch film and blend film) were put into an ultrasonic bath (Asonic, Ultrasonic bath), using constant 35 kHz frequency for 15 min [16].

Preparation of casting films

After the aspiration and the treatment, the mixtures (untreated and treated) were cast onto petri dishes (50 ml), spread thinly, uniformly and dried at 55 °C for 10 h. After the films were peeled off from the dishes, they were cooled at room temperature (23 °C; 55% RH). The films were stored in desiccators at 60% RH for further investigations.

Characterisation of the films

Film thickness

The thickness of the films was measured with a precision digital micrometre Mitutoyo Corporation, Japan, to the nearest 0.0001 µm at 5 random locations on each film.

Moisture content

Moisture content was determined by measuring the weight loss upon drying in a laboratory oven at 105 ± 1 °C until constant weight. Five samples per each film were tested and the results were expressed in percentage.

Water vapor permeability (WVP)

To determine the WVP of films, the ASTM E96 standard desiccant method was used [19]. The test cups were filled with silica gel (RH = 16% in the cup), where a sample was placed between the cup and the ring cover [20]. There was an air gap of 11 mm between the silica gel and the underside of the placed film. To ensure the best results of WVP, a silicone sealant was applied around the cup edge. The films with an exposed area of 50 cm² were tested at 90 ± 2% RH and 38 ± 2 °C for 24 h. Three replicates per each film were tested.

Film solubility (FS)

Water solubility of each film was determined as well. The samples (four samples per each film type) were dried at 105 °C for 24 h to determine the weight of the dry matter. Additional four samples of the same film type were placed in a 50 mL beaker containing 30 mL of distilled water. The beakers were covered with parafilm and stored in an environmental chamber for 1 h, where the climate conditions were 25 °C and 55% RH [21]. After that, the beakers were removed from the chamber, the films were peeled off from the beakers and gently rinsed with distilled water. All samples were then dried in an oven at 105 °C for 24 h. Three replicates per each film were tested. The total soluble matter-

film solubility (FS) was calculated using the following equation [21]:

$$FS (\%) = \frac{(mass\ of\ the\ film\ before\ test - mass\ of\ the\ film\ after\ test)}{mass\ of\ the\ film\ before\ test} \cdot 100$$

Mechanical properties

Tensile strength (TS) and elongation at break (E) of the films were determined on a tensile testing machine Instron 6022. The samples were analysed in standard atmosphere (temperature $23^{\circ}\text{C} \pm 1^{\circ}\text{C}$ and relative humidity $55\% \pm 2\%$). The cross speed head was 0.15 mm/s. Films of 6 cm in length and 0.7 cm in width were used, and a minimum of five probes for each sample was tested. During sample stretching, several load and elongation data per second were recorded until a break of the sample occurred.

Colour

The film colour was determined using the CIE colorimeter X-rite. The CIE Lab scale was used to determine L^* , a^* and b^* colour values. A standard plate was used as the standard ($L^* = 92.82$, $a^* = -1.24$, $b^* = 0.5$). Six measurements for each specimen at different locations on the samples were made. Before the colour measurements, the samples were conditioned at 55% RH and $25 \pm 2^{\circ}\text{C}$ for 72 h.

Total colour differences (ΔE), chroma (C) and hue angle (H) were calculated with the following equations [10, 21]:

$$\Delta E = \sqrt{(\Delta L^*)^2 + (\Delta a^*)^2 + (\Delta b^*)^2}$$

$$\Delta L^* = L^* - L_0^*$$

$$\Delta a^* = a^* - a_0^*$$

$$\Delta b^* = b^* - b_0^*$$

$$C = (a^*)^2 + (b^*)^2$$

$$H = \tan^{-1} \left(\frac{b^*}{a^*} \right) \quad \text{when } a^* > 0 \text{ and } b^* > 0$$

$$H = 180^{\circ} + \tan^{-1} \left(\frac{b^*}{a^*} \right) \quad \text{when } a^* < 0$$

$$H = 360^{\circ} + \tan^{-1} \left(\frac{b^*}{a^*} \right) \quad \text{when } a^* > 0 \text{ and } b^* < 0$$

where: L^* , a^* , b^* are the standard and L_0^* , a_0^* , b_0^* the sample colour parameters.

Fourier transform infrared spectroscopy (FTIR)

The FTIR spectra of the studied sample films were obtained on a Perkin Elmer spectrophotometer equipped with an attenuated total reflection (ATR) cell. The spectra were recorded over the range of $4000\text{--}800\text{ cm}^{-1}$, with a resolution of 4 cm^{-1} . For each spectrum, 146 consecutive scans were averaged.

Surface properties – Scanning electron microscope (SEM)

The SEM micrographs of the film surfaces were taken with a scanning electron microscope (JSM - 6060 LV). The instrument was operated at 10 kV, at a magnification of $400\times$.

Statistical analysis

The results for tensile properties, thickness, moisture, WVP and FS, given in the article, represent mean values \pm standard deviation. The analysis of variance-ANOVA was performed on the obtained results to establish significant differences.

RESULTS AND DISCUSSION

One of the major issues in using ultrasound in polymer processing is the controlled modification of the interaction between polymers without chemical modification. The results of previous research have shown that an ultrasonic treatment of the starch dispersion increased its solubility and clarity, but decreased viscosity [6, 15]. In this study, an ultrasonic treatment of the film solution was used in order to increase the solubility of composition components, which influences many film properties (strength, elongation, moisture and colour). The results showed that the ultrasonic treatment increased the moisture content and at the same time improved tensile properties. Generally, the film structure became stronger, more flexible and more even.

Thickness, moisture content, WVP and film solubility

The water vapour permeability (WVP) of films for food packaging should be as low as possible, because high WVP determines poor barrier properties. The thickness of films influences water vapour properties [17, 18]. The nature of films from biopolymers is mostly hydrophilic; therefore, the thickness influences the water barrier and the mechanical properties. In our research, the thickness (mean values) of films was used in the calculations for water vapour properties (TS). Table 1 shows a comparison of untreated and treated films and it can be seen that the chitosan-rice starch blend film treated with ultrasound exhibits better WVP than the untreated ones. From the literature it is known that glycerol is hydrophilic and improves moisture/barrier properties [20]. In our research, glycerol was added as a plasticiser, whereas the ultrasonic treatment had the biggest impact on WVP [20, 22]. From the obtained results it follows that the best water vapour properties are manifested by the chitosan-rice starch film treated with ultrasound ($3.37 \pm 0.29\text{ g mm/m}^2/\text{day kPa}$, i.e. by two times lower than the untreated sample). The same trend

was detected for the chitosan and rice-starch film. The WVP of untreated chitosan film decreased with the treatment from 9.11 to 8.47 g mm/m²/day kPa. Previous research has explained that chitosan films have high oxygen but poor water vapour barrier due to their hydrophilic character, which was confirmed in our research [20–23].

As expected, the values of the moisture content of the untreated films were higher than those of the treated ones. The highest moisture content was displayed by the untreated chitosan film (11.03%) and the lowest – by the treated blend film (9.0%). The ultrasonic treatment affected all films regarding moisture absorption, with a decrease between 0.5 and 1%. The decrease was not major, yet an impact on the solution and afterwards on other film properties was detected. The acoustic activation in a ultrasonic bath caused differences in the tested films. In the case of addition of glycerol, for all tested films the observed behaviour can be a result of an increase in free volume, and a consequent decrease in WVP and moisture content. The reason is the high content of glycerol, which was present at all samples. Water solubility is important for the films used in food packaging. Stuchell & Krochta explained in their research that blend films used for packaging maintained their integrity after 24 h of incubation, which indicates that rice starch and chitosan intra- and intermolecular network remained the same, and that only monomers and non-protein material were soluble in water [24]. The obtained results showed that the solubility of the films decreased with the ultrasonic treatment. As expected, the untreated rice starch film had the highest solubility (56%), which decreased with the ultrasonic treatment (49%), but the values still remained the highest among all tested samples. From Table 1 it follows that chitosan interacted with rice starch in the blend film; therefore, the solubility was lower for treated (30%) and untreated (35%) samples than for pure rice starch film. Both, the untreated (22%) and treated (18%) chitosan films had the lowest water solubility compared to the other film samples. The ultrasonic treatment decreased water solubility and moisture content of all treated films.

The equilibrium thickness of all samples as a function of moisture content and film solubility for chitosan and blend films is shown in Fig. 1. The results show that the ultrasonic treatment reduced the ability of the chitosan film to absorb water from 11.3% to 10.8% when thickness decreased. The film solubility was lower for both treated samples. The results suggest that the interaction of chitosan with rice starch, when a film is formed, limits film solubility, which, on its turn, reduces its moisture content. Chitosan strengthened the film structure of the blend mixture and solubility in water decreased when the thickness increased.

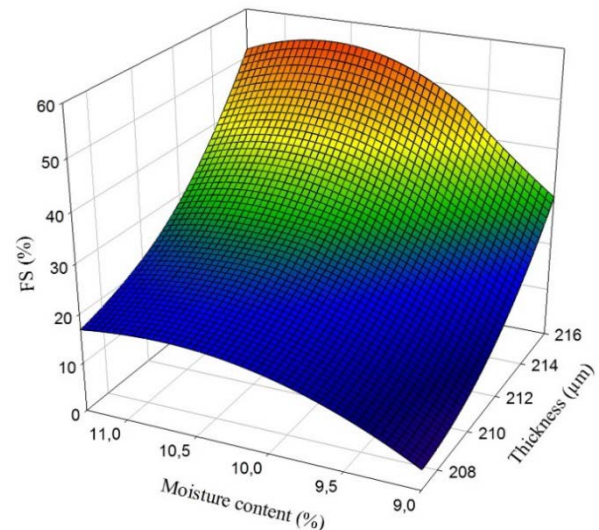


Fig. 1. Percentage of moisture content of chitosan and blend films (treated and untreated) as a function of thickness and film solubility.

Moisture content of rice starch films treated with ultrasound decreased as a function of thickness and water solubility (Fig. 2). In general, the treated films (rice starch and blend mixtures) showed decreased water solubility with respect to the percentage of moisture content and thickness. The studies of glycerol as a plasticiser have shown an increase in moisture content due to its hydrophilicity [20–23]. The presence of rice starch in the blend films can form highly cross-linked systems, preventing water molecules from penetrating into the composite films [23]. Such behaviour was confirmed in our

Table 1. Thickness, moisture content, water vapour properties (WVP) and film solubility (FS) of sample films.

	Sample	Thickness (μm)	Moisture content (%)	WVP (g mm/m ² /day kPa)	FS (%)
Untreated	Chitosan film	210 ± 2.5a	11.3 ± 0.55	9.11 ± 0.36b	22 ± 2.5
	Rice starch film	205 ± 5.0a	10.8 ± 0.69	6.45 ± 0.75b	56 ± 1.7
	Blend film	215 ± 3.3a	9.5 ± 0.23	7.92 ± 0.17b	35 ± 1.9
Ultrasound treated	Chitosan film	207 ± 6.7a	10.8 ± 0.47	8.47 ± 0.24b	18 ± 3.4
	Rice starch film	203 ± 4.2a	9.6 ± 0.18	5.45 ± 0.36b	49 ± 4.6
	Blend film	216 ± 1.2a	9.0 ± 0.78	3.37 ± 0.29b	30 ± 2.7

^a Mean of five replicates ± standard deviation; ^b Mean of three replicates ± standard deviation.

research due to the inclusion of glycerol and rice starch as well, since they interfere with cross-links, resulting in decreased water solubility.

Mechanical properties

Good mechanical properties such as tensile strength are very important for packaging films, due to the handling and shipping of packaged products. Elongation at break – flexibility is also very important. For such products, high tensile strength is required, but deformation and elongation should be adjusted according to the characteristics required for certain film applications. The mechanical properties of untreated films presented in the literature for chitosan and rice starch films were comparable to our results [10, 20]. The films with different components and treatment were flexible and with appropriate manageability. The results of the study of tensile strength and elongation at break of untreated and ultrasound treated films are presented in Fig. 3.

The results demonstrated that tensile strength increased with the ultrasonic treatment for all treated films. Better results of TS were obtained for treated

samples and the maximum occurred for the blend of chitosan-rice starch film. The values for untreated films are slightly higher, but still comparable to those reported in the literature [17].

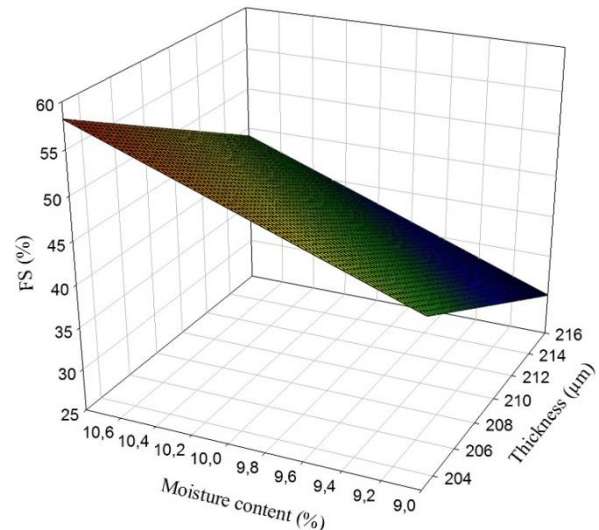


Fig. 2. Percentage of moisture content of rice starch and blend films (treated and untreated) as a function of thickness and film solubility.

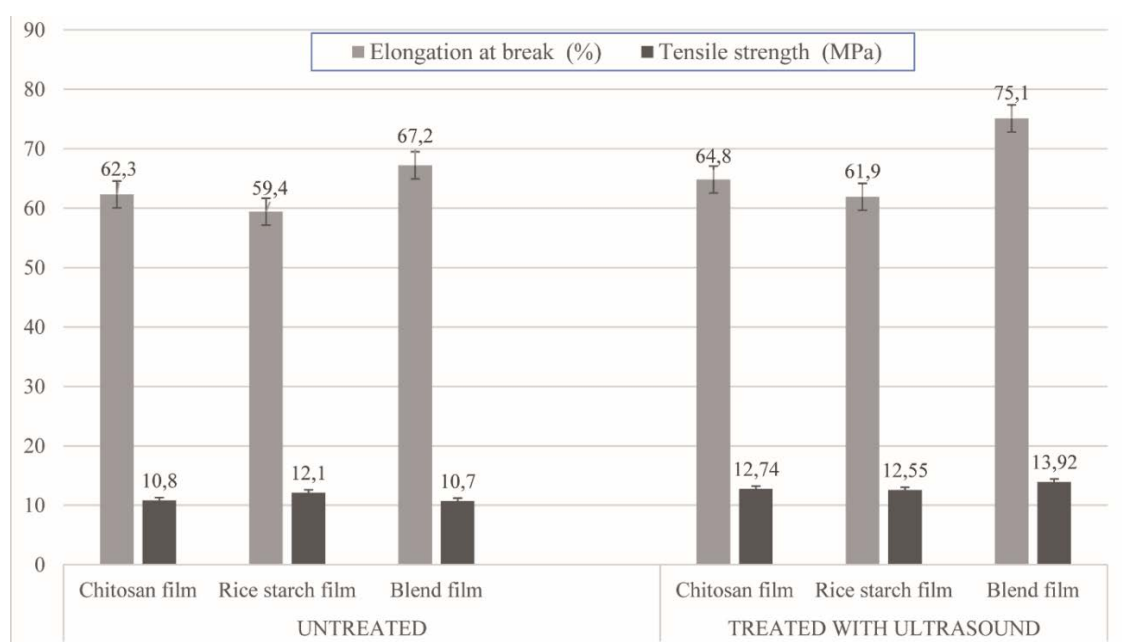


Fig. 3. Results of the study of tensile strength (TS) and elongation at break (E) of untreated and ultrasound treated films.

Table 2. Colour values (L^* a^* b^*), colour differences (ΔE), chroma (C) and hue angle (H) of untreated and ultrasound treated films.

	Sample	L^*	a^*	b^*	ΔE	C	H
Untreated	Chitosan film	84.06	-3.19	10.36	3.56	10.84	178.75
	Rice starch film	86.65	-4.07	9.88	6.28	10.67	178.89
	Blend film	88.92	-3.00	11.35	5.92	11.73	178.75
Ultrasound treated	Chitosan film	85.78	-2.05	9.22	2.36	9.45	178.68
	Rice starch film	91.66	-4.89	7.30	5.69	8.79	179.21
	Blend film	90.45	-2.78	9.07	5.50	9.49	178.75

The highest increase was detected for the blend of chitosan-rice starch film (30%), and for the chitosan film (18%). The treated rice starch film displayed a lower increase (4%). Elongation at break (E) is an indicator of film extensibility and is determined as the point when a film breaks at tensile testing. The values of the elongation at break were affected by the ultrasonic treatment. The highest elongation at break was obtained for blend films, which increased by 8% on ultrasonic treatment. For both rice starch and chitosan films elongation increased by 2.5%. The elongation values were higher for all samples due to the added plasticiser glycerol. Nevertheless, the elongation at break was better for all treated samples because of the increase in solubility and homogeneity of the film solutions, due to the acoustic activation in the ultrasonic bath.

Optical properties

The colour of films can be a factor in terms of consumer demands and it does not affect other analysed properties. The results are shown in Table 2. Generally, colour is an important factor of the appearance of packaging materials [25]. The total colour difference, chroma and hue angle were calculated from the colour values. The untreated chitosan films were more coloured than rice starch and blend films. It is known that chitosan has more yellowness compared to other tested samples in the research. From the L^* values which indicate lightness it can be seen that the treated samples are less coloured, lighter, especially the rice starch film. The a^* and b^* values vary significantly between the untreated and treated samples. All films include a

plasticiser which also affected the colour [10]. The hue angle was not significantly different among all sample films. The results of calculated chroma showed that the untreated samples have more yellowness than the treated ones.

FTIR analysis of films

Characteristic peaks were determined and compared with data from previously published research papers [4, 26, 27].

The spectra of untreated and treated chitosan and rice starch films are presented in Fig. 4. The spectra of the untreated films are similar to those published before [28]. In the FTIR spectrum of untreated chitosan films, peaks between 3000–3600 cm^{-1} are typical for OH stretching. The peak at 3269 cm^{-1} is an O-H stretch, at 2930 cm^{-1} it represents a CH_2 group and at 2880 cm^{-1} - CH_3 , the aliphatic group of chitosan. The smaller, hardly noticeable peak at 1635 cm^{-1} is a consequence of the C=O stretch of amide I, and the peaks at 1563 and 1565 cm^{-1} are N-H bending vibrations (amide II). An intensive peak at 1410 cm^{-1} suggests deformation vibrations of OH and CH groups, the peak at 1099 cm^{-1} is for glycosidic bonds and at 1016 cm^{-1} - for an ether group in the chitosan film. For the treated chitosan film, an increase in the peak intensity of the ether group at 1016 cm^{-1} is detected. The same higher intensity of peaks is detected for the peaks at 1096 cm^{-1} , 2932 cm^{-1} and 2881 cm^{-1} . In the FTIR spectrum of untreated rice starch film, a peak at 3230 cm^{-1} is detected, which presents the O-H stretch. The peak at 2900 cm^{-1} corresponds to the C-H stretch.

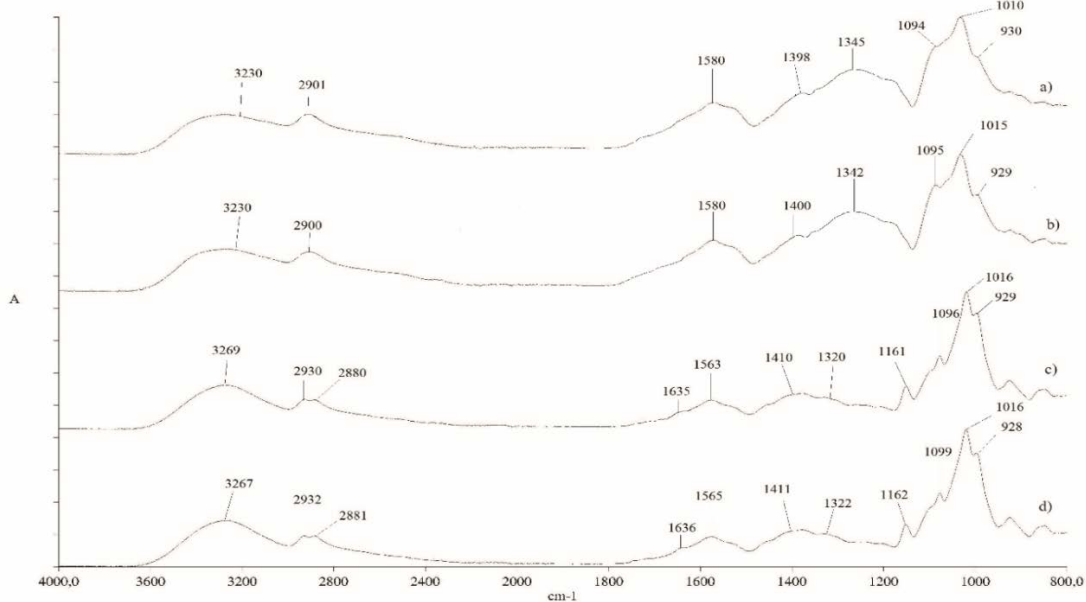


Fig. 4. FTIR spectra of untreated and ultrasound treated films: (a) untreated rice starch film, b) treated rice starch film, c) untreated chitosan film, d) treated chitosan film.

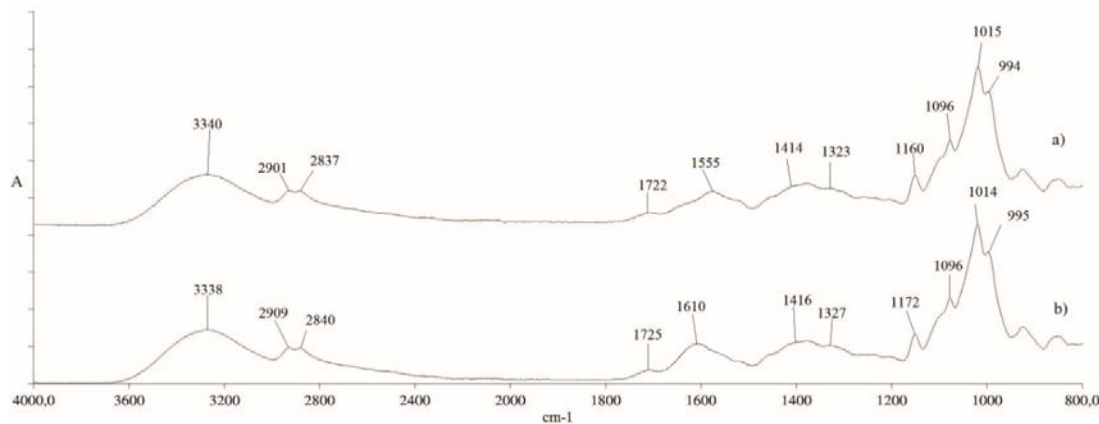


Fig. 5. FTIR spectra of (a) untreated and (b) ultrasound treated blend chitosan-rice starch films.

The peak at 1345 cm⁻¹ presents the O-H of water, whereas the 1400 cm⁻¹ and 1398 cm⁻¹ peaks result from the deformation vibrations of OH and CH groups. For the treated rice starch films, the effect of ultrasound on the film was the same as on chitosan. The intensity of peaks slightly increased, especially for the peaks between 1600 and 1000 cm⁻¹.

In the blend of rice starch-chitosan films, physical blends *versus* chemical interactions are affected by the changes in characteristic peaks [5]. From the spectra of untreated blend films presented in Fig. 5, a decrease in the amine peak intensity at 1555 cm⁻¹ and 1416 cm⁻¹ can be seen. The reason for the decrease is the smaller amount of chitosan in the blend film, compared to pure chitosan film. The region between 1600 cm⁻¹ and 900 cm⁻¹ shows some shifts of absorption bands, which indicate interactions between the macro chains of chitosan and rice starch. The peak at 1555 cm⁻¹ shifts to 1610 cm⁻¹, which suggests interactions between the hydroxyl group of rice starch and the amino group of chitosan [29]. The spectra of ultrasound treated blend film show small, yet noticeable changes in the intensities of peaks compared to the untreated blend film. The changes in the absorption bands of all ultrasound treated films were connected to the increase in the number of free mobile macromolecules rather than a breakage of starch molecules [30]. As predicted, the ultrasonic treatment improved the blend solution which became more homogeneous. It provided a dispersion capacity and as a result, more chain to chain interactions between polysaccharides were involved.

Surface characterisation

The effect of ultrasonic treatment on the surface of films was determined using a scanning electron microscope (SEM). SEM micrographs of untreated and treated films are presented in Fig. 6 (a-f). All figures show the surface of the films at 400× magnification and voltage 10 kV. The 10kV voltage

was used since at higher voltage, film samples would get damaged very quickly and the determination of the surface would not be correct. 400× magnification was used, as higher magnifications degrade the surface of the analysed films. The surface micrographs revealed a smooth, even surface for all treated films. As seen in Figure 6a, the untreated chitosan film is less smooth and not as even as the film treated with ultrasound (Fig. 6b). The same trend is seen in Figs. 6c and 6d, where the SEM micrographs of rice starch are shown. From Fig. 6c it can be seen that the untreated rice starch film has a more irregular surface than the chitosan film.

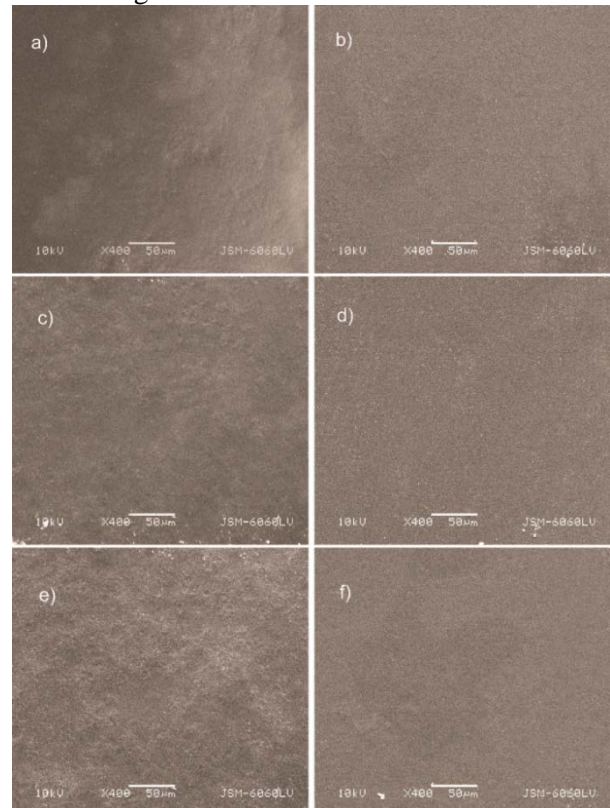


Fig. 6. SEM micrographs of untreated and ultrasound treated films: a) untreated chitosan film, b) treated chitosan film, c) untreated rice starch film, d) treated rice starch film, e) untreated chitosan-rice starch blend film, f) treated chitosan-rice starch blend film.

The untreated chitosan rice starch blend film had a less uniform, smooth and dense structure (Figs. 6e and 6f). The ultrasonic treatment improved the homogeneity of the surface, which is a good indicator of the better structural and mechanical properties, compared to the untreated films. In general, the ultrasonic treatment helps to obtain a smooth and homogeneous surface.

CONCLUSIONS

Chitosan, rice starch and chitosan-rice starch blend films were successfully prepared, and the solutions of films were successfully treated with ultrasound. The results showed that the ultrasonic treatment had a good impact on the preparation and properties of films. The surface of films improved for all treated films. The mechanical resistance of treated films was improved, especially for the blend film. By mixing these two polymers, the characteristics of the film improved and with an ultrasonic treatment, the properties got even better. The reaction between the two polymers in the blend film was confirmed by FTIR analysis. In addition, in blend films, a decrease in water vapour permeability was detected and this could be explained with the higher glycerol content of the chitosan-rice starch blend films. There has been a lot of research performed on chitosan and rice starch films, but less on improving blend films. New studies are necessary to find the best ultrasonic procedures (regarding treatment times and frequency) to prepare the films. One of the issues to be taken into account in further research on enhancing water barriers and tensile properties of blend chitosan-rice starch films treated with ultrasound is to prepare a bi-layer or laminated films in order to ensure more effective barriers against water transfer and better mechanical properties than blend films.

Acknowledgements: The author would like to thank the University of Ljubljana, Faculty of Natural Sciences and Engineering for its financial support and a colleague from the Faculty of Natural Sciences and Engineering, Jana Rozman, for her help at the preparation of films.

REFERENCES

- 1.J.M. Krochta, C.De Mulder-Johnston, *Food Technology*, **51**, 61 (1997).
- 2.R. J. Hernandez, *Food Engineering*, **22**, 495 (1994).
- 3.C. Caner, P. J Vergano, J. L. Wiles, , *Journal of Food Science*, **63**, 1049 (1998).
- 4.X. Y. Xu, K. M. Kim, M. A. Hanna, D. Nag, *Industrial Crops and Products*, **21**, 185 (2005).
- 5.R. H. Chen, J. H. Lin, *Carbohydrate Polymers*, **24**, 41 (1994).
- 6.T. Wittaya, Rice Starch-Based Biodegradable Films: Properties Enhancement, Structure and Function of Food Engineering, Prof. Ayman Amer Eissa (Ed.), ISBN: 978-953-51-0695-1, InTech, DOI: 10.5772/47751. Available from: <http://www.intechopen.com/books/structure-and-function-of-food-engineering/rice-starch-based-biodegradable-films-properties-enhancement>, 2016 (accessed 26.2.2016)
- 7.M. S. Rao, S. R. Kanatt, S. P. Chawla, A. Sharma, *Carbohydrate Polymers*, **82**, 1243 (2010).
- 8.M. B. Vásconez, S. K Flores, C.A. Campos, J. Alvarado, L. N. Gerschenson, *Food Research International*, **42**, 762 (2009).
- 9.J. W. Rhim, C. L. Weller, K. S. Ham, *Food Science and Biotechnology*, **7**, 263 (1998).
- 10.T. Bourtoom, M. S. Chinnan, *Food Science and Technology*, **41**, 1633 (2008).
- 11.M. Jaworska, K. Sakurai, P. Gaudon, E. Guibal, *Polymer International*, **2**, 198 (2003).
- 12.Z. Zhou, K. Robards, S. Helliwell, C. Blanchard, *International Journal of Food Science & Technology*, **37**, 849 (2002).
- 13.H. Dai, P. R. Chang, F. Geng, J. Yu, X. Ma, *Carbohydrate Polymers*, **79**, 306 (2010).
- 14.N. Follain, C. Joly, P. Dole, C. Bliard, *Carbohydrate Polymers*, **60**, 185 (2005).
- 15.Y. Z. Jenny, K. Kai, M. Raymond, K. Sandra, A. Muthupamidian, *Ultrasonics Sonochemistry*, **16**, 462 (2009).
- 16.W. J. Cheng, J. C. Chen, D. H. Liu, X. Q. Ye, F. S. Ke, *Carbohydrate Polymers*, **81**, 707 (2010).
- 17.S. Rivero, M. A. García, A. Pinotti, *Journal of Food Engineering*, **90**, 531 (2009).
- 18.K. Cooksey, K. Marsh, L. Doar, *Food Technology*, **53**, 60 (1999).
- 19.ASTM, Standard test methods for water vapor transmissions of materials, In: Annual book of ASTM standards, American Society for Testing and Materials, Philadelphia (1980).
- 20.P. C. Srinivasa, M. N. Ramesh, K. R. Kumar, R. N Tharanathan, *Journal of Food Engineering*, **63**, 79 (2004).
- 21.J. W. Rhim, S. I. Hong, H. M. Park, K. W. N. Perry, *Journal of Agricultural and Food Chemistry*, **54**, 5814 (2006).
- 22.A. B. Dias, C. M. O. Müller, F. D. S. Larotonda, J. Laurindo, *Journal of Cereal Science*, **51**, 213 (2010).
- 23.B. L. Butler, P. L. Vergano, R. F. Testin, J. M. Bunn, J. L. Wiles, *Journal of Food Science*, **61**, 953 (1996).
- 24.Y. M. Stuchell, J. M. Krochta, *Journal of Food Science*, **59**, 1332 (1994).
- 25.P. C. Srinivasa, M. N. Ramesh, K. R. Kumar, R. N. Tharanathan, *Carbohydrate Polymers*, **52**, 431 (2003).
- 26.Y. L. Guan, X. F. Liu, Y. P. Zhang, K. D. Yao, Study phase behavior on chitosan/viscose rayon blend film, *Journal of Applied Polymer Science*, **67**, 1965 (1998).
- 27.U. Vrabič Brodnjak, *Progress in Organic Coatings*, **103**, 93 (2017).

U. V. Brodnjak: Improvement of physical and optical properties of chitosan-rice starch films pre-treated with ultrasound

28. D. Bajer, H. Kaczmarek, *Progress on Chemistry and Application of Chitin and its Derivatives*, **15**, 17 (2010).
29. P. Meenakshi, S. E. Noorjahan, R. Rajini, U. Venkateswarlu, C. Rose, T. P. Sastry, *Bulletin of Material Science*, **25**, 25 (2002).
30. Y. Iida, T. Tuziuti, K. Yasui, A. Towata, T. Kozuka, *Innovative Food Science Emerging Technologies*, **9**, 140 (2008).

ПОДОБРЯВАНЕ НА ФИЗИЧНИТЕ И ОПТИЧНИТЕ СВОЙСТВА НА ФИЛМИТЕ ОТ ХИТОЗАН-ОРИЗОВО НИШЕСТЕ, ПРЕДВАРИТЕЛНО ТРЕТИРАНИ С УЛТРАЗВУК

У. Вр. Бродняк*

Люблянски Университет, Факултет по природни науки и инженерство, Департамент по текстил, графично изкуство и дизайн, Сњеженшика 5, SI-1000, Любляна, Словения

Получена на 3 април, 2017 г.; коригирана на 18 юни 2017 г.

(Резюме)

Прозрачни филми от хитозан, оризово нишесте и смес от хитозан-оризово нишесте се приготвят като се използва вода, ябълчена киселина и глицерол като пластификатор. Преди отливане, филмните разтвори са третирани с ултразвук. Целта на изследването е да се постигнат подобрени физически, оптични и повърхностни свойства на филмите. Резултатите показват, че ултразвуковото лъчение подобрява еластичността, устойчивостта на влага и прозрачността на филмите. При всички ултразвуково обработени филми нараства удължаването при скъсване и якостта на опън, особено при смесени филми. Освен това, съдържанието на влага показва намаление, пропорционално на увеличаването на дебелината при намаляваща разтворимост на филма при всички третирани пробы. Повърхността на необработения смесен филм е по-неравномерна в сравнение с филмите на хитозана и оризовото нишесте, които се подобряват след обльчването. Приготвянето на филмови разтвори с ултразвук е подобрена процедура за увеличаване на много свойства на биоразградими филми.

Removal of lead (Pb^{2+}) from synthetic wastewater using calcium pectate

D. Paliulis*, A. Krinickaitė

Department of Environmental Protection and Water Engineering, Vilnius Gediminas Technical University, Saulėtekio Ave. 11, LT-10223 Vilnius, Lithuania

Received May 9, 2017; Accepted October 1, 2017

The present work deals with the use of calcium pectate as a biosorbent for $Pb^{(II)}$ ions removal from aqueous solutions. Surface morphology of the adsorbent was analysed by scanning electron microscopy (SEM). The surface chemical nature of the biosorbent was studied by Fourier transform infrared spectroscopy (FTIR). The FTIR results revealed that amide, ether, alcohol and carbonyl functional groups are responsible for $Pb^{(II)}$ biosorption onto calcium pectate. Batch experiments were carried out to investigate the effects of pH, time, and initial metal ion concentration on the adsorption of $Pb^{(II)}$ ions by the biosorbent in synthetic wastewater. The optimum contact time and pH for the removal of $Pb^{(II)}$ ions were 480 min and pH 5.0, respectively. It was found that the maximum loading capacity of the biosorbent was $4.45\text{ mg}\cdot\text{g}^{-1}$ for $Pb^{(II)}$ ions. Results indicated that the mechanism of $Pb^{(II)}$ ions adsorption onto calcium pectate is ion exchange between $Ca^{(II)}$ and $Pb^{(II)}$ ions in the solution. The equilibrium data were analysed according to the linear forms of the Langmuir and Freundlich isotherms. Freundlich model gives a better fit than the Langmuir model. The results suggest that calcium pectate can be used as an effective, low cost, and eco-friendly green adsorbent for the removal of $Pb^{(II)}$ ions from aqueous solutions.

Keywords: Calcium pectate; Adsorption; Lead; Langmuir isotherm; Freundlich isotherm.

INTRODUCTION

Heavy metal pollution has become one of the most serious environmental problems today [1]. Lead and other heavy metals are often detected in industrial wastewaters originating from metal plating, mining activities, smelting, battery manufacture, tanneries, petroleum refining, paint manufacture, pesticides, pigment manufacture, printing and photographic industries, etc. Heavy metals are non-biodegradable and they can be accumulated in living tissues, causing various diseases and disorders; therefore they must be removed before discharge [2]. Many wastewater treatment techniques are used worldwide for pollutant removal from aqueous solutions such as reverse osmosis, coagulation, membrane filtration, ion exchange and adsorption. Among all techniques, adsorption is considered as the most suitable process, because of its simplicity and cost effectiveness [3]. Currently a high number of experimental studies are carried out where modified or synthetic adsorbents are used for removal of heavy metals from water, but there is still not enough data about biosorbent usage for this purpose. Biosorption can be used as a cost-effective and efficient technique for the removal of toxic heavy metals from wastewater. Waste materials from industries such as food processing and agriculture may act as biosorbents [4]. Different biosorbents are

tested for heavy metals removal form water, e.g. fruit wastes [4-6], fruit peels [7-13], watermelon rinds [14], passion fruit skins [15], garlic peels [16], chemically treated lemon residues [17], modified orange peels [18,19], chemically modified muskmelon peels [20].

The objective of this work was to determine the possibility of using calcium pectate as an effective adsorbent for the removal of $Pb^{(II)}$ ions from wastewater.

MATERIALS AND METHODS

Stock solutions of Pb ($1000\pm2\text{ ppm}$, Buck Scientific, USA) and Ca ($1000\pm2\text{ ppm}$, Carl Roth, Germany) were used for FAAS or GFAAS calibration. Standard solutions with the required $Pb^{(II)}$ concentrations ($0.5, 1.0, 2.5, 5.0\text{ mg L}^{-1}$) were prepared by appropriate dilution with deionized water. The pH of every solution was maintained at a desired value by adding 0.01 M NaOH or 0.01 M HNO_3 .

Adsorbent acquisition and preparation

The modified pectin type LM-101 AS, supplied by CP Kelco, Denmark was used in the experiments. This type of pectin was selected because of its low degree of esterification (36%), which displays a higher calcium sensitivity than pectins of higher degree of esterification. This enables the formation of calcium pectate gels [21]. In order to obtain a biosorbent with higher adsorption capacity the method suggested by Jakóbik-Kolon *et al.* [22] was

* To whom all correspondence should be sent:
E-mail: dainius.paliulis@vgtu.lt

selected. Obtained hydrogels were filtered through glass fiber filter with $0.45\text{ }\mu\text{m}$ pore size and washed with deionized water to remove excess of calcium. Then the beads were dried at 30°C for 72 h to obtain xerogels which were used for the adsorption and desorption of $Pb(\text{II})$.

Functional groups

A sample of the biosorbent was mixed with KBr and the functional groups were determined using a Perkin Elmer FTIR spectroscope.

Surface morphology

SEM examination of the biosorbent was done at 5 kV of accelerating voltage to study the surface texture and morphology of the biosorbent.

Adsorption procedure under dynamic conditions

$Pb(\text{II})$ solutions of desired concentrations (0.5, 1.0, 2.5, 5.0 mg L^{-1}) were prepared from the stock solution of Pb (1000 ± 2 ppm) by appropriate dilutions at different pH values (2.0, 3.0, 4.0 and 5.0). Higher pH values were avoided to prevent lead precipitation as hydroxide. Above precipitation pH (5.0) $Pb(\text{II})$ ions are removed by both adsorption and precipitation. For determination of the effect of contact time on the adsorption of $Pb(\text{II})$ from the solution, the experiments were conducted by varying the agitation time from 0.5 h to 8 h until equilibrium was reached at the most efficient pH of the solution containing the highest concentration of lead. In order to describe whether the adsorption is physical or chemical the calcium release was measured on an atomic absorption spectrometer. All adsorption experiments were carried out using 1.0 g L^{-1} of calcium pectate xerogel beads. They were added to 50 mL of $Pb(\text{II})$ solutions in bottles with screwed tops which were closed hermetically. The biosorbent was shaken at room temperature ($20 \pm 1^{\circ}\text{C}$) for selected time intervals at a speed of 20 rpm (RS12, Labos Shake-Gerhardt, Germany) and vacuum filtered through $0.45\text{ }\mu\text{m}$ glass fiber filter. The amount of $Pb(\text{II})$ ions adsorbed at a time t , q_t (mg g^{-1}), was calculated using the following formula:

$$q_t = \frac{(C_0 - C_t)V}{W} \quad (1)$$

where C_t (mg L^{-1}) is the liquid phase concentration of $Pb(\text{II})$ ions at any time, C_0 (mg L^{-1}) is the initial concentration of $Pb(\text{II})$ ions in the solution. V is the volume of the solution (L) and W is the mass of dry biosorbent (g).

Effect of metal concentration

The concentration of $Pb(\text{II})$ was determined by assessing the static $Pb(\text{II})$ adsorption from the aqueous solution.

Freundlich isotherm

Freundlich isotherm is widely applied in heterogeneous systems [18]. Freundlich isotherm is expressed as:

$$\log q_e = \log K_F + \frac{\log C_e}{n} \quad (2)$$

where q_e is the amount of adsorbate in the biosorbent at equilibrium (mg g^{-1}); K_F - Freundlich isotherm constant (mg g^{-1}); C_e - equilibrium concentration of $Pb(\text{II})$ (mg L^{-1}); n - adsorption intensity.

Langmuir isotherm

Langmuir isotherm is expressed as:

$$\frac{1}{q_e} = \frac{1}{Q_o} + \frac{1}{bQ_oC_e} \quad (3)$$

where q_e is the amount of adsorbate in the biosorbent at equilibrium (mg g^{-1}); Q_o - maximum monolayer coverage capacity (mg g^{-1}); b - Langmuir isotherm constant (L mg^{-1}); C_e - equilibrium concentration of $Pb(\text{II})$ (mg L^{-1}).

Analytical methods

Lead and calcium ion concentrations were determined using atomic absorption spectrometry (AAS; model Buck Scientific 210 VGP, USA) operated with an air-acetylene flame or graphite furnace, a slit of 0.7 mm at 283.2 and 400.7 nm wavelength, respectively.

Desorption procedure

After adsorption experiments the biosorbents were dried at $30 \pm 1^{\circ}\text{C}$ for 72 h and then mixed with 20 mL of 0.1 N HNO_3 solution. Samples were shaken on a RS-12 Rotoshake rotary shaker (Gerhard, Germany) for 0.5 h; 1 h; 4 h; 24 h at a speed of 20 rpm. After that the samples were filtered through glass fiber filter with $0.45\text{ }\mu\text{m}$ pore size. All experiments were conducted in triplicate and the mean of the three is presented. Blank samples (without $Pb(\text{II})$ ions) were used for validation studies. Concentrations of the $Pb(\text{II})$ ions in the blank solutions were below the detection limit.

RESULTS AND DISCUSSION

Imaging the surface of pectin gel beads using SEM microscope

The SEM image of calcium pectate xerogel was recorded (Fig 1). Though the beads seem to be oval in shape, the closer look reveals that their shape is uneven. The lighter colour shows salients and darker colour shows recesses. It is noticeable that the surface is irregular. One side of the bead is rougher than the other one. Steep slopes are also present. The biggest contrast between colours is at a zoom $\times 5000$ which indicates that even at very low levels there is significant roughness. However, the pores of the biosorbent are not seen here.

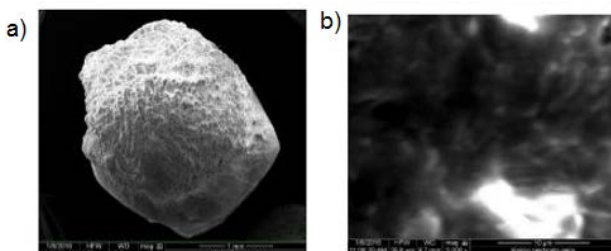


Fig. 1. SEM images of calcium pectate gel beads surface: a) $\times 40$; b) $\times 5000$.

Compared to the images recorded by Mata *et al.* [21], it is noticeable that the surface roughness is similar. Furthermore, authors' micrographs of the hydrogel revealed that, when hydrated, the gel bead pores open up and the structure becomes sponge-like. Thus, the pores open up and are visible in hydrogel state. The bead size was almost the same (about 3 mm) - two times bigger than that recorded by Mata *et al.* [21].

Functional groups of calcium pectate gel beads

The FTIR spectrum of calcium pectate xerogel was recorded and is shown in Fig. 2.

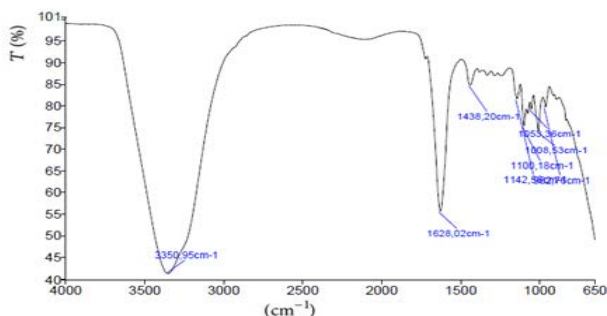


Fig. 2. FTIR spectrum of calcium pectate xerogel at 4000.0–650.0 cm^{-1} .

In the FTIR spectrum of calcium pectate xerogel, the peaks at 3350.95 cm^{-1} and 1628.02 cm^{-1} may be due to the presence of amide (N-H) groups. This bond is very important because highly amidated pectin does not need a lot of calcium to form gels.

The other groups are: ethers (C-O), alcohols (C-O), carbonyls (C=O).

Effect of initial pH on the adsorption of $Pb(II)$ ions

The effect of pH of the initial solution on the adsorption of $Pb(II)$ ions onto calcium pectate beads was studied by varying pH from 2.0 to 5.0 at 20 ± 1 $^{\circ}C$ (Fig. 3).

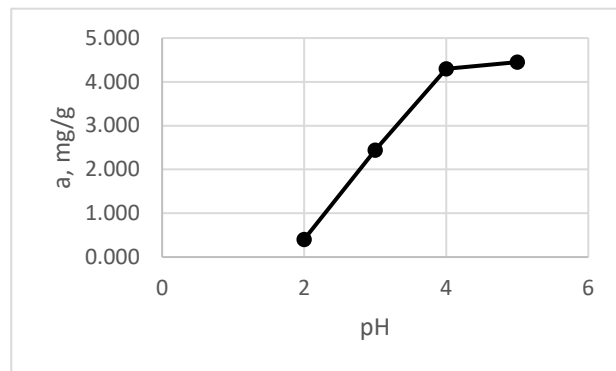


Fig. 3. Effect of pH on the adsorption of $Pb(II)$ onto biosorbent. $Pb(II)$ concentration = 5.0 $mg\ L^{-1}$, adsorbent:solution ratio = 1:1000 w:v, $T = 20 \pm 1$ $^{\circ}C$, 480 min contact time.

The results indicate that the uptake capacity for $Pb(II)$ ions increased from $0.41\ mg\ g^{-1}$ to $4.3\ mg\ g^{-1}$ in the pH range from 2.0 to 4.0. With further increase in pH of the solution from 4.0 to 5.0, the $Pb(II)$ uptake capacity increased from $4.3\ mg\ g^{-1}$ to $4.45\ mg\ g^{-1}$. The contact time was selected according to Mata *et al.* [22] and Gata-Jakobik *et al.* [23], where equilibrium contact time of 8 h was indicated. As optimal for $Pb(II)$ removal the pH range from 4.0 to 5.0 was considered.

Effect of initial $Pb(II)$ concentration on the adsorption of $Pb(II)$ ions

The effect of initial $Pb(II)$ concentration on the adsorption of $Pb(II)$ ions onto calcium pectate was evaluated by means of adsorption isotherms. For this study, Langmuir and Freundlich isotherm equations were used to predict adsorption capacities of $Pb(II)$ on calcium pectate. Figs. 4 and 5 show the Freundlich and Langmuir adsorption isotherms of $Pb(II)$ by calcium pectate beads at an initial pH of 5.0.

The minimum selected $Pb(II)$ concentration is 0.5 mg/L which is the limit concentration value in wastewaters to be discharged to a wastewater collection system, according to the respective legislation [23].

Results presented in Fig. 4 show that the removal rate of $Pb(II)$ ions can be described with the Freundlich isotherm.

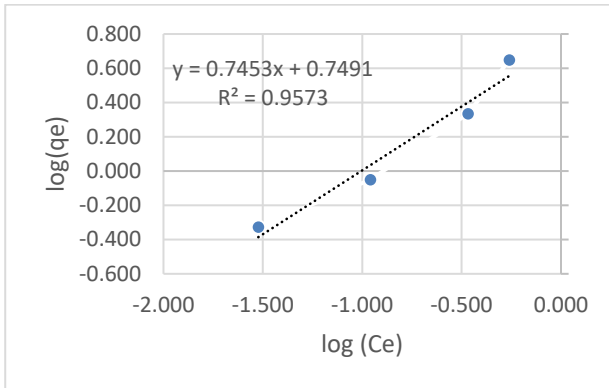


Fig. 4. Freundlich plots for Pb (II) adsorption at pH 5.0 onto the biosorbent. Adsorbent:solution ratio = 1:1000 w:v, T = 20±1 °C, 480 min contact, Freundlich isotherm parameters: n=1.342, K_F=5.612.

The Freundlich constant, K_F, unlike the Langmuir constant, Q_o, does not predict a saturation of the solid surface by the monolayer coverage of the adsorbate but it gives a relative measure of the adsorption capacity and estimates the bond strength. Favorable adsorption was registered because n was in the range of 1 < n < 10.

Results presented in Fig. 5 show that the removal rate of Pb(II) ions can be described with the Langmuir isotherm.

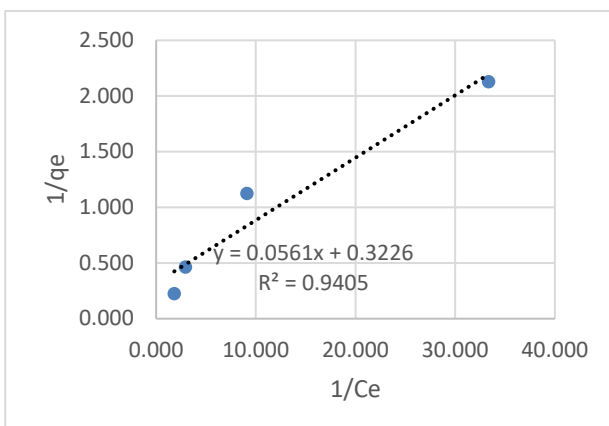


Fig. 5. Langmuir plots for Pb(II) adsorption at pH 5.0 onto the biosorbent. Adsorbent:solution ratio = 1:1000 w:v, T = 20±1 °C, 480 min contact, Langmuir isotherm parameters: Q_o=3.1, b=5.75.

According to Hamdi *et al.* [24], the separation factor (R_L) can be used to determine whether or not the adsorption process will be favorable. The values of R_L were between 0.258 and 0.034 at an initial concentration of Pb(II) ions of 0.5–5.0 mg L⁻¹. These values are between zero and one indicating that the adsorption was favorable. The Langmuir model is an indication of the surface homogeneity of the adsorbent. The values of R² were found to be near 1.0, showing favorable adsorption. The values of the correlation coefficients of the Langmuir and Freundlich isotherms indicate that these models fit

very well all adsorption equilibrium data throughout the studied experimental range. Therefore, it is assumed that adsorption involves a direct contact of metal ions onto the surface of biosorbent resulting in monolayer coverage. Freundlich model gives a better fit than the Langmuir model.

Effect of contact time on the adsorption of Pb(II) ions and the release of Ca(II) ions

Fig. 6 illustrates Pb(II) adsorption from synthetic wastewater as a function of contact time.

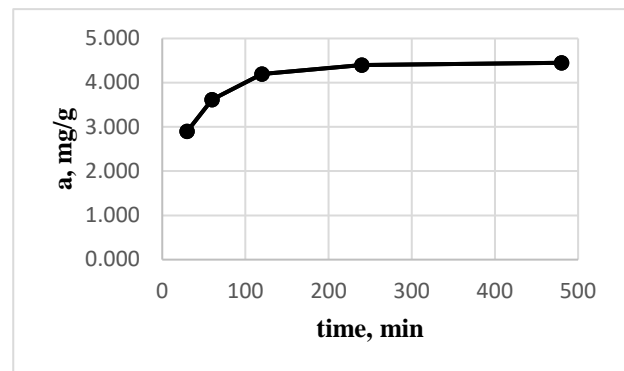


Fig. 6. Effect of contact time on Pb(II) adsorption at pH 5.0. Pb(II) concentration = 5 mg L⁻¹, adsorbent:solution ratio = 1:1000 w:v, T = 20±1 °C.

It is seen that the adsorption between 0.5 h and 8 h increased by 1.55 mg g⁻¹ Pb(II). After 120 min the adsorption rate slowed down (Fig. 6). Fig. 7 illustrates the effect of contact time on Ca(II) release from the biosorbent into solution at pH 5.0 at a Pb(II) concentration of 5 mg L⁻¹.

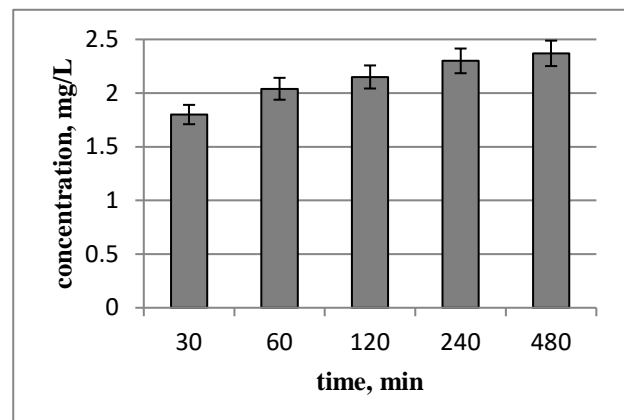


Fig. 7. Effect of contact time on calcium release from the biosorbent into solution at pH 5.0. Pb(II) concentration = 5 mg L⁻¹, adsorbent:solution ratio = 1:1000 w:v, T = 20±1 °C.

The contact time used in this experiment was 0.5 h; 1 h; 2 h; 4 h and 8 h. After the adsorption process was completed, calcium concentration was also determined. Mata *et al.* [25] have found a correlation between calcium release and metals uptake in

calcium alginate and calcium pectate gel beads. Experimental results obtained in the present work were similar to those of Mata *et al.* [25] (Fig. 7). This correlation indicated that the process is ion exchange-based adsorption. Webb [26] has shown that both physical and chemical adsorption may simultaneously occur on the surface. A layer of molecules may be physically adsorbed on top of an underlying chemisorbed layer. This suggests that after all calcium was replaced, physical adsorption might have taken place. This can indicate two theories. Firstly, it can be assumed that there is more than one mechanism in this adsorption. Ion exchange mechanism is responsible for the release of calcium into the solution, and physical adsorption can also take place, as the organic material tends to attract heavy metals. Secondly, as FTIR results show, this particular pectin is not sensitive to gelation in the presence of calcium ions. This means that lower calcium amounts are adsorbed in the biosorbent preparation stage. Therefore, both theories do not contradict each other and both can explain the obtained results.

Effect of contact time on the desorption of $Pb(II)$ ions

Desorption helps the recovery of $Pb(II)$ from the waste and the regeneration of the adsorbent in order to assess its potential as an adsorbent for commercial application. The desorption studies were carried out with the biosorbent after 8 h of adsorption. The results are presented in Fig. 8.

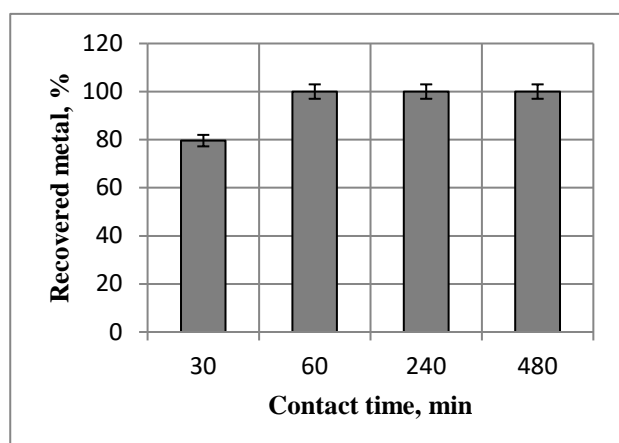


Fig. 8. Influence of contact time on the desorption of $Pb(II)$ from 0.1 g of biosorbent in 20 mL of 0.1 N HNO_3 solution.

The results (Fig. 8) revealed that full desorption of lead was achieved in 60 min. Mata *et al.* [21] obtained the same result for lead. However, Agata-Jakobik *et al.* [22] did not reach 100 % of desorption. According to Mata *et al.* [25] a part of lead was retained in the biosorbent after each desorption

cycle. Comparing to the desorption results of Isaac and Sivakumar [27] with apple peels, lead desorption was the same (almost 97 %) and equilibrium time was also 60 min. The equilibrium time for heavy metals removal using pectin is quite long (8 h) compared to other biosorbents (from 10 to 60 min depending on the particular natural biosorbent). However, the efficiency of $Pb(II)$ removal is higher compared to natural biosorbents.

Studies have shown (Figs. 4–7) that the adsorption efficiency of lead onto calcium pectate beads depends not only on contact time and concentration, but also on pH of the solution. The remarkable results obtained in this study prompt us to use calcium pectate beads as an adsorbent for the treatment of wastewater polluted with lead.

CONCLUSIONS

1. FTIR analysis revealed the presence of different functional groups in the biosorbent - amide N-H, ether (C-O), alcohol (C-O) and carbonyl (C=O) functional groups which participate in the adsorption process.

2. $Pb(II)$ uptake increases with an increase in contact time. The efficiency of Pb (II) adsorption increased from 58.0 to 89.0 % with an increase in contact time from 30 to 480 min. The adsorption equilibrium was achieved in 480 min.

3. A correlation was found between calcium release and metals uptake in calcium alginate and calcium pectate gel beads. This correlation indicated that the process is ion exchange-based adsorption.

4. Desorption from the biosorbent was influenced by the contact time. The desorption of $Pb(II)$ at equilibrium (100 %) was reached in 60 min.

5. This study showed that the Freundlich and Langmuir equations can be used to describe the adsorption phenomena of $Pb(II)$ onto calcium pectate gel beads.

REFERENCES

1. F. Fu, F. Q. Wang, *J. Environ. Manage.*, **92**, 418 (2011).
2. W. W. Ngah, M. A. K. M. Hanafiah, *Bioresour. Technol.*, **99**, 3948 (2008).
3. D. S. Malik, C. K. Jain, A. K. Yadav, *J. Global Biosci.*, **4**, 1829 (2015).
4. S. Schiewer, S. B. Patil, *Bioresour. Technol.*, **99**, 1903 (2008).
5. K. Kelly-Vargas, M. Cerro-Lopez, S. Reyna-Tellez, E. R. Bandala, J. L. Sanchez-Salas, *Phys. Chem. Earth, Parts A/B/C*, **37**, 29 (2012).
6. M. Thirumavalavan, Y. L. Lai, J. F. Lee, *J. Chem. Eng. Data*, **56**, 2255 (2011).
7. M. Torab-Mostaedi, M. Asadollahzadeh, A. Hemmati, A. Khosravi, *J. Taiwan Inst. Chem. Eng.*, **44**, 302 (2013).

8. J. Q. Albarelli, R. B. Rabelo, D. T. Santos, M. M. Beppu, M. A. A. Meireles, *J. Supercrit. Fluids*, **58**, 351 (2011).
9. M. A. Ashraf, A. Wajid, K. Mahmood, M. J. Maah, I. Yusoff, *Sci. Res. Essays*, **6**, 4064 (2011).
10. M. A. Ashraf, K. Mahmood, A. Wajid, M. J. Maah, I. Yusoff, In *Int. Conf. Food Eng. Biotechnol.*, **9**, 68 (2011).
11. R. Mallampati, L. Xuanjun, A. Adin, S. Valiyaveettil, *ACS Sustainable Chem. Eng.*, **3**, 1124 (2015)
12. F. Gönen, D. S. Serin, *Afr. J. Biotechnol.*, **11**, 1258 (2012).
13. S. Kamsonlian, S. Suresh, C. B Majumder, S. Chand, *Int. J. Sci. Technol. Manage.*, **2**, 7 (2011).
14. R. Lakshmiopathy, N. C. Sarada, *Int. J. Miner. Process.*, **122**, 65 (2013).
15. G. P. Gerola, N. V. Boas, J. Caetano, C. R. T. Tarley, Jr. A. C. Gonçalves, D. C. Dragunski, *Water, Air, Soil Pollut.*, **224**, 11 (2013).
16. S. Liang, X. Guo, Q. Tian, *Desal. Water Treat.*, **51**, 7171 (2013).
17. V. M. Marín-Rangel, R. Cortés-Martínez, R. A. Cuevas Villanueva, M. Garnica-Romo, H. E. Martínez-Flores., *J. Food Sci.*, **77**, 14 (2012).
18. N. Feng, X. Guo, S. Liang, Y. Zhu, J. Liu, *J. Hazard. Mater.*, **185**, 54 (2011).
19. N. C. Feng, X. Y. Guo, *Transactions of Nonferrous Metals Society of China*, **22**, 1231 (2012).
20. K. Huang, H. Zhu, *Environ. Sci. Pollut. Res.*, **20**, 4434 (2013).
21. Y. N. Mata, M. L. Blázquez, A. Ballester, F. González, J. A. Muñoz, *Chem. Eng. J.*, **150**, 301 (2009).
22. A. Jakóbik-Kolon, Andrzej K. Milewski, K. Mitko, L. Andrea, *Sep. Sci. Technol.*, **49**, 1688 (2014).
23. Order D1-515 *On the Approval of Regulation on Wastewater Management* of the Minister of Environment dated 8 October 2007 (*Official Gazette*, No. 110-4522, 2007).
24. N. Hamdi, S. Hamdaoui, E. Srasra, *Int. J. Environ. Res.*, **8**, 376 (2014).
25. Y. N. Mata, M. L. Blázquez, A. Ballester, F. González, J. A. Muñoz, *J. Hazard. Mater.*, **178**, 248 (2010).
26. P. A. Webb, *Micromeritics Instrument Corp. Technical Publications*, (2003).
27. C. P. J. Isaac, A. Sivakumar, *Desalin. Water Treat.*, **51**, 7709 (2013).

ОТСТРАНЯВАНЕ НА ОЛОВО (Pb^{2+}) ОТ СИНТЕТИЧНИ ОТПАДНИ ВОДИ С ИЗПОЛЗВАНЕ НА КАЛЦИЕВ ПЕКТАТ

Д. Палиулис, А. Кринискайтė

Департамент по защитата на околната среда, Технически университет Вилнюс Гедиминас, бул. Саулетекио 11, LT-10223 Вилнюс, Литва

Получена на 9 май, 2017 г.; коригирана на 1 октомври 2017 г.

(Резюме)

Настоящата работа се отнася до използването на калциев пектат като биосорбент за отстраняване на Pb (II) йони от водни разтвори. Повърхностната морфология на адсорбента е анализирана чрез сканираща електронна микроскопия (SEM). Повърхностната химична природа на биосорбента е изследвана чрез инфрачервена спектроскопия с Фурье трансформация (FTIR). Резултатите от FTIR показват, че амидни, етерни, алкохолни и карбонилни функционални групи са отговорни за Pb (II) биосорбцията върху калциев пектат. Проведени са количествени експерименти за да се изследват ефектите на pH, времето и началната концентрация на металните йони върху адсорбцията на Pb (II) йони от биосорбент в синтетичните отпадни води. Оптималното време за контакт и pH за отстраняване на Pb (II) йони са съответно 480 минути и pH 5.0. Установено е, че максималният капацитет на биосорбента е 4.45 mg g^{-1} за Pb (II) йони. Резултатите показват, че механизъмът на адсорбцията на Pb (II) йони върху калциев пектат е ионен обмен между Ca (II) и Pb (II) йони в разтвора. Данните за равновесието са анализирани в съответствие с линейната форма на изотермите на Langmuir и Freundlich. Моделът Freundlich е по-подходящ от модела Langmuir. Резултатите показват, че калциевият пектат може да бъде използван като ефективен, евтин и екологичен адсорбент за отстраняване на Pb (II) йони от водни разтвори.

Study of the possibility of using IXRF technique to detect the elements present in dust using Monte Carlo N Particles

H. R. Dehghan¹, A. Negarestani², M. R. Rezaie^{2,*}

¹Department of Photonics, Kerman Graduate University of Advanced Technology, P. O. Box 76315-117, Mahan, Iran

²Department Electrical and Computer Engineering, Kerman Graduate University of Advanced Technology, P. O. Box 76315-117, Mahan, Iran

Received November 15, 2016; Accepted April 12, 2017

Detecting heavy metals present in soil and dust as a major factor of environmental pollution has got a particular importance. An experimental (laboratory) method based on energy-dispersive X-ray fluorescence (EDXRF) technique was utilized so far to detect the elements. In this research, the Monte Carlo method based on the EDXRF technique was used to detect the elements. MCNPX2.7 code is based on Monte Carlo calculations and is able to trace 32 particles including photons within the range of X-rays and γ -rays. In this paper, the outcomes of multi-source EDXRF simulation technique were compared with the experimental results. The comparison shows that multi-source EDXRF technique(IXRF) is able to detect the percentage of elements present in soil and dust with a high compatibility.

Keywords: IXRF; Elements; Dust; EDXRF; Multi Source; MCNPX; Detection.

INTRODUCTION

Detecting the elements present in soil and the percentage of each component has got a particular importance from the aspect of agriculture, environmental pollution, agrology and mines discovery [1]. Different methods based on chemical decomposition and physical methods have been used for this purpose so far [2]. The most important chemical method CMB (Chemical Mass Balance) is not really capable of detecting dust and soil elements as the major pollution source [2]. The most efficient method is EDXRF which is a fast non-destructive method in which an X-ray system mostly of electron strip type is utilized [2]. EDXRF is being applied for detection of the elements present in soil [3-7]. MCNPX is a multi-task nuclear code offering the possibility of tracing a characteristic X-ray emission spectrum produced by collision of energetic photons, which is an atomic process. Accuracy of MCNPX code to detect the percentage of brass alloy has been investigated and verified by T. Trojek and T. Čechák [7]. In this research the possibility of using MCNPX with three radioactive sources, *viz.* ^{55}Fe (5.9 KeV), ^{241}Am (26.4, 59.6KeV) and ^{57}Co (122KeV), to detect the elements present in soil by the three source EDXRF method (IXRF)was studied.

MATERIALS AND METHODS

Purpose of the present research is the detection of the elements present in soil with the use of Monte Carlo N Particles (MCNPX) which is based on particles transportation using the Monte Carlo

method. Soil is a combination of Cu, Al, Ca, Co, Cr, Fe, K, Mn, Na, Ni, Pb, Rb, Si, Sr, Ti, V, Y, Zn, and Zr, each having its own specific X-ray spectrum. The energy emitted from the K layer is brought in Table 1 [9].

Ordinary soil contains different elements, most of which are in the $Z \leq 50$ range, however polluted soils and dust particles might have different elements in the range of $0 \leq Z \leq 100$. So far, one X-ray source has always been used for detection of the elements present in soil [10, 11]. Since each source emits X-rays with its particular energy spectrum, and the need for energy is to some extent higher than the atomic layer energy difference, so in order to precisely detect different elements, different sources are required. In this research, an attempt was made to use more than one source for detection of the elements present in soil and dust. Before producing any device, a fabrication feasibility study is needed. Atomic and nuclear codes are the best options for a fabrication feasibility study and MCNP is a credible nuclear code. This research was performed with the use of MCNP code in three phases, in each of which, a characteristic X-ray spectrum was obtained. In the first phase, γ -ray energy produced by three sources of ^{55}Fe (5.9KeV), ^{241}Am (26.4, 59.6KeV) and ^{57}Co (122KeV), was radiated separately to each element present in the soil. Then in the second phase, the elements included in a typical soil with certain percentages were separately irradiated by ^{55}Fe (5.9KeV), ^{241}Am (26.4, 59.6KeV) and ^{57}Co (122KeV). In the third phase, a radioactive source in form of a combination of ^{55}Fe (5.9KeV), ^{241}Am (26.4, 59.6KeV) and ^{57}Co (122KeV) sources irradiated the soil. The characteristic X-ray energy

* To whom all correspondence should be sent:

E-mail: mohamadreza45@gmail.com

spectrum in all three phases can be obtained in MCNP code with the use of tallies F_1 and F_2 in the specific input file of each phase. The input file description will be given in the following. The probability of emission in each energy range for each particle can be obtained with the use of MCNPX code and an input file was written for this purpose. An overview of the defined geometry in the input file is illustrated in Fig.1.

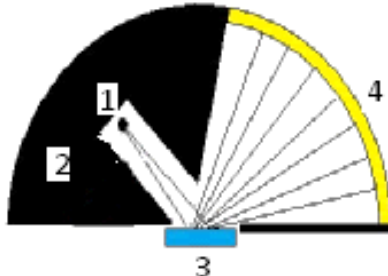


Fig. 1. The geometry considered in the simulation

In this geometry cell no.1 shows the point source with certain activity for sources with ^{55}Fe (5.9KeV), ^{241}Am (26.4,59.6KeV) and ^{57}Co (122KeV) energies, cell no.2 shows the source cover, cell no.3 shows the considered material (target) with optimal calculated thickness in each mode and for dimensions $2\times 2\text{cm}^2$, and cell no.4 shows a special shell defined as a detector. After radiation, the X-ray fluorescence spectrum will reach the internal surface of the cylindrical shell. Tally F_1 will provide the characteristic X-ray spectrum received by the detector. The number of particles was considered 108 in order to reach below 1% error. Splitting and Russian Roulette methods

were used to reduce variance, increase FOM and uniform SLOP in the output file of MCNPX. The percentage of elements present in a typical soil according to [9] is shown in Table 1.

RESULTS

Chemistry

The results of this simulation which was done in three phases with the use of tally F_1 are reported below. First, the characteristic X-ray spectrum of each element present in the soil, which was separately irradiated by γ -rays produced by three different sources of ^{55}Fe (5.9KeV), ^{241}Am (26.4,59.6KeV) and ^{57}Co (122KeV) was obtained and the results are shown in Table 1.

The comparison of theoretical and experimental results of Table 1 shows that MCNPX code has the capability of detecting each element separately with the use of EDXRF technique.

The soil with the mentioned element percentages in Table 1, was irradiated by different sources and the obtained EDXRF spectrum with the use of tally F_1 is shown in Figures 2 to 5.

The results show that ^{55}Fe (5.9KeV) can detect the elements in the $Z \leq 23$ range, whereas ^{241}Am (26.4,59.6KeV) is more appropriate to detect the elements in the $22 \leq Z \leq 40$ range.

Also, ^{57}Co (122KeV) is better for detection of heavy elements like lead. Eventually the X-ray spectrum of soil with the use of a composed source produced by ^{241}Am (59.6KeV), ^{55}Fe (5.9KeV) and ^{57}Co (122KeV) with different percentages which

Table1. The emission energy of K layer for elements in dust

Elements	K _α		K _β		Percent
	Experimental	MCNPX	Experimental	MCNPX	
Na	1.04	1.02	-----	-----	0.00755
Al	1.48	1.47	-----	-----	0.21326
Si	1.74	1.73	-----	-----	0.7024
K	3.31	3.38	-----	-----	0.04806
Ca	3.69	3.66	4.01	3.99	0.00247
Ti	4.5	4.5	4.93	4.91	0.00293
V	4.95	5.02	5.42	5.40	0.000133
Cr	5.41	5.4	5.94	5.91	0.000901
Mn	5.89	5.85	6.49	6.45	0.000926
Fe	6.4	6.36	7.05	7.02	0.0197
Co	6.93	6.88	7.64	7.61	0.0000123
Ni	7.48	7.5	8.26	8.24	0.000049
Cu	8.04	8.00	8.90	8.89	0.0000256
Zn	8.63	8.61	9.57	9.60	0.000133
Rb	13.39	13.4	14.96	14.92	0.00117
Sr	14.16	14.12	15.83	15.80	0.000102
Y	14.95	14.92	16.73	16.72	0.0002118
Zr	15.77	15.74	17.67	17.65	0.00005198
Pb	74.96	75.02	84.93	85.10	0.000225

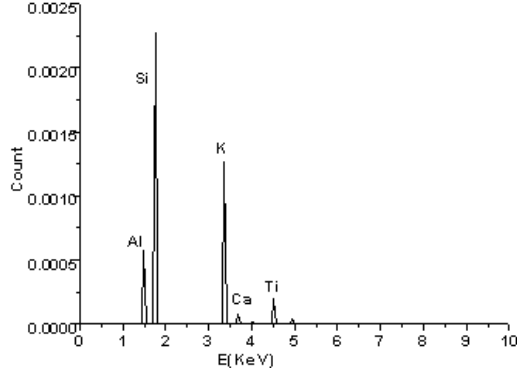


Fig. 2. The X-ray spectrum of a dust target at 5.9KeV (^{55}Fe source)

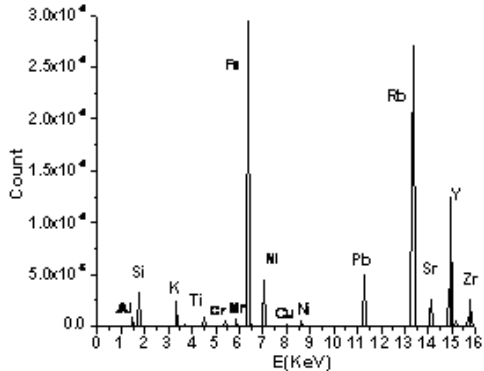


Fig. 3. The X-ray spectrum of a dust target at 26.4KeV (^{241}Am source)

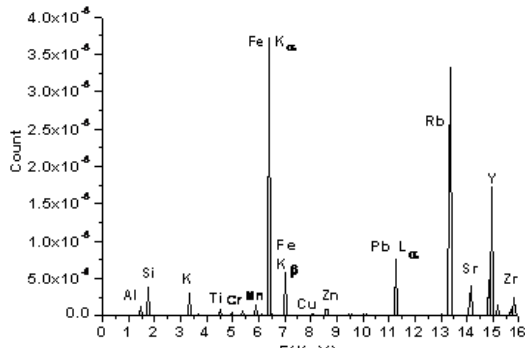


Fig. 4. The X-ray spectrum of a dust target at 59.6KeV (^{241}Am source)

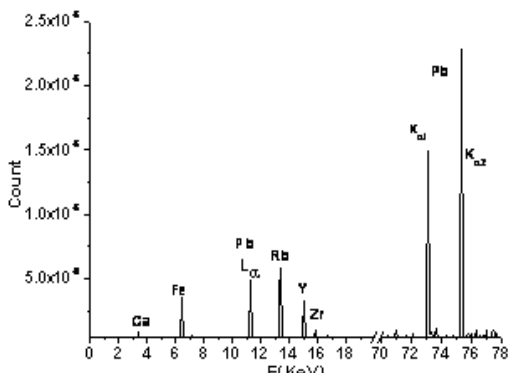


Fig. 5. The X-ray spectrum of a dust target at 122KeV (^{57}Co source)

have been obtained from MCNPX simulation code is according to figures 6 to 9. In these figures source

percentages have changed and the related spectrum was obtained accordingly. As can be seen in the figures and table 1, the spectrum shape depends on source percentages and percentage of the elements present in the compound. Comparing the detected elements by the multi-source EDXRF method(IXRF) with the present results for the elements in the soil shows that the introduced method is well able to detect the elements present in soil. Meanwhile, percentages of the elements obtained by this technique have a good compatibility with the percentages in soil. Percentage of elements in each mode is obtained according to the proportion of characteristic X-ray intensity in the compound to characteristic X-ray intensity obtained for the pure element. Afterwards, according to percentages of reported elements present in soil, the material of cell 1 was positioned by (2) and the EDXRF spectrum related to element admixture in soil was obtained (Figures 2 to 5).

M₁ card for the considered soil in MCNPX code is brought in Table 1. After executing the code, the obtained spectrum by the defined detector in MCNPX code with the three above mentioned sources is produced, which is shown in Figures 6 to 9.

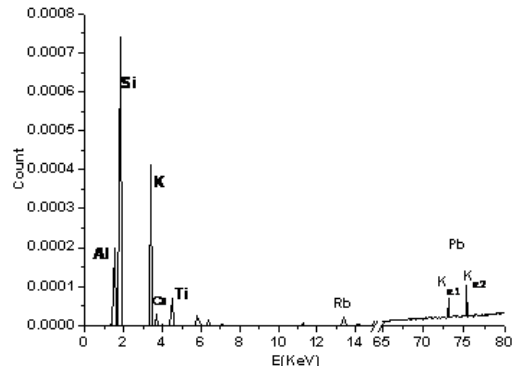


Fig. 6. The X-ray spectrum of a dust target at 5.9, 59.6, 122KeV equal percent (^{55}Fe , ^{241}Am , ^{57}Co source)

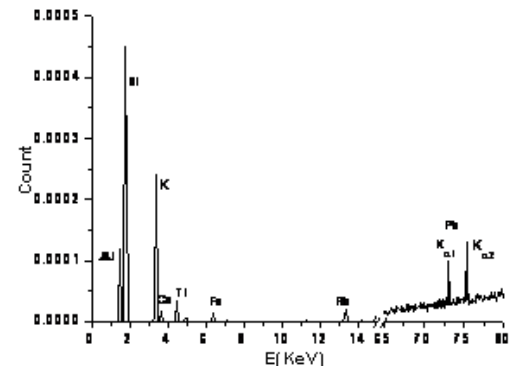


Fig. 7. The X-ray spectrum of a dust target at 5.9, 59.6, 122KeV 20,25,55 percent, respectively (^{55}Fe , ^{241}Am , ^{57}Co source)

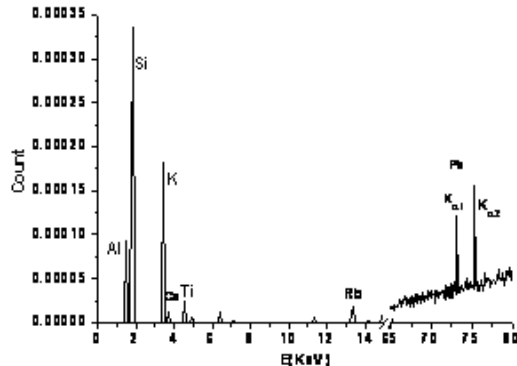


Fig. 8. The X-ray spectrum of a dust target at 5.9, 59.6, 122KeV 15,25,60 percent, respectively (⁵⁵Fe, ²⁴¹Am, ⁵⁷Co source)

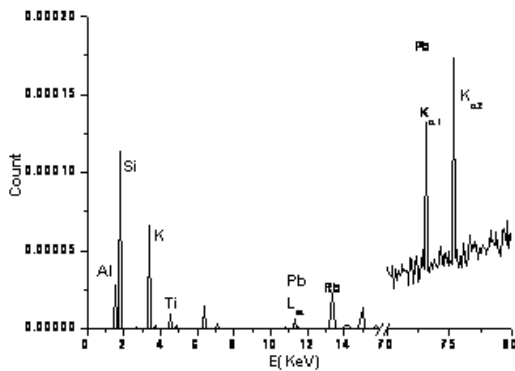


Fig. 9. The X-ray spectrum of a dust target at 5.9, 59.6, 122KeV 5,30,60 percent, respectively (⁵⁵Fe, ²⁴¹Am, ⁵⁷Co source)

CONCLUSIONS

One-source EDXRF technique is one of the most important techniques applied for detection of soil elements. In order to detect heavy elements present in soil with higher precision, the multi-source EDXRF(IXRF) technique was introduced in this research. To investigate functionality of the proposed technique, MCNPX nuclear code was utilized. Initially, the accuracy of the code in element detection was investigated and verified. Research outcomes show that in using sources of ⁵⁵Fe(5.9KeV) ²⁴¹Am(26.4KeV), ²⁴¹Am(59.6KeV) and also ⁶⁰Co(1173KeV) , for detection of soil elements within the $Z \leq 23$, $23 \leq Z \leq 40$ and $Z \geq 40$ ranges, ⁵⁵Fe(5.9KeV), ²⁴¹Am(26.4,59.6KeV) and ⁶⁰Co(1173KeV) are appropriate, respectively. The

reason of using three experimental sources is demonstrated by comparing the figures obtained with the code with the experimental results. The results show that the source with lower energy ⁵⁵Fe(5.9KeV), is appropriate for extraction of element spectra with atomic numbers between 11 and 19; the source (²⁴¹Am(26.4, 59.6KeV) is better for atomic numbers between 19 and 40 and the energetic source (⁶⁰Co1173, 1331KeV) is appropriate for detection of heavy metals like lead. The reason for this is the dependency of absorption cross-section and dispersion to energy.

Afterwards, with the use of IXRF technique, the emitted X-ray spectrum characteristic for the soil was obtained. The comparison between the results for the spectrum obtained by MCNPX with the experimental results, done by J. A. Bearden [9], shows that the IXRF technique has a good capability in detecting the elements present in soil with high precision.

REFERENCES

1. H. M. Agrawal, V. Singh, G.C. Joshi, M. Sudershan, A.K. Sinha, *Applied Radiation and Isotopes*, **69**, 969 (2011).
2. K.N. Yua, Z.L.L. Yeung, L.Y.L. Lee, M.J. Stokes, R.C.W. Kwok, *Applied Radiation and Isotopes*, **57**, 279 (2002).
3. J. A. Carrero, N. Goienaga, S.F.O. Vallejuelo, G. Arana, and J.M. Madariaga, *Spectrochimica Acta Part B*, **65**, 279(2010).
4. H. M. Agrawal, *Radiation Physics and Chemistry*, **81**, 1796 (2012).
5. S. Akbulut, U. Cevik, A.A. Van, K. De Wael, R. Van Grieken, *Chemosphere*, **96**, 16(2014).
6. F. M. Peinado, S.M. Ruano, M.B. González, C.E. Molina, *Geoderma*, **159**, 76(2010).
7. T. Trojek, T. Čechák, Nuclear Instruments and Methods in Physics Research B.,263, 72(2007)
8. B. P. Denise, MCNPX User Manual Version 2.6.0, Los Alamos National Laboratory, Los Alamos,2008.
9. J. A. Bearden, *Review of Modern Physics*,(1967)
10. A. N. Berlizov, D.A. Sharikov, H. Ottmar, H. Eberle, J. Galy, and K. Luetzenkirchen, *Nuclear Instruments and Methods in Physics Research A.*, **615**, 127 (2010).
11. F. Li, PhD Thesis, NCST, California, 2008.

ИЗСЛЕДВАНЕ НА ВЪЗМОЖНОСТИТЕ НА IXRF-ТЕХНИКА ЗА ОТКРИВАНЕТО НА ЕЛЕМЕНТИ В ПРАХ ПО МЕТОДА МОНТЕ-КАРЛО Н ЧАСТИЦИ

Х.Р. Деган¹, А. Негарестани², М.Р. Резаие^{2*}

¹Департамент по фотоника, Университет по авангардни технологии „Керман“, Махан, Иран

²Департамент по електро- и компютърно инженерство, Университет по авангардни технологии „Керман“, Махан, Иран

Постъпила на 15 ноември, 2016 г.; приета на 12 април, 2017 г.

(Резюме)

Откриването на тежки метали в почви и прах е важен фактор в изследването на замърсяването на околната среда. Досега за тази цел се използва лабораторен метод, основан на енерго-дисперсионна рентгенова флуоресценция (EDX-RF). За откриването на тези елементи в настоящето изследване се предлага методът Монте-Карло, основан на EDX-RF-техника. Кодът MCNPX2.7 се основава на Монте-Карло изчисления и е способен за трасиране на 32 частици (включително на фотони) в обхвата на рентгенови и γ -лъчи. В настоящата работа са сравнени резултатите на много-източникова симулация EDX-RF-техника (IXRF) с опитни резултати. Сравнението показва, че IXRF е в състояние да се откри процентното съдържание на елементите, налични в почвата и праха с голяма корелация.

Storage effect on phenolic content and antioxidant activity in selected fruit extracts

B. Radovanović^{1*}, A. Radovanović², V. Nikolić³, N. Manojlović⁴, J. Dimitrijević¹

¹Department of Chemistry, Faculty of Sciences and Mathematics, University of Niš, 18000 Niš, Serbia

²Faculty of Chemistry, University of Belgrade, 11000 Belgrade, Serbia

³Faculty of Technology, University of Niš, 16000 Leskovac, Serbia

⁴Faculty of Medical Sciences, University of Kragujevac, 34000 Kragujevac, Serbia

Received November 23, 2016; Accepted January 25, 2016

The objectives of this study were to investigate the influence of light and temperature on the content of phenolic compounds and its correlation with antioxidant activity in selected fruit extracts (strawberry (*Fragaria vesca*), blackberry (*Rubus fruticosus*), raspberry (*Rubus idaeus*), and sour cherry (*Prunus cerasus*)). The antioxidant capacity evaluated using 2,2-diphenyl-1-picrylhydrazyl radical (DPPH•) scavenging assays ranged from 90.87% to 96.50%. The content of target phenolic compounds showed high correlation with the antioxidant activity ($r^2 = 0.829$) and with the content of anthocyanins ($r^2 = 0.995$) of the investigated fruit extracts. Total phenol content was monitored in fruit extracts stored at 7 °C for 23 days and at room temperature (25 °C) for 90 days. All fruit extracts exhibited fluctuations in total phenol contents with an initial increase after 4 days, followed by a decrease at both storage temperatures. These changes were not significant during 23 days of storage and the investigated fruit extracts can be used as an easily accessible source of natural antioxidants in food and pharmaceutical supplements.

Keywords: Fruit extracts; antioxidant activity; phenolic composition; storage temperature.

INTRODUCTION

Many human diseases, like cancer, atherosclerosis and rheumatoid arthritis, as well as neurodegenerative diseases and ageing processes are caused by free radicals [1-3]. Epidemiological studies have indicated that frequent consumption of fruits and vegetables is associated with a lower risk of cardiovascular disease and cancer [4-8]. This protective role of fruits and vegetables had been attributed to their antioxidant compounds, such as phenolics, flavonoids, flavonols, anthocyanins, so natural antioxidants have gained increasing interest among consumers and scientific community [9].

Polyphenols are abundant micronutrients in our diet that have been credited with chemoprevention of diseases associated with oxidative stress. Over 8000 phenolic compounds have been identified from plant materials and they possess a wide spectrum of biochemical activities (antioxidant, antimicrobial, antimutagenic, anticancerogenic and ability to modify the gene expression) [10-16].

Fruits like strawberry, blackberry, raspberry and sour cherry are good sources of natural antioxidants and are traditionally used in diet [8]. Environmental factors like temperature, light and geographical area are very important for the development of red pigment in the fruit [16-20].

It has been reported that the freezing process decreased the total phenolic content and antioxidant capacity by 4-20 % in raspberries [21].

As antioxidant capacity is becoming an important parameter with respect to fruit and vegetable quality, it is of great interest to evaluate changes in antioxidant activity and total phenolic contents during storage of selected fruit extracts at elevated temperatures. This study was undertaken to investigate the effects of different temperatures on total phenolics and antioxidant capacity of extracts of raspberry (*Rubus idaeus*), blackberry (*Rubus fruticosus*), strawberry (*Fragaria vesca*), and sour cherry (*Prunus cerasus*), originating from Serbia (Rasinski region).

EXPERIMENTAL

Chemicals

2,2-Diphenyl-1-picrylhydrazyl (DPPH•) in free radical form was obtained from Sigma Chemical Co. (St. Louis, MO). Methanol, formic acid, gallic acid, catechin and quercetin were purchased from Merck Co (Germany). All reagents were of analytical grade.

Plant materials

Samples of strawberry, blackberry, raspberry and sour cherry were harvested in western Serbia (Rasinski region) at the commercial maturity stage. After harvest, the samples were immediately frozen and stored at -20 °C until analysis.

Preparation of extracts

Fruit extracts were obtained by grinding the berries (10 g) in 100 mL of methanol/water solution (70/30) at room temperature for 30 min. The mixture

* To whom all correspondence should be sent:

E-mail: blaga_radovanovic@yahoo.co.uk

© 2017 Bulgarian Academy of Sciences, Union of Chemists in Bulgaria 879

was stored at 7°C in the dark for 24 h and then centrifugated at 4000 rpm for 15 min.

Determination of total phenols, tartaric esters and flavonols

The total phenol content in the extracts was determined according to the Mazza and Miniati [9] procedure: 0.25 mL of extract and 0.25 mL of 0.1% HCl in 95% ethanol were mixed with 4.55 mL of 2% HCl and the absorbance was measured at 280, 320, 360 and 520 nm after incubation at room temperature for 5 min. Total phenol content was expressed as mg of galic acid equivalents /100 g of fruit (280 nm); tartaric esters - as mg catechin equivalent /100 g fruit (320 nm); flavonols - as mg quercetin equivalent/100 g fruit (360 nm).

Determination of monomeric anthocyanin

The total monomeric anthocyanin content in the fruit extracts was determined by the pH-differential absorbance method described by Giusti and Wrolstad [22]. Anthocyanins have maximum absorbance at a wavelength of 513 nm at pH of 1.0. The coloured oxonium form predominates at pH 1.0 and the colourless hemiketal form at pH 4.5. The pH-differential method is based on this reaction and permits accurate and rapid measurement of the total monomeric anthocyanins. Absorbance of the fruit extract was measured at 520 and 700 nm in potassium chloride buffer (pH 1.0) and sodium acetate buffer (pH 4.5) after incubation at room temperature for 15 min. Anthocyanin content was expressed in mg of cyanidin-3-glucoside equivalent (Cygl)/100 g fruit using the molar extinction coefficient of cyanidin-3-glucoside of 26900 L/mol cm and molar weight of 449.2 g/mol.

Determination of indices for anthocyanin pigment degradation, polymeric colour and browning

Indices for anthocyanin degradation of the fruit extracts can be derived using the pH-differential method described by Giusti and Wrolstad [22]. The absorbance at 420 nm of the disulphide-treated sample serves as an index for browning. The colour density of the control sample and the polymer colour of the disulphide-bleached sample are calculated as follows:

$$\text{Colour density} = [(A_{420\text{nm}} - A_{700\text{nm}}) + (A_{\lambda_{\text{max}}} - A_{700\text{nm}})]$$

The hue value is calculated as follows:

$$\text{Hue} = [(A_{420\text{nm}} - A_{700\text{nm}})/ (A_{\lambda_{\text{max}}} - A_{700\text{nm}})]$$

The ratio between polymerization color and colour density is used to determine the percentage of the colour that is contributed by the polymerized material.

Antioxidant activity

The antioxidant capacity was evaluated using 2,2-diphenyl-1-picrylhydrazyl radical (DPPH•) scavenging assays [1,3,12,15]. The antioxidant assay is based on the measurement of the loss of DPPH• colour by the change of absorbance at 517 nm caused by the reactions of DPPH• with the tested samples. The reaction was monitored on a UV/VIS spectrophotometer. Reaction solution was prepared by mixing 2.5 mL of diluted fruit extract with 1 mL of methanolic DPPH solution. The solution was kept in dark at room temperature for 20 min. Scavenging capacity of DPPH• in percent (%) of each fruit extract sample was calculated from the decrease in absorbance according to the relationship:

$$\text{Antioxidant capacity (\%)} = (1 - A_{\text{sample}} - A_{\text{blank}}/A_{\text{control}}) \times 100$$

where A_{control} is the absorbance of the control sample, A_{blank} is the absorbance of the diluted fruit extract sample and A_{sample} is the absorbance of the diluted fruit extract sample with DPPH radical.

Statistical analysis

Three analytical replicates were obtained from each sample fruit extract. Measurements were averaged, and results are given as mean \pm standard deviation (SD). The correlations between parameters were determined using analysis of variance (ANOVA) and quantified in terms of the correlation factor. One-way ANOVA was used to determine differences between measurements. Differences at $p < 0.005$ were considered to be significant.

RESULTS AND DISCUSSION

The quantity and the composition of phenolic compounds in fruits are influenced by genotype, storage conditions, extraction procedure, and environmental conditions. In red-coloured fruits, the phenolic content increases during the last ripening stage due to anthocyanins and flavonols accumulation, so it is very important to collect samples at equal ripening stages [11].

Fruit extracts show significant differences in anthocyanins content, since these pigments are responsible for the blue, purple, violet, and red colours of fruits. They are one of the major flavonoid classes. The major sources of anthocyanins in edible plants are the families *Vitaceae* (grape) and *Rosaceae* (cherry, plum, raspberry, strawberry, blackberry, apple, peach, etc.). Other plant families which contain anthocyanin pigments are *Solanaceae* (tamarillo and eggplant), *Saxifragaceae* (red and black currants), *Cruciferae* (red cabbage), and *Ericaceae* (blueberry and cranberry).

The concentrations of total phenols, tartaric esters, flavonols and anthocyanins in the investigated fruit extracts are presented in Table 1. Analysis of obtained results shows that the total phenol contents varied from 166.17 to 273.22 mg/100 g fruits; tartaric esters contents varied from 21.62 to 44.42 mg/100 g fruits; flavonols were between 9.21 and 24.42 mg/100 g fruits; and the monomeric anthocyanins varied from 26.02 to 121.95 mg/100 g fruits.

Similar results for phenol content in raspberry, strawberry, and blackberry extracts have been reported by other authors [10,13]. The highest concentrations of total phenols, tartaric esters and flavonols were found in sour cherry extract, followed by blackberry, strawberry and raspberry extract.

Sour cherry extract also contained the highest concentration of monomeric anthocyanins, followed by the blackberry extract. Significantly lower monomeric anthocyanin contents were recorded in strawberry and raspberry extracts. Data presented by other researchers from neighbouring countries for raspberry, strawberry and blackberry are similar to the results for anthocyanin content we obtained [13,14].

Polymeric colour has the lowest value in blackberry (12.20%), followed by raspberry and sour cherry. A higher value of polymeric colour is determined in strawberry (27.03%).

Table 1. Concentrations of total phenols, tartaric esters, flavonols, monomeric anthocyanins (mg/100 g fruit), polymeric color and antioxidant activity (%) of the investigated fruit extracts.

	Strawberry extract	Blackberry extract	Raspberry extract	Sour cherry extract
Total phenols	178.07 ± 3.62	230.00 ± 1.092	166.17 ± 2.07	200.01 ± 0.80
Tartaric esters	21.62 ± 0.08	24.81 ± 2.23	21.71 ± 0.85	44.42 ± 2.45
Flavonols	9.21 ± 0.11	18.06 ± 2.83	9.73 ± 0.42	24.42 ± 2.38
Monomeric anthocyanins	33.20 ± 0.20	84.16 ± 2.82	26.02 ± 2.80	121.95 ± 1.37
Polymeric colour	27.03 ± 0.68	12.20 ± 0.32	20.01 ± 0.80	21.14 ± 0.72
Antioxidant activity	90.87	94.80	92.70	94.13

Table 2. Correlation coefficients (r^2) of antioxidant activity, total phenols, tartaric esters, flavonols and anthocyanins assays of the investigated fruit extracts.

	DPPH•	Total phenols	Tartaric esters	Flavonols	Monomeric anthocyanins
DPPH•	1.000	0.829	0.254	0.607	0.792
Total phenols		1.000	0.658	0.909	0.995
Tartaric esters			1.000	0.893	0.682
Flavonols				1.000	0.928
Monomeric anthocyanins					1.000

The portion of anthocyanins in the total phenol content was evaluated by calculating the monomeric anthocyanins/total phenols ratio. Anthocyanins represent a significant portion in the total phenol content in sour cherry (0.61) and blackberry (0.37), following by strawberry (0.19). The portion of anthocyanins in raspberry (0.16) was considerably lower.

All fruit extracts exhibited significant antioxidant activity (Table 1). The strongest radical scavenging activity is displayed by blackberry (94.80%), sour cherry (94.13%), raspberry (92.70%) and strawberry (90.87%).

Correlation coefficients of antioxidant activity and contents of selected phenolic compounds in the fruit extracts are shown in Table 2. These results show significant correlations between total phenolics and monomeric anthocyanins content ($r^2 = 0.995$). There are strong correlations between antioxidant activity and total phenol content ($r^2 = 0.829$), antioxidant activity and anthocyanin content ($r^2 = 0.792$), flavonols and total phenols ($r^2 = 0.909$), flavonols and tartaric esters ($r^2 = 0.893$), and flavonols and anthocyanins ($r^2 = 0.928$) in the investigated fruit extracts (Table 2).

One group of selected fruit methanol extracts was kept at 7°C during 57 days, simulating a household situation where the fruit products are stored in the refrigerator. Another group of fruit methanol extracts was stored at room temperature (25°C), exposed to sunlight during 90 days.

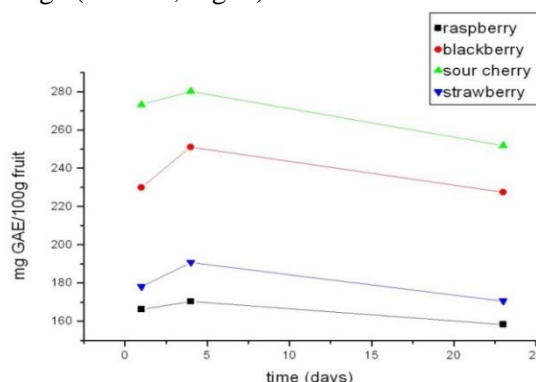
Table 3. Changes in the total phenol content of the investigated fruit extracts (mg GAE /100g fruit) at 7°C during 23 days.

Storage	Strawberry extract	Blackberry extract	Raspberry extract	Sour cherry extract
1 st day	198.07 ± 3.62	231.50 ± 1.09	166.17 ± 2.07	273.22 ± 4.38
4 th day	196.71 ± 3.06	230.13 ± 2.65	165.27 ± 3.10	272.24 ± 3.25
23 rd day	192.58 ± 2.31	227.47 ± 2.13	158.22 ± 2.10	270.56 ± 1.59

Table 4. Changes in the total phenol content of the investigated fruit extracts (mg GAE /100 g fruit) at 25°C, exposed to sun light, during 90 days.

Storage	Strawberry extract	Blackberry extract	Raspberry extract	Sour cherry extract
1 st day	198.07 ± 3.62	231.50 ± 1.09	166.17 ± 2.07	273.22 ± 4.38
4 th day	191.62 ± 3.08	224.52 ± 2.23	160.12 ± 2.81	272.15 ± 2.45
23 rd day	188.25 ± 2.11	211.28 ± 2.83	156.99 ± 2.42	270.78 ± 2.38
57 th day	186.15 ± 2.20	200.12 ± 2.82	142.02 ± 2.80	259.19 ± 1.37
90 th day	168.02 ± 168	198.50 ± 3.32	138.30 ± 1.80	232.43 ± 1.72

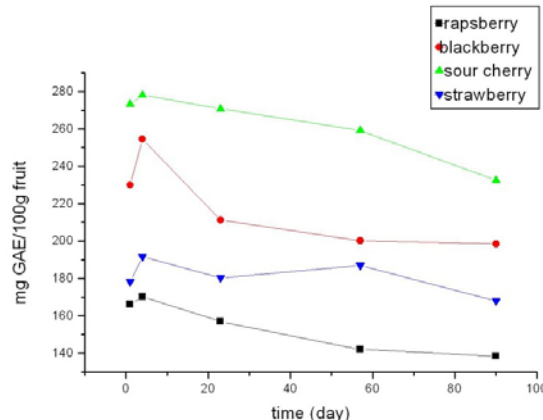
The changes in the total phenol contents of these samples are shown in Tables 3 and 4. During 23 days of storage at 7°C the changes in the total phenol concentrations were observed for all fruit extracts. The initial phenol contents of all samples increased after 4 days of storage. This increase in the phenol content in the first days of refrigerated storage was also observed by other authors [18,19]. This initial increase in the phenol content was followed by a decrease in the total phenol values at the end of storage (Table 3, Fig. 1).

**Fig. 1.** Effect of refrigerated storage on the total phenol content in selected fruit extracts.

In the second group of fruit extracts stored at room temperature and exposed to sunlight, an initial increase in phenol content after 4 days was also followed by a decrease in these values at the end of storage (Table 4, Fig. 2).

The total phenol concentration decrease in selected fruit extracts after 23 days of refrigerated storage was 4.2% in strawberry extract, 4.8% in raspberry extracts, 7.85% in sour cherry extracts and 1.1% in blackberry extracts.

The total phenol concentration decrease in selected fruit extracts after 23/90 days storage at room temperature and light was 1.23%/5.65% in strawberry extract, 5.53%/16.77% in raspberry extracts, 0.89%/14.93% in sour cherry extracts and 8.1%/13.7% in blackberry extracts.

**Fig. 2.** Storage effect of sunlight and room temperature on total phenol content in selected fruit extracts.

Total antioxidant capacity decrease in selected fruit extracts after 90 days of storage at room temperature was from 4.08% to 4.82%.

Total phenols in fruit extracts kept in the dark at 7°C were not significantly different from those exposed to sunlight and room temperature ($p < 0.005$) after 23 days of storage.

CONCLUSIONS

The results of the present study showed that the investigated fruit extracts displaying the highest content of phenolic compounds exhibited the greatest antioxidant activity. The highest content of total phenols and monomeric anthocyanins, as well as the highest antioxidant activity was observed in sour cherry, followed by blackberry, strawberry and raspberry. The contents of phenolic compounds showed a good correlation with the total antioxidant activity of all investigated fruit extracts. The changes in the total phenol content were not significant during 23 days of storage in refrigerator or room temperature. This indicates that the selected fruits can be used as an easily accessible source of natural antioxidants and as possible food and pharmaceutical supplements.

Acknowledgements: The research was supported by the Ministry of Education and Science of Serbia, project No. TR 034012.

REFERENCES

1. J. M. Heinonen, A. S. Meyer, E. N. Frankel, *J Agric. Food Chem.*, **4**, 4107 (1998).
2. M. S. M. Rufino, F. A. N. Fernandes, R. E. Alves, E. S. de Brito, *Food Chem.*, **114**, 693 (2009).
3. A. Turkoglu, M. Duru, N. Mecan, I. Kivrak, K. Gezer., *Food Chem.*, **101**, 267 (2007).
4. M. A. Lila, *J Biomed. Biotechnol.*, **5**, 306 (2004).
5. D. X. Hou, *Curr. Mol. Med.*, **3**, 149 (2003).
6. N. J. Temple, *Nutr. Res.*, **20**, 449 (2000).
7. T. Tsud, F. Horio, T. Osawa, *Biofactors*, **13**, 133 (2000).
8. H. Wang, G. Cao, R. L. Prior, *J. Agric. Food Chem.*, **50**, 3495 (1997).
9. G. Mazza, E. Miniati, *Vegetables and Grains*, CRC Press, Boca Raton, Florida, 1993.
10. L. Jakobek, M. Šeruga, M. M. Kosanović, I. Novak, *Agric. Cons. Scien.*, **72**, 301 (2007)..
11. R. M. Ferreyra, S. Z. Vina, A. Mugridge, A. R. Chaves, *Sci. spectrscopy*. In R. E. Wrolstad (Ed.). New York, Wiley, 2001. *Horticult.*, **112**, 27 (2007).
12. W. Kalt, C. V. Forney, A. Martin, R. J. Prior, *J. Agric. Food Chem.*, **47**, 4638 (1999).
13. D. Marinova, F. Ribarova, M. Atanasova, *J. Univ. Chem. Techn. Metall.*, **40**, 255 (2005).
14. G. E. Pantelidis, M. Vasilakakis, G. A. Manganaris, G. R. Diamantidis, *Food Chem.*, **102**, 777 (2007).
15. M. S. M. Rufino, F. A. N. Fernandes, R. E. Alves, E. S. de Brito, *Food Chem.*, **114**, 693 (2009).
16. J. F. Ayala-Zavala, S. Y. Wang, G. A. Gonzalez-Aguilar, *Lebensm.-Wiss.u -Technol.*, **37**, 687 (2004).
17. S. J. Wang, H. S. Lin , *J. Agric. Food Chem.*, **48**, 140 (2000).
18. J. Piljac-Žegarac, L. Valek, S. Martinez, A. Belščak, *Food Chem.*, **113**, 394 (2009).
19. C. Kevers, M. Falkowski, J. Tabart, J.O. Defraigne, J. Dommes, J. Pincemail, *J. Agric. Food Chem.*, **55**, 8596 (2007).
20. A. A. Van der Sluis, M. Dekker, M. A. J. S. Van Boekel, *J. Agric. Food Chem.*, **53**, 1073 (2005).
21. B. Ancos, E. M. Gonzales, P. Cano, *J. Agric. Food Chem.*, **48**, 4565 (2000).
22. M. M. Giusti, R. E. Wrolstad, Unit F1.2.1-13. *Anthocyanins. Characterization and measurement with UV-visible spectrscopy*. In R. E. Wrolstad (Ed.). New York, Wiley, 2001.

ЕФЕКТ НА СЪХРАНЕНИЕТО ВЪРХУ СЪДЪРЖАНИЕТО И АНТИОКСИДАНТНАТА АКТИВНОСТ НА ФЕНОЛИ В ИЗБРАНИ ПЛОДОВИ ЕКСТРАКТИ

Б. Радованович^{1*}, А. Радованович², В. Николич³, Н. Манойлович⁴, И. Димитриевич¹

¹Департамент по химия, Факултет по наука и математика, Университет Ниш, 18000 Ниш, Сърбия

²Факултет по химия, Белградски Университет, 11000 Белград, Сърбия

³Факултет по технология, Университет Ниш, 16000 Лесковац, Сърбия

⁴Факултет по медицински науки, Университет Крагуевац, 34000 Крагуевац, Сърбия

Получена на 23 ноември, 2016 г.; коригирана на 25 януари 2017 г.

(Резюме)

Целта на това изследване е да се изследва влиянието на светлината и температурата върху съдържанието на фенолни съединения и тяхната корелация с антиоксидантната активност в избрани плодови екстракти от ягода (*Fragaria vesca*), къпина (*Rubus fruticosus*), малина (*Rubus idaeus*) и вишна (*Prunus cerasus*). Антиоксидантният капацитет е оценен използвайки 2,2-дифенил-1-пикрилхидразилов радикал (DPPH-3) и е в диапазона от 90,87% до 96,50%. Съдържанието на изследваните фенолни съединения показва силна корелация с антиоксидантната активност ($r^2 = 0.829$) и със съдържанието на антоцианини ($r^2 = 0.995$) на изследваните екстракти от плодове. Общото съдържание на фенол се наблюдава в екстракти от плодове в продължение на 23 дни, съхранявани при 7 °C и 90 дни при стайна температура (25 °C). Всички плодови екстракти проявяват колебания в общото съдържание на фенол с първоначално увеличение след 4 дни, последвано от намаляване на общите фенолни стойности при двете температури на съхранение. Тези промени не са значителни по време на съхранение в продължение на 23 дни и изследваните екстракти от плодове могат да се използват като лесно достъпен източник на естествени антиоксиданти в хранителните и фармацевтичните добавки.

Preconcentration and determination of cadmium in some samples using solid phase extraction with slotted quartz tube flame atomic absorption spectrometry

Y. Arslan¹, D. Trak², E. Kendüzler^{2*}

¹*Mehmet Akif Ersoy University, Faculty of Arts & Sciences, Nanoscience and Nanotechnology Department, 15030 Burdur, Turkey*

²*Mehmet Akif Ersoy University, Faculty of Arts & Sciences, Chemistry Department, 15030 Burdur, Turkey*

Received December 2, 2016; Accepted June 23, 2017

In this study, a two-step preconcentration method is proposed for the determination of trace amounts of Cd(II). In the first preconcentration step, Amberlite CG-120 resin was used. After the separation and preconcentration of Cd(II), a slotted quartz tube was used for its FAAS determination. In this part, the slotted quartz tube was used as the second preconcentration step. Some experimental parameters influencing the separation and preconcentration of Cd(II) were separately optimized. The total enrichment factor was found to be 920 after the two steps of preconcentration and the detection limit was found to be 0.1 µg/L. Accuracy of the method was checked by analysing a standard reference material (Environmental Matrix Reference Material, Lake Water, TMDA-70.2). The proposed two-step preconcentration method was applied to the analysis of drinking water.

Keywords: cadmium; solid phase extraction; two-step preconcentration method; Amberlite CG-120 resin; slotted quartz tube; flame atomic absorption spectrometry.

INTRODUCTION

Elevated heavy metal concentrations in the atmosphere are caused by serious pollution from the industrialization activities [1]. The Environmental Protection Agency (EPA) proposed that cadmium is among thirteen toxic metal species in the priority pollutant list [2]. Cd is one of the most toxic elements for living organisms and it shows severe unwanted effects, especially on kidneys [3]. The half-life of Cd in the kidney is about 30 years. Therefore, the determination of Cd in different samples is very significant for food and environmental control [4].

Flame atomic absorption spectrometry (FAAS) [5], inductively coupled plasma optical emission spectrometry (ICP-OES) [6], inductively coupled plasma mass spectrometry (ICP-MS) [7], cold vapor generation atomic absorption spectrometry (CVG AAS) [8], graphite furnace atomic absorption spectrometry (GF-AAS) [9] and electrothermal atomic absorption spectrometry (ETAAS) [10] are the most proper techniques for the determination of Cd(II) with different sensitivity. Among the above techniques, FAAS has been the commonly preferred technique for the determination of some heavy metals at trace levels. However, the sensitivity of FAAS is inadequate for direct trace analysis. Preconcentration and/or separation methods are

often required before the FAAS analysis at trace levels [11].

There are several methods used for preconcentration and separation of Cd(II), such as solid-phase extraction (SPE) [12], non-dispersive ionic liquid based microextraction (NDILME) [13], multi-step cloud point extraction procedure (CPE) [14] and dispersive solid-phase extraction (DSPE) [10]. Among them, the SPE has been frequently used for the preconcentration and separation of elements from some matrices because of its simplicity, speed, low cost, and low consumption of reagents [15].

In recent years, ionic imprinted polymers (IIPs) [16], multiwalled carbon nanotubes (MWCNTs) [17], modified polyurethane foam [18] and modified silica gel [19] have been used for the preconcentration and separation of Cd(II) in some matrices prior to the its determination.

Additionally, there have been various applications to improve FAAS sensitivity in the detection step. One of the preferred devices called slotted quartz tube (SQT) was developed by Watling in 1977. Using the SQT device the sensitivity of FAAS has been increased from 2 to 5 fold depending on the element [20]. In the literature, there are some studies on the determination of metals at trace levels using the SQT-FAAS [21-23].

In this work, Cd(II) was enriched by a two-step preconcentration method. Amberlite CG-120 was employed as the adsorbent for the separation and preconcentration of Cd(II) (first preconcentration step). The functional groups of this resin are Na⁺

* To whom all correspondence should be sent:
E-mail: kenduzler@mehmetakif.edu.tr

form and sulfonic acid groups. The optimum pH values of this resin are in the range of ~0.4-10 [24]. In the first preconcentration step, some experimental parameters, such as pH, amount of adsorbent, sample volume and flow rate, eluent volume and flow rate for quantitative recovery of Cd(II) were optimized to obtain the best separation and/or preconcentration conditions. Furthermore, the SQT device was used together with the FAAS to further enhance the sensitivity of the system (second preconcentration step). The developed two-step preconcentration method (SPE and SQT device) was applied for the determination of Cd(II) in drinking water.

EXPERIMENTAL

Apparatus

In this study, the ATI UNICAM 939 model FAAS was used equipped with a deuterium lamp as background corrector, a Cd hollow-cathode lamp as light source (current, 8.0 mA; wavelength, 228.8 nm; bandwidth of the slit, 0.5 nm), acetylene flow rate, 1.1 L/min, slotted quartz tube with two slots (length of slotted quartz tube, 12 cm; length of top slot, 4 cm; length of lower slot, 5 cm). The pH values were controlled with a Thermo Orion 3 Stars Model pH meter.

Reagents

All chemicals were of analytical reagent grade and 18 MΩ.cm deionized water from a PURIS purification system (Model: Expe-UP Series) was used for the preparation of solutions. All glass vessels were cleaned before usage by soaking in 5% HNO₃ and then rinsed thoroughly with deionized water. 65% (w/w) HNO₃ and 60% (w/w) HClO₄ were obtained from Merck. 37% (w/w) HCl, was obtained from Riedel-de Haen.

Preparation of Cd(II) solution

Cd(NO₃)₂·4H₂O was supplied from Aldrich and a 1000 mg/L stock solution of Cd(II) was prepared by dissolving 0.280 g of Cd(NO₃)₂·4H₂O in 100 mL of deionized water. Working solutions of Cd(II) were prepared from the stock solution by dilution.

Column preparation

The glass column used in this study has 15 cm in length and 0.8 cm in internal diameter. In the preparation step of the column, a small glass wool wad was placed at the bottom of the column and 300 mg of Amberlite CG-120 resin was added on it. Afterwards, another small glass wool wad was

inserted onto the top of the resin. Before use, the Amberlite CG-120 resin in the column was washed consecutively with ethanol, 1 mol/L HCl, 1 mol/L HNO₃, and water. After each usage, the column was filled with deionized water and stored until the next experiment.

General procedure for the sorption of Cd(II) on the column

The column was firstly preconditioned at pH 1 using both 1 and 10% (w/w) HCl. 25 mL of a model solution containing 5 µg of Cd(II) was adjusted to pH 1 using both 1 and 10% (w/w) HCl. Then, the model solution was passed through the column at a flow rate of 5 mL/min. The adsorbed Cd(II) ions on the column were eluted with 5 mL of 3 mol/L HNO₃ at a flow rate of 1 mL/min. The eluent solution was analyzed by FAAS. The column filled with Amberlite CG-120 resin was used repeatedly after washing it with 10 mL of 3 mol/L HNO₃ solution and amply with deionized water.

Collection and preparation of samples

The developed two-step preconcentration method was applied to determine Cd(II) in drinking water. Commercial natural drinking waters were purchased from the local market in Burdur city, Turkey.

RESULTS AND DISCUSSION

In this study, Cd(II) was enriched by a two-step preconcentration method. Some experimental parameters of the first step, such as pH, amount of sorbent, concentration and type of eluent, sample and eluent flow rate, and sample volume were optimized. Then, some parameters of the second step using a SQT device, such as observation height (distance between the top of burner head and SQT device) and acetylene flow rate were optimized.

Effect of pH

pH is an important analytical parameter in the solid phase extraction of metal ions. In this study, the recovery values on the Amberlite CG-120 resin were determined at different pH values in the range of 1-5. As seen in Fig. 1, quantitative recovery of Cd(II) was obtained for all pH values in the range. pH 1 was chosen as the optimum pH value.

Effect of the amount of Amberlite CG-120 resin

The effect of the amount of Amberlite CG-120 resin is another significant parameter for an efficient extraction procedure. Different amounts of

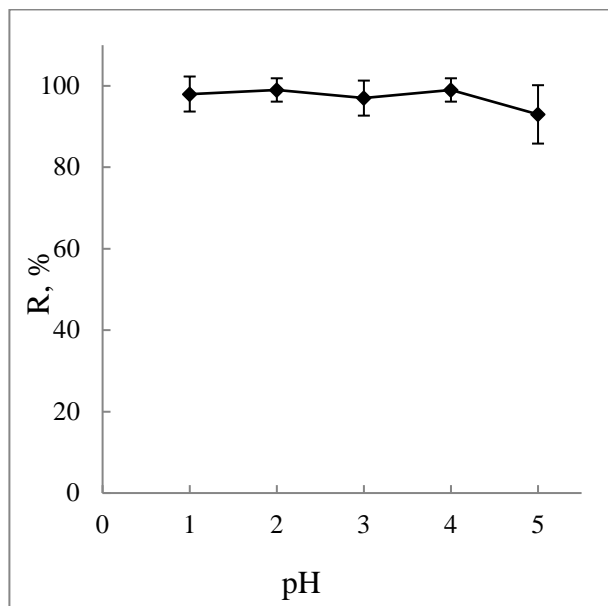


Fig. 1. Effect of pH on the recovery of Cd(II) on a column of Amberlite CG-120.

Amberlite CG-120 resin in the range from 0 to 500 mg were used and quantitative recoveries were obtained with 100 to 500 mg of Amberlite CG-120 resin. For quantitative recovery in the case of real samples, 300 mg of Amberlite CG-120 resin were used in further experiments.

Effect of type and volume of eluent

A series of eluent solutions, *viz.* 2 mol/L HNO₃, 2 mol/L HCl, 2 mol/L HClO₄ and ethanol, were employed in order to find out the suitable eluent type and volume. Quantitative recovery of Cd(II) was achieved with 10 mL of 2 mol/L HCl. After that, the optimum concentration and volume of HCl were optimized. To this purpose, various concentrations of HCl between 0.1 and 4.0 mol/L and volumes of 5 and 10 mL of HCl were taken. It was found that quantitative elution is achieved by using 5 mL of 3 mol/L HCl. Therefore, 5 mL of 3 mol/L HCl solution was employed in all studies.

Effect of flow rate of sample and eluent solution

The sample flow rate through the column is a substantial factor which influences both the recovery of analyte and the time of analysis. Thus, the flow rates of sample and eluent solution were investigated. The model solution was passed through the column at a flow rate changing from 0.25 to 5 mL/min. Quantitative recovery was obtained for all sample flow rates shown in Fig. 2 and 5 mL/min was chosen in order to shorten the analysis time. The eluent solution was passed through the Amberlite CG-120 resin at flow rates ranging from 0.25 to 2 mL/min. With all eluent

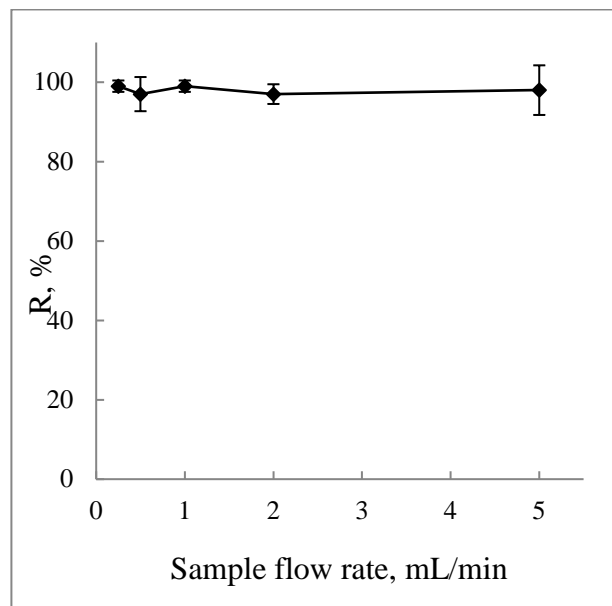


Fig. 2. The effect of sample flow rate on the recovery of Cd(II) on a column of Amberlite CG-120.

flow rates, quantitative recovery was achieved and 2 mL/min was selected to shorten the analysis time.

Effect of sample volume

For determining the enrichment factor of Cd(II), volumes of 25, 50, 100, 250, 500, 750 and 1000 mL of sample solution containing 5 µg Cd(II) were passed through the Amberlite CG-120 resin. The recovery of Cd(II) was quantitative for all sample volumes, as shown in Fig. 3.

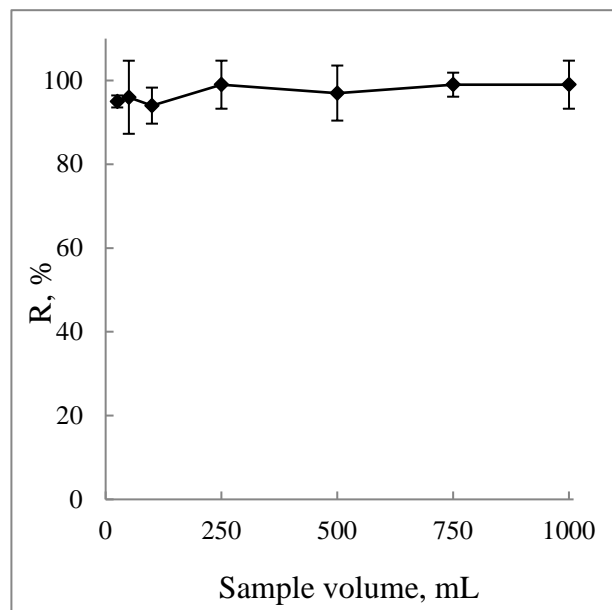


Fig. 3. Effect of sample volume on the recovery of Cd(II) on a column of Amberlite CG-120.

1000 mL was chosen as the optimum sample volume; and the eluent volume was chosen as 5 mL. In this way a preconcentration factor of 200 was achieved in the first preconcentration step of this proposed study.

Slotted Quartz Tube (SQT) optimizations

FAAS equipped with a SQT device was used for further improving sensitivity (second preconcentration step). The important parameters here - acetylene flow rate and observation height were optimized. The proper acetylene flow rate was identified as varying from 0.8 L/min to 1.4 L/min. At 1.1 mL/min acetylene flow rate, the maximum peak area for Cd(II) was obtained. The effect of the observation height on the Cd(II) signal in the range from 0.6 to 0.8 cm was studied. The optimum observation height was found to be 0.7 cm.

Matrix effects

Matrix effects should be investigated since accompanying ions present in the real samples may affect the analyte signal positively and/or negatively. For this, different cations prepared from salts with Cl^- , NO_3^- , SO_4^{2-} ions were added individually to the model solution of Cd(II) and then the proposed preconcentration method was applied. The results are given in Table 1. As can be seen, the proposed method is independent of matrix effects at the working concentrations of the selected elements.

Analytical figures of merit

In the proposed study, the equations of the calibration plots for FAAS and SQT-FAAS were found as $y=0.0682x+0.0004$ and $y=0.3156x+0.0076$, respectively. The comparison of the slopes of the calibration plots without and with SQT device yielded a 4.6-fold enrichment. In addition, using the Amberlite CG-120 resin, a 200-fold enrichment was

obtained. The total enrichment factor for Cd(II) determination using the two-step preconcentration method was found to be 920.

The limit of detection (LOD) was calculated using both Amberlite CG-120 resin and SQT device. For this reason, 25 mL of model solution containing 0.5 μg Cd(II) was passed through the Amberlite CG-120 resin. The retained Cd(II) on the Amberlite CG-120 resin was eluted by 25 mL of 3 mol/L HNO_3 . Then, the eluent was used for the determination of LOD (3s). LOD was found to be 0.1 $\mu\text{g}/\text{L}$ by the two-step preconcentration method ($N=11$).

Accuracy and analytical application

The accuracy of the method was evaluated by the determination of Cd(II) in the standard reference material, Environmental Matrix Reference Material, Lake Water, TMDA-70.2. The column was firstly preconditioned at pH 1.0. Then, 25 mL of standard reference material was adjusted to pH 1.0 and passed through the column. The elution of Cd(II) from the resin was performed using 3 mol/L HNO_3 . Then the eluent solution was analyzed using the SQT-FAAS method. Cd(II) concentration in the standard reference material was found to be $142 \pm 8 \mu\text{g}/\text{L}$ with a relative error of 1.4% based on four replicate measurements at the 95% confidence level, which is a good agreement with the certified value of $140 \pm 9 \mu\text{g}/\text{L}$. Therefore, it seems that the proposed two-step preconcentration method is useful for the preconcentration of trace levels of Cd(II) in the presence of other metal ions which shows the applicability of the method.

The proposed two-step preconcentration method was also applied for the determination of Cd(II) in drinking water and the accuracy of the method was checked by the determination of the recovery of spiked Cd(II) in the drinking water, as shown in Table 2.

Table 1. Effect of some ions on the recovery of Cd(II).

Ion	Concentration (mg/L)	R* (%)	Ion	Concentration (mg/L)	R* (%)
Na^+	1	98±5	Cu^{2+}	1	97±4
	5	95±4		5	96±3
	50	95±3		50	93±1
K^+	1	98±2	Mn^{2+}	1	96±2
	5	95±2		5	98±4
	50	96±3		50	100±3
Mg^{2+}	1	100±4	Al^{3+}	1	93±3
	5	97±6		5	93±2
	50	101±6		50	96±1
Fe^{3+}	1	100±1	Co^{2+}	1	94±2
	5	97±5		5	95±1
	50	92±1		50	94±5

* $\bar{x} \pm s$, ($N=3$)

Table 2. Determination of Cd(II) in drinking water (N=3).

Added Cd(II), $\mu\text{g/L}$	Found, $\bar{x} \pm \frac{\text{ts}}{\sqrt{N}} \mu\text{g/L}$	Relative error, %
-	N.D. ^a	-
10	9.6 \pm 1.7	-4
20	20.2 \pm 1.5	+1

^a N.D.: Not detected**Table 3.** Determination of Cd(II) in drinking water (N=3).

Study	pH	EF ^a	Resin type	Sample volume, mL	Measuring instrument	LOD, $\mu\text{g/L}$	Ref.
1	4.8	160	Duolite XAD-761 resin	800	FAAS	0.38	[25]
2	8	250	Mini-column packed with sulfur	500	FAAS	0.2	[26]
3	6	282	Multiwalled carbon nanotubes/poly(2-amino thiophenol) nanocomposites	2200	FAAS	0.3	[27]
4	8.5	80	Column packed with sulfur powder modified with 2-mercaptopbenzothiazole	200	CVG-AAS	4.6.10 ⁻³	[8]
This study	1	920	Amberlite CG-120	1000	SQT-FAAS	0.1	-

CONCLUSIONS

In conclusion, the suggested two-step preconcentration method (solid-phase extraction with Amberlite CG-120 resin and SQT) is a rapid, simple, economic, accurate and precise method for the preconcentration and determination of Cd(II) in different environmental samples. This method possesses several advantages. For example, there is no necessity of using buffer and chelating agents for the separation and preconcentration of Cd(II). The method has a high enhancement factor, high tolerance limit for matrix ions, low detection limit and works in a strongly acidic medium. The analytical performance of the proposed method is compared with that of other preconcentration methods in the literature, as shown in Table 3.

REFERENCES

1. A. S. Amin, A. A. Gouda, *Food Chem.*, **132**, 518 (2012).
2. F. Omidi, M. Behbahani, M. K. Bojdi, S. J. Shahtaheri, *J. Magn. Magn. Mater.*, **395**, 213 (2015).
3. B. Yang, Q. Gong, L. Zhao, H. Sun, N. Ren, J. Qin, J. Xu, H. Yang, *Desalination*, **278**, 65 (2011).
4. A. M. H. Shabani, S. Dadfarnia, Z. Dehghani, *Talanta*, **79**, 1066 (2009).
5. H. Xu, Y. Wu, J. Wang, X. Shang, X. Jiang, *J. Environ. Sci.*, **25**, 45 (2013).
6. M. S. El-Shahawi, A. S. Bashammakh, M. I. Orief, A. A. Alsibaai, E. A. Al-Harbi, *J. Ind. Eng. Chem.*, **20**, 308 (2014).
7. N. Zhang, B. Hu, *Anal. Chim. Acta*, **723**, 54 (2012).
8. N. Pouurreza, K. Ghanemi, *J. Hazard. Mater.*, **178**, 566 (2010).
9. Md. I. ul Hoque, D. A. Chowdhury, R. Holze, A. Chowdhury, Md. S. Azam, *J. Environ. Chem. Eng.*, **3**, 831 (2015).
10. J. Á. Méndez, J. B. García, S. G. Martín, R. M. P. Creciente, C. H. Latorre, *Spectrochim. Acta B*, **106**, 13 (2015).
11. E. V. Oral, İ. Dolak, H. Temel, B. Ziyadanogullari, *J. Hazard. Mater.*, **186**, 724 (2011).
12. S. A. Rezvania, A. Soleymanpour, *J. Chromatogr. A*, **1436**, 34 (2016).
13. Naeemullah, T. G. Kazi, M. Tuzen, F. Shah, H. I. Afridi, D. Citak, *Anal. Chim. Acta*, **812**, 59 (2014).
14. Naeemullah, T. G. Kazi, M. Tuzen, *J. Ind. Eng. Chem.*, **35**, 93 (2016).
15. H. Lü, H. An, Z. Xie, *Int. J. Biol. Macromol.*, **56**, 89 (2013).
16. M. C. Barciela-Alonso, V. Plata-García, A. Rouco-López, A. Moreda-Piñeiro, P. Bermejo-Barrera, *Microchem. J.*, **114**, 106 (2014).
17. M. Krawczyk, M. Jeszka-Skowron, *Microchem. J.*, **126**, 296 (2016).
18. N. Burham, *Desalination*, **249**, 1199 (2009).
19. H. Lü, H. An, X. Wang, Z. Xie, *Int. J. Biol. Macromol.*, **61**, 359 (2013).
20. İ. Demirtaş, S. Bakırdere, O. Y. Ataman, *Talanta*, **138**, 218 (2015).
21. M. Yaman, İ. Akdeniz, *Anal. Sci.*, **20**, 1363 (2004).
22. G. Kaya, M. Yaman, *Talanta*, **75**, 1127 (2008).
23. S. X. Li, F. Y. Zheng, Y. C. Li, T. S. Cai, J. Z. Zheng, *J. Agr. Food. Chem.*, **60**, 11691 (2012).
24. T. Pasinli, A. E. Eroğlu, T. Shahwan, *Anal. Chim. Acta*, **547**, 42 (2005).
25. H. Ciftci, *Desalination*, **263**, 18 (2010).
26. H. Parham, N. Pourreza, N. Rahbar, *J. Hazard. Mater.*, **163**, 588 (2009).
27. M. R. Nabid, R. Sedghi, A. Bagheri, M. Behbahani, M. Taghizadeh, H. A. Oskooie, M. M. Heravi, *J. Hazard. Mater.*, **203**, 93 (2012).

**ПРЕ-КОНЦЕНТРИРАНЕ И ОПРЕДЕЛЯНЕ НА КАДМИЙ В НЯКОИ ПРОБИ ЧРЕЗ
ТВЪРДО-ФАЗНА ЕКСТРАКЦИЯ И ПЛАМЪКОВА АТОМНО-АБСОРБЦИОННА
СПЕКТРОФОТОМЕТРИЯ (FAAS)**

Я. Арслан¹, Д. Трак², Е. Кенджюзлер^{2*}

*1 Университет „Мехмет Акиф Ерсой“ Факултет за изкуства и наука, Департамент по нанонауки и
нанотехнологии, 15030 Бурдур, Турция*

*21 Университет „Мехмет Акиф Ерсой“, Факултет за изкуства и наука, Департамент по химия, 15030 Бурдур,
Турция*

Постъпила на 11 април, 2016 г.; коригирана на 23 юни, 2017 г.

(Резюме)

В тази работа се предлага дву-степенно пре-концентриране з определянето на след от Cd(II). За първото пре-концентриране се използва йонообменна смола Amberlite CG-120. След разделянето и пре-концентрирането кадмият се определя чрез FAAS в тясна кварцова кювета. Кюветата се използва за вто пре-концентриране. Отделно са оптимизирани някои експерименални параметри влияещи на пре-концентрирането и разделянето на Cd(II). Факторът на обогатяване е определен на 920 след две степени на пре-концентрация, а границите на откриване са 0.1 µg/L. Точността на метода е проверена чрез анализа на стандартни референтни материали (Environmental Matrix Reference Material, Lake Water, TMDA-70.2). Предложената дву-степенна процедура е приложена за анализа на питейна вода.

A comparative study on the ionization constants of a Schiff's base in different environments by multiwavelength UV-Vis spectroscopy

K. Alizadeh*, H. Soltani-Afarani

Faculty of Chemistry, Lorestan University, Khorramabad, Iran

Received May 11, 2015; Accepted June 12, 2017

In the present study, the Schiff's base 5-bromo-2-[(2-mercaptophenyl)imino] methylphenol was covalently immobilized on agarose, cellulose acetate and sol-gel membranes. A multiwavelength spectrophotometric method was applied to study the acidity constants of immobilized and dissolved forms of the mentioned compound in universal buffer solutions of various pH, recorded over the wavelength range 200–800 nm. The protolytic equilibrium constants, spectral profiles, concentration diagrams and number of components were calculated. Not unexpectedly, different apparent pK_a values were obtained. The values of the acidity constants of 5-bromo-2-[(2-mercaptophenyl)imino] methylphenol were different in various environments. The reason was that solute properties, such as ionization constants, depend on the composition and properties of its surrounding sphere, therefore they are very sensitive to membrane components.

Keywords: Schiff's base; Acid dissociation constants; Spectrophotometry; Principal components analysis; Environments.

INTRODUCTION

The accurate determination of pK_a values is often required in various chemical and biochemical areas and its vital importance is in understanding the distribution, transport behavior, binding to receptors and mechanism of action of certain pharmaceutical preparations. The acidity constants of organic reagents play a fundamental role in many analytical procedures such as acid-base titration, complex formation, different extraction procedures like SPE, ISEs, in optodes and pH sensors.

Different methodologies have been proposed for the experimental determination of acid dissociation constants including $^1\text{H-NMR}$ spectroscopy [1], capillary electrophoresis [2], FT-IR spectrometry [3], UV-VIS absorption and fluorescence spectrophotometry [4] and potentiometry [5]. Among these techniques, UV-Vis spectrophotometry has been utilized for the determination of pK_a values of acidic substances due to its high sensitivity (10^{-6} M) [6]. Here, the compound under investigation must possess chromophore(s) in proximity to the ionization center(s) so that the protonated and deprotonated species exhibit sufficient spectral dissimilarity [7]. If the molar absorption coefficients of the ionizing species are known, the pK_a values can be computed by fitting the spectral data obtained at a particular wavelength channel to established equations [6]. However, this method suffers from some limitations. For instance, the absorption data of the fully deprotonated and protonated forms cannot be obtained if these species are not stable within 1-pH

units of the pK_a values. Furthermore, the calculation may be difficult to apply for multi-protic substances with overlapping pK_a values. Recently, different chemometric methods based on factor analysis have been developed for multi-wavelength spectrophotometric determination of overlapping acidity constants. Programs and algorithms used for the determination of acidity constants from absorbance data are SQUAD [8], SPECFIT [9] and DATAN 2.1 [10-12]. Fortunately, these problems can be solved very satisfactorily by combining the data obtained in the spectrometric determinations with multivariate analysis and non-linear regression [13].

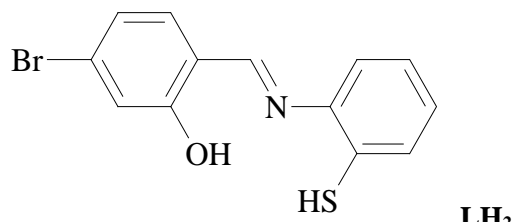


Fig. 1. Molecular structure of the compound used in this work.

In continuation of our research in this field [14, 15], this work was undertaken to determine the acidity constants, concentration distribution diagrams and pure spectra of the species involved in the Schiff's base, 5-bromo-2-[(2-mercaptophenyl)imino] methylphenol **LH₂**, (Fig. 1), covalently immobilized on agarose, triacetyl cellulose (photographic film tape) and sol-gel glass film membranes at 25 °C in aqueous solutions, using a spectrophotometric method.

* To whom all correspondence should be sent:
E-mail: Alizadehkam@yahoo.com

EXPERIMENTAL

Materials and instruments

The Schiff's base **LH₂** with the chemical name 5-bromo-2-[(2-mercaptophenyl)imino]methylphenol, was synthesized and purified as reported [16, 17]. Other chemicals were of reagent grade, purchased from Fluka or Merck.

A Jenway (USA) model 3020 pH meter with a combined glass electrode was used for pH determinations after calibration against standard Merck buffers. A Shimadzu (Japan) model 1650PC double-beam spectrophotometer was used for recording the electronic absorption spectra.

The multivariate analysis Add-in for excel was downloaded for PCA analysis [13] from the Centre for chemometrics website at <http://www.chm.bris.ac.uk/org/chemometrics/addins>, and the other data treatments were performed in MATLAB for Windows (Mathworks, Version 7.10) [18].

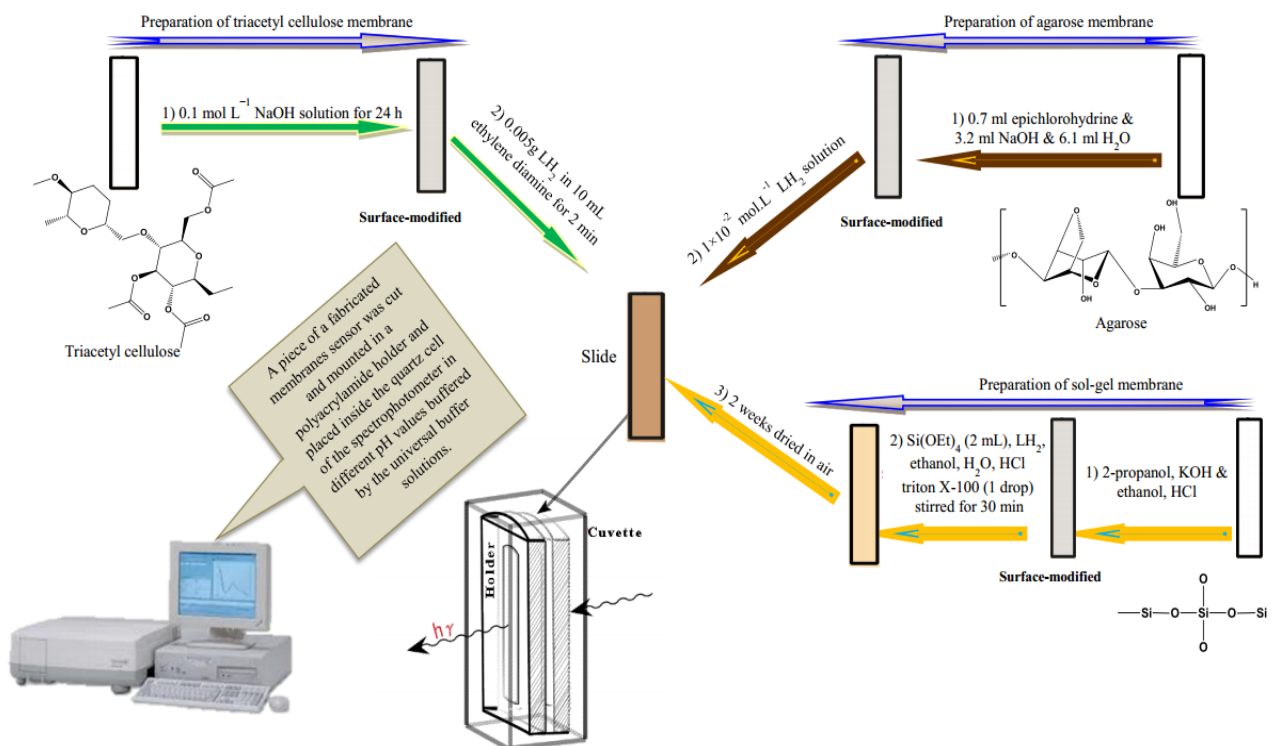
Procedures

A method described elsewhere was used for constructing transparent triacetyl cellulose, agarose and sol-gel membranes with a sensing layer of **LH₂**, as presented in Scheme 1 [19-24]. For analysis, about 2 ml of a sample buffered by a universal buffer was transferred into a 1 cm quartz cell

equipped with a membrane sensor. A home-made polyacrylamide holder was used for holding the membranes inside the quartz cells of the spectrophotometer. To obtain the UV-Vis spectra of the dissolved forms of **LH₂**, 2.5 mL of 5.0 × 10⁻⁵ M **LH₂** in universal buffer solutions of various pH were measured over the wavelength range from 200 to 800 nm. The concentration values of the immobilized **LH₂** on membranes with different composition were calculated by absorbance measurements at the maximum wavelength and same pH in comparison to those of their standard soluble forms.

RESULTS AND DISCUSSION

In the present study, the Schiff's base 5-bromo-2-[(2-mercaptophenyl)imino]methylphenol, **LH₂**, is considered as a di-protic solute. The mentioned structure presents two ionizable OH and SH groups. In this case, ring 1 and ring 2 are conjugated via an imine linkage, thus deprotonation of the OH group of one ring system should appreciably affect the ionization of the SH group of the other. To determine the acid dissociation constants of this molecule, its UV-Vis spectra were recorded at various pH. Using chemometric methods one can analyse the whole spectra, thereby utilizing all spectral information, which considerably reduces the level of error and the result could be even



Scheme 1. Experiment setup for absorbance measurements.

further improved. Therefore, multiwavelength spectrometry can be a powerful alternative for systems where a single wavelength is applied for every component. The approach is superior to any single-point measurement since several hundreds of data points per spectrum can be treated simultaneously. So the obtained acidity constants are more reliable and precise than those obtained by previous methods [14, 25, 26].

The resulting absorbance spectra were recorded for the protonated form of LH_2 at different pH values of the universal buffer. Sample plots in Fig. 2 show the corresponding spectra of LH_2 immobilized in agarose and photographic film.

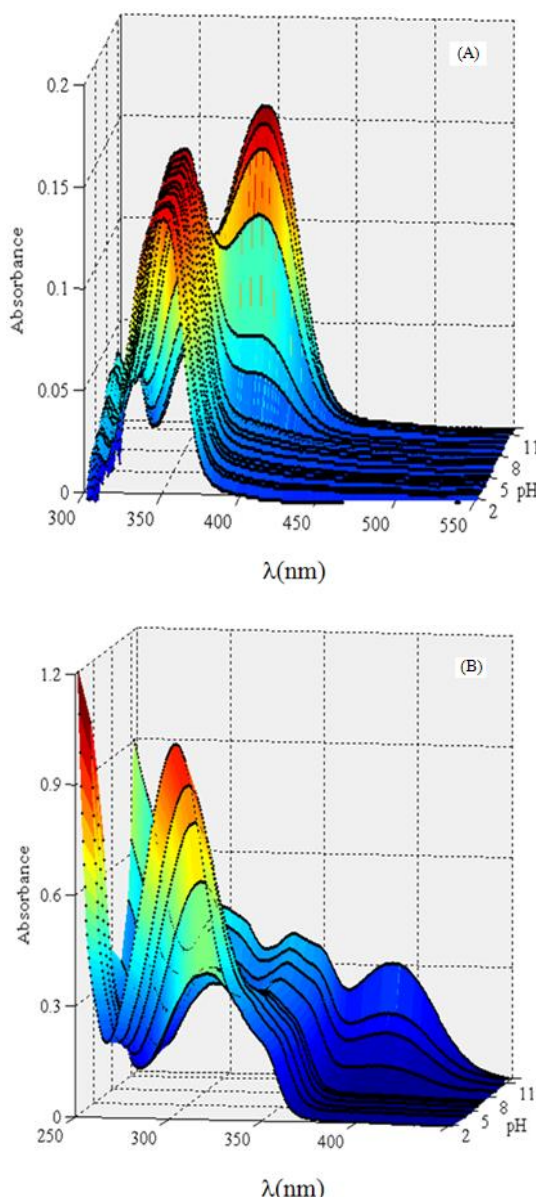


Fig. 2. UV-Vis absorption spectra of LH_2 immobilized in photographic film (A) and agarose (B) membranes as a function of pH.

The most suitable wavelengths in the UV region in the low and in the high pH range with their corresponding molar absorption coefficients ($L \text{ mol}^{-1} \text{cm}^{-1}$) for the compound LH_2 in various environments are summarized in Table 1. Absorption maxima (λ_{\max}) in the UV region observed for LH_2 in the different systems are assigned to $\pi \rightarrow \pi^*$ transition of the benzenoid system towards the other ring present in its structure.

Table 1. Absorption maxima (λ_{\max}) and molar absorption coefficients of 5-bromo-2-[(2-mercaptophenyl)imino] methylphenol in various environments. The shorter and longer wavelength bands are observed in the low and in the high pH range, respectively.

Entry	System	$\lambda_{\max}(\text{nm})$	Molar absorption coefficient
1	Triacetyl cellulose membrane(photographic film)	345,	32000,
		394.5	30000
2	Agarose membrane	303.5,	30400,
		392.5	10100
3	Sol-gel glass	304.5,	27400,
		370	10000
4	Aqueous solution	395.5,	18100,
		452	17880

A fundamental question is how many spectroscopically active species are present in this experiment? To answer this question principal components analysis (PCA) was performed on the data matrix. The observed rank of the data matrix was three or two depending on the composition and properties of its surrounding sphere like aqueous solution, agarose, cellulose acetate and sol-gel membranes. Although the rank of a matrix is a mathematical concept, in the ideal case it corresponds to the number of present species. Cross-validation is also a complementary method to determine the number of PCs. A simple graphical approach is to take the number of PCs, where the graphs of PRESS or RSS are level off, see Figure 3. As seen in Fig. 3, there are two or three significant factors in the corresponding plots.

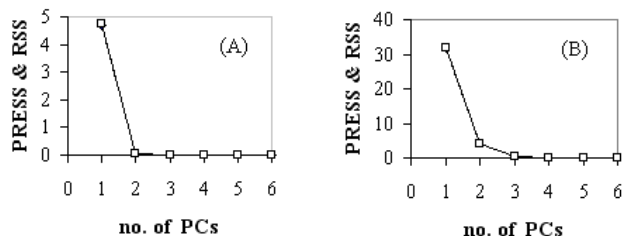
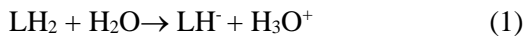


Fig. 3. Plots of PRESS & RSS vs. principal components for LH_2 immobilized in photographic film (A) and agarose (B) membranes.

These factors could be attributed to the protogenic species available in the dissociation equilibria of the mentioned compound [25, 26].

The two successive acid-base equilibria of the compound used in this work in different environments are represented by the following equations:



where LH_2 is the neutral form of the molecule, LH^- (deprotonated form of LH_2) is the monoanion species and L^{2-} (deprotonated form of LH^-) is the dianion solute. The equilibrium constants that characterize the ionization reactions described in equations (1) and (2) are indicated as K_1 and K_2 , respectively. The reaction described in Eq. (1) predominates in the low pH range, while the second ionization reaction occurs in the high pH range [26, 27].

The monoprotic and diprotic acid-base equilibrium models were developed by combination of Beer law and law of mass action which can be summarized in a matrix equation as $\text{Y} = \text{CA} + \text{R}$. A Matlab-based program for nonlinear regression with Newton-Gauss-Levenberg/Marquardt (NGL/M) algorithm was used [18]. This model was used by minimization of the sum of squares to fit experimental data and to calculate the pure spectra, distribution diagrams and acid dissociation constants of the mentioned molecule in various environments.

If two chemical equilibria (three species, i.e., LH_2 , LH^- and L^{2-}) are apparent at various pH values the following model has been used. It is shown here in corresponding final matrix notation.

$$\text{Y} = \text{C} \times \text{A} + \text{R}$$

$$\downarrow \text{pH} \left[\begin{array}{c} \xrightarrow{\text{Spectrum}} \\ \text{Abs} \\ \text{Y} \\ \text{Data Matrix} \\ (\text{n pH} \times \text{n} \lambda) \end{array} \right] = \text{C}_{\text{tot}} \left[\begin{array}{c} \xrightarrow{\text{Concentration Profile}} \\ \alpha_1 \quad \alpha_2 \quad \alpha_3 \\ \vdots \quad \vdots \quad \vdots \\ \alpha_{\text{n}} \quad \alpha_{\text{n}} \quad \alpha_{\text{n}} \\ (\text{n pH} \times 3) \end{array} \right] \times \left[\begin{array}{c} \xrightarrow{\text{Pure Components Spectra}} \\ \varepsilon_1^{\lambda} \quad \varepsilon_1^{\lambda'} \quad \varepsilon_1^{\lambda''} \quad \dots \\ \varepsilon_2^{\lambda} \quad \varepsilon_2^{\lambda'} \quad \varepsilon_2^{\lambda''} \quad \dots \\ \vdots \quad \vdots \quad \vdots \\ \varepsilon_{\text{n}}^{\lambda} \quad \varepsilon_{\text{n}}^{\lambda'} \quad \varepsilon_{\text{n}}^{\lambda''} \quad \dots \\ (3 \times \text{n} \lambda) \end{array} \right] + \left[\begin{array}{c} \xrightarrow{\text{Residual Matrix}} \\ \text{R} \\ (\text{n pH} \times \text{n} \lambda) \end{array} \right]$$

Another model for a sole chemical equilibrium is represented here:

$$\text{Y} = \text{C} \times \text{A} + \text{R}$$

$$\downarrow \text{pH} \left[\begin{array}{c} \xrightarrow{\text{Spectrum}} \\ \text{Abs} \\ \text{Y} \\ \text{Data Matrix} \\ (\text{n pH} \times \text{n} \lambda) \end{array} \right] = \text{C}_{\text{tot}} \left[\begin{array}{c} \xrightarrow{\text{Concentration Profile}} \\ \alpha_1 \quad \alpha_2 \\ \vdots \quad \vdots \\ \alpha_{\text{n}} \quad \alpha_{\text{n}} \\ (\text{n pH} \times 2) \end{array} \right] \times \left[\begin{array}{c} \xrightarrow{\text{Pure Components Spectra}} \\ \varepsilon_1^{\lambda} \quad \varepsilon_1^{\lambda'} \quad \varepsilon_1^{\lambda''} \quad \dots \\ \varepsilon_2^{\lambda} \quad \varepsilon_2^{\lambda'} \quad \varepsilon_2^{\lambda''} \quad \dots \\ \vdots \quad \vdots \quad \vdots \\ \varepsilon_{\text{n}}^{\lambda} \quad \varepsilon_{\text{n}}^{\lambda'} \quad \varepsilon_{\text{n}}^{\lambda''} \quad \dots \\ (2 \times \text{n} \lambda) \end{array} \right] + \left[\begin{array}{c} \xrightarrow{\text{Residual Matrix}} \\ \text{R} \\ (\text{n pH} \times \text{n} \lambda) \end{array} \right]$$

Three principal components were observed in aqueous solution, agarose and sol-gel membranes using multiwavelength spectrometry at various pH, which are equal to three chemical species in the

spectrum. In the other membrane (photographic film) two chemical species were observed in the corresponding spectrum (Figs. 4 and 5). In order to show the compatibility of the proposed model with the experimental data, in the best case utilizing the sum of squares and the dimensions of the corresponding experimental data matrix, i.e. a & b was calculated $[\text{ssq}/(\text{a} \times \text{b})]^{1/2} = 0.004$ which is a good indication for the compatibility of experimental data with model.

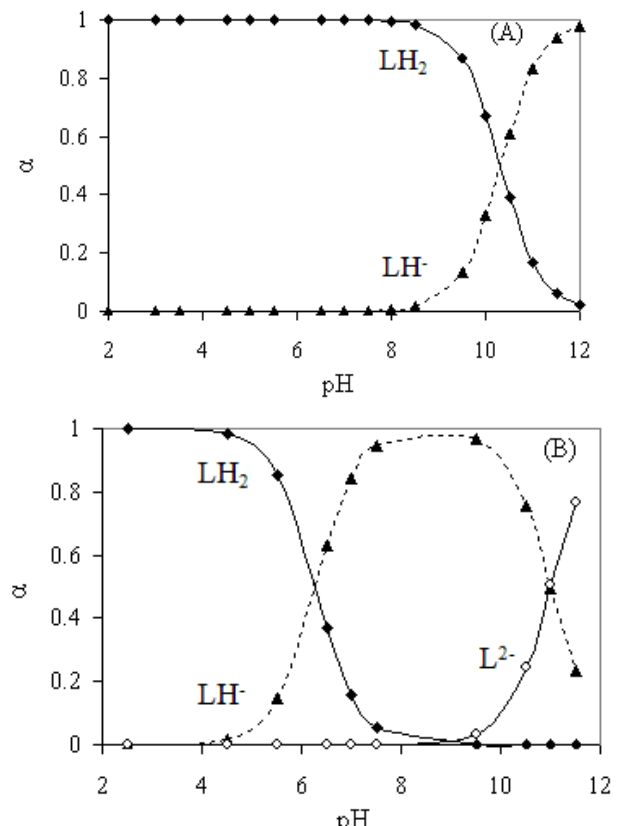


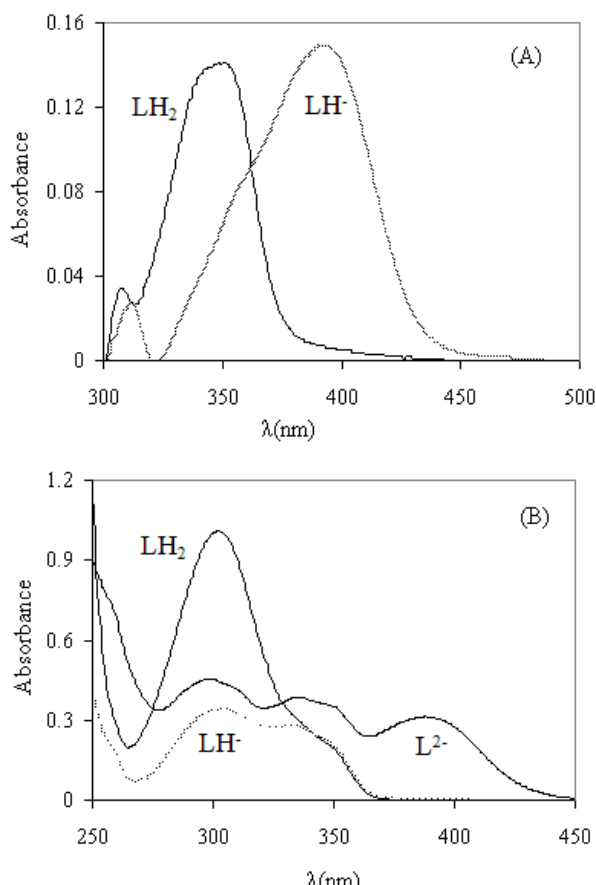
Fig. 4. Distribution diagrams of LH_2 immobilized in photographic film (A) and agarose (B) membranes at different pH values.

As shown in Table 2, different pK_a values were obtained for the immobilized forms of LH_2 on agarose and on sol-gel membranes. The same results were found for the dissolved form. This can be related to the relatively high hydrophilicity of agarose and sol-gel permitting faster diffusion of protons in the membrane. Therefore, the response is fast and hydrogen release is easier, leading to a decrease in pK_a values during the deprotonation process.

Also, the authors believe that the environment of the photographic film may well change the pore size and result in a prolonged response time of the sensor to hydrophilic species, then a sole pK_a will be obtained at various pH values.

Table 2. Determination of experimental pK₁, pK₂ values of the title compound in various environments.

Entry	Environment	Number of present species	pK ₁	pK ₂
1	Triacetyl cellulose membrane ^a	2	10.312±0.004	----
2	Agarose membrane	3	6.265±0.010	11.000±0.013
3	Sol-gel glass	3	7.040±0.020	11.211±0.015
4	Aqueous solution	3	6.764±0.010	11.115±0.021

^aPhotographic film**Fig. 5.** Pure spectra of each assumed species of LH₂ immobilized in photographic film (A) and agarose (B)membranes.

CONCLUSIONS

In this work the acidity constants of 5-bromo-2-((2-mercaptophenyl)imino)methylphenol covalently immobilized on agarose, triacetyl cellulose and sol-gel membranes at different pH values were studied by a multiwavelength spectrophotometric method. A model based on the Newton-Gauss-Levenberg/Marquardt (NGL/M) algorithm was used to find the minimum of the sum of square function values to fit experimental data and to calculate the ionization constants, the pure spectrum profiles of each chemical species and the concentration profiles of the mentioned molecule in several environments. The influence of composition and properties of environments on the obtained values of the studied molecular structure was investigated.

Acknowledgements: The authors gratefully acknowledge the support of this study by the College of Science, Lorestan University.

REFERENCES

1. A. Blasco, C. A. Bunton, S. Bunel, C. Ibarra, E. Moraga, *Int. J. Food Microbiol.*, **35**, 163 (1997).
2. S. K. Poole, S. Patel, K. Dehring, H. Workman, C. F. Poole, *J. Chromatogr.*, **A1037**, 445 (2004).
3. A. Lachenwitzer, N. Li, J. Lipkowsky, *J. Electroanal. Chem.*, **532(1)**, 85 (2002).
4. S. Rouhani, R. Rezaei, H. Sharghi, M. Shamsipur, G. Rounaghi, *Microchem. J.*, **52**, 22 (1995).
5. A. Moghimi, R. Alizadeh, A. Shokrollahi, H. Aghabozorg, M. Shamsipur, A. Shockravi, *Inorg. Chem.*, **42(5)**, 1616 (2003).
6. A. Albert, E. P. Serjeant, *The Determination of Ionization Constants*, Chapman and Hall, London, 1984.
7. A. Avdeef, K. Y. Tam, *J. Pharma. Biomed. Anal.*, **20**, 631 (1999).
8. J. Havel, M. Meloun, in: *Computation Methods for the Determination of Formation Constants*, D. J. Leggett (eds.), Plenum Press, New York, 1985.
9. H. Gammp, M. Maeder, C. J. Meyer, A.D. Zuberbuhler, *Talanta*, **32**, 1133 (1985).
10. J. Ghasemi, A. Niazi, M. Kubista, A. Elbergali, *Anal. Chim. Acta*, **455**, 335 (2002).
11. L. Antonov, G. Gorgov, V. Petrov, M. Kubista, J. Nygren, *Talanta*, **49(1)**, 99 (1999).
12. J. Nygren, A. Elbergali, M. Kubista, *Anal. Chem.*, **70**, 4841 (1998).
13. <http://www.chm.bris.ac.uk/org/chemometrics/addins>.
14. M. Shamsipur, B. Maddah, B. Hemmateenejad, S. Rouhani, K. Haghbeen, K. Alizadeh, *Spectrochim. Acta Part A*, **70**, 1 (2008).
15. K. Alizadeh, A.R. Ghiasvand, M. Borzoei, S. Zohrevand, B. Rezaei, P. Hashemi, M. Shamsipur, B. Maddah, A. Morsali, K. Akhbari, I. Yavari, *J. Mol. Liq.*, **149**, 60 (2009).
16. R. Hahn, W.A. Herrmann, G.R.J. Artus, M. Kleine, *Polyhedron*, **14**, 2953 (1995).
17. M. Behpour, S. M. Ghoreishi, N. Soltani, M. Salavati-Niasari, M. Hamadanian, *Corrosion Sci.*, **50**, 2172 (2008).
18. M. Maeder, Y. M. Neuhold, *Practical Data Analysis in Chemistry*, Elsevier Science, Amsterdam, 2007.
19. P. Hashemi, M. M. Abolghasemi, K. Alizadeh, R. Afzari-Zarjani, *Sens. Actuators B*, **129**, 332 (2008).
20. A. Safavi, M. Bagheri, *Sens. Actuators B*, **90**, 143 (2003).

21. E. Wang, K. F. Chow, V. Kwan, T. Chin, C. Wong, A. Bocarsly, *Anal. Chim. Acta*, **495**, 45 (2003).
22. M. K. Amini, T. Momeni-Isfahani, J. H. Khorasani, M. Pourhossein, *Talanta*, **63**, 713 (2004).
23. A. A. Ensafi, M. Bakhshi, *Sens. Actuators B*, **96**, 435 (2003).
24. P. Hashemi, M. Hosseini, K. Zargoosh, K. Alizadeh, *Sens. Actuators B*, **153**, 24 (2011).
25. A. Niazi, A. Yazdanipour, J. Ghasemi, M. Kubista, *Collect. Czech. Chem. Commun.*, **71**, 1 (2006).
26. R. Kellner, R. M. Mermel, M. Otto, M. Valcárcel, H. M. Widmer, *Analytical Chemistry*, WILEY-VCH, 2nd ed., Weinheim, 1999.
27. K. Alizadeh, S. Seyyedi, M. Shamsipur, S. Rouhani, K. Haghbeen, *Spectrochim. Acta A*, **74(3)**, 691 (2009).

СРАВНИТЕЛНО ИЗСЛЕДВАНЕ НА ЙОНИЗАЦИОННИТЕ КОНСТАНТИ НА ШИФОВА БАЗА В РАЗЛИЧНИ СРЕДИ ЧРЕЗ UV-Vis СПЕКТРОСКОПИЯ С ПОЛИХРОМАТИЧНА ДЪЛЖИНА НА ВЪЛНАТА

К. Ализаде*, Х. Солтани-Афарани

Факултет по химия, Университет Лорестан, Хорамабад, Иран

Получена на 11 май, 2015 г.; коригирана на 12 юни 2017 г.

(Резюме)

В настоящото изследване Шифовата база 5-брому-2-([(2-меркаптофенил)имино]метил)фенол е ковалентно имобилизирана върху агароза, целулозен ацетат и зол-гел мембрани. Приложен е полихроматичен спектрофотометричен метод за изследване на константите на киселинност на имобилизираните и разтворените форми на споменатото съединение в универсални буферни разтвори с различно pH в областта на дължини на вълните 200-800 нм. Протолитните равновесни константи, спектралните профили, диаграмите на концентрациите, както и броят на компонентите са изчислени. Не неочаквано бяха получени забележимо различни рKa стойности. Константите на киселинност на 5-брому-2-([(2-меркаптофенил)имино]метил)фенол се различават една от друга в различни среди. Причината е, че свойствата на разтвореното вещество, катостойност на йонизационните константи, зависят от състава и свойствата на заобикалящата го сфера, поради което са много чувствителни към мембранныте компоненти.

Investigation of biodegradation and growth kinetics of dairy wastewater in a batch reactor

T. T. Bayram¹, A. Nuhoğlu², E. Aladağ^{1*}

¹Department of Environmental Engineering, Faculty of Engineering, Van Yuzuncu Yıl University, Van, Turkey

²Department of Environmental Engineering, Faculty of Engineering, Ataturk University, Erzurum, Turkey

Received April 19, 2017; Accepted June 8, 2017

In this study, biodegradation of dairy wastewater was investigated under aerobic conditions in a batch reactor. A minimum concentration of 100 mg L⁻¹ and a maximum concentration of 1000 mg L⁻¹ of COD in the wastewater were used. The culture substrate removal kinetics was followed and the specific growth rate was fitted to the Monod model. The kinetic coefficients K_S and μ_{\max} were found to be 46.55 mg L⁻¹ and 0.0344 h⁻¹, respectively. The regression coefficient was 0.99. The compatibility of actual and predicted results of microbial growth and substrate removal was compared with this model. Results indicated that predicted and actual values fitted each other with 89% compatibility.

Keywords: Dairy wastewater; Biological treatment; Aerobic processes; Batch reactor; Bio-kinetic parameters.

INTRODUCTION

Wastewater pollution is increasing as a result of rapid industrialization and increasing human population. This inhibits the metabolic function of aquatic life and ecological balance. Usable water reserves are consistently being contaminated, as a result of which the water turns unusable. When such a situation is encountered, wastewater needs to be treated and serious precautions must be taken.

Wastewater produced during the dilution of milk and dairy products in the dairy industry is among the substantial pollution sources for natural aquatic environments. Considerably different treatment systems have been developed in order to treat wastewater released from the dairy and dairy products industry but generally physicochemical and biological methods are reported in the literature [1-6].

This study proposes investigating of the biological COD removal performance from dairy wastewater under aerobic conditions in a batch system and comparing the compatibility of predicted (proposed by the model) and actual (experimental) values for the removal of organic material and the growth of microorganisms with the Monod model.

EXPERIMENTAL

Materials

All chemicals used in the study were purchased from Merck and Sigma. Wastewater was collected from the pilot dairy production and processing plant operated by Ataturk University Agriculture Faculty

Food Engineering Department. The plant produces several products including feta cheese, cheddar (kashar), thread cheese (civil), yoghurt, pasteurized milk, daily milk and ice cream. The plant capacity is approximately 900 kg day⁻¹ of milk and dairy products. The wastewater capacity of the plant ranges between 1.5–2 m³ wastewater ton⁻¹ processed milk. Activated sludge samples were taken from the secondary settling tank of the wastewater treatment facility in Erzincan city and used for the adaptation of microorganisms to wastewater by feeding with dairy industry wastewater. The experiments were carried out in a completely mixed batch reactor with a working volume of 2.0 L. Experimental setup can be seen in Fig. 1. Aeration was provided by means of air bubble diffusers at a volumetric flow rate of 1 vvm. During the experiments, pH, temperature and stirring rate were adjusted to 7±1, 25±1 °C and 300 rpm, respectively.

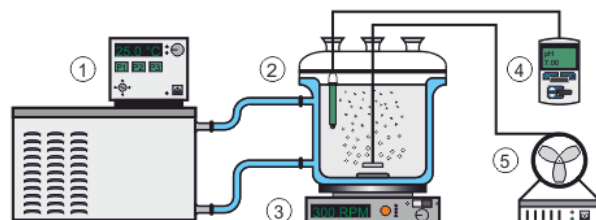


Fig. 1. Schematic diagram of the batch reactor system
(1) Water circulator, (2) Batch reactor, (3) Magnetic stirrer, (4) pH meter, (5) Air pump.

Method

The COD analysis was carried out using the methods stated in the Standard Methods [7]. The microorganisms concentrations were measured spectrophotometrically using Spekol 1100 (Analytik Jena AG). The calibration curve was prepared at the

* To whom all correspondence should be sent:
E-mail: erdinaladag@gmail.com

wavelength of 525 nm and the concentration of the microorganisms was determined using that curve. The pH and temperature of the medium were continuously controlled using a WTW multiline P4 multi-parameter measurement device.

RESULTS AND DISCUSSION

Effect of initial concentration on biodegradation

Batch experiments were conducted by adding wastewater with COD concentrations of 100, 250, 500, 750 and 1000 mg L⁻¹ to the medium. Biodegradation of different initial wastewater concentrations *versus* time is shown in Fig. 2. It can be seen that when COD concentration increased from 100 to 1000 mg L⁻¹, the time of biodegradation raised from 10 to 48 h.

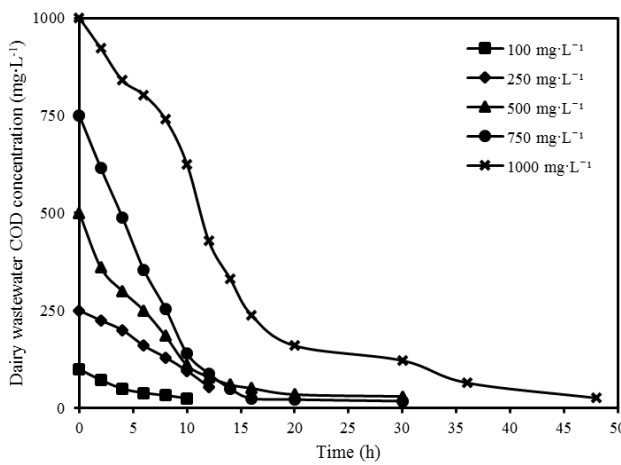


Fig. 2. Biodegradation of different initial COD concentrations in wastewater *versus* time.

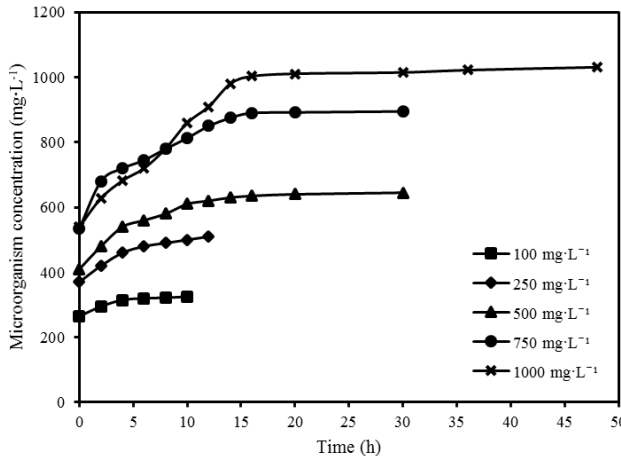


Fig. 3. Microorganisms concentrations as a function of time at different initial dairy COD concentrations in wastewater

Effect of initial concentration on the growth of the culture

Fig. 3 shows microorganisms concentrations as a function of time at different initial dairy wastewater concentrations. According to the experimental results, the maximum specific growth rate was registered at a COD concentration of 1000 mg L⁻¹.

Modeling the growth kinetics of the microorganisms

One of the most important points to be taken into consideration when determining growth kinetics of microorganisms is to adopt an equation showing the relationship between the specific growth rate and the substrate concentration.

$$\frac{dX}{dt} = \mu X \quad (1)$$

Equation (1), where X is the biomass concentration (mg L⁻¹), was used to calculate the specific growth rate of microorganisms. The constant μ which represents the specific growth rate (h⁻¹) can be estimated through linearization of the equation. The plotted data of the linearized results are shown in Fig. 4. The constant μ can be obtained from the linear interception of $\ln(X)$ *versus* t .

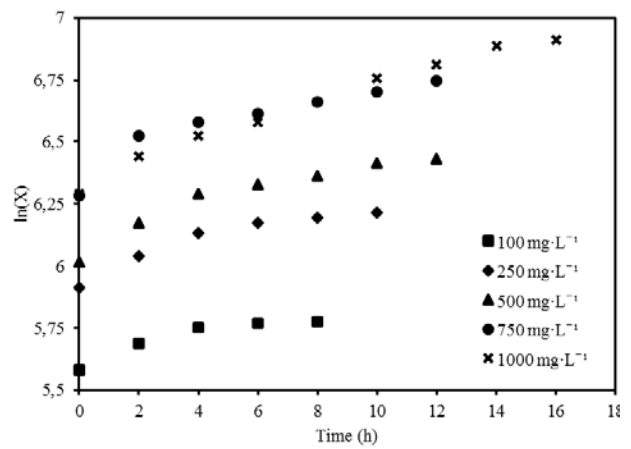


Fig. 4. Variation of microorganisms concentration *versus* time.

The microbial growth can be represented by a simple Monod equation [8].

$$\mu = \frac{\mu_{max} S}{K_S + S} \quad (2)$$

where μ is the specific growth rate (h⁻¹), S is the substrate concentration (mg L⁻¹), μ_{max} is the maximum specific growth rate (h⁻¹), K_S is the half saturation coefficient (mg L⁻¹). As can be seen, the Monod equation has two kinetic parameters μ_{max} and K_S . Numeric values of these two parameters should be calculated and used in the mathematical modeling

studies. A non-linear regression method was used instead of a linear method to calculate the numeric values. The most important point to be considered in the calculation of parameters using a nonlinear regression method is to draw the best fitting curve using the experimental data. Non-linear estimation module of the Statistical Package for the Social Sciences (SPSS) software was used for nonlinear regression calculation. K_s and μ_{max} were determined to be 46.55 mg L^{-1} and 0.0344 h^{-1} , respectively. The regression coefficient was found to be 0.99 for both estimated and experimental μ values. The curve drawn based on these values and experimental data is presented in Fig. 5.

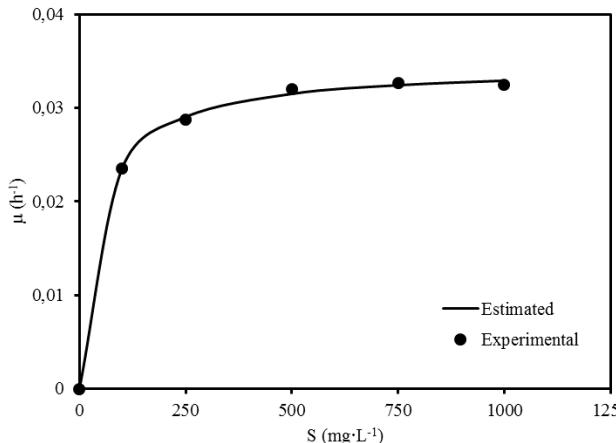


Fig. 5. Predicted and actual specific growth rate.

It is known that the removal rate of an organic compound is a function of its molecular structure, the species of microorganisms that use it as a carbon and energy source and the time required by these microorganisms to develop the necessary enzymes for its utilization. In Table 1 a comparison is given between growth kinetic parameters discussed in the literature including this study.

Table 1. Comparison of the growth kinetic parameters discussed in literature

System	K_s (mg L ⁻¹)	μ_{max} (h ⁻¹)	Reference
Batch reactor	46.55	0.0344	This study
MSBR	174	0.070	[9]
AS	141	0.018	[10]
Two-phase anaerobic	134	0.412	[11]
Anaerobic digestion	420	0.032	[12]

Kinetic coefficients found in previous studies show great variations when compared to the values obtained from the pilot facility wastewater in this study and depend on its characteristics. All compounds involved in dairy industry wastewater are biodegradable. About the lower K_s values

calculated is, it can be said that the wastewater has higher organic material content and lower biodegradation rate in comparison with other studies.

In the study [11], μ_{max} was reported to be 0.412 h^{-1} and it was stated that the mixed culture used for the treatment of dairy wastewater adapted more rapidly to wastewater and more quickly consumed the carbon sources.

Evaluation of the compatibility of biodegradation with the model

The mathematical model of the system was numerically solved determined by means of the coefficients in the Monod model obtained using the 8.3.18 version of Berkeley Madonna software program and simultaneously solving Equations (3) and (4) considering the Runge-Kutta method.

$$\frac{dS}{dt} = -\frac{\mu_{max} SX}{[K_s + SY]} \quad (3)$$

$$\frac{dX}{dt} = \frac{\mu_{max} SX}{K_s + S} - bX \quad (4)$$

By simultaneously solving Equations (3) and (4), the variables of substrate removal and microbial growth in the reactor with time were also determined using the model. The curve fit module of Berkeley Madonna software was used to reduce deviations between the coefficients calculated in the model and the experimentally measured values. The software was operated by considering the ranges for microorganisms decay rate (b) from 0.001 to 0.003 h⁻¹ and the yield coefficient (Y) from 0.25 to 0.75 (mg microorganism.mg⁻¹ substrate). Best compatibility was observed when the values of b and Y were entered into the program as 0.001 h^{-1} and $0.52 \text{ (mg microorganism.mg}^{-1} \text{ substrate)}$, respectively. The model was operated at initial COD concentration in the wastewater of 1000 mg.L^{-1} and the graph obtained is given in Fig. 6. It can be seen from the figure that estimated and actual values are compatible with each other. Table 2 shows the specific growth rate and the regression coefficients for different initial wastewater COD concentrations. The profiles found using the same model kinetic coefficients for removal of substrate and growth of microorganism gave better results for the substrate, while the values of some microorganism profiles showed deviations. A lower increase in the concentration of microorganisms was calculated than that predicted by the model. This situation can be explained by the occurring biofilm on the wall of the continuously stirred reactor. Even though great

care was taken to prevent such a situation, it can be stated that the measured microorganisms concentration does not accurately reflect the increase in the amount of microorganisms in the reactor.

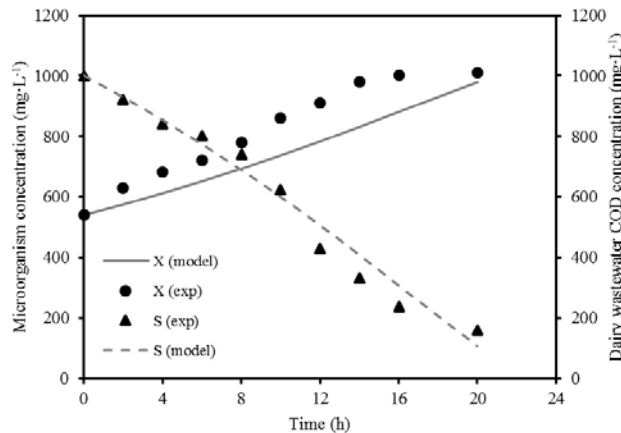


Fig. 6. Predicted versus actual values of dairy wastewater COD removal at initial concentration (S) of 1000 mg L⁻¹ and microbial growth (X).

Table 2. Specific growth rate and regression coefficients for different initial wastewater COD concentrations.

S (mg L ⁻¹)	100	250	500	750	1000
μ (h ⁻¹)	0.024	0.029	0.032	0.033	0.033
R ²	0.89	0.90	0.92	0.88	0.94

Mathematical models are extensively used in the optimum design and control of any given process since effects of operational parameters on system performance can be estimated through such models without any experimental work. Mathematical models offer significant advantages for the estimation of the performance in biological wastewater treatment systems where days or even months are needed to find balance conditions even if only one parameter is changed. For microbial growth, even simple models dependent on Monod criteria can give accurate results for scaling a reactor [13, 14].

CONCLUSIONS

In this study, the biological COD removal performance from dairy wastewater under aerobic conditions was investigated in a batch system and the compatibility of predicted (proposed by model) and actual (experimental) values for the removal of organic material and the growth of microorganisms using the Monod model were compared.

Batch experiments were carried out with 100, 250, 500, 750 and 1000 mg L⁻¹ initial COD concentrations. The equilibrium time at an initial concentration of 100 mg L⁻¹ is 10 h and at an initial concentration of 1000 mg L⁻¹ - 48 h. The Monod

kinetic parameters K_s and μ_{max} were calculated to be 0.0344 h⁻¹ and 46.55 mg L⁻¹, respectively. The regression coefficient was 0.99 for the curve drawn by using the Monod equation and the values of the kinetic parameters. Taking into consideration the results above, it can be concluded that the kinetic parameters relationships derived from the batch experiments and proposed by the model were compatible with each other. Additionally, it can be stated that the dairy wastewater is easily biodegradable by the microorganisms.

Acknowledgements: This study was financially supported by the Ataturk University Scientific Research Fund through project no BAP-2008/155. The authors gratefully acknowledge the funding from Ataturk University.

REFERENCES

- V. Golob, A. Vinder, M. Simonič, *Dyes and Pigments*, **67** (2), 93-97 (2005).
- J. Groeneweg, B. Sellner, W. Tappe, *Water Research*, **28** (12), 2561-2566 (1994).
- P. A. Mateos, Depuración aerobia de vertidos lácteos en régimen discontinuo: influencia de las condiciones de operación. Universidad de Sevilla (1993).
- J. Quiroga, L. Romero, D. Sales, E. Nebot, *Chemical and Biochemical Engineering Quarterly*, **8** (2), 53-61 (1994).
- J. Quiroga, J. Perales, L. Romero, D. Sales, *Chemosphere*, **39** (11), 1957-1969 (1999).
- S. Pavlostathis, E. Giraldo-Gomez, *Critical Reviews in Environmental Science and Technology*, **21** (5-6), 411-490 (1991).
- W. E. Federation, A. P. H. Association, Standard methods for the examination of water and wastewater. American Public Health Association (APHA): Washington, DC, USA (2005).
- K. Kovárová-Kovar, T. Egli, *Microbiology and Molecular Biology Reviews*, **62** (3), 646-666 (1998).
- J. Kaewsuk, W. Thorasampan, M. Thanuttamavong, G. T. Seo, *Journal of Environmental Management*, **91** (5), 1161-1168 (2010).
- F. Carta-Escobar, J. Pereda-Marin, P. Alvarez-Mateos, F. Romero-Guzmán, M. D. Barrantes, *Biochemical Engineering Journal*, **22** (2), 117-124 (2005).
- Y. Yu, C. L. Hansen, S. Hwang, *Biotechnology and Bioengineering*, **78** (2), 147-156 (2002).
- W. Hu, K. Thayanithy, C. Forster, *Process Biochemistry*, **37** (9), 965-971 (2002).
- E. Metcalf, H. P. Eddy, G. Tchobanoglous, *Wastewater engineering: treatment, disposal and reuse*. McGraw-Hill, New York (1991).
- M. Safoniuk, *Chemical Engineering*, **111** (7), 10-12 (2004).

ИЗСЛЕДВАНЕ НА БИОРАЗГРАЖДАНЕТО И КИНЕТИКАТА НА РАСТЕЖА НА МЛЕЧНИТЕ ОТПАДНИ ВОДИ В СТАНДАРТЕН РЕАКТОР

Т. Т. Байрам¹, А. Нуходлу², Е. Аладаг^{1*}

¹Катедра по Инженерство на околната среда, Факултет по инженерство, Юзунку Гил Университет, Van, Турция

²Департамент по Инженерство на околната среда, Факултет по инженерство, Ататюрк Университет, Erzurum, Турция

Получена на 19 април, 2017 г.; коригирана на 8 юни 2017 г.

(Резюме)

В това проучване биоразграждането на млечните отпадъчни води е изследвано при аеробни условия в стандартен реактор. Използвани са концентрации от минимум 100 и максимум 1000 mg L⁻¹ COD в отпадните води. Кинетиката на отстраняване на субстратната култура и специфичната скорост на растеж са пригодени към Monod модел. Кинетичните коефициенти K_S и μ_{max}, са съответно 46.55 mg L⁻¹ и 0.0344 h⁻¹. Регресионният коефициент е 0.99. Съвместимостта на действителните и прогнозираните резултати от микробния растеж и отстраняването на субстрата са сравнени с помощта на този модел. Резултатите показват, че съответствието между прогнозираните и действителните стойности е 89%.

Cytotoxicity and DNA binding of copper (II) and zinc (II) complexes of flavonoids: quercitrin, myricitrin, rutin

B. Atabey-Ozdemir¹, O. Demirkiran², U. Yildiz¹, I. O.Tekin³, B. Coban*¹

¹Bülent Ecevit University, Faculty of Arts and Sciences, Department of Chemistry, Zonguldak, 67100, Turkey.

²Trakya University, Faculty of Pharmacy, Department of Pharmacognosy, Edirne, 22100, Turkey

³Bülent Ecevit University, Faculty of Medicine, Department of Immunology, Zonguldak, 67100, Turkey.

Received December 20, 2016; Accepted May 27, 2017

Flavonoids: quercitrin, myricitrin and rutin and their metal complexes were comparatively investigated for binding to DNA by means of spectrophotometric methods and DNase activities were evaluated via agarose gel electrophoresis of pBR322. Free flavonoids bind to DNA in an intercalative mode, but Cu(II) complexes of these flavonoids bind even stronger due to the electrostatic interaction of the metal in addition to the intercalation. Flavonoids show protective effect against DNA cleavage in the presence of peroxide. However, Cu(II) and Zn(II) complexes of these flavonoids cause multiple scissions on the DNA backbone. In addition, Cu(II) complexes of the flavonoids have stronger DNase activity. Moreover, myricitrin was found two times more cytotoxic when combined with metal ions (Cu^{2+} or Zn^{2+}) than when used alone against peripheral blood mononuclear cells.

Keywords: Flavonoids, DNA binding, DNase activity, Cytotoxicity, Cu(II) complex, Zn(II) complex.

INTRODUCTION

Interaction between DNA and drug molecules is a very popular subject [1-3] especially for the designing of new DNA-targeted drugs and their *in vitro* screening.

Flavonoids are non-nutritive compounds present in plants, and have a broad spectrum of pharmacological activities. Quercetin (2-(3,4-dihydroxyphenyl)-3,5,7-trihydroxy-chromen-4-one), and myricetin 2-(3,4,5-trihydroxyphenyl)-3,5,7-trihydroxy-chromen-4-one) (Table 1), some of the most abundant natural flavonoids, are present in various vegetables and fruits, and their average human daily intake is estimated to be 16–25 mg/person [4]. They are also some of the main active components of many natural Chinese traditional medicines (CTM). The flavonoids frequently occur as glycosides, quercitrin (quercetin-3-O-L-rhamnoside), myricitrin (myricetin-3-O-L-rhamnoside) and rutin (quercetin-3-O-D-rutinoside) (Fig. 1) being the most common flavonol glycosides in the human diet [5]. Flavonoids, especially quercitrin (Q), myricitrin (M) and rutin (R), are capable of scavenging reactive oxygen species (ROS) and chelating iron ions which play a vital role in initiating free radical reactions, and suppressing the generation of hydroxyl radicals in the Fenton reaction [6-9]. Myricitrin and rutin have been found to have anticancer properties against prostate cancer and malignant gliomas [10, 11].

In this context, it is generally considered that these flavonoids form coordination complexes with

some essential trace metals, and it is believed that this is the active form of the compounds, which is medicinally beneficial [12]. Flavonoids are known to react with various metal cations to form stable compounds which have demonstrable antibacterial properties and antitumor activity [13-15]. Given that some metal ions, especially transition metals, not only play vital roles in a vast number of widely differing biological processes, but also may be potentially toxic in their free state, the studies of interactions between flavonoid–metal complexes and DNA are important to further the understanding of the pharmacology of flavonoids. Complexes of different transition metals including copper and zinc were investigated and all metal complexes showed stronger DNA binding ability and were more active against cancer cell lines in respect to free flavonoid [16-23].

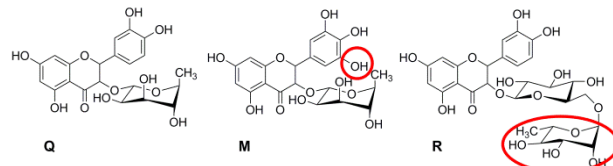


Fig. 1. Flavonoids, especially quercitrin (Q), myricitrin (M) and rutin (R),

Many techniques, such as UV–Vis spectrophotometry [24], fluorescence spectroscopy [25, 26], circular dichroism spectroscopy [27], mass spectrometry [28], and voltammetry [29] have been used to study the binding between metal complexes and DNA.

* To whom all correspondence should be sent:

E-mail: burakcoban@yahoo.com

In this work, the interactions of flavonoids: Q, M and R and their metal complexes with calf thymus (CT)-DNA were comparatively investigated with the aid of absorption and fluorescence spectrophotometry and their DNase activity was investigated against pBR322 plasmid DNA via agarose gel electrophoresis assays. In addition, cytotoxicity of myricitrin alone and in combination with metal ions was evaluated.

EXPERIMENTAL

All reagents and solvents were of commercial origin and were used without further purification unless otherwise noted. Solutions of calf thymus DNA (CT-DNA purchased from Sigma) in 50 mM ammonium acetate (pH 7.5) had a UV-Vis absorbance ratio of 1.8–1.9: 1 at 260 and 280 nm ($A_{260}/A_{280} = 1.9$), indicating that the DNA was sufficiently free of protein [30]. The concentration of DNA was determined spectrophotometrically using a molar absorptivity of $6,600 \text{ M}^{-1} \text{ cm}^{-1}$ (260 nm) [30]. Double-distilled water was used to prepare buffers. Stock solution of CT-DNA was stored at 4 °C and used within 4 days.

Physical measurements

UV-Vis spectra were recorded with a Varian Cary 100 spectrophotometer and emission spectra were recorded with a Perkin Elmer LS 55 fluorescence spectrometer at room temperature.

Absorption and emission titrations

For the absorption and emission titrations, flavonoids and metals (about 1 mmol) were dissolved in a minimum amount of DMSO (0.5 mL), and were then diluted in 5 mM ammonium acetate buffer, pH 7.5 to a final concentration of 20 µM. Titrations were performed in a 10-mm stoppered quartz cell by using a fixed concentration of the compound (20 µM; flavonoid alone and in combination with (1:1) Cu²⁺ or Zn²⁺ ion), to which the CT-DNA stock solution was added in increments of 1 µL to a DNA-to-compound concentration ratio of 6:1. Analysis was performed by means of a UV-Vis or fluorescence spectrophotometer by recording the spectrum after each addition of DNA. Compound-DNA solutions were incubated for 10 min before the spectra were recorded. A control solution of 20 µM of the drug in the same buffer was treated in the same manner. Cell compartments were thermostated at 25 ± 0.1 °C.

For emission intensity measurements, the excitation wavelength was fixed and the emission range was adjusted before the measurements. Ammonium acetate (5 mM), pH 7.5 buffer was used

as a blank to make preliminary adjustments. All measurements were performed with a 5-nm entrance slit and a 5-nm exit slit. The complexes were excited at 383 and 400 nm, respectively; the emission spectra were monitored between 710 and 740 nm.

Competitive studies

The competitive behavior of each compound with ethidium bromide (EB) was investigated by fluorescence spectroscopy in order to examine whether the compound is able to displace EB from the DNA-EB complex.

DNA was pretreated with EB at a DNA-to-EB concentration ratio of 50:1 at 27 °C for 30 min to prepare the initial DNA-EB complex. The intercalating effect of the compounds with the DNA-EB complex was studied by adding a certain amount of a solution of the compounds in increments to the solution of the DNA-EB complex. The influence of each addition of compounds to the solution of the DNA-EB complex was estimated by recording the change in the fluorescence peak at 640 nm. To study the competitive binding of the compounds with EB, the latter was excited at 453 nm in the presence of DNA alone, as well as in the presence of the compounds.

DNAse activity by gel electrophoresis

Gel electrophoresis experiments were performed using pBR322 negatively supercoiled plasmid DNA and 1 % agarose gels together with a tris(hydroxymethyl)aminomethane-borate-EDTA running buffer solution (10 mL) containing 0.1 µg pBR322 together with different amounts of **1** and **2** (0, 20, 40, 60, 100 and 200 µM) in 50 mM ammonium acetate buffer, pH 7.5 were prepared at 0 °C and incubated at 36 °C for 1 h in the dark. Prior to the samples being loaded onto the gel, 2.5 mL of 0.25 % bromophenol blue loaded buffer and sucrose in water (40 % w/v) was added to the reaction mixtures. Gels were obtained at room temperature by using a Thermo midi horizontal agarose gel electrophoresis system and applying a potential of 35 V for 4 h. The resulting gels were stained with EB solution (0.5 µg mL⁻¹) for 45 min, after which they were soaked in water for further 20 min. Gels were visualized under UV light and photographed.

Cytotoxicity assays

Peripheral blood mononuclear cells from healthy individuals were activated with phytohemagglutinin for proliferation and treated with 150 and 1,500 µg of myricitrin in combination with (1:1) metal ion (Cu²⁺ or Zn²⁺). Cells were

incubated at 37 °C for 48 h in a humidified incubator in 5 % CO₂ atmosphere in RPMI-1640 supplemented with 10 % fetal bovine serum, 100 U/mL penicillin, and 100 µg/mL streptomycin for viability analysis using propidium iodide (PI) staining and flow cytometry. A 100-µL cell suspension was used for each sample. Cells were stained with PI according to the manufacturer's instructions, and their viability was measured in a Coulter FC500™ flow cytometer (Beckman-Coulter).

RESULTS

All three flavonoids have very similar UV spectra with an absorption peak at 360 nm wavelength. Addition of metal ions caused the absorption peak to shift to around 400 nm and a slight hypochromic effect is seen in Fig. 2.

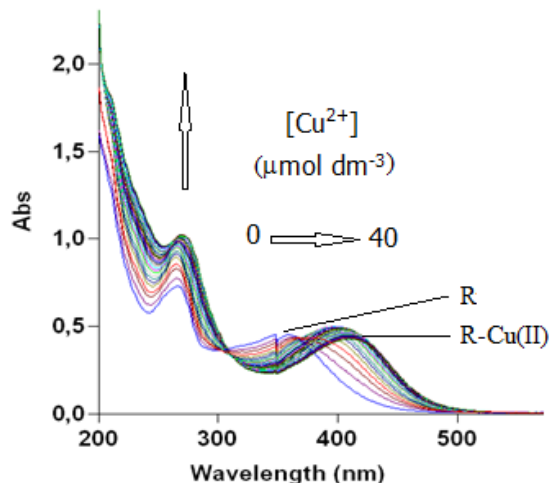


Fig. 2. Absorption spectra of rutin in 50 mM ammonium acetate buffer on gradual additions of Cu²⁺ at pH 7.0 at 298 K. [Rutin]= 20 µM, [Cu²⁺]= 0-40 µM. Arrows indicate the absorbance and wavelength changes with increase in Cu²⁺ concentration.

Very low hypochromic and bathochromic effects were seen after the addition of DNA to the free flavonoid solutions (Fig. 3). The hypochromicity and bathochromic shift increased when Cu(II) complexes of flavonoids were titrated with DNA solution (Fig. 4). Their intrinsic binding constants (K_b) were calculated as Q–Cu(II): $2.62 \pm 0.25 \times 10^5 \text{ M}^{-1}$; M–Cu(II): $1.80 \pm 0.20 \times 10^5 \text{ M}^{-1}$; R–Cu(II): $1.02 \pm 0.10 \times 10^5 \text{ M}^{-1}$.

The competitive titrations of ethidium bromide (EB) dye and flavonoid–Cu(II) species in the presence of DNA are shown in Fig. 5. According to the spectra, EB fluorescence intensity was decreased by the addition of flavonoid–Cu(II) complexes.

The potential of the Cu(II) and Zn(II) complexes to cleave DNA was studied by agarose gel electrophoresis using pBR322 plasmid DNA. When circular DNA is subjected to gel electrophoresis,

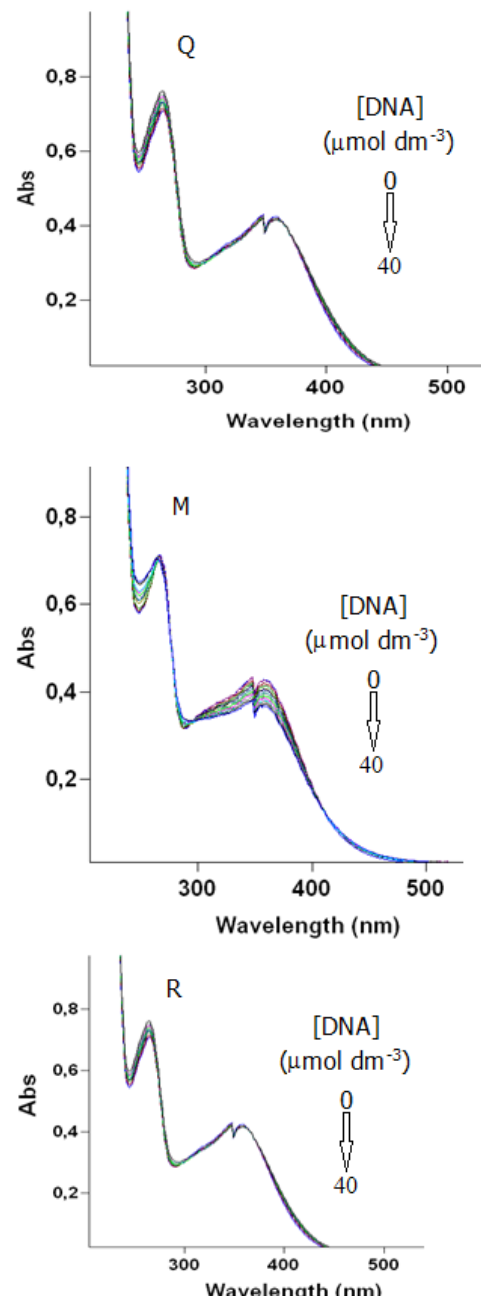


Fig. 3. Absorption spectra of free flavonoids Q, M and R in 50 mM ammonium acetate buffer on gradual additions of calf thymus DNA at pH 7.0 at 298 K. [flavonoid]= 20 µM, [ct-DNA]= 0-40 µM. Arrows indicate the absorbance changes with increase in ct-DNA concentration.

relatively fast migration will be observed for the supercoiled form (form I). If scission occurs on one strand (nicked circular), the supercoiled form will relax to generate a slower moving open circular form (form II). If both strands are cleaved, a linear form (form III) that migrates between the two forms will be generated [31].

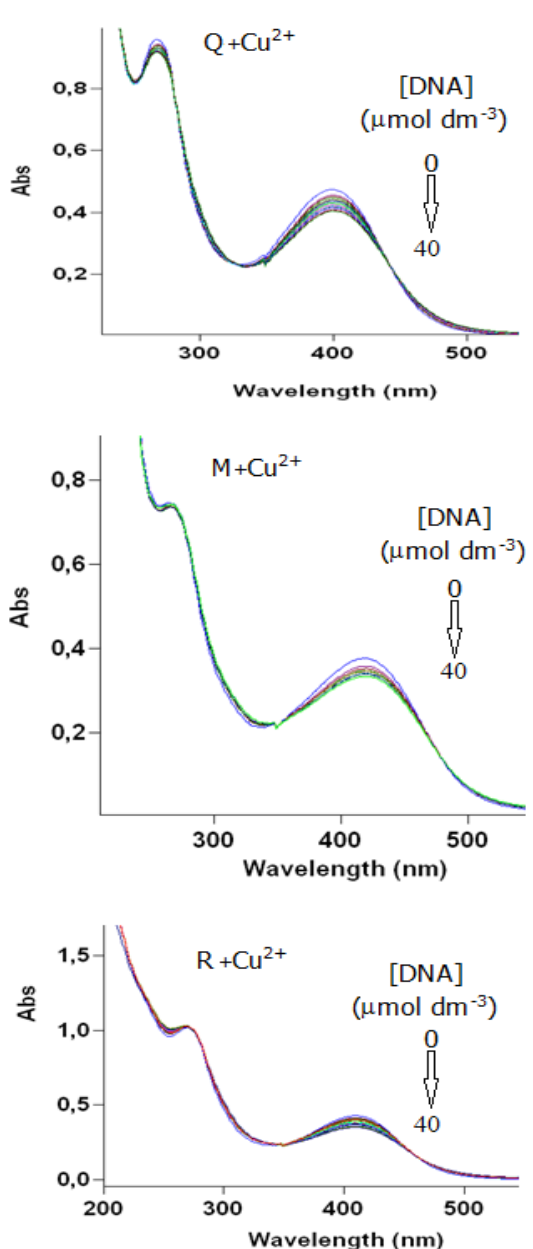


Fig. 4. Absorption spectra of Cu(II) complexes of Q, M and R in 50 mM ammonium acetate buffer on gradual additions of calf thymus DNA at pH 7.0 at 298 K. [Cu(II) complex] = 20 μM , [ct-DNA] = 0–40 μM . Arrows indicate the absorbance changes with increase of ct-DNA concentration.

Fig. 6 shows the separation of pBR322 by gel electrophoresis after incubation with Q, M and R, respectively. Lane 1 is the control having only DNA. The flavonoids, as expected, were unable to cleave the DNA as shown in lanes 2–4. Lane 5 is negative control DNA incubated with peroxide solution, a small proportion of DNA cleavage can be seen as formation of form II. Addition of flavonoids will

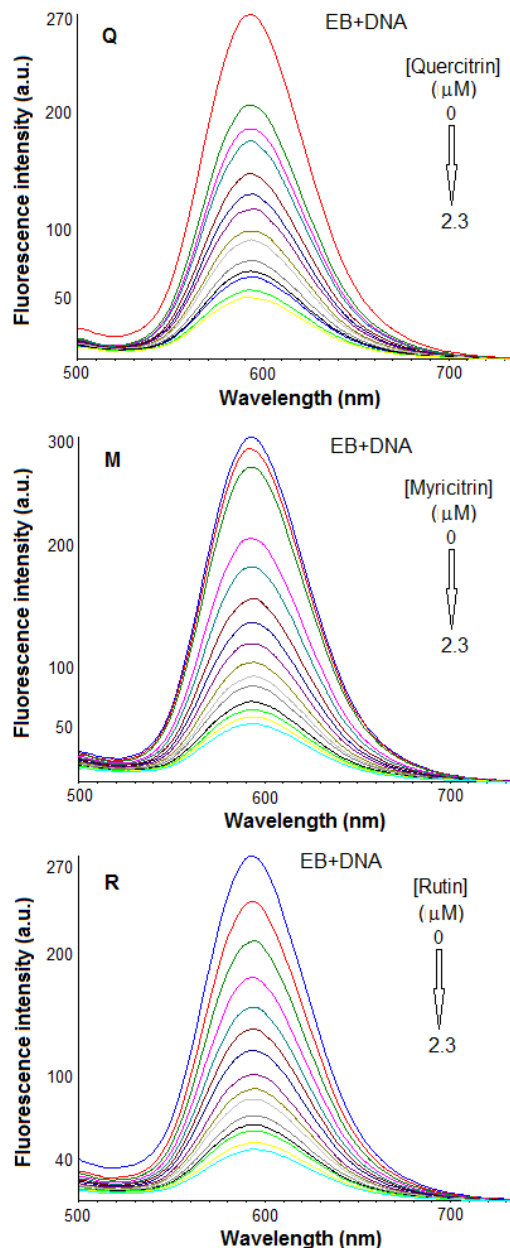


Fig. 5. Fluorescence spectra of the competition between Cu(II) complexes of Q, M and R and ethidium bromide (EB) at 298 K. [EB] = 20.0 μM and [ct-DNA] = 100.0 μM at $\lambda_{\text{exc}} = 363$ nm. [Complex] = 0.2, 0.4, 0.6, 0.8, 1.0, 1.2, 1.4, 1.55, 1.7, 1.9, 2.1, 2.3 μM .

reduce the DNA cleavage in the lanes 6–8 indicating that free flavonoids protect DNA from peroxide damage.

When plasmid DNA was treated with Cu(II) and Zn(II) complexes of flavonoids, a very small fraction of form II was formed indicating a mild DNA damage (not shown on the pictogram). Peroxide addition makes the comparison easier to understand.

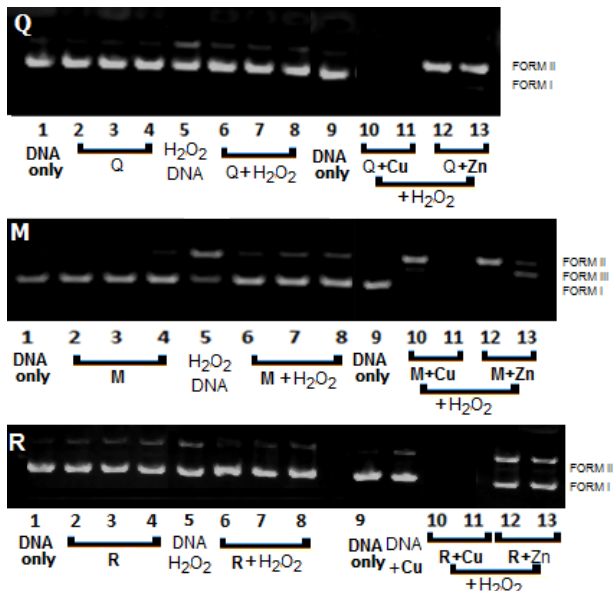


Fig. 6. Agarose gel electrophoresis pictogram showing the cleavage pattern of pBR322 plasmid DNA (50 μ g) with varying concentrations of flavonoids **Q**, **M** and **R** or their Cu²⁺ or Zn²⁺ complexes at 37 °C for 12 h of incubation. Lanes 1 and 9: DNA control, lanes 2-4: 50, 100, 500 μ M flavonoid, lane 5: peroxide, lanes 6-8: 50, 100, 500 μ M flavonoid+peroxide, lanes 10,11: 50, 500 μ M flavonoid-Cu²⁺ complex+peroxide, lanes 12,13: 50, 500 μ M flavonoid-Zn²⁺ complex+peroxide.

Following lanes cover the metal complexes of the flavonoids incubated with DNA (10-13) in the presence of peroxide. Cu(II) complexes caused multiple scissions on the plasmid DNA backbone and therefore small DNA fragments cannot be seen in the gel (lanes 10 and 11) whereas, Zn(II) complexes also cleave plasmid DNA producing form II of all DNA incubated with the Q-Zn(II) and R-Zn(II) complexes (for Q and R: lanes 12 and 13) [32]. With the addition of higher concentrations of M-Zn(II) complex a fraction of form III was also formed (M: lane 13). These observations suggest that Cu(II) complexes caused greater damage to plasmid DNA in comparison to the Zn(II) complexes of the three flavonoids.

Table 1 Cytotoxicity assay results of Myricitrin at two different concentrations in presence and absence of Cu and Zn.

	M (g/L)	M+Zn (g/L)	M+ Cu (g/L)	Zn (g/L)	Cu (g/L)	Control*
	0.15	1.5	0.15	1.5	0.15	1.5
Dead cells (%)	9.1 ± 0.2	10.8 ± 0.5	16.5 ± 1.0	22.5 ± 1.9	17.7 ± 1.8	26.8 ± 2.8
						14.9 ± 0.6
						0.1 ± 0.3

*No compounds were used. Results are expressed as means ± SD ($n = 3$)

In the cytotoxicity assay results shown in Table 1, dead cells were presented as percentages and concentrations of the compounds were chosen as 0.15 and 1.5 g L⁻¹ and in the control try no

compounds were used (no dead cells were expected). Dose-dependent cell death was registered for this assay.

DISCUSSION

The spectral changes (the absorption peak shifted to 400 nm) upon addition of Cu(II) ions (or Zn(II) ions) to the flavonoid solutions indicate that 1:1 stable complexes were formed (Fig. 1) [14, 23]. The interaction of the free flavonoids with DNA was classical intercalation revealed by the observation of very low hypochromic and bathochromic effects in the spectrum (Fig. 2) and this is in accordance with literature findings [18]. In addition, Cu(II) complexes of these flavonoids interacted with DNA in the same manner but stronger hypochromic and bathochromic effects were measured (a decrease in the absorption peak at ~400 nm wavelength with a small red shift ~1-4 nm) (Fig. 3). This may be explained by allowing the planar flavonoid part of the complex to bind DNA by intercalation between the base pairs, as well as by addition of the Cu(II) cation electrostatically interacting with the negatively charged phosphate backbone. The binding values are comparable with the literature values [20]. The most hydrophobic flavonoid Q has the highest binding constant; the additional -OH group in M and the additional monosaccharide in R slightly reduced the binding constants of the latter flavonoids. As a control experiment, the interaction between DNA and the Cu(II) ions was studied (Fig. 7a) and the resulting hyperchromic effect on the spectra indicates that Cu(II) ions bind DNA electrostatically by an external binding mode.

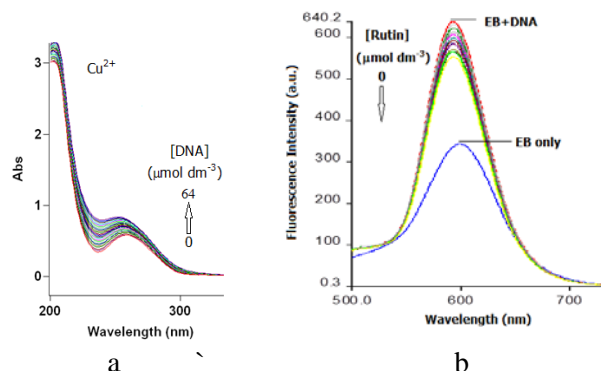


Fig.7. a: (left) The interaction between DNA and the Cu(II) ions; b: (right) The displacement of EB by the R studied by using fluorescent spectroscopy.

The intercalated EB was displaced from the EB-DNA complex by the flavonoid:Cu(II) species (Fig. 4). The strength of the displacement can be summarized as Q-Cu(II) > M-Cu(II) > R-Cu(II). This displacement was in accordance with the absorption spectral results, as well as with the

literature data [20]. In addition, when the free flavonoid (R) was used in place of metal complex the displacement of EB by the flavonoid was very weak (Fig. 7b). This exchange reaction was supported by the results from cyclic voltammetry studies from which the equilibrium formation constant for the Q-Cu(II) complex binding to DNA was found to be about 2.05 times larger than that of its free form [20]. This result is also in accordance with the UV titration findings.

DNAse activities of the flavonoids and their metal complexes were compared and the same displacement was found as Q > M > R. The results suggested that the Cu(II) complexes were more reactive than the Zn(II) complexes (Fig. 5). This may be due to the advanced redox cycling activity of Cu(II) vs Zn(II), where cuprous ions (Cu^{+}) formed *in situ* can convert H_2O_2 to hydroxyl radicals and binding of the complex to DNA provides centers for generation of hydroxyl radicals close to sites susceptible to breakage [33]. Thus, the quercitrin-Cu(II) complex has caused the highest level of damage and the rutin-Zn(II) complex produced the lowest level of damage to plasmid DNA. Similar results were obtained in the literature [34].

According to the results in Table 1, there is a concentration-dependent raise of cell death for each trial and the flavonoid (M) was two times more potent when it was in combination with a metal ion (Cu^{2+} or Zn^{2+}) compared to the flavonoid used alone. This result supports the results of spectrophotometric titrations and electrophoretic assay. Cell deaths may probably be due to DNA binding of the compounds.

DNA protective effects of the flavonoids have been extensively studied [35, 36]. However, cytotoxicity of these flavonoids against cancer cells has also been reported as mainly due to their binding ability to DNA [11, 37, 38]. The anticancer activities of flavonoid metal complexes were found to be even greater than those of the sole flavonoid. The binding abilities of flavonoid-metal complexes to DNA were studied and their intercalative binding mode and cytotoxicity to certain cancer cell lines were reported [22, 39, 40].

CONCLUSIONS

In conclusion, absorption spectroscopy studies demonstrated that a 1:1 Q:Cu(II) complex was formed in appropriate mixtures of the ligand and the metal ion, and that this complex was stabilized by intercalation between the base pairs of DNA (binding constant, $K_b = (1.82 \pm 0.20) \times 10^5 \text{ M}^{-1}$). A competitive reaction, monitored by fluorescence spectroscopy, between fluorescent probe, ethidium

bromide (EB) dye, DNA and Q-Cu(II) showed that the intercalated EB was displaced from the EB-DNA complex by the Q-Cu(II) species. In both spectrophotometric studies flavonoid-Cu(II) complexes bind DNA stronger than the actual flavonoid. Very similar results were found by electrophoresis of the plasmid DNA in the presence of the flavonoids, flavonoid-Cu(II) complexes and flavonoid-Zn(II) complexes with or without peroxide addition. While free flavonoids do not show DNA damage they even protect against peroxide damage, as indicated in the literature. Both metal complexes of the flavonoids create much stronger DNA damage while Cu(II) complexes show higher DNAse activities. In the cytotoxicity assay myricitrin showed two times higher potency when combined with metal ions (Cu^{2+} or Zn^{2+}) which is consistent with the other results reported here.

Acknowledgements: We are grateful for the support of Bulet Ecevit University with grant #2014-72118496-05 and Trakya University with grant number TUBAP-2014/17.

REFERENCES

- S. Grguric-Sipka, R. Vilaplana, J. Perez, M. Fuertes, C. Alonso, Y. Alvarez, T. Sabo, F. Gonzalez-Vilchez, *J. Inorg. Biochem.*, **97**, 215 (2003).
- S. Rauf, J. Gooding, K. Akhtar, M. Ghauri, M. Rahman, M. Anwar, A. Khalid, *J. Pharm. Biomed. Anal.*, **37**, 205 (2005).
- N. Ljubijankić, A. Zahirović, E. Turkušić, E. Kahrović, *Croat. Chem. Acta*, **86**, 215 (2013).
- M. Hertog, P. Hollman, M. Katan, D. Kromhout, *Nutr. Cancer*, **20** 21 (1993).
- N. Cook, S. Samman, *J. Nutr. Biochem.*, **7**, 66 (1996).
- I. Afanas'ev, A. Dorozhko, A. Brodslui, V. Kostyuk, A. Potapovitch, *Biochem. Pharmacol.*, **38**, 1763 (1989).
- V. Kostyuk, A. Potapovich, *Arch. Biochem. Biophys.*, **355**, 43 (1998).
- V. Kostyuk, A. Potapovich, S. Speransky, G. Maslova, *Free Radic. Biol. Med.*, **21**, 487 (1996).
- S. Sekaran, S. Kandaswamy, K. Gunasekaran, E. Perumal, F.Y. Afsar Basha, B.J. Madhan Mohan, A. Jagadeesan, *J. Biochem. Mol. Toxicol.*, **26**, 522 (2012).
- B.L. Santos, A.R. Silva, B.P.S. Pitanga, C.S. Sousa, M.S. Grangeiro, B.O. Fragomeni, P.L.C. Coelho, M.N. Oliveira, N.J. Menezes-Filho, M.F.D. Costa, R.S. El-Bachá, E.S. Velozo, G.P. Sampaio, S.M. Freire, M. Tardy, S.L. Costa, *Food Chem.*, **127**, 404 (2011).
- R. Xu, Y. Zhang, X. Ye, S. Xue, J. Shi, J. Pan, Q. Chen, *Food Chem.*, **138**, 48 (2013).
- X. Zhu, H. Mao, *Chin. Traditional Med.*, **28**, 373 (1997).
- A. Bravo, J. Anacona, *Trans. Metal Chem.*, **26**, 20 (2001).

14. J. Zhou, L. Wang, J. Wang, N. Tang, *Trans. Metal Chem.*, **26**, 57 (2001).
15. J. Zhou, L. Wang, J. Wang, N. Tang, *J. Inorg. Biochem.*, **83**, 41 (2001).
16. G. Dehghan, J.E.N. Dolatabadi, A. Jouyban, K.A. Zeynali, S.M. Ahmadi, S. Kashanian, *DNA Cell Biol.*, **30**, 195 (2011).
17. Q. Guo, J. Yuan, J. Zeng, X. He, D. Li, *J. Mol. Struct.*, **1027**, 64 (2012).
18. C.D. Kanakis, P.A. Tarantilis, M.G. Polissiou, S. Diamantoglou, H.A. Tajmir-Riahi, *Cell Biochem. Biophys.*, **49**, 29 (2007).
19. B. Neto, A. Lapis, *Molecules*, **14**, 1725 (2009).
20. Y. Ni, S. Du, S. Kokot, *Anal. Chim. Acta*, **584**, 19 (2007).
21. C. Santini, M. Pellei, V. Gandin, M. Porchia, F. Tisato, C. Marzano, *Chem. Rev.*, **114**, 815 (2013).
22. J. Tan, B. Wang, L. Zhu, *Bioorg. Med. Chem.*, **17**, 614 (2009).
23. N.E.A. Ikeda, E.M. Novak, D.A. Maria, A.S. Velosa, R.M.S. Pereira, *Chem-Biol. Interact.*, **239**, 184 (2015).
24. B. Coban, U. Yildiz, *Appl. Biochem. Biotech.*, **172**, 248 (2014).
25. D. Wang, X. Wang, C. Zhang, Y. Ma, X. Zhao, *J. Agric. Food Chem.*, **59**, 7405 (2011).
26. B. Coban, U. Yildiz, A. Sengul, *J. Biol. Inorg. Chem.*, **18**, 461 (2013).
27. J. Talib, C. Green, K.J. Davis, T. Urathamakul, J.L. Beck, J.R. Aldrich-Wright, S.F. Ralph, *Dalton Trans.*, 1018 (2008).
28. S.F. Ralph, J.L. Beck, R. Gupta, T. Urathamakul, M.M. Sheil, J.R. Aldrich-Wright, *J. Inorg. Biochem.*, **96**, 214 (2003).
29. I. Kocak, U. Yildiz, B. Coban, A. Sengul, *J. Solid State Electrochem.*, **19**, 2189 (2015).
30. Y.-J. Liu, Z.-H. Liang, Z.-Z. Li, J.-H. Yao, H.-L. Huang, *J. Organometal. Chem.*, **696**, 2728 (2011).
31. J.K. Barton, A.L. Raphael, *J. Am. Chem. Soc.*, **106**, 2466 (1984).
32. B. Coban, I.O. Tekin, A. Sengul, U. Yildiz, I. Kocak, N. Sevinc, *J. Biol. Inorg. Chem.*, **21**, 163 (2016).
33. A.S.H. Li, B. Bandy, S.S. Tsang, A.J. Davison, *Free Radic. Biol. Med.*, **30**, 943 (2001).
34. T. Jun, W. Bochu, Z. Liancai, *Bioorg. Med. Chem. Lett.*, **17**, 1197 (2007).
35. S.A. Aherne, N.M. O'Brien, *Nutr. Cancer*, **34**, 160 (1999).
36. X. Li, W. Mai, D. Chen, *J. Chin. Chem. Soc.*, **61**, 383 (2014).
37. M. Qin, Y. Luo, X.-B. Meng, M. Wang, H.-W. Wang, S.-Y. Song, J.-X. Ye, R.-L. Pan, F. Yao, P. Wu, G.-B. Sun, X.-B. Sun, *Vascul. Pharmacol.*, **70**, 23 (2015).
38. R.D. Snyder, P.J. Gillies, *Environ. Mol. Mutagen.*, **40**, 266 (2002).
39. J. Tan, L. Zhu, B. Wang, *BioMetals*, **23**, 1075 (2010).
40. I.E. León, J.F. Cadavid-Vargas, A. Resasco, F. Maschi, M.A. Ayala, C. Carbone, S.B. Etcheverry, *J. Biol. Inorg. Chem.*, **21**, 1009 (2016).

ЦИТОТОКСИЧНОСТ И ДНК-СВЪРЗВАНЕ НА МЕДНИ (II) И ЦИНКОВИ (II) КОМПЛЕКСИ НА ФЛАВОНОИДИ: КУЕРЦИТРИН, МИРИЦИТРИН, РУТИН

Б. Атабей-Оздемир¹, О. Демиркиран², У. Йилдиз¹, И.О. Текин³, Б. Джобан*¹

¹Университет „Бюлент Еджевит“, Факултет за изкуство и наука, Департамент по химия, Зонгулдак, Турция

²Тракийски университет, Факултет по фармация, Департамент по фармакогнозия, Одрин 22100, Турция.

³Университет „Бюлент Еджевит“, Факултет по медицина, Департамент по имунология, Зонгулдак 67100, Турция

Постъпила на 20 декември, 2016 г.; приета на 27 май, 2017 г.

(Резюме)

Направено е сравнително изследване на flavonoidите куерцитрин, мирицитрин и рутин и техните метални комплекси за свързването им с спектрофотометрични методи и ДНК-азната активност с агарозна електрофореза на pBR322. Свободните flavonoidи се свързват с ДНК по интеркалационен механизъм, но медните комплекси Cu(II) се свързват по-здраво поради електростатични взаимодействия. Flavonoidите имат защитно действие срещу разкъсването на ДНК в присъствие на водороден пероксид. Обаче комплексите с Cu(II) и Zn(II) с тези flavonoidи предизвиква срязващо на скелета на ДНК. Освен това, медните комплекси с flavonoidите имат силна ДНК-азна активност. Мирицитринът е два пъти по-цитотоксичен, когато е комбиниран с метални йони (Cu^{2+} и Zn^{2+}) отколкото самостоятелно използван спрямо кръвни моно-нуклеарни клетки.

DNA binding by copper (II) complexes of semithiocarbazone containing ligands

B. Coban^{*1}, N. Eser¹, I. Babahan²

¹Bülent Ecevit University, Faculty of Arts and Sciences, Department of Chemistry, Zonguldak, 67100, Turkey.

²Adnan Menderes University, Faculty of Arts and Sciences, Department of Chemistry, Aydin, 09010, Turkey.

Received December 23, 2016; Accepted May 30, 2017

DNA binding properties of two previously synthesized copper complexes of *vic*-dioximes bearing thiosemicarbazone units (*2E*)-2-[4-(dimethylamino)benzylidene]-*N*-[(1*Z*,2*E*)-*N*-hydroxy-2-(hydroxyimino)ethanimidoyl]hydrazine carbothioamide (**1**) and (*2E*)-2-[4-(diethylamino)benzylidene]-*N*-[(1*Z*,2*E*)-*N*-hydroxy-2-(hydroxyimino)ethanimidoyl]hydrazine carbothioamide (**2**), were investigated using absorption spectroscopy, fluorescence spectroscopy, and agarose gel electrophoresis methods. Experimental studies suggested that the complexes bind to DNA through intercalation. Their intrinsic binding constants (K_b) were calculated as **1**: $5.50 \pm 0.25 \times 10^4 \text{ M}^{-1}$; **2**: $2.10 \pm 0.18 \times 10^5 \text{ M}^{-1}$. These complexes also promote the cleavage of plasmid pBR322, both in the absence and presence of hydrogen peroxide.

Keywords: Cu(II) complex, thiosemicarbazone, *vic*-dioxime, DNA, intercalation

INTRODUCTION

Interaction between DNA and drug molecules is a very popular subject [1-3], especially for the designing of new DNA-targeted drugs and their *in vitro* screening. The biochemistry of thiosemicarbazones has received considerable attention because of their promising biological implications, and structural diversity. The chemistry of transition metal complexes of thiosemicarbazone ligands has also been of interest, primarily due to their bioinorganic relevance. The potential biological benefits of this class of complexes have been found to include antibacterial, antimarial, antiviral, and antitumour activities [4-10]. Dioximes have also been applied to analytical, biological, pigment, and medicinal chemistry applications. In particular, they have been found to play an important role in coordination chemistry, mainly due to their planar structure stabilized by hydrogen bonding interactions [5, 11, 12].

Many techniques, such as UV-vis spectrophotometry, fluorescence spectroscopy, circular dichroism spectroscopy, mass spectrometry, and voltammetry have been used to study the binding between metal complexes and DNA [13-17].

In this work, the interactions of previously synthesized [5] thiosemicarbazone containing ligands and their Cu(II) complexes with calf thymus (CT)-DNA were comparatively investigated with the aid of the absorption and fluorescence spectroscopy and their DNase activity was investigated against pBR322 plasmid DNA via agarose gel electrophoresis assays.

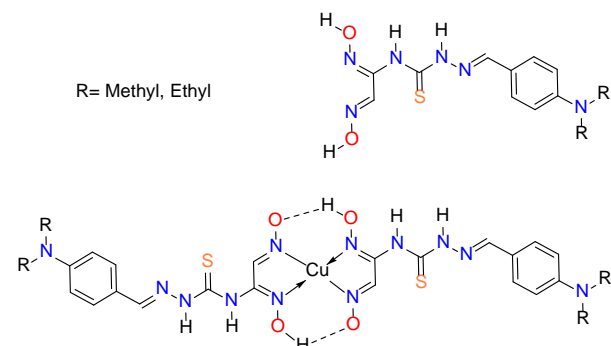


Fig. 1. Chemical structures of ligands **LH1** and **LH2** and complexes **1** (CuL1_2) and **2** (CuL2_2).

EXPERIMENTAL

The ligands and the complexes were prepared according to the literature [5]. All reagents and solvents were of commercial origin and used without further purification unless otherwise noted. Solutions of calf thymus DNA (CT-DNA purchased from Sigma) in 50 mM ammonium acetate (pH 7.5) had a UV-Vis absorbance ratio of 1.8–1.9: 1 at 260 and 280 nm ($A_{260}/A_{280} = 1.9$), indicating that the DNA was sufficiently free of protein [16]. The concentration of DNA was determined spectrophotometrically using a molar absorptivity of $6,600 \text{ M}^{-1} \text{ cm}^{-1}$ (260 nm) [16]. Double distilled water was used to prepare buffers. Stock solution of CT-DNA was stored at 4 °C and used within 4 days.

Physical measurements

UV-Vis spectra were recorded with a Varian Cary 100 spectrophotometer and emission spectra were recorded with a Perkin Elmer LS 55 fluorescence spectrometer at room temperature.

* To whom all correspondence should be sent:
E-mail: burakcoban@yahoo.com

Absorption and emission titrations

For the absorption and emission titrations, ligands and Cu(II) complexes (about 1 mmol) were dissolved in a minimum amount of DMSO (0.5 mL), and were then diluted in 5 mM ammonium acetate buffer, pH 7.5) to a final concentration of 20 μ M. Titrations were performed in a 10-mm stoppered quartz cell by using a fixed concentration of the compound (20 μ M), to which the CT-DNA stock solution was added in increments of 1 μ L to a DNA-to-compound concentration ratio of 6:1. Analysis was performed by means of a UV-Vis or fluorescence spectrophotometer by recording the spectrum after each addition of DNA. Compound-DNA solutions were incubated for 10 min before the spectra were recorded. A control solution of 20 μ M of the drug in the same buffer was treated in the same manner. Cell compartments were thermostated at 25 \pm 0.1°C.

For emission intensity measurements, the excitation wavelength was fixed and the emission range was adjusted before the measurements. Ammonium acetate (5 mM), pH 7.5 buffer was used as a blank to make preliminary adjustments. All measurements were performed with a 5-nm entrance slit and a 5-nm exit slit. The complexes were excited at 383 and 400 nm, respectively; the emission spectra were monitored between 710 and 740 nm.

Competitive studies

The competitive behavior of each compound with ethidium bromide (EB) was investigated by fluorescence spectroscopy in order to examine whether the compound is able to displace EB from the DNA-EB complex.

DNA was pretreated with EB at a DNA-to-EB concentration ratio of 50:1 for 30 min at 27 °C to prepare the initial DNA-EB complex. The intercalating effect of the compounds with the DNA-EB complex was studied by adding a certain amount of a solution of the compounds in increments to the solution of the DNA-EB complex. The influence of

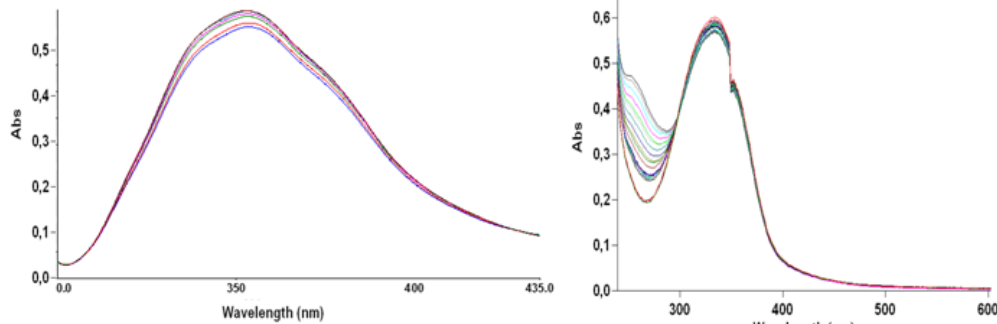


Fig. 2. Absorption spectra of the complexes in 50 mM ammonium acetate buffer on gradual additions of calf thymus DNA at pH 7.0 and 298 K. [complex] = 20 μ M, [ct-DNA] = 0-40 μ M. Arrows indicate the absorbance changes with increase in ct-DNA concentration.

each addition of compounds to the solution of the DNA-EB complex was estimated by recording the change in the fluorescence peak at 640 nm. To study the competitive binding of the compounds with EB, the latter was excited at 453 nm in the presence of DNA alone as well as in the presence of the compounds.

DNAse activity by gel electrophoresis

Gel electrophoresis experiments were performed using pBR322 negatively supercoiled plasmid DNA and 1 % agarose gel together with a tris(hydroxymethyl)aminomethane-borate-EDTA running buffer solution. Reaction mixtures (10 mL) containing 0.1 μ g pBR322 together with different amounts of **1** and **2** (0, 5, 500 μ M) in 50 mM ammonium acetate buffer, pH 7.5 were prepared at 0 °C, were then incubated at 36 °C for 1 h and 24 h in the dark and for 1 h with the addition of 2 μ L of 30 % hydrogen peroxide solution. Prior to the samples being loaded onto the gel, 2.5 mL of 0.25 % bromophenol blue loaded buffer and sucrose in water (40 % w/v) was added to the reaction mixtures. Gels were obtained at room temperature by using a Thermo midi horizontal agarose gel electrophoresis system and applying a potential of 35 V for 4 h. The resulting gels were stained with EB solution (0.5 μ g mL⁻¹) for 45 min, after which they were soaked in water for further 20 min. Gels were visualized under UV light and photographed.

RESULTS AND DISCUSSION

Both ligands have very similar UV spectra with an absorption peak around 280-360 nm wavelength. Addition of DNA caused very little or no change in the absorption spectra seen in Fig 5.

Very low hypochromic and bathochromic effects are seen in the electronic absorption spectra of the complexes upon addition of DNA (Fig 2). The hypochromicity and bathochromic shift increased when the complexes were titrated with DNA solution (Fig 2).

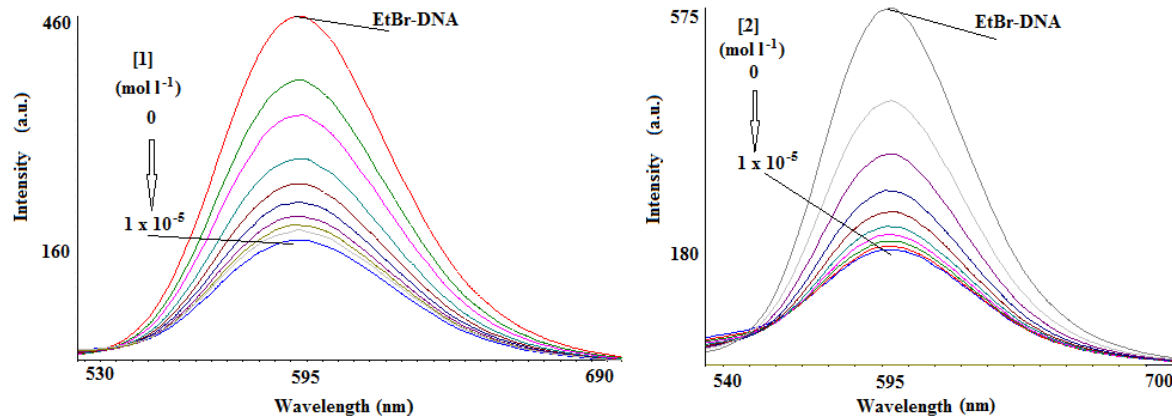


Fig. 3. Fluorescence spectra of the competition between complexes and ethidium bromide (EB) at 298 K. [EB] = 20.0 μM and [ct-DNA] = 100.0 μM at $\lambda_{\text{exc}} = 363 \text{ nm}$. [Complex] = 0.5–10.0 μM .

In the absence of DNA, the complexes **1** and **2** emit weak luminescence in ammonium acetate buffer at ambient temperature, with a maximum at 383 and 455 nm, respectively. On addition of CT-DNA, the emission intensity slightly increases (Fig 6).

The competitive titrations of ethidium bromide (EB) dye and complexes in the presence of DNA are shown in Fig 3. According to the spectra, EB fluorescence intensity was decreased by the addition of complexes.

The potentials of the complexes to cleave DNA were studied by agarose gel electrophoresis using pBR322 plasmid DNA. When circular DNA is subjected to gel electrophoresis, relatively fast migration will be observed for the supercoiled form (form I). If scission occurs on one strand (nicked circular), the supercoiled form will relax to generate a slower moving open circular form (form II). If both strands are cleaved, a linear form (form III) that migrates between the two forms will be generated [15]. Fig 4a shows the separation of pBR322 by gel electrophoresis after 1 h incubation of lanes 1–6 and 24 h incubation of lanes 7–12 with the complexes. Lanes 1, 4, 7, 10 are controls, having only DNA. The plasmid DNA was cleaved by the complexes and a small portion of form II was produced (lanes 2–3 and 5–6) in 1 h but a larger portion of the plasmid DNA was converted to form II by 24 h incubation by the complexes (lanes 8–9 and 11–12). In Fig 4b, lane 1 is the control, having only DNA and lane 2 is the negative control DNA incubated with peroxide solution. Addition of complexes caused DNA cleavage in the lanes 3–8. A small portion of form II was produced by the complexes at 10 mM concentration. However, at the highest concentration of **2**, plasmid DNA was extensively damaged, multiply occurred in the DNA backbone and therefore small DNA fragments cannot be seen in the gel.

The complexes exhibit strong interaction compared with their corresponding ligands. There were very weak interactions of the ligands with DNA. The binding strengths of the ligands and complexes to CT-DNA were determined by calculating the binding constant (K_b) using the equation:

$$[\text{DNA}] / (\varepsilon_a - \varepsilon_f) = [\text{DNA}] / (\varepsilon_b - \varepsilon_f) + 1/K_b (\varepsilon_b - \varepsilon_f)$$

The absorption coefficients ε_a , ε_f , and ε_b correspond to $A_{\text{obs}}/[\text{complex}]$, the extinction coefficient for the free complex, and the extinction coefficient for complex in the fully bound form, respectively. The plot of $[\text{DNA}] / (\varepsilon_a - \varepsilon_f)$ versus $[\text{DNA}]$ gives a slope of $1/(\varepsilon_a - \varepsilon_f)$ and an intercept of $1/K_b (\varepsilon_b - \varepsilon_f)$. The binding constants indicate that the complexes bind to CT-DNA. In addition, the complexes interacted with DNA in an intercalative manner because hypochromic and bathochromic effects were measured (a decrease in the absorption peak at $\sim 400 \text{ nm}$ wavelength with a small red shift $\sim 1 \text{ nm}$) (Fig. 2). This may be explained by allowing the planar 4-diethylaminobenzene ring of the ligand binding to DNA by intercalation between the base pairs. Their intrinsic binding constants (K_b) were calculated as **1**: $5.50 \pm 0.25 \times 10^4 \text{ M}^{-1}$; **2**: $2.10 \pm 0.18 \times 10^5 \text{ M}^{-1}$. The binding values are comparable with the literature values [8]. The more hydrophobic complex **2** has a higher binding constant. The binding constants were much smaller than those of classical intercalators, thus, the interaction would be explained as partial intercalation. As a control experiment, the interaction between DNA and Cu(II) ions was studied (Fig 7) and the resulting hyperchromic effect and absence of bathochromic effect on the spectra indicates that Cu(II) ions bind DNA electrostatically with an external binding mode [18,19].

The aqueous solutions of the complexes emitted weak luminescence but addition of DNA increased the luminescence intensity indicating that the complexes interact with CT-DNA and are protected

by the hydrophobic environment inside the DNA helix reducing the accessibility of solvent water molecules to the complex and the mobility of the complex is restricted at the binding site, leading to a decrease in the vibrational modes of relaxation (Fig 6).

The intercalated EB was displaced from the EB–DNA complex by the complexes (Fig 3). The strength of the displacement can be summarized as **2** > **1**. This displacement was in accordance with the UV titration findings where the hydrophobicity of the N-ethyl compound would be higher than that of N-methyl.

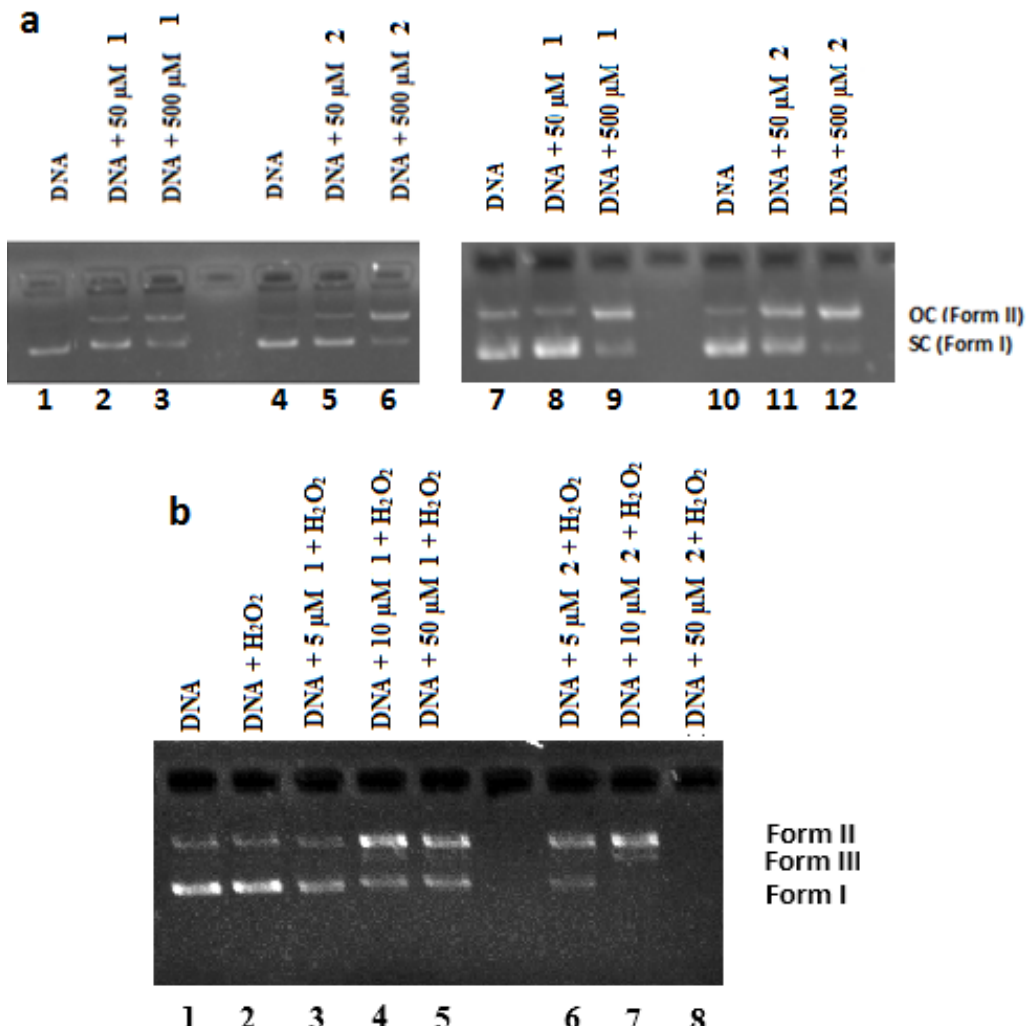


Fig. 4. Agarose gel electrophoresis pictogram showing the cleavage pattern of pBR322 plasmid DNA (50 µg) with 50 and 500 µM concentrations of the complexes at 37 °C **a**. Lanes 1-6 for 1h incubation and lanes 7-12 for 24 h incubation. **b**. Effect of additional peroxide: lane 1: DNA control, lane 2: peroxide, lanes 3-5 and 6-8: peroxide+5, 10, 50 µM of complexes **1** and **2**, respectively.

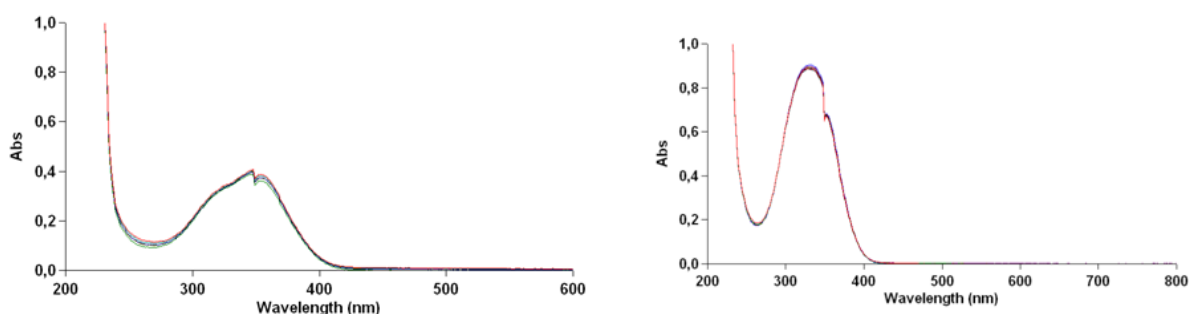


Fig 5. Absorption spectra of Ligands **L1H** (left) and **L2H** (right) in 50 mM ammonium acetate buffer on the gradual additions of calf thymus DNA at pH 7.0 at 298 °K. [ligand] = 20 µM, [ct-DNA] = 0-40 µM. Arrows indicate the absorbance changing with increase of ct-DNA concentration

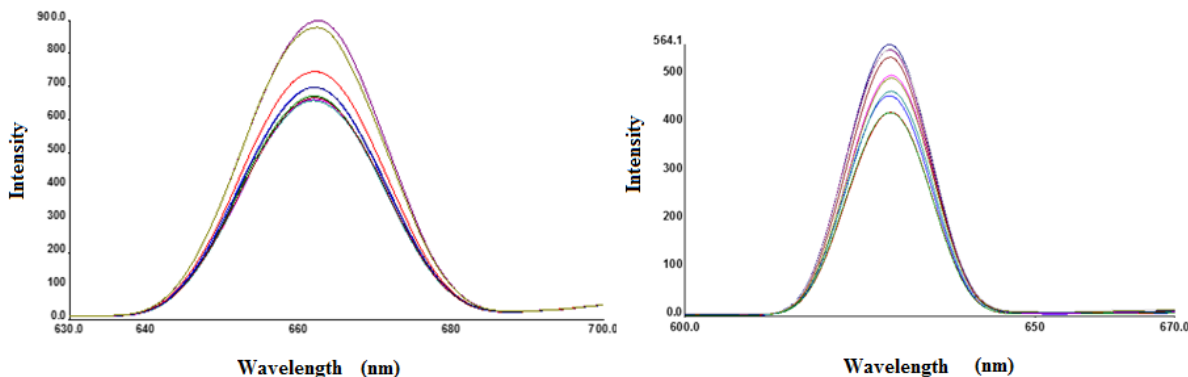


Fig. 6. Emission spectra of **1** (left) and **2** (right) (10 μM) in ammonium acetate buffer at 25 $^{\circ}\text{C}$ in the presence of 0–20 μM calf thymus-DNA. The intensity increases with increasing DNA concentration in both cases. The complexes were excited at 400 and 380 nm, respectively; the emission spectra were monitored between 660 and 600 nm

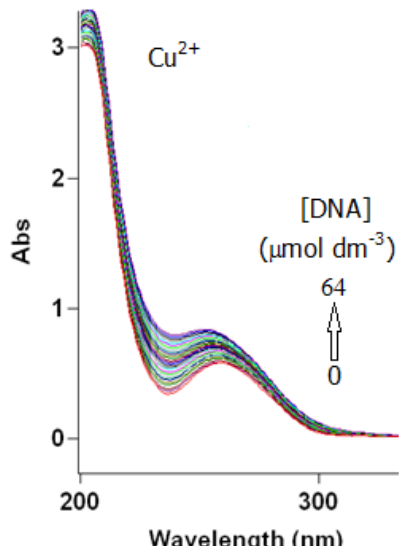


Fig. 7. Absorption spectra of calf thymus DNA in 50 mM ammonium acetate buffer on the gradual additions of Cu^{2+} at pH 7.0 at 298 $^{\circ}\text{K}$. $[\text{ct-DNA}] = 100.0 \mu\text{M}$, $[\text{Cu}^{2+}] = 6, 12, 18, 24, 30, 35, 41, 47, 53, 58, 64 \mu\text{M}$. Arrows indicate the absorbance changing with increase of Cu^{2+} concentration

CONCLUSIONS

DNAse activities of the complexes were compared and the same displacement was found as **2** > **1**. The complexes show strong DNAse activity in the presence of peroxide (Fig 4). This may be due to the advanced redox cycling activity of Cu(II) where *in situ* formed cuprous ions (Cu^{+}) can convert H_2O_2 to hydroxyl radicals and binding of the complex to DNA provides centers for generation of hydroxyl radicals close to sites susceptible to breakage [20]. Thus, the more hydrophobic complex gives a higher level of damage to plasmid DNA.

In conclusion, the absorption and fluorescence spectroscopy studies demonstrated that the complexes **1** and **2** interacted with DNA base pairs (binding constant, $K_b = (1.82 \pm 0.20) \times 10^5 \text{ M}^{-1}$). A competitive reaction, monitored by fluorescence spectrophotometry, between fluorescent probe, ethidium bromide (EB) dye, DNA and complexes showed that the intercalated EB was displaced from the EB–DNA complex by **1** and **2**. According to both spectrophotometric studies, the complexes bind DNA stronger than the actual ligand. Very similar results were found by electrophoresis of the plasmid DNA in the presence of the complexes with and without peroxide addition. The complexes induced strong DNA damage in the presence of peroxide and **2** has better DNAse activity as expected from the spectrophotometric studies.

Acknowledgements: We are grateful for the support of Bülent Ecevit University with grant #2015-72118496-07.

REFERENCES

1. S. Grguric-Sipka, R. Vilaplana, J. Perez, M. Fuertes, C. Alonso, Y. Alvarez, T. Sabo, F. Gonzalez-Vilchez, *J. Inorg. Biochem.*, **97**, 215 (2003).
2. N. Ljubijankić, A. Zahirović, E. Turković, E. Kahrović, *Croat. Chem. Acta*, **86**, 215 (2013).
3. S. Rauf, J. Gooding, K. Akhtar, M. Ghauri, M. Rahman, M. Anwar, A. Khalid, *J. Pharm. Biomed. Anal.*, **37**, 205 (2005).
4. A.A. Al-Amiry, Y.K. Al-Majedy, H. Abdulreazak, H. Abood, *Bioinorg. Chem. Appl.*, Article ID 483101, 6 pages (2011).
5. İ. Babahan, A. Özmen, N. Orhan, D. Kazar, E.H. Değirmenci, *Bioorg. Chem.*, **53**, 92 (2014).

6. J.S. Casas, M.S. García-Tasende, J. Sordo, *Coord. Chem. Rev.*, **209**, 197 (2000).
7. X. Du, C. Guo, E. Hansell, P.S. Doyle, C.R. Caffrey, T.P. Holler, J.H. McKerrow, F.E. Cohen, *J. Med. Chem.*, **45**, 2695 (2002).
8. M.A. Hussein, T.S. Guan, R.A. Haque, M.B.K. Ahamed, A.M.S.A. Majid, *Polyhedron*, **85**, 93 (2015).
9. A.I. Matesanz, C. Hernández, P. Souza, *J. Inorg. Biochem.*, **138**, 16 (2014).
10. G. Pelosi, *Open Crystallogr. J.*, **3**, 16 (2010).
11. B. Dede, İ. Özmen, F. Karipçin, M. Cengiz, *Appl. Organometal. Chem.*, **23**, 512 (2009).
12. A. Sengul, H. Agac, B. Coban, E. Eroglu, *Turk. J. Chem.*, **35**, 25 (2011).
13. A. Arslantas, A.K. Devrim, M. Sözmen, H. Necefoglu, *Rasayan J. Chem.*, **3**, 201 (2010).
14. B. Coban, I.O. Tekin, A. Sengul, U. Yildiz, I. Kocak, N. Sevinc, *J. Biol. Inorg. Chem.*, **21**, 163 (2016).
15. B. Coban, U. Yildiz, *Appl. Biochem. Biotech.*, **172**, 248 (2014).
16. B. Coban, U. Yildiz, A. Sengul, *J. Biol. Inorg. Chem.*, **18**, 461 (2013).
17. I. Kocak, U. Yildiz, B. Coban, A. Sengul, *J. Solid State Electrochem.*, **19**, 2189 (2015).
18. R.F. Pasternack, E.J. Gibbs, J.J. Villafranca, *Biochem.*, **22**, 2406 (1983).
19. S.-P. Tang, L. Hou, Z.-W. Mao, L.-N. Ji, *Polyhedron*, **28**, 586 (2009).
20. A.S.H. Li, B. Bandy, S.S. Tsang, A.J. Davison, *Free Radic. Biol. Med.*, **30**, 943 (2001).

КОМПЛЕКСИ НА ДНК С МЕД (II) И ЛИГАНДИ ОТ СЕМИКАРБАЗОНИ

Б. Джобан *¹, Н. Есер¹, И. Бабахан²

¹ Университет „Бюлент Еджевит“, Факултет за изкуство и наука, Департамент по химия, Зонгудак, Турция

² Университет „Аднан Мендерес“, Факултет за изкуство и наука, Департамент по химия, Айдин 09010, Турция

Постъпила на 23 декември, 2016 г.; коригирана на 30 май, 2017 г.

(Резюме)

Изследвани са свързвашите свойства на ДНК на два предварително синезирани медни комплекса от *vic*-диоксими, носещи тиосемикарбазониони единици (*2E*)-2-[4-(диметиламино)бензилиден]-*N*-(*1Z,2E*)-*N*-хидрокси-2-(хидрокси-инино)станимидоил]хидразин карбо-тиоамид (**1**) и (*2E*)-2-[4-(диетиламино)бензилиден]-*N*-(*1Z,2E*)-*N*-хидрокси-2-(хидроксиимино)станимидоил] хидразин карботиоамид (**2**). Изследванията са извършени с помощта на абсорбционна спектроскопия, флуоресцентна спектроскопия и агароза-гел-електрофореза. Експерименталните изследвания предполагат свързването на комплексите с ДНК чрез интеркалация. Техните присъщи константи на свързване (K_b) са изчислени на **1**: $5.50 \pm 0.25 \times 10^4 \text{ M}^{-1}$; на **2**: $2.10 \pm 0.18 \times 10^5 \text{ M}^{-1}$. Тези комплекси подпомагат разкъсването на плазмида pBR322, в присъствие и отсъствие на водороден пероксид.

Liquid-liquid extraction studies of ruthenium(III) from malonate medium using *n*-octylaniline as an ion-pairing reagent: study of catalyst and alloys

A. P. Gaikwad, V. J. Suryavanshi, M. A. Anuse*

Analytical Chemistry Laboratory, Department of Chemistry, Shivaji University, Kolhapur-416004, Maharashtra, India

Received October 18, 2016; Accepted June 2, 2017

Herein we have developed a solvent extraction system for ruthenium(III) by using 0.1 M *n*-octylaniline in 0.05 M malonate medium at pH 3.5. Various operational parameters like pH, reagent concentration, weak organic acid, equilibrium time, and loading capacity of extractant were optimized for the quantitative recovery of ruthenium(III). Stoichiometry of the extracted species was resolved by the slope ratio analysis method. The extraction takes place by formation of an ion-pair complex between the $[\text{CH}_3(\text{CH}_2)_7\text{C}_6\text{H}_4\text{NH}_3]^+_{(\text{org})}$ species and the $[\text{Ru}(\text{C}_3\text{H}_2\text{O}_4)_2]^-_{(\text{aq})}$ species. The association of these two species yielded the uncharged neutral extractable species $[\text{CH}_3(\text{CH}_2)_7\text{C}_6\text{H}_4\text{NH}_3^+ \text{Ru}(\text{C}_3\text{H}_2\text{O}_4)^-]^2_{(\text{org})}$. The stoichiometry of the extracted species was found to be 1: 2: 1 (metal: acid: extractant). The soundness of the proposed method was checked by extracting ruthenium(III) from binary and ternary mixtures and various catalysts were also investigated.

Keywords: Liquid-liquid extraction, *n*-Octylaniline, Ruthenium(III), Sodium malonate, Catalyst.

INTRODUCTION

Ruthenium is a very rare element that is found about 10^{-8} % on earth's crust. Chondrite and especially iron meteorites contain high amounts of ruthenium ($1-6 \times 10^{-4}$ %). Ruthenium also occurs in alliance with other platinum group metals [1]. Ruthenium is a rare polyvalent hard white transition metal. Small amount of ruthenium can impart hardness to platinum and palladium. The resistivity to corrosion of titanium was noticeably increased by a small amount of ruthenium [2]. Ruthenium is a versatile catalyst. It is used to remove H_2S from oil in oil refineries [3]. The use of ruthenium is compatible with semiconductor processing techniques; therefore, it is used as a material for microelectronics [4]. Ruthenium is very hard and corrosion resistant, therefore it is used for coating of electrodes by the chloralkali process, the outcome of the process gives chlorine and caustic soda which are applicable for a wide range of industrial and domestic applications. The application of ruthenium in alloys of aircraft turbine blades will reduce the CO_2 impact of air travel on the environment in the future. If present prototypes are doing well, its high temperature stability and high melting point will permit elevated temperatures and thus more efficient burning of aircraft fuel [5]. Recently, platinum group metals (PGMs), particularly ruthenium and its chlorocomplexes, have been largely used for the catalytic oxidation of organic compounds. Organometallic ruthenium carbene and allenylidene complexes are efficient catalysts for olefin

metathesis [6]. Generally, ruthenium complexes have better resistance to hydrolysis and have more choosy action on tumors. Ruthenium and its alloys have a well-known application in jewelry [1]. The increasing applications of ruthenium in various fields have made it compulsory to develop a simple, inexpensive and sensitive method for its separation and determination.

In current days a variety of reagents have been considered for liquid-liquid extraction of ruthenium(III). 2-Mercaptobenzimidazole is used as extractant for ruthenium(III) in n-butanol [7]; 3-hydroxy-2-methyl-1-phenyl-4-pyridone [8], Cyanex 921 [9], Cyanex 923, Cyanex 471, Cyanex 272, LIX 54, LIX860N-I [10] are reported for solvent extraction. Bis (2-ethylhexyl) phosphoric acid [11, 12] and tributylphosphate [13] extract the nitrosyl-ruthenium complex in dodecane. Solvent extractions using high molecular weight amines (HMWA) turn more and more popular in modern years. The HMWA are well-known as liquid anion exchangers, which combine several advantages of liquid-liquid extraction and ion exchange. High molecular weight amines (HMWA) reported for ruthenium(III) extraction are: Alamine 336 [14], Alamine 300, Aliquat 336 [10], N-octylamine [15]. Extraction of ruthenium from HCl media has been performed with N,N'-dimethyl-N,N'-dicyclo-hexylmalonamide (DMDCHMA) dissolved in 1,2-dichloroethane [16]. Alkyylaniline hydrochloride [17] extracts ruthenium from chloride or sulfate medium into toluene. The oxygenated and hydrocarbon solvents like methyl isobutyl ketone

* To whom all correspondence should be sent:

E-mail: maanuse@gmail.com

Table 1. Evaluation of earlier reported extraction methods with the present method

Sr. No	Extractant	Medium	Diluent	Strippant	Determination method	Equilibration time, min	Ref.
1	0.1M Cyanex 921	4 M HCl	Toluene	0.5M Na ₂ SO ₄	Spectrophotometry	15	9
2	Alamine 336 (15% A336 + 5% decanol)	1 M HCl	Kerosene	Na ₂ CO ₃	ICP-AES	20	14
3	<i>n</i> -Octylaniline 5%	1 M HCl	Xylene	2% NaCl	Spectrophotometry	1	15
4	N, N'-Dimethyl-N, N'-dicyclohexylmalonamide 0.3 M	7 M HCl	1,2 DCE	Water	Spectrophotometry	30	16
5	Aliquat 336 (15%) + LIX 54 (1%)	4 M HCl	Kerosene/dodecane	0.35M NaCl/2M NH ₃ +3M NH ₄ Cl	ICP-AES	20	44
6	N- <i>n</i> -octylaniline 4%	0.05 M HCl	Chloroform	1 M HCl	Spectrophotometry	--	45
7	25% Aliquat 336/ 25% Alamine 336	6 M HCl	Xylene	Na ₂ CO ₃	Spectrophotometry	15	46
8	<i>n</i> -Octylaniline	Sodium malonate pH = 3.5	Xylene	2% NaCl: 1M HCl (4:1)	Spectrophotometry	5	PM

PM = Present method

(MIBK) [18], paraffin oil [19], mixture of isoamyl alcohol and isobutyl methyl ketone [20] have also been used as extractants for ruthenium. Ruthenium (III) from purex process is separated using paraffin oil in nitric acid medium but it is necessary to oxidize Ru to RuO₄ by addition of ceric nitrate before extraction [19]. Mixture of isoamyl alcohol and MIBK in 1:1 ratio extracts ruthenium in the presence of a large excess of platinum but iridium interferes with the extraction procedure [20]. Attempts have also been made to selectively separate ruthenium (III) from associated elements with P-50 oxime [21], di(2-ethylhexyl) sulfoxide [DHSO] [22]. The various investigated systems are presented in Table 1 to review the literature in terms of various extractants used and special characteristics regarding those systems. Previously we have reported liquid-liquid extraction techniques for the separation of various metals [23-31]. Development of a new extraction system for extraction of ruthenium(III) especially in weak organic acid solutions is a topic of great interest. The target of this effort is to investigate the extraction properties of *n*-octylaniline with respect to noble metals such as ruthenium(III) from weak organic acid media. In the present investigation, the *n*-octylaniline-malonate system was considered for the extraction of ruthenium(III) as a function of diverse physicochemical parameters. The proposed technique is applied for the rapid and selective separation of ruthenium(III) from associated metal ions in their binary mixtures. In addition to that, this technique was also tested for isolation and determination of ruthenium(III) from various real samples like catalysts and a synthetic mixture.

EXPERIMENTAL

Apparatus

Absorbance measurement was carried out with a digital UV-visible spectrophotometer model Optizen- α (Mecasys Co., Ltd Korea) with a 10 mm quartz cell. Elico digital pH meter model SL-127 with combined glass electrode was utilized for the pH measurement. Digital balance Mettler Toledo (Model ML 204/AOI, Switzerland) was used for the weighing purpose.

Reagents

Standard ruthenium(III) solution

A solution of ruthenium(III) was prepared by dissolving 1.0 g of ruthenium chloride hydrate (Johnson Matthey, UK) in 1.0 M HCl, diluting with water to 250 mL in a standard volumetric flask and standardizing [32]. The required working solution (200 µg/ mL) of ruthenium(III) was prepared by diluting the above solution in a standard volumetric flask with water.

4'-Chloro-PTPT

1-(4'-Chlorophenyl)-4,4,6-trimethyl-(1H,4H)-pyrimidine-2-thiol (4'-chloro-PTPT) was synthesized by the reported method of Mathes [33-36] and was used for the spectrophotometric determination of ruthenium(III). The solutions of diverse ions were prepared in water or dilute HCl by dissolving their AR grade salts. Doubly distilled organic solvents were used for the extraction study and doubly distilled water was used throughout.

n-Octylaniline

n-Octylaniline was synthesized by the reported method of Pohlandt's [37] and its working (0.1 M) solution was prepared by dissolving a weighed quantity of *n*-octylaniline with xylene in a 100 mL standard volumetric flask.

General procedure for extraction and determination of ruthenium(III)

To a solution containing 200 μg of ruthenium(III) in a 25-mL standard volumetric flask sodium malonate was added to obtain 0.05 M solution. The pH of the aqueous phase was adjusted to 3.5 with dilute HCl and NaOH solutions. The aqueous phase was shaken with 10 mL of 0.1 M *n*-octylaniline in xylene for 5 min. The phases were allowed to separate, the organic phase was used to back extract ruthenium(III) with a 4:1 combination of 2 % NaCl and 1.0 M HCl. The back extracted aqueous phase was evaporated to moist dryness, dissolved in a minimum amount of *aqua regia* and evaporated with two 2 mL portions of concentrated HCl to remove oxides of nitrogen. The resulting solution of ruthenium(III) was diluted with 0.1 M HCl and was determined spectrophotometrically by the 4'-chloro-PTPT method [38]. All experiments were repeated on an average five times.

RESULTS AND DISCUSSION

Influence of pH on the extraction of ruthenium(III)

The effect of pH on the quantitative extraction of ruthenium(III) was investigated in the pH range from 0.5 to 10. The extraction was carried out with 0.1 M *n*-octylaniline in xylene. The phase ratio (aq: org) was kept 2.5:1 and both phases were equilibrated for 5 min.

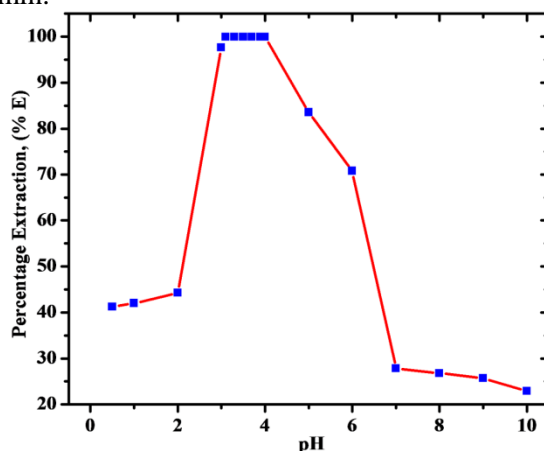


Fig. 1. Influence of pH on the extraction of ruthenium(III). Conditions: Ru(III) = 200 $\mu\text{g}/\text{mL}$, sodium malonate = 0.05 M, extractant = *n*-octylaniline (0.1 M) in xylene, shaking time = 5 min, strippant = 2 % NaCl + 1 M HCl (4: 1)

Fig. 1 shows that quantitative extraction of ruthenium(III) takes place in the pH range from 3.1 to 4.0. As pH increases above 4.0, the extraction of ruthenium(III) decreases due to the lack of formation of ion-pair complex. Therefore, further extractions were carried out at pH 3.5.

Influence of reagent concentration

To find out the optimum concentration of reagent required for the quantitative extraction of ruthenium(III), *n*-octylaniline in the range of 0.01 - 0.15 M was investigated. Other physicochemical parameters like pH, period of equilibration and type of diluent were kept constant and extraction was carried out. As reagent concentration increased, there was an increase in ruthenium(III) extraction. The quantitative extraction of ruthenium(III) was observed in the range from 0.09 M to 0.13 M *n*-octylaniline in xylene (Fig. 2). Therefore, 10 mL of 0.1 M *n*-octylaniline in xylene was adopted for the general extraction procedure.

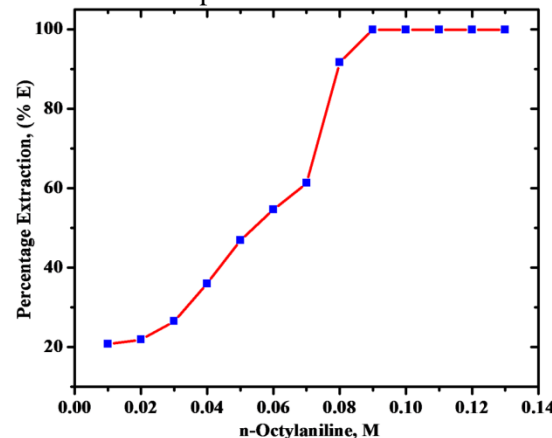


Fig. 2. Influence of *n*-octylaniline concentration. Conditions: Ru(III) = 200 $\mu\text{g}/\text{mL}$, pH = 3.5, sodium malonate = 0.05 M, shaking time = 5 min, strippant = 2 % NaCl + 1 M HCl (4: 1)

Effect of weak organic acid concentration

The extraction of ruthenium(III) was carried out in the presence of varying concentrations of sodium malonate, sodium succinate and sodium salicylate as weak acid media (Fig. 3) at pH 3.5 with 0.1 M *n*-octylaniline in xylene. It was observed that the extraction of ruthenium(III) starts at 0.01 M and becomes quantitative in the range of 0.04 M - 0.055 M for sodium malonate, beyond that the extraction decreased. Other weak organic acids such as salicylate and succinate showed incomplete extraction of ruthenium(III). Thus, for further experimental work 0.05 M malonate was adopted.

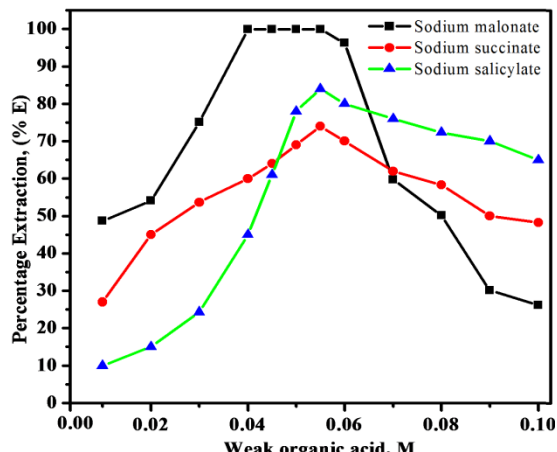


Fig. 3. Influence of weak organic acid concentration. Conditions: Ru(III) = 200 µg/ mL, pH = 3.5, extractant = *n*-octylaniline (0.1 M) in xylene, shaking time = 5 min, strippant = 2 % NaCl + 1 M HCl (4: 1)

Effect of diluents

In this study, the extraction of ruthenium(III) was carried out by applying various aromatic and aliphatic organic diluents. It was found that xylene, toluene and benzene showed quantitative extraction of ruthenium(III); there was incomplete extraction in methyl isobutyl ketone (93.04 %), *n*-butyl alcohol (42.2 %) and no extraction in chloroform, amyl alcohol, amyl acetate, 1, 2-dichloroethane and carbon tetrachloride (Table 2). Therefore, xylene was used as solvent throughout the experiment.

Table 2. Extraction of ruthenium(III) with various diluents

Solvent	Dielectric constant, (ϵ)	Percent extraction, (% E)	Distribution ratio, (D)
Xylene*	2.30	99.9	2497.5
Toluene	2.38	99.9	2497.5
Benzene	2.27	99.9	2497.5
Methyl isobutyl ketone (MIBK)	13.10	93.1	33.73
<i>n</i> -Butyl alcohol	17.80	42.2	1.82
Chloroform	4.80	No extraction	-
Amyl alcohol	13.90	No extraction	-
Amyl acetate	4.80	No extraction	-
1,2-Dichloro ethane	10.50	No extraction	-
Carbon tetrachloride	2.24	No extraction	-

Conditions: Ruthenium(III) = 200 µg/ mL, pH = 3.5, aq: org ratio = 2.5: 1, sodium malonate = 0.05 M, strippant = 2 % NaCl + 1 M HCl (4:1).

* Recommended for the general extraction procedure,

Influence of stripping reagents

Ruthenium(III) laden organic phase was back extracted with various stripping agents (Table 3). Ruthenium(III) was quantitatively stripped with a mixture of 2 % NaCl and 10 mL 1.0 M HCl (3 ×

Table 3. Effect of stripping agents on ruthenium(III) recovery

Strippant	Concentration	% Recovery	Distribution ratio, (D)
HCl	Concentrated (2 × 10 mL)	99.9	2497.5
HBr	Concentrated (2 × 10 mL)	99.9	2497.5
2% NaCl + 1 M HCl*	40 mL + 10 mL	99.9	2497.5
Ammonia	7 M (3 × 10 mL)	34.5	1.31
Ammonia + NH ₄ Cl	2 M + 3 M (2 × 10 mL)	43.0	2.74
NaOH	1 M (2 × 10 mL)	60.8	3.87
KOH	1 M (2 × 10 mL)	55.8	3.15
H ₂ O	2 × 10 mL	-	-
NH ₄ Cl	2 % (3 × 10 mL)	26.3	0.89

Conditions: Ruthenium(III) = 200 µg/ml, pH = 3.5, aq: org ratio = 2.5: 1, extractant = 0.1 M *n*-octylaniline in xylene, sodium malonate = 0.05 M.

* Recommended for the general extraction procedure,

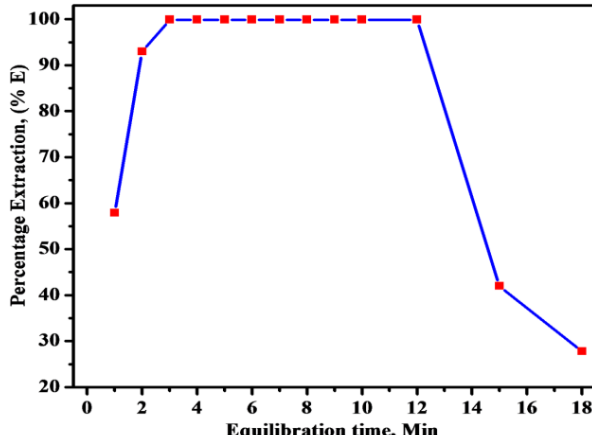
10 mL). However, the back extraction of ruthenium(III) from the extract was incomplete with other reagents like acetate buffer, sodium hydroxide, ammonia and potassium hydroxide. In the recommended procedure, a mixture of 2 % NaCl and 10 mL 1.0 M HCl was applied for the quantitative recovery of ruthenium(III) from the loaded organic phase.

Influence of equilibration time

The equilibration time required for the complete extraction of ruthenium(III) was studied by equilibrating the aqueous and the organic phase from 1 to 18 min. The extraction of ruthenium(III) increased with time, and became quantitative over a period of 3 min equilibration of the solutions, but with prolonged equilibration (over 12 min, Fig. 4) the percent extraction of ruthenium(III) decreased due to the dissociation of the ion-pair complex. Thus, 5 min of equilibration time was kept throughout the study of ruthenium(III) extraction.

Metal loading capacity of *n*-octylaniline

Varying concentrations of ruthenium(III) (50 – 2000 µg) were extracted with 0.1 M *n*-octylaniline in xylene (10 mL) from 0.05 M sodium malonate medium at pH 3.5. It was observed that 10 mL of 0.1 M *n*-octylaniline can quantitatively extract 500 µg of ruthenium(III) from the aqueous phase. Beyond the amount of 500 µg the extraction decreased. Therefore, 200 µg of ruthenium(III) was chosen for the extraction study.

**Fig. 4.** Function of equilibration period

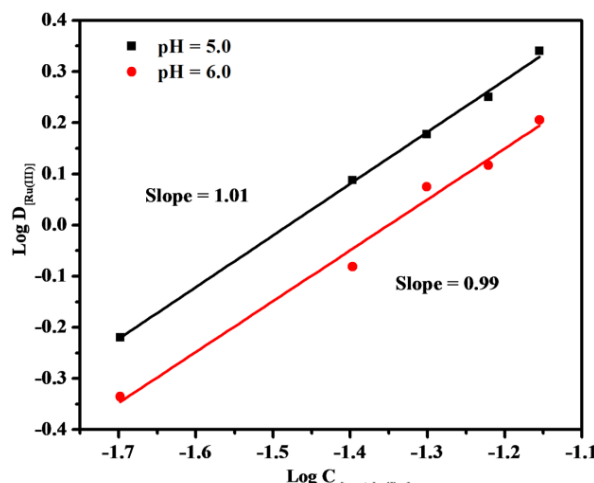
Conditions: Ru(III) = 200 $\mu\text{g}/\text{mL}$, sodium malonate = 0.05 M, pH = 3.5, extractant = *n*-octylaniline (0.1 M) in xylene, strippant = 2 % NaCl + 1 M HCl (4:1)

Effect of aqueous to organic volume ratio

The influence of various ratios of aqueous to organic phase was investigated. The various phase ratios were studied to optimize the ratio for quantitative extraction of ruthenium(III). The results show a quantitative aqueous/organic (A/O) phase ratio between 1:1 and 4:1. Above the 4:1 ratio there was a decrease in extraction due to the worse availability of reagent. Therefore, in the recommended extraction procedure, the phase ratio was maintained at 2.5:1.

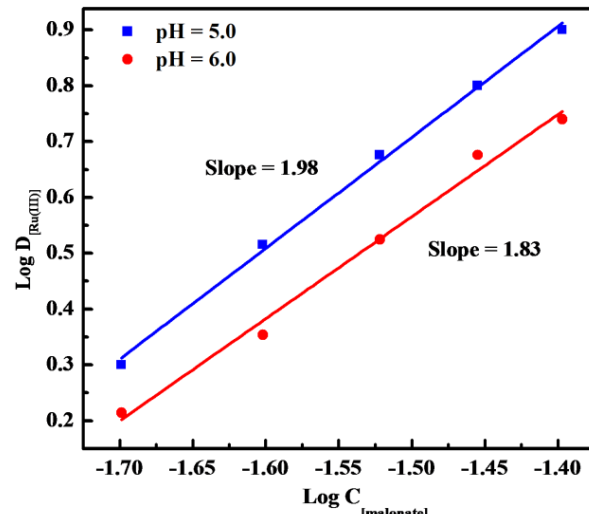
Stoichiometry of extracted species

The nature of the extracted complex species was determined by using log D - log C plots. The graph of $\log D_{[\text{Ru(III)}]}$ vs $\log C_{[\text{n-octylaniline}]}$ at a fixed sodium malonate concentration (0.05 M) was found to be linear having slopes of 1.01 and 0.99 at pH 5.0 and 6.0, respectively (Fig. 5).

**Fig. 5.** Log-log plot of $\log D_{[\text{Ru(III)}]}$ versus $\log C_{[\text{n-octylaniline}]}$ at a fixed malonate concentration.

Also the graph of $\log D_{[\text{Ru(III)}]}$ vs $\log C_{[\text{malonate}]}$ at a fixed *n*-octylaniline concentration (0.1 M) was

linear and the slope values were 1.98 and 1.83 at pH 5.0 and 6.0, respectively (Fig. 6).

**Fig. 6.** Log-log plot of $\log D_{[\text{Ru(III)}]}$ versus $\log C_{[\text{malonate}]}$ at a fixed *n*-octylaniline concentration.

The probable composition of the extracted species was calculated to be 1: 2: 1 (metal: acid: extractant). The possible mechanism of extraction appears to be as follows: protonated *n*-octylaniline forms the cationic species $[\text{CH}_3(\text{CH}_2)_7\text{C}_6\text{H}_4\text{NH}_3]^+_{(\text{org})}$ while malonate (bidentate ligand) combines with ruthenium(III) to form the anionic species $[\text{Ru}(\text{C}_3\text{H}_2\text{O}_4)_2]^-_{(\text{aq})}$ and both of them associate to form an ion-pair of the type $[\text{CH}_3(\text{CH}_2)_7\text{C}_6\text{H}_4\text{NH}_3^+ \text{Ru}(\text{C}_3\text{H}_2\text{O}_4)_2]_{(\text{org})}$ which, being neutral, constitutes an extractable species.

The possible extraction mechanism of the ion-pair complex is as follows:



APPLICATIONS

Effect of diverse ions

The influence of a large number of cations and anions on the extraction of 200 $\mu\text{g}/\text{mL}$ of ruthenium(III) with *n*-octylaniline was investigated by the recommended procedure. The tolerance limit of individual diverse ions was set so that the error in percent recovery was not more than $\pm 2\%$. The proposed method shows a high tolerance limit over various cations and anions. Some interfering cations are masked to increase the tolerance limit. Rhodium(III) and Pd(II) are masked with 25 mg of tartrate and Ir(III) with 25 mg of oxalate. Gold(III) is masked with 10 mg of bromide (Table 4). Ascorbate, thiourea, citrate and thiocyanate interfere with the extraction procedure.

Table 4. Effect of foreign ions on the extraction of ruthenium(III).

Tolerance limit, mg	Foreign ion added
50	Tartrate, oxalate, fluoride, acetate
25	Bromide, EDTA, Mg(II)
15	Fe(III), Zn(II), Mo(VI), Se(IV), Ba(II), Ce(IV)
10	Iodide, Ni(II), Co(II), U(VI), Hg(II)
5	Cu(II), Pb(II), Cr(VI), Bi(III), Te(IV), Cd(II)
2	Phosphate, Tl(I), Ca(II), Al(III), Cr(III), Cd(II),
1	Ag(I), Pt(IV), Os(VIII)
0.5	Rh(III) ^a , Pd(II) ^a , Ir(III) ^b , Au(III) ^c

Conditions: Ruthenium(III) = 200 µg/mL, pH = 3.5, extractant = 0.1 M *n*-octylaniline, aq: org ratio = 2.5: 1, sodium malonate = 0.05 M in xylene, strippant = 2 % NaCl + 1 M HCl (4:1)

^a Masked by 25 mg of tartrate,

^b Masked by 25 mg of oxalate,

^c Masked by 10 mg of bromide

Table 5. Separation of ruthenium(III) from binary mixtures

Metal ions	Amount taken, µg	Average recovery*, %	Chromogenic ligand	Ref
Ru(III)	200	99.8	-	
Pd(II) ^a	200	99.7	4'-Chloro PTPT	[38]
Ru(III)	200	99.8	-	
Pt(IV)	300	99.2	SnCl ₂	[39]
Ru(III)	200	99.8	-	
Ir(III) ^b	100	98.6	SnCl ₂ - HBr	[39]
Ru(III)	200	99.8	-	
Rh(III) ^a	200	99.7	SnCl ₂ + KI	[39]
Ru(III)	200	98.0	-	
Os(VIII)	200	99.3	Thiourea	[39]
Ru(III)	200	99.8	-	
Au(III) ^c	200	98.8	SnCl ₂	[39]
Ru(III)	200	99.7	-	
Fe(III)	1000	98.8	Thiocyanate	[39]
Ru(III)	200	99.8	-	
Cu(II)	2000	98.8	4'-Chloro-PTPT	[40]
Ru(III)	200	99.7	-	
Co(II)	1000	98.8	Thiocyanate	[41]
Ru(III)	200	99.8	-	
Ni(II)	5000	98.8	DMG	[41]
Ru(III)	200	99.8	-	
Se(IV)	300	98.8	4'-Bromo-PTPT	[42]
Ru(III)	200	99.8	-	
Te(IV)	200	98.8	4'-Bromo-PTPT	[43]

*Average of six determinations

^a Masked by 25 mg of tartrate,

^b Masked by 25 mg of oxalate,

^c Masked by 10 mg of bromide

Separation of ruthenium(III) from binary mixtures

The method allows the separation of ruthenium(III) from binary mixtures with some associated metal ions such as Os(VIII), Pt(IV), Cu(II), Fe(III), Co(II), Ni(II), Se(IV) and Te(IV).

The proposed method was successfully used for the separation of ruthenium(III) from these associated metal ions, under the optimum extraction conditions while all other added metal ions remained quantitatively in the aqueous phase where they were determined spectrophotometrically by standard methods [38-43]. Ruthenium(III) was back extracted from the organic phase and determined by spectrophotometry with the 4'-chloro- PTPT method (Table 5). At the same conditions of extraction of ruthenium(III), some metals like Rh(III), Pd(II), Ir(III) and Au(III) were co-extracted. Therefore, prior to the extraction of ruthenium(III), rhodium(III) and Pd(II) were masked with 25 mg of tartrate, Ir(III) was masked with 25 mg of oxalate and Au(III) was masked with 10 mg of bromide. The masked metal ions remained in the aqueous phase; they were demasked with perchloric acid followed by hydrochloric acid. Then the residue was dissolved in 10 mL of water and the aqueous phase was evaporated to almost dryness to completely remove traces of acid. The residue containing Rh(III), Pd(II), Ir(III) and Au(III) was analyzed spectrophotometrically by standard methods.

Separation of ruthenium(III) from ternary mixtures

The selectivity of the proposed extraction method was increased by using an appropriate masking agent for added metal ions. A ternary mixture of ruthenium(III), palladium(II) and rhodium(III) was extracted from 0.05 M malonic acid at pH 3.5 with 10 mL of 0.1 M *n*-octylaniline in xylene by masking Pd(II) and Rh(III) with tartrate (25 mg). It was found that ruthenium(III) was extracted while palladium(II) and rhodium(III) remained unextracted. Ruthenium(III) was stripped with 2% of NaCl and 1.0 M HCl (4:1) and determined by the recommended procedure [38].

The aqueous phase containing palladium(II), rhodium (III) and excess of malonic acid was decomposed by the addition of concentrated hydrochloric acid, and sodium malonate was added up to 0.03 M. Rhodium(III) was extracted quantitatively with 10 mL of 0.1 M *n*-octylaniline in xylene at pH 9.0. Rhodium(III) was stripped from the organic phase with 1.0 M hydrochloric acid (2×10 mL) and determined spectrophotometrically using the stannous chloride-potassium iodide method [39]. The malonate from the aqueous phase was decomposed with concentrated hydrochloric acid and the residue was extracted with 0.1 M hydrochloric acid. The aqueous phase was made 0.085 M with respect to sodium salicylate and

Table 6. Sequential separation of ruthenium(III) from a ternary mixture

Metal ion	Amount taken, μg	Aqueous phase (25 mL)	Stripping agent	Determination method	Recovery*, %	Ref
Ru(III)	200	0.05 M Malonate pH = 3.5	2 % NaCl + 1 M HCl (4: 1)	4'-Chloro PTPT	99.8	[39]
Rh(III) ^c	200	0.03 M Malonate pH = 9.0	1 M HCl (2 \times 10 mL)	SnCl ₂ + KI	99.7	[40]
Pd(II) ^a	200	0.085 M Salicylate pH = 1.5	5 M Ammonia (3 \times 10 mL)	4'-Chloro PTPT	99.7	[39]

^aAverage of six determinations^a Masked by 25 mg of tartrate

extraction of palladium(II) was carried out with 10 mL of 0.07 M *n*-octylaniline at pH 1.5. Palladium(II) extracted from the organic phase was stripped with 5.0 M ammonia (2 \times 10 mL) and determined spectrophotometrically with 4'-chloro- PTPT [38] (Table 6).

Determination of ruthenium(III) in synthetic mixtures

The proposed method was used for the extraction and determination of ruthenium(III) from malonate media at pH 3.5 in various ternary mixtures (Table 7).

Table 7. Determination of ruthenium(III) in synthetic mixtures

Synthetic mixture Ions	Ruthenium(III) found, μg	Amount of ruthenium(III) extracted, %	RSD, %
Ru(III)	200		
Pd(II) ^a	100	197.0	98.5
Pt(IV)	100		
Ru(III)	200		
Ir(III) ^b	100	198.7	99.3
Rh(III) ^a	100		
Ru(III)	200		
Ni(II)	100	197.0	98.5
Au(III) ^c	100		
Ru(III)	200		
Co(III)	200	198.7	99.3
Fe(III)	200		
Ru(III)	200		
U(VI)	100	197.5	98.7
Te(IV)	100		

^a Masked by 25 mg of tartrate, ^b Masked by 25 mg of oxalate, ^c Masked by 10 mg of bromide

RSD = Relative standard deviation

Ruthenium(III) was quantitatively extracted with 0.1 M *n*-octylaniline in xylene while Pt(IV), Ni(II), Te(IV), Fe(III), Co(II), U(VI) remained unextracted in the aqueous phase. Rh(III) and Pd(II) were masked with 25 mg of tartrate and Ir(III), and Au(III) with 25 mg of oxalate and 10 mg of bromide, respectively. The extracted ruthenium(III) was 920

stripped and determined spectrophotometrically by the 4'-chloro-PTPT method.

Analysis of ruthenium(III) in catalysts samples

Ruthenium(III), activated carbon and 0.1 g of alumina were added to 20 mL of *aqua regia*. The solution was heated to evaporate till moist dryness. The nitric acid was removed by evaporating with two 5 mL portions of hydrochloric acid. The solution was then filtered and diluted to 100 mL in a volumetric flask. An aliquot of the diluted solution was used for the analysis of ruthenium(III) content by the developed method. The results obtained were found in good agreement with the certified value (Table 8).

CONCLUSIONS

- I. The extraction equilibria of ruthenium(III) and sodium malonate were investigated systematically using *n*-octylaniline in xylene.
- II. The results demonstrated that *n*-octylaniline is an excellent reagent for the extraction of ruthenium(III) from malonate media at pH 3.5 compared with some other high-molecular-weight amines and organophosphorus compounds. Further, *n*-octylaniline has good regeneration and loading capacities.
- III. The extractability of ruthenium(III) in presence of other associated elements was investigated. The proposed method was applied for the separation of ruthenium(III) from binary mixtures of associated transition metal ions and other rare earths.

REFERENCES

1. J. A. Rard, *Chem. Rev.*, **85**, 555 (1985).
2. C. R. Hamond, The elements in Lide, D.R., ed., *CRC Handbook of Chemistry and Physics*, 86th Edition, Boca Raton (FL), CRC press, (2005).
3. A. D. Richards, A. Rodger, *Chem. Soc. Rev.*, **36**, 471 (2007).
4. K. Daibin, I. Seigo, W. Bernard, K. Cedric, M. Jacques-E, H. Baker, R. Zakeeruddin, M. Shaik, G. Michael, *J.American Chem. Soc.*, **128**, 4146 (2006).
5. K. R. Seddon, *Platinum Metals Review*, **40**, 128 (1996).

6. S. Atak, M.S. Celik, *Innovations in mineral and coal processing*, Taylor and Francis 1998. CRC Press, ISBN 9789058090133 - CAT# RU41050.
7. T. M. Bahrainwala, Z. R. Turel, *J. Radioanal. Nucl. Chem.*, **237**, 175 (1998).
8. V. Druskovic, V. Vojkovic, T. Antonic, *Croat. Chem. Acta.*, **78**, 617 (2005).
9. A. Mhaske, P. Dhadke, *Hydrometallurgy*, **63**, 207 (2002).
10. S. Kedari, M. T. Coll, A. Fortuny, E. Goralska, A. M. Sastre, *Sep. Sci. Technol.*, **40**, 1927 (2005).
11. G. Yan, J. Aistad, *J. Radioanal. Nucl. Chem.*, **201**, 191 (1995).
12. G. Yan, J. Aistad, *J. Radioanal. Nucl. Chem.*, **196**, 287 (1995).
13. A. M. Rozen, N. A. Kartasheva, Z. N. Nikolotova, *Radiokhimiya*, **37**, 232 (1995).
14. E. Goralska, M. T. Coll, A. Fortuny, C. S. Kedari, A. M. Sastre, *Sol. Extr. Ion Exch.*, **25**, 65 (2007).
15. T. N. Lokhande, G. B. Kolekar, M. A. Anuse, M. B. Chavan, *Sep. Sci. Technol.*, **35**, 153 (2000).
16. P. Malik, A. P. Paiva, *Sol. Extr. Ion Exch.*, **29**, 176 (2011).
17. V. G. Torgov, M. G. Demidova, T. M. Korda, T. M. Korda, N. K. Kalish, R. S. Shulman, *Analyst*, **121**, 489 (1996).
18. O. X. Rong, W. J. Duan, H. R. Li, R. N. Chen, S. Q. Liu, J. L. Ye, Z. Huang, X. H. Gu, *Fenxi Shiyanshi*, **13**, 37 (1994).
19. M. Kenj, *J. Nucl. Sci. Technol.*, **27**, 262 (1990).
20. Z. Aneva, S. Arpadyan, I. Kalaidzhieva, *Anal. Chim. Acta.*, **236**, 385 (1990).
21. E. Jackson, *Miner. Eng.*, **9**, 469 (1996).
22. C. H. Shen, B. R. Bao, Y. Z. Bao, G. D. Wang, J. Qian, Z. B. Cao, *J. Radioanal. Nucl. Chem.*, **178**, 91 (1994).
23. B. T. Khogare, G. S. Kamble, A. N. Kokare, S. B. Zanje, V. J. Suryavanshi, M. A. Anuse, P. B. Piste, B. N. Kokare, *J. Environ. Chem. Engg.*, **4**, 3075 (2016).
24. A. Kokare, V. Suryavanshi, S. Zanje, G. Kore, M. Anuse, *Anal. Methods*, **8**, 6158, (2016).
25. S. B. Zanje, A. N. Kokare, V. J. Suryavanshi, G. D. Kore, B. T. Khogare, M. A. Anuse, *J. Trace Analysis Food Drug*, **24**, 1 (2016).
26. V. J. Suryavanshi, R. R. Pawar, M. A. Anuse, G. N. Mulik, *Anal. Methods*, **7**, 2497 (2015).
27. V. J. Suryavanshi, M. M. Patil, S. B. Zanje, A. N. Kokare, G. D. Kore, M. A. Anuse, G. N. Mulik, *Sep. Sci. Technol.*, **51**, 1690 (2016).
28. V. J. Suryavanshi, M. M. Patil, A. N. Kokare, S. B. Zanje, R. R. Pawar, M. A. Anuse, G. N. Mulik, *J. Chin. Chem. Soc.*, **63**, 694 (2016).
29. S. B. Zanje, A. N. Kokare, V. J. Suryavanshi, D. P. Waghmode, S. S. Joshi, M. A. Anuse, *Spectrochim. Acta Part A*, **169**, 223 (2016).
30. A. Gaikwad, S. Jagatap, V. Suryavanshi, S. Kolekar, M. Anuse, *Int. J. Anal. Bioanal. Chem.*, **3**, 42 (2013).
31. V. J. Suryavanshi, M. M. Patil, S. B. Zanje, A. N. Kokare, A. P. Gaikwad, M. A. Anuse, G. N. Mulik, *Russian J. Inorg. Chem.*, **62**, 256 (2017).
32. F. E. Beamish, J. C. Van Loon, *Analysis of noble metals: overview and selected methods*, Academic Press INC, London, (1977).
33. R. A. Mathes, F.D. Stewart, F. J. Swedish, *J. Am. Chem. Soc.*, **70**, 1452 (1948).
34. R. A. Mathes, F. D. Stewart, *J. Am. Chem. Soc.*, **72**, 1879 (1950).
35. R. A. Mathes, F. D. Stewart, 2-Mercapto-3-amino-3, 6-dihydro-pyrimidines, *U. S. Patent*, 26, 535 (1950).
36. R. A. Mathes, *J. Am. Chem. Soc.*, **75**, 1747-1748 (1953).
37. C. Pohlandt, *Talanta*, **26**, 199 (1979).
38. M. A. Anuse, M. B. Chavan, *Chem. Anal.*, (Warsaw), **29**, 409 (1984).
39. E. B. Sandell, *Colorimetric determination of traces of metals*, 3rd Ed. Interscience, New York, pp 503, 519, 702, 774, 781, 524 (1965).
40. M. A. Anuse, S. R. Kuchekar, M. B. Chavan, *Ind. J. Chem.*, **25A**, 1041 (1986).
41. Z. Marczenko, *Spectrophotometric determination of elements*, Ellis Horwood Limited, Chichester, pp 229, 370 (1976).
42. G. B. Kolekar, M. A. Anuse, *Res. J. Chem. Environ.*, **2**, 9 (1998).
43. G. B. Kolekar, M. A. Anuse, *Bull. Chem. Soc. Jpn.*, **71**, 859 (1998).
44. C.S. Kedari, M. T. Coll, A. Fortuny, *Hydrometallurgy*, **82**, 40 (2006).
45. S. J. Kokate, S. R. Kuchekar, *J. Saudi Chem. Soc.*, **14**, 41 (2010).
46. S. Panigrahi, T. Dash, K. C. Nathsarma, K Sarangi, *Sep. Sci. Technol.*, **49**, 545 (2014).

ТЕЧНО-ТЕЧНА ЕКСТРАКЦИЯ НА РУТЕНИЙ (III) В СРЕДА НА МАЛОНАТ ПРИ ИЗПОЛЗВАНЕТО НА N-ОКТИЛАНИЛИН КАТО ЙОН-СВЪРЗВАЩ АГЕНТ:
ИЗСЛЕДВАНЕ НА КАТАЛИЗATORA И СПЛАВИ

А.П. Гаикуад, В.Дж. Сурияванши, М.А. Анусе*

Лаборатория по аналитична химия, Департамент по химия, Университет „Шиваджи“, Колхапур -416004,
Махарацра, Индия

Постъпила на 18 октомври, 2016 г.; коригирана на 2 юни, 2017 г.

(Резюме)

Ние разработихме система за течна екстракция на рутений (III), използвайки 0.1 М n-октиланилин в среда на 0.05 М малонат при pH 3.5. Оптимизирани са различни работни параметри като pH, концентрации на реагентите, време за установяване на равновесието и капацитет на екстрагента за количественото определяне. Стехиометрията на екстрагираните вещества бе определена от наклона на правата линия. Екстракцията се извършва при формирането на ионни двойки комплекси между $[CH_3(CH_2)_7C_6H_4NH_3]^{+}_{(org)}$ и $[Ru(C_3H_2O_4)_2]^{-}_{(aq)}$. Асоциирането на тези два йона води до неутрален незареден компонент $[CH_3(CH_2)_7C_6H_4NH_3^+ Ru(C_3H_2O_4)^-]_{(org)}$. Стехиометрията на екстрагираните компоненти е 1: 2: 1 (метал: киселина: екстрагент). Валидността на предложения метод е проверена чрез екстракцията на рутений (III) от бинарни и тройни смеси и са изследван и различни катализатори.

Chemical composition and bioactive properties of the essential oil of *Rhinanthus angustifolius* subsp. *grandiflorus*

A. A. Kaya^{1*}, O. Üçüncü², S. M. İlter², C. Baltacı², S. Öztürk¹

¹ School of Health, Gümüşhane University, TR-29100 Gümüşhane, Turkey

² Department of Food Engineering, Faculty of Engineering and Natural Sciences, Gümüşhane University, TR-29100 Gümüşhane, Turkey

Received December 9, 2016; Accepted May 26, 2017

In this study, the chemical composition and antimicrobial activities of the essential oil of the *Rhinanthus angustifolius* subsp. *grandiflorus* plant were investigated. Essential oil was obtained from all parts of the plant by hydrodistillation and was analyzed by GC-FID and GC-MS. 31 components representing 99.46% of the total oils were characterized. The main components of these species were found to be 2,3-dihydro-5-methyl-1H-indene (25.14%), α -cubebene (19.27%), 1-hexadecene (15.59%) and hexadecanoic acid (12.14%). The antimicrobial activity of the isolated essential oil was investigated. Antimicrobial activity was observed against *B. cereus*, *E. coli*, *E. coli* O157:H7 and *S. Aureus* microorganisms. Moreover, an effect on the fermentations of *B. cereus*, *E. coli*, *E. coli* O157:H7 and *S. Aureus* was detected.

Keywords: *Rhinanthus angustifolius* subsp. *grandiflorus*, Essential oil, GC-FID/MS, Antimicrobial activity, Phenolic content.

INTRODUCTION

Rhinanthus L. (Scrophulariaceae) consists of 30–40 species of hemi-parasitic annual herbs most of which are widespread in Europe [1,2]. *Rhinanthus* was formerly classified in Scrophulariaceae but, later it was suggested to be included into Orobanchaceae [3,4]. *Rhinanthus angustifolius* C. C. Gmelin is a very variable species and consists of three subspecies [1]. *R. angustifolius* subsp. *grandiflorus* is easily recognized from other subspecies by its leaf size (longer than 8 mm). The genus is represented by a subspecies (*Rhinanthus angustifolius* C. C. Gmelin subsp. *grandiflorus* (Wallr.) D. A. Webb) in the flora of Turkey [5]. The species of *Rhinanthus* is used in folk medicine for treating eye complaints caused by certain bacteria kinds [6]. An iridoid glucoside, 6'-O-benzoylshanzhiside methyl ester, was isolated from *R. angustifolius* [7]. Some scientists have found that alcoholic extracts of *R. angustifolius* have strong antibacterial activities [8].

Rhinanthus L. of Scrophulariaceae family has 40 natural species in Europe, North Africa, North Asia and North America. These are annual or perennial herbaceous or brier plants [9,10]. The *Rhinanthus angustifolius* subsp. *grandiflorus* plant used in this study is a non-endemic *Rhinanthus* taxon of the family mostly found in the northern parts of the Eastern Anatolia region and has bell-shaped yellow flowers. The flowers of the *R. angustifolius* subsp. *grandiflorus* plant are used as a medicine for treating ear complaints by people in Anatolia [11].

Studies in the literature show that some *Rhinanthus* species (*Rhinanthus angustifolius*, *Rhinanthus rumelicus* Velen. and *Rhinanthus serotinus* (Schönh.) Oborny) contain natural compounds such as flavonoids, anthocyanines, anthraquinones and saponins which have certain biological activities [8,12,13]. However, no study was found on the chemical composition or biological activities of the essential oil of the *R. angustifolius* subsp. *grandiflorus* plant. This study investigates the chemical composition of *Rhinanthus angustifolius* found in Turkey and the antibacterial, antifungal and antioxidant properties of its essential oil extract.

EXPERIMENTAL

Studies conducted

Rhinanthus angustifolius subsp. *grandiflorus* was collected from the shores of Lake Limni, district of Torul, Province of Gümüşhane (approximately 1800 m) in July 2013. The plant material was identified by Dr. Mutlu Gültepe and stored under number KTUB-508 in the Karadeniz Technical University. Real samples were filtered through 0.45 μm nylon filter membranes (Varian, USA).

Clevenger-type hydrodistillation process

Collected plant material was shade-dried and weighed 76 g. Dried plants were broken into small pieces with a blender, put into a flask with 800 mL of pure water and heated for 3 h in a Clevenger-type water steam distillation apparatus. The resulting steam was cooled at -15 $^{\circ}\text{C}$ and 20 mg (w/w 0.026%) of essential oil was obtained. The essential oil was taken into a brown vial with 1 mL hexane of HPLC

* To whom all correspondence should be sent:

E-mail: afsinkaya@hotmail.com

quality, dried over anhydrous Na_2SO_4 and stored at -5 $^{\circ}\text{C}$ for analysis [14].

GC and GC-MS analyses

GC-MS and GC-FID analyses were performed in accordance with the literature [15].

Identification of components

In order to determine the chemical content of the essential oil, each compound was firstly determined using the WILEY and NIST libraries of the computer performing the mass spectrum analysis and then by comparing their retention times with alkene standards ($\text{C}_7\text{-C}_{30}$) and literature data [16-18].

Antimicrobial activity analysis

All test microorganisms were obtained from the Food Engineering Laboratory of Gümüşhane University. Antimicrobial activities of the essential oil extract were determined using the agar diffusion method against *Aeromonas hydrophila* ATCC 7965, *Bacillus cereus* ATCC 33019, *Bacillus subtilis* ATCC 6633, *Enterobacter cloacea* ATCC 13047, *Escherichia coli* ATCC 11230, *Escherichia coli* O157:H7 ATCC 33150, *Klebsiella pneumoniae* ATCC 13883, *Listeria monocytogenes* ATCC 7644, *Proteus vulgaris* ATCC 13319, *Pseudomonas aeruginosa* ATCC 17853, *Salmonella typhimurium* ATCC 14028, *Staphylococcus aureus* ATCC 25923, *Saccharomyces cerevisiae* BC 5461, *Candida albicans* ATCC 1223, *Aspergillus niger*, *Aspergillus flavus* and *Penicillium*. Extracts were prepared from stock solutions by dissolving in hexane (1000 ppm) [19,20].

Agar diffusion method

All microorganisms were developed in a nutrient broth at 37°C for 18 h. *C. albicans*, *S. cerevisiae*, *A. niger*, *A. flavus* and *Penicillium* were developed in a malt extract broth at 27°C for 42 h. Microorganisms developed by cooling sterile nutrient agar and malt extract agar to 45°C were inoculated (1%) and poured to petri plates. Once agars solidified, wells with a diameter of 5 mm were opened on agars. Pre-extracted samples were added to wells (50 μL). Hexane was used for control. Then, the petri plates were incubated at 37°C for 24 h for bacteria and at 27°C for 48 hours for fungi. Antimicrobial activity was determined by measuring the inhibition zones of test microorganisms [21] in mm.

Antioxidant activity tests

Determination of free radical scavenging activity

The free radical scavenging activity value was found by the DPPH method. A DPPH solution prepared with 4 mL of 0.1 mM methanol was added to the essential oil extract of *Rhinanthus angustifolius* subsp. *grandiflorus*. The mixture was kept at room temperature in dark for 30 min and measured against methanol at 517 nm. Measurements were repeated in five parallels and averaged [22]. % Inhibition results were calculated using the formula:

$$\% \text{ Inhibition} = (\text{Control Absorbance} - \text{Sample Absorbance}) / \text{Control Absorbance} \times 100$$

Total Phenolic Content

The Folin-Ciocalteu method was used for determination of total phenolic content [20]. In summary, pre-extracted materials were taken to 40 μL test tubes and then 2.4 mL of pure water was added. 200 mL of Folin-Ciocalteu phenolic reagent, 600 mL of sodium carbonate solution and 760 mL of pure water were added to the mixture. The mixture was stirred for 15 sec. Reduction of Folin-Ciocalteu reagent results in a blue color in alkaline environment. The absorbance was measured at 765 nm after 2 h of incubation. All measurements were performed in five parallels and averaged. The chart used in the calculations is shown in Figure 1. The results are presented as GAE/L [23].

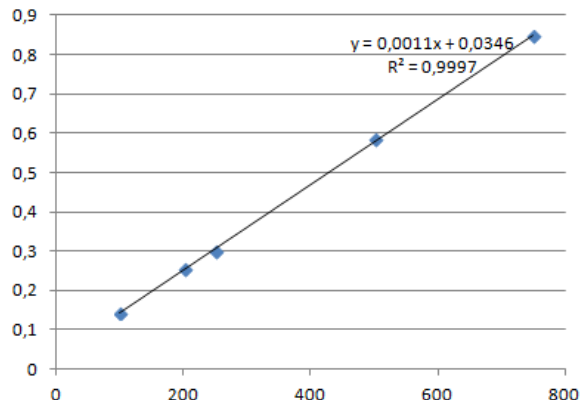


Fig. 1. Gallic acid curve used for total phenolic content determination

RESULTS AND DISCUSSION

As a result of the hydrodistillation applied to 76 g of dried *Rhinanthus angustifolius* subsp. *grandiflorus* plant, 20 mg of essential oil was obtained with a yield of 0.026%. 31 compounds at a rate of 99.46% were identified in the chemical structure of the essential oil by comparing the results of the GC-MS analysis with the literature. As seen in

Table 1, the identified compounds are divided into 6 groups as terpene or terpene-like, aldehydes, alcohols, esters, acids and other compounds. The main components of the essential oil were found to

be 2,3-dihydro-5-methyl-1H-indene, (25.137%), α -cubebene (19.27%), 1-hexadecane (15.59%) and hexadecanoic acid (12.14%)

Table 1. Identified chemical content of the *Rhinanthus angustifolius* subsp. *grandiflorus* plant

No	Retention Time, min	Name of Compound	% Area	Experimental RI
<i>Terpene or terpene-like</i>				
1	25.53	α -Cubebene	19.27	1309
2	27.02	Copaene	3.12	1344
3	28.97	β -Damascenone	0.45	1389
4	31.72	(E)-6,10-Dimethyl-5,9-undecadien-2-one,	0.54	1455
5	33.19	β -Cyclocitrylideneacetone	0.19	1490
6	34.76	(E)-3-(4,8-Dimethyl-3,7-nonadienyl)-furan	1.02	1536
7	46.40	Perhydrofarnesyl acetone	1.89	1847
8	61.50	Methyl dehydroabietate	0.59	2339
<i>Aldehydes</i>				
9	26.14	2,4-Decadienal	1.18	1324
10	27.94	2-Undecenal	0.31	1365
11	59.33	1,2,3,4,4a,9,10,10a-Octahydro-1,4a-dimethyl-7-(1-methylethyl)-[1R-(1 α ,4a β ,10a α)]-1-phenanthrenecarboxaldehyde	0.54	2262
<i>Alcohols</i>				
12	9.75	1-Okten-3-ol	0.94	944
13	10.02	6-Methyl-2-heptanol,	0.38	952
<i>Esters</i>				
14	37.54	2,2,4-Trimethyl-3-carboxyisopropyl pentanoic acid isobutyl ester	0.27	1599
15	47.26	Phthalic acid, diisobutyl ester	0.36	1873
16	51.29	Hexadecanoic acid, ethyl ester	0.09	1995
17	57.50	Phthalic acid, isohexyl 3-methylbut-3-enyl ester	0.67	2198
18	59.96	1-Phenanthrenecarboxylic acid, 7-ethenyl-1,2,3,4,4a,4b,5,6,7,8,10,10a-dodecahydro-1,4a,7-trimethyl methyl ester [1R-(1 α ,4a β ,4b α ,7 α ,10a α)]-	3.82	2286
<i>Acids</i>				
19	33.59	Adamantane-1-carboxylic acid	1.05	1501
20	50.33	Hexadecanoic acid	12.14	1964
<i>Other compounds</i>				
21	12.86	Indane	0.30	1026
22	16.33	2,3-Dihydro-5-methyl-1H-indene	25.13	1129
23	29.07	N-Methylbenzamid	0.63	1391
24	37.17	15-nor-Funebran-3-one	0.27	1591
25	38.02	1-Hexadecene	15.59	1613
26	41.74	3-Cyclohexyl-undecane	0.59	1717
27	46.14	Galaxolide	2.59	1839
28	48.20	n-Nonadecane	0.37	1900
29	54.55	Heneicosane	1.51	2100
30	60.37	Tricosane	2.92	2300
31	66.41	Pentacosane	1.26	2500
		Total	99.46	

Table 2. Antimicrobial activity results (in mm) of the essential oil of *Rhinanthus angustifolius* subsp. *grandiflorus*

Bacteria	1%	2%	5%	10%
<i>A. hydrophila</i>	-	-	-	-
<i>B. cereus</i>	12.01±0.10	10.24±0.10	-	-
<i>B. subtilis</i>	-	-	-	-
<i>Ent. cloacae</i>	-	-	-	-
<i>E. coli</i>	10.64±0.10	8.19±0.15	-	-
<i>E.coli O157:H7</i>	13.13±0.10	10.20±0.10	8.56±0.10	-
<i>K. pneumoniae</i>	-	-	-	-
<i>L.monocytogenes</i>	-	-	-	-
<i>P. vulgaris</i>	-	-	-	-
<i>Pseu. aeruginosa</i>	-	-	-	-
<i>Sal. typhimurium</i>	-	-	-	-
<i>S. aureus</i>	8.14±0.10	-	-	-
<hr/>				
Fungi				
<i>Sac. cerevisiae</i>	5.01±0.15	-	-	-
<i>C. albicans</i>	7.19±0.10	-	-	-
<i>A.niger</i>	-	-	-	-
<i>A.flavus</i>	-	-	-	-
<i>Penicillium</i>	-	-	-	-

Inhibition levels of the essential oil extracts of *Rhinanthus angustifolius* subsp. *grandiflorus* against test bacteria and fungi are given in Table 2. In the antimicrobial study, inhibition zones increased as the concentration of extracts increased. Essential oil extracts showed strong antimicrobial activity at concentrations of 1000 ppm and 500 ppm. Essential oil of *Rhinanthus* plant was found to show antimicrobial activity against *B. cereus*, *E. coli*, *E.coli O157:H7* and *S. aureus*. It was effective against *Sac. cerevisiae* and *C. albicans* fungi, whereas it showed no antifungal activity for the fungi studied in the present work.

It was found that the essential oil extract had high antioxidant activity. The essential oil extract of *Rhinanthus angustifolius* subsp. *grandiflorus* was found to have 53.92% DPPH radical scavenging activity against yellow-colored diphenylpicrylhydrazine.

The total phenolic activity of the essential oil extract of *R. angustifolius* subsp. *grandiflorus* was found to be 630.19 GGA/L. Due to its high phenolic content, the plant can be used in daily diet or in functional foods. It was found that antioxidants found in medicinal plants have biological effects in addition to being safe and effective.

CONCLUSIONS

In this work, we describe the chemical composition and antimicrobial activities of *Rhinanthus angustifolius* subsp. *grandiflorus* essential oil. 31 components obtained from all parts of the plant by hydrodistillation were analyzed by GC-FID and GC-MS. This is the first study in the literature on antioxidant and antimicrobial properties of the *Rhinanthus* plant found in the flora of Turkey.

This study may contribute to future research on bioactive properties of the plant.

Acknowledgements: This study was supported within the scope of the project no. 13.F5115.02.2 by the Scientific Research Projects Unit of Gümüşhane University (GÜBAP). We would like to thank Dr. Mutlu GÜLTEPE, who performed plant identification.

REFERENCES

1. R.Soó, D. Webb, L. Rhinanthus, in: Flora Europaea, T. Tutin, V. Heywood, N. Burges, D. Valentine, D. Moore (Eds), vol. 3. Cambridge University Press, Cambridge, UK, 1972, p 276.
2. T. Talve, M.E. McGlaughlin, K. Helenurm, L.E. Wallace, T. Oja, *Plant Biology*, **16**, 495 (2014).
3. R.G. Olmstead, P.A. Reeves, *Ann. Missouri. Bot. Gard.*, **82**, 176 (1995)
4. R.G. Olmstead, C.W. de Pamphilis, A.D. Wolfe, N.D. Young, W.J. Elisons, P.A. Reeves, *Amer. J. Bot.*, **88**, 348 (2001).
5. I.C. Hedge, (), Rhinanthus L. in: Flora of Turkey and the East Aegean Islands, P.H. Davis, (Eds), vol. 6. Edinburgh University Press, Edinburgh, 1978 p 777.
6. O. Polunin, Flowers of Europe - A Field Guide. Oxford University Press, New York, 1969.
7. Y. Takeda, K. Tamura, T. Matsumoto, H. Terao, M. Tabata, T. Fujita, G. Honda, E. Sezik, E. Yeşildat, *Phytochemistry*, **33**, 623 (1993).
8. C. Usta, A.B. Yıldırım, A.U. Turker, *Biotechnology & Biotechnological Equipment*, **28**, 306 (2014).
9. P.H. Davis, Flora of Turkey and The East Aegean islands, vol. 5. Edinburgh University Press, Edinburgh, 1988, p 67.

10. A. Güner, N. Özhatay, T. Ekim, K.H.C. Başer, Flora of Turkey and The East Aegean islands, vol. 5. Edinburgh University Press, Edinburgh, 2000, p11.
11. T. Baytop, Türkiyede Bitkilerle Tedavi, İstanbul Üniversitesi, İstanbul, 1999, p187.
12. I.M. Imbreia, A.L. Nicolin, F. Imbreia, *Research Journal of Agricultural Science*, **44**, 178 (2012).
13. M. Kozieradzka-Kiszkurowska, J. Bohdanowicz, *Acta Biologica Cracoviensis Series Botanica*, **55**, 99 (2013).
14. Z. Tunalier, N. Kirimer, K.H.C. Başer, *Chem. Nat. Comp.*, **38**, 43 (2002).
15. O. Üçüncü, N. Yaylı, C. Volga, N. Yaylı, S. Terzioğlu, *Asian J. Chem.*, **21**, 6569 (2009).
16. R.P. Adams, Identification of essential oil components by gas chromatography/mass spectrometry. Allured Publishing Corporation Carol Stream, USA 1995.
17. N. Kahriman, C.G. Albay, N. Dogan, A. Usta, S.A. Karaoğlu, N. Yaylı, *Asian J. Chem.*, **22**, 6437 (2010).
18. H.D. Skaltsa, C. Demetzos, D. Lazari, M. Sokovic, *Phytochemistry*, **64**, 743 (2003).
19. Z.A. Maksimovic, S. Dordevic, M. Mraovic, *Fitoterapia*, **76**, 112 (2005).
20. O. Sağdıç, M. Özcan, *Food Control*, **14**, 141 (2003).
21. C. Perez, M. Pauli, P. Bazerque, *Acta Biologiae et Medicina Experimentalis*, **15**, 113 (1990).
22. C. Sanchez-Moreno, J.A. Larrauri, F. Saura-Calixto, *Journal of the Science of Food and Agriculture*, **76**, 270 (1998).
23. N. Gámez-Meza, J.A. Noriega-Rodríguez, L.A. Medina-Juárez, J. Ortega-García, R. Cázares-Casanova, O. Angulo-Guerrero, *Journal of the American Oil Chemists' Society*, **76**, 1445 (1999).

ХИМИЧЕН СЪСТАВ И БИОАКТИВНИ СВОЙСТВА НА ЕСЕНЦИАЛНО МАСЛО ОТ *Rhinanthus angustifolius* subsp. *grandiflorus*

А.А. Кая^{1*}, О. Ючюнчю², Ш.М. Илтер², К. Балтаджъ², С. Йозтюрк¹

¹ Здравен колеж, Университет в Гюмюшхане, TR-29100 Гюмюшхане, Турция

² Департамент по хранителни технологии, Факултет по инженерство и природни науки, Университет в Гюмюшхане, TR-29100 Гюмюшхане, Турция

Постъпила на 9 декември, 2016 г.; приета на 26 май, 2017 г.

(Резюме)

В това изследване са изследвани химичния състав и анти-микробните свойства на сенциално масло от *Rhinanthus angustifolius* subsp. *grandiflorus*. Маслото е извлечено от всички органи на растението чрез дестилация с водна пара и е анализирано по методите GC-FID и GC-MS. Охарактеризирани са тридесет и един компонента представляващи 99.46% от общото количество масло. Главните компоненти са 2,3-дихидро-5-метил-1Н-инден (25.14%), α-кубебен (19.27%), 1-хексадекен (15.59%) and хексадеканова киселина (12.14%). Анти-микробната активност на изолираното есенциално масло е изпитана върху микроорганизмите *B. cereus*, *E. coli*, *E. coli* O157:H7 и *S. Aureus*. Освен това е определен и ефекта му върху ензимите на *B. cereus*, *E. coli*, *E. coli* O157:H7 и *S. Aureus*.

GC analysis in evaluation of changes in fatty acids content of selected fats during storage and heating

R. Kowalski^{1*}, G. Kowalska², U. Pankiewicz¹, M. Sujka¹, K. Kałwa¹

¹Department of Analysis and Evaluation of Food Quality, University of Life Sciences in Lublin, 8 Skromna Street, 20-704 Lublin, Poland

²Central Laboratory of Agroecology, University of Life Sciences in Lublin, Dobrzańskiego Street, 20-262 Lublin, Poland

Received October 5, 2016; Accepted July 27, 2017

The purpose of the paper was the comparison of quantitative changes in fatty acids composition in selected fats (soybean, sunflower, rapeseed, and olive oils, as well as margarine, butter and porcine lard) during their storage and heating. Comparison of quantitative analysis results expressed as absolute fatty acids amounts ($\text{g } 100 \text{ g}^{-1}$ – internal standard addition method) with their relative contents after summing up the analyzed components to 100% (internal normalization method), is presented. Experimental data revealed a great differentiation between quantitative results of particular fatty acids groups expressed as absolute amounts ($\text{g } 100 \text{ g}^{-1}$), and as percentages assuming that the sum of fatty acids in a sample was 100%. In general, the obtained results indicated that long-term storage at both ambient and elevated temperature led to a decrease in SFA, MUFA and PUFA contents ($\text{g } 100 \text{ g}^{-1}$ of sample) in the triacylglycerols fraction. Comparison of absolute and relative contents indicated that more credible results could be achieved only by means of analytical techniques based on internal standard addition or other analytically-equivalent methods that can give a full quantitative representation of the absolute amounts of substances tested.

Keywords: Fats, fatty acid methyl ester, gas chromatography, heating, quality, storage.

INTRODUCTION

Dietary fats are the most concentrated source of energy, fat-soluble vitamins and essential unsaturated fatty acids (UFA). They also build their own tissues and take part in the synthesis of some biologically active substances (eicosanoids), namely prostaglandins counted among tissue hormones.

Fatty acids contained in fats are oxidized in tissues, producing appropriate amounts of energy, or are utilized for building body components. Fatty acids are components of cellular membranes and cellular organelles affecting their permeability for nutrients that are transferred to human organism cells.

Plant oils are essential for human diet due to UFA content [1–8]. High level of unsaturation of fatty acids present in oils is required by nutritionists, and at the same time, it makes great problems for food technologists due to their higher susceptibility to oxidation. Oxidation processes in fats cause worsening of the sensory quality of food products and decrease their nutritional value; final products of these processes cause ageing of the organism, as well as take part in the etiology of such diseases as coronary vessels disturbances and tumors [9]. Moreover, hydrolysis and polymerization processes can occur during fat warming. Intensity of these

changes depends on temperature, time and way of heating. Polymerization is the most undesired conversion taking place during fat warming, namely long-term or repeated one. It was found that heating of plant-origin oils containing linoleic acid both in the air and under nitrogen atmosphere, besides dimers and polymers, also formed monomers of cyclic structure (which are counted to agents probably responsible for pathogenesis), and fatty acids of unidentified structure [10]. Products formed during the above mentioned transformations of fatty acids are stable and are not a typical triacylglycerols fraction of fatty acids that may be determined by means of GC technique after saponification and esterification.

There are many studies dealing with changes of fatty acids composition in stored or heated fats [11–17]. Unfortunately, they do not contain full quantitative evaluation of particular fatty acids in triacylglycerols, but only give their percentage assuming the sum in a fat to be 100%. Such quantitative evaluation leads to some result incorrectness, which is particularly apparent in the case of significant amounts of very durable oxidized or polymerized substances formed during fat storage or heating.

Therefore, the purpose of the paper was the analysis of quantitative changes in fatty acids composition in selected fats available on the market during their storage and heating. Moreover, a

* To whom all correspondence should be sent:
E-mail: radoslaw.kowalski@up.lublin.pl

relative comparison of quantitative analysis results expressed as absolute fatty acids amounts ($\text{g}/100 \text{ g}$ – internal normalization method) with their relative contents after totalling the analysed components to 100% (internal standard addition method), is presented in the paper.

EXPERIMENTAL

Fats

Selected fats of plant and animal origin, purchased in a store, were the material for study: soybean oil, sunflower oil, rapeseed oil, olive oil, margarine, butter, porcine lard. Aliquots of 20 g fats were placed in glass bulbs of 50 ml capacity, marked in accordance with Table 1, and then subjected to experimental factors action: heating in a thermostat at 120°C with long-term storage at various temperatures (-22°C in dark; +4°C in dark; ambient with daylight). Samples for analyses were taken from thermostatically processed fats after 120, 192, and 288 h of high-temperature action, and after 70 and 140 days of storage at -22°C, +4°C and ambient temperature.

Table 1. Samples designation

Sample	Sample
1	Raw oil – control
2	Fat heated at +120°C – 120 h
3	Fat heated at +120°C – 192 h
4	Fat heated at +120°C – 288 h
5	Fat stored at ambient temperature – 70 days
6	Fat stored at ambient temperature – 140 days
7	Fat stored at +4°C – 70 days
8	Fat stored at +4°C – 140 days
9	Fat stored at -25°C – 70 days
10	Fat stored at -25°C – 140 days

Analytical methods

Aliquots of 300 μl of heptadecanoic acid (Sigma) solution in hexane (10 mg ml^{-1}) were added to weighed samples of the fats (about 50 mg). Fat saponification and fatty acids esterification (with 14% methanolic solution of BF_3) was performed according to standards IUPAC-AOAC-963.22 [18] and AOAC 969.33 [19]. The quantitative composition of FAMES was determined by GC (FID). The quantitative analysis was performed on the basis of calibration curves for a FAMES standard mixture (C14 – C20) within the concentration range of 0.1 – 80.0 $\text{g}/100 \text{ g}^{-1}$ [20–22]. Water presence in the studied fats was taken into account in the obtained results.

Gas chromatography

GC was performed on a Unicam 610 Series gas chromatograph equipped with a flame-ionization

detector and a 60 m (0.25 mm i.d.) column coated with a 0.25 μm film of HP-23. A temperature gradient was applied (160°C for 1 min, then incremented by 2.75°C min^{-1} to 215°C, held at 215°C for 2 min, then incremented by 40°C min^{-1} to 230°C and held at 230°C for 2 min). The injection port and detector temperatures were 270°C; split ratio 1:50. Hydrogen was used as carrier gas at a flow rate of 43 m s^{-1} .

RESULTS AND DISCUSSION

Figs. 1–7 present the results of fatty acids contents in the examined fats during their storage and heating. Data in Table 2 reveal a great differentiation between the quantitative results of particular fatty acid groups presented as absolute amounts ($\text{g}/100 \text{ g}^{-1}$) and as percentages assuming that the sum of fatty acids in a sample was 100% (internal normalization method).

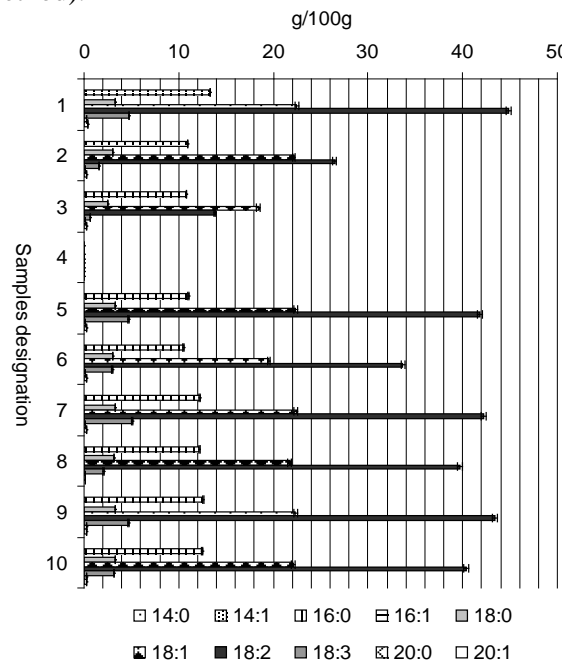


Fig. 1. Fatty acids contents in soybean oil stored under different conditions and heated at +120°C (designations as in Table 1). 14:0, myristic acid; 14:1, myristoleic acid; 16:0, palmitic acid; 16:1, palmitoleic acid; 18:0, stearic acid; 18:1, oleic acid; 18:2, linoleic acid; 18:3, α -linolenic acid; 20:0, arachidonic acid; 20:1, eicosenoic acid.

In general, the obtained results indicated that long-term storage at ambient temperature and heating led to a decrease in SFA, MUFA and PUFA contents ($\text{g}/100 \text{ g}^{-1}$ of sample) in the triacylglycerols fraction, which is probably associated with the increase in polymerized and oxidized forms levels at the absence of mass exchange between the experimental system and the surroundings – the weight of stored or heated fat remains constant.

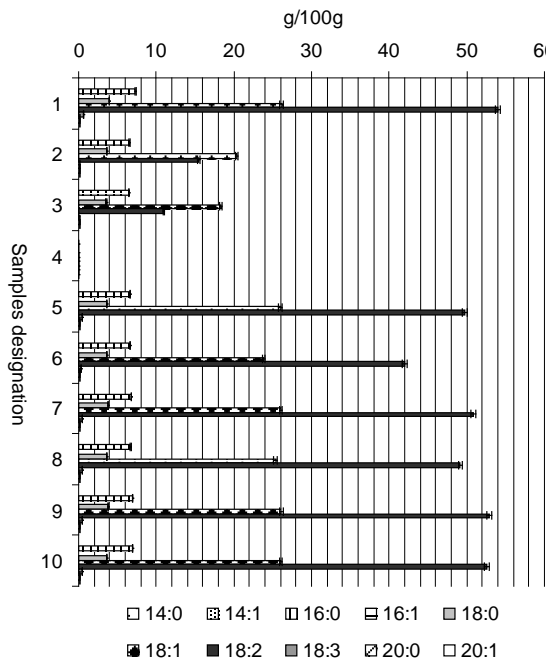


Fig. 2. Fatty acid contents in sunflower oil stored under different conditions and heated at +120°C (designations as in Table 1). 14:0, myristic acid; 14:1, myristoleic acid; 16:0, palmitic acid; 16:1, palmitoleic acid; 18:0, stearic acid; 18:1, oleic acid; 18:2, linoleic acid; 18:3, α -linolenic acid; 20:0, arachidonic acid; 20:1, eicosenoic acid.

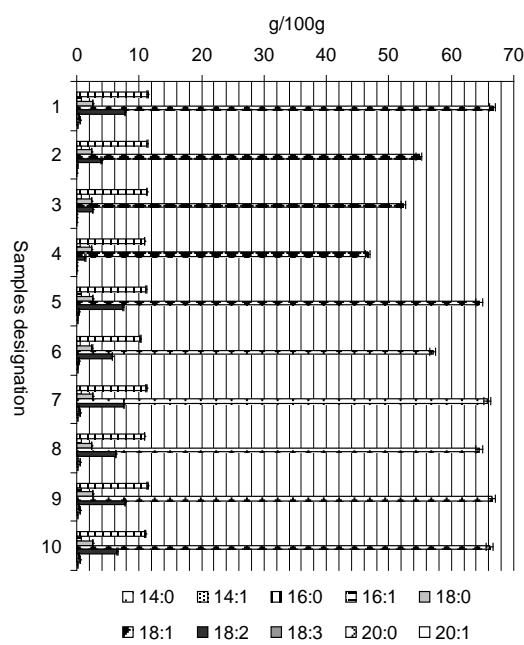


Fig. 4. Fatty acid contents in olive oil stored under different conditions and heated at +120°C (designations as in Table 1). 14:0, myristic acid; 14:1, myristoleic acid; 16:0, palmitic acid; 16:1, palmitoleic acid; 18:0, stearic acid; 18:1, oleic acid; 18:2, linoleic acid; 18:3, α -linolenic acid; 20:0, arachidonic acid; 20:1, eicosenoic acid.

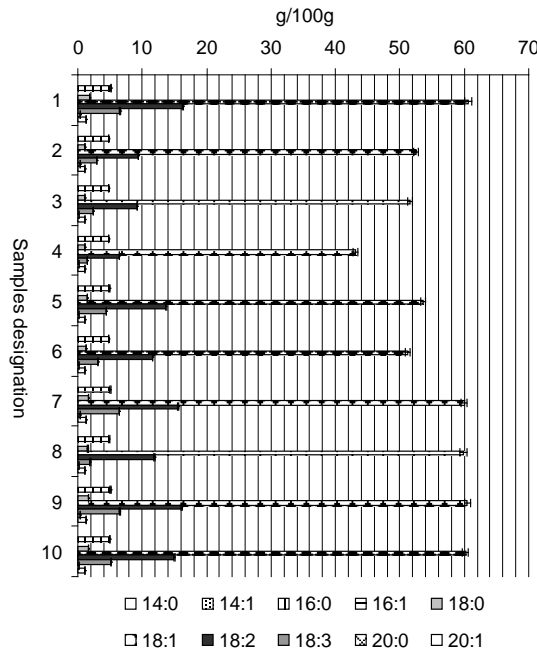


Fig. 3 Fatty acid contents in rapeseed oil stored under different conditions and heated at +120°C (designations as in Table 1). 14:0, myristic acid; 14:1, myristoleic acid; 16:0, palmitic acid; 16:1, palmitoleic acid; 18:0, stearic acid; 18:1, oleic acid; 18:2, linoleic acid; 18:3, α -linolenic acid; 20:0, arachidonic acid; 20:1, eicosenoic acid.

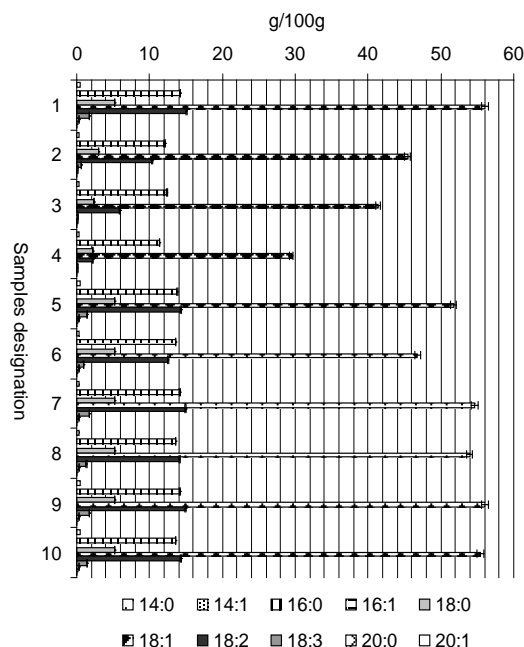


Fig. 5. Fatty acid contents in margarine stored under different conditions and heated at +120°C (designations as in Table 1). 14:0, myristic acid; 14:1, myristoleic acid; 16:0, palmitic acid; 16:1, palmitoleic acid; 18:0, stearic acid; 18:1, oleic acid; 18:2, linoleic acid; 18:3, α -linolenic acid; 20:0, arachidonic acid; 20:1, eicosenoic acid.

Data on above changes, expressed as a percentage of total fatty acids, indicate that the shares of SFA and MUFA increased, but PUFA percentage in fats shows a decreasing tendency due to experimental conditions.

Relative comparison of both data forms from Table 2 indicates that more credible information can be achieved in that type of experiment applying

analytical techniques based on internal standard addition or other analytically-equivalent methods. When interpreting the obtained results from quantitative analysis based on the assumption that the sum of fatty acids in the studied fraction is 100%, a major error is committed, because only semi-quantitative information on fatty acid profile in the studied sample can be obtained in this case.

Table 2. Changes in quantitative composition of particular fatty acids groups in fats stored under different conditions and heated at +120°C (designations as in Table 1). * - sample's state of matter resembling "gum-resin"

Fat	Sample	Fatty acid groups					
		SFA		MUFA		PUFA	
		g 100 g ⁻¹ of sample	Percentage	g 100 g ⁻¹ of sample	Percentage	g 100 g ⁻¹ of sample	Percentage
Soybean oil	1	16.88±0.15	18.89±0.17	22.81±0.30	25.55±0.33	49.57±0.55	55.53±0.61
	2	14.23±0.13	21.90±0.20	22.40±0.29	34.64±0.45	28.03±0.31	43.35±0.48
	3	13.48±0.12	28.76±0.26	18.61±0.24	40.00±0.52	14.43±0.16	31.02±0.34
	4	*	*	*	*	*	*
	5	14.48±0.13	17.28±0.16	22.57±0.29	27.00±0.35	46.55±0.51	55.68±0.61
	6	13.69±0.12	19.47±0.18	19.72±0.26	28.15±0.37	36.66±0.40	52.32±0.58
	7	14.71±0.13	17.35±0.16	22.64±0.29	26.75±0.35	47.27±0.52	55.86±0.61
	8	14.48±0.13	19.73±0.18	20.93±0.27	28.62±0.37	37.72±0.41	51.58±0.57
	9	15.12±0.14	17.56±0.18	22.66±0.29	26.37±0.34	48.13±0.53	56.03±0.62
	10	14.95±0.13	18.45±0.16	22.35±0.29	27.65±0.36	43.53±0.48	53.85±0.59
Sunflower oil	1	11.42±0.10	12.35±0.11	26.37±0.34	28.55±0.37	54.58±0.60	59.09±0.65
	2	10.40±0.09	22.17±0.20	20.52±0.27	44.13±0.57	15.58±0.17	33.51±0.37
	3	10.17±0.09	25.43±0.23	18.52±0.24	46.76±0.61	10.91±0.12	27.56±0.30
	4	*	*	*	*	*	*
	5	10.47±0.09	12.03±0.11	26.19±0.34	30.16±0.39	50.17±0.55	57.79±0.64
	6	10.38±0.09	13.47±0.12	24.06±0.31	31.32±0.41	42.37±0.47	55.16±0.61
	7	10.74±0.10	12.14±0.11	26.24±0.34	29.71±0.39	51.35±0.56	58.13±0.64
	8	10.51±0.09	13.35±0.12	24.35±0.32	31.02±0.40	43.62±0.48	55.58±0.61
	9	11.01±0.10	12.10±0.11	26.32±0.34	28.99±0.38	53.46±0.59	58.89±0.65
	10	10.82±0.10	11.98±0.11	26.24±0.34	29.10±0.38	53.11±0.58	58.90±0.65
Rapeseed oil	1	7.25±0.07	7.85±0.07	61.87±0.80	67.27±0.87	22.86±0.25	24.86±0.27
	2	6.22±0.06	8.50±0.08	53.64±0.70	74.26±0.97	12.37±0.14	17.13±0.19
	3	6.14±0.06	8.61±0.08	52.69±0.68	74.72±0.97	11.68±0.13	16.57±0.18
	4	6.08±0.05	10.32±0.09	44.18±0.57	75.99±0.99	7.88±0.09	13.55±0.15
	5	6.72±0.06	8.37±0.08	54.74±0.71	68.79±0.89	18.12±0.20	22.77±0.25
	6	6.27±0.06	8.49±0.08	52.22±0.68	71.26±0.93	14.79±0.16	20.18±0.22
	7	6.95±0.06	7.81±0.07	59.41±0.77	67.14±0.87	22.13±0.24	25.01±0.28
	8	6.57±0.06	8.27±0.07	58.65±0.76	74.16±0.96	13.87±0.15	17.54±0.19
	9	7.02±0.06	7.74±0.07	60.56±0.79	67.07±0.87	22.72±0.25	25.17±0.28
	10	6.81±0.06	7.89±0.07	59.01±0.77	68.70±0.89	20.08±0.22	23.38±0.26
Olive oil	1	14.53±0.13	16.04±0.14	67.64±0.88	74.92±0.97	8.11±0.09	8.98±0.10
	2	13.79±0.12	18.78±0.17	55.56±0.72	75.65±0.99	4.09±0.04	5.57±0.06
	3	13.66±0.12	19.74±0.18	53.01±0.69	76.59±1.02	2.54±0.03	3.67±0.04
	4	13.32±0.12	21.52±0.19	47.21±0.61	76.26±0.99	1.38±0.02	2.22±0.02
	5	13.94±0.13	15.95±0.14	65.34±0.85	74.96±0.97	7.89±0.09	9.05±0.10
	6	12.98±0.12	16.80±0.15	57.88±0.75	75.27±0.98	6.04±0.07	7.85±0.09
	7	14.19±0.13	16.13±0.15	65.44±0.85	74.73±0.97	7.94±0.09	9.07±0.10
	8	13.74±0.12	16.44±0.16	62.92±0.82	75.73±1.00	6.42±0.07	7.73±0.09
	9	14.39±0.13	15.92±0.15	67.50±0.88	74.94±1.02	8.18±0.09	9.09±0.10
	10	13.97±0.13	16.05±0.16	65.82±0.86	75.97±1.01	6.85±0.08	7.91±0.09

Table 2. Continued

Fat	Samples	Fatty acid groups					
		SFA		MUFA		PUFA	
		g 100 g ⁻¹ of sample	Percentage	g 100 g ⁻¹ of sample	Percentage	g 100 g ⁻¹ of sample	Percentage
Margarine	1	20.21±0.18	21.72±0.20	56.02±0.73	60.26±0.78	16.73±0.18	18.00±0.20
	2	15.64±0.14	21.77±0.20	45.43±0.59	63.39±0.82	10.95±0.12	15.28±0.17
	3	15.14±0.14	24.30±0.22	41.31±0.54	66.49±0.86	6.04±0.07	9.72±0.11
	4	14.01±0.13	30.65±0.28	29.52±0.38	64.99±0.84	2.19±0.02	4.82±0.05
	5	19.76±0.18	22.73±0.20	51.76±0.67	59.65±0.78	15.68±0.17	18.07±0.20
	6	19.45±0.18	24.45±0.22	46.79±0.61	58.99±0.77	13.46±0.15	16.97±0.19
	7	20.08±0.18	22.68±0.20	52.06±0.68	58.92±0.77	16.61±0.18	18.80±0.21
	8	19.44±0.17	22.72±0.20	50.90±0.51	59.59±0.75	15.47±0.17	18.11±0.20
	9	20.14±0.18	22.53±0.20	52.87±0.41	59.24±0.76	16.66±0.18	18.67±0.21
	10	19.55±0.18	22.40±0.20	52.26±0.39	60.00±0.80	15.70±0.17	18.03±0.20
Butter	1	46.75±0.42	51.37±0.46	39.24±0.33	43.13±0.56	4.99±0.05	5.48±0.06
	2	41.82±0.38	54.56±0.49	31.58±0.46	41.24±0.54	3.17±0.03	4.14±0.05
	3	38.11±0.34	53.73±0.48	30.24±0.41	42.69±0.55	2.49±0.03	3.51±0.04
	4	38.32±0.34	58.92±0.53	25.72±0.41	39.60±0.51	0.92±0.01	1.41±0.02
	5	34.64±0.31	47.07±0.42	35.36±0.39	48.10±0.63	3.52±0.04	4.78±0.05
	6	33.15±0.30	48.78±0.44	31.39±0.48	46.25±0.60	3.33±0.04	4.90±0.05
	7	45.62±0.41	56.00±0.50	31.22±0.46	38.35±0.50	4.56±0.05	5.60±0.06
	8	44.94±0.40	56.94±0.51	30.28±0.53	38.39±0.50	3.64±0.04	4.62±0.05
	9	46.37±0.42	52.65±0.47	36.73±0.48	41.73±0.54	4.93±0.05	5.60±0.06
	10	45.56±0.41	53.80±0.48	35.10±0.46	41.48±0.54	3.97±0.04	4.69±0.05
Porcine lard	1	40.51±0.36	44.56±0.40	40.86±0.53	44.97±0.58	9.49±0.10	10.45±0.11
	2	33.73±0.30	45.79±0.41	37.08±0.48	50.39±0.66	2.78±0.03	3.77±0.04
	3	32.89±0.30	48.51±0.44	33.13±0.43	48.92±0.64	1.71±0.02	2.52±0.03
	4	26.41±0.24	47.53±0.43	28.07±0.36	50.60±0.66	0.99±0.01	1.79±0.02
	5	37.11±0.33	43.58±0.39	39.23±0.51	46.10±0.60	8.75±0.10	10.28±0.11
	6	34.21±0.31	46.04±0.41	33.00±0.43	44.46±0.58	7.01±0.08	9.44±0.10
	7	36.32±0.33	42.26±0.38	40.74±0.53	47.43±0.62	8.82±0.10	10.27±0.11
	8	35.90±0.32	45.19±0.41	35.88±0.47	45.21±0.59	7.58±0.08	9.55±0.11
	9	39.84±0.36	44.32±0.40	40.59±0.53	45.17±0.59	9.42±0.10	10.48±0.12
	10	37.71±0.34	43.57±0.39	39.90±0.52	46.12±0.60	8.89±0.10	10.28±0.11

Such analytical procedure is correct only in routine qualitative evaluation, but it has to take into account other parameters, i.e. color, acidic number, peroxide number, anisidine number, Totox index or oil oxidation stability determined by means of Rancimat test. It should be underlined that the above mentioned parameters not always can characterize the utilization value of a fat. Flaczyk *et al.* [23] and Wroniak *et al.* [24] did not find direct influences of the peroxide content in the studied oils on their oxidation stability. Despite the very high Totox index for olive oil and sunflower oil, those fats were characterized by the highest oxidation stability in the Rancimat test. Therefore, the quantitative analysis by means of GC technique with internal standard and calibration in temperature and storage tests is much simpler and faster, and it supplies more detailed information on the changes in the studied fat composition. However, GC method with internal

standard may seem insufficient in routine qualitative evaluation of single fat samples, because there are no reference norms (what levels of fatty acids are desirable for a given product). Thus, in that case, the qualitative and quantitative composition of fresh and stored oils, as well as oils subjected to various thermal processing operations should be determined. It should also be underlined that a proper selection of internal standard or standards, reference material (certified mixture of triacylglycerols) along with validation of the whole analysis is necessary in such procedures. That type of evaluation could be a basis for determining the limiting values for particular fatty acids, which would serve for routine qualitative analysis of various fats.

The experiment revealed that the least changes were found in samples stored at -25°C and +4°C, which depended on the storage time. The most apparent changes in fatty acids contents were

recorded in samples stored at ambient temperature. Fats heated in a thermostat at +120°C were characterized by a dynamic decrease in fatty acids concentrations. Oils containing polyunsaturated fatty acids (sunflower

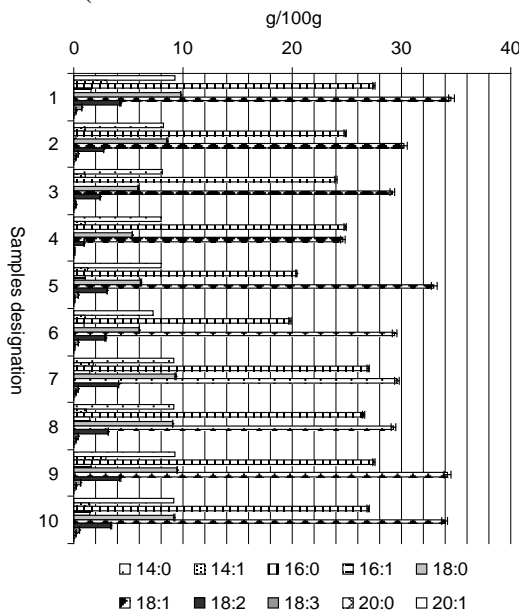


Fig. 6. Fatty acid contents in butter stored under different conditions and heated at +120°C (designations as in Table 1). 14:0, myristic acid; 14:1, myristoleic acid; 16:0, palmitic acid; 16:1, palmitoleic acid; 18:0, stearic acid; 18:1, oleic acid; 18:2, linoleic acid; 18:3, α -linolenic acid; 20:0, arachidonic acid; 20:1, eicosenoic acid.

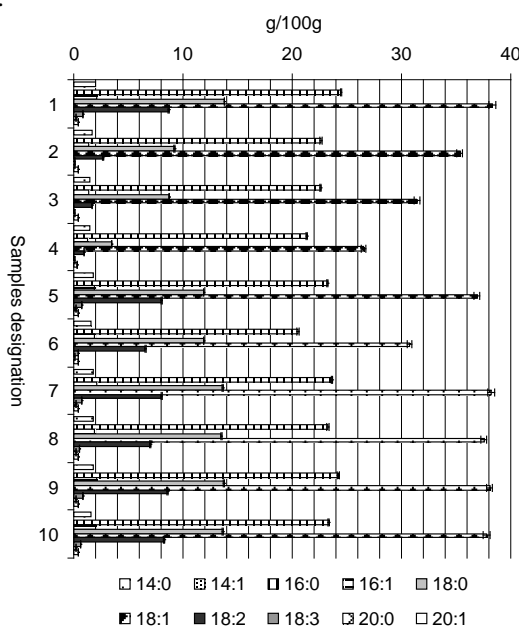


Fig. 7. Fatty acid contents in porcine lard stored under different conditions and heated at +120°C (designations as in Table 1). 14:0, myristic acid; 14:1, myristoleic acid; 16:0, palmitic acid; 16:1, palmitoleic acid; 18:0, stearic acid; 18:1, oleic acid; 18:2, linoleic acid; 18:3, α -linolenic acid; 20:0, arachidonic acid; 20:1, eicosenoic acid.

and soybean oils) were particularly susceptible to high-temperature effects: losses of fatty acids contents were respectively about 53% and about 43% after 192 h of heating. Intensive oxidation of these oils, resulting in conversion of the oils into liquids with very high viscosity, like resin, took place after 288 h of samples treatment at high temperature. Besbes *et al.* [14] found that palm oil heated at 120°C for 48 h had significantly higher viscosity than unheated one, which was undoubtedly affected by polymerization and formation of high-molecular-weight compounds including carbon–carbon and carbon–oxygen–carbon bridges between fatty acids [25, 26].

As follows from the data in Figs. 1–7 related to the high temperature treatment, the most positive composition of fatty acids was recorded in butter, with loss of fatty acids at about 26.0% after 288 h of heating; in olive oil with loss of about 28.4%; in rapeseed oil with loss of about 33.8%; and in porcine lard with loss of about 35.4% after 288 h of heating. Margarine was characterized by about 47.5% decrease in fatty acids concentration after 288-h heating.

The obtained results confirm the fact that among others, the fatty acid composition and the presence of additional substances (water) and natural antioxidants (phenolic compounds, tocopherols, squalen) determine fat's stability [27–29]. It is well known that fats rich in saturated fatty acids (animal-origin fats) are a group that is best resistant to oxidation, whereas plant-origin oils containing a high percentage of oleinic acid (one double bond) are good for frying, because they are not so susceptible to oxidation as sunflower or soybean oils (rich in linoleic acid) [30].

Summarizing, the GC technique with internal standard is suitable for evaluation of the quantitative changes occurring in fatty acids of fats being heated and stored. Furthermore, introducing that method as an alternative in fast qualitative assessment of edible fats is proposed after working out the detailed reference norms, which is going to be the subject of a further study.

CONCLUSIONS

- Results indicate that the semi-quantitative GC method giving only the percentage of particular fatty acids assuming that their sum is 100%, does not supply correct information for evaluation of changes occurring in stored and heated fats.

- It was found that the GC method with internal standard is appropriate for assessing the quantitative changes in fatty acids in heated and stored fats.

REFERENCES

1. A. Christophe, Effects of feeding a supplement of γ -linolenic acid containing oils with fish oil on the fatty acid composition of serum phospholipids in healthy volunteers. In: Huang YS, Mills DE (eds.) γ -Linolenic acid, metabolism and its roles in nutrition and medicin. AOCS Press. Champaign, IL, 1996, p. 168.
2. J. C. Philips, Y. S. Huang, Natural sources and biosynthesis of γ -linolenic acid: an overview. In: Huang YS, Mills DE (eds.) γ -Linolenic acid, metabolism and its roles in nutrition and medicin. AOCS Press. Champaign, IL, 1996, p. 1.
3. H. J. Wille, J. Wang, Enzymatic enrichment of γ -linolenic acid from black currant seed oil. In: Huang YS, Mills DE (eds.) γ -Linolenic acid, metabolism and its roles in nutrition and medicin. AOCS Press. Champaign, IL, 1996, p. 33.
4. M. Markrides, R. A. Gibson, Are long-chain polyunsaturated fatty acids essential nutrients in infancy? In: Riemersma RA, Armstrong R, Kelly RW, Wilson R (eds.) Essential fatty acids and eicosanoids. AOCS Press. Champaign, IL, 1998, p. 136.
5. H. Okuyama, M. Z. Huang, M. Miyazaki, S. Watanabe, T. Kobayashi, A. Nagatsu, J. Sakakibara, Two factors in fats and oils that affect survival time of Stroke-Prone spontaneously hypertensive rats: n – 6/n – 3 ratio and minor components. In: Riemersma RA, Armstrong R, Kelly RW, Wilson R (eds) Essential fatty acids and eicosanoids. AOCS Press. Champaign, IL, 1998, p. 273.
6. W. Rafflenbeul, *Eur. J. Lipid Sci. Tech.* **103**, 315 (2001).
7. A. Kammel-Eldin, N. V. Yanishlieva, *Eur. J. Lipid Sci. Tech.* **104**, 825 (2002).
8. V. A. Ziboh, Y. H. Cho, I. Mani, S. D. Xi, *Arch. Pharm. Res.* **25**, 747 (2002).
9. I. F. F. Benzie, *Int. J. Food Sci. Nutr.* **47**, 233 (1996).
10. Š. Ziemiański, *Żyw. Człow. i Metabol.*, **24(2)**, 35 (1997).
11. A. I. Méndez, E. Falqué, *Food Control*, **18**, 521 (2007).
12. J. A. Pereira, S. Casal, A. Bento, M. B. P. P. Oliveira, *J. Agr. Food Chem.*, **50**, 6335 (2002).
13. J. R. Morelló, M. J. Motilva, M. J. Tovar, M. P. Romero, *Food Chem.*, **85**, 357, (2004).
14. S. Besbes, C. Blecker, C. Deroanne, G. Lognay, N. E. Drira, H. Attia, *Food Chem.*, **91** 469 (2005).
15. M. R. Ramírez, R. Cava, *LWT-Food Sci. Tech.* **38**, 726 (2005).
16. M. R. Ramírez, D. Morcuende, M. Estévez, R. C. López, *Food Chem.* **92**, 159 (2005).
17. K. Stránský, M. Zarevúcka, Z. Wimmer, *Food Chem.* **92**, 569 (2005).
18. AOAC 963.22 Methyl esters of fatty acids in oils and fats, in Official Methods of Analysis of the AOAC, 17th ed., AOAC International Arlington-Virginia USA, 2000.
19. AOAC 969.33 Fatty acids in oils and fats, in Official Methods of Analysis of the AOAC, 17th ed., AOAC International Arlington-Virginia USA, 2000.
20. R. Kowalski, *Acta Chromatogr.* **18**: 15 (2007).
21. R. Kowalski, *Food Chem.*, **112**, 820 (2009).
22. R. Kowalski, *J. Food Qual.*, **33**, 269 (2010).
23. E. Flaczyk, M. Rudzińska, D. Górecka, B. Szczepaniak, S. Klimczak, J. Korczak, *Rośl. Oleiste–Oilseed Crops* **25**, 213 (2004).
24. M. Wroniak, M. Kwiatkowska, K. Krygier, *Żyw. Nauka Tech. Jakość* **2(47)**, 46 (2006).
25. U. Bracco, A. Dieffenbacher, L. Kolarovic, *J. Amer. Oil Chem. Soc.* **58**, 6 (1981).
26. S. G. Stevenson, M. Vaisey-Genser, N. A. Eskin, J. *Amer. Oil Chem. Soc.* **61**, 1102 (1984).
27. A. Koski, E. Psomiadou, M. Tsimidou, A. Hopia, P. Kefalas, K. Wähälä, M. Heinonen *Eur. Food Res. Technol.* **214**, 294 (2002).
28. M. Matuszewska, M. Wroniak, M. W. Obiedziński, K. Krygier, *Thuszcze Jadaj.*, **35(3–4)**, 77 (2000).
29. E. Szukalska, Selected issues of fat oxidation. *Thuszcze Jadaj.*, **38**, 42 (2003).
30. P. Moszczyński, *Zdrowa Żywn.* **64(2)**, 4 (2004).

ГАЗ-ХРОМАТОГРАФСКИ АНАЛИЗ ПРИ ОПРЕДЕЛЯНЕТО НА ИЗМЕНЕНИЯТА В СЪДЪРЖАНИЕТО НА МАСТНИ КИСЕЛИНИ В ИЗБРАНИ МАЗНИНИ ПО ВРЕМЕ НА СЪХРАНЕНИЕ И НАГРЯВАНЕ

Р. Ковалски^{1*}, Г. Ковалска², У. Панкиевич¹, М. Суйка¹, К. Калва¹

¹Департамент по анализ и оценка на качеството на храните, Университет за науките на живота, 20-704 Люблин, Полша

²Централна лаборатория по агроекология, Университет за науките на живота, 20-262 Люблин, Полша

Постъпила на 5 октомври, 2016 г.; приета на 27 юли, 2017 г.

(Резюме)

Целта на настоящата работа е сравнението на количествените промени в състава на мастни киселини в избрани мазнини (от соя, слънчоглед, рапица, зехтин, както и маргарин, масло и свинска мас) при тяхното съхранение и нагряване. Сравнението е като абсолютни количества ($g\ 100\ g^{-1}$ по метода на стандартната добавка) с тяхните относителни количества след сумиране на анализираните компоненти към 100% (вътрешен метод на нормализация). Експерименталните данни разкриват големи разлики между количествените резултати за определени групи киселини ($g\ 100\ g^{-1}$) и като процентно съдържание. Общо взето, получените резултати показват, че дългосрочното съхраняване при стайна или повишена температура води до намаляване на съдържанието на насытени (SFA) и ненаситени (MUFA и PUFA) ($g\ 100\ g^{-1}$ проба) във фракцията от триглицеридите. Сравнението на абсолютни и относителни съдържания показва, че по-достоверни резултати може да се постигнат само при използването на аналитична техника, основана на вътрешната стандартна добавка или други еквивалентни методи, даващи пълно количествено представяне на абсолютните количества.

Preparation of modified diatomite filler *via* a starch-fatty acid complex coating method for improvement of paper strength properties

W. Shang^{1,2}, X. Qian^{1*}, H. Liang²

¹ Key Laboratory of Bio-based Material Science and Technology of Ministry of Education, Material Science and Engineering College, Northeast Forestry University, Harbin 150040, China.

² College of Chemistry Engineering, Northeast Electric Power University, Jilin 132012, China.

Received 24 August, 2017, Revised November 15, 2017

In this work, diatomite particles were modified to improve the bondability of diatomite particles with pulp fibers *via* a starch-fatty acid complex coating method. The SEM results illustrated that the surface of the modified diatomite particles was covered by the complex coatings. The coating efficiency of the starch-fatty acid complex on diatomite surface was up to 98%. Modified diatomite had good shear resistance. Compared with the handsheet filled unmodified diatomite, the handsheet filled with modified diatomite had higher strength properties and smaller bulk. The higher zeta potential and larger particle size of modified diatomite were responsible for the higher retention of modified diatomite filler. This work provided a technical support for the application of diatomite as a novel papermaking filler.

Key words: Starch-fatty acid complex; Modified diatomite; Paper; Strength properties

INTRODUCTION

It has been a long history of using mineral fillers in paper industry. Many kinds of mineral fillers have been used, such as kaolin, calcium carbonate, talcum powder and titanium dioxide [1–5]. The application of fillers in paper industry is an active area of research and development [1–3]. Papermakers expect that higher filler content in the paper would improve the cost competitiveness of paper products. The increase of filler content in paper can reduce the energy demand and improve the optical and printing properties of paper [2–6]. Over the past few decades, all of the above improvements provide considerable benefits for paper industry [7–11].

Fillers are second only to pulp fibers as raw materials in paper industry. However, the use of fillers has a negative impact on the strength properties of the paper, especially at high filler addition levels [13–17]. One of the prominent problems in the use of fillers is that some strength properties of paper such as tensile, tear, folding, and stiffness usually decrease with the increase in filler addition level [2,18–25]. These adverse effects are due to the fact that fillers interfere with the hydrogen bonding of fibers, thereby reducing the physical properties of paper [2,30].

Because of the above mentioned adverse effects, researchers have developed some techniques to overcome these shortcomings [7,19–22]. Many methods have been experimented, including filler preflocculation, [3,4,8] synthesis of fillers with various structures and functions [9–12], surface modification, lumen loading [10–18], and composite fillers. In recent years, filler modification has been an active area of research, because it has the potential to significantly increase the content of filler in the paper [23–26]. The surface modification of the filler for improving the hydrogen bonding between fibers has attracted more and more attention.

It has been reported that starch is suitable for surface modification of papermaking fillers because its chemical structure is similar to that of cellulose. Starch is often used as a dry additive to increase the bonding strength between fibers [19–21]. Starch can be attached to the filler surface in order to improve the bondability between fillers and fibers, and thereby to enhance paper strength. It has been widely used for the modification of clay and calcium carbonate fillers [22–30]. Yoon and Deng prepared a new clay–starch composite filler and claimed more than 100% increase in the tensile strength of the paper at a high addition level [22,23,29,33]. Zhao *et al.* prepared a starch-modified filler by spray drying and evaluated this technology at pilot or full scale [30,34].

Diatomite is a low-cost, environmentally friendly and natural micro/nanostructured material

* To whom all correspondence should be sent:
E-mail: qianxueren@aliyun.com

derived from sedimentary silica, and has cylindrical and plate morphology with well-developed mesoporous and/or macroporous structure [31]. The use of diatomite as a novel papermaking filler is low, but it has become an increasingly important research area. Compared with traditional papermaking fillers, diatomite as a kind of novel papermaking filler has many advantages, such as light weight, high porosity, low wire wear and good adaptability. It is very interesting and important to study whether starch can be used to modify diatomite for improving the strength properties of paper.

In this work, diatomite particles were modified *via* a starch-fatty acid complex coating method. The basic characteristics of the modified diatomite particles including coating efficiency, particle size, ζ potential and shear resistance were evaluated. Meanwhile, the effect of modified diatomite filler on handsheet strength properties and filler retention was investigated.

EXPERIMENTAL

Materials

Analytical methods

Diatomite filler was provided by Hongyuan Co., China. Palmitic acid was purchased from Damao Co., China. Cationic polyacrylamide (Percol 182) was supplied by BASF (China) Co. Bleached hardwood kraft pulp board was supplied by Mudanjiang Hengfeng Paper Co., China. The pulp board was beaten to a beating degree of 45 °SR in a Valley beater. Raw corn starch was supplied by Ruixing Group Co., China.

Preparation of starch-fatty acid complex modified diatomite

Diatomite particles were modified using a starch-fatty acid complex coating method. Raw corn starch suspension (3%) was cooked at 90 °C for 1 h, and then the pH of the cooked starch solution was adjusted to 11 using 0.3 mol/L sodium hydroxide solution. Subsequently, a certain amount of palmitic acid (on the basis of starch) was added to the cooked starch solution and further cooked at 90 °C for 30 min, to form a mixture of palmitic acid and starch. Dry diatomite particles were put into a 500 mL beaker, and then a certain amount of deionized water was added to the beaker, to form a diatomite slurry with a concentration of 150 g/L. The diatomite slurry was dispersed by mixing with a stirrer for 10 min, and then the mixture of palmitic acid and starch was added to the diatomite slurry

and stirred for 10 min. The above mixture was poured into a twofold volume of hydrochloric acid solution with a pH of 2, and kept at room temperature for 3 h. The supernatant was collected to measure the total organic carbon (TOC), and the precipitate was washed with deionized water until neutral. Finally, the resultant precipitates were dried at 90 °C for about 3 h. Starch-fatty acid modified diatomite samples with different starch/diatomite ratios were obtained by the above preparation procedure.

Characterization of filler

The surface morphology of the filler was observed by a JSM6510A scanning electron microscope (SEM). The sample was coated with gold before observation.

The ζ potential of the diatomite filler was analyzed using Malvern Zetasizer 3000.

The coating efficiency (CE, %) of the starch-fatty acid complex on the diatomite surface was evaluated by the content of total organic carbon (TOC) in the supernatant determined by a TOC analyzer (Liqui TOC). CE was calculated by the following formula:

$$CE (\%) = [(W_i - W_d)/W_i] \times 100 \quad (1)$$

where, W_i and W_d (g) are the weights of the initial starch-fatty acid complex and the starch-fatty acid complex dissolved in the supernatant, respectively.

The particle size of the filler was analyzed by a particle size analyzer (OMEC LS-POP). After the filler suspension was well dispersed, the particle size was measured.

The shear resistance of the modified diatomite was evaluated by the following method. The modified diatomite suspension was mechanically stirred with an OA2500 stirrer at two stirring speeds (1000 rpm for 70 min and 2000 rpm after 70 min). One sample was taken every 10 min and the particle size was measured with the particle size analyzer.

Preparation of handsheets and determination of physical properties

Different dosages of unmodified or modified diatomite filler and 0.04 wt% (on the basis of filler) of Percol-182 used as retention aid were added to 1% bleached hardwood kraft pulp suspension. After adding retention aid and filler the slurry was stirred for 25 s, the handsheet with a target grammage of 150 g/m² was prepared with a ZQJ1-B handsheet former. All handsheets were dried at 105 °C for 15 min on a sheet dryer. The handsheets were then conditioned at 50±2% RH and 23±1 °C overnight.

Physical properties of the handsheets were determined according to TAPPI Test Methods.

Determination of filler retention in handsheets

The content of ash in handsheets was measured by ashing in a muffle furnace at 575 ± 25 °C for 6 h. The filler retention (FR , %) was calculated by the following formula:

$$FR (\%) = [W_a / (A \times W_f)] \times 100 \quad (2)$$

where, W_a (g) is the weight of ash in the handsheets, and W_f (g) is the weight of the filler added. A is the weight fraction of diatomite in the filler. The value of A is equal to 1 for unmodified filler.

RESULTS AND DISCUSSION

When starch is gelatinized in the presence of fatty acid, the amylose from the starch granules forms a helical inclusion complex with the fatty acid [32]. The complex of starch-fatty acid can be dissolved in alkali aqueous solution. After adding the slurry of diatomite to the complex, diatomite particles are fully mixed with the complex. When the mixture is poured into hydrochloric acid solution with pH of 2, the starch-fatty acid complex precipitates. Thus, the precipitated starch-fatty acid complex is *in situ* coated individual diatomite particles or diatomite aggregates, and hence a modified diatomite filler is obtained.

The surface morphology of unmodified and modified diatomite filler particles was observed by SEM, and the images are shown in Figure 1. Unmodified diatomite had numerous micropores on the surface (Figure 1a), but the surface of modified diatomite was fully covered and no micropores were visible (Figure 1b), which illustrated that the surface of modified diatomite was coated by the starch-fatty acid complex.

The retention and flocculation of the diatomite filler in pulp fiber networks are affected by the ζ potential of the diatomite particles. In this work, the ζ potentials of unmodified and starch-fatty acid complex modified diatomite fillers with different dosages of fatty acid were measured, and the results are shown in Table 1. The ζ potential of unmodified diatomite is -63.12 mV. However, the ζ potential increased after the diatomite was modified with the starch-fatty acid complex. Furthermore, the ζ potential increased with the increase in fatty acid dosage.

For instance, the ζ potential of modified diatomite was -45.26 mV at a fatty acid dosage of 5%, and the ζ potential increased to -10.13 mV

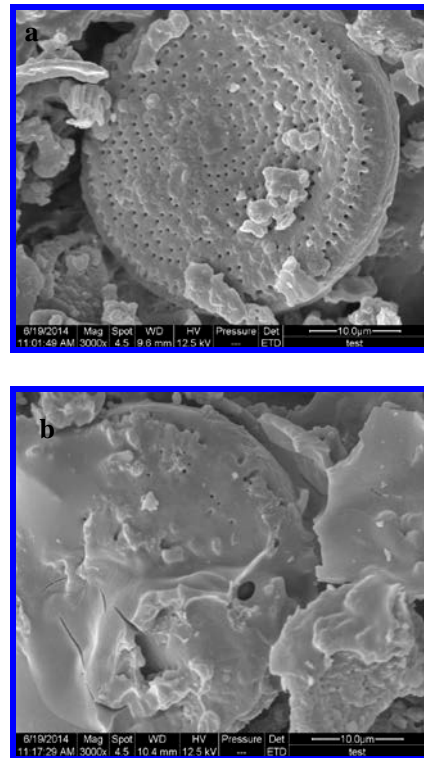


Fig. 1. SEM images of unmodified (a) modified (b) diatomite filler.

Table 1. ζ Potential of starch-fatty acid complex modified diatomite filler

Sample no.	Condition	ζ Potential (mV)
1	Unmodified diatomite	-63.12
2	Starch: diatomite, 1:4; fatty acid, 5%	-45.26
3	Starch: diatomite, 1:4; fatty acid, 10%	-22.28
4	Starch: diatomite, 1:4; fatty acid, 20%	-10.13
5	Starch: diatomite, 1:8; fatty acid, 10%	-24.36
6	Starch-fatty acid complex (fatty acid, 10%)	-7.52

when fatty acid dosage was 20%. It is primarily because the high ζ potential (-7.52 mV) of the starch-fatty acid complex can significantly contribute to the increase of the ζ potential of the modified diatomite. Because the ζ potential of the starch-fatty acid complex was far higher than that of diatomite, the ζ potential increased when diatomite was coated with starch-fatty acid complex.

For modified diatomite, it is very important to effectively utilize the starch-fatty acid complex. If the utilization efficiency of the starch-fatty acid complex is low, no good coating could be formed on the surface of diatomite. In this research, the CE

of the starch-fatty acid complex on the surface of diatomite was measured, and the results are shown in Table 2. It was found that about 98% of the starch-fatty acid complex was coated on the surface of diatomite. Fatty acid dosage had almost no effect on *CE*, which revealed that 5% fatty acid was enough to effectively utilize the starch-fatty acid complex. Filler particle size is very important because it affects filler retention and paper physical properties. The particle size of unmodified diatomite was about 5.5 μm , but the size increased to 10–20 μm after modification. The shear resistance of the filler directly affects the particle size of the filler.

Table 2. *CE* of starch-fatty acid complex on the surface of diatomite

Sample no.	Condition	TOC (ppm)	<i>CE</i> (%)
	Fatty acid (%)		
Starch:	Diatomite		
1	1:4	5	61.25 98.02
2	1:4	10	59.42 97.97
3	1:4	15	58.35 97.89
4	1:4	20	57.15 97.80
5	1:8	10	57.52 98.03

The shear resistance of modified diatomite is very important for its application, because the filler must pass through a high-shear zone in papermaking system. Therefore, it is necessary to study the shear resistance of modified diatomite. The change of the size of modified diatomite with stirring time is shown in Figure 2. The particle size of modified diatomite was kept unchanged for 70 min at a stirring speed of 1000 rpm. For the filler of modified diatomite with a low starch/diatomite ratio (less than 1:4), the particle size was only slightly decreased with prolonging stirring time after 70 min at a stirring speed of 2000 rpm. The results indicated that the starch-fatty acid complex modified diatomite filler had a high shear resistance.

The physical properties of filled handsheets are shown in Figures 3–5. All strength properties of handsheets decreased with increasing filler dosage, which is in agreement with the general knowledge about the influence of filler addition on handsheet strength properties. However, the strength properties of handsheets with modified diatomite filler were far higher than those of handsheets filled with unmodified diatomite at any filler addition level.

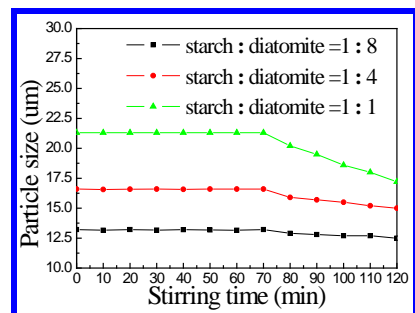


Fig. 2. Change in particle size of modified diatomite with stirring time. Note: the stirring speed is 1000 rpm for 70 min and it is 2000 rpm after 70 min. Fatty acid dosage is 10%.

Furthermore, the handsheets filled with modified diatomite with a higher starch/diatomite ratio had higher strength properties, especially for tensile and tearing strengths. This was because diatomite modified at a higher starch/diatomite ratio was coated with a larger amount of starch-fatty acid complex.

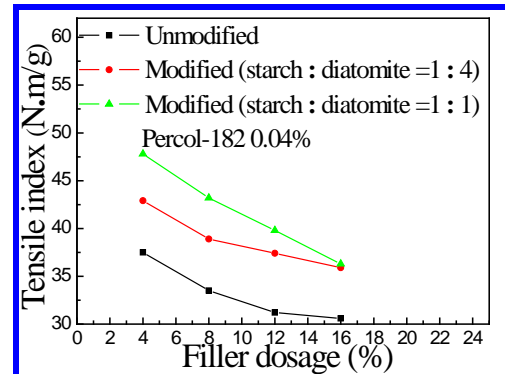


Fig. 3. Effect of filler dosage on the tensile index of filled handsheets.

The effect of filler addition level on the bulk of the handsheet is shown in Figure 6. The bulk of the handsheet increased with the increase of filler addition level. Meanwhile, the bulk of modified diatomite filled handsheet was lower than that of unmodified diatomite filled handsheet.

It indicated that the starch-fatty acid complex coatings on the surface of diatomite could improve the bondability of diatomite particles with pulp fibers. Generally, the smaller the bulk, the higher is the strength. Therefore, the bulk data were well in agreement with the strength data. All the above results indicated that starch-fatty acid complex modified diatomite can improve the strength properties of filled handsheets.

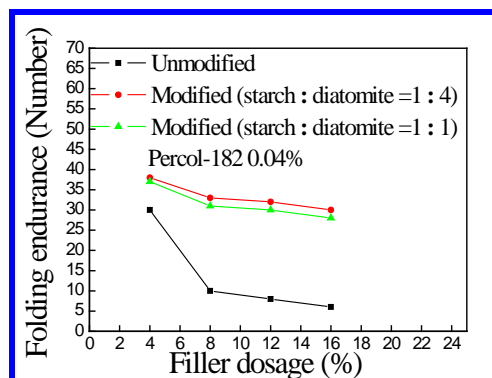


Fig. 4. Effect of filler dosage on the folding endurance of filled handsheets.

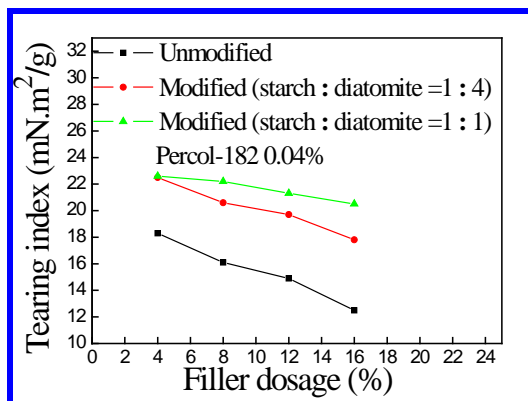


Fig. 5. Effect of filler dosage on the tearing index of filled handsheets.

The effect of filler dosage on filler retention is shown in Figure 7. The filler retention (*FR*) decreased with increasing filler dosage, which is in agreement with the general knowledge about the influence of filler addition level on *FR*. However, the *FR* of the modified diatomite filler was higher than that of the unmodified diatomite filler.

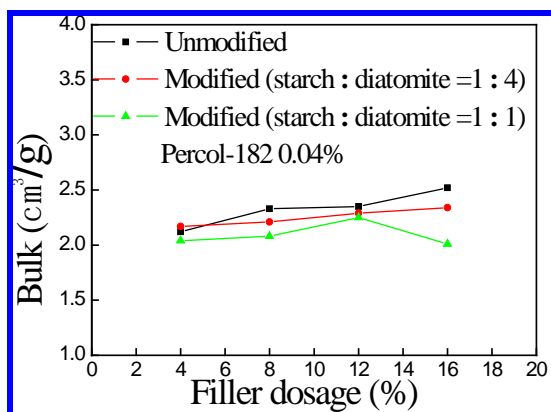


Fig. 6. Effect of filler dosage on the bulk of filled handsheets.

In addition, the *FR* of the modified diatomite filled handsheet was less affected by the filler addition level compared with the unmodified diatomite filled handsheet. It is primarily because that the particle size of starch-fatty acid complex modified diatomite was much larger than that of unmodified diatomite. Furthermore, as mentioned earlier, the modified diatomite has a higher ζ potential compared with the unmodified diatomite, which was also responsible for the high retention of modified diatomite.

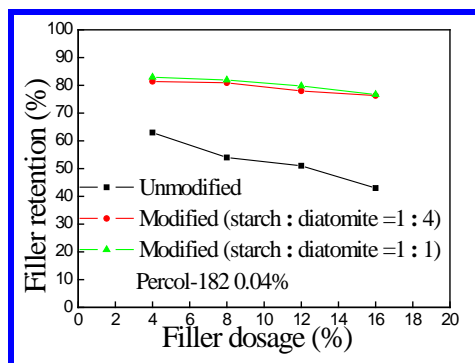


Fig. 7. Effect of filler dosage on filler retention.

CONCLUSION

Diatomite filler was successfully modified via a starch-fatty acid complex coating method. The SEM images showed that the surface of modified diatomite particles was covered by the complex of starch-fatty acid coatings. The coating efficiency (*CE*) was as high as 98%. The modified diatomite had larger particle size and higher ζ potential compared with the unmodified diatomite. The modified diatomite had good shear resistance. Compared with the handsheet filled with unmodified diatomite, the handsheet filled with modified diatomite displayed higher strength properties and smaller bulk. The retention of modified diatomite filler was higher than that of unmodified diatomite due to its larger particle size and higher ζ potential.

Acknowledgements: This work was financially supported from the Science and technology development project of Jilin Province and the Science and technology development project of Jilin City.

REFERENCES

- Y. Deng, P. Jones, L. McLain, J. A. Ragauskas, *Tappi J.*, **9**, 31 (2010).
- K. Koivunen, H. Alatalo, P. Silenius, *J. Mater., Sci.*, **45**, 3184 (2010).

3. S. Li , S. Wang, *Journal Of Northeast Dianli University*, **03**, 69 (2016).
4. V. S. Chauhan, N. K. Bhardwaj, *Tappi J.*, **13**, 17 (2014).
5. S. W. Mabee, R. Harvey, *Proceedings of TAPPI Papermakers Conference, Vancouver, BC, Canada, April*, 2000.
6. J. Shen, Z. Song, X. Qian, *BioResources*, **4**, 1190 (2009).
7. L. Liu, Y. Huang, K. Lu, *Journal Of Northeast Dianli University*, **06**, 95 (2015).
8. S. W. Mabee, *Proceedings of TAPPI Papermakers Conference, Cincinnati, OH, USA, March* (2001).
9. H. Yang, L. Qiu, X. Qian, J. Shen, *BioResources*, **8**, 5449 (2013).
10. S. Song, M. Zhang, Z. He, J. Z. Li, Y. Ni, *Ind. Eng. Chem. Res.*, **51**, 16377 (2012).
11. S. C. Vipul, K. B. Nishi, *Ind. Eng. Chem. Res.*, **53**, 11622 (2014).
12. Y. Zhang, J. Li, W. Li, *RSC Adv.*, **5**, 85673 (2015).
13. R. Juuso, D. M. Katarina, K. Jonna, C. M. Thad, *Cellulose*, **22**, 4003 (2015).
14. J. Fan, Y. Cao, T. Li, J. Li, X. Qian, J. Shen, *ACS Sustain Chem Eng.*, **3**, 1866 (2015).
15. Y. Deng, S. Y. Yoon, J. A. Ragauskas, *US Patent No. US2008/087396 A1*, (2008).
16. X. Huang, X. Qian,; J. Li, S. Lou, J. Shen, *Carbohydrate Polymers*, **117**, 78 (2015).
17. X. Huang, J. Shen, X. Qian, *Carbohydrate Polymers*, **98**, 931 (2013).
18. Y. Zhang, L. Lv, C. Shi, *Journal Of Northeast Dianli University*, **05**, 17 (2015).
19. S. Bratskaya, S. Schwarz, G. Petzold, T. Liebert, T. Heinze, *Ind. Eng. Chem. Res.*, **45**, 7374 (2006).
20. C. Gaiolas, P. Mendes, M. S. Silva, A. P. Costa, M. N. Belgacem, *Appita J.*, **58**, 282 (2005).
21. T. Lv, L. Dong, Y. Shi, et al., *Journal Of Northeast Dianli University*, **02**, 51 (2016).
22. S. Y. Yoon, Y. Deng, *Ind. Eng. Chem. Res.*, **46**, 4883 (2007).
23. S. Y. Yoon, Y. Deng, *Tappi J.*, **5**, 3 (2006).
24. J. Shen, Z. Q. Song, X. R. Qian, *Appita J.*, **62**, 360 (2009).
25. Cao, S.; Song, D.; Deng, Y.; Ragauskas, A. J. *Ind. Eng. Chem. Res.*, **50**, 5628 (2011).
26. H. Fan, S. Wang, J. Liu, *BioResources*, **9**, 5883 (2014).
27. Y. Sang, M. McQuaid, P. Englezos, *BioResources*, **7**, 354 (2012).
28. H. Fan, D. Wang, W. Bai, J. Liu, *BioResources*, **7**, 3317 (2012).
29. S. Y. Yoon, Y. Deng, *J. Appl. Polym. Sci.*, **100**, 1032 (2006).
30. Y. Zhao, Z. Hu, A. J. Ragauskas, Y. Deng, *Tappi J.* **4**, 3 (2005).
31. X. Ye, S. Kang, H. Wang, H. Li, Y. Zhang, G. Wang, H. Zhao, *J. Hazard. Mater.*, **289**, 210 (2015).
32. S. Meng, Y. Ma, J. Cui, D. W. Sun, *Starch-Stärke*, **66**, 809 (2014).
33. Y. Zhang, Y. Sun, H. Zhang, *Journal of Northeast Dianli University*, **06**, 67 (2014).
34. W. Shang, X. Meng, Y. Tan, *Journal of Northeast Dianli University*, **03**, 55 (2015).

ПОЛУЧАВАНЕ НА МОДИФИЦИРАН ДИАТОМИТЕН ПЪЛНИТЕЛ ЧРЕЗ НАНАСЯНЕ НА КОМПЛЕКС ОТ НИШЕСТЕ И МАСТНА КИСЕЛИНА ЗА ПОДОБРЯВАНЕ НА ЗДРАВИНАТА НА ХАРТИЯ

У. Шанг^{1,2}, Кс. Киан^{1*}, Х. Лианг²

¹ *Лаборатория по биоматериалознание и технология при Министерството на образованието, Колеж по материалознание и инженерство, Североизточен университет по горско стопанство, Харбин 150040, Китай.*

² *Колеж по инженерна химия, Североизточен университет по електрическа енергия, Джилин 132012, Китай.*

Получена на 24 август, 2017 г.; Ревизирана на 15 ноември, 2017 г.

(Резюме)

Диатомитовите частици са модифицирани за подобряване на свързвашите им свойства с влакната на хартиения пулп чрез нанасяне на комплекс от нишесте и мастна киселина. Резултатите от SEM анализа показват, че повърхността на модифицираните диатомитови частици е покрита с комплексния слой. Ефективността на покриване с комплекса от нишесте и мастна киселина е до 98%. Модифицираният диатомит проявява високо съпротивление на срязване. В сравнение с хартиени листове, пълни с немодифициран диатомит, тези пълни с модифициран диатомит имат по-голяма здравина и по-малък обем. По-високият зета потенциал и по-големият размер на частиците на модифицирания диатомит са причина за по-доброто задържане на модифицирания диатомитов пълнител. Настоящото изследване предлага техническо потвърждение на приложението на диатомит като нов пълнител в хартиеното производство.

Influence of sensitizing treatment on the corrosion resistance of Incoloy 028 alloy

Z.Q. Yu¹, G.S. Zhou¹, S.D. Zhu^{2*}, J.M. Li³, L.J. Li⁴

¹ School of Materials Science and Engineering, Xi'an Jiaotong University, Xi'an, China

² School of Materials Science and Engineering, Xi'an Shiyou University, Xi'an, China

³ School of Mechanical Engineering, Zhengzhou University of Science and Technology, Zheng'zhou, China

⁴ School of Chemistry & Chemical Engineering, Xi'an Shiyou University, Xi'an, China

Received August 29, 2017, Revised November 15, 2017

The influence of the precipitated phases on Incoloy 028 alloy was investigated *via* a sensitizing treatment at various sensitizing times and temperatures, weight loss and electrochemical testing methods were used, and the influence of the precipitated phases on the corrosion resistance on Incoloy 028 alloy was discussed on the basis of the significant characteristics of the polarization curves and Nyquist plots. The results showed that the corrosion resistance of Incoloy 028 was influenced by the precipitated phases; the corrosion rate of Incoloy 028 alloy initially increased and then decreased with the increasing sensitizing temperature; the most severe corrosion occurred at 900 °C; and the elemental contents of Cr and Mo in the corrosion area were lower than those in the non-corroded area on the alloy surface, indicating that the corrosion resistance on the precipitated phase area was weakened.

Key words: Incoloy 028 alloy, Sensitizing treatment, Precipitated phases, Corrosion resistance, Potentiodynamic polarisation curve, Electrochemical impedance spectrometry.

INTRODUCTION

Ni-Fe-Cr alloys possess good resistance to a wide variety of corrosive environments in industrial processes such as chemical and petrochemical processing, marine engineering, oil/gas production and transport, and in nuclear reactors [1-3]. The demand for Ni-Fe-Cr alloys is increasing, and materials with excellent mechanical properties are required [4,5].

Incoloy 028 is a Ni-Fe-Cr alloy with addition of molybdenum, copper, and titanium, which has replaced many other alloys due to its superior local corrosion resistance. It is high-alloyed austenitic steel having excellent resistance to stress corrosion cracking and localized attacks such as pitting and crevice corrosion [5-9]. Many efforts have been made to understand the corrosion behavior [8-12].

Nickel-based alloys also are widely utilized in locations where severe corrosion attacks. However, the influence of precipitated phases on Incoloy 028 alloy by a sensitizing heat treatment has rarely been investigated in relation to CO₂ corrosion in the oil/gas industry. It is important to understand the corrosion resistance of Incoloy 028 alloy at various sensitizing temperatures by using weight loss and electrochemical tests.

EXPERIMENTAL

Specimen preparation

All specimens were made of the nickel-based alloy Incoloy 028 with original chemical

composition of (wt.%): C 0.01, Si 0.41, Mn 1.06, P 0.022, S 0.002, N 0.056, Ni 30.3, Cr 27.6, Mo 3.5, Cu 0.95, and Fe balance. Specimen slices with a size of 30 × 15 × 1.5 mm were processed for corrosion immersion tests, while the electrochemical test specimens were φ 8 × 6 mm rods embedded in epoxy resin with an exposed working area of 0.685 cm². A new specimen was used for each experiment, and prior to the electrochemical tests, the working surfaces were wet-ground with SiC sand paper of up to 1200 grits, followed by ultrasonic cleaning in acetone and final rinsing in deionized water.

All specimens were of nickel-based alloy Incoloy 028 treated through a solid-solution process at 1180 °C for 2 h with subsequent water-cooling. Then, some specimens were treated through sensitizing heat treatment at 700, 800, 900, and 1000 °C for 2 h, with subsequent air-cooling. Other specimens were treated through sensitizing heat treatment at 900 °C for 0.5, 2, and 5 h.

Weight loss corrosion test

The prepared specimens were weighed using an electronic balance with a precision of 0.1 mg, and then placed in a constant-temperature water bath. The solution was deoxygenated by bubbling pure N₂ for 4 h before the introduction of CO₂, and the CO₂ gas was bubbled to the water bath during the corrosion test in the range of 30 - 70 °C. The corrosion tests were carried out for 15 days under static conditions. The test solution came from oilfield produced water, with main ionic concentrations of 12.16 g L⁻¹ of Cl⁻, 0.43 g L⁻¹ of

To whom all correspondence should be sent:

E-mail: zhudsxt@126.com

SO_4^{2-} , 0.27 g L⁻¹ of HCO_3^- , 0.14 g L⁻¹ of Ca^{2+} , and 8.16 g L⁻¹ of K^+ and Na^+ . Five samples were tested for each experimental condition. After each test, specimens were rinsed with distilled water and ethanol, and were then divided into two groups. The specimens in group one were descaled with Clark solution (20 g of Sb_2O_3 + 50 g of SnCl_2 + 1 L of 36.5 wt.% HCl), after which the weight loss was measured. The specimens in group two were not descaled, but dried and stored in a desiccator until the analysis with scanning electron microscopy (SEM) and X-ray diffraction (XRD) was performed.

Electrochemical corrosion test

The test solution was 3.5% NaCl, de-aerated by purging with nitrogen prior to the test. The electrochemical tests were conducted by polarization and EIS methods in a conventional three-electrode cell.

The polarization tests were applied to the working electrode at a scan rate of 0.2 mV s⁻¹ from -0.3 mV to 0.3 mV vs. SCE with respect to the open-circuit potential. The EIS measurements were carried out at the open-circuit potential using 5 mV amplitude perturbation at a frequency range of 100 kHz - 10 mHz. Each experiment was performed at least twice at 20 °C. The ZView software was used to analyze the EIS data.

RESULTS AND DISCUSSION

Corrosion immersion test

Corrosion rate

Figure 1 shows the influence of temperature on the corrosion rate (CR) of Incoloy 028. The CR increased with the increase in temperature. The CR of the Incoloy 028 alloy initially increased, and then decreased with increasing sensitizing temperature. The most severe corrosion occurred in the specimen sensitized at 900 °C for 2 h.

In addition, under identical temperature conditions, the CR of the Incoloy 028 treated at 900 °C increased with the increase in sensitizing time from 0.5 to 5 h, as shown in Fig. 2. These results indicate that the number of precipitated phases in the specimens for various sensitizing times played a role in corrosion rate.

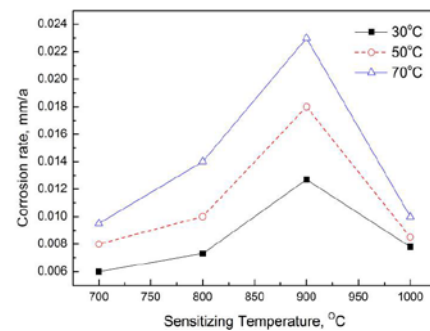


Fig. 1. Influence of temperature on corrosion rates of Incoloy 028 treated at various sensitizing temperatures for 2 h.

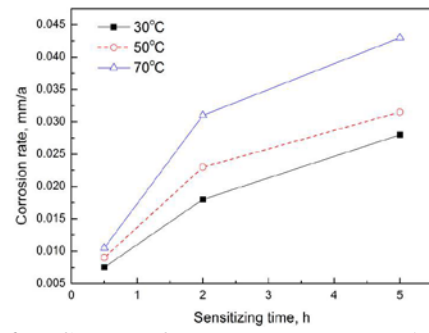


Fig. 2. Influence of temperature on corrosion rates of Incoloy 028 treated at 900 °C for various sensitizing times.

Corrosion characterisation

The surface morphology is shown in Fig. 3a. It can be seen that pitting corrosion occurred on the surface of Incoloy 028, which could be explained by a second-phase precipitation in the local surface area for the specimen sensitized at 900 °C leading to a diminishing of corrosion-resistance of Incoloy 028. Figs. 3b and 3c present the energy-dispersive spectroscopy (EDS) plots, the corrosion products included elements such as Fe, Cr, Ni, Mo, C, O, Si, and small amounts of Ca, Ba, and Cl. It was determined that the main phases in all corrosion products were FeCO_3 and small sediment compounds such as SiO_2 and CaCO_3 . In contrast, the contents of both Cr and Mo in the corrosion area were lower than those on the alloy surface. This result indicates that the corrosion attack preferentially took place in the area of precipitated phases, i.e., the area containing low amounts of Cr and Mo.

XRD spectra shown in Fig. 4 further reveals that the peaks were γ -phase in the substrate, which is demonstrated by the presence of the corrosion product FeCO_3 due to the superior anti-corrosion performance of Incoloy 028.

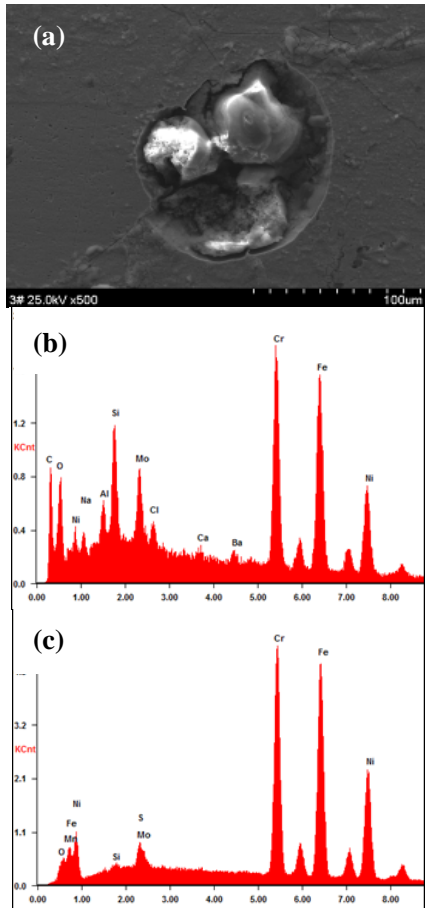


Fig. 3. Surface characterization of Incoloy 028 treated for 2 h at sensitizing temperature of 900 °C after corrosion test at 70 °C. (a) SEM; (b) EDS of corrosion area; (c) EDS of alloy surface.

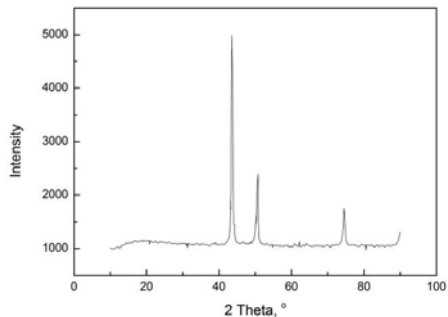


Fig. 4. XRD spectrum of the corrosion product on Incoloy 028 treated at 900 °C for 2 h after corrosion test at 50 °C.

Electrochemical test

Polarization

Figure 5 shows the Tafel polarization curves of Incoloy 028. The anodic branches of the polarization curves had similar characterization, which indicates that the anodic reaction maintains the same corrosion mechanism. It is evident that the corrosion potential initially moved in a more negative direction, and then moved in a positive direction, indicating that the self-corrosion tendency initially increased and then decreased with

increasing sensitizing temperature. The corrosion current density of Incoloy 028 at 900 °C was higher than those at 700, 800, and 1000 °C under the same conditions. This result is in accordance with the result from the weight loss method mentioned above. The cathodic branch slopes (b_c) were close to the corresponding anodic branch slopes (b_a), so it can be proven that the corrosion process is controlled by the combined effects between anodic dissolution and cathodic diffusion.

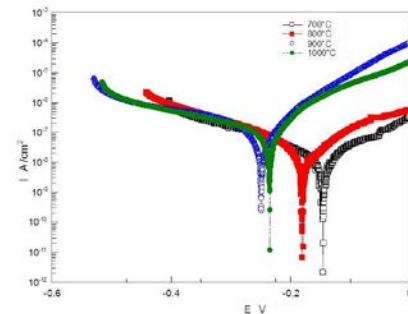


Fig. 5. Polarization curves of Incoloy 028 treated at various sensitizing temperatures in 3.5% NaCl solution at 20 °C for 2 h.

Figure 6 shows the Tafel polarisation curves of Incoloy 028. The polarization curves moved in the positive direction, indicating that the thermodynamic effect accelerated the transfer rates of corrosive species and the corrosion reactions at temperatures ranging from 20 to 50 °C. It is worth noting that the anodic branch slopes were similar, while the cathodic branch slopes increased with increasing temperature, which indicates that the entire corrosion process was predominantly controlled by cathodic reactions when the testing temperature increased.

Figure 7 shows the Nyquist plots of Incoloy 028 treated at various sensitizing temperatures in 3.5% NaCl solution at 20 °C for 2 h. There was one depressed capacitive loop in the intermediate frequency region. The diameter of the capacitive loop decreased when the sensitizing temperature increased, and the minimum diameter was for the specimen sensitized at 900 °C.

The corresponding equivalent circuit model is shown in Fig. 8. In this model, R_s is the solution resistance between the working electrode and reference electrode and R_t is the charge transfer resistance of the corrosion reaction. The CPE-n of Incoloy 028 is close to 1, which indicates the presence of an approximately ideal capacitor. CPE- Y_0 represents the base admittance of the CPE and the changes in its values indicate that the adsorption layer and/or corrosion film demonstrate no significant difference. As expected, the value of R_t decreased with the increase of the sensitizing temperature, especially at 900 °C, i.e., the corrosion resistance decreased. The

results are in good accordance with that obtained from the Tafel polarization.

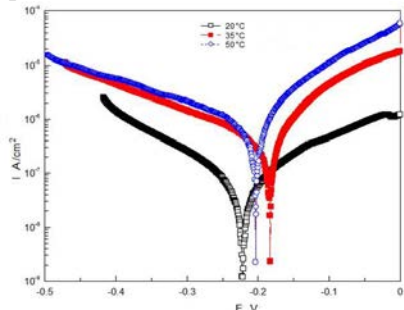


Fig. 6. Influence of temperature on polarization curves of Incoloy 028 treated at sensitizing temperature of 800 °C in 3.5% NaCl solution for 2 h.

EIS measurements

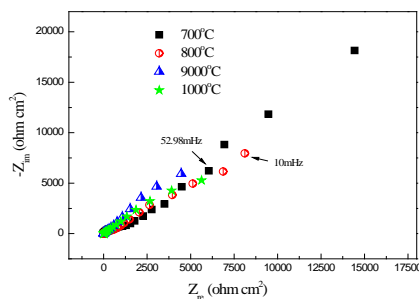


Fig. 7. Nyquist plots of Incoloy 028 treated at various sensitizing temperatures in 3.5% NaCl solution at 20 °C for 2 h.

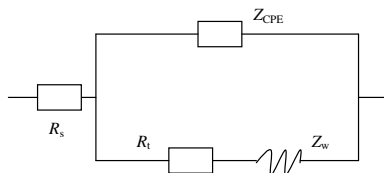


Fig. 8. The equivalent circuit model corresponding to the Nyquist plots of Incoloy 028 under various conditions.

CONCLUSION

The corrosion rate of Incoloy 028 firstly increased, then decreased with the increasing sensitizing temperature; the specimen sensitized at 900 °C underwent the most severe corrosion. The corrosion processes were controlled by the combined effects between anodic dissolution and

cathodic diffusion. The corrosion potential of Incoloy 028 shifted to more negative values before changing direction to positive values with the increasing sensitizing temperature, while the corrosion current density of the specimen sensitized at 900 °C was higher than that sensitized at 700, 800, and 1000 °C. And the minimum diameter of the capacitive loop was obtained from the specimen sensitized at 900 °C, and the charge transfer resistance decreased with the increase in the sensitizing temperature, especially at 900 °C.

Acknowledgements: The authors would like to thank the Youth Science and Technology New Star Plan of Shaanxi Province (2016KJXX-13, 2017KJXX-49), Scientific Research Program Funded by Shaanxi Provincial Education Department (17JS113), Xi'an Science and Technology Program (2017081CG/RC044 (XASY003, XASY004))

REFERENCES

1. A. Thomas, M. El-Wahabi, J. M. Cabrera and J. M. Prado, *J. Mater. Process. Technol.*, **177**, 469 (2006).
2. B.A. Baker, *Proceedings of NACE Corrosion/2006*, Houston, TX, paper No. 06229.
3. J. Kawakita, S. Kuroda, T. Fukushima, T. Kodama, *Corros. Sci.*, **45**, 2819 (2003).
4. Y.Y. Chen, L.B. Chou, H.C. Shih, *Mater. Sci. Eng. A.*, **396**, 129 (2005).
5. T. Bellezze, G. Roventi, R. Fratesi, *Surf. Coat. Technol.*, **155**, 221 (2002).
6. S.Y. Lu, Nickel Based and Iron-Nickel Based Corrosion Resistant Alloy, Chemical Industry Press, Beijing, 1989.
7. S.A. Al-Fozan, A.U. Malik, *Desalination*, **228**, 61 (2008).
8. J.L.J. Soler, D.J. Baxter, J.F. Norton, *Corrosion*, **55**, 1191 (1999).
9. S. Ghosh, T. Ramgopal, *Proceedings of NACE Corrosion/2004*, Houston, TX, paper No. 04231.
10. P. Crook, M. L. Caruso, *Proceedings of NACE Corrosion/2004*, Houston, TX, paper No. 04221.
11. C. Y. Sun, G. Liu, Q. D. Zhang, R. Li, L. L. Wang, *Mater. Sci. Eng. A*, **595**, 92 (2014).
12. F. G. Meng, J. X. Dong, M. C. Zhang, Z. H. Yao, *Chin. J. Nonferrous Met.*, **24**, 432 (2014).

ВЛИЯНИЕ НА СЕНСИБИЛИЗИРАЩАТА ОБРАБОТКА ВЪРХУ КОРОЗИОННАТА УСТОЙЧИВОСТ НА СПЛАВТА Incoloy 028

З. Ю¹, Г. Жоу¹, С. Жу^{2*}, Дж. М. Ли³, Л. Дж. Ли⁴

¹ Факултет по материалознание и инженерство, Университет Сиан Джсаатонг, Сиан, Китай

² Факултет по материалознание и инженерство, Университет Сиан Шиоу, Сиан, Китай

³ Училище по машиностроение, Университет за наука и технологии в Джънджоу, Джънджоу, Китай

⁴ Училище по химия и инженерна химия, Университет Сиан Шиоу, Сиан, Китай

Получена на 29 август, 2107 г.; Коригирана на 15 ноември 2017 г.

(Резюме)

Изследвано е влиянието на утаените фази върху сплавта Incoloy 028 чрез сенсибилизираща обработка при различна температура и време. Използвани са методи на загуба на тегло и електрохимични методи. Влиянието на утаените фази върху корозионната устойчивост на сплавта Incoloy 028 е дискутирано на основата на значимите характеристики на поляризационните криви и графиките на Nyquist. Резултатите показват, че корозионната устойчивост на сплавта Incoloy 028 се влияе от утаените фази, като скоростта на корозия първоначално нараства, след което намалява с повишаване на температурата на сенсибилизация и най-силна корозия се наблюдава при 900°C. Съдържанието на Cr и Mo в областта на корозия е по-ниско от това в некородиралата област върху повърхността на сплавта, което сочи, че областта с утаени фази е отслабена.

Influence of nano-serpentine mineral powder as a lubricating additive on the high-temperature tribological properties of metal friction pairs

Z. N. Jia^{1*}, Y. Y. Yang², X. W. Qi², X. M. Song¹

¹Hebei Instrument & Meter Engineering Technology Research Center, Chengde, 067000 P. R. China;

²National Defense Key Laboratory Key Laboratory of mechanical structure and Materials Science under extreme conditions, Yanshan University, Qinhuangdao, 066004 P. R. China

Received August 24, 2017; Accepted November 1, 2017

High-temperature tribological properties of 45 steel friction pairs were investigated, and nano-serpentine mineral powder (nano-serpentine), nano-serpentine mineral powder + nano-lamellar expandable graphite (Nano-EG + nano-serpentine) were used as mineral oil additives, respectively. By means of SEM, TEM and EDS, the worn surface morphology and composition distribution on the contact surfaces with different lubricating additives at high temperature were compared and analyzed. The results show that under high-temperature conditions, using nano-serpentine mineral powder and Nano-EG combined as lubricating oil additives, a self-repairing transfer film is formed. At an early high-temperature friction stage, the friction coefficient decreases with time, which leads to better anti-friction properties. As regards wear resistance, the high-temperature friction tribological properties of 45 steel with a Nano-EG + nano-serpentine additive were superior to those with only nano-serpentine mineral powder additive, which is mainly due to the combination of the good self-lubrication property of Nano-EG and the self-repairing effect of the nano-serpentine mineral powder.

Keywords: High temperature; Nano-serpentine; Surface morphology; Self-repairing film; Tribological properties

INTRODUCTION

High-temperature friction, as the name implies, refers to the friction and wear problems at high temperature, which mainly includes two aspects: one is the continuous operation of the machine at a higher temperature; the second is the machine working at a higher temperature periodically. Typical for the former case are aircraft engines, space vehicles and different metallurgical equipment. For the latter case, tribological problems usually appear in certain circumstances such as lean oil leakage/oil cutting-off. Especially, under insufficient lubrication conditions, the contact parts of relative motion may lead to temporarily high temperature.

Problems about high temperature friction and wear are mainly solved through surface engineering technology (PVD/PVC coating, laser cladding layer, carburizing/nitrogen technology, etc.), lubricating materials and wear-resistant materials. Especially, in the case of oil shortage, how to reduce the friction and wear of the kinematic pair is one of the research topics of high temperature tribological design, which is important not only for the normal operation of the machine, but also to the reliability and service life of the friction pairs.

Using surface engineering technology, Liu, Deng *et al.* co-workers studied the friction and wear properties of five PVD nitride coatings at 200–700°C and found that the five kinds of coatings would cause oxidation wear at high temperature [1]. Of all

coatings, AlTiN was most adapted to high temperature, high speed and heavy load. At the same time, the different hardness and chemical activity caused different wear mechanisms. The research on the high temperature friction and wear properties of Ni-P alloy coating by Li *et al.* showed that a Ni-P alloy layer prepared by electric brush plating technology could effectively improve the tribological properties of the specimen at 450 °C [2]. Zhang and Ceng used grid laser quenching and low-temperature ion sulphurizing technology to treat 42MnCr52 steel surface. Because of the increase in hardness and oil storage function of the porous sulfide layer, processed samples have significant antifriction and wear resistance properties [3]. The friction and wear properties of Fe-Al/TiC laser cladding layer against Si₃N₄ ball were studied by Wang and Gao [4]. It was found that delamination wear is the high-temperature wear mechanism of the cladding layer.

From the lubrication technology and materials matching, Li and Xiong used laser surface texturing technology to etch micropores on the surface of nickel-based material in order to store lubricating oil, and utilized plasma surface alloying technology to diffuse Mo or multi-permeate Mo/N on the microporous surface to improve the surface wear resistance [5–7]. Sun and Qiao found that SiO₂ nanoparticles could significantly enhance the high-temperature wear resistance properties of rapeseed oil at 500 °C [8]. The friction coefficient is only 0.16 and the wear loss is reduced by more than 80%. Yao and Yue found that friction and wear performances of double imidazole ionic liquid with alkyl chain are significantly better than with ether

To whom all correspondence should be sent:

E-mail: ysujia@163.com

chain at 250 °C. Shortening the chain length of double imidazole ionic liquid is beneficial to the tribological properties [9].

To improve the wear resistance of materials, TiB₂-SiC multiphase ceramics was *in situ* synthesized by Zhou and Xiao [10]. The results showed that the physical properties and the high-temperature tribological properties of SiC ceramics are improved, and high temperature oxidation is the main wear mechanism. Through the research of the high-temperature friction and wear properties of PCD tools, Al₂O₃/TiC ceramic cutting tools and carbide tools, Zhang and Deng revealed the high-temperature friction and wear mechanism of typical hard-brittle material tools [11], and provided a theoretical basis for the design and selection of tool materials. High-temperature friction and wear behavior of M50 high-speed steel were investigated by Liu [12]. The results showed that the combined action of friction heat and ambient temperature causes a semi-molten state of the contact surfaces above 400 °C. As an inevitable result, a layer of metal film is formed during the sliding process, which is the main reason for reducing the friction coefficient.

Nano mineral serpentine powder, as a lubricating oil additive, showed good tribological properties and its self-repairing behavior has been confirmed by some scholars [13-16]. In this paper, nano expanded graphite with lamellar structure (Nano-EG) was used as antifriction agent, nano mineral serpentine powder (nano-serpentine) as lubricating oil additive (self-repairing agent). The tribological properties of steel/steel friction pairs at high temperature were studied by corresponding experimental design in order to reduce friction and wear of metal pairs in case of oil cutting-off.

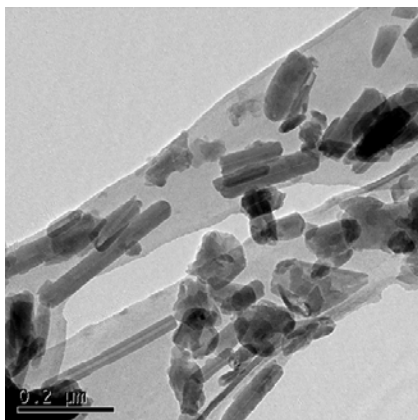


Fig. 1. TEM image of nano-serpentine powder

EXPERIMENTAL

Nano-serpentine powder was prepared by mechanical milling and Nano-EG by ultrasonic cavitation. A certain amount of nano-serpentine powder and/or Nano-EG was added to the base oil. By electromagnetic stirring the lubricating oil with nano additives was obtained. Figs. 1 and 2 show the TEM (JEM-2010, JEOL company, Japan) image of nano-serpentine and the SEM (S-4800 SEM, Hitachi company, Japan) image of Nano-EG, respectively. From Fig. 1 it is seen that the nano-serpentine powder mainly shows two kinds of shapes: one is approximately spherical (diameter is less than 100 nm), the other is a long column type (diameter is less than 50 nm). As can be seen from Fig. 2, the lamellar structure of expanded graphite is removed, and its thickness is less than 25 nm.

The lubricating oil with different additives was put into the oil tank located on the lower base of the testing machine, and then the friction pair was placed in a high-temperature insulation box for heating to 350°C. The tribological tests were carried by using MMU-5G high temperature friction and wear tester (Jinan Jingcheng Test Technology Co.) at a load test of 200 N, 400 N and 800 N, and a speed of 346 r/min. The upper and lower specimens were 45 steel, respectively. The other test details can be found elsewhere [15, 16]. In order to reduce the dispersion of test results, each test was repeated three times under the same conditions. The antifriction and wear resistance of the friction pairs with different lubricating oil additives at high temperature were determined. Meanwhile, the wear mechanism was discussed by means of SEM and EDS.

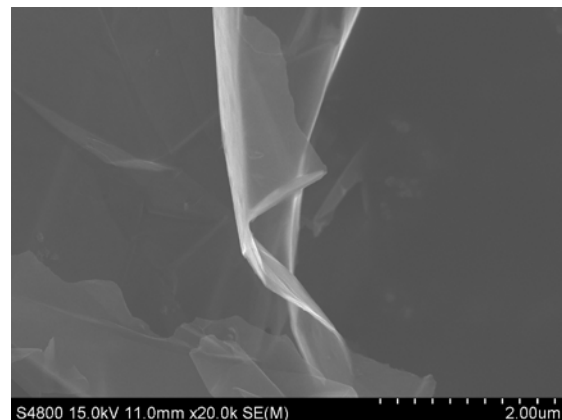


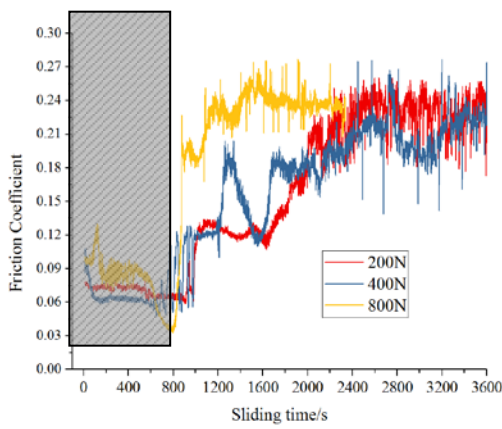
Fig. 2. SEM image of Nano-EG

RESULTS AND DISCUSSION

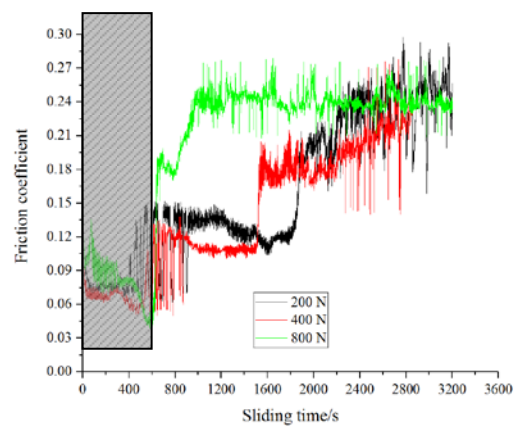
Fig. 3 shows the friction coefficient-time history curve of friction pairs with different additives. According to the figure, it can be seen that the friction coefficient is characterized by three obvious stages under high temperature. In the initial stage of wear, the friction coefficient is small and gradually decreases. After a period of time, the friction coefficient rises suddenly and enters a relatively stable platform. Then the friction coefficient continues to increase and fluctuates at higher values. Compared to Fig. 3a and 3b, where the additive is Nano-EG+ nano-serpentine, the duration of the first stage is longer than that of nano-serpentine additive, and the antifriction effect is better. At present, the global air disasters that caused by oil supply disruptions of aircraft engine lubrication system occur frequently [17-19]. When oil cutting-off of the aircraft lubricating system takes place, the sustained flight capability has become the focus of attention. After oil cutting-off, the carrying capacity of bearings under full load operation conditions is very important for the safety of the aircraft. For example,

the turbine spindle bearings of aircraft in the design, it is required to work 30 s under oil cutting-off in normal flight conditions [20]. Through the tribological tests, the lubricating oil by adding nano repairing agent and self lubricant can not only effectively meet this requirement, but also greatly prolong the working time of the engine.

Fig. 4 illustrates the wear of the upper and lower specimens with different additives. The negative value means that the mass after the test is not reduced, but increased to some degree. It is obvious that under the conditions of low and medium load, there is a small amount of negative wear loss for the lower specimens and a small amount of wear loss for the upper specimens. However, under high load negative wear loss appears for both upper and lower samples. Compared with Fig. 4a and 4b, it is seen that when nano-serpentine is added, the wear loss of the upper and lower samples is higher under higher load. When the contact load was 800 N, the maximum negative wear loss of the upper specimens was registered, and the mass increase reached 0.069 g and 0.076 g, respectively.

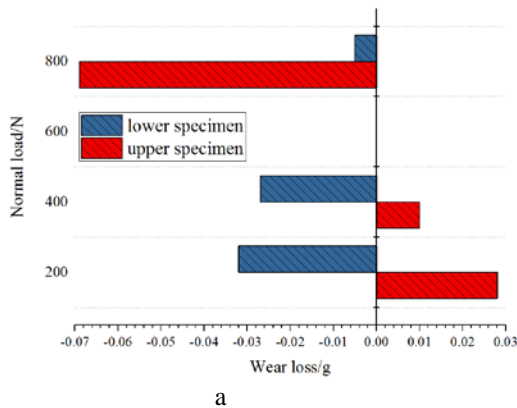


a

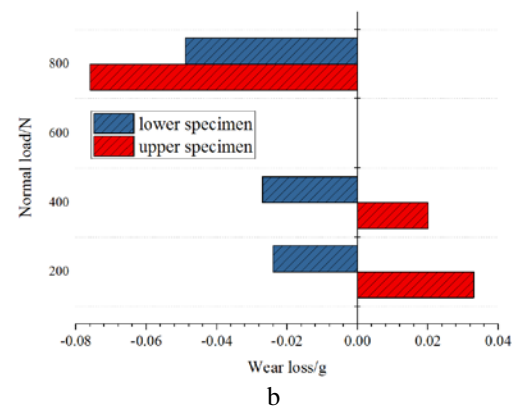


b

Fig. 3. History curve of friction coefficient-time with different additives: a) Nano-EG + nano-serpentine powder, b) nano-serpentine powder



a



b

Fig. 4. Comparison of wear loss of specimens with different additives: a) Nano-EG + nano-serpentine powder, b) nano-serpentine powder

Meanwhile, when the additive was Nano-EG + nano-serpentine or nano-serpentine, the mass of the lower specimens increased to 0.005 g and 0.051 g, respectively. This is because Nano-EG as self-lubricating additive could hinder the spreading of nano-serpentine on the contact surface so that the process of chemical reaction occurred on the contact surface [15, 16]. From the point-of-view of metal self-repairing and reduced wear of the surface, Nano-EG + nano-serpentine or nano-serpentine as lubricating oil additives not only did not lead to a phenomenon of obvious wear under the conditions of oil cutting-off at high temperature, but could also effectively improve the contact state and fit between friction pairs.

Fig. 5 shows the SEM image of the worn surface morphology when the additive is nano-serpentine. As shown in Fig. 5a, the surface wear is mainly based on a slight ploughing effect and adhesion under light load conditions. Under medium load, the wear morphology is smooth and the adhesion wear is the main wear form, as shown in Fig. 5b. When the load is large, the wear morphology of the specimens is mainly a plastic flow. Due to the heavy tangential

force, the self-repairing film formed on the worn surface forms cracks (red arrows in the figure), as shown in Fig. 5c. Fig. 6 shows the SEM worn surface morphology when the additive is Nano-EG+ nano-serpentine. As can be seen from the figure, the addition of Nano-EG significantly improves the wear form of contact surface. At different loads, the wear surface is relatively smooth. When the load is small, the slight adhesive wear is the main, as shown in Fig. 6a). Under medium load, the worn surface is mainly composed of minor ploughing and a small amount of adhesion, as shown in Fig. 6b). When the load is large, the wear is changed into adhesive wear. Also, due to the larger tangential force the self-repairing film formed on the worn surface also appeared cracks (red arrow in the figure), as shown in Fig. 6c). Because of the addition of Nano-EG, the wear forms with different lubricating oil additive are different. Nano-EG with the self-lubrication property improves the wear resistance of the contact surface and also weakens the ploughing effect of nano-serpentine on the contact surface. Fig. 7 shows the local EDS energy spectrum analysis of the worn surface topography for different additives (Fig. 7a and b).

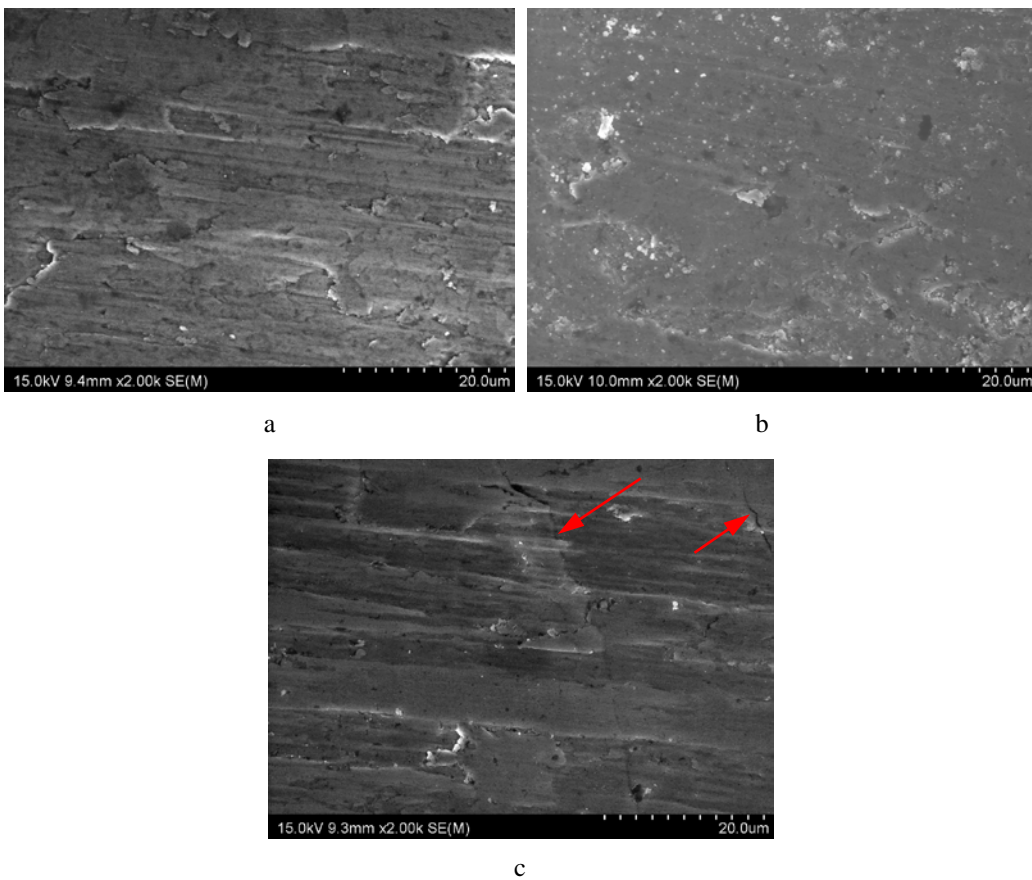


Fig. 5. Morphology of the worn surfaces with nano-serpentine additive at different loads: a) 200N, b) 400 N, c) 800N

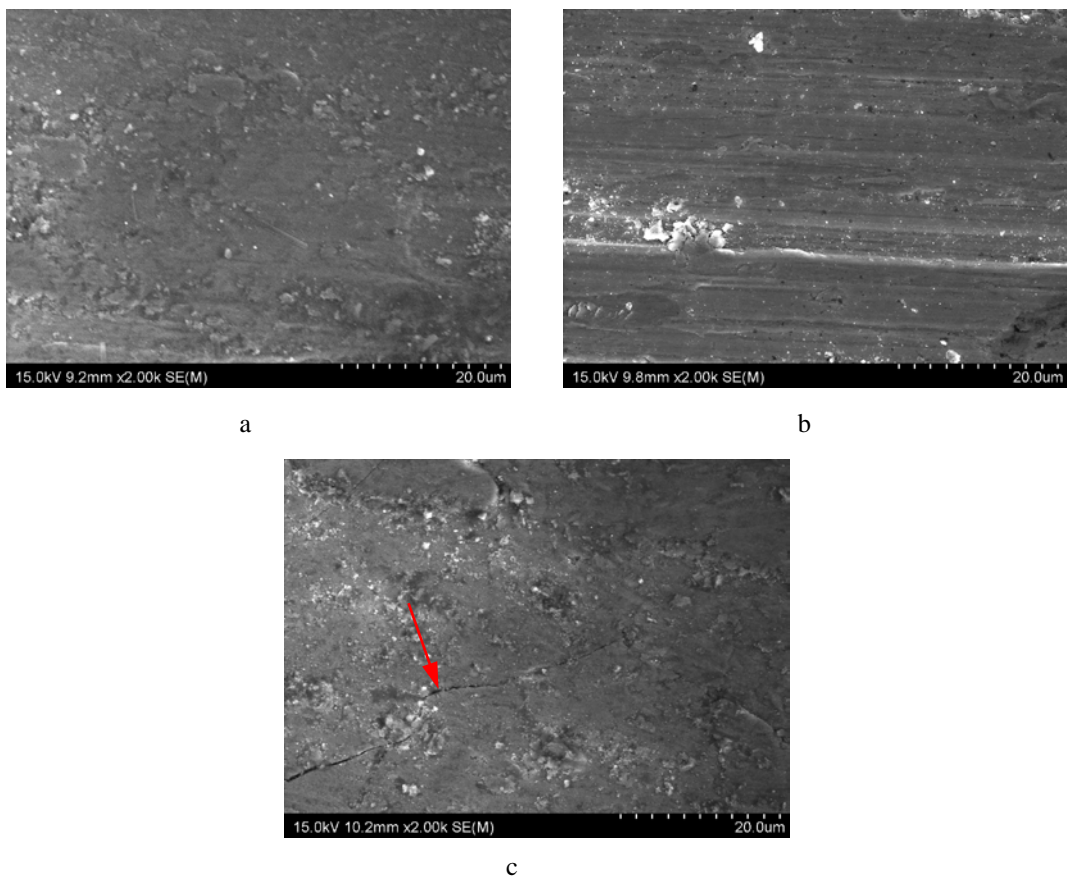


Fig. 6. Morphology of the worn surfaces with Nano-EG + nano-serpentine additives at different loads:
a) 200N, b) 400 N, c) 800N

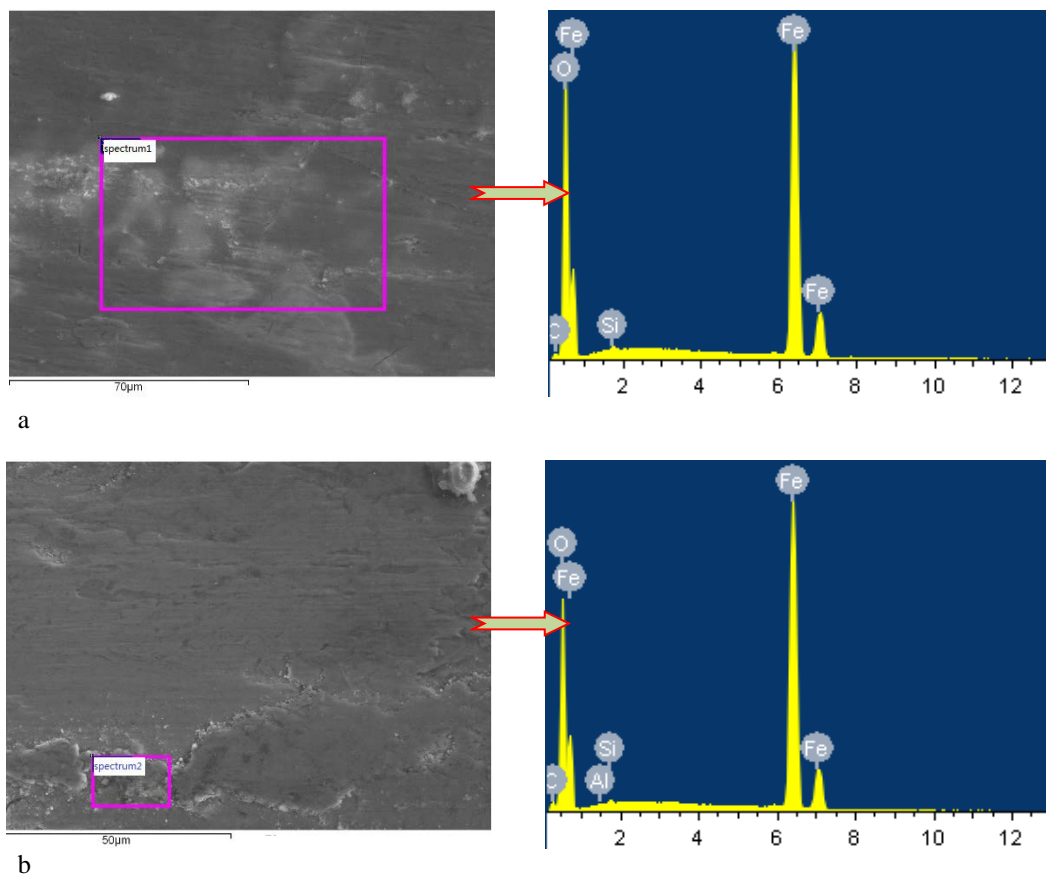


Fig. 7. Energy spectrum analysis of worn surface with different additives: a) nano-serpentine powder, b) Nano-EG + nano-serpentine powder

The characteristic element Mg of serpentine in energy spectrum not found, which indicates that in the friction test process, the magnesium iron has been replaced by iron [15, 16]. At the same time, oxygen atoms appear in the spectrum, which shows that the chemical reaction occurs in the process of friction. There are two possible ways to introduce oxygen atoms. One is decom-position product silica during heat treatment and hydrolysis of serpentine powder under high temperature condition, two is a chemical reaction between the oxygen atoms and iron. According to the friction coefficient curve mentioned above, the friction coefficient tends to relative stable value with the test time. The results show that the variation of the friction coefficient is mainly controlled by the chemical reaction at the friction interface. According to Fig. 4, the larger the external load is, the more easily the additives are deposited on the interface and the chemical reaction occurs on the friction surface. Therefore, varying degrees of mass increase for the upper and lower specimens appear.

CONCLUSIONS

The paper investigated the high temperature tribological properties of metal friction pair with Nano-EG and nano-serpentine mineral powder as lubricate additives. Some conclusions are as follows:

1) The addition of nano-serpentine mineral powder and Nano-EG into the lubricating oil could effectively improve the wear resistance of the metal friction pair under high temperature condition. More important, in the initial period of friction, the friction coefficient decreased with the running time, which is very beneficial to alleviate/reduce the friction and wear problems caused by oil cutting-off at short time under high temperature.

2) The varying degrees of wear loss for the upper and lower specimens appeared. Lubricating additive material was transferred to the contact surfaces, which is the nature of the wear resistance can be improved.

3) The high temperature tribological properties of metal friction pairs were influenced by kind of additives. When the nano-serpentine mineral powder was added, the wear form was mainly composed of plough and adhesive wear. However, when Nano-EG and nano-serpentine were added, slight adhesive wear was the main wear form.

4) With nano-serpentine used as lubricating oil additive together with Nano-EG, the tribological properties of the friction pairs at high temperature were superior to those with nano-serpentine mineral

powder only. It is mainly because Nano-EG has good self-lubrication property (better antifriction effect), and nano-serpentine mineral powder has a self-repairing effect on the contact surface.

Acknowledgements: The authors gratefully acknowledge the assistance of the Key Laboratory of Fundamental Science of Mechanical Structure and Material Science under Extreme Condition for National Defense. Furthermore, special thanks are given to the Natural Science Foundation of Hebei Province (Grant No. E2016411005).

REFERENCES

1. A. H. Liu, J. X. Deng, H. B. Cui, S. P. Li, J. Zhao, *Transactions of Materials and Heat Treatment*, **33** (6), 147 (2012).
2. Z. M. Li, S. Q. Qian, W. Wang, J. H. Liu, *Acta Metallurgica Sinica*, **46** (7), 867 (2010).
3. P. Zhang, Q. Q. Zeng, Z. H. Cai, Q. Li, *Journal of Academy of Armored Force Engineering*, **24** (1), 75 (2010).
4. Y. H. Wang, Z. Q. Gao, X. N. Zhang, Q. F. Li, *Materials for Mechanical Engineering*, **5** (5), 39 (2011).
5. Z. J. Huang, D. S. Xiong, J. L. Li, M. L. Liu, *Journal of Materials Protection*, **44** (6), 28 (2011).
6. J. L. Li, D. S. Xiong, Z. Wan, *Transactions of Non-ferrous Metals Society of China*, **17** (S1), 99 (2007).
7. J. L. Li, D. S. Xiong, J. F. Dai, *Transactions of Nonferrous Metals Society of China*, **S3**, 171 (2005).
8. X. F. Sun, Y. L. Qiao, K. Wang, S. N. Ma, *Journal of Academy of Armored Force Engineering*, **22** (1), 80 (2008).
9. M. H. Yao, Y. Y. Yue, Y. M. Zhang, Y. Q. Xia, F. Zhou, Y. M. Liang, *Journal of Tribology*, **31** (5), 485 (2011).
10. S. Q. Zhou, H. N. Xiao, G. Y. Li, *Lubrication Engineering*, **32** (7), 59 (2007).
11. H. Zhang, J. X. Deng, Z. Wu, X. Ai, J. Zhao, *Journal of Tribology*, **31** (4): 369 (2011).
12. Z. M. Liu, *Journal of Tribology*, **17** (1), 38 (1997).
13. Y. S. Jin, *China Surface Engineering*, **23** (1), 45 (2010).
14. F. Gao, Y. Xu, B. S. Xu, P. J. Shi, *Journal of Tribology*, **31** (5), 431 (2011).
15. X. W. Qi, Z. N. Jia, Y. L. Yang, B. L. Fan, *Tribology International*, **44** (7–8), 805 (2011).
16. X. W. Qi, L. Lu, Z. N. Jia, Y. L. Yang, H. R. Liu, *Tribology International*, **49** (11), 53 (2012).
17. A. Tauqir, I. Salam, A. U. Haq, A. Q. Khan, *Engineering Failure Analysis*, **7** (2), 127 (2000).
18. Park M, *Engineering Failure Analysis*, **9** (6), 673 (2002).
19. I. Salam, A. Tauqir, A. U. Haq, A. Q. Khan, *Engineering Failure Analysis*, **5** (4), 261 (1998).
20. G. Hamburg, P. Cowley, R. Valor, *Lubrication Engineering*, **37** (7), 407 (1981).

ВЛИЯНИЕ НА НАНОСЕРПЕНТИНОВ МИНЕРАЛЕН ПРАХ КАТО СМАЗОЧНА ДОБАВКА ВЪРХУ ТРИБОЛОГИЧНИТЕ СВОЙСТВА НА ТРИЕЩИ СЕ ДВОЙКИ МЕТАЛИ

Ж. Жиа¹, Ю.Ю. Янг², Кс.У. Ки², Кс.М. Сонг¹

¹Хебей център за изследване на инструментални инженерни технологии, Ченгде, 067000 Н. Р. Китай;

²Национална лаборатория по отбрана за механична структура и материалознание при екстремни условия,
Яншан Университет, Кинхуангдао, 066004 Н. Р. Китай

Получена на 24 август, 2017 г.; Приета на 1 ноември, 2017 г.

(Резюме)

Изследвани са високотемпературните трибологични свойства на 45 триещи се стоманени двойки с използване на наносерпентинов минерален прах (наносерпентин) и смес от наносерпентин и наноламелен разширяем графит като минерални маслени добавки. С помощта на SEM, TEM и EDS е изследвана морфологията на износените повърхности и съставът им с използване на различни смазочни добавки при висока температура. Резултатите показват, че при високотемпературни условия с използване на смес от наносерпентин и наноламелен разширяем графит се получава саморегулиращ се трансферен филм. В ранен етап на високотемпературното трение коефициентът на трение намалява с времето, което води до по-добри антифрикционни свойства. По отношение на съпротивлението на износване, високотемпературните трибологични свойства на 45 двойки стомана с добавка от наносерпентин и наноламелен разширяем графит са по-добри от тези с използване само на наносерпентин, което се дължи на комбинацията от добри смазващи свойства на наноламелния разширяем графит и саморегулиращия ефект на наносерпентиновия минерален прах.

Identification of Clenbuterol by MALDI-TOF Mass Spectrometry

Q. Huo^{1,2}, T. Zhou¹, J. He¹, J. Q. Xue^{3,4*}

¹Biochemical Engineering College of Beijing Union University, Beijing, China

²Beijing; Beijing Key Laboratory of Biomass Waste Resource Utilization, Beijing, China

³Division of Nuclear Technology and Applications, Institute of High Energy Physics, Chinese Academy of Sciences, Beijing, China

⁴Beijing Engineering Research Center of Radiographic Techniques and Equipment, Beijing, China

Received August 16, 2017; Accepted November 6, 2017

Matrix-assisted laser desorption ionization time-of-flight mass spectrometry (MALDI-TOF-MS) was used to analyze macromolecular compounds. The present study focused on how to use MALDI for determination of small molecules such as clenbuterol, and how to explore the matrix to improve the sensitivity. The macromolecular 1,2,3,4-tetrakis(3',4'-hydroxyphenyl) thiophene matrix not only absorbed the laser energy but also caused sample desorption ionization. At the same time, it did not produce interfering ions of low molecular weight. Moreover, when perfluoro C₆₀ was added to the matrix, sensitivity was improved.

Keywords: matrix-assisted laser ionization; clenbuterol; matrix; sensitivity.

INTRODUCTION

The MALDI-TOF systems have evolved considerably since the first commercial version was introduced by Shimadzu in 1988 [1-3]. Matrix-assisted laser desorption/ionization (MALDI) is a soft ionization technique used in mass spectrometry, allowing the analysis of biomolecules (biopolymers such as proteins, peptides and sugars) [4-6] and large organic molecules (such as polymers, dendrimers and other macromolecules) [7,8], which tend to become fragile and fragmented when ionized by more conventional ionization methods. The strength of MALDI-TOF-MS lies in the ability to generate a molecule profile representing a large number of molecules expressed by the specific organism tested. This introduces a high level of molecule multiplex testing with results in minutes. The molecule profile can be used for microbial identification, detecting specific strains, and detection of antibiotic-resistant markers [9, 10].

The MALDI process starts by adding the sample to a metal target slide. A matrix solution is then applied to the sample, resulting in formation of crystals. A focused laser beam, either in the UV or IR range, can “evaporate” compounds from the solid phase; the sample is ionized with a laser pulse where the absorption of high energy by the matrix crystals results in vaporization of the molecules that are accelerated by a voltage gradient through the time-of-flight tube. The velocity of the molecules through the time-of-flight tube is inversely

proportional to the size and charge of the molecule. As the molecules separate based on size and charge, smaller molecules reach the detector first, followed by larger molecules, resulting in the creation of a series of peaks named spectra. It was said that a MALDI-TOF instrument in a shared proteomics facility can easily be set up to handle hundreds of analyses per day [11-13].

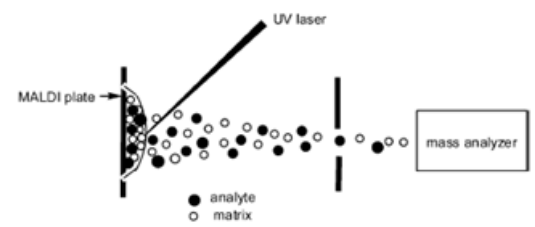


Fig. 1. Scheme graph of MALDI-TOF MS

The matrix is the core of the MALDI study. The matrix should meet the following conditions: (1) to be miscible with the measured object, diluting the analyte, reducing the force between the molecules, and preventing the formation of molecular clusters; (2) to be stabilized under the vacuum existing; (3) to strongly absorb the laser light source; (4) to be able to protect the sample towards the laser irradiation, the energy transfer to the analyte not directly destroying the structure of the analyte; (5) to provide protons by proton transfer to promote analyte ionization; (6) to provide the volume flow, where analyte molecules are thrown. Different types of compounds should be generally used in different matrices. For MALDI, the selection of matrix has a significant impact on the final results of the experiments; the choice of

* To whom all correspondence should be sent:

E-mail: jqxue @ihep.ac.cn

the matrix is also related with the formation of the fragment ions. By now, there is still no perfect theoretical guidance on how to choose the matrix for the different samples [14,15].

Clenbuterol is a class of animal drugs which are β -agonists; there are several kinds of drugs such as ractopamine, clenbuterol, etc. When clenbuterol is added to the food, carcass lean meat of animals can be increased with reduced food use and the meat be sold with reduced costs. However, clenbuterol will produce side effects to human body; an excessive intake will produce abnormal physiological responses such as nausea, dizziness, muscle tremors, palpitations, increased blood pressure and other symptoms of poisoning. Ministry of Agriculture has issued documents (No.176, No.193 Notice and No.1519 Ordinance) prohibiting the use of β -agonists as feed additives. Clenbuterol in animal feed is often detected by GC-MS, HPLC, ELISA and LC-MS/MS [16,17].

When the molecular weight of the sample is less than 400, the matrix (a small-molecule compound) commonly used in MALDI-TOF MS will produce ionization, leading to a mass spectrum of the small-molecule compounds existing in a large number of hetero-peaks that cannot be described. Hetero-peaks have a very strong mass discrimination effect, lead to small-molecule compounds which are not easily ionized to molecular ions. So the main purpose of the study is to find a matrix which is not only able to absorb laser energy but also can ionize the sample, at the same time not generating interfering ions of low molecular weight. In this way we will be able to take advantage of MALDI-TOF MS analysis of different types of small-molecule compounds [18].

EXPERIMENTAL

Materials

Matrix: 1,2,3,4-tetrakis (3',4'-hydroxyphenyl) thiophene (provided by the Institute of Chemistry, Chinese Academy of Sciences); α -cyano-4-hydroxy cinnamic acid (CCA) (Aldrich Co.); perfluoro C₆₀ (provided by the Institute of Chemistry, Chinese Academy of Sciences).

Solvents: ethanol, tetrahydrofuran (THF) (Beijing Chemical Factory); Milli Q ultrapure water.

Ionization reagents: sodium chloride; trifluoroacetic acid (Beijing Chemical Factory).

Samples: ractopamine; salbutamol; clenbuterol; terbutaline (Beijing Antai advanced technology development Co.).

Laboratory instruments and parameter settings

Instrument: Bruker autoflex MALDI-TOF MS equipped with a semiconductor laser, wavelength 355 nm, maximum power 200 μ J, attenuation 25% -45% of the laser operation. The delay leads and reflected working mode were used, delay time was 35000 ns, delayed extraction voltage 14.5 Kv, acceleration voltage 19 Kv, reflector voltage 20 kV. 150 superimposed scan signals formed the mass spectrum.

Configuration of sample, matrix, and ionized solution

Ractopamine, salbutamol, clenbuterol and terbutaline samples were dissolved in aqueous ethanol solution (ethanol:water=1:1), the concentration of the solution was 10⁻² mol/L; 1,2,3,4-tetrakis (3',4'-hydroxyphenyl) thiophene or α -cyano-4-hydroxy cinnamic acid (CCA) matrix was weighed, dissolved in aqueous ethanol solution (ethanol:water=1:1), the concentration of the solution was 10⁻³ mol/L; sodium chloride or trifluoroacetic acid ionizing solutions were weighed, dissolved in aqueous ethanol solution (ethanol:water=1:1), the concentration of the solution was 10⁻⁵ mol/L.

Sample preparation

The sample solution, 3 μ L of the matrix solution, and 1 μ L of ionizing reagent (if necessary) were thoroughly mixed, a 0.5 μ L droplet was placed on a clean stainless steel sample target, and after the solvent was evaporated, the crystalline sample was sent to the mass spectrometer for analysis.

RESULTS AND DISCUSSION

Matrix choice

As shown in Fig. 2, 1,2,3,4-tetrakis (3',4'-hydroxyphenyl)-thiophene contains eight phenolic hydroxyl groups which can provide a large number of protons in the ionization process; the protons are transferred to the sample molecules, so that sample ionization occurs.

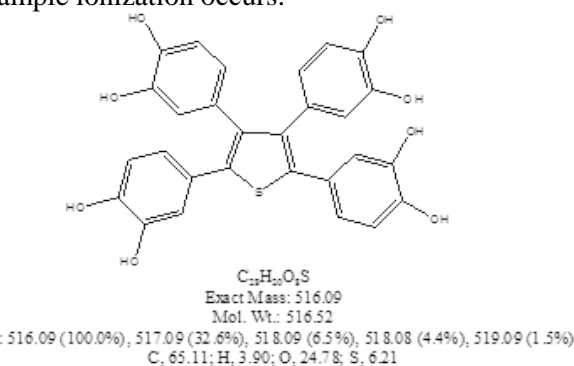


Fig. 2. 1, 2, 3, 4 – tetrakis (3', 4'-hydroxyphenyl) thiophene structure

Furthermore, 1, 2, 3, 4 – tetrakis (3',4'-hydroxyphenyl) thiophene has a relatively large molecular weight (516.09) which can be effectively reduced to produce a large number of hetero-peaks in the region of Da less than 400.

The UV absorption diagram of 1,2,3,4-tetrakis (3',4'-hydroxyphenyl) thiophene is shown in Fig. 3. UV laser absorption by the sample molecules is at 355 nm.

When terbutaline was determined by the MALDI-TOF mass spectrum, the concentration of the matrix solution was 10^{-3} mol/L, terbutaline sample solution concentration was 10^{-2} mol/L, sodium chloride concentration was 10^{-5} mol/L, solvent: ethanol:water =1:1.

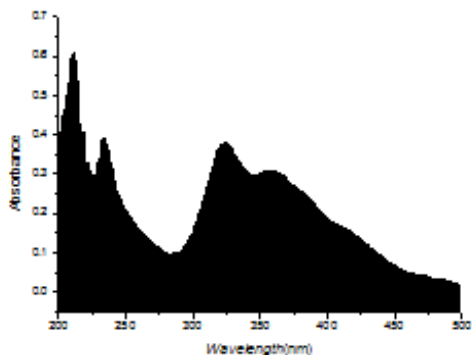


Fig. 3. 1,2,3,4-tetrakis (3',4'-hydroxyphenyl) thiophene UV absorption diagram

As shown in Fig. 4A, the 1,2,3,4-tetrakis (3',4'-hydroxyphenyl) thiophene matrix displays a protonated $[M + H]^+$ peak, but in Fig. 4 B, the CCA matrix shows a large number of impurity peaks within the detection area and no sample peak.

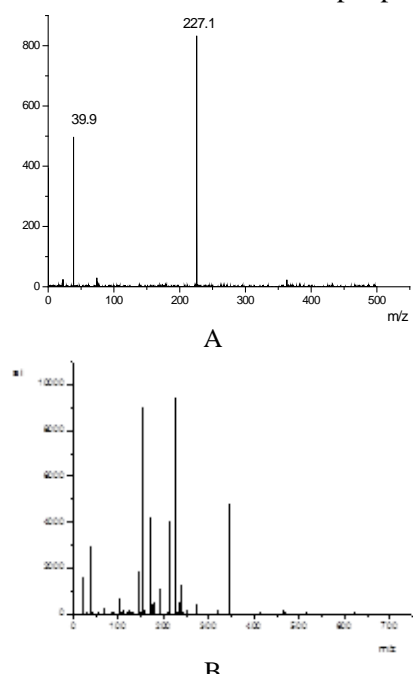


Fig. 4. MALDI-TOF mass spectrum of terbutaline in different matrices. A: 1,2,3,4-tetrakis (3',4'-dihydroxyphenyl) thiophene matrix; B: CCA matrix

Although few sample peaks can be found in the spectrum, the intensity of the sample peaks is lower and completely submerged in the impurity peaks.

Improvement of the matrix sensitivity

As shown in Fig. 5 A, when the sample solution is diluted to a certain concentration, sample salbutamol solution concentration is 10^{-8} mol/L under the same conditions, there is no apparent signal peak in the detection area using 1,2,3,4-tetrakis (3',4'-dihydroxy phenyl) thiophene as a matrix. Although few sample peaks can be found, the intensity of the peaks is lower and they are completely submerged in the impurity peaks. In Fig. 5 B and C, when using the mixture of 1,2,3,4-tetrakis (3',4'-dihydroxyphenyl) thiophene and perfluoro C₆₀ as a matrix, the interfering peaks in the whole region are greatly reduced.

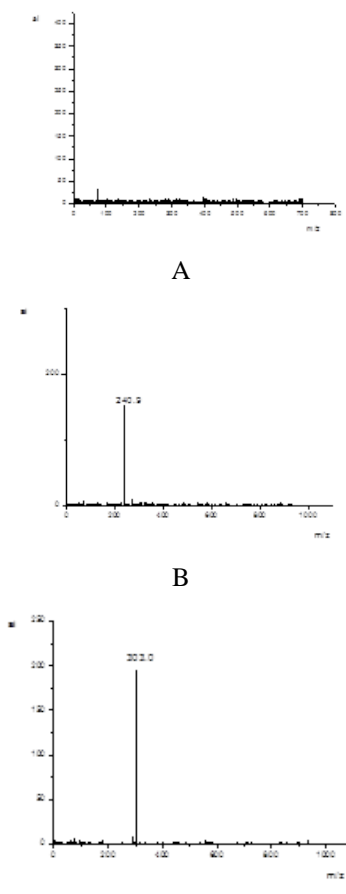


Fig. 5. MALDI-TOF mass spectrum for clenbuterol in different matrices. A: 1,2,3,4-tetrakis (3',4'-dihydroxyphenyl) thiophene matrix-salbutamol; B: Mixture of 1,2,3,4-tetrakis (3',4'-dihydroxyphenyl) thiophene and perfluoro C₆₀ matrix-salbutamol; C: Mixture of 1,2,3,4-tetrakis (3',4'-dihydroxyphenyl) thiophene and perfluoro C₆₀ matrix-ractopamine.

MALDI can determine macromolecules only; if the sample is a small molecule, a macromolecular matrix should be selected. However, a

macromolecular matrix has poor sensitivity: when the concentration of the sample solution is less than 10^{-8} mol/L it cannot produce a volume flow and significant signal peaks cannot be obtained.

In order to compensate for this deficiency, perfluoro C₆₀ was added to the matrix. Perfluoro C₆₀ has more hydrophobic characteristics, its structure is shown in Fig. 6. It can lock the sample in drops thus greatly increasing the sample concentration.

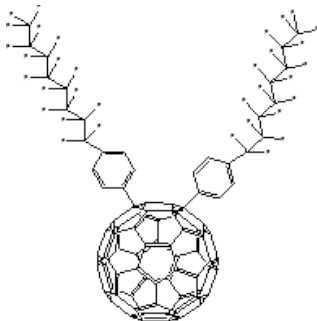


Fig. 6. Perfluoro C₆₀ structure

Because of its hydrophobicity, the adsorption force of the sample at the target surface becomes weak, and the sample is easier sputtered from the target surface. Perfluoro C₆₀ UV absorption diagram is shown in Fig. 7. The UV laser absorption at 355 nm can be absorbed by the sample molecules. The volume flow can be produced at lower energy. This is a good solution to the problem of poor sensitivity. Therefore, the 1,2,3,4-tetrakis (3',4'-hydroxyphenyl) thiophene mixed with the sample solution was added dropwise to the target surface uniformly covered with perfluoro C₆₀ and subjected to MALDI analysis.

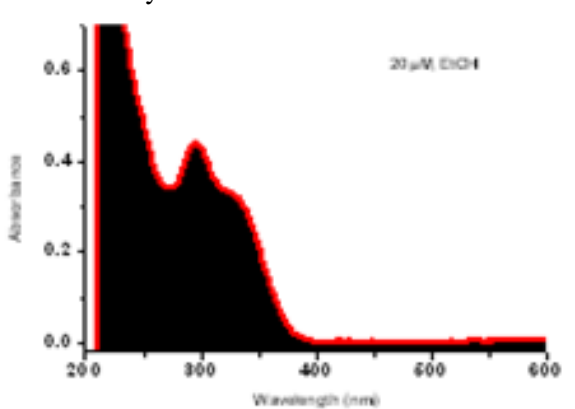


Fig. 7. Perfluoro C₆₀ UV absorption diagram

When the concentration of the sample solution is less than 10^{-8} mol/L, GC-MS and LCMS cannot detect a signal in the sample and MALDI-TOF mass spectrometry should be used.

Analysis of clenbuterol

Ractopamine, salbutamol, clenbuterol and terbutaline were analyzed by MALDI-TOF MS in 958

this experiment, the results are shown in Table 1 and Fig. 8.

In a mixture of 1,2,3,4-tetrakis (3',4'-dihydroxy phenyl) thiophene and perfluoro C₆₀ as a matrix with a concentration of 10^{-3} mol/L, clenbuterol concentration in the sample solution of 10^{-2} mol/L, sodium chloride concentration of 10^{-5} mol/L and solvent: ethanol:water=1:1, MALDI-TOF MS can quickly and accurately determine the molecular weight of clenbuterol.

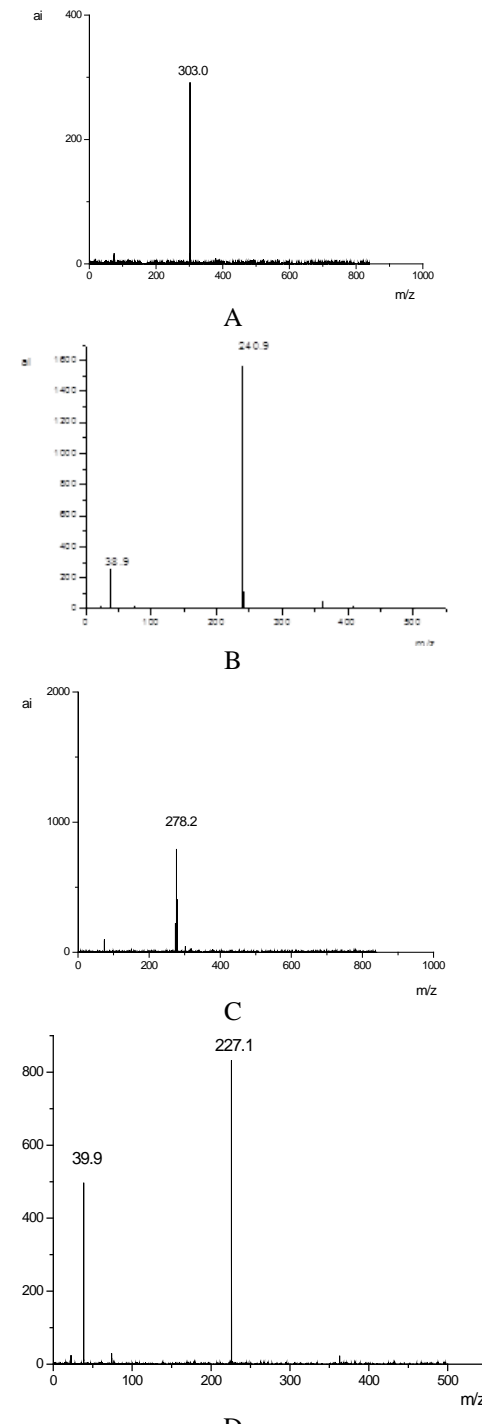


Fig. 8. The clenbuterol MALDI-TOF Mass Spectrum
A: ractopamine; B: salbutamol; C: clenbuterol; D: terbutaline

Table 1. The determination table of clenbuterol

Name	Structure	Formula	Theoretical molecular weight	Detection molecular weight
Ractopamine		C ₁₈ H ₂₃ NO ₃	301.38	303.0
Salbutamol		C ₁₃ H ₂₁ NO ₃	239.31	240.9
Clenbuterol		C ₁₂ H ₁₈ Cl ₂ N ₂ O	277.19	278.2
Terbutaline		C ₁₂ H ₁₉ NO ₃	225.29	227.1

CONCLUSION

This paper explores the matrix-assisted laser ionization time-of-flight mass spectrometry (MALDI-TOF MS) analysis of the small-molecule compound clenbuterol. MALDI-TOF MS has the advantages of high sensitivity, high throughput, simple operation and short analysis time. It is suitable for analysis of a variety of compounds. Using the new macromolecular matrix 1,2,3,4-tetrakis (3',4'-hydroxyphenyl) thiophene, not only a good sample can be mixed to provide a large number of protons, but also to transfer energy. Interference peaks were greatly reduced in the mass spectrum.

When the sample solution was diluted to 10⁻⁸ mol/L, the sample was not easily peeled off from the target surface, the macromolecular matrix had poor sensitivity, therefore, perfluoro C₆₀ was introduced. Perfluoro C₆₀ can lock the sample in drops of water, thereby greatly increasing sample concentration and ease of sputtering the sample from the target surface. This improved the macromolecular matrix sensitivity. The sample molecular weight was accurately measured, the error was within the allowable range, and almost no impurity peaks were present in the mass spectra. Results indicated that MALDI-TOF MS has a wide range of development and application. By taking advantage of MALDI-TOF MS high sensitivity, the presence of clenbuterol in food can be quickly and accurately detected, thus providing food security.

Acknowledgements: This work was financially supported by the National Natural Science Foundation of China (Grants No. 11475020, 8151114029 and 11475198), Chaoyang District collaborative innovation project (Grant No. XC1608).

Abbreviations: MALDI-TOF-MS: Matrix assisted laser desorption ionization time-of-flight mass spectrometry, CCA: α-cyano-4-hydroxy cinnamic acid.

REFERENCES

- 1.J. Wu, P. Zhang, *Instrumentation Analysis Monitoring*, **2**, 28 (2010).
- 2.J. Han, L.S.H. Sheng, *Chinese Journal of Pharmaceutical Analysis*, **3**, 30 (1998).
- 3.Y. W. Tian, J. P. Xie, *Tobacco Science & Technology*, **3**, 20 (2007).
- 4.J. Chalupová, M. Raus, M. Sedlářová, M. Sebela, *Biotechnology advances*, **32**, 230(2014).
- 5.Fenselau C, Demirev P A. *Mass Spectrom Rev*, **20**, 157 (2001).
- 6.V. Ryzhov, C . Fenselau, *Anal. Chem.*, **73**, 746 (2001).
- 7.G. Impallomeni, M . Giuggrida, T. Barauzzi, M. Giuseppe, B. Alberto, *Biomacromolecules* **3**, 835 (2002).
- 8.R. Duchateau, W. J. Wouter, Van Meerendonk, L .Yajjou, B. Bastiaan, C. Cor, G. GertJan, *Macromolecules* **39**, 7900 (2006).
- 9.C. Fenselau, P. A. Demirev, *Mass Spectrom. Rev.* **20**, 157 (2001).
- 10.V. Ryzhov, C. Fenselau, *Anal. Chem*, **73**, 746 (2001).
- 11.R. C. Beavis *Fresenius J. Anal. Chem.*, **343**, 25(1992).
- 12.Daniel C. Liebler: *Introduction to Proteomics: tools for the new biology*. Humana Press, 2002
- 13.A. Wertes, G. Lrinyi, R. Gijbels, *Anal. Chem.*, **65**, 2389 (1993).
- 14.Rachel R. Ogorzalek L. *Sample Preparation in Biological Mass Spectrometry*, 715 (2011).
- 15.Pasch H, Pizzi A, Rode K. *Polymer*. **42**, 7531 (2001).
- 16.<http://zh.wikipedia.org/wiki/%E7%98%A6%E8%82%89%E7%B2%BE>
- 17.C. Maltin, D. Balcerzak, R. Tilley, D. Margaret, *Proceedings of the Nutrition Society*, **62**, 337(2003).
- 18.F. Beate, S. Celestina, R. Grit, S. Rosmarie, S. Jürgen, *Journal of Biochemical and Biophysical Methods*, **70**, 689 (2007).

ИДЕНТИФИЦИРАНЕ НА КЛЕНБУТЕРОЛ С ПОМОЩТА НА MALDI-TOF МАССПЕКТРОМЕТРИЯ

К. Хюо^{1,2}, Т. Жоу¹, Ж. Хе¹, Ж. Ксие^{3,4*}

¹ Колеж по биохимично инженерство на Пекинския съюзен Университет, Пекин, Китай

² Пекинска лаборатория за оползотворяване на отпадни биоресурси, Пекин, Китай

³ Отдел по ядрена технология и приложение, Институт по високоенергийна физика, Китайска академия на науките, Пекин, Китай

⁴ Пекински инженерен изследователски център по радиографски техники и оборудване, Пекин, Китай

Получена на 16 август, 2017 г.; Приета на 6 ноември 2017 г.

(Резюме)

Матрично-асистирана лазерна десорбционна йонизация на времепролитаща масспектрометрия (MALDI-TOF-MS) е използвана за анализ на макромолекулни съединения. Настоящото изследване се фокусира върху използването на MALDI за определяне на малки молекули като кленбутерол и използване на матрицата за повишаване на чувствителността. Макромолекулната матрица на 1,2,3,4-тетракис (3',4'-хидроксифенил) тиофен не само абсорбира лазерната енергия, но също води до десорбционна йонизация на пробата. В същото време тя не дава нискомолекулни пречещи иони. Добавянето на перфлуоро C₆₀ към матрицата води до повишаване на чувствителността.

Quality grading system of Jadeite-Jade green based on three colorimetric parameters under CIE standard light sources D₆₅, CWF and A

GuoYing*

School of Gemology, China University of Geosciences, Beijing, China

Received June 1, 2016; Accepted May 25, 2017

The article deals with the color changes appearing under different light sources due to the individual and combined effects of lightness, hue and chroma. As a result, a green color grading system is created based on color evaluation from its appearance. We tested the color of 277 pieces of green jadeite specimens using Color i5 spectrophotometer based on CIE 1976 L*a*b* uniform color space and Munsell color matching system. It was concluded that the CIE standard light source D₆₅ is more suitable for assessing jadeite-jade green compared with the CIE standard light sources CWF and A. After the alternate use of light sources D₆₅ and A, the color shows a slight yellow tone. While the light source changed from D₆₅ to CWF, the lightness of jadeite-jade green decreased sharply. The jadeite-jade green concentrates on the lightness scope of (5.64, 61.96), and most of them focus on the scope of moderate to brighter lightness of (30, 60). It is shown that the optimal green of jadeite-jade is deep and dark. The support vector machine (SVM) predicts that 20 of 35 unclassified jadeite-jade cabochons should have a corresponding level based on the color green grading system of jadeite-jade. Taking into account the combination of theory and practice, the conclusion is drawn that the color green grading system of jadeite-jade should be calculated in the CIE 1976 L*a*b* uniform color space combined with the Munsell color system for physical color comparison.

Keywords: Jadeite-Jade green, CIE standard light source, Color grade, Quality grading of Jadeite-Jade green

INTRODUCTION

Jadeite-jade is the uncrowned king of all kinds of jade, and it is the latest representative of China jade culture which lasts for thousands of years, and is eagerly pursued by modern Chinese. But because of the structure of polycrystalline aggregation and almost the whole range of transparency and color, jadeite-jade quality evaluation, especially color evaluation is always an unrevealed problem. Gemologists from the world have tried many ways for several decades, but the effect is not ideal, such as jargons combined with industry experience and commercial estimation. Strong, intense, vivid, right and even are the terms widely spread in hundreds of years for the qualitative evaluation of jadeite-jade color standard, for example apple green, vivid green. Although experts can appraise jadeite-jade according to their experience, due to the lack of modern quantitative analysis, it could not be used as the color grading standard. Based on color evaluation, Gem Dialogue is recommended by the American association of Gem stone (AGS). It is composed of 21 pieces of transparent color scales and transparent black-grey, opaque black-white and transparent brown masks, respectively. Each of these 21 color scales has 10 strips with different color chroma, and each of these 3 masks has 10 strips with different grey level from black to white,

so a total of 60000 kinds of color chip combinations will be formed together with color scale and mask. However, this color specification system is supported by subjective evaluation by the naked eye and lacks a complete theoretical system, so to evaluate the different combinations of color scale and color mask, there is no only color scheme for the same color sample. On account of this, China gem faculties attempted to try unified standards to regulate jadeite-jade quality evaluation, and encourage industry. But with the booming development of jewelry industry and rapid gemological progress, these standards also gradually exposed some problems [1,2]. The provincial standard Jadeite-jade Jewelry Grading was issued in 2003 from the Yun Nan province, with the help of Gem Dialogue (GIA) and Gem Set (GIA). A photo album was issued according to the two most widely used international color description and classification systems of gemstones. But this does not avoid the disadvantage of subjective quantitative description and the practical problems such as color fades through ageing; therefore it is not good for color difference presentation of high-quality jadeite-jade color. Another example is the GB/T 23885-2009 Jadeite Grading issued in 2009 [3], which is an attempt to evaluate and classify the quality of jadeite-jade color. While not applied in the jewelry industry, it still takes an abandoned CIE 1931 two-dimensional

* To whom all correspondence should be sent:
E-mail: guoying@cugb.edu.cn

color system as the theoretical basis. In that system the color tone is described as a dominant wavelength, the color purity or excitation purity (P_e) is described as chroma, Gem Dialogue grey scale is described as lightness, and Gem Dialogue is regarded as the color matching system. The standard appendix B illustrates that jadeite-jade (green color) color evaluation should employ a spectral photometric method of color measurement with an alternative standard light source A (color temperature 2856K) or D (color temperature of D_{65} is 6504K). It is well known that the color temperature difference of different light sources, background color difference of different chroma and different illumination intensity can affect the jadeite-jade color appearance apparently, which leads to additional color and illuminant metamerism [4-10], and especially to high chroma color.

EXPERIMENTAL

Materials

277 pieces of cabochon jadeite-jade with smooth surface, fine texture and good purity were selected as samples. All gemstones were sized from $6\text{mm} \times 8\text{mm} \times 5\text{mm}$ to $8\text{mm} \times 10\text{mm} \times 7\text{mm}$ that is below the upper limit of the national standard $50\text{mm} \times 30\text{mm} \times 50\text{mm}$. They displayed even color within the range from bluish green to vivid green to yellowish green, with continuous changing of color shade and depth.

Analytical methods

Spectrophotometer Color i5 was used to collect reflective signals from the jadeite-jade surface via the integrating sphere. Testing conditions: geometry D\8 tri-beam simultaneous SCE, specular component setting-excluded (SCE), light source D_{65} with light source A and CWF calibrated, measurement time < 2.5 sec (flash & data acquisition), spectral range 360 to 750 nm, wavelength interval 10 nm, voltage 240V, current 50~60HZ.

The research followed three steps: firstly, the three-dimensional coordinates L^* , a^* , b^* of jadeite-jade green were quantitatively tested in the CIE 1976 $L^*a^*b^*$ uniform color space, so the distance of each couple of points could be calculated to show their color difference; secondly, based on that, the color metamerism characteristics could be confirmed, and the color evaluation system would be set up while the lightness is taken as the primary factor; thirdly, with the correction of most popular color system Munsell, the final color grading system of jadeite-jade green is formed which has 5

grades from the top grade to the last, and is in accordance with international gem color grading system.

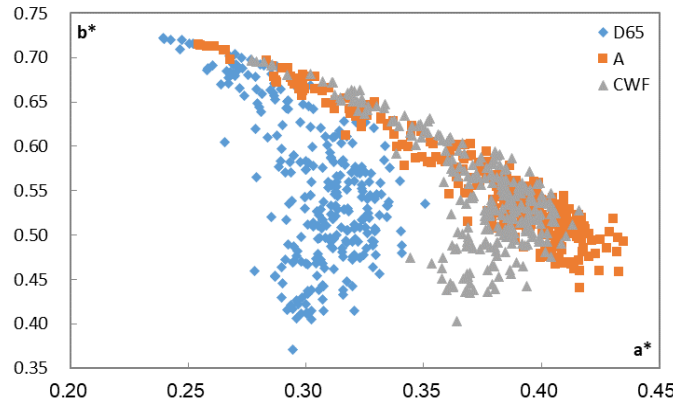
RESULTS AND DISCUSSION

Jadeite-jade Green under Different Light Source

For a specific CIE observer and standard light source, if two jadeite-jade color with same tristimulus values have different spectral power distribution within the visible spectrum, these two color called metamerism color [11]. Its measurement includes alternating standard observer and alternating light source, while the method of light source alternation is often used, especially for small size gemstone samples.

For the sake of significantly different color distribution of jadeite-jade green under three CIE standard light sources it is required that the contribution to jadeite-jade color appearance from the smoothness of the spectral power distribution curve and the effect on the color rendering should be analyzed. The plot areas of L^* , a^* , b^* are significantly different, and with the temperature increase they gradually move toward the blue area, as shown in Figure 1.

It is confirmed that the CIE standard light source A is more suitable for the performance of low chroma or bluish green samples for its orange to red background, and as a result it benefits the chroma promotion of green with the naked eye because its orange-red background significantly turns jadeite-jade green into a warm color. CIE standard light source CWF is more suitable for the performance of jadeite-jade bluish green, its light yellow and light fluorescence can promote stone chroma and make the color greener. CIE standard light source D_{65} is more suitable for the performance of lightness and transparency of jadeite-jade green because of its high color temperature and slight blue background, such as for nearly colorless and transparent glass-like samples with fine texture. But D_{65} is not suitable for the performance of jadeite-jade green with blue tone, because it will reduce the chroma of green especially compared with the other two CIE standard light sources. China National Standard GB/T23885-2009 "Jadeite-Jade Grading" defines that the upper limit of color temperature of the light source should be below 5503K, that is, the CIE standard light source D_{55} . Both D_{55} and D_{65} are the light sources recommended by CIE to simulate the sun light, so they exhibit very close appearance of CIE standard green and CIE high chroma green with small color difference less than 3, which belongs to the just perceivable range by the naked

**Fig. 1.** Chromatic diagram of Jadeite-Jade green under 3 CIE standard light sources D₆₅, A and CWF**Table 1.** Imitation of CIE Standard green color under different light sources

	D ₆₅ (6504K)	A(2856K)	CWF(4500K)	D ₅₅ (5503K)
CIE standard green				
CIE 1976 L*a*b*	56, -32, 0 55, 149, 133	52.49, -29.08, -9.85 33, 138, 140 509 nm	53.43, -22.20, 1.59 84, 140, 125	55.54, -31.67, -1.68 51, 149, 136
Main-wavelength color difference	— —	ΔE _{D65-A} =10.86	ΔE _{D65-CWF} =10.26	ΔE _{D65-D55} =1.77
CIE standard high chroma green				
CIE 1976 L*a*b*	56, -45, 0 0, 154, 133	51.22, -43.30, -12.72 0, 141, 141 534 nm	52.34, -33.28, 0.82 39, 134, 124	55.40, -45.00, -2.08 0, 151, 134
Main-wavelength color difference	— —	ΔE _{D65-A} =13.69	ΔE _{D65-CWF} =12.31	ΔE _{D65-D55} =2.16

Table 2. Correlation coefficients of the mean values of L*, a*, b*, C* and \bar{h}_0 under 3 measuring light sources

\overline{L}^*				\overline{a}^*			\overline{b}^*			\overline{C}^*			\overline{h}_0		
D ₆₅	D ₆₅	A	CWF	D ₆₅	A	CWF	D ₆₅	A	CWF	D ₆₅	A	CWF	D ₆₅	A	CWF
D ₆₅	1	—	—	1	—	—	1	—	—	1	—	—	1	—	—
A	0.999	1	—	0.988	1	—	0.991	1	—	0.987	1	—	0.979	1	—
CWF	1	0.999	1	0.986	0.995	1	0.967	0.954	1	0.980	0.948	1	0.925	0.930	1

$$\Delta E_{2000} = \sqrt{\left(\frac{\Delta L'}{k_L S_L}\right)^2 + \left(\frac{\Delta C'}{k_C S_C}\right)^2 + \left(\frac{\Delta H'}{k_H S_H}\right)^2 + R_T \left(\frac{\Delta C'}{k_C S_C}\right) \left(\frac{\Delta H'}{k_H S_H}\right)}$$

CIE 2000

$$\Delta E_{LAB} = \sqrt{(\Delta L^*)^2 + (\Delta a^*)^2 + (\Delta b^*)^2}$$

CIE LAB

eye. Consequently, D₅₅ can act as a light source for jadeite-jade evaluation, as shown in Table 1.

Considering the light source and the characteristics of jadeite-jade green, each CIE standard light source has its advantages for their different spectral power distribution. The conclusion can be drawn: compared with CIE standard light sources A and CWF, the light source D₆₅ is more suitable for the jadeite-jade green evaluation.

The analysis of the impact from different CIE standard light sources on jadeite-jade green should be done from lightness (L*), chromaticity coordinates (a* and b*), chroma (C*) and hue angle (h_0), respectively based on the CIE 1976 L*a*b uniform color space, as shown in Table 2.

The color differences from the light source alteration were calculated in pairs.

CIE 2000 formula is the latest color difference

formula recommended by CIE, including not only also a cross-function which is similar to the BFD formula. So, as a result, the capability of the neutral gray color prediction is improved. But because of the low resolution of green, the basic color difference has the greatest influence on the color difference from Δa^* and the color appears as lightly yellowish. Formula CIE LAB is used within the uniform color space instead of CIE 2000, the results are shown in table 3.

Table 3. General averages of ΔE^* , ΔL^* , Δa^* , Δb^* , ΔC^* , Δh_0 obtained with 277 pieces of jadeite-jade according to 3 measuring light sources

	$\overline{\Delta E^*}$	$\overline{\Delta L^*}$	$\overline{\Delta a^*}$	$\overline{\Delta b^*}$	$\overline{\Delta C^*}$	$\overline{\Delta h_0}$
$D_{65} \rightarrow A$	8.36	1.89	-3.63	7.30	7.46	-3.94
$D_{65} \rightarrow A$	8.33	0.78	-8.05	-1.98	3.93	9.07
$A \rightarrow CWF$	10.33	-1.11	-4.42	-9.27	-3.53	13.01

Compared with the CIE standard light source D_{65} , the lightness of jadeite-jade green decreased greatly under A, and this is obviously the result of the decrease in color temperature from D_{65} to A (6504K to 2856K). The sharp increase of chromaticity coordinates a^* reveals a change to the direction of red, while the sharp decrease of chromaticity coordinates b^* reveals a change to the direction of blue. And for the sake of the greatest influence on color difference from Δb^* , the color appearance shows a slight yellow tone after light source alteration from D_{65} to A.

The lightness of jadeite-jade green decreased sharply when the light source changed from D_{65} to CWF, which is related to the decrease in color temperature from 6504K to 4150K. The sharp increase of chromaticity coordinates a^* reveals a change to the direction of red tone, while the light increase of chromaticity coordinates b^* reveals a change to the direction of yellow tone. For the sake of the greatest influence on color difference from Δa^* , the color appears lightly yellowish green after light source alteration. The different color temperature of the different light sources has an effect on jadeite-jade green, for example, if under the same illuminance, the lightness and chroma of green will gradually increase with the increase in color temperature of the light source. The color appearance of jadeite-jade changes is obviously accompanied by changes in light source illuminance. As a result, with the increase in light source illuminance, both visual chroma and visual lightness would increase, and both color saturation and lightness would also increase (Hunt effect and Stevens effect). Jadeite-jade green can appear brighter when illuminated by a high illuminance

lightness, chroma and hue weighed function, but light source, and the color grade can be noticed by the naked eye.

This illustrates that the light source alteration ($D_{65} \rightarrow A$, $D_{65} \rightarrow CWF$, $A \rightarrow CWF$) has little impact on the lightness, while it has bigger impact on the chromaticity coordinates and chroma, and has the biggest impact on hue angle. So, it is concluded that the green tones can present obvious visual difference in the process of light source conversion.

Grade by lightness

Under the circumstance of standard light source A, the dominant wavelengths λ of the 277 pieces of cabochon jadeite-jade were tested in the range of 513-562 nm. The dominant wavelengths of 58 samples were higher than 550 nm and were not graded as green according to Jadeite Grading, though they showed apparent vivid green with the naked eye. The chroma of 219 pieces of jadeite-jade was calculated and graded. 13 pieces of jadeite-jade were not classified to any chroma level for the sake of $P_e < 10$.

Jadeite Grading introduces a grey scale of Gem Dialogue, and grades 206 pieces of green jadeite-jade chroma at four levels consequently, that is, 19 pieces of V1 with $G < 10$, 113 pieces of V2 with $10 \leq G < 30$, 55 pieces of V3 with $30 \leq G < 50$, and 19 pieces of V4 with $G \geq 50$.

The results revealed that compared with the equal lightness L^* of yellowish green jadeite-jade, there is a little grey tone in the visual effect, and black/grey masks are always used with the grey scale range of 10-40. Lightness of yellowish green usually belongs to V2, while the grey scale is significantly stronger only when the color is dark, such as jargons of "Yin green" and "Melon-Peel green". Among them the yellowish green of jadeite-jade with $L^* \in (38, 55)$ is the main source of V1, and is also the main source of high-quality green jadeite-jade, such as "Huang-Yang green". The value of low-lightness jadeite with grey scale $G \geq 30$ (especially $G \geq 50$) will decrease.

In the uniform color space CIE 1976 $L^*a^*b^*$, CIE stipulates that the lightness of green and high chroma green is 56, the lightness of yellowish green and high chroma yellowish green is 65, that is $L^*=56$ while green jadeite-jade has optimum chroma $C^*=45$, and $L^*=65$ while yellowish green jadeite-jade has optimum chroma $C^* \in (16.40, 49.20)$.

Through the measurement of Color i5, the lightness of 206 pieces of jadeite-jade green

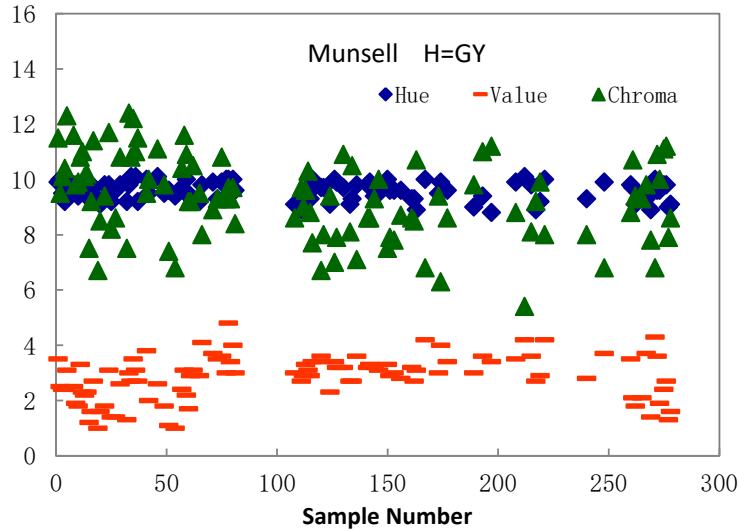


Fig. 2. Color parameters of 105 pieces of jadeite-jade greenish yellow under Munsell color system

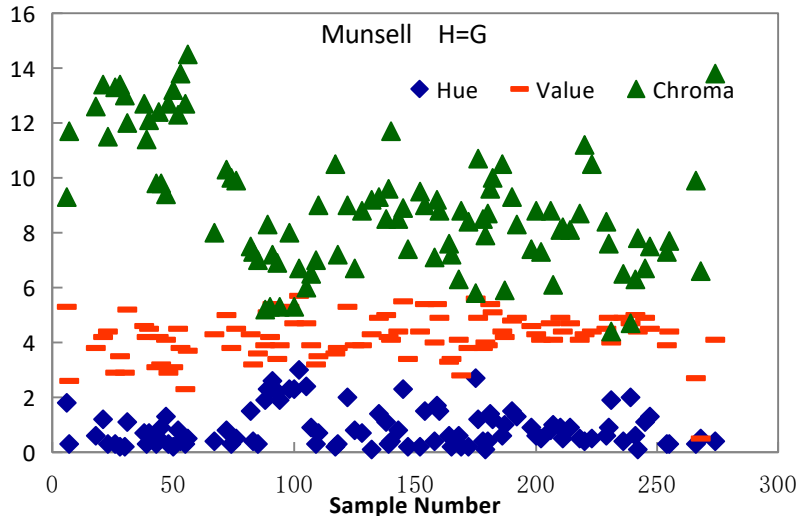


Fig. 3. Color parameters of 101 pieces of jadeite-jade green under Munsell color system

concentrates on the scope $L^* \in (5.64, 61.96)$, and most of them focus on the scope of moderate to brighter $L^* \in (30, 60)$, but failed to meet the best green lightness. This agrees with the deep tone of visual effect of jadeite-jade vivid green or yellowish green. Through comparison of samples and Munsell color chips, the better moderate lightness is testified adequately, see Figs. 2 and 3. They illustrate that the optimal color of jadeite-jade green has a relative low lightness, meaning that the optimal green of jadeite-jade is a little deep and dark, but not the standard green of color science.

Quality grading of jadeite-jade green

According to Jadeite Grading, the quality of color green of 206 pieces of jadeite-jade should be graded into 5 levels from excellent (12 pieces) to very good (71 pieces), good (22 pieces), fair (51 pieces) and poor (15 pieces), described as the acronyms EX, VG, G, F and P. Other 35 pieces did not belong to any level. According to the known

level of samples, the tested lightness and chroma data of 206 samples, using Support Vector Machines (SVM) the vacancy levels in Table 3 and 35 unknown level samples were predicted, see Table 4.

Table 4. Evaluation sheet of jadeite-jade green color

	Ch1	Ch2	Ch3	Ch4	Ch5
V1	EX	EX	VG	G	G _p
V2	VG	VG	G	F	G _p
V3	F	F	F	P	P
V4	F _p	F _p	F _p	P	P

Note: G_p and F_p are SVM predicted level G and F

SVM is put forward by Vapnik in the mid-1990s, based on a statistical theory, an application of the theory of VC dimension and structural risk minimization principle, with the aid of optimization methods [12,13] such as a machine learning algorithm. It has unique advantages in solving small samples, nonlinear and high dimensional pattern recognition problems [14]. But its performance by

Table 5. Grade F by prediction and evaluation of jadeite-jade green color

Predicted Level F	16# Pe=84.6 G=50	9# Pe=79.0 G=50	22# Pe=77.8 G=50	10# Pe=92.1 G=50	49# Pe=85.6 G=50	60# Pe=89.3 G=50	20# Pe=88.4 G=50	27# Pe=91.1 G=60	262# Pe=93.0 G=50
Known Level F	273# Pe=86.2 G=40	42# Pe=83.3 G=40	265# Pe=71.5 G=40	13# Pe=73.6 G=40	14# Pe=74.5 G=30	12# Pe=80.5 G=40	59# Pe=78.8 G=40	55# Pe=89.2 G=30	4# Pe=85.9 G=30
Predicted Level F	49# Pe=85.6 G=50	198# Pe=19.4 G=10	236# Pe=14.9 G=10	192# Pe=18.7 G=10	230# Pe=18.3 G=10	159# Pe=18.1 G=10	6# Pe=18.4 G=10	102# Pe=17.0 G=10	
Known Level F	261# Pe=85.1 G=40	158# Pe=25.4 G=20	167# Pe=25.2 G=20	160# Pe=20.0 G=10	210# Pe=20.4 G=10	181# Pe=22.3 G=10	89# Pe=25.8 G=10	122# Pe=26.9 G=10	

Table 6. Level G by prediction and evaluation of jadeite-jade green color

Known level F	82# Pe=16.9 G=20		247# Pe=17.2 G=20		154# Pe=18.5 G=20	
Measured Level F	127# Pe=41.1 G=20		67# Pe=30.4 G=20		145# Pe=26.4 G=8	

the error penalty parameter c and its greater influence on the form of kernel function and its parameters, applied to many kinds of classification was not good enough, so the classification accuracy should be improved [15,16].

The model trained by SVM is verified by the test set samples, its accuracy is 86.21%, and can be used to do prediction [17], and the unasserted levels are listed in Table 4. There are 35 pieces of unasserted samples. 19 of them with $Pe \in (65, 100)$

and $G \in (50, 100)$ are graded as level F, while among the rest, 16 with $Pe \in (10, 20)$, $G \in (10, 20)$, 9 pieces are graded as level G and 7 pieces are graded as level F. The quality of jadeite-jade green rapidly decreased with reduced lightness, so good quality jadeite-jade usually has a fancy intense color, which corresponds to the experimental prediction. Only the prediction of Ch5-V2 is a little higher than what it should be at level F even below.

Compared with computer color simulation, the results of level F and G of color grade predicted by SVM are listed in Tables 5 and 6. Predicted 9 pieces of F samples and 6 pieces of G samples did not match the corresponding color close to already known levels of the samples. Although SVM prediction is possible, this proves that the existing green jadeite-jade grading system has obvious flaws.

CONCLUSIONS

When the color temperature of the light source gradually increases, stone color turns little by little to blue. Compared with the CIE standard light source D₆₅, the lightness of jadeite-jade green greatly decreased under CWF and A, which can obviously present visual difference. Taking into account light source and samples, D₆₅ is more suitable as the light source for jadeite-jade green compared with the sources CWF and A.

As an independent colorimetric parameter, lightness is relatively in accordance with the visual effect of jadeite-jade green, e.g., the optimal color of jadeite-jade green is not the standard green of color science, but a little deep and dark.

There are 3 problems in the current jadeite grading systems: 1. Some good-quality green jadeite-jade, as “Fu-Rong” jadeite-jade, could not be included in the grading system, because its green and yellowish green is with the main wavelength more than 550nm; the second is green under naked eye but with relative low excitement purity (Pe<10), it always has the typical color of “Jin-Si” jadeite-jade. 2. For all color parameters considered separately, the weight of their contribution to the color is not comprehensively taken into account. As a result, some good-quality green samples under naked eye are out of the grading system. 3. There are 35 samples predicted by SVM, 17 and 3 pieces of them predicted as level F and G, respectively, that are matched with already known levels, so they can be involved in the jadeite grading system; but the other 9 and 6 pieces of them are predicted as level F and G, respectively, that are unmatched with already known levels, so there are obviously some disadvantages in the current system.

Gem quality evaluation of green [18] is a complex system. Gem colors will be simultaneously determined by the lighting source, observation conditions (including the background) and its own conditions. So the first factor is the light source effect [19,20]. The second factor is the impact on the visual lightness of the green color under neutral background, and if possible, all psychological factors such as color constancy

should be considered. Because of the dependency of hue and chroma, the relative independent lightness should be first considered when the object color is taken into account [21], and then the weights of their respective contributions to the color appearance should be comprehended to make an operable color grading system of jadeite-jade.

Based on the combination of theory and practice, CIE 1976 L*a*b* uniform color space is recommended as measuring system, and Munsell color system is recommended as object matching system.

REFERENCES

1. Bureau of Technical Supervision of the Quality of Yunnan Province. DB53/T 102-2002 Local Standard in Yunnan Province-Jadeite Jewelry Grading. *Beijing: Standards Press of China*, 2002-11-1.
2. Bureau of Technical Supervision of the Quality of Yunnan Province. DB53/T 302-2009 Local Standard in Yunnan Province-Jadeite Jewelry Quality Grade Evaluation. *Beijing: Standards Press of China*, 2010-3-1.
3. GB/T 23885-2009, Jadeite Grading, China National Bureau of Technical Supervision. Chinese National Standards. *Beijing: Standards Press of China*, 2009-6-1.
4. E. C. Fuchs, K. Gatterer. *Central European Journal of Chemistry*, **6**(4), 497 (2008).
5. H. Xu, M. R. Luo, B. Rigg. Evaluating the Quality of Daylight Simulators Using Metameric Samples. *9th Congress of the International Colour Association*, **4421**, 697-700 (2002).
6. S. H. Kim, Y. K. Lee, B. S. Lim, S. H. Rhee, H. C. Yang. *Dental Materials*, **23**(3):374-379(2007).
7. Z. J. Li, R. S. Berns. *Color Research and Application*, **32**(4), 293 (2007).
8. M. E. L. Leow, W. K. M. Ng, B. P. Pereira, A. K. Kour, R. W. H. Pro. *Prosthetics and Orthotics International*, **23**(2), 174 (1999).
9. L. D. Carstensen. *Color Research and Application*, **20**(2), 131 (1995).
10. D. C. Rich, J. Jalilali, *Color Research and Application*, **20**(1), 29 (1995).
11. M. Melgosa, E. Hita, *Optik (Jena)*, **107**, 5 (1997).
12. R. Li, Y. E. Shiwei, Z. Z. Shi, *Acta Electronica Sinica*, **30**(5), 745 (2002).
13. B. Gou, X. W. Huang, SVM *Journal of Data Acquisition & Processing*, **21**(3), 334 (2006).
14. Z. W. Xing, H. Zhang, Machine. *Computer Technology and Development*, **22**(6), 247 (2012).
15. G. H. Feng, *Computer Engineering and Applications*, **47**(3), 123 (2011).
16. X. X. Niu, K. H. Yang, *Information Technology*, **11**, 19 (2006).
17. Q. Y. Zhang, X. L. Feng, H. L. Long, J. J. Suo, D. D. Zhang, L. Z. Xu, L. Xu, *Acta Chimica Sinica*, **70**(8), 989 (2012).
18. Y. Guo, X. Li, H. M. Du, H. J. Sun, Green Color Appreciation of Gemstones Based on CIE 1976

- L*a*b*. 2011 International Conference on Multimedia and Signal Processing, Guilin, Guangxi China, May 14-15, 2011, DOI:10.1109/CMSP.47.2011
19. H. Wang, Y. Guo, Y. Zhang, Key Engineering Materials, **492**, 374 (2011).
20. Y. Guo, J. Zhang, T. Mo. Advanced Materials Research, **177**, 620 (2010).
21. H. M. Du, Y. Guo. Optical influence of different standard illuminants on green nephrite's color From Manasi. Proceedings of Conference 7844 Semiconductor Lasers, Solid State Lighting & Applications, **7844**, 784411 (2010).

СИСТЕМА ЗА ОЦЕНКА НА ЗЕЛЕНИЯ ЦВЯТ НА ЖАДЕИТ-НЕФРИТ НА ОСНОВАТА НА ТРИ КОЛОРИМЕТРИЧНИ ПАРАМЕТРА НА СИЕ СТАНДАРТНИ СВЕТЛИННИ ИЗТОЧНИЦИ D₆₅, CWF И А

Гуо Инг*

Училище по гемология, Университет по геонауки, пекин, Китай

Потъпила на 1. юни 2016; Приета на 25. май 2017

(Резюме)

Изследвани са промените в цвета при облъчване с различни светлинни източници, като е оценено влиянието на факторите светлост, оттенък и хрома поотделно и заедно. В резултат е създадена система за оценка на цвета, основаваща се на външния вид. Изследван е цветът на 277 образци от зелен жадеит-нефрит с помощта на спектрометър Color i5 на основата на еднородното цветово пространство CIE 1976 L*a*b* и системата на Munsell за цветово съвпадение. Резултатите показват, че стандартният СИЕ светлинен източник D₆₅ е по-подходящ за оценка на зеления цвят на жадеит-нефрит в сравнение със стандартните източници CWF и А. След последователно използване на източниците D₆₅ и А, цветът показва лек жълт нюанс. Когато източникът се сменя от D₆₅ на CWF, светлостта на жадеит-нефритовия зелен цвят рязко намалява. Светлостта на зеления цвят на образците от жадеит-нефрит е в областта (5.64-61.96), като по-голямата част е със средна до висока светлост (30-60). Показано е, че оптималният цвят на жадеит-нефрита е дълбок и тъмен. Помощният векторен инструмент предсказва, че 20 от 35 некласифицирани кабошони от жадеит-нефрит би трябвало да са на съответното ниво от системата за оценка на зеления цвят. Имайки пред вид комбинацията от теория и практика е направен изводът, че системата за оценка на зеления цвят на жадеит-нефрита трябва да се одновременно еднородното цветово пространство СИЕ 1976 L*a*b* в съчетание с цветовата система на Munsell за физично сравняване на цвета.

Study on the water resistance performance of floor rockmass under different fracture combinations

H.L. Yu¹, J.M. Zhu^{2*}, Y.S. Zhang^{1,3}, W.Q. Zhang^{1,3}, Zh.Ch. Wang⁴

¹College of Mining and Safety Engineering, Shandong University of Science and Technology, Qingdao 266590, China

²Department of Resources and Civil Engineering, Shandong University of Science and Technology, Taian 271019, China

³State Key Laboratory of Mining Disaster Prevention and Control Co-founded by Shandong Province and the Ministry of Science and Technology, Shandong University of Science and Technology, Qingdao 266590, China

⁴School of Civil and Safety Engineering, Dalian Jiaotong University, Dalian 116028, China

Received August 24, 2017; Accepted November 1, 2017

To obtain the water resistance performance of floor strata under different rock layers and fracture combinations, the propagation mechanisms of different crack combinations in floor strata under mining conditions were simulated by using singular elements. The propagation path of twin cracks under different situations was given by the minimum plastic zone theory according to the change of the fracture factor and the plastic strain of different strata combination cracks under the influence of fault, water pressure and mining. The shortest length of the rock bridge between twin cracks after bursting in different strata combination was obtained. The water resistance performance of every strata combination was analyzed. It was shown that the water resistance performance of the floor strata under the combination soft-soft-hard-hard upward is the worst while the combination of alternating soft-hard is the best. The fracture factor combination and the plastic strain of the crack will reach maximum when mining near to it, and the crack is mostly easy to extend. The shortest length of the rock bridge between the twin cracks after bursting is under the combination of soft rock layers below and hard rock layers above while it is the longest under the combination of alternating soft-hard. The length of the rock bridge between the twin cracks after bursting will be shortened when considering the water pressure inside the crack and fault, which results in a decrease in rock water resistance performance. This paper will provide a reference for floor water inrush prediction in fractured rock mass.

Keywords : Floor strata , Fracture combination , Minimum plastic zone , Propagation path , Water resistance performance

INTRODUCTION

Since the floor aquifuge in pressure mining plays a role of blocking the confined water, the water resistance performance of the aquifuge is a very important parameter. Due to the difference of the comprehensive petrofabric, physical, mechanical, and hydraulic characteristics between the floor strata and the engineering geology, their mechanism and characteristics of rock mass failure are different under various geological stress; the mechanism, physical process and genetic types of the strong seepage channel formation which could induce the ordovician limestone water inrush are different too, then the water resistance performance differences between different strata combination are shown [1-2]. Floor water inrush is the interaction result of various factors, such as the geological structure, mining pressure, water pressure, the characteristics of aquifuge, etc. [3-4]. The fracture in the floor strata combination will cause plastic failure under the influence of mining, fault and water pressure; the further expansion of plastic zone leads to an increase in the permeability of rock

mass near the cracks, making the cracks interconnected, and a water inrush channel will form under the action of high-pressure water. To realize the mining safety on the confined water, the influence of various factors should be comprehensively considered. Domestic and foreign scholars put forward a lot of theories such as "water inrush coefficient" [5-6], "concept of relative thickness of aquifuge" [7], "strong seepage channel" [8-9], "water-rock stress" [10], "zero position destruction and *in-situ* fissures" [11], "key stratum theory" [12], "down three zone theory" [13-14] and so on. In these theories the mechanism and prediction methods of water inrush were revealed from all aspects, and the direction of mining fissure extension search becomes critical in the formation mechanism of water inrush channel. In this paper, the crack in different floor strata combinations was simulated using the singular unit in the finite element, considering the influence of mining, strata construction, high-pressure water. Propagation direction of cracks in different floor strata combination was searched using a minimum criterion of the plastic zone, and the crack and rock combination was obtained which is the most easy to form the water inrush channel. It has important

* To whom all correspondence should be sent:

E-mail: 330729788@qq.com

theoretical significance for many mining cracks extension mechanism analysis, coal floor strata's water resistance performance evaluation and accurate analysis, and to ensure the mining safety under pressure.

Criterion of crack propagation and the simulation method

Crack fracture criterion selection

The underground rock fracture is I-II mixed mode fracture under combined compression-shear loading, as shown in Fig. 1.

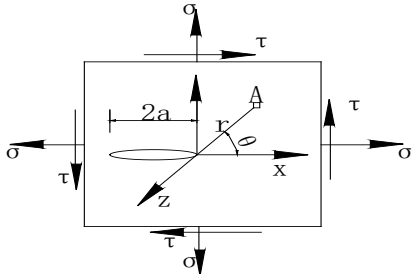


Fig.1. Mechanism of crack under compression-shear combination conditions

According to the Griffith criterion, when the maximum stress intensity factor K_{\max} reaches K_{IC} , the energy released by the crack propagation is enough to provide for all its extension needs, and the cracks will further extend, the total strain energy release rate G_C and the crack propagation resistance R_C should meet the formula below:

$$G_t = G_I + G_{II} + G_{III} \geq R_c \quad (1)$$

For I - II type combined loading:

$$\begin{cases} G_I = \frac{(1-\nu^2)K_I^2}{E} \\ G_{II} = \frac{(1-\nu^2)K_{II}^2}{E} \\ G_{III} = 0 \end{cases} \quad (2)$$

So the criterion of fracture is the formula:

$$K_I^2 + K_{II}^2 = K_{\max}^2 = K_c^2 \quad (3)$$

Where: K_I and K_{II} are the type I and type II stress intensity factors of crack, respectively. When meeting $K_I^2 + K_{II}^2 \geq K_c^2$, crack extension will occur.

From the energy conservation and transformation of the crack propagation, we can conclude that the existence of the crack tip plastic zone is an important factor to anti-crack, the plastic work of the crack propagation has close

relationship with the material fracture toughness, and in the same plastic zone, in which direction the plastic zone width is the shortest (refers to the shortest distance between the crack tip and the edge of the plastic zone), the crack will propagate most easily from this direction [15].

Under the combined stress state, the stress field of a certain point near the crack tip is as below:

$$\sigma_x = \frac{K_I}{\sqrt{2\pi r}} \cos \frac{\theta}{2} (1 - \sin \frac{\theta}{2} \sin \frac{3\theta}{2}) - \frac{K_{II}}{\sqrt{2\pi r}} \sin \frac{\theta}{2} (2 + \cos \frac{\theta}{2} \cos \frac{3\theta}{2}) \quad (4)$$

$$\sigma_y = \frac{K_I}{\sqrt{2\pi r}} \cos \frac{\theta}{2} (1 + \sin \frac{\theta}{2} \sin \frac{3\theta}{2}) + \frac{K_{II}}{\sqrt{2\pi r}} \sin \frac{\theta}{2} \cos \frac{\theta}{2} \cos \frac{3\theta}{2} \quad (5)$$

$$\tau_{xy} = \frac{K_I}{\sqrt{2\pi r}} \cos \frac{\theta}{2} \sin \frac{\theta}{2} \cos \frac{3\theta}{2} + \frac{K_{II}}{\sqrt{2\pi r}} \cos \frac{\theta}{2} (1 - \sin \frac{\theta}{2} \sin \frac{3\theta}{2}) \quad (6)$$

Where: A is a certain point in the stress-strain field near the crack tip; r is the distance from point A to the crack tip; θ is the angle between A and X axis.

As the normal stress at the crack tip is equal to or greater than the effective yield stress, the material near this area enters the plastic state, the plastic deformation will take place, and the plastic zone will be formed eventually. The range of the plastic zone can be determined by yield condition of the material.

According to the Von Mises yield condition:

$$(\sigma_1 - \sigma_2)^2 + (\sigma_2 - \sigma_3)^2 + (\sigma_3 - \sigma_1)^2 = 2\sigma_s^2 \quad (7)$$

Using the relationship of the stress invariants:

$$\begin{aligned} \sigma_1 + \sigma_2 + \sigma_3 &= \sigma_x + \sigma_y + \sigma_z \\ \sigma_1\sigma_2 + \sigma_2\sigma_3 + \sigma_3\sigma_1 &= \sigma_x\sigma_y + \sigma_y\sigma_z + \sigma_z\sigma_x - \tau_{xy}^2 - \tau_{yz}^2 - \tau_{zx}^2 \\ \sigma_1\sigma_2\sigma_3 &= \sigma_x\sigma_y\sigma_z + 2\tau_{xy}\tau_{yz} - \sigma_x\tau_{yz}^2 - \sigma_y\tau_{xz}^2 - \sigma_z\tau_{xy}^2 \end{aligned}$$

the function (7) changes to:

$$(\sigma_x - \sigma_y)^2 + (\sigma_y - \sigma_z)^2 + (\sigma_z - \sigma_x)^2 + 6(\tau_{xy}^2 + \tau_{yz}^2 + \tau_{zx}^2) = 2\sigma_s^2 \quad (8)$$

Substituting the functions (4-6) into the equation (8), the mini-plastic zone displacement can be expressed as:

$$r = \frac{9}{2\sigma_s^2} \left[\left(\frac{5}{36} + \frac{1}{18} \cos \theta - \frac{1}{12} \cos^2 \theta \right) K_{\bullet}^2 + \left(\frac{1}{3} \cos \theta \sin \theta - \frac{1}{9} \sin^2 \theta \right) K_{\bullet} K_{\bullet}^2 + \left(\frac{5}{36} - \frac{1}{8} \cos \theta + \frac{1}{4} \cos^2 \theta \right) K_{\bullet}^2 \right] \quad (9)$$

Under this yield condition, the crack will develop along the direction of the shortest distance r_{min} , namely, the crack extension direction will be determined by the conditions below:

$$\begin{cases} \frac{\partial r}{\partial \theta} = 0 \\ \frac{\partial^2 r}{\partial \theta^2} > 0 \end{cases} \quad (10)$$

For the multiple crack penetration, in this paper, according to the calculated extension direction of crack, the extended distance of two adjacent crack tip after fracture was obtained, then the minimum distance between the rock bridge of the cracks after fracture in different strata combination was determined by its coordinates.

Special element method of stress intensity factor

Too much degrees of freedom are needed to solve the stress intensity factor by using a general element, only by increasing the element number to make the approximate displacement field and its first derivative field infinitely approach the corresponding real field, the convergence can be guaranteed. General finite element cannot satisfy the convergence condition, because the displacement derivative of the exact solutions is unbounded in the crack tip. To make the displacement model reflecting the singularity, at the crack tip to switch to a special finite element. Thus there is no need to refine the grid, but the accuracy of the solution can greatly improve. In ANSYS, the stress intensity factor under plane strain conditions uses a special isoparametric element "PLANE82" which has mid-side nodes. "PLANE82" element around the crack tip degenerates into "PLANE2" element, each one has a node at the crack tip, at the same time removes the middle node to the quarterpoint, which can make the corner into singularity. The stress intensity factor of the crack tip can be determined by this element, as is shown in Figs. 2 and 3.

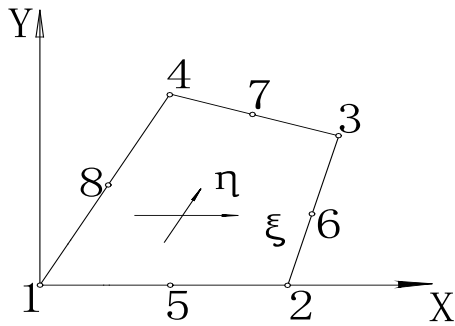


Fig. 2. Isoparametric element

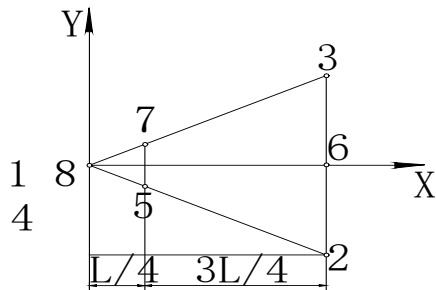


Fig. 3. Singular element

By the transformation below:

$$\begin{cases} x = \sum_{i=1}^8 N_i(\xi, \eta) x_i \\ y = \sum_{i=1}^8 N_i(\xi, \eta) y_i \end{cases} \quad (11)$$

To map the element to regular square space (ξ, η), $-1 \leq \xi \leq 1$, $-1 \leq \eta \leq 1$, the corresponding shape functions of node i are:

$$N_i = \left[\begin{array}{l} (1+\xi\xi_i)(1+\eta\eta_i) - (1-\xi^2)(1+\eta\eta_i) - \\ (1-\eta^2)(1+\xi\xi_i) \end{array} \right] \xi_i^2 \eta_i^2 / 4 + \\ (1-\xi^2)(1+\eta\eta_i)(1-\xi_i^2)\eta_i^2 / 2 + \\ (1-\eta^2)(1+\xi\xi_i)(1-\eta_i^2)\xi_i^2 / 2 \quad (12)$$

The coordinate of node i in the XY coordinate system is (x_i, y_i) , but in the transformation system (ξ, η) is (ξ_i, η_i) . The corner node is $\xi_i, \eta_i = \pm 1$, the middle node is $\xi_i, \eta_i = 0$, the displacement is as below:

$$\begin{cases} u = \sum_{i=1}^8 N_i(\xi, \eta) u_i \\ v = \sum_{i=1}^8 N_i(\xi, \eta) v_i \end{cases} \quad (13)$$

The η is -1 in the side 1-2, the shape function is:

$$\begin{cases} N_1 = \frac{1}{2}\xi(1-\xi) \\ N_2 = \frac{1}{2}\xi(1+\xi) \\ N_5 = 1 - \xi^2 \end{cases} \quad (14)$$

Substitution of the functions (14) into the equations (6, 7),

$$x = -\frac{1}{2}\xi(1-\xi)x_1 + \frac{1}{2}\xi(1+\xi)x_2 + (1-\xi^2)x_5 \quad (15)$$

Taking $x_1 = 0$, $x_2 = L$, and removing the middle node 5 from the usual position to the quarter, taking $x_5 = L/4$, then

$$x = \frac{L}{4}(1+\xi)^2 \quad (16)$$

$$\xi = -1 + 2\sqrt{\frac{x}{L}} \quad (17)$$

The displacement is:

$$\begin{aligned} u &= -\frac{1}{2}\xi(1-\xi)u_1 + \frac{1}{2}\xi(1+\xi)u_2 + (1-\xi^2)u_5 \\ &= -\frac{1}{2}(-1+2\sqrt{\frac{x}{L}})(2-2\sqrt{\frac{x}{L}}) + \frac{1}{2}(-1+2\sqrt{\frac{x}{L}})(2\sqrt{\frac{x}{L}})u_2 + \\ &\quad (4\sqrt{\frac{x}{L}} - 4\frac{x}{L})u_5 \end{aligned} \quad (18)$$

So the strain of x direction is:

$$\begin{aligned} \varepsilon_x &= \frac{\partial u}{\partial x} = \frac{\partial \xi}{\partial x} \frac{\partial u}{\partial \xi} = -\frac{1}{2}(\frac{3}{\sqrt{xL}} - \frac{4}{L})u_1 + \\ &\quad \frac{1}{2}(-\frac{1}{\sqrt{xL}} + \frac{4}{L})u_2 + (\frac{2}{\sqrt{xL}} - \frac{4}{L})u_5 \end{aligned} \quad (19)$$

Reducing the side 1-4 of the quadrilateral in Fig. 2 into a tip, then the quadrilateral turned into a six nodes triangle whose mid-side nodes are at the quarter, as shown in Figure 3.

The η is equal to the zero on the X axis,

$$\begin{aligned} x &= -\frac{1}{4}(1+\xi)(1-\xi)L - \frac{1}{4}(1+\xi)(1-\xi)L + \frac{1}{2}(1-\xi^2)\frac{L}{4} + \\ &\quad \frac{1}{2}(1+\xi)L + \frac{1}{2}(1-\xi^2)\frac{L}{4} = \frac{L}{4}(1+\xi^2) \end{aligned} \quad (20)$$

For the opening mode crack:

$$\begin{cases} U = \frac{K_I}{8G} \sqrt{\frac{2\rho}{\pi}} \left[(2k-1) \cos \frac{\theta}{2} - \cos \frac{3\theta}{2} \right] \\ V = \frac{K_I}{8G} \sqrt{\frac{2\rho}{\pi}} \left[(2k-1) \sin \frac{\theta}{2} - \sin \frac{3\theta}{2} \right] \end{cases} \quad (21)$$

For the shear crack in plane:

$$\begin{cases} U = -\frac{K_{II}}{8G} \sqrt{\frac{2\rho}{\pi}} \left[(2k+3) \sin \frac{\theta}{2} + \sin \frac{3\theta}{2} \right] \\ V = -\frac{K_{II}}{8G} \sqrt{\frac{2\rho}{\pi}} \left[(2k-3) \cos \frac{\theta}{2} + \cos \frac{3\theta}{2} \right] \end{cases} \quad (22)$$

Where: G is shear elastic modulus $k = 3 - 4\nu$, ν is Poisson ratio; ρ is the distance from crack nearby to the crack tip (not more than $10-2L$); θ is the rupture angle of crack.

Substituting the node displacement obtained into functions (9) and (10), the stress fracture factor of the crack could be estimated. This isoparametric element algorithm which contains rigid motion and constant strain mode meets the necessity of convergence, in that it can get very good effect only needing a few elements.

Propagation mechanism of multiple cracks under different floor strata structure

Establishment of numerical model

The numerical model width is 400 m and the height is 295 m considering that the 6th coal thickness is 3 m, buried depth is 375 m and the inclination nearby horizontal. Overburden thickness of 6th coal is 170 m, the overburden-pressure according to the gravity load $p = \gamma H$, and this is the free boundary. The floor strata of the 6th coal are 125 m, the aquifuge h is 55 m, the confined water pressure $P_w = 3MPa$, the bottom boundary is the limit vertical displacement, applying level constraints on the model lateral boundary. In order to consider the water resistance performance of the strata comprehensively, different combination models containing strata, fault, fissure and water pressure were set up, as shown in Figure 4. The length of each crack is 6 m, located in the two bottom layers, respectively. The coordinates of crack tip 2 are (198.0, 108.08), the crack tip 3 is (198.04, 113.78). The inclination of crack 1-2 is 59.470. The inclination of crack 3-4 is 58.50. There are four procedures of rock combination from bottom to top: a) 2346 (soft rock, hard rock, hard rock, soft rock), b) 4326 (soft rock, soft rock, hard rock, hard rock), c) 2364 (soft rock, hard rock, soft rock, hard rock), d) 2643 (hard rock, hard rock, soft rock, soft rock). Divided into two kinds of working conditions, respectively, considering fault and water pressure in the fracture of 1 Mpa. The length of work face along the incline direction is 200 m, the step length of the step excavation is 10 m, so there are 21 steps to mine the work face. The changes of the stress intensity factor and the plastic strain of the crack under different conditions were obtained.

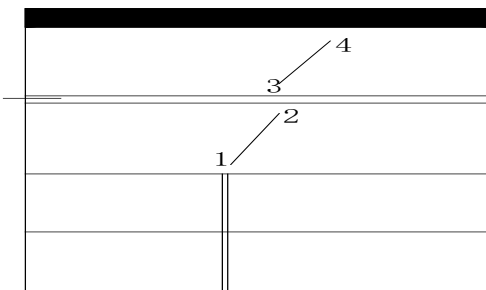


Fig. 4. Schematic diagram of the two arbitrary angle cracks in the aquifuge containing fault

Selection of rock mechanic parameters

The Drucker-prager yield criterion is used for the rock layers. The computational mechanic parameters of each strata are shown in Table 1.

Calculation results analysis

Fracture factor change rule of the crack under different condition

The fracture factor change curves of the crack under different conditions are shown in Figs. 5-8, by the graphs it can be seen:

(1) For the fracture factor value K_I of crack tip 2, it increases gradually, reaches the maximum value when the working face advances to 20 m distance from the crack tip, and then it suddenly decreases, and achieves the minimum when the working face advances to the middle of it. Then, the value of the K_I increases gradually and levels off. The value of K_{II} slowly decreases at first, reaches the minimum when the working face advances 40 m. Then, K_{II} increases slowly, achieves the maximum value when the working face advances to 30 m distance from the crack tip. Finally, it decrease gradually, achieves the minimum value at a distance from the crack about 10 m. When the working face advances to the middle, K_{II} suddenly increases to the maximum and then tends to be stable. Considering K_I , K_{II} comprehensively, the value of K_c reaches maximum when the working face advances to a 20 m distance from the crack tip, that is to say, the crack will be destroyed most easily here. When the working face advances to the middle, the K_c is at the minimum, then it increases and tends to be stable. The change trends of fracture factors K_I and K_{II} at crack tip 3 are similar to the

crack tip 2, only the value of K_I and K_{II} reaches the maximum at 10 m from the crack tip.

(2) For the same kind of rock combinations, the crack propagation will change greatly, when considering the effect of 1 MPa water pressure in the crack and the fault below the crack. Under the action of fault and water pressure, the fracture factor values K_I and K_{II} of the crack will increase and the crack is easier to break, just the change of the trend curve pattern is small. The effect order from large to small is: the combination action of fault and hydraulic pressure, bearing 1 MPa water pressure in the crack, only affected by faults, only affected by mining. It can be seen that when there are fault and water pressure in the crack in the floor strata, it is easier to damage the crack.

(3) For different rock combinations, the change trend curves of K_I , K_{II} are roughly the same, but have different values, different ease of crack fracture. When the rock combination from bottom to top is 4326 (soft rock, soft rock, hard rock, hard rock), the crack is the easiest to destroy. When the rock combination is 2643 (hard rock, hard rock, soft rock, soft rock), the crack is the most difficult to destroy.

(4) Considering K_I , K_{II} comprehensively, the value of K_I is much larger than of K_{II} , the crack destroy is mainly composed of tensile and compression failure. The crack 3-4 affected by mining is larger than crack 1-2.

Table 1. Mechanical parameters of each strata

Rock character	Thickness of layer /m	Elastic modulus /GPa	Poisson ratio	Density t/m ³	Cohesion /MPa	Angle of internal friction/°	Compressive strength /MPa	Tension strength /MPa	Number of rock characters
Limestone	70	14	0.24	2.76	4	38	30	1.79	1
Arenaceous shale	14.8	2.2	0.23	2.57	2.9	36	11	0.7	2
Kern stone	13.2	6.2	0.15	2.65	4	39	15	0.98	3
Fine sandstone	12.6	7.5	0.13	2.65	5	42	22	1.1	4
Weak interlayer	0.7	0.7	0.34	2.35	0.6	32	3.5	0.1	5
Mudstone	12.4	2.8	0.23	2.60	3	24	10	0.7	6
Coal	2.7	1.2	0.36	1.40	1	25	3.2	0.03	7
Mudstone	3.5	2.7	0.24	2.60	2.9	25	9.8	0.65	8

Coalescence mechanism of multi-cracks

Under the influence of mining and geological structure, multiple cracks will expand and interconnect each other, which makes the permeability greatly enhanced.

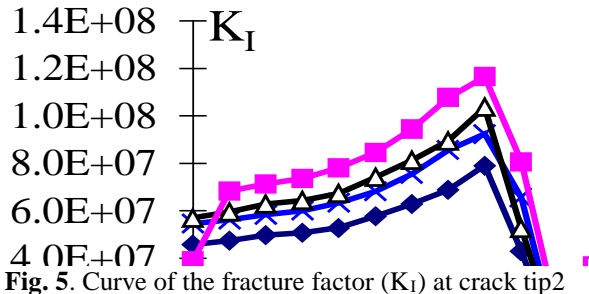


Fig. 5. Curve of the fracture factor (K_I) at crack tip2

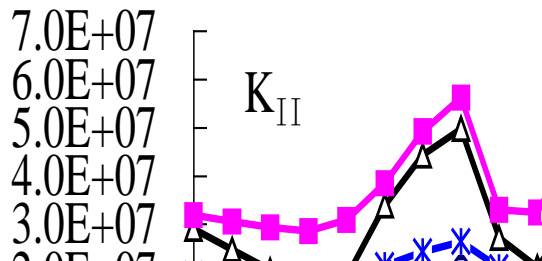


Fig. 6. Curve of the fracture factor (K_{II}) at crack tip2

This paper mainly studies the shortest length of the rock bridge of two cracks after damage under different conditions.

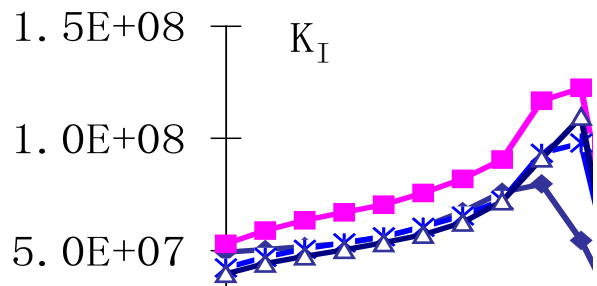


Fig. 7. Curve of the fracture factor (K_I) at crack tip3

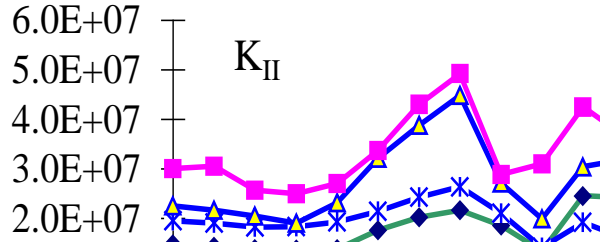


Fig. 8. Curve of the fracture factor (K_{II}) at crack tip3

Firstly, the maximum principal stress value of the factor combination $\sqrt{K_I^2 + K_{II}^2}$ under different strata combination is substituted in equation (5) to obtain σ_s , then σ_s is substituted and the fracture factors K_I and K_{II} of the time step in equation (6), obtain any two floor strata crack propagation path under different rock combination according to equation (7), determine the coordinate after crack destroyed of point 2 and 3, according to which the shortest distance of rock bridge between the crack tip 2 and 3 after the crack damaged is obtained. The results are shown in Table 2.

Table 2. Results of propagation route under different floor combinations

Rock layer	Combination of construction	Failure angle of second crack tip /°	Mini-plastic zone displacement /m	Failure angle of third crack tip /°	Mini-plastic zone displacement /m	Displacement of rock bridge after failure /m
2346	Normal	68.58	1.28	51.57	1.30	3.715803
	Fault	65.94	1.29	51.15	1.31	3.65223
	Water pressure in crack	77.6	1.297	55.03	1.32	3.507769
	Fault, Water pressure in crack	78.37	1.30	54.85	1.33	3.483808
2364	Fault	63.09	1.24	60.11	1.28	3.685071
	Fault, Water pressure in crack	60.1	1.29	65.46	1.30	3.5991
2643	Fault	74.01	1.292	55	1.32	3.655416
	Fault, Water pressure in crack	61.99	1.305	59.53	1.34	3.530717
4326	Fault	67.38	1.298	57.51	1.33	3.591298
	Fault, Water pressure in crack	74.37	1.31	62.37	1.35	3.386976

As can be seen from the table:

(1) The fault and the water pressure in the crack have a certain influence on the crack propagation under the condition of the same rock combination. The minimum plastic zone is the maximum when the crack is affected by both the fault and the water pressure; when there is 1 Mpa water pressure in the crack takes the second place; and reaches the minimum when there is no structure in rock. It can be seen that the crack under the combined effect of fault and water pressure in the cracks is easiest to be damaged and the water resistance performance is the worst, however, the connection capacity of the cracks is worst when it is affected by mining only and the water resistance performance is best.

(2) The minimum plastic zone range of crack tip 3 is larger than of crack tip 2, that is to say, the upper crack is more strongly affected by mining.

(3) By comparison of different strata combinations, the minimum plastic zone range of the floor strata combination 4326 is the maximum under the same conditions and the length of the rock bridge between cracks after destroyed is the minimum; the combination 2643 takes the second place; the minimum plastic zone range combination 2364 is the minimum and the length of the rock bridge is the maximum. It can be seen that the water resistance performance of combination 4326 is the worst, on the contrary, the 2364 is the best.

CONCLUSIONS

In this paper different crack combinations in floor strata under mining conditions were simulated using a singular element, the two cracks propagation paths under different situations were given using the minimum plastic zone theory according to the change of the fracture factor and the plastic strain of different strata combination cracks under influence of fault, water pressure and mining, the shortest length of the rock bridge between the two cracks after bursting in different strata combination was obtained, and the water resistance performance of every strata combination was analyzed. The conclusion is that: the water resistance performance of the floor strata under the combination of soft-soft-hard-hard upward is the worst while the combination of alternating soft-hard is the best. The fracture factor combination and the plastic strain of the crack will reach maximum when mining is performed near to it, and the crack is the easiest to destroy. The length of the rock bridge between the two cracks after bursting is

the shortest under the combination soft below and hard above, while it is the longest under the combination of alternating soft-hard. The length of the rock bridge between the two cracks after bursting will be shortened when considering the water pressure inside the crack and fault, which results in the decrease of rock water resistance performance. This paper provides a reference for floor water inrush prediction in fractured rock mass.

Acknowledgements: The authors would like to thank the financial support by the National Natural Science Foundation of China (Grant No. 41472281) and Scientific Research Foundation of Shandong University of Science and Technology for Recruited Talents (No 2014RCJJ041).

REFERENCES

1. M. Feng, X. Mao, Q. Zhu, *Journal of Mining & Safety Engineering*, **27**(3), 404 (2010).
2. Y. Gao, Sh. Liu, B. Lv, K. Li, *Journal of Mining & Safety Engineering*, **33**(4), 624 (2016).
3. S. Peng, J. Wang. Safety coal mining above the confined aquifer. Beijing: China Coal Industry Publishing House, 91–111, (2001).
4. Q. Wu, B. Li, *Journal of China Coal Society*, **41**(9), 2143 (2016).
5. W. Qiao, W. Li, C. Zhao, *Chinese Journal of Rock Mechanics and Engineering*, **28**(12), 2466 (2009).
6. B. Li, H. Liu, X. Liu, *Journal of Hebei University of Engineering (Natural Science Edition)*, **28**(3), 68 (2011).
7. Q. Liu, W. Li, H. Chai, Q. Guo, Sh. Sun, *Mining Safety & Environmental Protection*, **42**(1), 64 (2015).
8. Zh. Li, C. Zhai, L. Li, *Journal of Central South University (Science and Technology)*, **46**(5), 1806 (2016).
9. R. Liu, D. Cao, D. Hu, *Hydrogeology & Engineering Geology*, **43**(1), 105 (2016).
10. L. Shi, *Journal of Shandong University of Science and Technology (Natural Science)*, **28**(3), 17 (2009).
11. J. Sun, L. Wang, H. Hou, *Journal of China University of Mining & Technology*, **42**(4), 560 (2013).
12. W. Li, J. Yang, *Coal Mining Technology*, **15**(5), 45 (2010).
13. X. Yu, L. Shi, J. Wei, *Journal of Shandong University of Science and Technology (Natural Science)*, **25**(4), 14 (2006).
14. W. Sun, Sh. Zhang, L. Zhu, *Mining Safety & Environmental Protection*, **43**(3), 100 (2016).
15. Sh. Yin, The theory and application of fracture and damage. Beijing, Tsinghua University press, 1992.

ИЗСЛЕДВАНИЯ ВЪРХУ ВОДОУСТОЙЧИВОСТТА НА СТРАТИФИЦИРАНИ СКАЛНИ МАСИ ПРИ РАЗЛИЧНИ УСЛОВИЯ НА РАЗРУШАВАНЕ

Х.Л. Ю¹, Ж.М. Жу^{2*}, И.С. Джан^{1,3}, У.К. Джан^{1,3}, Ж.Ч. Уан⁴

¹ Колеж по минно инженерство, Шандонг Университет за наука и технология, Кингдао 266590, Китай

² Департамент по ресурси и гражданско инженерство, Шандонг Университет за наука и технология, Таян 271019, Китай

³ Държавна лаборатория по предотвратяване и контрол на минни инциденти към провинция Шандонг и Министерство за наука и технология, Кингдао 266590, Китай

⁴ Факултет по гражданско инженерство, Далян Жиаотонг Университет, Далян 116028, Китай

Получена на 24 август, 2017 г.; Приета на 1 ноември, 2017 г.

(Резюме)

За определяне на водоустойчивостта на дълни слоеве под различни скални пластове са симулирани механизмите на разпространение на пукнатините на слоевете при минна експлоатация с помощта на сингуларен елемент. Пътят на разпространение на двойни пукнатини при различни случаи е определен с помощта на теорията за минимална пластична зона според промяната на фактора на пропукване и пластичното напрежение на комбинации от различни слоеве под влияние на нарушения, водно налягане или минна експлоатация. Определена е най-късата дължина на скалния мост между двойни пропуквания при различни комбинации на слоевете. Анализирано е водното съпротивление на комбинации от различни слоеве. Показано е, че водното съпротивление на дълни слоеве при комбинация от меки-меки-твърди-твърди слоеве е най-лошо, а при комбинация меки-твърди – най-добро. Факторът на пропукване и пластичното напрежение на пропукването са максимални при близки минни дейности, като пропукването най-лесно се разширява. Дължината на скалния мост между две пропуквания е най-малка когато отдолу се намират меки скали, а отгоре – твърди скали и най-голяма когато се сменят последователно меки и твърди скали. Дължината на скалния мост намалява като се вземе предвид водното налягане в пукнатината и нарушението, което води до намаляване на водното съпротивление. Статията дава възможност за предсказване на водния напор в пропукани скални маси.

Stagnation point nanofluid flow along a stretching sheet with non-uniform heat generation/absorption and Newtonian heating

B. K. Mahatha¹, R. Nandkeolyar^{2*}, M. Das¹, P. Sibanda³

¹Department of Mathematics, School of Applied Sciences, KIIT University, Bhubaneswar-751024, India

²School of Mathematics, Thapar University, Patiala-147001, India

³School of Mathematics, Statistics & Computer Science, University of KwaZulu-Natal, Private Bag X01, Scottsville 3209, Pietermaritzburg, South Africa

Received November 10, 2014; Accepted February 6, 2017

The non-uniform heat generation/absorption and Newtonian heating effects on the steady two-dimensional laminar stagnation point boundary layer nanofluid flow past a stretching sheet in the presence of an external uniform magnetic field is investigated. The nanofluid is assumed to be viscous, incompressible and electrically conducting. The effects of Brownian motion and thermophoretic diffusion are taken into account. The governing non-linear partial differential equations are transformed to a set of ordinary differential equations in similarity form which are then solved using Spectral Relaxation Method (SRM). The effects of pertinent flow parameters on the flow, heat and nanoparticle concentration are studied with the help of graphs and tables. The nanofluid model presented in the paper has significant applications in the fluid engineering process where simultaneous effects of heat generation and convecting heating of the bounding surface take place such as in heat exchangers and nuclear reactor cooling.

Keywords: Brownian motion, Magnetic field, Nanofluid, Newtonian heating, Non-uniform heat generation/absorption, Stagnation point, Thermophoresis.

INTRODUCTION

Nanofluids are fluids with suspended nanosized (typically 1-100nm in size) particles of metals such as copper and gold, oxides such as alumina, silica, copper oxide, carbides and carbon nanotubes etc. The base fluids are water, oils, ethylene glycol, biofluids, polymer solutions and some lubricants. Nanofluids are potentially useful in heat transfer devices such as in microelectronics, fuel cells, automobiles, pharmaceutical processes, and hybrid-powered engines, engine cooling/vehicle thermal management, domestic refrigerator, chiller, heat exchanger, nuclear reactor coolant, in grinding, in space technology, and in defense and ships [1]. Nanofluids are reported to exhibit enhanced thermal conductivity and convective heat transfer coefficient compared to the base fluid [2]. Choi et al. [3] concluded that addition of small amount (less than 1% by volume) of nanoparticles to conventional heat transfer liquids increased the thermal conductivity of the fluid upto approximately two times. Choi [4] was the first who used the term nanofluids to refer the fluids with suspended nano-sized particles. Later, it was revealed by Buongiorno [5] that the enhancement in the thermal conductivity occurs due to the presence of Brownian and thermophoretic diffusions in the flow field.

Flow of a viscous, incompressible, and electrically conducting fluid over a continuously

stretching surface under the influence of a transverse magnetic field finds applications in a variety of engineering processes such as in polymer extrusion process which involves cooling of a molten liquid being stretched into a cooling systems. The cooling liquid used and the rate of stretching are the main factors for the fluid mechanical properties of the penultimate product in these processes. Flow of the fluids, having better electromagnetic properties, such as polyethylene oxide, polyisobutylene solution in cetane can be controlled by applying external magnetic fields. A considerable attention must be given to control the rate of stretching of the extrudate rather than cooling liquids to accomplish the properties expected for outcome. Crane [6] was the first to analyze boundary layer flow of the Newtonian fluid caused solely by the linear stretching of an elastic sheet moving in its own plane with velocity proportional to the distance from the fixed point. Nadeem et al [7] presented a numerical investigation of three-dimensional flow of a water-based nanofluid over an exponentially stretching sheet. Ibrahim and Shankar [8] studied the boundary layer flow and heat transfer of a nanofluid over a permeable stretching sheet in the presence of an external magnetic field, slip boundary condition and thermal radiation. The effect of magnetic field on stagnation point nanofluid flow and heat transfer over a stretching sheet was discussed by Ibrahim et al. [9]. They showed that the heat transfer rate at the surface increases with the magnetic parameter when

* To whom all correspondence should be sent:

E-mail: rajnandkeolyar@gmail.com

the free stream velocity exceeds the stretching sheet velocity. Qasim et al. [10] investigated magnetohydrodynamic flow of a ferrofluid along a stretching cylinder with velocity slip and prescribed surface heat flux. The boundary layer flow of a nanofluid due to an exponentially permeable stretching sheet with external magnetic field was studied by Bhattacharyya and Layek [11].

The temperature dependent heat source/sink has significant contributions on the heat transfer characteristics. Temperature differences between the surface and ambient-fluid are encountered in several engineering applications. Nandepannavar et al. [12] studied the flow and heat transfer of a viscous and incompressible fluid over a non-linearly stretching sheet in the presence of non-uniform heat source and variable wall temperature. They numerically solved the problem for the case of non-linearly stretching sheet by shooting technique with a fourth-order Runge-Kutta method while an analytical solution was presented for the case of linearly stretching sheet. It was concluded that the cumulative effect of the temperature dependent and space dependent heat generation/absorption is significant on heat transfer characteristics. Pal [13] investigated the influence of Hall current and thermal radiation on the flow and heat transfer characteristics of a viscous, incompressible, and electrically conducting fluid over an unsteady stretching permeable surface in the presence of an externally applied magnetic field. The two-dimensional stagnation point flow of nanofluid toward an exponentially stretching sheet with non-uniform heat generation/absorption was investigated by Malvandi et al. [14]. They observed that the increase in the heat generation causes the heat transfer rate to decrease. The problem of heat and mass transfer in unsteady MHD boundary layer flow of a nanofluid over a stretching sheet with a non-uniform heat source/sink was considered by Shankar and Yirga [15]. There are several other studies [16, 17] which discussed the effects of non-uniform heat generation/absorption under different conditions. In these studies the fluid was considered to be viscoelastic. Goyal and Bhar-gava [18] presented numerical simulation of the MHD boundary layer flow of a viscoelastic nanofluid past a stretching sheet in the presence of partial slip and temperature dependent heat source/sink. In a comment, Mastroberardino [19] demonstrated that the analytical results reported by Nandeppanavar et al. [20] were incorrect. He then presented the valid solutions of the governing ordinary differential equations for the fluid flow and temperature field using the homotopy analysis method.

There are several practical situations where the bottom wall is subjected to convective heating using a hot fluid situated on the other side of the wall. The heat transfer taking place due to such arrangement is referred as Newtonian heating. Newtonian heating process from the bottom wall has applications in many engineering devices such as, in heat exchanger where the conduction in the solid tube wall is influenced by the convection in the fluid past it, conjugate heat transfer around fins where the conduction within the fin and the convection surrounding the fluid must be analyzed simultaneously to obtain important design information, and convection flows setup when the bounding surfaces absorbs heat by solar radiation. Uddin et al. [21] investigated the steady two dimensional MHD laminar free convective boundary layer flow of an electrically conducting Newtonian nanofluid over a vertical plate in a quiescent fluid taking into account the Newtonian heating boundary condition. Makinde et al. [22] presented the combined effects of buoyancy force, convecting heating, Brownian motion and thermophoresis on the stagnation point flow and heat transfer of an electrically conducting nanofluid towards a stretching sheet under the influence of transverse magnetic field. The complex interaction between the electrical conductivity and that of nanoparticles in the presence of a magnetic field in a boundary layer flow past a convectively heated flat surface was discussed by Makinde and Mutuku [23]. They observed that the presence of nanoparticles greatly enhance the magnetic susceptibility of nanofluids as compared to the conventional base fluid.

Motivated from the above studies, the authors intend to investigate the effects of non-uniform heat generation and Newtonian heating effects on the steady two dimensional laminar stagnation point boundary layer nanofluid flow past a stretching sheet in the presence of an external uniform magnetic field. The nanofluid model includes the effect of Brownian diffusion and thermophoresis forces. The governing nondimensionalized equations in similarity form are solved using spectral relaxation method (SRM).

FORMULATION OF THE PROBLEM

We consider the steady two dimensional stagnation point laminar boundary layer flow of a viscous, incompressible, and electrically conducting nanofluid past a stretching sheet. The x axis is taken along the stretching sheet while the y axis is normal to the sheet. The surface of the sheet is stretched with a velocity proportional to the distance along x axis

keeping the origin as fixed. Thus, the fluid flow is induced due to the stretching velocity, say $U_w = ax$, of the sheet. The fluid flow is permitted by an external uniform magnetic field B_0 which acts in y -direction. The fluid outside the boundary layer is also assumed to have a velocity U_∞ . The surface of the sheet is convectively heated by a hot fluid of temperature T_f and the concentration of the nanoparticle at the surface is C_w while the values at free stream temperature and nanoparticle concentration are T_∞ and C_∞ , respectively.

Assuming that the induced magnetic field effects are negligible and there is no external electric field applied to the system, so that the effect of polarization of electric field is neglected, the equations governing the nanofluid velocity, nanofluid temperature and nanoparticle volume friction, are given by

$$\frac{\partial u}{\partial x} + \frac{\partial v}{\partial y} = 0 \quad (1)$$

$$u \frac{\partial u}{\partial x} + v \frac{\partial u}{\partial y} = U_\infty \frac{dU_\infty}{dx} + v \frac{\partial^2 x}{\partial y^2} - \frac{\sigma B_0^2}{\rho_0} (u - U_\infty) \quad (2)$$

$$u \frac{\partial T}{\partial x} + v \frac{\partial T}{\partial y} = \alpha \frac{\partial^2 T}{\partial y^2} + \tau \left[D_B \frac{\partial C}{\partial y} \frac{\partial T}{\partial y} + \frac{D_T}{T_\infty} \left(\frac{\partial T}{\partial y} \right)^2 \right] + \frac{q'''}{(\rho c)_f} \quad (3)$$

$$u \frac{\partial C}{\partial x} + v \frac{\partial C}{\partial y} = D_B \frac{\partial^2 C}{\partial y^2} + \frac{D_T}{T_\infty} \frac{\partial^2 T}{\partial y^2} \quad (4)$$

where u and v are the velocity components along the x and y axes, respectively, C and T are nanoparticle concentration and nanofluid temperature, respectively, ν is the kinematic viscosity, σ is electrical conductivity, α is the thermal diffusivity of the fluid, D_B is the Brownian diffusion coefficient, D_T is the thermophoretic diffusion coefficient and $\tau = \frac{(pc)_p}{(pc)_f}$ is the ratio between the effective heat capacity of the nanoparticle material and heat capacity of the fluid with ρ being the density, and c being the specific heat at constant pressure. The subscripts p and f are used to denote the physical properties of nanoparticles and base fluid, respectively.

In Eq. (3), q''' is the space and temperature dependent internal heat generation/absorption (non-uniform heat source/sink) which can be expressed as

$$q''' = \left(\frac{k U_w(x)}{x \nu} \right) \left[A^* \frac{u(T_f - T_\infty)}{U_\infty(x)} + B^*(T - T_\infty) \right] \quad (5)$$

where A^* and B^* are the parameters of the space and temperature dependent internal heat generation/absorption. It is to be noted that A^* and

B^* are positive to internal heat source and negative to internal heat sink, ν is the kinematic viscosity.

The boundary conditions for the problem are

$$u = U_x(x) = ax, \quad v = 0, \quad -k \frac{\partial T}{\partial y} = h(T_f - T), \quad C = C_w \text{ at } y = 0; \quad u \rightarrow U_\infty(x) = bx, \quad v \rightarrow 0, \quad T \rightarrow T_\infty, \quad C \rightarrow C_\infty, \quad \text{as } y \rightarrow \infty. \quad (6)$$

We introduce the following dimensionless quantities

$$\psi(x,y) = \sqrt{b\nu}xf(\eta), \quad \theta = \frac{(T-T_\infty)}{(T_f-T_\infty)}, \quad \phi = \frac{(C-C_\infty)}{(C_w-T_\infty)}$$

$$\text{where } \eta = \sqrt{\frac{b}{\nu}}y, \quad (7)$$

where η is the dimensionless stream function, and the above transformation is chosen in such a way that $u = \partial\psi/\partial y$ and $v = -\partial\psi/\partial x$.

Using the above transformation, the equation of continuity (1) is automatically satisfied and we obtain from Eqs. (2)-(5), as

$$\begin{aligned} f &= 0, & f' &= \epsilon, & \theta' &= -Bi(1-\theta), \\ \phi &= 1 \text{ at } \eta = 0, & f' &\rightarrow 1, & \theta &\rightarrow 0, & \phi &\rightarrow 0 \text{ as } \eta \rightarrow \infty. \end{aligned} \quad (11)$$

In the above equations, primes denote differentiation with respect to η and the parameters are defined as

$$\begin{aligned} Pr &= \frac{\nu}{\alpha}, & Nb &= \frac{(pc)_p D_B (c_w - c_\infty)}{(pc)_f \nu}, \\ \epsilon &= \frac{a}{b}, & Le &= \frac{\nu}{D_B}, & Nt &= \frac{(pc)_p D_T (T_f - T_\infty)}{(pc)_f T_\infty \nu}, \\ Bi &= \frac{h}{k} \sqrt{\frac{\nu}{b}}, \end{aligned}$$

where $E > 0$ is for a stretching sheet and $E < 0$ is for a shrinking sheet. Further, Pr is the Prandtl number, Le is the Lewis number, Nb is the Brownian motion parameter, and Nt is the thermophoresis parameter.

The physical quantities of interest are the local skin friction coefficient C_{fx} , the local Nusselt number Nu_x and the local Sherwood number Sh_x which are defined as

$$C_{fx} = \frac{\tau_w}{\rho U_\infty^2}, \quad Nu_x = \frac{x q_w}{k(T_f - T_\infty)}, \quad Sh_x = \frac{x q_m}{D_B(C_w - C_\infty)},$$

where the surface shear stress τ_w , the local heat flux q_w , and the local mass flux q_m are given by

$$\begin{aligned} \tau_w &= \mu \left(\frac{\partial u}{\partial y} \right)_{y=0}, & q_w &= -k \left(\frac{\partial T}{\partial y} \right)_{y=0}, \\ q_m &= -D_B \left(\frac{\partial C}{\partial y} \right)_{y=0}, \end{aligned}$$

with μ and k being the dynamic viscosity and thermal conductivity of the nanofluids, respectively. Using the similarity variables (7), we obtain

$$(Re_x)^{1/2} C_{fx} = f''(0), \quad (12)$$

$$(Re_x)^{-1/2} Nu_x = -\theta'(0), \quad (13)$$

$$(Re_x)^{-1/2} Sh_x = -\phi'(0), \quad (14)$$

where $Re_x = \frac{U_{\infty}x}{v}$ is the local Reynolds number.

SOLUTION TECHNIQUE

The spectral relaxation method (SRM) (see Motwa and Makukula [24], Kameswaran et al. [25]) is employed to solve the Eqs. (8)-(10) subject to the boundary conditions (11). The method uses the Gauss-Seidel approach to decouple the system of equations. In the framework of SRM method the iteration scheme is obtained as

$$f'_{r+1} = p_r, \quad f_{r+1}(0) = 0 \quad (15)$$

$$p''_{r+1} + f_{r+1}p'_{r+1} - Mp_{r+1} = p_r^2 - M - 1, \quad (16)$$

$$\begin{aligned} \theta''_{r+1} + Prf_{r+1}\theta'_{r+1} + \epsilon B^*\theta_{r+1} \\ = -[PrNb\theta'_r\phi'_r + PrNt\theta'^2_r + \epsilon A^*f'_{r+1}], \end{aligned} \quad (17)$$

$$\phi''_{r+1} + Lef_{r+1}\phi'_{r+1} = -\frac{Nt}{Nb}\theta''_{r+1}. \quad (18)$$

The boundary conditions for the above iteration scheme are

$$p_{r+1}(0) = \epsilon, \quad p_{r+1}(\infty) \rightarrow 1, \quad (19)$$

$$\theta'_{r+1}(0) = -B\{1 - \theta_{r+1}(0)\}, \quad \theta_{r+1}(\infty) \rightarrow 0, \quad (20)$$

$$\phi_{r+1}(0) = 1, \quad \phi_{r+1}(\infty) \rightarrow 0. \quad (21)$$

In order to solve the decoupled equations (15)-(18), we use the Chebyshev spectral collocation method. The computational domain $[0, L]$ is transformed to the interval $[1, 1]$ using $\eta = L(\xi + 1)/2$ on which the spectral method is implemented. Here L is used to invoke the boundary conditions at $\xi = 0$. The basic idea behind the spectral collocation method is the introduction of a differentiation matrix which is used to approximate the derivatives of the unknown variables at the collocation points as the matrix vector product of the form

$$\frac{df_{r+1}}{d\eta} = \sum_{k=0}^N D_{lk} f_r(\xi_k) = Df_r, \quad l = 0, 1, 2, \dots, N, \quad (22)$$

where $N + 1$ is the number of collocation points (grid points), $D = 2/L$, and $f = [f(\xi_0), f(\xi_1), \dots, f(\xi_N)]^T$ is the vector function at the collocation points. Higher-order derivatives are obtained as powers of D , that is,

$$f_r^{(p)} = D^p f_r, \quad (23)$$

where p is the order of the derivative.

Applying the spectral method to equations (15)-(18), we obtain

$$A_1 f_{r+1} = B_1, \quad f_{r+1}(\xi_N) = 0, \quad (24)$$

$$A_2 p_{r+1} = B_2, \quad p_{r+1}(\xi_N) = \epsilon, \quad p_{r+1}(\xi_0) = 1 \quad (25)$$

$$\begin{aligned} A_3 \theta_{r+1} &= B_3, \quad \theta'_{r+1}(\xi_N) \\ &= -Bi\{1 - \theta_{r+1}(\xi_N)\}, \quad \theta_{r+1}(\xi_0) = 0 \end{aligned} \quad (26)$$

$$A_4 \Phi_{r+1} = B_4, \quad \phi_{r+1}(\xi_N) = 1, \quad \phi_{r+1}(\xi_0) = 0 \quad (27)$$

where,

$$A_1 = D, \quad B_1 = p_r, \quad (28)$$

$$A_2 = D^2 + \text{diag}(f_r)D + \text{diag}(-M)I, \quad (29)$$

$$B_2 = p_r^2 - (M - 1), \quad (29)$$

$$A_3 = D^2 + \text{diag}(P_r f_r)D + \text{diag}(\epsilon B^*)I, \quad (30)$$

$$B_3 = -[P_r Nb\phi'_r\theta'_r + PrNt\theta'^2_r + \epsilon A^*f'_{r+1}], \quad (30)$$

$$A_4 = D^2 + \text{diag}(Lef_2)D, \quad B_4 = -\frac{Nt}{Nb}\theta''_{r+1}, \quad (31)$$

In equations (28)-(31), \mathbf{I} is an identity matrix and $\text{diag}[\cdot]$ is a diagonal matrix, all of size $(N + 1) \times (N + 1)$ where N is the number of grid points, \mathbf{f} , \mathbf{p} , Θ , and Φ are the values of the functions f , p , θ and ϕ , respectively, when evaluated at the grid points and the subscript r denotes the iteration number.

The initial guesses, to start the SRM scheme for equations (15)-(18), are chosen as

$$\begin{aligned} f_0(\eta) &= \eta + e^{-\eta} - e^{-\epsilon\eta}, \\ p_0(\eta) &= 1 - e^{-\eta} + \epsilon e^{-\epsilon\eta}, \\ \theta_0(\eta) &= \frac{1}{2}e^{-\eta B_i} \phi_0(\eta) = e^{-\eta}. \end{aligned} \quad (32)$$

ERROR ANALYSIS

The error in the iteration scheme is assessed by taking the norm of the difference in the values of functions between two successive iterations. For each iteration scheme, we define the following maximum error Ed at the $(r + 1)$ th iteration level

$$Ed = \max \left(\|z_{1,r+1} - z_{1,r}\|_{\infty}, \|z_{2,r+1} - z_{2,r}\|_{\infty}, \dots, \|z_{m,r+1} - z_{m,r}\|_{\infty} \right), \quad (33)$$

where z_i ; $i = 1, 2, \dots, m$ are the governing unknown functions in the nonlinear system. It is observed from Fig 1 that the error Ed decreases rapidly with an increase in the number of iterations, which ascertain us the convergence of iteration schemes. It may be noted from

Fig 1 that about 50 iterations are required to obtain an accuracy of up to 10^{-12} in nanofluid velocity, temperature, and species concentration. The unknowns are calculated, for a given number of collocation points N , until the following criteria for convergence is satisfied at iteration r

$$E_d \leq \epsilon,$$

where E is the convergence tolerance level. The effect of the number of collocation points N is examined in order to select the smallest value of N which gives a consistent solution to the error level E .

This is achieved by repeatedly solving the governing equations using the above iteration schemes with different values of N until the consistent solution is reached.

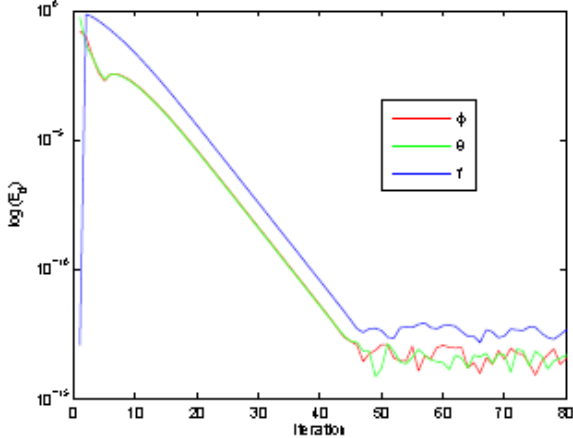


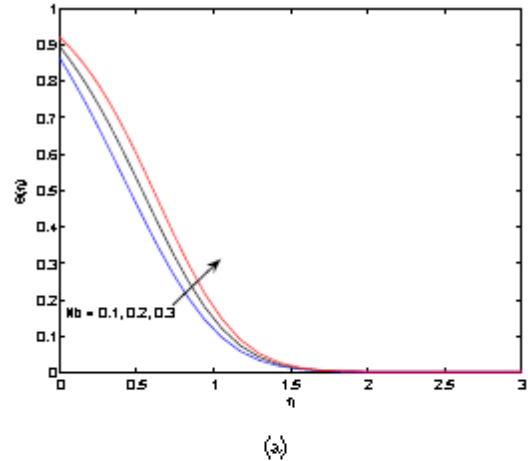
Fig. 1. Maximum error in f , θ , and ϕ versus number of iterations.

RESULTS AND DISCUSSION

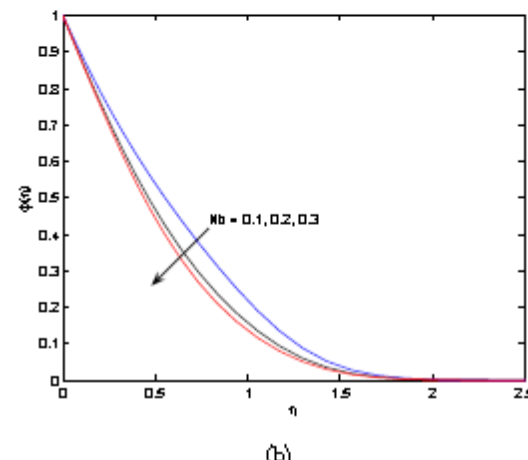
The steady two dimensional laminar stagnation point boundary layer flow of a viscous, incompressible, and electrically conducting nanofluid past a stretching sheet in the presence of an external magnetic field is investigated with a view to analyze the effects of non-uniform heat generation/absorption and Newtonian heating. In order to analyze the effects of several flow parameters viz. the magnetic parameter M , Brownian motion parameter Nb , thermophoresis parameter Nt , heat generation/absorption parameter A^* and B^* , and the Biot number Bi , the profiles of nanofluid velocity f , nanofluid temperature θ , and nano-particle concentration φ are depicted graphically in Figs. 2- 6 while the values of coefficient of skin-friction, Nusselt number, and Sherwood number are tabulated in Table 1.

In Figs. 2 and 3, the effects of Brownian motion parameter Nb and thermophoresis parameter Nt on the nanofluid temperature and nanoparticle concentration are visualized. These are the two important effects which perturb the heat transfer characteristics of the fluid significantly due to the presence of nanoparticles in the flow field. The increase in Brownian motion parameter Nb measures an increase in the Brownian motion of the nano-sized particles present in the fluid. It is observed that the increase in Brownian motion of the nanoparticles causes an increase in the nanofluid temperature and a decrease in nanoparticle concentration within the boundary layer region. This is the cumulative effect due to transfer of heat from the surface to the fluid and the kinematic energy gained by the nanoparticle due to Brownian motion. The Brownian motion of

nanoparticles transfers the surface heat to the fluid while the nanoparticles gain higher kinematic energy which contributes to the thermal energy of the fluid. Also there is a movement of the nanoparticles from the high temperature region towards the low temperature region and as a result the concentration of the nanoparticles within the boundary layer region decrease with the increase Brownian motion of the nanoparticles. It is concluded from Fig. 3, that the increase in thermophoretic parameter Nt increases the nanofluid temperature. The increase in the temperature is viewed as a result of the thermophoresis force by which a nanoparticle pushes the other nanoparticles away from the heated surface which in turn generates thermal energy due to the collision of nanoparticles. On the other hand, the effect of thermophoretic force on nanoparticle concentration is only significant in a region away from the surface where it increases with the increase in thermophoretic force.



(a)



(b)

Fig. 2. The effect of Brownian motion parameter Nb on (a) the fluid temperature θ and (b) the species concentration φ , when $M = 2$, $E = 0.1$, $Le = 5$, $Pr = 5$, $Bi = 5$, $Nt = 0.1$, $A^* = 0.5$, and $B^* = 0.5$.

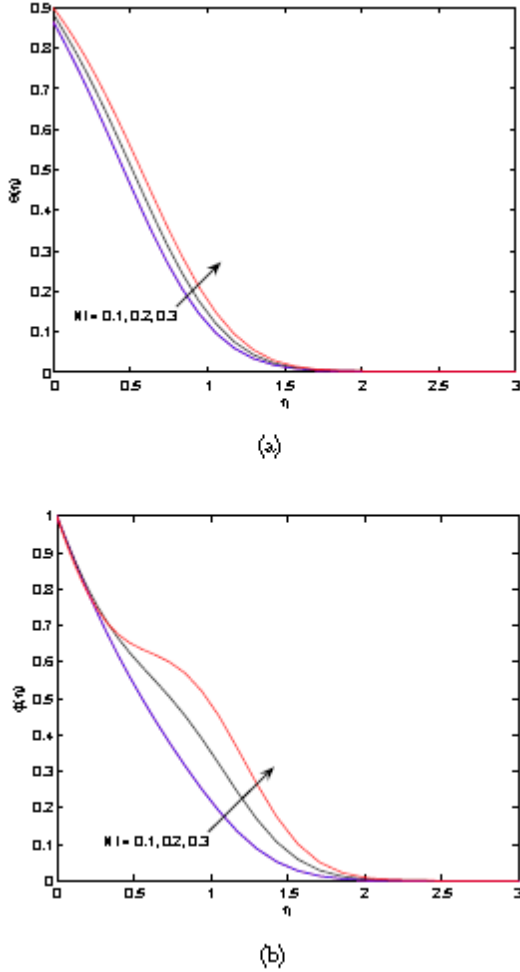


Fig. 3. The effect of Thermophoresis parameter Nt on (a) the fluid temperature θ and (b) the species concentration φ , when $M = 2$, $E = 0.1$, $Le = 5$, $Bi = 5$, $Nb = 0.1$, $Pr = 5$, and $B^* = 0.05$.

Fig. 4 displays the effect of space dependent heat generation/absorption parameter A^* and temperature dependent heat generation/absorption parameter B^* on the nanofluid temperature and nanoparticle concentration within the boundary layer region. An increase in $A^* > 0$, $B^* > 0$ contribute in the generation of thermal energy and hence the nanofluid temperature increases while an increase in $A^* < 0$, $B^* < 0$ takes the thermal energy from the system and the nanofluid temperature decreases. As the nanofluid temperature increases, with increasing A^* and B^* , diffusion of nanoparticles take place from the high temperature region to the low temperature region and as a result the nanoparticle concentration within the boundary layer decreases which is depicted in Fig. 4(b).

The surface of stretching sheet is convectively heated by a hot fluid via Newtonian heating process. The effect of this heating is measured by the non-dimensional parameter Bi , and is captured in Fig. 5.

It is clearly observed that the nanofluid temperature increases with the increase in convective heating of the surface. Also there is an increase in the nanoparticle concentration with the increase in convective heating of the surface.

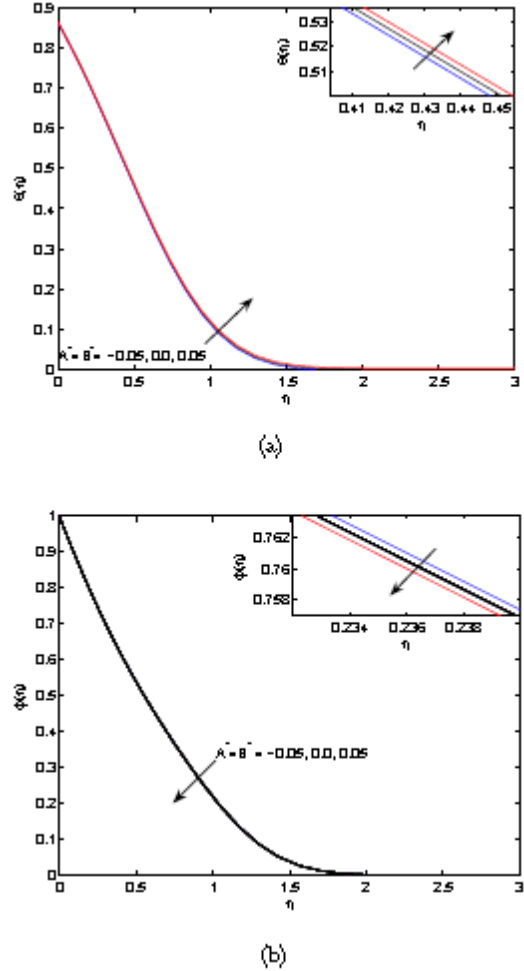
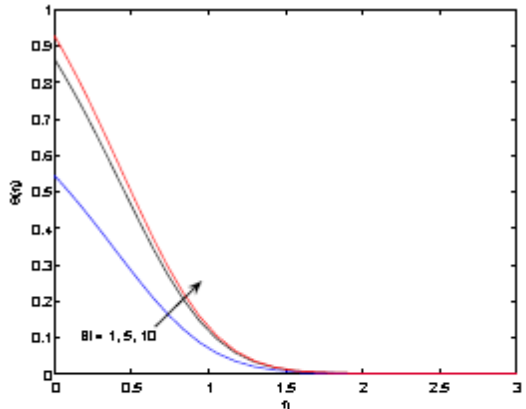
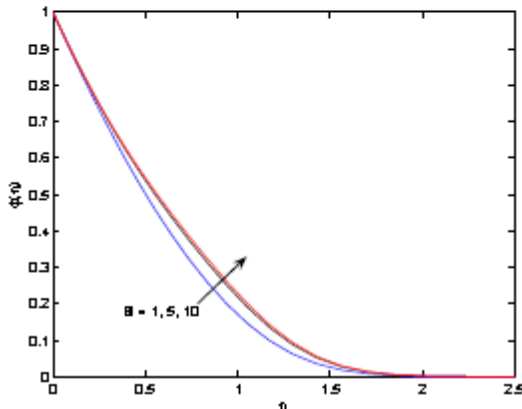


Fig. 4. The effect of space dependent heat source/sink A^* and temperature dependent heat source/sink B^* on (a) the fluid temperature θ and (b) the species concentration φ , when $M = 2$, $E = 0.1$, $Le = 5$, $Bi = 5$, $Nt = Nb = 0.1$, and $Pr = 5$.

The effect of magnetic parameter M is presented in Fig. 6. An increase in magnetic parameter measures the increase in the strength of the externally applied magnetic field. Interestingly, it is observed that the incasing in magnetic parameter causes a flow acceleration while it decreases the nanofluid temperature and nano-particle concentration. This is an opposite effect with the usual effect of magnetic field because in most of the cases the application of an external magnetic field gives rise to a resistive force, known as Lorentz force. However the obtained results are in agreement with the results of Ibrahim et al. [9]. Thus, in order to delay the boundary layer formation the magnetic field strength should be decreased appropriately.



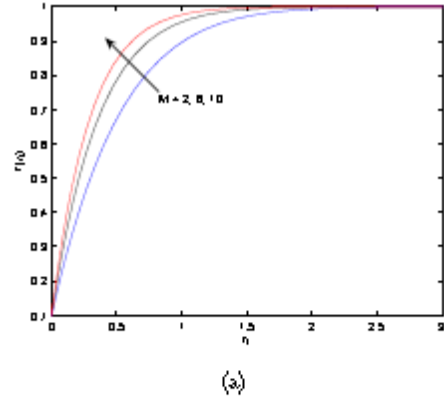
(a)



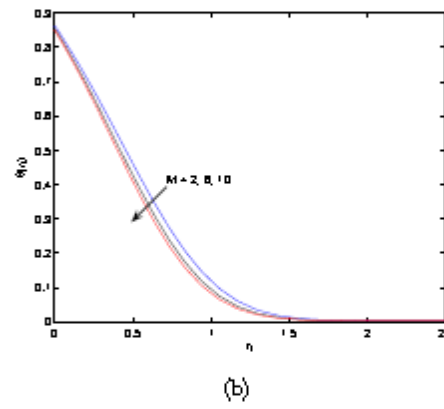
(b)

Fig. 5. The effect of Biot number Bi on (a) the fluid temperature θ and (b) the species concentration φ , when $M = 2$, $E = 0.1$, $Le = 5$, $Nb = Nt = 0.1$, $Pr = 5$, $A^* = 0.05$, and $B^* = 0.05$.

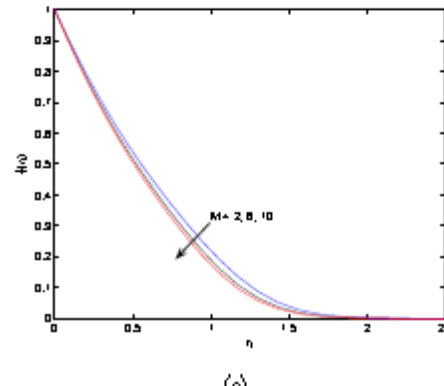
It is perceived from Table 1 that an increase in the magnetic field causes an increase in the coefficient of skin-friction which is due to the increase in the tangential force taking place as a result of increasing velocity. It is observed that the Nusselt number, which measures the rate of heat transfer from the surface, increases with increasing values of M and Bi , while it decreases with increasing values of Nb , Nt and $A^* = B^*$. This implies that the rate of heat transfer from the surface increases with an increase in the magnetic field and convective heating of the surface while the effects of Brownian motion, thermophoresis and heat generation/absorption is to decrease the rate of heat transfer from the surface. It may also be noted that the nanoparticle mass transfer increases with the increase in magnetic field, Brownian motion, thermophoresis, and heat generation/absorption while it is reversely affected by an increase in the convective heating at the surface.



(a)



(b)



(c)

Fig. 6. The effect of magnetic parameter M on (a) the fluid velocity $f t$, (b) the fluid temperature θ and (c) species concentration φ when $Le = 5$, $Pr = 5$, $Bi = 5$, $E = 0.1$, $Nb = Nt = 0.1$, $A^* = 0.05$, and $B^* = 0.05$.

CONCLUSIONS

The effects of space/temperature dependent non-uniform heat generation/absorption and Newtonian heating on the flow of a viscous, incompressible, and electrically conducting nanofluid past a stretching sheet is studied. The space dependent and temperature dependent heat generation have increasing effect on the nanofluid temperature while the heat absorption has a decreasing effect. However, the observed effects were found to be very less in these cases. The Newtonian heating at the surface of the sheet has an increasing effect on the nanofluid temperature and nanoparticle

concentration and the effect on the nanofluid temperature is significant. One of the interesting results of the present study is the increasing effect of the magnetic field on the nanofluid velocity and an opposite one on the nanofluid temperature where these two physical quantities behave opposite to their usual trend with a change in the strength of the applied magnetic field. Thus in physical problems of the type as presented in this study, it is worthwhile to have a lesser applied magnetic field, as this will delay the boundary layer formation in the flow-field and will also decrease the skin-friction coefficient and rate of heat transfer from the surface.

Table 1. Effects of different parameters on coefficient of local skin-friction C_{fx} , local Nusselt number Nu_x , and local Sherwood number Sh_x .

M	BI	NB	$NTA^* = B^*$	$C_{fx}\sqrt{RE_x}$	$NU_x/\sqrt{RE_x}$	$SH_x/\sqrt{RE_x}$
2	5	0.1	0.1	0.05	1.7104942	0.682568
6					2.482135450	0.725279741
10					3.065835750	0.749335331
	1				1.7104942	0.455541371
	5				1.7104942	0.682568
10					1.7104942	0.72469558
	0.1				1.7104942	0.682568
	0.2				1.7104942	0.527392751
	0.3				1.7104942	0.397449151
	0.1				1.7104942	0.682568
	0.2				1.7104942	0.589630761
	0.3				1.7104942	0.5069898
	0.05				1.7104942	0.691489461
	0				1.7104942	0.687039391
	0.05				1.7104942	0.682568

Acknowledgement: Authors of the paper gratefully acknowledge the suggestion of the reviewers which helped them to improve the quality of the paper in its present form.

REFERENCES

- W. J. Minkowycz, E. M. Sparrow, J. P. Abraham, *Nanoparticle Heat Transfer and Fluid Flow*, CRC Press, 2012.
- S. Kakac, A. Pramuanjaroenkij, *International Journal of Heat and Mass Transfer*, **52**, 3187 (2009).
- S. U. S. Choi, Z. G. Zhang, W. Yu, F. E. Lockwood, E. A. Grulke, *Appl. Phys. Lett.*, **79**, 2252 (2001).
- S. U. S. Choi, Enhancing thermal conductivity of fluids with nanoparticles,, in: The Proceedings of the 1995 ASME International Mechanical Engineering Congress and Exposition, San Francisco, USA, ASME, FED 231/MD 66, 1995, p. 99
- J. Buongiorno, *J. Heat Transfer*, **128**, 240 (2006).
- L. J. Crane, Flow past a stretching plate, *Z. Angew. Math. Phys.*, **21**, 645 (1970).
- S. Nadeem, R. U. Haq, Z. H. Khan, *Alexandria Eng. J.*, **53**, 219 (2014).
- W. Ibrahim, B. Shankar, *Computers and fluids*, **75**, 1 (2013).
- W. Ibrahim, B. Shankar, M. M. Nandeppanavar, *Int. J. Heat Mass Transf.*, **56**, 1 (2013).
- M. Qasim, Z. Khan, W. Khan, I. A. Shah, *PLoS ONE*, **9**(1), e83930. (2014)
- K. Bhattacharyya, G. Layek, *Physics Research International* **2014** (2014) 592536.
- M. M. Nandeppanavar, K. Vajravelu, M. S. Abel, C.-O. Ng, *Int. J. Heat Mass Transf.*, **54**, 4960 (2011).
- D. Pal, *Comput. Math. Appl.*, **66**, 1161 (2013).
- A. Malvandi, F. Hedayati, G. Domairry, *J. Thermodynamics* 2013, Article ID: 764827, (2013).
- B. Shankar, Y. Yirga, *Int. J. Math. Comp. Sci. Eng.*, **7**(12) 935 (2013).
- M. Abel, P. Siddheshwar, M. M. Nandeppanavar, *Int. J. Heat Mass Transf.*, **50**, 960 (2007).
- M. S. Abel, M. N. Mahantesh, *Comm. Nonlinear Sci. Numer. Simulat.* **14**, 2120 (2009).
- M. Goyal, R. Bhargava, *ISRN Nanotech.* 2013, 931021, (2013) .
- A. Mastroberardino, *Commun. Nonlinear Sci. Numer. Simulat.*, **19**, 1638 (2014) .
- M. M. Nandeppanavar, K. Vajravelu, M. S. Abel, *Comm. Nonlinear Sci. Numer. Simulat.*, **16**(9), 3578 (2011).
- M. J. Uddin, W. A. Khan, A. I. Ismail, *PLOS One*, **7**(11), 1 (2012). doi:10.1371/journal.pone.0049499.
- O. D. Makinde, W. A. Khan, Z. H. Khan, *Int. J. Heat Mass Transf.*, **62**, 526 (2013).
- O. D. Makinde, W. N. Mutuku, *U.P.B. Sci. Bull., Series A*, **76**(2), 181 (2014).
- S. S. Motsa, Z. G. Makukula, *Cent. Eur. J. Phys.*, **11**(3), 363 (2013).
- P. Kameswaran, P. Sibanda, S. S. Motsa, *Boundary Value Problems* 2013, 242 (2013).

НАНОФЛУИДЕН ПОТОК С ТОЧКА НА СТАГНАЦИЯ ПО ПРОТЕЖЕНИЕ НА
РАЗТЕГЛЯЩА СЕ ПЛАСТИНА С НЕЕДНАКВО ГЕНЕРИРАНЕ / ПОГЛЪЩАНЕ НА
ТОПЛИНА И НЮТОНОВО НАГРЯВАНИ

Б. К. Махата¹, Р. Нандкейоляр^{2*}, М. Дас¹, П. Сибанда³

¹ Катедра по математика, Училище по приложни науки, Университет КИИТ, Бхубанешвар-751024, Индия

² Училище по математика, Университет Тапар, Патяла-147001, Индия

³ Училище по математика, статистика и компютърни науки, Университет Куа Зулу-Натал, Скотсвил 3209,
Питермариибург, Южна Африка

Получена на 10 ноември, 2014 г.; приета на 6 февруари, 2017 г.

(Резюме)

Разглеждат се неравномерното генериране / абсорбция на топлина и ефектите на Нютоново нагряване върху постоянния двумерен ламинарен граничен слой на стагнация на нанофлуид преминаващ разтягаща се пластина в присъствието на външно унифицирано магнитно поле. Предполага се, че нанофлуидът е вискозен, несвиваем и електрически проводим. Ефектите от Брауновото движението и термофоретичната дифузия са взети под внимание. Управляващите нелинейни частни диференциални уравнения се трансформират в набор от обикновени диференциални уравнения, които се решават с помощта на спектралния метод на релаксация (SRM). Ефектите от съответните параметри на потока, топлината и концентрацията на наночастици се изследват с помощта на графики и таблици. Представеният нанофлуиден модел има значителни приложения при инженерни процеси с течение, при които се осъществява едновременен процес на генериране на топлина и конвективно нагряване на граничната повърхност, като топлообменници и охлаждане на ядрен реактор.

Mathematical modeling of thin-layer microwave drying of corn husk and investigation of powder properties

A. Akdoğan¹, G. Çalışkan Koç^{*2}, S. N. Dirim²

¹ *Gümüşhane University, Engineering and Natural Sciences Faculty, Food Engineering Department, Gümüşhane, Turkey*

² *Ege University, Engineering Faculty, Food Engineering Department, Izmir, Turkey*

Received September 15, 2016; Accepted April 29, 2017

The aim of this study is to investigate the effect of different microwave powers on the drying kinetics of chopped corn husks and to determine the properties of the corn husk powder obtained after grinding the dried product. The drying behavior of corn husks was determined using eleven commonly used thin-layer models. The obtained powders were analyzed for moisture content, water activity, color, tapped and bulk densities, wettability, flowability, and cohesiveness. In addition, the effective moisture diffusivity and activation energy of corn husks were calculated from drying data. From the analysis of the results, the drying rate and the drying time of corn husk slices considerably decreased with increasing microwave power. Among all used drying models, the Page model was found to satisfactorily describe the kinetics of microwave drying of corn husk. The effective moisture diffusivity values ranged from 2.264×10^{-10} to $8.941 \times 10^{-10} \text{ m}^2\text{s}^{-1}$.

Keywords: corn husk; microwave drying; agricultural waste; modeling; activation energy.

INTRODUCTION

Corn is one of the main agricultural products all over the world. Corn husks consist of thin cellulose-rich leafy sheets that cover the corn cob. Corn husks are an important by-product of the corn processing industry and have been either used as animal food or are returned to the harvested field. On the average, the husks contain 382 g cellulose, 445 g hemicellulose, 66 g lignin, 19 g protein, and 28 g ash per kg of dry matter [1]. Utilization of corn husks may potentially reduce environmental pollution and provide further profits to the farmers [2].

The main aim of drying which is one of the oldest food preservation techniques is to allow longer periods of storage, minimize packaging requirements, and transportation costs [3]. Drying can be accomplished using many techniques, e.g., microwave drying. In a microwave drying system, the microwave energy has an internal heat generative capacity and can easily penetrate the interior layers to directly absorb the moisture in the sample. The quick energy absorption causes rapid evaporation of water. Theoretically, microwave drying technique can reduce the drying time period [4]. In fact, the dehydration kinetics is important for the design and optimization of the drying process [5]. During drying, the determination of the rate of water removal and the effect of drying conditions on this rate is important and expressed in terms of drying models. Thin-layer drying equations which are

practical, provide sufficiently good results and are important in mathematical modeling of drying [6]. Thin-layer drying is the process of drying in one layer of sample particles or slices.

Corn is one of the leading harvested crops in the world and corn husks constitute a large amount. Proper methods of treatment of husks will reduce the environmental pollution and at the same time, valuable nutrient sources in the husks will be saved. Considering the possible treatment methods, drying is the most suitable one. By drying, the stability of husks against chemical and biological decomposition will be increased and the amounts of waste material will be decreased. Although electrical methods, such as microwave drying, are considered to be expensive applications in waste treatment, high drying rates and feasibility of the drying systems for designs and different scales promote their use in future applications. According to the literature, corn husks were used as a substrate for fermentation of bioethanol and citric acid. Since the fermentation systems are to be well controlled for substrate composition and quality, use of dried materials will be more advantageous in those systems. In addition, there are few studies on the determination of the effective moisture diffusivity of the microwave drying process. The aims of this study are to observe the effects of different microwave powers on the drying kinetics of corn husks, to fit the experimental data to thin-layer drying models to estimate the model parameters and finally to determine the powder properties of corn husks.

* To whom all correspondence should be sent:
E-mail: gulsah.caliskan@ege.edu.tr

EXPERIMENTAL DETAILS

Materials

Fresh corns were obtained from a local supermarket in Izmir, Turkey. The husks were removed, washed, sorted, and sliced into a thickness of 0.48 ± 0.02 mm.

Microwave drying

Experiments were performed in a domestic microwave oven (Arçelik MD 595, Turkey) at 2450 MHz with a maximum output power of 900W. Ten grams of sample was taken and placed in the oven. Drying experiments were performed at five different microwave powers (180, 360, 540, 720, and 900 W). For determination of the moisture loss, the samples together with the tray were taken out at uniform intervals and weighed using a digital balance with 0.01 g precision (Ohaus AR2140, USA). Drying process was ended when constant weight was recorded. The powder was obtained by grinding the dried material in a home type blender (Tefal Smart, MB450141, Turkey).

Mathematical modeling of drying data

The moisture ratio values (MR) were calculated using the obtained moisture content values from drying experiments for all microwave powers. The dimensionless moisture ratio can be calculated using the equation (1);

$$MR = \frac{M_t - M_e}{M_0 - M_e} \quad (1)$$

Where M_t , M_0 , and M_e are the moisture contents at any time, initial, and equilibrium (kg water/ kg dry matter), respectively.

Drying data were fitted to eleven (Lewis, Page, Modified Page I, Henderson and Pabis, Modified Henderson and Pabis, Logarithmic, Midilli, Modified Midilli, Two-term, Two-term Exponential, and Wang and Singh) well-known thin layer drying models. Nonlinear regression analysis was used to evaluate the parameters of the selected model using statistical software SPSS 16.0 (SPSS Inc., Chicago, IL, USA). The goodness of fit was determined using the coefficient of determination (R^2), the root mean square error (RMSE), and the reduced chi-square (χ^2). The high values of the coefficient of determination (R^2), the low values of the root mean square error (RMSE) and the reduced chi-square (χ^2) were chosen for the goodness of fit [6]. The effective moisture diffusivity was calculated by using Eq. 2 [7]:

$$MR = \frac{M_t - M_e}{M_0 - M_e} = \frac{8}{\pi^2} \sum_{n=0}^{\infty} \frac{1}{(2n+1)^2} \exp\left(-\frac{(2n+1)^2 \pi^2 D_{eff}}{4L^2} t\right) \quad (2)$$

where D_{eff} is the effective moisture diffusivity and L is the thickness of corn slices. For long drying times only the first term ($n=1$) of the series can be used, so the Eq. (3) can be written as:

$$MR = \frac{M_t - M_e}{M_0 - M_e} = \frac{8}{\pi^2} \exp\left(-\frac{\pi^2 D_{eff}}{4L^2} t\right) \quad (3)$$

Eq. (3) could be simplified to a straight-line equation as Eq. (4) [3,7, 8];

$$\ln(MR) = \ln\left(\frac{8}{\pi^2}\right) - \left(\frac{D_{eff}\pi^2}{4L^2}\right) t \quad (4)$$

Physical analysis and analysis of powder properties

The moisture content of fresh corn husks and microwave dried corn husk powders was determined according to AOAC [9]. Water activity was measured using Testo-AG 400, Germany water activity measurement device. The color values of corn husks (L^* , a^* and b^* values) were measured with a Minolta CR-400 Colorimeter, Japan. Total color change (ΔE) of microwave dried corn husks with respect to fresh corn husks was calculated by using Eq. 5;

$$\Delta E = \sqrt{\Delta L^2 + \Delta a^2 + \Delta b^2} \quad (5)$$

For the determination of tapped and bulk densities, flowability and cohesiveness the methods of Jinapong et al. [10] were used. The average wettability time of microwave dried corn husk powders was determined using the method of Goula and Adamopoulos [11].

Data were analyzed using statistical software SPSS 16.0 (SPSS Inc., Chicago, IL, USA). The data were also subjected to analysis of variance (ANOVA) and Duncan's multiple range test ($\alpha=0.05$) to determine the difference between means. The drying experiments were replicated twice and all analyses were triplicated.

RESULTS AND DISCUSSION

Results of Physical Analysis

The moisture contents and color values (L^* , a^* , and b^*) of fresh corn husks were found to be $76.95 \pm 5.07\%$ (wet basis, wb), and 73.58 ± 1.33 , -3.97 ± 0.46 , and 18.73 ± 1.79 , respectively. The results of the physical analyses applied to corn husk powder and the total color change are given in Table 1.

Table 1. Results of the physical analyses applied to microwave dried corn husk powders.

Properties	Microwave Power (Watt)				
	180	360	540	720	900
Moisture Content (% wb)	11.53±0.20 ^b	7.59±1.87 ^a	7.12±0.37 ^a	5.96±0.31 ^a	6.52±0.68 ^a
Water Activity	0.40±0.03 ^b	0.38±0.02 ^b	0.30±0.02 ^a	0.29±0.04 ^a	0.26±0.01 ^a
ΔE	9.92±0.13 ^b	8.68±0.36 ^a	8.30±0.70 ^a	10.80±0.29 ^c	9.55±0.31 ^b

^{a-c} Different letters in the same row indicate a significant difference between averages at P<0.05.

The results showed that the microwave drying process removed about 90% of the water from fresh corn husks at microwave powers between 360W-900W. Moisture contents and water activity values of microwave dried corn husk powder decreased according to increasing microwave power due to a high transfer rate at high microwave power. However, an increase in microwave power from 720W to 900W caused a slight increase in the moisture content due to structural changes. The decrease in moisture content was not found statistically significant for microwave powers between 360 and 900 W (P>0.05). The water activity values of corn husks are within acceptable limits for safe storage of products. The lowest color change was observed from the drying experiment at 540W. Chua and Chou [12] studied the color change in carrots at microwave powers of 100, 300, and 500 W and determined the lowest color change at 500 W microwave power. In a study by Ozkan *et al.* [13], it was reported that considering the color change of microwave dried (90-1000W) spinach at energy levels of 500, 650, and 700W, the measured color values were very close to those of the fresh spinach. The result of this study is consistent with the studies of Chua and Chou [12] and Ozkan *et al.* [13].

Effect of different microwave powers on the drying kinetics of corn husks

The drying behavior of corn husks was determined from the mass loss in the samples of known initial moisture content (76.95±5.07% (wb)).

As expected, drying time of corn husk samples decreased with increasing microwave power, and so it was observed that drying time of the samples at 540W was less than half of the drying time at 180W. The drying rates were calculated (kg water/kg dry matter.min) and plotted against the moisture ratio (kg water/kg dry matter) for drying of corn husk slices as shown in Fig. 1. The drying rates increased with the increase in microwave output power and the highest values of the drying rate were obtained during the experiment at 900W. Constant drying rate periods ranged between 1.13 and 1.85 kg water/ (kg dry matter.min)⁻¹ for microwave powers between 180 and 900 W, respectively. Constant rate period was followed by a falling rate period for all microwave powers.

In order to describe the drying kinetics of corn husks, eleven different semi-empirical models were fitted to experimental data and the summary of model parameters of thin-layer drying models, as well as the statistical results (R^2 , RMSE, and χ^2) are presented in Table 2. It was reported that the most suitable thin-layer drying model is that which provides the highest R^2 value and the lowest RMSE and χ^2 values [14]. In this study, the coefficient of correlation (R^2) was one of the primary criteria for selecting the best model to define the microwave drying behavior of corn husk slices. Calculated R^2 values were found to be 0.999 for Page, Modified Henderson and Pabis and Two-term Exponential models.

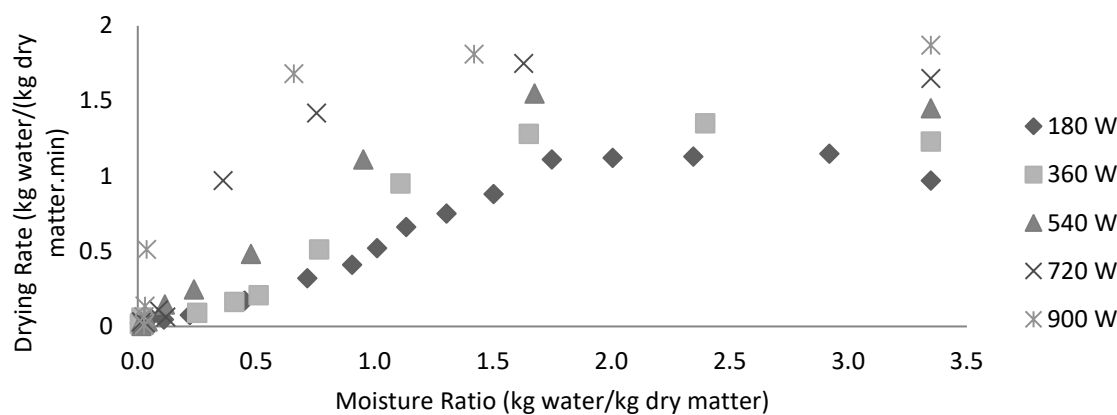


Fig. 1. Variation of the drying rate (kg water / (kg dry matter min⁻¹)) as a function of the moisture ratio (kg water/kg dry matter) for different microwave powers.

Table 2. Coefficients of the model equations obtained from the statistical analysis of drying data.

Model	P(W)	Model Constants					R ²	χ ²	RMSE	
(MR = e ^{-kt})	180	k=0.448					0.997	2.819E-04	0.01636	
	360	k=0.845					0.996	4.217E-04	0.01966	
	540	k=1.335					0.999	8.449E-05	0.00872	
	720	k=1.394					0.999	8.720E-03	0.00320	
	900	k=2.009					0.999	4.839E-05	0.00651	
(MR = e ^{-k(t)ⁿ})	180	k=0.406	n=1.095				0.999	9.457E-05	0.00948	
	360	k=0.794	n=1.159				0.999	1.619E-05	0.00385	
	540	k=1.335	n=0.985				0.999	8.182E-05	0.00858	
	720	k=1.697	n=1.002				0.999	1.143E-05	0.00319	
	900	k=2.069	n=1.084				0.999	6.021E-06	0.00230	
Modified Page I (MR = e ^{(-kt)ⁿ})	180	k=4.176	n=0.107				0.997	2.823E-04	0.01638	
	360	k=0.967	n=0.874				0.996	4.216E-04	0.01966	
	540	k=1.134	n=0.996				0.999	8.450E-05	0.00872	
	720	k=0.963	n=1.148				0.999	2.691E-03	0.04891	
	900	k=1.489	n=1.349				0.999	4.838E-05	0.00651	
Henderson and Pabis (MR = ae ^{-kt})	180	k=0.459	a=1.027				0.998	2.151E-04	0.01429	
	360	k=0.863	a=1.023				0.997	3.599E-04	0.01816	
	540	k=1.332	a=0.997				0.999	8.357E-05	0.00867	
	720	k=1.395	a=1.000				0.999	1.152E-05	0.00320	
	900	k=2.013	a=1.002				0.999	4.773E-05	0.00646	
Modified Henderson and Pabis (MR = ae ^{-kt} + be ^{-gt} + ce ^{-ht})	180	a=1.084	b=-0.042	c=-0.042	k=0.435	g=42.097	h=0.084	0.999	5.415E-05	0.00717
	360	a=-1.588	b=-1.588	c=4.187	k=0.548	g=0.549	h=0.608	0.999	1.223E-04	0.01059
	540	a=7.647	b=7.426	c=-14.077	k=1.106	g=1.133	h=1.106	0.999	7.950E-05	0.00846
	720	a=-0.774	b=0.790	c=0.978	k=0.144	g=0.153	h=1.423	0.999	7.693E-06	0.00262
	900	a=-3.737	b=2.369	c=2.369	k=1.490	g=1.582	h=1.583	0.999	1.089E-05	0.00309
Logarithmic (MR = ae ^{-kt} + c)	180	k=0.427	a=1.040	c=-0.024				0.999	9.336E-05	0.00942
	360	k=0.804	a=1.040	c=-0.024				0.998	1.987E-04	0.01350
	540	k=1.307	a=1.001	c=-0.006				0.999	7.000E-05	0.00794
	720	k=1.002	a=1.384	c=-0.002				0.999	9.422E-06	0.00289
	900	k=1.979	a=1.007	c=-0.005				0.999	3.237E-05	0.00532
Midilli (MR = ae ^{-kt} + bt)	180	k=0.440	a=1.018	b=-0.002				0.999	1.114E-04	0.01029
	360	k=0.832	a=1.018	b=-0.004				0.998	2.355E-04	0.01469
	540	k=1.319	a=0.996	b=-0.002				0.999	7.198E-05	0.00805
	720	k=1.388	a=1.000	b=0.000				0.999	1.235E-05	0.00331
	900	k=2.001	a=1.002	b=-0.001				0.999	3.960E-05	0.00589
Modified Midilli (MR = e ^{-kt} + bt)	180	k=0.431	b=-0.003				0.999	1.348E-04	0.01132	
	360	k=0.816	b=-0.004				0.997	2.671E-04	0.01565	
	540	k=1.324	b=-0.001				0.999	7.292E-05	0.00810	
	720	k=1.389	b=0.000				0.999	1.209E-05	0.00328	
	900	k=1.998	b=-0.001				0.999	4.016E-05	0.00593	
Two Term (MR = ae ^{-k₁t} + be ^{-k₂t})	180	k ₁ =0.459	k ₂ =-0.459	a=0.545	b=0.482		0.998	2.151E-04	0.01429	
	360	k ₁ =0.863	k ₂ =0.863	a=0.516	b=0.508		0.999	3.600E-04	0.01816	
	540	k ₁ =1.332	k ₂ =1.332	a=0.396	b=0.601		0.999	8.357E-05	0.00867	
	720	k ₁ =1.395	k ₂ =1.395	a=0.318	b=0.682		0.999	1.152E-05	0.00320	
	900	k ₁ =2.013	k ₂ =2.013	a=0.507	b=0.495		0.999	4.773E-05	0.00646	
Two Term Exponential (MR = ae ^{-kt} + (1 - a)e ^{-kat})	180	k=0.547	a=1.561				0.999	1.005E-04	0.00977	
	360	k=1.100	a=1.681				0.999	1.677E-05	0.00392	
	540	k=1.355	a=1.127				0.999	8.439E-05	0.00872	
	720	k=1.421	a=1.147				0.999	1.136E-05	0.00318	
	900	k=2.382	a=1.519				0.999	5.973E-06	0.00229	
Wangh and Singh (MR = 1 + at + bt ²)	180	a=-0.289	b=0.020				0.968	3.060E-03	0.05392	
	360	a=-0.521	b=0.065				0.965	3.727E-03	0.05845	
	540	a=-0.692	b=0.110				0.904	1.007E-02	0.09519	
	720	a=-0.755	b=0.132				0.920	8.923E-03	0.08906	
	900	a=-0.928	b=0.193				0.882	1.435E-02	0.11204	

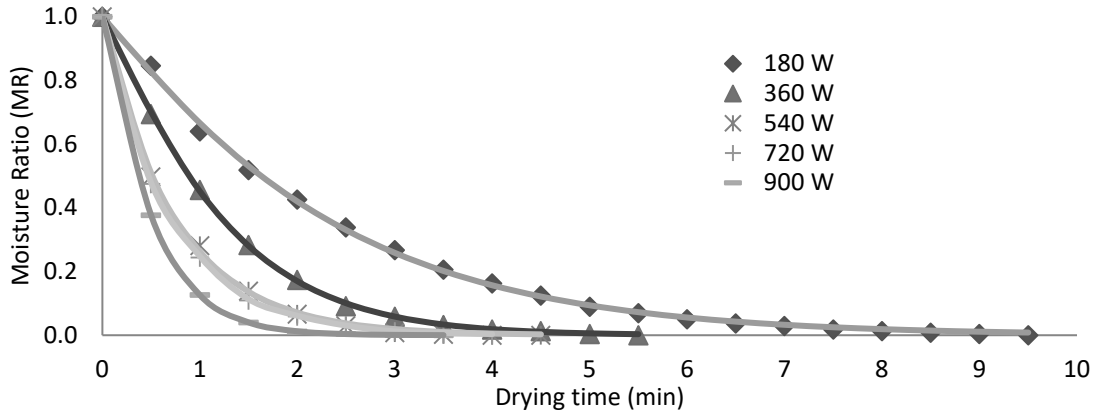


Fig. 2. Experimental and predicted moisture ratio values obtained by the Page model.

As a result of statistical analysis, the Page model was found to be the most appropriate one with a higher value of the coefficient of determination (R^2) and lower reduced chi-square (χ^2) and root mean square error (RMSE). The Page model represents a non-linear relationship between $\ln(MR)$ and drying time. The experimental and predicted moisture ratio values obtained using the Page model are given in Fig. 2. In addition, Arabhosseini *et al.* [15] reported that small numbers of the model parameters are preferable to find a relationship between the parameter values and the drying conditions, which is valid for the Page model. Several researchers reported that the Page model was chosen to determine the hot air drying behavior of black tea [8], microwave vacuum and hot air drying behavior of mint [3], microwave drying behavior of *Pandanus amaryllifolius* leaves [16], microwave drying behavior of spinach [13], hot air drying behavior of bay leaves [17], convective drying behavior of parsley [14], hot air drying behavior of tarragon leaves [15].

Effective moisture diffusivity values for drying of corn husks

The effective moisture diffusivities (D_{eff}) of microwave dried corn husks were calculated from the Fick's diffusion model and the results are given in Table 3. Chopped corn husks were placed in the microwave oven as a thin layer. That can be assumed as an infinite slab. L is taken as the thickness of the corn husk layer in Eqs. (2-4). As can be seen from Table 3 the D_{eff} values increased with increasing microwave powers, as expected.

Table 3. Effective moisture diffusivity values of the microwave dried corn husks.

Microwave Output Power (W)	D_{eff} ($m^2.s^{-1}$)	R^2
180	2.264E-10	0.9803
360	4.132E-10	0.9886
540	5.393E-10	0.9975
720	5.999E-10	0.9828
900	8.941E-10	0.9980

Panchariya *et al.* [8] investigated the drying kinetics of black tea between 80 and 120 °C in hot air and the effective moisture diffusivities varied from 1.141×10^{-11} to $2.98 \times 10^{-11} m^2.s^{-1}$ over the temperature range. Similarly, Doymaz [3] reported that the effective moisture diffusivities of mint for the temperature range 35-60°C ranged between 3.067×10^{-9} and $1.941 \times 10^{-8} m^2.s^{-1}$. Several researchers studied the microwave treatment of leafy plants such as mint and *Pandanus amaryllifolius* leaves which have a similar structure with corn husks. Ozbek and Dadali [18] reported that the effective moisture diffusivities of mint varied from 0.3982×10^{-10} to $2.0732 \times 10^{-10} m^2.s^{-1}$ for the power range from 180 to 900 W. Similarly, Rayaguru and Routray [16] calculated the D_{eff} value for *Pandanus amaryllifolius* as 1.99×10^{-7} - $5.35 \times 10^{-8} m^2.s^{-1}$ for the power range from 180 to 720 W.

In processes where energy is involved, the temperature dependence of the reaction rates is expressed in terms of the Arrhenius equation. In the microwave drying process, where the temperature cannot be measured accurately, Arrhenius equation can be used as the modified form given in Eq. (6) [18]:

$$k = k_0 \exp\left(-E_a \frac{m}{P}\right) \quad (6)$$

where k is the drying rate constant obtained using Page equation (min^{-1}). k_0 is the pre-exponential constant (min^{-1}). E_a is the activation energy (W.g^{-1}). P is the microwave power (W) and m is the mass of sample (g).

In the above-referred paper [18], the modified Arrhenius equation was used to define the dependence of a reaction rate constant on $m.P^{-1}$ where the mass of dried sample was increasing at constant microwave power. The same form of the equation was used in this study with the difference that the mass of the sample was kept constant while the microwave power used for drying operation was changed.

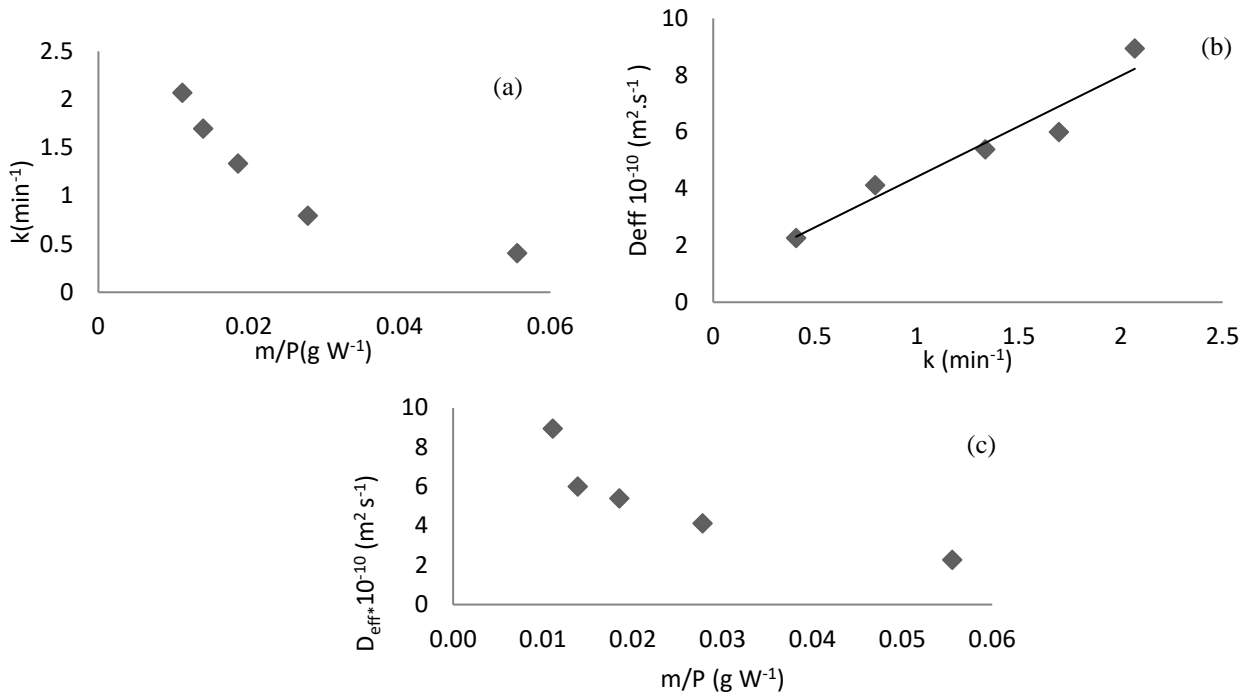


Fig. 3. (a) Relationship between the drying rate constant (k) of Page model and the sample mass /power ratio, (b) Relationship between the drying rate constant (k) and the effective moisture diffusivity (D_{eff}) for microwave drying of corn husks (■ calculated data; - model), (c) Relationship between the effective moisture constant and the sample mass.

The relationship between k and $m.P^{-1}$ is shown in Fig. 3a. Reduced chi-square (χ^2), RMSE and coefficient of determination (R^2) were found to be 0.01669, 0.1119 and 0.972, respectively. The k_0 and E_a values were estimated to be 3.443 min^{-1} and 49.350 W.g^{-1} , respectively. It was observed that the value of the drying rate constant (k) increased with the increase in microwave output power. By considering the Page model and the modified form of the Arrhenius equation together, (using the calculated value of k in the Page model) the constant n was found to be 1.065 as an arithmetical average for microwave drying of corn husk, and so it is possible to estimate the moisture ratio for a specific time or *vice versa*. The relationship between the drying rate constant (k) and the effective moisture diffusivity (D_{eff}) for microwave drying of corn husks is also shown in Fig. 3b. The result is consistent with that of Ozban and Dadali [18]. The researchers reported that the drying curve becomes steeper with the increase in microwave output power which indicates a faster drying of the product.

The activation energy was calculated by using the modified Arrhenius type exponential model as given in Eq. (7) [18]:

$$D_{\text{eff}} = D_0 \exp \left(-E_a \frac{m}{P} \right) \quad (7)$$

where D_{eff} is the effective moisture diffusivity ($\text{m}^2.\text{s}^{-1}$), D_0 is the pre-exponential factor ($\text{m}^2.\text{s}^{-1}$), E_a is the activation energy (W.g^{-1}), P is the microwave power (W) and m is the mass of the sample (g). Similarly, the relationship between D_{eff} and m/P is given in Fig. 3c. Reduced chi-square (χ^2). RMSE and coefficient of determination (R^2) were found to be 1.331×10^{-20} , 9.989×10^{-11} and 0.924, respectively. D_0 and E_a were estimated as $9.678 \times 10^{-10} \text{ m}^2.\text{s}^{-1}$ and 27.149 W.g^{-1} , respectively.

Results for powder properties

Dried products are usually ground to uniform size for further utilization. In this study, powdered form of dried corn husks was aimed to be suitable for different applications. The results for the powder properties of microwave dried corn husk powders are shown in Table 4. The tapped and bulk density values of corn husk powders range between 135-299 and 176-349 kg/m³, respectively. Average wettability time (s) of husk powders decreased with increasing microwave power. This might be caused by the effect of the residual moisture content. Goula and Adamopoulos [11] reported that the residual moisture content, which significantly affects the operational conditions of the powder, affects wettability. The flowability and cohesiveness properties of microwave dried corn husk powders in

Table 4. Powder properties of the microwave dried corn husk powders.

Properties	Microwave Power (Watt)				
	180	360	540	720	900
Tapped density (kg/m ³)	200±9.8 ^b	135±3.8 ^a	240±2.9 ^b	229±11.2 ^b	299±7.9 ^c
Bulk density (kg/m ³)	240±7.9 ^b	176±4.6 ^a	284±13.5 ^b	267±0.1 ^b	349±10.8 ^c
Wettability (s)	497.5±3.5 ^e	268.5±4.9 ^d	121.0±1.4 ^b	184.5±9.2 ^c	48.5±13.4 ^a
Flowability (CI)	Very good	Fair	Good	Very good	Very good
Cohesiveness (HR)	Low	Intermediate	Low	Low	Low

^{a-e} Different letters in the same row indicate a significant difference between averages at P<0.05

terms of Carr Index and Hausner ratio were evaluated. The classification of powder flowability based on the Carr index (CI) is very good (<15), good (15-20), fair (20-35), bad (35-45), and very bad (>45).

The powder cohesiveness based on the Hausner Ratio (HR) is classified as low (<1.2), intermediate (1.2-1.4), and high (>1.4) [10]. According to powder properties, flowability and cohesiveness values of husk powders were generally found to be very good and low, respectively. These results showed the acceptability of the obtained powders for easy flowing and easy dosage to be used in powder formulations.

CONCLUSIONS

Drying kinetics of corn husk powders were investigated in a domestic microwave oven at different microwave powers (180-900W). Depending on the analysis of the results, a considerable falling drying rate was observed and the drying time of corn husk slices decreased with increasing microwave power. By evaluation of the eleven semi-empirical drying models by comparing the coefficient of determination (R^2), reduced chi-square (χ^2) and root mean square error (RMSE), Page equation was found to satisfactorily describe the kinetics of microwave drying of corn husks. The drying rate constant (k) of the Page model generally increased with increasing microwave powers.

REFERENCES

- Y.D. Hang, E.E. Woodams, *LWT – Food Sci. Technol.*, 32: 208-210, (1999).
- S. Huda, Y. Yang, *Macromol. Mater. Eng.*, 293,3:235-243, (2008).
- I. Doymaz, *J. Food Eng.*, 74,3: 370-375, (2006).
- Z. Wang, J. Sun, F. Chen, X. Liao, X. Hu, *J. Food. Eng.*, 80,2:536-544, (2007).
- M. Planinic', D. Velic', S. Tomas, M. Bilic, A. Bucic', *Eur. Food Res. Technol.*, 221,446–451, (2005).
- Z. Erbay, F. Icier, *J. Food Eng.*, 91,4:533-541, (2009).
- J. Crank, 2nd Ed., Clarenden Press, Oxford, UK, (1975).
- P.C. Panchariya, D. Popovic, A.L. Sharma, *J. Food Eng.*, 52, 349-351, (2002).
- AOAC, vol. II. 15th ed. Association of Official Analytical Chemists. Arlington, VA, (1990).
- N. Jinapong, M. Suphantharika, P. Jamnong, *J. Food Eng.*, 84, 2:194-205, (2008).
- A.M. Goula, K.G. Adamopoulos, *Drying Technol.*, 26,6: 726-737, (2008).
- J.K. Chua, K.S. Chou, *Int. J. Food Sci. Technol.*, 40,23–39, (2005).
- I.A. Ozkan, B. Akbudak, N. Akbudak, *J. Food Eng.*, 78,2: 577-583, (2007).
- E. Kavak Akpinar, Y. Bicer, F. Cetinkaya, *J. Food Eng.*, 75, 3:308-315, (2006).
- A. Arabhosseini, W. Huisman, A. van Boxtel, J. Müller, *Ind. Crops Prod.*, 29, 1: 53-59, (2009).
- K. Rayaguru, W. Routray, *Int. Food Res. J.*, 18,3:1035-1042, (2011).
- T. Gunhan, V. Demir, E. Hancioglu, A. Hepbasli, *Energ. Convers. Manage.*, 46,11-12: 1667-1679, (2005).
- B. Özbek, G. Dadali, *J. Food Eng.*, 83,4:541-549, (2007).

МАТЕМАТИЧНО МОДЕЛИРАНЕ НА МИКРОВЪЛНОВО СУШЕНЕ В ТЪНЪК СЛОЙ НА ЦАРЕВИЧНИ ОБВИВКИ И ИЗСЛЕДВАНЕ СВОЙСТВАТА НА ПРАХА

А. Акдоган¹, Г. Чалъшкан Коч^{*2}, С.Н. Дирим²

¹ Университет в Гюмюшхане, Факултет по инженерство и природни науки, Департамент по хранителни технологии, Гюмюшхане, Турция

² Университет „Еге“, Инженерен факултет, Департамент за хранителни технологии, Измир, Турция

Постъпила на 15 септември, 2016 г.; коригирана на 29 април, 2017 г.

(Резюме)

Целта на тази работа е да се изследва ефекта на микровълновата енергия на кинетиката на сушенето на нарязани обивки и да се определят свойствата на получения прах след сушенето. Процесът на сушенето е изследван с помощта на 11 общо-приети тънкослойни модели. Получените прахове са анализирани за влагосъдържание, водна активност, цвят, плътност, омокряемост, течливост, кохезивност. Допълнително ефективният коефициент на дифузия на влагата и активиращата енергия на обивките е изчислена от данните за сушенето. Резултатите показват, че скоростта и времето на сушене значително намаляват с повишаването на микровълновата енергия. Между всички използвани модели този на Page е намерен като най-задоволителен за описание на кинетиката на микровълновото сушене на царевичните обивки. Ефективният коефициент на дифузия на влагата варира от 2.264×10^{-10} до $8.941 \times 10^{-10} \text{ m}^2\text{s}^{-1}$.

Ultrasound-assisted dispersive liquid-liquid microextraction with HPLC-UV for the simultaneous determination of Diclofenac potassium and Indomethacin in serum and plasma samples: Experimental design and optimization

N. Chamkouri¹, V. Zare-Shahabadi^{2*}, A. Niazi¹

¹Department of Chemical Engineering, Tehran Science and Research Branch, Islamic Azad University, Tehran, Iran

¹Department of chemistry, faculty of sciences, Islamic Azad university, Arak Branch, Arak, Iran.

²Department of Chemistry, College of Chemical Engineering, Mahshahr Branch, Islamic Azad University, Mahshahr, Iran.

Received May 30, 2016; Accepted June 5, 2017

In this work, a rapid, simple, and environmentally friendly method based on ultrasound-assisted dispersive liquid-liquid microextraction (UADLLME) was proposed for simultaneous determination of diclofenac potassium and indomethacin in serum and plasma samples. High performance liquid chromatography with UV detection (HPLC-UV) was used. The experimental conditions, including pH of sample solution, type of extraction solvent, time of ultrasound, centrifugation condition and ionic strength were investigated and optimized. After screening out the factors with insignificant effect, the remaining factors were optimized using the Central Composite Design. Under the optimal conditions, detection limit were found as 1.09 and 2.18 ng mL⁻¹ for diclofenac potassium and indomethacin respectively and relative standard deviations (RSD) of the analysis less than 3% ($n= 5$) and detection. Mean recoveries of both in human plasma and serum samples were in the ranges of 92–99%. UADLLME - HPLC-UV was successfully applied for the simultaneous determination of diclofenac potassium and indomethacin in human plasma and serum samples.

Keywords: Ultrasound-assisted emulsification-microextraction, diclofenac potassium, indomethacin, Human serum and plasma samples, HPLC-UV.

INTRODUCTION

Diclofenac potassium and indomethacin are nonsteroidal anti-inflammatory drugs (NSAIDs). They have been widely used to treat fever and a variety of conditions that cause pain and inflammation [1]. Beside of their widely use, there are unwanted side effects such as indigestion, ulcers and bleeding parts of the gastrointestinal tract along with liver, kidney and heart problems [2-4]. Therefore, monitoring NSAID drug concentrations are considered an important issue in pharmacokinetic and medicine studies for improving the toxicological management of long-term NSAID therapy [5-7].

Several chromatographic methods have been described for determination of NSAIDs in biological samples, such as capillary electrophoresis (CE) [8-10], high-performance thin-layer chromatography (HPTLC) [11], high-performance liquid chromatography [12-14] and gas chromatography (GC) [15-17]. Sample preparation methods such as Dispersive liquid-liquid extraction(DLLE) [18, 19], dispersive liquid-liquid microextraction based on solidification of floating organic droplets (DLLE-SFO) [14], solid-phase extraction(SPE) [13], hollow fiber-based liquid phase microextraction (HF-

LPME) [17, 20], and stir bar-sorptive extraction (SBSE) [21] are needed when biological samples are to be analysis for NSAIDs.

Dispersive liquid-liquid microextraction (DLLME) was reported by Rezaee et al. [22] as an effective method among the microextraction methods for preconcentration and separation of organic and inorganic specimens. It has several advantages including simplicity of operation, rapidity, high recovery, low consumption of organic solvents, simplicity of experiment, and low cost [23]. In ultrasound assisted -DLLME (UADLLME), the mixture a microvolume of solvents is rapidly injected into the sample to extract analytes. Mass transfer process in the above extraction procedure was accelerated by ultrasonic radiation, caused to introduce a new method named. The consequence is a very efficient and fast analyte extraction. After mass transfer, the two phases can be readily separated by centrifugation [22].

George E. P. Box (1950s) introduced response surface methodology (RSM) -a factorial design based method for collection of statistical techniques- that has been used in the modeling and optimization of some processes [24-25]. Different types of RSM such as three-level factorial design, central composite design (CCD), and Box-Behnken design (BBD) and have different properties and

* To whom all correspondence should be sent:
E-mail: valizare@gmail.com

characteristics. Different types of CCD are such as Central Composite Circumscribed (CCC), Central Composite Inscribed (CCI), and Central Composite Face-centered (CCF). Finally, it is a good way to graphically illustrate the relation between different experimental variables and the response(s) [25].

The goal of this work is simultaneous determination of diclofenac potassium and indomethacin in human serum and plasma samples by HPLC-UV after preconcentration by UADLLME. Experimental variables affecting the extraction efficiency, including pH of sample solution, volume of extraction and dispersive solvent, and ultrasound time were considered and optimized using the central composite design.

EXPERIMENTAL

Materials and Reagents

All analytical-reagent grade of the drugs (>99%) were purchased from Sigma Aldrich (Steinheim, Germany). The stock solutions (500 ng mL^{-1}) were prepared by dissolving appropriate amount of each drug in methanol. The working solutions were prepared by diluting of the stock solutions with methanol. Methanol (HPLC-grade) was purchased from Merck (Darmstadt, Germany). Deionized water produced by Milli-Q system (Millipore, Bedford, MA, USA). All of the standard solutions were stored at 4°C and brought to ambient temperature just prior to use. Throughout the experimental runs, all the solvents, calibration, and real samples were filtered through $0.45 \mu\text{m}$ nylon filter membranes (Varian, USA).

Instrumentation

The chromatography measurements were carried out by a KNAUER HPLC system equipped with a micro vacuum degasser, HPLC column (C18 250 mm \times 4.6mm, 5 μm), and UV detector set to record absorbance at 254 nm. The pH was measured using a pH meter (Metrohm 827, Switzerland) combined with a glass electrode. A 320R Hettich centrifuge (Germany) and a digital 10P ultrasonic bath (Sonorex, Germany) were also used. The MINITAB 16 was used for experimental design, analysis and subsequent regression analysis.

Extraction procedure

The real samples in this study were collected from human serum and plasma samples orthopedic patient volunteers at Taleghani medical center (Abadan, Iran) and then stored at $5\text{--}8^\circ\text{C}$ until analysis (female, age 27 ± 3.1 years; and male, age 24 ± 5.0 years). Human samples were prepared using the UADLLME method. To aliquots of 1 mL human

sample a solution containing 200 μL of 1% TCA was added for protein precipitation. 200 μL of sample was placed in centrifuge vial and 100 μL of 0.01 M phosphate buffer (pH= 4.5) was added. Then, 80 μL of n-hexane and 10 μL of methanol were injected into the sample solution and shaken manually. The vial was immersed in an ultrasonic, sonicated for 2 min, and shaken manually. A cloudy solution was centrifuged for 6 min at 3000 rpm in order to disrupt the emulsions and separate both phases. After centrifugation extraction, the organic phase on the bottom of the tube was collected with a Hamilton microsyringe. Finally, 10 μL of the obtained mixture was injected into the separation system.

RESULTS AND DISCUSSION

Calibration line preparation for caffeine analysis

In order to establish a sensitive and simple analytical method for the simultaneous analysis of selected NSAIDs, all affecting experimental variables were investigated and optimized. These variables were pH, type and volume of extraction solvent, type and volume of dispersive solvent, time of ultrasound, conditions of centrifuging step, ionic strength were studied and optimized. After screening out the factors with insignificant effect, the remaining factors were optimized using the Central Composite Design.

Optimization of chromatographic condition

The main of this work is to HPLC determination of diclofenac potassium and indomethacin after extraction and preconcentration by UADLLME. Two variables including type of mobile phase and column oven temperature were optimized with the hope to find both analytes. Mixtures of acetonitrile/water, acetonitrile/methanol/water, and methanol/ water with different pH values were studied. The best symmetry of the peak shapes was found in the mobile phase containing methanol and water with pH value of 4.5. Formic acid was used to adjust pH of the mobile phase in all experiments. It was found that during the chromatographic analysis increasing the ratio of water to methanol caused to elute efficiently the analytes from the column. Effect of column oven temperature was also studied in the range of 20-30 $^\circ\text{C}$ with the selected mobile phase and flow rate of 1.0 mL min $^{-1}$. According to the results, temperature of 25 $^\circ\text{C}$ was found to be optimal and used in the subsequent analysis. It should be mentioned that changing the flow rate of mobile phase did not affect the chromatographic peaks. Scheme of the gradient used in the HPLC analysis

are presented in Table 1.

Table 1. Scheme of the gradient used in the HPLC analysis.

Time(min)	%H ₂ O (pH 3.5)	%MeOH
0	40	60
2	45	55
3	45	55
5	40	60
7	30	70
10	30	70

Optimization of the extraction parameters using one-at-a time method

The extraction efficiency of UADLLME method depends on some important analytical parameters. In order to optimize the experimental parameters on the response, two methods were applied. The variables pH of the sample solution, type and volume of extraction solvent, type and volume of dispersive solvent, centrifugation time, ultrasound extraction time, and ionic strength were investigated and optimized using one-factor-at-a time.

The variables pH, type of.....were studied and optimized pH of sample solution

pH of the sample solution is one of the factors studied in this study. Effect of pH on the response of drugs, phosphate buffers in the range of 2.0 - 6.0 were investigated. According to the obtained results, it can be concluded that response of drugs were increased when the sample pH was decreased to 4.5. It was found, at low pH, the considered drugs were not in ionic form in solution. The results are shown in Fig. 1. Finally, pH of 4.5 was select as the optimum pH sample solution for the following experiments.

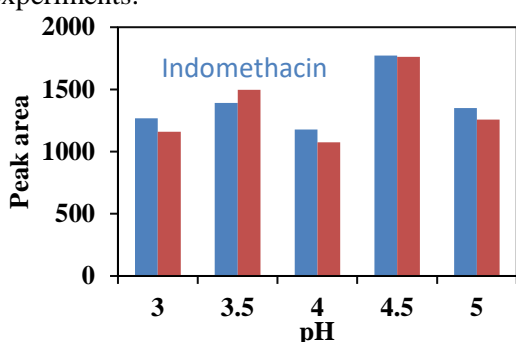


Fig. 1. Effect of pH sample solution on the response of drugs (200 (ng mL⁻¹)).

Selection of extraction solvent and dispersive solvent

One of the most important analytical parameter in UADLLME methods selection of suitable extraction solvent [23]. The extraction solvent has to meet some properties such as lower density than that of

water, low solubility in water, and high extraction capability of the target analytes. Different extraction solvents including n-hexane, 1-octanol, chlorobenzene, and dichloromethane and different dispersive solvents including methanol, acetonitrile, ethanol and acetone were studied. Among them, n-hexane was chosen as the best extraction solvent and methanol was chosen as the best dispersive solvent, because it had higher recoveries in comparison with the others. To obtain the highest response, volume of the extraction solvent and dispersive solvent had to be optimized. Finally, volume of them extraction and dispersive solvents was changed in the range of 10.0 to 100.0 μ L and 5.0 to 40.0 μ L respectively. The results are shown in Fig. 2.a-b. The optimum volumes of extraction solvent and dispersive solvents for both drugs were found 80.0 μ L and 10 μ L respectively.

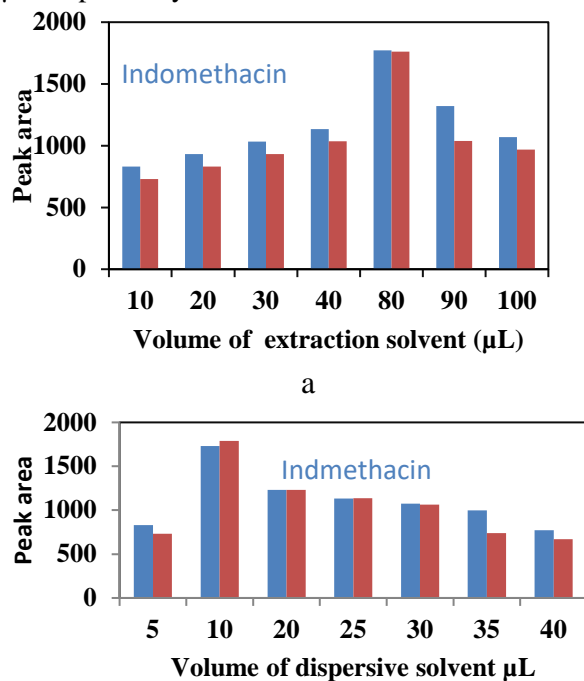


Fig. 2. Effect of extraction solvent volume on the recoveries of drugs. Conditions: sample solution, 5 mL of 200 (ng mL⁻¹) of each drugs; pH sample solution: 4.5.

In this method, to improve the homogeneity, effect of time and temperature of ultrasound to help mixing the solvents and sample solution were investigated with a series of experiments. Ultrasound radiation might affect recoveries due to its own affecting on both emulsification and mass transfer process. Temperature affects organic solvent solubility in water and distribution coefficients as well as the emulsification phenomenon. Time and temperature was studied in the range of 0-5 min and different temperatures ranging from 20 °C - 35 °C. Maximum response were obtained after

ultrasonication for 2 min and 25 °C no improvement was achieved by further ultrasonication. Ultrasound could generate the emulsion quickly and make rapidly a very large contact surface area between the extraction phase and the aqueous phase. Finally, 2 min was found to be the optimum time. It is clear from the results shown in this fig. that emulsification at ambient temperature helps to reach higher response. Therefore, this temperature was taken in the extraction step. At lower temperature, response decreased due to decrease in mass transfer phenomenon.

Effect of centrifugation condition

Centrifugation was required to break down the emulsion and accelerate the phase-separation process. In this method, extraction time is defined as the interval time between injection of the dispersive and extraction solvents to the sample and the start of centrifugation. Centrifugation time was investigated in the range of 1-7 min, whereas centrifuging rate was kept at 3000 rpm. Fig.3. shows that response of the drugs were increased by increasing centrifugation time up to 6 min and decreased after that. This time was chosen at the best.

Ionic strength

Effect of ionic strength varies in different extraction methods and, therefore, it should be study. Influence of ionic strength was investigated by adding different amounts of NaNO₃, NaCl, and KH₂PO₄ 0–10% (w/v) to the aqueous drugs solution to be extracted. The results indicated that the response was approximately constant at different ionic strengths. Finally No significant variation was seen in the extraction efficiencies of target analytes.

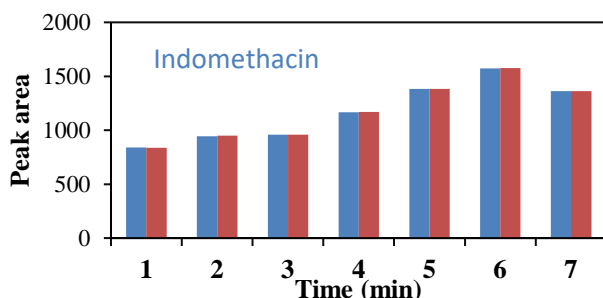


Fig. 3. Effect of centrifugation extraction time on the response of drugs. Conditions: sample solution, 5 mL of 200 (ng mL⁻¹) of each drugs; pH sample solution: 4.5; volume and type of extracting solvent: 1-octanol, 80.0 μL; ultrasonication extraction time: 2 min, ultrasound temperature 25 °C.

Optimization of the variables using the Central composite design

According to the results obtained from study of

one-factor-at-a time, four independent variables including volume of extraction solvent (X₁), dispersive solvents (X₂), pH (X₃), time of ultrasound (X₄) were found to be significant. These parameters were further studied by the Central composite design. A set of 46 runs were chosen based on this design and performed randomly. Variables, assigned levels, and the corresponding Central composite design are shown in Table 2 and Table 3. The response variable for diclofenac potassium (Y₁) indomethacin (Y₂) and the tested variables were related by the following equations.

Table 2. Factors and their levels in Central Composite design.

Factors	Level		
	Low	Center	High
V _{extraction} μL X ₁	-1	0	1
V _{dispersive} μL X ₂	70	80	90
pH* X ₃	5	10	15
Time X ₄	3.0	4.0	5.0
	1	2	3

*Time of ultrasound (min)

Table 3. Factors and their levels in Central Composite design and obtained result for each run.

Run no	Variables				Absorbance	
	X1	X2	X3	X4	Y1	Y2
1	0	0	0	-2	0.737	1.109
2	1	1	1	-1	0.652	0.878
3	0	0	-2	0	1.098	1.347
4	0	0	0	0	0.999	1.4985
5	-1	-1	-1	1	0.642	0.963
6	0	0	0	0	0.881	1.3215
7	1	1	-1	-1	1.003	1.5045
8	-1	1	1	1	0.996	1.494
9	0	0	0	0	1.001	1.5015
10	-1	1	1	-1	0.885	1.3275
11	1	-1	1	1	1.007	1.5105
12	0	0	0	0	0.989	1.4835
13	0	-2	0	0	0.994	1.491
14	0	0	2	0	1.003	1.5045
15	-1	1	-1	-1	1.012	1.518
16	-1	1	-1	1	0.862	1.257
17	-1	-1	1	-1	0.659	0.9885
18	1	-1	-1	1	1.022	1.533
19	0	2	0	0	1.007	1.5105
20	1	-1	1	-1	0.994	1.491
21	-1	-1	-1	-1	0.555	0.8325
22	1	1	-1	1	0.863	1.2945
23	0	0	0	0	1.036	1.554
24	0	0	0	2	0.645	0.9675
25	-2	0	0	0	0.83	1.215
26	0	0	0	0	0.872	1.308
27	1	1	1	1	0.544	0.816
28	1	-1	-1	-1	0.909	1.181
29	2	0	0	0	0.779	1.003
30	-1	-1	1	1	0.871	1.196
31	0	0	0	0	1	1.381

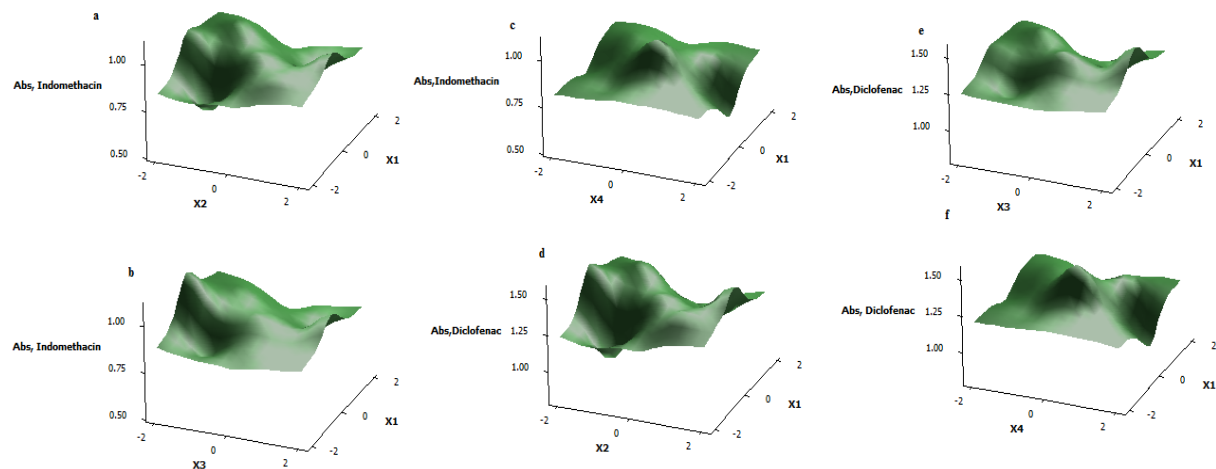


Fig. 4. Response surfaces plot for the Central composite design for indomethacin (a) (x_1) V extraction μL – (x_2) V dispersive μL , (b) (x_1) V extraction μL – (x_3) pH, (c) (x_1) V extraction μL – (x_4) time of ultrasound, and Central composite design for diclofenac (d) (x_1) V extraction μL – (x_2) V dispersive μL , (e) (x_1) V extraction μL – (x_3) pH, (f) (x_1) V extraction μL – (x_4) time of ultrasound.

Analysis of variance (ANOVA) was applied to evaluate the statistical significance of the model. F-test was used to estimate the statistical significance of all terms in the polynomial equation within 95% confidence interval [24-25]. The resulted model had R² and F-value of 0.99 and, respectively. The summary of the ANOVA is shown in Table 4. The result showed the value of R² of 0.8. This finding means that the stabilized model was able to explain 0.81 of the results (or of the variability of the response). After generation of the polynomial equations that relate the absorbance to the independent variables, genetic algorithm was employed to optimize of the process. Response surface curves facilitate investigating the interaction between the independent variables and finding the optimal level for each variable, as well. These curves are represented in Fig. 4. All of factors found effective in one-factor at a time study were appear in the eq. 1 and, eq. 2 therefore, had significant effect on the response. Based on the resulted model, it was found that volume of extraction solvent, dispersive solvents, pH, and time of ultrasound were found to be significant effect on the response.

Optimum values of the tested variables for analysis of both analytes were found to be as follows: volume of extraction solvent μL ($X_1=79$

μL), volume of dispersive solvent μL ($X_2=10 \mu\text{L}$), pH ($X_3=4.3$), and time of ultrasound ($X_4=2.2 \text{ min}$).

Analytical features of proposed method

Under the optimal conditions, analytical features of the proposed method including limit of detection (LOD), limit of quantification (LOQ), dynamic range, enrichment factor (EF), and relative standard deviations (RSD) were investigated. Results are shown in Table 4. A good linear relationship is displayed between the corresponding peak areas and the concentrations of the both drugs based on the correlation coefficients.

Comparison of the parameters obtained in this work with those reported in the literature is given in Table 6. It is obvious that analytical features of the proposed procedure are comparable or better than the others reported for diclofenac potassium and indomethacin determination.

Chromatograms of solutions containing mixture of both under the optimal conditions are shown in Fig. 6a-b. Chromatograms two-dimensional chromatograms of the extracted indomethacin (50 ppb) and diclofenac (10 ppb) in serum samples and indomethacin (200 ppb) and diclofenac (100 ppb) in plasma samples after spiking.

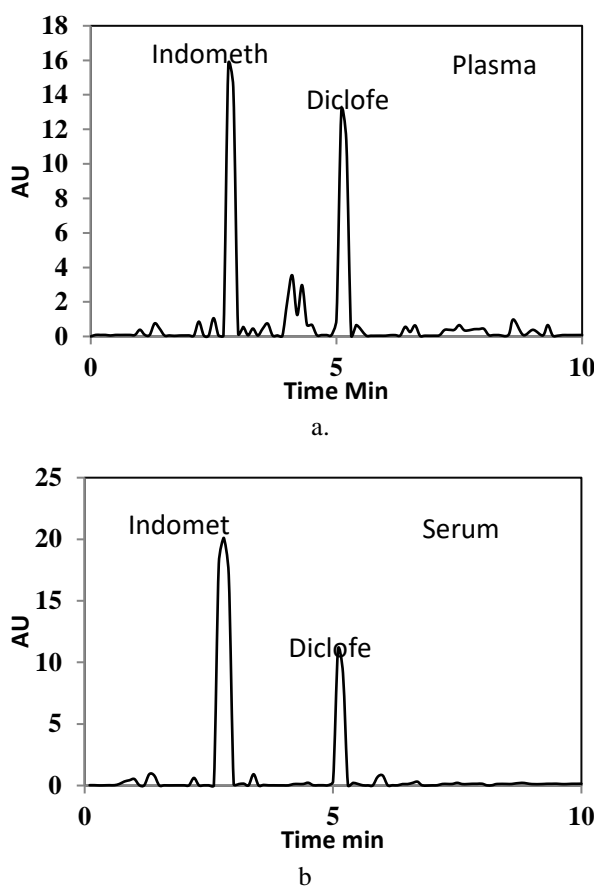
Table 4. Statistical parameters and figures of merit for determination of analytes in samples by applying UADLLME method.

Drugs	LOD (ng mL^{-1})	Dynamic range (ng mL^{-1})	EF*	LOQ (ng mL^{-1})	RSD (%)
Indomethacin	2.18	5-500	210	6.09	1.11
Diclofenac	1.09	5-1000	2800	3.55	2.07

*Average Enrichment factor

Table 6. comparison of this study and the reported different methods for the determination of diclofenac and Indomethacin

Method	Appratus	Analyte	LOD ngmL ⁻¹	RSD %	EF	Ref
HF-LPME	HPLC-DAD	Diclofenac	52.9	1.3	1060	12
DLLME-SFO	HPLC	Diclofenac	5.2	-	-	14
USAEME	HPLC-DAD	Diclofenac, Indomethacin	1.09, 2.18	1.11, 2.007	210,-2800	

**Fig. 6.** Chromatograms two-dimensional chromatograms of the extracted indomethacin (50 ppb) and diclofenac (10 ppb) in serum samples and indomethacin (200 ppb) and diclofenac (100 ppb) in plasma samples after spiking.*Application of the proposed method to real samples*

To evaluate performance of the proposed method, determination of diclofenac potassium and indomethacin in human serum and plasma samples was carried out under the optimized conditions. The results are collected in Table 7. Mean recoveries in human samples were in the ranges of 92–99%. The recoveries demonstrated that the matrixes have negligible effect on the quantification of these compounds and the method is accurate within the desired range. The obtained results revealed ability of the proposed method for the determination of diclofenac potassium and indomethacin in human serum and plasma samples.

Table 7. Added and Found indomethacin and diclofenac concentrations (ng mL⁻¹) in serum samples (R1-R3) and plasma sample (R4-R6).

Samples		Indomethacin	Diclofenac
R1*	Added	0	0
	Found	45.1	68.9
R2*	Recovery%		
	Added	50.0	10.0
R3*	Found	96.5	73.2
	Recovery%	98.54	92.77
R4**	Added	100.0	50.0
	Found	144	112.8
R5**	Recovery%	99.3	94.94
	Added	0	0
R6**	Found	9.0	12.5
	Recovery%		
R5**	Added	200.0	100.0
	Found	206.7	110.1
R6**	Recovery%	98.56	97.86
	Added	200	5
R6**	Found	206.7	18.2
	Recovery%	98.56	96.70

*Serum ** plasma(n=3)

CONCLUSIONS

A new method has been proposed for the simultaneous determination of diclofenac potassium and indomethacin in human serum and plasma samples using HPLC-UV after optimization by UADLLME. The proposed method has advantages such as; simplicity of operation, low consumption of organic solvents, good reproducibility and gives a precise, highly sensitive and selective procedure with good LODs.

Acknowledgements: The authors would like to acknowledge the support of Islamic Azad University, Ark Branch.

REFERENCES

- 1.R. Liu, J.L. Zhou, A. Wilding, *Journal of Chromatography A*, **1022**(1), 179 (2004).
- 2.C.K.S. Ong, P. Lirk, C.H. Tan, R.A. Seymour, *Clinical medicine & research*, **5**(1), 19 (2007).
- 3.U. Kotowska, J. Kapelewska, J. Sturgulewska, *Environmental Science and Pollution Research*, **21**(1), 660 (2014).

4. E. Dinç, C. Yücesoy, F. Onur, *Journal of pharmaceutical and biomedical analysis*, **28**(6), 1091 (2002).
5. M.M. Sena, Z.F. Chaudhry, C.H. Collins, R. J. Poppi, *Journal of pharmaceutical and biomedical analysis*, **36**(4), 743 (2004).
6. G. Escandar, A. Bystol, A. Campiglia, *Analytica Chimica Acta*, **466**(2), 275 (2002).
7. L. Moberg, G. Robertsson, B. Karlberg, *Talanta*, **54**(1), 161 (2001).
8. C. Simó, A. Gallardo, J. San Román, C. Barbas, A. Cifuentes, *Journal of Chromatography B*, **767**(1), 35 (2002).
9. Z. Shihabi, M. Hinsdale, *Journal of Chromatography B*, **683**(1), 115 (1996).
10. F.K. Główka, M. Karaźniewicz, *Analytica chimica acta*, **540**(1), 95 (2005).
11. T.K. Save, D. Parmar, P.V. Devarajan, *Journal of chromatography B*, **690**(1), 315 (1997).
12. M.R. Payán, M.Á.B. López, R. Fernández-Torres, J. L. Pérez Bernal, M. C. Mochón., *Analytica chimica acta*, **653**(2), 184 (2009).
13. A. Bakkali, E. Corta, L.A. Berrueta, B. Gallo, F. Vicente, *Journal of Chromatography B*, **729**(1-2), 139 (1999).
14. D.S.M. Shukri, M.M. Sanagi, W.A.W. Ibrahim, N.N.Z. Abidin, H.Y. Aboul-Enein, *Chromatographia*, **78**(15-16), 987 (2015).
15. D. Borrey, E. Meyer, W. Lambert, S. Van Calenbergh, C. Van Peteghem, A.P. De Leenheer, *Journal of Chromatography A*, **910**(1), 105, (2001).
16. A. Azzouz, E. Ballesteros, *Journal of Chromatography B*, **891**(1), 9 (2012).
17. A. Sarafraz-Yazdi, A. Amiri, G. Rounaghi, Eshtiagh-Hosseini, *Journal of Chromatography B*, **908**(1), 67 (2012).
18. D.S.M. Shukri, M.M. Sanagi, W.A.W. Ibrahim, N.N.Z. Abidin, H.Y. Aboul-Enein, *Chromatographia*, **78**(15-16), 987 (2015).
19. U. Alshana, N.G. Ertaş, N. Göger, *Food chemistry*, **138**(2), 890 (2013).
20. M.R. Payán, M.Á.B. López, R. Fernández-Torres, M.V. Navarro, M.C. Mochón, *Talanta*, **79**(3), 911 (2009).
21. P.L. Kole, J. Millership, J.C. McElnay, *Journal of pharmaceutical and biomedical analysis*, **54**(4), 701 (2011).
22. M.D. Luque de Castro, F. Priego-Capote, *Talanta*, **72**, 321 (2007).
23. H. Chen, J. Ying, H. Chen, J. Huang, L. Liao, *Chromatographia*, **68**, 629 (2008).
24. M. Ghaedi, H. Mazaheri, S. Khodadoust, S. Hajati, M.K. Purkait, *Spectrochimica Acta Part A*, **135**, 479 (2015).
25. N. Chamkouri, A. Niazi, V. Zare-Shahabadi, *Spectrochimica Acta Part A*, **156**, 105 (2016).

ЕДНОВРЕМЕННО ОПРЕДЕЛЯНЕ НА ДИКЛОФЕНАК-КАЛИЙ И ИНДОМЕТАЦИН С ПРОБИ ОТ СЕРУМ И ПЛАЗМА С ПОМОЩТА НА ЕДНОВРЕМЕННИ УЛТРАЗВУКОВА ДИСПЕРСИОННА ТЕЧНО-ТЕЧНА МИКРО-ЕКСТРАКЦИЯ И HPLC-UV. ПЛАНИРАН ЕКСПЕРИМЕНТ И ОПТИМИЗАЦИЯ

Н. Чамкури¹, В. Заре-Шахабади^{2*}, А. Ниязи¹

¹Департамент по инженерна химия, Научно-изследователски клон в Техеран, Исламски университет „Азад“, Техеран, Иран

¹Департамент по химия, Научен факултет, Исламски университет „Азад“, Клон Арак, Иран

²Департамент по химия, Колеж по инженерна химия, Клон Махшахр, Исламски университет „Азад“, Махшахр, Иран

Постъпила на 30 май, 2016 г.; приета на 5 юни, 2017 г.

(Резюме)

В тази работа се предлага бърз, прост и екологично съобразен метод за едновременното определяне на диклофенак-калий и индометацин в serum и плазма. Методът се основава на ултразвукова дисперсионна течно-течна микроякстракция. Определянето става с високо-ефективна течна хроматография с UV-датчик. Експерименталните условия (рН на разтворите, вида екстрагент, времетрането на ултразвуковото третиране, условията на центрофугиране и йонната сила) са изследвани и оптимириани. След отсяването на незначителните, останалите фактори са оптимизирани чрез централен композиционен план. Границите на откриване на диклофенак-калий и индометацин при оптималните условия са съответно 1.09 и 2.18 ng mL^{-1} . Относителното стандартно отклонение (RSD) при анализите беше под 3% ($n = 5$). Средните добиви в човешка плазма и serum бяха в интервала 92–99%.

AUTHOR INDEX

- Abdel-Hady F., Mazher A. K., Alzahrani A., Hamed M., An inverse approach in designing a humidifier for humidification-dehumidification desalination process.....469
- Abedi M. R., See Kazemi et al.449
- Akdoğan A., Çalışkan Koç G., Dirim S. N., Mathematical modeling of thin-layer microwave drying of corn husk and investigation of powder properties.....986
- Aladağ E., See Bayram et al.896
- Alam S., See Rehman et al.816
- Al-Degs Y., See Gergov et al.410
- Al-Fahami K.H., See Ewais et al.569
- Ali Ahmed. D., See Sadoudi et al.68
- Ali N., See Khan et al.320
- Aliev K., See Ebadi et al.540
- Alin A., See Gergov et al.410
- Alizadeh K., Soltani-Afarani H., A comparative study on the ionization constants of a Schiff's base in different environments by multiwavelength UV-Vis spectroscopy.....890
- Alzahrani A., See Abdel-Hady et al.469
- Amin M. M., Khanahmad H., Teimouri F., Sadani M., Karami M. A., Rahimmanesh I., Improvement of biodegradability of explosives using anaerobic-intrinsic bioaugmentation approach735
- Amrollahi M. A., See Bagherpoor et al.483
- Amrollahi M. A., See Emtiazi et al.478
- An Shi J., See Qing et al.171
- Andelković D., See Kostić et al.360
- Andelković T., See Kostić et al.360
- Andries C., Manea M., Pocanschi C. L., Pui A., Drochioiu G., Gradinaru V. R., Coordination behavior of Coenzyme A towards gold ions: Spectroscopic, mass spectrometric and microbiological studies621
- Angelova S. E., See Nikolova-Mladenova et al.800
- Angelova V. T., Valcheva V., Vassilev N., Buyukliev R., Mihaylova R., Momekov G., Synthesis, *in vitro* antiproliferative and antimycobacterial activity of thiazolidine-2,4-dione and hydantoin derivative..643
- Antonov A. S., See Damov et al.589
- Anuse M. A., See Gaikwad et al.914
- Arjmand F., Shafiei F., Modeling of the physicochemical properties of aliphatic alcohols using topological indices and quantitative structure-property relationship852
- Arnaudov L., See Rangelov et al.422
- Arslan Y., Trak D., Kendüzler E., Preconcentration and determination of cadmium in some samples using solid phase extraction with slotted quartz tube flame atomic absorption spectrometry884
- Arvind Narayan S., See Shobana et al.347
- Ashraf S., See Rehman et al.823
- Atabey-Ozdemir B., Demirkiran O., Yildiz U., Tekin I. O., Coban B., Cytotoxicity and DNA binding of copper (II) and zinc (II) complexes of flavonoids: quercitrin, myricitrin, rutin.....901
- Aydin M., See Şimşek et al.82
- Babahan I., See Coban et al.908
- Bagherpoor S., Amrollahi M. A., An efficient ultrasound-promoted method for the synthesis of xanthene derivatives483
- Baharestan F., See Sadeghi et al.330
- Bai H. L., Wang J., Liu C. M., Chromatography of separation and qualitative, quantitative analysis biflavonoids from crude extract of *Selaginella tamariscina*658
- Baiseitov D. A., Tulepov M. I., Sasykova L. R., Gabdrashova Sh. E., Essen G. A., Kudaibergenov K. K., Mansurov Z. A., Sorption capacity of the oil sorbents for removing of thin films of oil.....335
- Baiseitov D. A., Tulepov M. I., Sasykova L. R., Gabdrashova Sh. E., Magazova A. N., Dalelkhanuly O., Kudyarova Zh. B., Mansurov Z. A., Catalytic hydrogenation of coal of the kazakhstan fields in presence of polymers600
- Baltacı C., See Kaya et al.923
- Banaszczak E. W., See Szymański et al.339
- Bandi R. K., Waghmare A., Hindupur R. M., Pati H. N., A simple, efficient and scalable synthesis of substituted bis-arylchloromethanes.....79
- Bayram T. T., Nuhoglu A., Aladağ E., Investigation of biodegradation and growth kinetics of dairy wastewater in a batch reactor.....896
- Begum I., See Rehman et al.493
- Bin H., See Zhenzhi et al.210, 217
- Bing Chen Q., See Qing et al.171
- Bojić A., See Kostić et al.360
- Bojinova A. S., See Nalimova et al.121
- Bošković I. D., Đukić D. A., Mašković P. Z., Mandić L. G., Phytochemical composition and biological activity of *Echium italicum* L. plant extracts836
- Boyadjiev B., Boyadjiev Chr., New models of industrial column absorbers. 1.Co-current absorption processes711
- Boyadjiev B., Boyadjiev Chr., New models of industrial Column Absorbers. 2.Counter-current absorption process720
- Boyadjiev B., Boyadjiev Chr., New models of industrial column chemical reactors706
- Boyadjiev Chr., See Boyadjiev et al.706, 711, 720
- Brodnjak U. Vr., Improvement of physical and optical properties of chitosan-rice starch films pre-treated with ultrasound859
- Buyukliev R., See Angelova et al.643
- Çalışkan Koç G., See Akdoğan et al.986
- Cao R.-w., See Feng et al.685
- Chai Y. R., See Li et al.697
- Chamkouri N., Zare-Shahabadi V., Niazi A., Ultrasound-assisted dispersive liquid-liquid microextraction with HPLC-UV for the simultaneous determination of Diclofenac potassium and Indomethacin in serum and plasma samples: Experimental design and optimization994

Chaulia S. N., Synthesis, spectroscopic characterisation and biological activity studies of Co(II), Ni(II), Cu(II) and Zn(II) metal complexes with azo dye ligand derived from 4,4'-diaminodiphenylether and 5-sulpho salicylic acid.....	46
Chehardoli G., See Sajjadifar et al.....	87
Chen B., See Yun et al.....	288
Chen F., See Xin et al	145
Chen H. N., See Jia et al.	190
Chen H., See He et al.....	193
Chen H., See Sun et al.	234
Chen H.-L., See Song et al.....	245
Chen J., Wen J., The degradation and corrosion characteristics of blended amine solution in the coal bed methane decarburation process.....	669
Chilev C., See Simeonov et al.	399
Chorukova E. Y., See Simeonov et al.....	430
Christoskova St. G., See Slavova et al.	761
Coban B., Eser N., Babahan I., DNA binding by copper (II) complexes of semithiocarbazole containing ligands.....	908
Coban B., See Atabey-Ozdemir et al.....	901
Cong X., See Li et al.....	250
Cvetković T., See Kostić et al.....	360
Dai S. J., See Sun et al.	678
Dai Z-D., See Song et al.	245
Dalelkhanuly O., See Baiseitov et al.	600
Damov K. S., Jordanov I. P., Antonov A. S., Iliev M. T., Characterization of aerodispersed systems with increased concentration according to the kinematic viscosity and mass density of their aerosol phase	589
Darbandi H., See Kiyani et al.	562
Das M., See Mahatha et al.	977
Daşdan D. Ş., See Fidan et al.....	742
Davaajav Ya., See Purevsuren et al.	34
De Luca M., See Gergov et al.....	410
Dehghan H. R., Negarestani A., Rezaie M. R., Study of the possibility of using IXRF technique to detect the elements present in dust using Monte Carlo N Particles.....	874
Demirkiran O., See Atabey-Ozdemir et al.....	901
Denchev D. D., See Simeonov et al.....	430
Dharmaraja J., See Shobana et al.....	347
Dhaveethu Raja J., See Vadivel et al.	26
Dimitrijević J., See Radovanović et al.	879
Dimitrov D. I., See Petrova et al.	115
Dimitrov D. Tz., See Nalimova et al.	121
Dimitrov M., See Tsvetkova et al.	384
Dimitrov O. S., See Koseva et al.	366
Dirim S. N., See Akdoğan et al.....	986
Dishovsky N. T., See Malinova et al.	436
Dobrucka R., The biological synthesis of anatase titanium dioxide nanoparticles using <i>Arnicae anthodium</i> extract.....	595
Dobruzhaliiev D. G., See Nikolova et al.....	807
Đorđević D., See Matović-Purić et al.	390
Dospasliev L., Ivanova M., Spectrophotometric investigations on liquid-liquid extraction systems containing cobalt and tetrazolium salts. Application of the developed method for analysis of the cobalt content of biological samples (mushrooms and tobaccos).....	787
Doychinova M., See Gergov et al.	410
Doymaz İ., See Ismail et al.	92
Draganova K. I., See Mantcheva et al.	371
Drochioiu G., See Andries et al.	621
Du T., See Zeng et al.	176
Đukić D. A., See Bošković et al.	836
Dzimbova T. A., See Sapundzhi et al.	768
Ebadi A. G., Hisoriev H., Aliev K., Measurement of some chemical and Biochemical parameters in <i>Cladophora glomerata</i> L. from Farahabad Region of Iran.....	540
Ebadi A. G., Hisoriev H., Bio-oil production from fast pyrolysis of <i>Cladophora glomerata</i> in a fluidized bed reactor	504
Ebrahimi M., See Kazemi et al.	449
E-Habib F., See Riaz et al.	354
Ejaz R., See Rehman et al.	20
Eliyas A. E., See Zaharieva et al.	652
Emre F. B., Okuşluk F., Tekin S., Sandal S., Investigation on the effect of nano-TiO ₂ synthesized by the hydrothermal method on LNCaP cancer cells	664
Emtiazı H., Amrollahi M. A., Mg(ClO ₄) ₂ -catalyzed one-pot synthesis of 2-amino-4H-chromenes and dihydropyrano[c]chromenes	478
Engstler J., See Ismail et al.	62
Erkmen J., Effect of residual gases in the electrodialysis cell on mass transfer	611
Eser N., See Coban et al.	908
Essen G. A., See Baiseitov et al.	335
Ewais H. A., Ismail I. M., Al-Fahami K.H., Kinetic studies on the formation of silver nanoparticles by reduction of silver(I) with glucose in aqueous and micellar media	569
Farman M., See Riaz et al.	354
Fei Z. H., See Ke et al.	635
Feng Y.-l., Yu L.-j., Cao R.-w., Adsorption of Copper ions by Montmorillonite/Sodium Humate/N-Isopropyl Acrylamide composite.....	685
Feodorova Y. N., See Mantcheva et al.	371
Fidan İ., Daşdan D. Ş., Karaman F., Kaban Ş., Surface characterization of thiazolidinone derivatives by inverse gas chromatography	742
Firdos A., Tariq A. R., Imran M., Niamat I., Kanwal F., Mitu L., Antioxidant potential of black pepper extract for the stabilization of sunflower oil.....	31
Frankowska M., See Szymański et al.	339
Gabdashova Sh. E., See Baiseitov et al.	335, 600
Gaikwad A. P., Suryavanshi V. J., Anuse M. A., Liquid-liquid extraction studies of ruthenium(III) from malonate medium using n-octylaniline as an ion-pairing reagent: study of catalyst and alloys.....	914
Gandova V., See Petrova et al.	115
Gao H., See Huang et al.	17
Gao Y., See Wang et al.	228
Gece G., Theoretical basis for the corrosion inhibition feature of Argan oil.....	846
Genadiev V., See Purevsuren et al.	34

Georgiev D., See Vlaev et al.....	775
Georgieva A. Ts., See Nalimova et al.....	121
Gergov G., Alin A., Doychinova M., De Luca M., Simeonov V., Al-Degs Y., Assessment of different PLS algorithms for quantification of three spectrally overlapping drugs.....	410
Gil'mundinov Sh. A., See Sassykova et al.....	583
Glavchev I. K., See Purevsuren et al.....	34
Glavcheva-Laleva Z. I., See Purevsuren et al.....	34
Gradinaru V. R., See Andries et al.....	621
Grigorova E., Khristov M., Stoycheva I., Tsyntsarski B., Nihtanova D., Markov P., Effect of activated carbons derived from apricot stones or polyolefin wax on hydrogen sorption properties of MgH ₂	109
Guan Y., See Lu et al.....	161
Gündüz M. G., See Şimşek et al.....	82
Guo J. J., See Xu et al.....	264
Guo J. J., See Yang et al.....	269
Guo J. J., Zhang R. B., Yang N., Design and evaluation of the microfluidic magnetic isolating method for aquaculture pathogens detection	276
Hadjieva B., See Tsvetkova et al.....	377
Hamed M., See Abdel-Hady et al.....	469
Han J., See Huang et al.....	17
Han W.-Y., See Lu et al.....	161
Hao X.-P., See Zhang et al.....	134
Hasan A. A., Magnetohydrodynamic stability of self-gravitating compressible resistive rotating streaming fluid medium.....	487
Hassanabadi A., See Sadeghi et al.....	330
Hassani A. H., See Rahbari et al.....	455
Hayat T., See Khan et al.....	320
He J., See Huo et al.....	955
He M., Zhu W., Liu F., Chen H., Droplet characteristic adjustment method based on LEM for 3D electronic printing.....	193
Hindupur R. M., See Bandi et al.....	79
Hisoriev H., See Ebadi et al.....	504, 540
Hristov D. S., Velikov S. K., Vodenicharov V. E., Tsanova-Savov S. P., Ribarova F. T., Evaluation of chemical composition, energy and biological value of typical Bulgarian traditional foods.....	782
Hu L.-Sh, Sun B.-F., Experimental studies on a horn-shaped booster pellet.....	829
Hu Y. B., See Jia et al.....	190
Hu Y., See Zeng et al.....	176
Huang D., See Huang et al.....	17
Huang G. L. , Gao H., Yi C., Huang D., Han J., Study on the synthesis of 2,3,4,6-O-tetraacetyl- α -D-glucopyranosyl bromide.....	17
Huang J., See Zeng et al.....	176
Huang Z., See Zeng et al.....	176
Hubenov V. N., See Simeonov et al.....	430
Huo Q., Zhou T., He J., Xue J. Q., Identification of Clenbuterol by MALDI-TOF Mass Spectrometry	955
Idakieva K., See Mileva et al.....	11
Ignatova K., Marcheva Y., Composition and structure of Ni-Co coating depending on the ratio of Ni and Co in a citrate electrolyte	313
Iliev M. T., See Damov et al.....	589
İlter Ş. M., See Kaya et al.....	923
Imran M., See Firdos et al.....	31
Imran M., See Rehman et al.....	493
Iqbal M., See Riaz et al.....	354
Ismail I. M., See Ewais et al.....	569
Ismail N., Joshi R., Engstler J., Schneider J. J., Improved hydrogen storage capacity of CNTs synthesized in presence of iron catalyst using arc discharge method in air atmosphere	62
Ismail O., Kipcak A. S., Doymaz İ., Piskin S., Thin-layer drying kinetics of nectarine slices using IR, MW and hybrid methods	92
Itoua Bl.V., Ogunniyi D. S., Ongoka P., Petrov L., Effect of fumaric acid on the properties of alkyd resin and palm oil blend.....	127
Ivanov B. B., See Nikolova et al.....	807
Ivanova M., See Dospatliev et al.....	787
Ivanova S., See Tsvetkova et al.....	377, 384
Janani H., See Rezvani et al.....	74
Jawaherneshan N., See Sajjadifar et al.....	87
Javid A. H., See Rahbari et al.....	455
Jia J., See Xu et al.....	264
Jia Y. J., Su W. X., Hu Y. B., Chen H. N., Pt doped TiO ₂ (Pt-TiO ₂) sol gel thin films.....	190
Jia Z. N., Yang Y. Y., Qi X. W., Song X. M., Influence of nano-serpentine mineral powder as a lubricating additive on the high-temperature tribological properties of metal friction pairs.....	948
Jiang R., Yu H., Wang L., Limitations of measurements of supercritical CO ₂ sorption isotherms on coals with manometric equipment—A theoretical description	509
Jiao Tu Y., Wu H., Determination of metal ions by ultrasound-assisted hollow fiber liquid-phase microextraction technique	151
Jing D., See Yuan et al.....	282
Jordanov I. P., See Damov et al.....	589
Joshi R., See Ismail et al.....	62
Jovičić D., See Matović-Purić et al.....	390
Joz-Yarmohammadi F., See Kazemi et al.....	449
Jugović Z., See Matović-Purić et al.....	390
Kabaivanova L. V., See Simeonov et al.....	430
Kaban Ş., See Fidan et al.....	742
Kadinov G. B., See Zaharieva et al.....	652
Kafi A., See Sadeghi et al.....	330
Kałwa K., See Kowalski et al.....	928
Kaneva N. V., See Nalimova et al.....	121
Kanwal A., See Rehman et al.....	493
Kanwal F., See Firdos et al.....	31
Kanwal F., See Rehman et al.....	493
Kara İ., Yalçinkaya Ö., Evaluation of persistence of gunshot residue (GSR) using graphite furnace atomic absorption spectrometry (GFAAS) method	101
Karahan M., See Vural et al.....	557
Karakirova Y. G., Nakagawa K., Yordanov N. D., Investigation of sugar irradiated with He, Ne and C ions for dosimetric purposes	629
Karaman F., See Fidan et al.....	742

Karami M. A., See Amin et al.	735
Karvar S., Rezagholipour Dizaji H., Unidirectional growth of $\text{CoNi}(\text{SO}_4)_2 \cdot 12\text{H}_2\text{O}$ single crystal by Sankaranarayanan–Ramasamy (SR) method	608
Kaya A. A., Üçüncü O., İlter Ş. M., Baltacı C., Öztürk S., Chemical composition and bioactive properties of the essential oil of <i>Rhinanthus angustifolius</i> subsp. <i>Grandiflorus</i>	923
Kazemi F., Zamani H. A., Joz-Yarmohammadi F., Ebrahimi M., Abedi M. R., Application of 1, 4-diaminoanthraquinone as a new selectophore material for construction of potentiometric iron (III)-selective electrode	449
Ke C. Z., Wang N., Li W. X., Shi W. Z., Fei Z. H., Adsorption properties of 4-Phenylphenol in aqueous solution with adsorption resins chemically modified.	635
Ke C.-Y., See Zhang et al.	134
Kecili A., See Sadoudi et al.	68
Kendüzler E., See Arslan et al.	884
Khan A., See Riaz et al.	354
Khan S. U., Ali N., Hayat T., Analytical and numerical study of the diffusion of chemically reactive species in an Eyring-Powell fluid over an oscillatory stretching surface	320
Khanahmad H., See Amin et al.	735
Khristov M., See Grigorova et al.	109
Kindekov I., See Mileva et al.	11
Kipcak A. S., See Ismail et al.	92
Kiradzhiyska D. D., See Mantcheva et al.	371
Kiyani H., Darbandi H., One-pot three-component synthesis of 1-amidoalkyl-2-naphthols in the presence of phthalimide- <i>N</i> -sulfonic acid.....	562
Kökpınar Ö., See Şimşek et al.	82
Kononova I. E., See Nalimova et al.	121
Koseva I. I., Tzvetkov P. T., Yordanova A. S., Marychev M. O., Dimitrov O. S., Nikolov V. S., Preparation of chromium doped LiAlSiO_4 glass-ceramics	366
Kostić I., Andelković T., Andelković D., Bojić A., Cvetković T., Pavlović D., Quantification of DEHP into PVC components of intravenous infusion containers and peritoneal dialysis set before and after UV-A treatment	360
Kostova B. D., See Slavkova et al.	792
Kowalska G., See Kowalski et al.	928
Kowalski R., Kowalska G., Pankiewicz U., Sujka M., Kalwa K., GC analysis in evaluation of changes in fatty acids content of selected fats during storage and heating	928
Krastev D., See Mileva et al.	11
Krasteva L. K., See Nalimova et al.	121
Krinickaitė A., See Paliulis et al.	868
Kroumova E. Tz., See Simeonov et al.	430
Kudaibergenov K. K., See Baiseitov et al.	335
Kudyarova Zh. B., See Baiseitov et al.	600
Kumar S., See Sharma et al.	309
Lai W. L., See Liu et al.	199
Li B., See Xiong et al.	499
Li D., See Zeng et al.	176
Li J. M., See Yu et al.	943
Li L. J., See Yu et al.	943
Li L., See Xiong et al.	499
Li M., Cong X., Chemical changes and the mechanisms in the sintering process of sea silt	250
Li T., Xu W. H., Chai Y. R., Wang Z. Y., Xie D. T., Differences of Cd uptake and expression of Cd-tolerance related genes in two varieties of ryegrasses	697
Li W. X., See Ke et al.	635
Li W., See Yun et al.	288
Li W., See Zeng et al.	176
Li Z., See Yang et al.	269
Liang H., See Shang et al.	936
Liang X., See Sun et al.	234
Libo N., See Zhenzhi et al.	210
Lihareva N., Petrov O., Tzvetanova Y., Modelling of Cs^+ uptake by natural clinoptilolite from water media	577
Liu J.-L., See Zhang et al.	134
Liu C. M., See Bai et al.	658
Liu F., See He et al.	193
Liu J., Zeng X., Zhou D., Zhao Y., Pan X., Environmental safety assessment on chlorination by-products in brine discharged from desalination plant	157
Liu L., See Liu et al.	199
Liu W. G., See Sun et al.	678
Liu Y. G., Zhang Y., Yan J., Xu Y. J., Rheological properties of RHMOD-INVERT™—A Study on a novel oilbased drilling fluid with high thixotropy	527
Liu Y., Liu L., Shi G., Shi J., Lai W. L., Research on the synthesis and characterization of abiraterone acetate	199
Lu Y.-J., Wu X.-M., Guan Y., Zhang S.-L., Wang J.-L., Zhao J.-X., Han W.-Y., Shen Z.-Q., Optimization of cell culture for H9N2 subtype AIV and establishment of high-yield cell strain	161
Lujie C., See Zhenzhi et al.	210
Ma D., See Song et al.	534
Ma X., See Zhong et al.	520
Magazova A. N., See Baiseitov et al.	600
Mahatha B. K., Nandkeolyar R., Das M., Sibanda P., Stagnation point nanofluid flow along a stretching sheet with non-uniform heat generation/absorption and Newtonian heating	977
Mahmud T., See Rehman et al.	20
Malinova A., Dishovsky N. T., Tzanev A. Tz., Study on the influence of devulcanization conditions on the reclaim-based vulcanizates operation characteristics	436
Mandić L. G., See Bošković et al.	836
Manea M., See Andries et al.	621
Manojlović N., See Radovanović et al.	879
Mansurov Z. A., See Baiseitov et al.	335, 600
Mantcheva R. D., Kiradzhiyska D. D., Feodorova Y. N., Draganova K. I., Biocompatibility of aluminium alloys and anodic Al_2O_3	371
Mao H. P., See Yang et al.	269
Marcheva Y., See Ignatova et al.	313

Markov P., See Grigorova et al.....	109
Marychev M. O., See Koseva et al.	366
Mašković P. Z., See Bošković et al.	836
Mašković P., See Matović-Purić et al.	390
Matović-Purić I., Pecarski D., Jugović Z., Jovičić D., Đorđević D., Mašković P., Comparative study of some biochemical parameters of the fungi <i>Mucor plumbeus</i> , <i>Aspergillus niger</i> and <i>Trichoderma harzianum</i>	390
Mazher A. K., See Abdel-Hady et al.	469
Mehrgan M. R., See Rahbari et al.....	455
Merouani H., Ounissi A., Ouddai N., DFT study of nitrogenated heterocycles of six and seven links .	690
Mihailova S. N., See Simeonov et al.	430
Mihalev K., See Petrova et al.	115
Mihaylova R., See Angelova et al.	643
Milanov P. B., See Sapundzhi et al.....	768
Milenova K. I., See Zaharieva et al.	652
Mileva M. , Raynova Y., Kindekov I., Krastev D., Idakieva K., In vitro investigation of the antioxidant properties of Cancer pagurus hemocyanin	11
Ming G. Z., See Zhenzhi et al.....	217
Mitu L., See Firdos et al.	31
Mitu L., See Rehman et al.	20, 493, 816
Mitu L., See Shobana et al.	347
Mitu L., See Vadivel et al.	26
Momekov G. Tz., See Slavkova et al.....	792
Momekov G., See Angelova et al.	643
Momekova D. B., See Slavkova et al.	792
Moshnikov V. A., See Nalimova et al.	121
Mustafaeva Z., See Vural et al.....	557
Nakagawa K., See Karakirova et al.	629
Nalibayeva A., See Sassykova et al.	583
Nalimova S. S., Kononova I. E., Moshnikov V. A., Dimitrov D. Tz., Kaneva N. V., Krasteva L. K., Syuleyman S. A., Bojinova A. S., Papazova K. I., Georgieva A. Ts., Investigation of the vapor-sensitive properties of zinc oxide layers by impedance spectroscopy.....	121
Namkhainorov J., See Purevsuren et al.	34
Nandkeolyar R., See Mahatha et al.....	977
Narayan S. A., See Vadivel et al.....	26
Negarestani A., See Dehghan et al.....	874
Nenkova S. K., See Radoykova et al.	40
Nenkova S., See Raicheva et al.	139
Niamat I., See Firdos et al.....	31
Niazi A., See Chamkouri et al.	994
Nihtanova D., See Grigorova et al.	109
Nikolić V., See Radovanović et al.	879
Nikolov R., See Raicheva et al.	139
Nikolov V. S., See Koseva et al.	366
Nikolova D. S., Ivanov B. B., Dobružhaliev D. G., Optimal energy management in brewing	807
Nikolova-Mladenova B. I., Angelova S. E., Synthesis of 5-nitrosalicylaldehyde based hydrazones and DFT-calculations of their structure and reactivity	800
Norouzi B., Tajjedin S., Application of modified carbon paste electrode with multiwall carbon nanotube as a simple and an effective catalyst for determination of cefixime in real samples.....	729
Nuhoglu A., See Bayram et al.	896
Obreshkova D., See Tsvetkova et al.....	377, 384
Ogunniyi D. S., See Itoua et al.	127
Okuşluk F., See Emre et al.	664
Ongoka P., See Itoua et al.	127
Ouddai N., See Merouani et al.	690
Ounissi A., See Merouani et al.	690
Öztürk S., See Kaya et al.....	923
Paliulis D., Krinickaitė A., Removal of lead (Pb_2^+) from synthetic wastewater using calcium pectate	868
Pan Q., See Zhang et al.	134
Pan X., See Liu et al.	157
Pankiewicz U., See Kowalski et al.	928
Papazova K. I., See Nalimova et al.	121
Pati H. N., See Bandi et al.	79
Pavlović D., See Kostić et al.	360
Pecarski D., See Matović-Purić et al.	390
Pelit Arayici P., See Vural et al.	557
Pencheva N. S., See Sapundzhi et al.	768
Peng Shao X., See Qing et al.	171
Peng X., See Xiong et al.	499
Petrov L., See Itoua et al.	127
Petrov O., See Lihareva et al.	577
Petrov P. D., See Slavkova et al.	792
Petrova I., Shikov V., Gandova V., Mihalev K., Dimitrov D. I., Spectrophotometric and thermodynamic study on the co-pigmentation interaction between strawberry anthocyanins and quercetin in model systems.....	115
Ping L. L., Tao Y. J., Friction stir welding automatic effect on building the microstructure and properties of highnickel steel.....	239
Piskin S., See Ismail et al.	92
Pocanschi C. L., See Andries et al.	621
Pui A., See Andries et al.	621
Purevsuren B., Davaajav Ya., Namkhainorov J., Glavcheva-Laleva Z. I., Genadiev V., Glavchev I. K., Pyrolysis of animal bone, characterization of the obtained char and tar and application of bone tar for crosslinking of epoxy resin	34
Qi X. W., See Jia et al.	948
Qian J., See Zeng et al.	176
Qian X., See Shang et al.	936
Qing Wei L., Yan Jiang X., An Shi J., Zhou Zhao W., Peng Shao X., Bing Chen Q., Sun Y., Study on dust-catching and inhibiting microorganism ability of <i>Jacaranda mimosifolia</i> under the same condition of compare experiment	171
Radeva G., See Raicheva et al.	139
Radovanović A., See Radovanović et al.	879
Radovanović B., Radovanović A., Nikolić V., Manojlović N., Dimitrijević J., Storage effect on phenolic content and antioxidant activity in selected fruit extracts.....	879
Radojkova T. Hr., Nenkova S. K., Valchev I. V., Monomeric phenolic compounds from hydrolyzed waste lignocellulosic materials	40
Rahbari K., Hassani A. H., Mehrgan M. R., Javid A. H., Evaluating the performance of decision-making units using hybrid neural network model for	

predicting the performance and data envelopment analysis approach Case study: Khuzestan steel company treatment plant	455
Rahimmanesh I., See Amin et al.....	735
Raicheva L., Radeva G., Nenkova S., Nikolov R., Adsorption characteristics of activated carbon obtained from residual hydrolyzed lignin	139
Rangelov A., Arnaudov L., Stoyanov S., Spassov T., Gelatinization of industrial starches studied by DSC and TG	422
Rasheed S., See Rehman et al.....	493
Rasool N., See Riaz et al.	354
Rather S. U., Corrosion study of ferrites prepared by hydrothermal method	444
Rauf A., See Rehman et al.....	20
Raynova Y., See Mileva et al.	11
Rehman R., Alam S., Mitu L., Diamond green dye adsorptive removal from water by carrot pulpy waste and potato peels.....	816
Rehman R., Ashraf S., Analysis of caffeine contents in commercial beverages and tea samples of Pakistan using UV/Visible spectrometry.....	823
Rehman R., Mahmud T., Ejaz R., Rauf A., Mitu L., Sorptive removal of Direct Blue-15 dye from water using <i>Camellia sinensis</i> and <i>Carica papaya</i> leaves.	20
Rehman S., Rasheed S., Imran M., Kanwal A., Kanwal F., Begum I., Mitu L., Sunflower and soybean oil stabilized with natural extracts of turnip's peel....	493
Rezagholipour Dizaji H., See Karvar et al.....	608
Rezaie M. R., See Dehghan et al.	874
Rezvani A. R., Janani H., Rostami-Charati F., Skelton B. W., Synthesis of a new five-coordinate ternary copper (II) complex: crystal structure and spectral studies	74
Riaz M., Rasool N., Iqbal M., Tawab A., E-Habib F., Khan A., Farman M., Liquid chromatography-electrospray ionization-tandem mass spectrometry (LC-ESI-MS/MS) analysis of <i>Russelia equisetiformis</i> extract	354
Ribarova F. T., See Hristov et al.....	782
Rostami-Charati F., See Rezvani et al.	74
Sadani M., See Amin et al.	735
Sadeghi B., Baharestan F., Kafi A., Hassanabadi A., Clean, simple and efficient synthesis of spiro-2-amino-4H-pyran-3-carbonitrile via $\text{HBF}_4\text{-SiO}_2$ nanoparticles: a green protocol	330
Sadoudi R., Ali Ahmed. D., Trache M., Kecili A., Studies of the physico-chemical characteristics and fatty acid composition of commercially available Algerian frying edible oils	68
Şafak C., See Şimşek et al.	82
Sajjadifar S., Zolfigol M. A., Javaherneshan N., Chehardoli G., Comparison between acetic acid and propanoic acid as a solvent/catalyst in the indolenines synthesis: an approach without any indole by-product	87
Sandal S., See Emre et al.	664
Sankarganesh M., See Vadivel et al.....	26
Sapundzhi F. I., Dzimbova T. A., Pencheva N. S., Milanov P. B., Modeling of the relationship between biological activity of delta-selective enkephalin analogues and docking results by polynomials.....	768
Saso L., See Tsvetkova et al.....	384
Sassykova L. R., Nalibayeva A., Gil'mundinov Sh. A., Development of technology of synthesis of catalysts for neutralization of emissions of the industry and motor transport	583
Sassykova L. R., See Baiseitov et al.	335, 600
Schneider J. J., See Ismail et al.	62
Shafiei F., See Arjmand et al.	852
Shang W., Qian X., Liang H., Preparation of modified diatomite filler via a starch-fatty acid complex coating method for improvement of paper strength properties	936
Sharma D. K., Kumar S., A facile synthesis of 3-chloro-2-phenyl-4H-chromen-4-ones using grinding technique at room temperature	309
Shen Z.-Q., See Lu et al.	161
Shi G., See Liu et al.	199
Shi J., See Liu et al.	199
Shi W. Z., See Ke et al.	635
Shikov V., See Petrova et al.	115
Shobana S., See Vadivel et al.	26
Shobana S., Subramaniam P., Dharmaraja J., Arvind Narayan S., Mitu L., Stability studies on solution equilibria of $\text{Zn}(\text{II})$ pyrimidine nucleus bases.....	347
Shopska M. G., See Zaharieva et al.	652
Sibanda P., See Mahatha et al.	977
Simeonov E., Yaneva Z., Chilev C., Investigation of the mechanism and kinetics of extraction from plant materials	399
Simeonov I. S., Denchev D. D., Kabaivanova L. V., Kroumova E. Tz., Chorukova E. Y., Hubenov V. N., Mihailova S. N., Different types of pretreatment of lignocellulosic wastes for methane production.....	430
Simeonov V., See Gergov et al.	410
Şimşek R., Gündüz M. G., Şafak C., Kökpınar Ö., Aydin M., Free radicals properties of some gamma-irradiated organic compounds.....	82
Siwek R., See Szymański et al.	339
Skelton B. W., See Rezvani et al.	74
Slavkova M. Iv., Momekova D. B., Kostova B. D., Momekov G. Tz., Petrov P. D., Novel dextran/ β -cyclodextrin and dextran macroporous cryogels for topical delivery of curcumin in the treatment of cutaneous T-cell lymphoma.....	792
Slavova I. A., Christoskova St. G., Stoyanova M. K., Catalytic oxidation of Rhodamine B in aqueous solutions with sulphate radicals over $\text{Co}_3\text{O}_4/\text{MgO}$ and $\text{CoFe}_2\text{O}_4/\text{MgO}$	761
Soltani-Afarani H., See Alizadeh et al.	890
Song G., See Song et al.	245
Song J., Dai Z-D., Song G., Chen H.-L., Study on the nonisothermal crystallization behaviorof polyvinyl alcohol/montmorillonite composite by DSC analysis	245
Song W., Ma D., Wu K., Zhu Y., Wu J., Yu B., Core-flooding experimental study of oil displacement by using sulfate-reducing bacteria	534
Song X. M., See Jia et al.	948

Spassov T., See Rangelov et al.	422
Stoyanov S., See Rangelov et al.	422
Stoyanova M. K., See Slavova et al.	761
Stoycheva I., See Grigorova et al.	109
Su W. X., See Jia et al.	190
Subramaniam P., See Shobana et al.	347
Sujka M., See Kowalski et al.	928
Sun B.-F., See Hu et al.	829
Sun J., See Yang et al.	269
Sun L., Liang X., Wang Q., Chen H., Material composition detection using an image segment with an improved artificial bee colony algorithm	234
Sun W. H., Dai S. J., Liu W. G., Yu L. T., Study on removing impurity from magnesite ore by two step reverse flotation. Study on removing impurity by two step reverse flotation	678
Sun Y., See Qing et al.	171
Sun Y., See Yun et al.	288
Suryavanshi V. J., See Gaikwad et al.	914
Syuleyman S. A., See Nalimova et al.	121
Szymański A., See Szymański et al.	339
Szymański M., Banaszczak E. W., Siwek R., Frankowska M., Szymański A., Caffeine release from selected pharmaceutical preparation....	339
Tajjedin S., See Norouzi et al.	729
Tang Y., See Wang et al.	228
Tao Y. J., See Ping et al.	239
Tariq A. R., See Firdos et al.	31
Tawab A., See Riaz et al.	354
Teimouri F., See Amin et al.	735
Tekin I. O., See Atabay-Ozdemir et al.	901
Tekin S., See Emre et al.	664
The 4th Asia-Pacific Conference on Engineering Technology (APCET 2016)	183
The Institute of Chemical Engineering at the Bulgarian Academy of Sciences – 30 years recap	5
Tian J., See Zhong et al.	520
Trache M., See Sadoudi et al.	68
Trak D., See Arslan et al.	884
Tsanova-Savov S. P., See Hristov et al.	782
Tsvetkov M. P., See Zaharieva et al.	652
Tsvetkova D. D., Ivanova St. A., Saso L., Obreshkova D., Dimitrov M., Estimation of linearity and precision of the HPLC-HILIC method for analysis of estradiol hemihydrate	384
Tsvetkova D., Obreshkova D., Ivanova S., Hadjieva B., Evaluation of the separation of steroids in combined forms by RP HPLC with UV-detection and gas chromatography	377
Tsyntsarski B., See Grigorova et al.	109
Tulepov M. I., See Baiseitov et al.	335, 600
Tzanev A. Tz., See Malinova et al.	436
Tzvetanova Y., See Lihareva et al.	577
Tzvetkov P. T., See Koseva et al.	366
Üçüncü O., See Kaya et al.	923
Vadivel M., Shobana S., Narayan S. A., Mitu L., Dhaveethu Raja J., Sankarganesh M., Optimization of process conditions and characterization of ethylene-propylene-diene rubber with bismaleimide	26
Valchev I. V., See Radoykova et al.	40
Valcheva V., See Angelova et al.	643
Vassilev N., See Angelova et al.	643
Velikov S. K., See Hristov et al.	782
Vlaev S. D., Georgiev D., Shear on particles exposed to backswept mixing flow with a view to stress-sensitive cell response	775
Vodenicharov V. E., See Hristov et al.	782
Vural P., Karahan M., Pelit Arayici P., Mustafaeva Z., Radiation induced formation of poly (N-isopropyl acrylamide)-bovine serum albumin covalent conjugates and their immunogenicity	557
Waghmare A., See Bandi et al.	79
Wan B., See Wang et al.	204
Wang G., Gao Y., Tang Y., Research on the mechanism for chemical clogging and its effect on the stability of tailing dam.....	228
Wang H., See Xin et al.	145
Wang J., See Bai et al.	658
Wang J., See Zeng et al.	176
Wang J.-L., See Lu et al.	161
Wang L., See Jiang et al.	509
Wang L., Wan B., Research on the physics-of-the failure model for corrosion damage accumulation under a multi-level stress profile based on the acceleration factor.....	204
Wang N., See Ke et al.	635
Wang Q., See Sun et al.	234
Wang Z. Y., See Li et al.	697
Wang Zh. Ch., See Yu et al.	969
Wei X., See Zhong et al.	520
Wen J., See Chen et al.	669
Weng L., See Xiong et al.	499
Wu H., See Jiao et al.	151
Wu J., See Song et al.	534
Wu K., See Song et al.	534
Wu X.-M., See Lu et al.	161
Xie D. T., See Li et al.	697
Xin Y., Wang H., Chen F., Synthesis and anti-plant pathogenic fungal activity of novel benzofuran-2-carboxamide derivatives	145
Xiong Z., Li B., Li L., Peng X., Yin Y., Weng L., Reaction mechanisms between acrylamide and mercaptan in high temperature system with different humidity.....	499
Xu C., See Xu et al.	264
Xu P. F., See Yang et al.	269
Xu P. F., Yang N., Jia J., Xu C., Guo J. J., A kind of integrated microfluidic system for rapid pathogenic botrytis cinerea detection.....	264
Xu W. H., See Li et al.	697
Xu Y. J., See Liu et al.	527
Xue J. Q., See Huo et al.	955
Xue L., See Yun et al.	288
Xuexin Y., Preparation and functional properties of maltose ester lactate.....	256
Yahui B., Gas-liquid flows in porous media and coupling effects	617
Yalçinkaya Ö., See Kara et al.	101
Yan J., See Liu et al.	527

Yan Jiang X., See Qing et al.....	171
Yan P., See Yuan et al.	185, 282
Yaneva Z., See Simeonov et al.	399
Yang F., See Zhang et al.	134
Yang N., Li Z., Sun J., Xu P. F., Guo J. J., Mao H. P., Interference analysis for pesticide residue photometric detection based on integrated microfluidic chip	269
Yang N., See Guo et al.	276
Yang N., See Xu et al.	264
Yang Y. Y., See Jia et al.	948
Yi C., See Huang et al.	17
Yildiz U., See Atabay-Ozdemir et al.	901
Yin Y., See Xiong et al.	499
Ying G., Quality grading system of Jadeite-Jade green based on three colorimetric parameters under CIE standard light sources D ₆₅ , CWF and A	961
Yordanov N. D., See Karakirova et al.	629
Yordanova A. S., See Koseva et al.	366
Yu B., See Song et al.	534
Yu H. L., Zhu J. M., Zhang Y. S., Zhang W. Q., Wang Zh. Ch., Study on the water resistance performance of floor rockmass under different fracture combinations	969
Yu H., See Jiang et al.	509
Yu L. T., See Sun et al.	678
Yu L.-j., See Feng et al.	685
Yu Z. Q., Zhou G. S., Zhu S. D., Li J. M., Li L. J., Influence of sensitizing treatment on the corrosion resistance of Incoloy 028 alloy	943
Yuan A., See Zeng et al.	176
Yuan Z., Yan P., Hydroxyl radical scavenging activity of microparticles prepared from solid fermentation by edible-medicinal fungi	185
Yuan Z., Yan P., Jing D., Optimization of fermenting conditions for antioxidant activity and yield of polysaccharides from mushroom solid fermentation	282
Yun T., Chen B., Li W., Sun Y., Xue L., Using point cloud data for tree organ classification and real leaf surface construction	288
Zaharieva K. L., Milenova K. I., Shopska M. G., Tsvetkov M. P., Eliyas A. E., Kadinov G. B.,	
Photocatalytic ability of abiotic and biotic materials for discoloration of malachite green and reactive Black 5 dyes	652
Zamani H. A., See Kazemi et al.	449
Zare-Shahabadi V., See Chamkouri et al.	994
Zeng X., See Liu et al.	157
Zeng Y., Li W., Huang J., Huang Z., Wang J., Qian J., Yuan A., Du T., Hu Y., Li D., Study on new rural domestic sewage treatment technology based on CASS and VBF.....	176
Zhang Q.-Z., Liu J.-L., Yang F., Hao X.-P., Ke C.-Y., Pan Q., Zhang X.-L., Density functional theory based study of the heat of polymerization of olefins	134
Zhang R. B., See Guo et al.	276
Zhang S.-L., See Lu et al.	161
Zhang W. Q., See Yu et al.	969
Zhang X.-L., See Zhang et al.	134
Zhang Y. S., See Yu et al.	969
Zhang Y., See Liu et al.	527
Zhao J.-X., See Lu et al.	161
Zhao Y., See Liu et al.	157
Zhengming , See Zhenzhi et al.G.	210
Zhenzhi G., Bin H., Ming G. Z., Numerical analysis of surface cracks of spherical explosive with a cushion	217
Zhenzhi G., Bin H., Zhengming G., Libo N., Lujie C., Study on the influence of different clearance on the crack of PBX explosive	210
Zhong K., Tian J., Wei X., Ma X., The performance test and evaluation of rock asphalt modified asphalt and mixture.....	520
Zhou D., See Liu et al.	157
Zhou G. S., See Yu et al.	943
Zhou T., See Huo et al.	955
Zhou Zhao W., See Qing et al.	171
Zhu J. M., See Yu et al.	969
Zhu S. D., See Yu et al.	943
Zhu W., See He et al.	193
Zhu Y., See Song et al.	534
Zolfigol M. A., See Sajjadifar et al.	87

АВТОРСКИ УКАЗАТЕЛ

- Ма С., виж Джун и др..... 526
Абдел-Хади Ф., Мазхер А. К., Алзахрани А., Хамед М., Обратен подход за конструиране на овлажнител за процеси на обезсоляване с овлажняване/изсушаване..... 477
Абеди М. Р., виж Каземи и др. 454
Айдън М., виж Шимшек и др. 86
Акдоган А., Чальшкан Koch Г., Дирим С. Н.,
Математично моделиране на микровълново сущене в тънък слой на царевични обивки и изследване свойствата на праха..... 993
Аладаг Е., виж Байрам и др. 900
Алам С., виж Рехман и др. 822
Ал-Дегс Я., виж Гергов и др. 421
Алзахрани А., виж Абдел-Хади и др. 477
Али Ахмед Д., виж Садуди и др. 73
Али Н., виж Хан и др. 330
Алиев К., виж Ебади и др. 544
Ализаде К., Солтани-Афарани X., Сравнително изследване на йонизациянните константи на Шифова база в различни среди чрез UV-Vis спектроскопия с полихроматична дължина на вълната 895
Алин А., виж Гергов и др. 421
Ал-Фахами К. Х., виж Еуаис и др. 576
Амин М. М., Канахмад X., Теймури Ф., Садами М.,
Карами М. А., Рахимманеш И., Подобрена биодеградация на експлозиви чрез анаеробно биоускоряване 741
Амролахи М. А., виж Багерпур и др. 486
Амролахи М. А., виж Емтиази и др. 482
Ангелова С. Е., виж Николова-Младенова и др.... 806
Ангелова Т., Вълчева В., Василев Н., Буюклиев Р.,
Михайлова Р., Момеков Г., Синтез, *ин vitro* антитролиферативна и антимикобактериална активност на тиазолидин-2,4-дион и хидантоинови производни..... 651
Андрис К., Маня М., Поканчи К. Л., Пуи А.,
Дрокиоу Г., Градинару В. Р., Координационни отнасяния на Коензим А спрямо златни йони: спектроскопски, мас-спектрометрични и микробиологични изследвания..... 628
Анделькович Д., виж Костич и др. 365
Анделькович Т., виж Костич и др. 365
Антонов А. С., виж Дамов и др. 594
Анусе М. А., виж Гаикуад и др. 922
Арвинд Нааян С., виж Шобана и др..... 353
Арджманд Ф., Шафиеи Ф., Моделиране на физикохимичните свойства на алифатни алкохоли, използвайки топологични индекси и количествена връзка структура-свойства 858
Арнаудов Л., виж Рангелов и др..... 429
Асгарпана Дж., виж Реза Резвани и др. 78
Атабей-Оздемир Б., Демиркиран О., Йилдиз У.,
Текин И. О., Джобан Б., Цитотоксичност и ДНК-свързване на медни (II) и цинкови (II) комплекси на flavonoidи: куерцитрин, мерицитрин, рутин 907
Ашраф С., виж Рехман и др..... 828
Бабахан И., виж Джобан и др. 913
Багерпур С., Амролахи М. А., Ефикасен ултразвуков метод за синтез на ксантенови производни..... 486
Бай Х. Л., Ванг Дж., Лю Ц. М., Хроматография на разделянето, качествения и количествения анализ на бифлавоноиди в сирови екстракти от *Selaginella tamariscina* 663
Байрам Т. Т., Нуходгул А., Аладаг Е., Изследване на биоразграждането и кинетиката на растежа на млечните отпадни води в стандартен реактор .900
Байсейтов Д. А., Тулепов М. И., Сасикова Л. Р.,
Габдрашова Ш. Е., Есен Г. А., Кудайбергенов К. К., Мансуров З. А., Сорбционен капацитет на сорбент за отстраняването на тънки слоеве от петрол 338
Байсейтов Д. А., Тулепов М. И., Сасикова Л. Р.,
Габдрашова Ш. Е., Магазова А. Н., Далелханули О., Кудярова Ж. Б., Мансуров З. А., Катализично хидриране на въглища от казахстански находища в присъствие на полимери 607
Балтаджъ К., виж Кая и др..... 927
Банашчак Е. В., виж Шимански и др. 346
Банди Р. К., Вагмар А., Хиндупур Р. М., Пати Х. Н.,
Проста, ефективна и мащабирана синтеза на субституирани бис-арил-хлорометани 81
Бахарестан Ф., виж Садеги и др. 334
Бегун И., виж Рехман и др..... 498
Бин Х., виж Женжи и др. 216, 227
Божинова А. С., виж Налимова и др. 126
Божич А., виж Костич и др. 365
Бошкович И. Д., Джукич Др. А., Машкович П. З.,
Мандич Л. Г., Фито-химичен състав и биологична активност на екстракти от *Echium italicum L.* 845
Бояджиев Б., Бояджиев Хр., Нови модели на индустритални колонни абсорбери. 1.Правоточни абсорбционни процеси 719
Бояджиев Б., Бояджиев Хр., Нови модели на индустритални колонни абсорбери. 2.Противоточни абсорбционни процеси 728
Бояджиев Б., Бояджиев Хр., Нови модели на индустритални колонни химични реактори..... 710
Бояджиев Хр., виж Бояджиев и др. 710, 719, 728
Бродняк У. Вр., Подобряване на физичните и оптичните свойства на филмите от хитозан-оризово нишесте, предварително третирани с ултразвук 867
Буюклиев Р., виж Ангелова и др..... 651
Вагмар А., виж Банди и др. 81
Вадивел М., Шобана С., Нааян С. А., Миту Л.,
Дхавеетху Раджа Дж., Санкарганеш М.,
Оптимизация на условията на процеса и охарактеризиране на каучук от етилен-пропилен-диен с бис-малеинимид..... 30
Ван Дж.-Л., виж Лю и др. 170
Ванг Дж., виж Бай и др. 663
Ванг К., виж Сун и др. 238

Василев Н., виж Ангелова и др.	651
Великов С. К., виж Христов и др.	786
Вен Дж., виж Чен и др.	677
Влаев С. Д., Георгиев Д., Скорости на сръзване върху частици при разбъркване с дъгообразни лопатки със значение на физиологията на микроорганизми, чувствителни към механично напрежение	781
Воденичаров В. Е., виж Христов и др.	786
By К.-М., виж Лю и др.	170
Вурал П., Каракан М., Пелит Араиджи П., Мустафаева З., Радиационно индуцирано образуване на ковалентно спрегнати поли-(п- изопропил акрилат)-албумини от говежди серум и тяхната имуногенност	562
Вълчев И. В., виж Радойкова и др.	45
Вълчева В., виж Ангелова и др.	651
Вън Л., виж Сюон и др.	503
Вю Х., виж Тю и др.	156
Г. Инг., Система за оценка на зеления цвят на джадеит-нефрит на основата на три колориметрични параметри на CIE стандартни светлинни източници D65, CWF и A	968
Габдрашова Ш. Е., виж Байсейтов и др.	338, 607
Гаикуад А. П., Суриявианши В. Дж., Анусе М. А., Течно-течна екстракция на рутений (III) в среда на малонат при използването на п-октиланилиин като йон-свързващ агент: изследване на катализатора и сплави	922
Гандрова В., виж Петрова и др.	120
Гао И., виж Уанг и др.	233
Гао Х., виж Хуанг и др.	19
Гедже Г., Теоретична основа за характеристиката на инхибиране на корозията на арганово масло	851
Генадиев В., виж Пуревсурен и др.	39
Георгиев Д., виж Влаев и др.	781
Георгиева А. Ц., виж Налимова и др.	126
Гергов Г., Алин А., Дойчинова М., Де Лука М., Симеонов В., Ал-Дегс Я., Оценка на различни PLS алгоритми за количествено определяне на три спектрално припокриващи се лекарства	421
Гильмундинов Ш., виж Сасикова и др.	588
Главчев И. К., виж Пуревсурен и др.	39
Главчева-Лалева З. И., виж Пуревсурен и др.	39
Градинару В. Р., виж Андрис и др.	628
Григорова Е., Христов М., Цинцарски Б., Стойчева И., Нихтянова Д., Марков П., Ефект на активни въглени, получени от кайсиеви костишки или полиолефинов въскът върху сорбционните свойства по отношение на водород на MgH ₂	114
Гуан Ю., виж Лю и др.	170
Гуо Дж. Дж., виж Ксу и др.	268
Гуо Дж. Дж., виж Ян и др.	275
Гуо Дж. Дж., Джан Р. Б., Ян Н., Проектиране и оценка на метод с микро-флуидна изолация за откриване на патогени в аквакултури	281
Гюндюз М. Г., виж Шимшек и др.	86
Давааджав Я., виж Пуревсурен и др.	39
Дай З.-Д., виж Сонг и др.	249
Дай С. Дж., виж Сун и др.	684
Далелханули О., виж Байсейтов и др.	607
Дамов К. С., Йорданов И. П., Антонов А. С., Илиев М. Т., Охарактеризиране на аеродисперсни системи с повищена концентрация по кинематичния вискозитет и масовата плътност на аерозолната им фаза	594
Дарбанди Х., виж Кияни и др.	568
Дас М., виж Махата и др.	985
Де Лука М., виж Гергов и др.	421
Деган Х. Р., Негарестани А., Резаие М. Р., Изследване на възможностите на IXRF-техника за откриването на елементи в прах по метода на Монте-Карло N частици	878
Демиркиран О., виж Атабей-Оздемир и др.	907
Денчев Д. Д., виж Симеонов и др.	435
Джавахернешан Н., виж Саджадифар и др.	91
Джавид А. Х., виж Раҳбани и др.	468
Джан И. С., виж Ю и др.	976
Джан И., виж Лиу и др.	533
Джан Р. Б., виж Гуо и др.	281
Джан У. К., виж Ю и др.	976
Джанани Х., виж Реза Резвани и др.	78
Джао У. Д., виж Уей и др.	175
Джия Дж., виж Ксу и др.	268
Джия И. Дж., Хе М. У., Чен Х. Н., Тънки филими от TiO ₂ , получени по зол-гел метода и дотирани с платина (Pt-TiO ₂)	192
Джобан Б., виж Атабей-Оздемир и др.	907
Джобан Б., Есер Н., Бабахан И., Комплекси на ДНК с мед (II) и лиганди от семикарбазони	913
Джоз-Ярмохамади Ф., виж Каземи и др.	454
Джорджевич Д., виж Матович-Пурич и др.	398
Джоши Р., виж Исмаил и др.	67
Джу И., виж Сун и др.	539
Джукич Др. А., виж Бошкович и др.	845
Джун К., Тиан Дз., Уей С., Ма С., Тест за ефективност и оценката на шистоасфалт, модифициран асфалт и смеси	526
Джън Д., виж Юан и др.	287
Дзимбова Т. А., виж Сапунджи и др.	774
Дзън Ю., Ли У., Хуан Дж., Хуан Д., Циен Д., Юан А., Ду Т., Ху Я., Ли Д., Проучване на нова технология за обработка на селски битови отпадни води на базата на CASS и VBF	182
Дзян Р., Ю Х., Уан Л., Ограничения на измерванията на свръхкритичните изотерми за сорбция на CO ₂ върху въглища с манометрично оборудване - теоретично описание	519
Дзян С., виж Уей и др.	175
Димитриевич И., виж Радованович и др.	883
Димитров Д. И., виж Петрова и др.	120
Димитров Д. Ц., виж Налимова и др.	126
Димитров М., виж Цветкова и др.	389
Димитров О. С., виж Косева и др.	370
Дирим С. Н., виж Акдоган и др.	993
Дишовски Н. Т., виж Малинова и др.	443
Добруджалиев Д. Г., виж Николова и др.	815
Добруцка Р., Биологична синтеза на наночастици от титанов диоксид (анатаз) чрез екстракт от <i>Arnicae anthodium</i>	599

Доймаз И., виж Исмаил и др.....	100
Дойчинова М., виж Гергов и др.	421
Доспатлиев Л., Иванова М., Спектрофотометрично изследване на системи за течно-течна екстракция, съдържащи кобалт и тетразолиеви соли. Прилагане на разработения метод за определяне съдържанието на кобалт в биологични преби (гъби и тютюн)	791
Драганова К. И., виж Манчева и др.	376
Дрокиоу Г., виж Андрис и др.	628
Ду Т., виж Дъзън и др.....	182
Дхавестху Раджа Дж., виж Вадивел и др.....	30
Дхармаджада Дж., виж Шобана и др.	353
Ебади А. Г., Хисориев Х., Алиев К., Измерване на някои химични и биохимични параметри в <i>Cladophora glomerata L.</i> от региона на Фараҳабад в Иран.....	544
Ебади А. Г., Хисориев Х., Производство на биомасло чрез бърза пиролиза на <i>Cladophora Glomerata</i> в реактор с кипящ слой.....	508
Ебрахими М., виж Каземи и др.	454
Елияс Ал. Ел., виж Захариева и др.....	657
Емре Ф. Б., Окушлук Ф., Текин С., Сандал С., Изследване на ефекта на наночастици от TiO_2 , синтезирани по хидротермалния метод върху LnCap-ракови клетки	668
Емтиази Х., Амролахи М. А., Едностадийна синтеза на 2-амино-4Н-хромени и дихидропирано [с] хромени, катализирана от $Mg(ClO_4)_2$	482
Енгстлер Й., виж Исмаил и др.....	67
Еркмен Дж., Ефект на остатъчните газове върху масопренасянето в клетка за електродиализа..	616
Есен Г. А., виж Байсейтов и др.....	338
Есер Н., виж Джобан и др.	913
Еуаис Х. А., Исмаил И. М., Ал-Фахами К. Х., Кinetични изследвания по образуването на сребърниnano-частици чрез редукция на сребро (I) с глюкоза във водни и мицеларни среди.....	576
Жанг К.-Ж., Лю Дж.-Л., Янг Ф., Хао С.-П., Ке К.-Ю., Пан С., Жанг Кс.-Л., Изследване на топлината на полимеризация на олефини с помощта на теорията на пътностния функционал (DFT) ..	138
Жанг Кс.-Л., виж Жанг и др.....	138
Жанг С.-Л., виж Лю и др.....	170
Жао Дж.-К., виж Лю и др.	170
Жао Ю., виж Лиу и др.	160
Женгминг Г., виж Женжи и др.	216
Женжи Г., Бин Х., Женгминг Г., Либо Н., Лужие К., Изследване на влиянието на отстраняването на пукнатини при РВХ-експлозиви.....	216
Женжи Г., Бин Х., Минг Г. З., Числен анализ на повърхностни пукнатини при сферични експлозиви с амортизор.....	227
Жиа Ж., Янг Ю. Ю., Ки Кс. У., Сонг Кс. М., Влияние на наносерпентинов минерален прах като смазочна добавка върху трибологичните свойства на триещи се двойки метали	954
Жоу Т.	960
Жоу Г.	947
Жу Д., виж Лиу и др.	160
Жу Ж. М., виж Ю и др.	976
Жу С.	947
Жу У., виж Хе и др.	198
Замани Х. А., виж Каземи и др.	454
Заре-Шахабади В., виж Чамкури и др.	1000
Захариева К. Л., Миленова К. И., Шопска М. Г., Цветков М. П., Елияс Ал. Ел., Кадинов Г. Б., Фотокаталитична способност на абиотични и биотични материали за обезцветяване на малахитово зелено и реактивно черно 5 багрила..	657
Зенг К., виж Лиу и др.	160
Золфигол М. А., виж Саджадифар и др.	91
Иванов Б. Б., виж Николова и др.	815
Иванова М., виж Доспатлиев и др.	791
Иванова С., виж Цветкова и др.	383
Иванова Ст. А., виж Цветкова и др.	389
Игнатова К., Марчева Й., Състав и структура на Ni-Co покрития в зависимост от съотношението на Ni и Co в цитратен електролит	319
Идакиева К., виж Милева и др.	16
Йи С., виж Хуанг и др.,.....	19
Йилдиз У., виж Атабей-Оздемир и др.	907
Икбал М., виж Риаз и др.	359
Илиев М. Т., виж Дамов и др.	594
Илтер Ш. М., виж Кая и др.	927
Имран М., виж Рехман и др.	498
Имран М., виж Фирдос и др.	33
Ин И., виж Сюн и др.	503
Йовичич Д., виж Матович-Пурич и др.	398
Йозтурк С., виж Кая и др.	927
Йорданов И. П., виж Дамов и др.	594
Йорданов Н. Д., виж Каракирова и др.	634
Йорданова А. С., виж Косева и др.	370
Исмаил И. М., виж Еуаис и др.	576
Исмаил Н., Джоши Р., Енгстлер Й., Шнайдер Й. Й., Подобрен капацитет на въглеродни нанотръби (cnt) за складиране на водород при дъгово изпразване във въздух в присъствие на железен катализатор.....	67
Исмаил О., Кипчак А. С., Доймаз И., Пишkin С., Кинетика на сушене на тънки слоеве от нектарини при IR, MW и хибридни методи	100
Итуа Бл. В., Огуний Д. С., Онгока П., Петров Л., Влияние на фумаровата киселина върху свойствата на смеси на алкидна смола и палмово масло	133
Кабаиванова Л. В., виж Симеонов и др.	435
Кабан Ш., виж Фидан и др.	749
Кадинов Г. Б., виж Захариева и др.	657
Каземи Ф., Замани Х. А., Джоз-Ярмохамади Ф., Ебрахими М., Абеди М. Р., Приложение на 1, 4-диаминоантрахинон като нов селектофорен материал за производството на потенциометричен Fe(III)-селективен електрод	454
Калва К., виж Ковалски и др.	935
Канаҳмад Х., виж Амин и др.	741
Канвал Ф., виж Фирдос и др.	33
Кануал А., виж Рехман и др.	498

- Кануал Ф., виж Рехман и др..... 498
 Кара И., Ялчинкая О., Оценяване на трайността на остатъци от изстrelи (GSR) с атомно-абсорбционна спектрофотометрия в графитна пещ (GFAAS) 108
 Каракирова Й. Г., Накагава К., Йорданов Н. Д., Изследване на захар облечена с Не, Ne и С иони за дозиметрични цели 634
 Караман Ф., виж Фидан и др. 749
 Карами М. А., виж Амин и др. 741
 Караджан М., виж Вурал и др. 562
 Карвар И. С., Резаголипур Дизаджи Х., Еднопосочен растеж на единичен монокристал от $\text{CoNi}(\text{SO}_4)_2 \cdot 12\text{H}_2\text{O}$ по метода на Sankaranarayanan-Ramasamy (SR) 610
 Кафи А., виж Садеги и др. 334
 Кая А. А., Ючюнчю О., Илтер Ш. М., Балтаджъ К., Йозтюрк С., Химичен състав и биоактивни свойства на етерично масло от *Rhinanthus angustifolius* подвид *Grandiflorus* 927
 Ке К.-Ю., виж Жанг и др. 138
 Ке Ц., Уанг Н., Ли В., Ши У., Фей З., Адсорбционни свойства на 4-фенилфенол във воден разтвор с химически модифицирана адсорбционна смола 642
 Кендюзлер Е., виж Арслан и др. 889
 Кецили А., виж Садуди и др. 73
 Ки Кс. У. 954
 Киан Кс., виж Шанг и др. 942
 Киндеков Ив., виж Милева и др. 16
 Кипчак А. С., виж Исмаил и др. 100
 Кираджийска Д. Д., виж Манчева и др. 376
 Кияни Х., Дарбанди Х., Едно-стадийна трикомпонентна синтеза на 1-амидоалкил-2-нафтоли в присъствие на фталимид-*n*-суlfонова киселина 568
 Ковалска Г., виж Ковалски и др. 935
 Ковалски Р., Ковалска Г., Панкиевич У., Суйка М., Калва К., Газ-хроматографски анализ при определянето на изменениета в съдържанието на мастни киселини в избрани мазнини по време на съхранение и нагряване 935
 Кононова И. Е., виж Налимова и др. 126
 Косева Й. И., Цветков П. Ц., Йорданова А. С., Маричев М. О., Димитров О. С., Николов В. С., Получаване на дотирана с хром стъклокерамика съдържаща LiAlSiO_4 370
 Костич И., Андъелкович Т., Андъелкович Д., Божич А., Цветкович Т., Павлович Д., Количествено определяне на DEHP в компоненти от интравенозни системи и прибори за перитониална диализа от PVC преди и след третиране с ултравиолетови лъчи 365
 Костова Б. Д., виж Славкова и др. 799
 Кринискайте А., виж Палиулис и др. 873
 Крумова Е. Ц., виж Симеонов и др. 435
 Кръстев Д., виж Милева и др. 16
 Кръстева Л. К., виж Налимова и др. 126
 Ксу К., виж Ксу и др. 268
 Ксу П. Ф., виж Ян и др. 275
 Ксу П. Ф., Ян Н., Джия Дж., Ксу К., Гуо Дж. Дж., Интегрирана микрофлуидна система за бързо откриване на патогените *Botrytis cinerea* 268
 Ксуе Ж. 960
 Крюексин И., Получаване и функционални свойства на малтозо-лактатен естер 263
 Кудайбергенов К. К., виж Байсейтов и др. 338
 Кудярова Ж. Б., виж Байсейтов и др. 607
 Кумар С., виж Шарма и др. 312
 Кънева Н. В., виж Налимова и др. 126
 Къокпинар Й., виж Шимшек и др. 86
 Лаи У. Л., виж Лю и др. 203
 Ли Б., виж Сун и др. 503
 Ли В., виж Ке и др. 642
 Ли Д., виж Дъзън и др. 182
 Ли Дж. М. 947
 Ли З., виж Ян и др. 275
 Ли Л. Дж. 947
 Ли Л., виж Сун и др. 503
 Ли М., Цонг С., Химични промени и механизми на синтеруването на морска тиня 255
 Ли Т., Су У. Х., Чай И. Р., Уанг З. И., Сие Д., Разлики в усвояването на Cd и експресията на Cd-толерантни гени в две разновидности на райграс 705
 Ли У., виж Дъзън и др. 182
 Ли У., виж Юн и др. 296
 Лианг Х., виж Сун и др. 238
 Лианг Х., виж Шанг и др. 942
 Либо Н., виж Женжи и др. 216
 Лиу Дж., Зенг К., Жу Д., Жао Ю., Пан К., Екологична оценка на безопасността на вторични продукти на хлориране в саламура, изхвърлена от инсталация за обезсоливане 160
 Лиу И. Г., Джан И., Ян Дз., Сю И. Дж., Реологични свойства на RHMOD-INVERT™ - изследване на нова сондажна течност на основата на масло с висока тиксотропия 533
 Лиу Ф., виж Хе и др. 198
 Лихарева Н., Петров О., Цветанова Я., Моделиране на йонен обмен на Cs^+ с природен клиноптиолит във водни разтвори 582
 Лужие К., виж Женжи и др. 216
 Лю Дж.-Л., виж Жанг и др. 138
 Лю И., Лю Л., Ши Г., Ши Дж., Лаи У. Л., Изследвания и охарактеризиране на абираторон-ацетат 203
 Лю Л., виж Лю и др. 203
 Лю У. Г., виж Сун и др. 684
 Лю Ц. М., виж Бай и др. 663
 Лю Ю.-Дж., Ву К.-М., Гуан Ю., Жанг С.-Л., Ван Дж.-Л., Жао Дж.-К., Хан В.-Ю., Шен Ж.-Ц., Оптимизация на клетъчна култура на H9N2 подтип на AIV и установяване на клетъчен щам с висок добив 170
 Ма Д., виж Сун и др. 539
 Магазова А. Н., виж Байсейтов и др. 607
 Мазхер А. К., виж Абдел-Хади и др. 477
 Малинова П. А., Дишовски Н. Т., Цанев А. Ц., Изследване влиянието на условията на

девулканизация върху експлоатационните характеристики на вулканизати на базата на регенерат	443	чувствителните към изпарения свойства на слоеве от цинков оксид	126
Мандич Л. Г., виж Бошкович и др.	845	Намхайноров Дж., виж Пуревсурен и др.	39
Манойлович Н., виж Радованович и др.	883	Нандкейоляр Р., виж Махата и др.	985
Мансуров З. А., виж Байсейтов и др.	338	Нарайян С. А., виж Вадивел и др.	30
Мансуров З. А., виж Байсейтов и др.	607	Негарестани А., виж Деган и др.	878
Манчева Р. Д., Кираджийска Д. Д., Феодорова Я. Н., Драганова К. И., Биосъвместимост на алуминиеви сплави и аноден Al_2O_3	376	Ненкова С. К., виж Радойкова и др.	45
Маня М., виж Андрис и др.	628	Ненкова С., виж Райчева и др.	144
Мао Х. П., виж Ян и др.	275	Ниамат И., виж Фирдос и др.	33
Маричев М. О., виж Косева и др.	370	Николич В., виж Радованович и др.	883
Марков П., виж Григорова и др.	114	Николов В. С., виж Косева и др.	370
Марчева Й., виж Игнатова и др.	319	Николов Р., виж Райчева и др.	144
Маскович П., виж Матович-Пурич и др.	398	Николова Д. Ст., Иванов Б. Б., Добруджалиев Д. Г., Оптимално управление на енергията в пивоварството	815
Матович-Пурич И., Печарски Д., Югович З., Йовичич Д., Джорджевич Д., Маскович П., сравнително изследване на някои биохимични параметри на гъби <i>Mucor plumbeus</i> , <i>Aspergillus niger</i> и <i>Trichoderma harzianum</i>	398	Николова-Младенова Б. И., Ангелова С. Е., Синтез на хидразони, получени от 5- нитросалицилалдехид и DFT-изчисления за тяхната структура и реакционна способност	806
Махата Б. К., Нандкейоляр Р., Дас М., Сибанда П., Нанофлуиден поток с точка на стагнация по протежение на разтегляща се пластина с нееднакво генериране / погълщане на топлина и Нютоново нагрявани	985	Нихтянова Д., виж Григорова и др.	114
Махмуд Т., виж Рехман и др.	25	Ниязи А., виж Чамкури и др.	1000
Машкович П. З., виж Бошкович и др.	845	Нороузи В., Таджедин С., Приложение на електрод с въглеродна паста, модифициран с многостенни въглеродни нанотръби като прост и ефективен катализатор за определянето на цефиксим в реални преби	734
Мерган М. Р., виж Раҳбани и др.	468	Нухоглу А., виж Байрам и др.	900
Меруани Х., Униси А., Уддаи Н., DFT-изследване на нитрирани хетероциклини съединения с шест и седем връзки	696	Обрешкова Д., виж Цветкова и др.	383, 389
Миланов П. Б., виж Сапунджи и др.	774	Огуний Д. С., виж Итуа и др.	133
Милева М., Райнова Ю., Киндеков Ив., Кръстев Д., Идакиева К., Ин витро изследване на антиоксидантните свойства на хемоцианин от рак <i>Cancer pagurus</i>	16	Окушлук Ф., виж Емре и др.	668
Миленова К. И., виж Захариева и др.	657	Онгока П., виж Итуа и др.	133
Минг Г. З., виж Женжи и др.	227	Павлович Д., виж Костич и др.	365
Миту Л., виж Вадивел и др.	30	Палиулис Д., Кринискайте А., Отстраняване на олово (Pb_2^+) от синтетични отпадни води с използване на калциев пектат	873
Миту Л., виж Рехман и др.	25, 498, 822	Пан К., виж Лиу и др.	160
Миту Л., виж Фирдос и др.	33	Пан С., виж Жанг и др.	138
Миту Л., виж Шобана и др.	353	Панкиевич У., виж Ковалски и др.	935
Михайлова Р., виж Ангелова и др.	651	Папазова К. И., виж Налимова и др.	126
Михайлова С. Н., виж Симеонов и др.	435	Пати Х. Н., виж Банди и др.	81
Михалев К., виж Петрова и др.	120	Пелит Араиджи П., виж Вурал и др.	562
Момеков Г. Цв., виж Славкова и др.	799	Пенчева Н. С., виж Сапунджи и др.	774
Момеков Г., виж Ангелова и др.	651	Петров Л., виж Итуа и др.	133
Момекова Д. Б., виж Славкова и др.	799	Петров О., виж Лихарева и др.	582
Мошников В. А., виж Налимова и др.	126	Петров П. Д., виж Славкова и др.	799
Мустафаева З., виж Вурал и др.	562	Петрова И., Шиков В., Гандова В., Михалев К., Димитров Д. И., Спектрофотометрично и термодинамично изследване на ко- пигментационни взаимодействия между антоциани от ягоди и кверцетин в моделни системи	120
Надери Н., виж Реза Резвани и др.	78	Печарски Д., виж Матович-Пурич и др.	398
Накагава К., виж Каракирова и др.	634	Пинг Л. Л., Тао И. Дж., Ефект на твърдо-фазното заваряване върху образуването на	244
Налибаева А., виж Сасикова и др.	588	микроструктурата и свойствата на виско- качествена никелова стомана	244
Налимова С. С., Кононова И. Е., Мошников В. А., Димитров Д. Ц., Кънева Н. В., Кръстева Л. К., Сюлейман Ш. А., Божинова А. С., Папазова К. И., Георгиева А. Ц., Изследване на измерени по метода на импедансна спектроскопия на	628	Пишкин С., виж Исмаил и др.	100
	628	Поканчи К. Л., виж Андрис и др.	628
	628	Пуи А., виж Андрис и др.	628

Пуревсурен Б., Давааджав Я., Намхайноров Дж., Главчева-Лалева З. И., Генадиев В., Главчев И. К., Пиролиза на животински кости, характеризиране на получените въглен и катран и прилагането на костен катран за омрежване на епоксидна смола	39
Пън С., виж Сюон и др.....	503
Радева Г., виж Райчева и др.	144
Радованович А., виж Радованович и др.....	883
Радованович Б., Радованович А., Николич В., Манойлович Н., Димитриевич И., Ефект на съхранението върху съдържанието и антиоксидантната активност на феноли в избрани плодови екстракти	883
Радойкова Т. Х., Ненкова С. К., Вълчев И. В., Мономерни фенолни съединения от отпадъчни хидролизни лигноцелуцозни материали	45
Райнова Ю., виж Милева и др.	16
Райчева Л., Радева Г., Ненкова С., Николов Р., Адсорбционни характеристики на активен въглен получен от отпадъчен технически хидролизиран лигнин.....	144
Рангелов А., Арнаудов Л., Стоянов С., Спасов Т., Гелиране на индустриски нишестета, изследвано с ДСК и ТГ	429
Расуул Н., виж Риаз и др.	359
Ратхер С. У., Изследване на корозията на ферити, пригответи по хидротермален метод	448
Рауф А., виж Рехман и др.....	25
Рахбани К., Хасани А. Х., Мерган М. Р., Джавид А. Х., Хибриден подход на невронна мрежа и анализ на обхвата на данните за оценка и предсказване на ефективността на единици за вземане на решение на пример на система за пречистване на индустриски отпадъчни води на компания за преработка на стомана в Хузестан....	468
Рахимманеш И., виж Амин и др.	741
Рашийд С., виж Рехман и др.....	498
Реза Резвани А., Джанани Х., Ростами-Чарати Ф., Скелтън Б. У., Надери Н., Асгарпанах Дж., Синтеза на нов третичен мед (II) комплекс: кристална структура и спектрални изследвания	78
Резаголипур Дизаджи Х., виж Карвар и др.	610
Резаие М. Р., виж Деган и др.	878
Рехман Р., Алам С., Миту Л., Отстраняване на баргилото диамантено зелено от води чрез адсорбция върху отпадъчна морковена пулпа и картофени обелки.....	822
Рехман Р., Ашраф С., Анализ на съдържанието на кофеин в търговски напитки и проби от чай с помошта на УВ-спектрометрия	828
Рехман Р., Махмуд Т., Риаз Р., Рауф А., Миту Л., Сорбционно отстраняване на багрилото директно синьо-15 от вода използвайки листа от <i>Camellia sinensis</i> и <i>Carica papaya</i>	25
Риаз М., Расуул Н., Икбал М., Таяб А., Хабиб Ф. Е., Хан А., Фарман М., Анализ на екстракт от <i>Russelia equisetiformis</i> чрез течна хроматография,	
съчетана с електроспрей-йонизация и мас-спектрометрия (LC-ESI-MS/MS).....	359
Риаз Р., виж Рехман и др.....	25
Рибарова Ф. Т., виж Христов и др.	786
Ростами-Чарати Ф., виж Реза Резвани и др.....	78
С., Рашийд С., Имран М., Кануал А., Кануал Ф., Бегун И., Миту Л., Сълънчогледови и соеви масла, стабилизирани с естествени екстракти от кори на ряпа	498
Садами М., виж Амин и др.....	741
Садеги Б., Бахарестан Ф., Кафи А., Хасанабади А., Чист, прост и ефективен синтез на спиро-2-амино-4Н-пиран-3-карбонитрил чрез наночастици $\text{HBF}_4\text{-SiO}_2$: зелен протокол.....	334
Саджадифар С., Золфигол М. А., Джавахернешан Н., Чехардоли Г., Сравнение между оценката и пропановата киселина като разтворител/катализатор в синтезата на индоленини: подход без индолови странични продукти	91
Садуди Р., Али Ахмед Д., Траче М., Кецили А., Изследване на физико-химичните характеристики и състава от мастни киселини на търговски алжирски хранителни растителни масла	73
Сакар Дасдан Д., виж Фидан и др.....	749
Сандал С., виж Емре и др.	668
Санкарланеш М., виж Вадивел и др.....	30
Сапунджи Ф. И., Дзимбова Т. А., Пенчева Н. С., Миланов П. Б., Моделиране на връзката между биологичната активност на делта-селективни енкефалинови аналоги и резултати от молекулен докинг с полиноми	774
Сасикова Л. Р., виж Байсейтов и др.....	338, 607
Сасикова Л. Р., Налибаева А., Гильмундинов Ш., Разработване на технология за синтез на катализатори за обезвреждане на емисии в индустрията и автотранспорта	588
Сасо Л., виж Цветкова и др.	389
Сибанда П., виж Махата и др.	985
Сивек Р., виж Шимански и др.	346
Сие Д., виж Ли и др.	705
Симеонов В., виж Гергов и др.....	421
Симеонов Е., Янева З., Чилев Ч., Изследване на механизма и кинетиката на екстракция от растителни сировини	409
Симеонов И. С., Денчев Д. Д., Кабаиванова Л. В., Крумова Е. Ц., Чорукова Е. И., Хубенов В. Н., Михайлова С. Н., Различни начини на предварително третиране на лигноцелулозни отпадъци за продукция на метан	435
Син Я., Уанг Х., Чен Ф., Синтеза на нови бензофуран-2-карбоксамидови производни и тяхната активност спрямо патогенни гъбички.	150
Скелтън Б. У., виж Реза Резвани и др.....	78
Славкова М. Ив., Момекова Д. Б., Костова Б. Д., Момеков Г. Цв., Петров П. Д., Нови макропорести криогелове от декстран/β-циклодекстрин и декстран за дермално доставяне	

на куркумин при лечение на кожен Т-клетъчен лимфом.....	799
Славова И. А., Христоскова Ст. Г., Стоянова М. К., Каталитично окисление на Родамин В във водни разтвори със сулфатни радикали върху $\text{Co}_3\text{O}_4/\text{MgO}$ и $\text{CoFe}_2\text{O}_4/\text{MgO}$	767
Солтани-Афарани Х., виж Ализаде и др.	895
Сонг Г., виж Сонг и др.	249
Сонг Дж., Даи З.-Д., Сонг Г., Чен Х.-Л., Изследване на неизотермичната кристализация на композити от поли-винилов алкохол с монтморилонит чрез диференциална сканираща калориметрия (DSC)	249
Сонг Кс. М.	954
Спасов Т., виж Рангелов и др.	429
Стойчева И., виж Григорова и др.	114
Стоянов С., виж Рангелов и др.	429
Стоянова М. К., виж Славова и др.	767
Су У. Х., виж Ли и др.	705
Субраманиам П., виж Шобана и др.	353
Суйка М., виж Ковалски и др.	935
Сун Б. Ф., виж Ху и др.	835
Сун Дж., виж Ян и др.	275
Сун И., виж Уей и др.	175
Сун Л., Лианг Х., Ванг К., Чен Х., Определяне строежа на материали по сегменти на образи с помощта на алгоритъм „изкуствена пчелна колония“.....	238
Сун У. Х., Даи С. Дж., Лю У. Г., Ю Л. Т., Изследване върху отстраняването на замърсявания от магнезитова руда чрез двустепенна обратна флотация.....	684
Сун У., Ма Д., У К., Джу И., У Дж., Ю Б., Експериментално изследване на изместването на нефт с помощта на сулфат-редуциращи бактерии при изпитание със заливане на скална ядка....	539
Сун Ю., виж Юн и др.	296
Суриявианши В. Дж., виж Гаикуад и др.	922
Сю И. Дж., виж Лиу и др.	533
Сю Л., виж Юн и др.	296
Сюлейман Ш. А., виж Налимова и др.	126
Сюн З., Ли Б., Ли Л., Пън С., Ин И., Вън Л., Реакционни механизми между акриламид и меркаптан при високотемпературна система с различна влажност	503
Таджедин С., виж Нороузи и др.	734
Танг И., виж Уанг и др.	233
Тао И. Дж., виж Пинг и др.	244
Тарик А. Р., виж Фирдос и др.	33
Таяб А., виж Риаз и др.	359
Теймури Ф., виж Амин и др.	741
Текин И. О., виж Атабей-Оздемир и др.	907
Текин С., виж Емре и др.	668
Тиан Дз., виж Джун и др.	526
Трак Д., виж Арслан и др.	889
Траче М., виж Садуди и др.	73
Тулепов М. И., виж Байсейтов и др.	338, 607
Тю Дж., Вю Х., Определяне на метални иони чрез ултразвук-подпомагана течна микроекстракционна техника с кухи влакна ...	156
У Дж., виж Сун и др.	539
У К., виж Сун и др.	539
Уан Б., виж Уан и др.	209
Уан Д., виж Дъзън и др.	182
Уан Ж. Ч., виж Ю и др.	976
Уан Л., виж Дзян и др.	519
Уан Л., Уан Б., Изследване на натрупването на корозионни дефекти при много-степенно напрежение с ускорение с модела „physics-of-failure“	209
Уанг Г., Гао И., Танг И., Анализ на влиянието на химическото задърстване и просмукване върху стабилността на хвостохранилищата	233
Уанг З. И., виж Ли и др.	705
Уанг Н., виж Ке и др.	642
Уанг Х., виж Син и др.	150
Уддаи Н., виж Меруани и др.	696
Уей Л., Дзян С., Шай Д. А., Джоу У. Д., Шао С. П., Чън Ц., Сун И., Проучване на прахоулавянето и способността за инхибиране на микроорганизми на <i>Jacaranda mimosifolia</i> при еднакви условия на експеримент за сравнение	175
Уей С., виж Джун и др.	526
Униси А., виж Меруани и др.	696
Фарман М., виж Риаз и др.	359
Фей З., виж Ке и др.	642
Фенг И. И., Ю Л. Дж., Цао Р. У., Адсорбция на медни иони от композит от монтморилонит/натриев хумат/п-изопропилакриламид.....	689
Феодорова Я. Н., виж Манчева и др.	376
Фидан И., Сакар Дасдан Д., Караман Ф., Кабан Ш., Повърхностно охарактеризиране на тиазолидинонови производни с обратна газова хроматография	749
Фирдос А., Тарик А. Р., Имран М., Ниамат И., Канвал Ф., Миту Л., Антиоксидантен потенциал на екстракт от черен пипер за стабилизирането на сълнчогледово масло	33
Франковска М., виж Шимански и др.	346
Хабиб Ф. Е., виж Риаз и др.	359
Хаджиева Б., виж Цветкова и др.	383
Хамед М., виж Абдел-Хади и др.	477
Хан А., виж Риаз и др.	359
Хан В.-Ю., виж Лю и др.	170
Хан Дж., виж Хуанг и др.	19
Хан С. У., Али Н., Хаят Т., Аналитично и числено изследване на дифузията на химически активни вещества във флуид на Eyring-Powell над надлъжно осцилираща повърхност	330
Хао С.-П., виж Жанг и др.	138
Хасан А. А., Магнитохидродинамична стабилност на самогравитираща, свиваема, резистивна, въртяща се поточна среда	492
Хасанабади А., виж Садеги и др.	334
Хасани А. Х., виж Раҳбани и др.	468
Хаят Т., виж Хан и др.	330
Хе Ж.	960
Хе М. У., виж Джия и др.	192

Хе М., Жу У., Лиу Ф., Чен Х., Метод за настройка на размера на капките по LEM-метода за 3D електронно печатане	198
Хиндупур Р. М., виж Банди и др.	81
Хисориев Х., виж Ебади и др.....	508, 544
Христов Д. С., Великов С. К., Воденичаров В. Е., Цанова-Савова С. П., Рибарова Ф. Т., Оценка на химичния състав, енергията и биологичната стойност на типични традиционни Български храни	786
Христов М., виж Григорова и др.....	114
Христоскова Ст. Г., виж Славова и др.	767
Ху Л. Ш., Сун Б. Ф., Експериментално изследване на рого-образни взривни капсули.....	835
Ху Я., виж Дъзън и др.	182
Хуан Д., виж Дъзън и др.	182
Хуан Дж., виж Дъзън и др.	182
Хуанг Г. Л., Гао Х., Йи С., Хуанг Д., Хан Дж., Изследване на синтезата на 2,3,4,6-О-тетраацетил- α -D-глюкопиранозил бромид	19
Хуанг Д., виж Хуанг и др.	19
Хубенов В. Н., виж Симеонов и др.	435
Хуо К., Жоу Т., Хе Ж., Ксеу Ж., Идентифициране на кленбутерол с помощта на MALDI-TOF масспектрометрия	960
Цанев А. Ц., виж Малинова и др.	443
Цанова-Савова С. П., виж Христов и др.	786
Цао Р. У., виж Фенг и др.	689
Цветанова Я., виж Лихарева и др.	582
Цветков М. П., виж Захарieva и др.	657
Цветков П. Ц., виж Косева и др.	370
Цветкова Д., Иванова Ст. А., Сасо Л., Обрешкова Д., Димитров М., оценка на линейността и точността на HPLC-HILIC-метод за анализ на естрадиол хемихидрат	389
Цветкова Д., Обрешкова Д., Иванова С., Хаджиева Б., Оценка на разделянето на стероиди в комбинирани форми чрез RP HPLC с UV-детекция и газова хроматография.....	383
Цветкович Т., виж Костич и др.	365
Циен Д., виж Дъзън и др.	182
Цинцарски Б., виж Григорова и др.....	114
Цонг С., виж Ли и др.	255
Чай И. Р., виж Ли и др.	705
Чальшкан Koch Г., виж Акдоган и др.	993
Чамкури Н., Заре-Шахабади В., Ниязи А., Едновременно определяне на диклофенак-калий и индометацин с преби от serum и плазма с помощта на едновременни ултразвукова дисперсионна течно-течна микро-екстракция и HPLC-UV. Планиран експеримент и оптимизация	1000
Чаулия С. Н., Синтеза, спектроскопско охарактеризиране и биологична активност на Co(II), Ni(II), Cu(II) и Zn(II) метални комплекси с лиганди от азо-багрило, получено от 4,4'-диаминодифенилтер и 5-сулфосалицилова киселина.....	61
Чен Дж., Вен Дж., Характеристики на деградация и корозия за разтвор на смес от амиини при	
отнемането на въглерода от метан в слой въглища	677
Чен Ф., виж Син и др.	150
Чен Х. Н., виж Джия и др.	192
Чен Х., виж Сун и др.....	238
Чен Х., виж Хе и др.	198
Чен Х.-Л., виж Сонг и др.	249
Чехардоли Г., виж Саджадифар и др.	91
Чилев Ч., виж Симеонов и др.	409
Чорукова Е. И., виж Симеонов и др.	435
Чън Б., виж Юн и др.	296
Чън Ц., виж Уей и др.	175
Шай Д. А., виж Уей и др.	175
Шанг У., Киан Кс., Лианг Х., Получаване на модифициран диатомитен пълнител чрез нанасяне на комплекс от нищесте и мастна киселина за подобряване на здравината на хартия	942
Шао С. П., виж Уей и др.	175
Шарма Д. К., Кумар С., Проста синтеза на 3-хлоро-2-фенил-4Н-хромен-4-они с използването на смилане при стайна температура	312
Шафак Дж., виж Шимшек и др.	86
Шафиеси Ф., виж Арджманд и др.	858
Шен Ж.-Ц., виж Лю и др.	170
Ши Г., виж Лю и др.	203
Ши Дж., виж Лю и др.	203
Ши У., виж Ке и др.	642
Шиков В., виж Петрова и др.	120
Шимански А., виж Шимански и др.	346
Шимански М., Банащак Е. В., Сивек Р., Франковска М., Шимански А., Освобождаване на кофеин от избрани фармацевтични препарати	346
Шимшек Р., Гюндюз М. Г., Шафак Дж., Къокпинар Й., Айдън М., Свойства на свободните радиали на някои гама-обълчени органични съединения...	86
Шнайдер Й. Й., виж Исмаил и др.	67
Шобана С., виж Вадивел и др.	30
Шобана С., Субраманиам П., Дхармараджа Дж., Арвинд Нааян С., Миту Л., Изследвания на стабилността на равновесието в разтвори на Zn(II)-комpleksi с пиrimидинови бази	353
Шопска М. Г., виж Захариева и др.	657
Ю Б., виж Сун и др.	539
Ю З., Жоу Г., Жу С., Ли Дж. М., Ли Л. Дж., Влияние на сенсибилизиращата обработка върху корозионната устойчивост на сплавта Incoloy 028	947
Ю Л. Дж., виж Фенг и др.	689
Ю Л. Т., виж Сун и др.	684
Ю Х. Л., Жу Ж. М., Джан И. С., Джан У. К., Уан Ж. Ч., Изследвания върху водоустойчивостта на стратифицирани скални маси при различни условия на разрушаване	976
Ю Х., виж Дъзън и др.	519
Юан А., виж Дъзън и др.	182
Юан Дж., Ян П., Джън Д., Оптимизация на условията за твърдо-фазна ферментация на гъби	

във връзка с тяхната антиоксидантна активност и добива на полизахариди	287
Юан З., Ян П., Способност за остраняване на хидроксилни радикали от микрочастици, получени при твърдо-фазна ферментация на едливи медицински гъби	189
Югович З., виж Матович-Пурич и др.	398
Юн Т., Чън Б., Ли У., Сун Ю., Сю Л., Използване на точкови данни в облак за класификацията на органите и реалния строеж на листата на дървета	296
Ючюнчю О., виж Кая и др.	927
Ялчинская О., виж Кара и др.	108
Ян Дз., виж Лиу и др.	533
Ян Н., виж Гуо и др.	281
Ян Н., виж Ксу и др.	268
Ян Н., Ли З., Сун Дж., Ксу П. Ф., Гуо Дж. Дж., Мао Х. П., Интерференчен анализ за фотометричното определяне на остатъци от пестициди с интегрални микро-флуидни чипове	275
Ян П., виж Юан и др.	189, 287
Янг Ф., виж Жанг и др.	138
Янг Ю. Ю.	954
Янева З., виж Симеонов и др.	409
Яхуи Б., Течение газ-течност в поръзона среда и свързани ефекти.....	620

SUBJECT INDEX

1-(2-hydroxyphenyl)-3-phenylpropane-1,3-diones.....	309
1,4-dihydropyridines.....	82
1-amidoalkyl-2-naphthol	562
2,3,4,6-O-tetraacetyl- α -D-glucopyranosyl bromide	17
2,4,6-trinitrotoluene	735
2-amino-4H-chromenes	478
2H-chromene	643
2-naphthol	483
3-chloro-2-phenyl-4H-chromen-4-ones	309
3D electronic printing	193
3H-indole	87
4-Hydroxycoumarin.....	478
4-Phenylphenol.....	635
5-nitrosalicylaldehyde.....	800
abiraterone acetate	199
absorption and emission spectra	366
acetic acid	87
acid dissociation constants.....	890
acrylamide	449, 685
activated carbon	139
activation energy.....	986
adsorption	20, 509, 635, 868
adsorption isotherms	635
aerobic processes	896
aerosols	589
Aghbashlo et al. model	92
agricultural waste.....	986
algae.....	504
Algeria	67
aliphatic alcohols	852
alkaline treatment.....	40
alkyd resin.....	127
Al-Si-Zr	371
Amberlite CG-120 resin	884
amentoflavone	658
anaerobic digestion	430
animal bone.....	34
anodized aluminium.....	371
anthocyanins	115
antimicrobial activity	923
antimycobacterial activity	643
antioxidant	449, 669
antioxidant activity	493, 879
antioxidant potential	30
antioxidant properties	11
anti-plant pathogenic fungal activity	145
antiproliferative/cytotoxic effects	643
application	787
aquaculture pathogens	276
argan oil	846
arylyhydrazones.....	800
artificial bee colony	234
artificial neural networks (ANN).....	455
<i>Aspergillus niger</i>	390
asphalt mixture	520
Au complexes	621
austenite	239
average concentration model	706, 711, 720
azo compounds.....	46
B3LYP/6-31G	134
backswung impeller.....	775
ball milling	109
batch reactor	807, 896
benzofuran-2-carboxamide.....	145
BET isotherm	139
beverages.....	823
BHA	30
BHT	30
bioaugmentation	735
biocompatibility	371
biodegradable polymers	859
biogenic material	652
bio-kinetic parameters	896
biological activity	836
biological study	46
biological treatment	896
biological value	782
biologically active compounds	79
biomethane yield	430
bio-oil	504
bipolar membrane.....	611
Black pepper.....	30
blend	127
blend films	859
blended amine	669
block carriers	583
bone char and tar	34
bone pyrolysis	34
booster pellet	829
bootstrap method	410
<i>Brassica rapa</i>	493
brewing	807
brine	157
Brownian motion	977
building materials	239
Bulgarian traditional foods	782
by-products	157
cadmium	697, 884
cadmium uptake	697
caffeic acid	354
caffeine	339, 823
caffeine-tannins complex	339
calcium pectate	868
<i>Camellia sinensis</i>	20
<i>Cancer pagurus</i> hemocyanin	11
capture efficiency	276
carbon nanotubes	62
<i>Carica papaya</i> leaves	20
carrot pulpy waste	816
CASS	176
catalyst	62, 583, 600, 914
catechin	354
cefixime	729
cell cultures	371
CFD	775
char	504

characterization.....	67
chemical.....	250
chemical and biochemical parameters	540
chemical clogging.....	228
chemical composition	313
chemical effects	320
chemical reaction.....	706
chlorination.....	157, 309
chlorine	250
chromium doped glass-ceramics.....	366
CIE standard light source.....	961
<i>Cladophora glomerata</i>	504, 540
clearance contact.....	210
clenbuterol	955
clinoptilolite.....	577
Co	787
CO ₂	509
CO ₂ sequestration	509
Co ₃ O ₄ /MgO	761
coal	509, 600
co-current flows	711
Coenzyme A	621
CoFe ₂ O ₄ /MgO.....	761
colloidal dispersions	775
color grade	961
column apparatus.....	706, 711, 720
combined forms	377
compressible	487
computational study.....	46
computer dynamic simulation.....	176
computer modelling	768
convection-diffusion model	706, 711, 720
co-pigmentation	115
copper (II) complex	74
copper ion	685
core-flooding experiment.....	534
corn husk.....	986
corrosion	204, 444, 669
corrosion inhibition.....	846
corrosion resistance	943
counter-current flows	720
coupling effect	617
crack	210, 217
cryogel	792
crystallization behavior.....	245
Cs ⁺ ion exchange	577
CTCL local therapy	792
Cu(II) complex	901, 908
curcumin	792
cytotoxicity	901
dairy wastewater	896
data envelopment analysis	455
De Luca method.....	410
decarburization	669
dehumidification	469
delta opioid receptor	768
Density Functional Theory (DFT)	134
desalination	157, 469
descriptor dual	690
design.....	469
desorption	635
detection	874
detergent	390
devulcanization conditions	436
dextran	792
DFT	846
DFT calculation.....	690, 800
di-(2-ethylhexyl) phthalate (DEHP)	360
diamond green dye	816
diclofenac potassium	994
dihydropyrano[c]chromenes	478
Direct Blue-15 dye	20
discharged	157
DNA	908
DNA binding	901
DNAse activity	901
droplet characteristic adjustment	193
drying properties	127
DSC	26
DSC analysis	245
dust	874
dynamic adsorption	635
dynamic monitoring	617
<i>Echium italicum L.</i>	836
edible-medicinal fungi	185
EDXRF	874
effective diffusion coefficient	399
efficiency	455
electrochemical impedance spectrometry	943
electrodialysis	611
electrooxidation	729
elements	874
emulsifier	256
emulsion	527
energy	782
enolizable systems	331
environmental samples	151
environments	890
EOR	534
EPDM-g-BMI	26
EPR dosimetry	629
EPR, Free radicals	82
equilibrium	577
equilibrium constant	115
error model	269
ESI-MS	658
ESI-MS/MS	354
essential oil	923
estradiol	377
estradiol hemihydrate	384
ethoxyl-oleyl-cetyl alcohol	390
ethylene-propylene-diene rubber	26
experimental design	436
extraction	40, 658
Eyring-Powell fluid	320
Farahabad region	504, 540
fast pyrolysis	504
fats	928
fatty acid methyl ester	928
ferrites	444

finite difference scheme.....	320
firearm investigation.....	101
flame atomic absorption spectrometry.....	151, 884
flavonoids.....	901
floor strata.....	969
fluidized bed	504
food.....	449
food chemistry	782
forensic sciences.....	101
formatting	264
fracture combination.....	969
Freundlich isotherm.....	868
friction stir welding.....	239
fruit extracts.....	879
frying vegetable oils	67
fumaric acid.....	127
gamma-irradiation.....	82
gap contact.....	217
gas	611
gas absorption	720
gas chromatography.....	377, 928
gas flood	617
gas sensors	121
gas-liquid flows	617
GC-FID/MS	923
gelatinization	422
goethite	652
green chemistry.....	331
grinding technique	309
growth from solution	608
gunshot residues	101
H9N2 AIV	161
HBF ₄ -SiO ₂ NPs.....	331
heat integration	807
heat of polymerization	134
heat tanks	807
heating	928
heat-moisture treatment	422
heavy ion.....	629
high nickel steel	239
high shear.....	527
high temperature	948
high thixotropy	527
high-performance liquid chromatography	339
Homotopy analysis method	320
HPLC-HILIC	384
HPLC-UV	994
human serum.....	994
humatic acid sodium	685
humidification.....	469
hybrid drying	92
hydantoin	643
hydrating/dehydrating	109
hydrogen storage.....	62
hydrogen storage capacity	109
hydrogenation	600
hydrothermal method.....	444, 664
hydroxyl radical	185
image segment	234
immunization	557
impedance	264
impedance spectroscopy.....	121
Incoloy 028 alloy.....	943
indolenine.....	87
indomethacin	994
industry.....	583
inhibite microorganism	171
initiation capacity	829
injection slug	534
insensitive main charge	829
INT	787
integrated microfluidic	264
intercalation.....	908
intrinsic bioremediation.....	735
inverse gas chromatography	742
ion-selective electrode.....	449
IR drying	92
Iran	504, 540
iron chelating activity	11
iron chelators	800
irradiation	557, 629
IRT gene	697
isotherm.....	816
IXRF	874
<i>Jacaranda mimosifolia</i>	171
Jadeite-Jade green	961
J-Integral	210, 217
ketones, aliphatic	87
kinematic viscosity	589
kinetic models	816
kinetics	399, 577
kinetics and mechanism	569
kinetics of deposition	313
Langmuir isotherm	20, 868
laser beam scan	589
lead	868
leaf surface reconstruction	288
lepidocrocite	652
Lewis acid	483
Lewis acid-base constants	742
LiAlSiO ₄	366
limited volume	589
linearity	384
linoleic acid	846
liquid-liquid extraction	914
L-lactic acid	256
LNCaP	664
low viscosity	527
lumped element modeling	193
macroporous sponges	792
magnesite ore	678
magnesium perchlorate	478
magnetic field	977
magnetic isolation	276
magnetogravitational	487
malachite green	652
malononitrile	331
maltose	256
maltose ester lactate	256
mass density	589

mass spectrometry	621
mass transfer	611
material composition detection	234
material testing	859
matrix	955
matrix-assisted laser ionization	955
MCNPX	874
MDCK	161
mechanical activation	600
medical devices	360
mercaptans	449
metal chelates	347
metal ions	151
methyl protocatechuate	354
Mg-C nanocomposites	109
micelles	569
microfluidic	269
microfluidic chip	276
microwave drying	986
minimum plastic zone	969
mixed ligand	74
mixing	775
MLR method	852
modeling	399, 986
modified asphalt	520
modified diatomite	936
modified electrode	729
molecular docking	768
molecular electrostatic potential	800
molecules reactivity	690
montmorillonite	245
montmorillonite modification	685
morphology	313
motor transport	583
MTT assay method	664
<i>Mucor plumbeus</i>	390
multi source	874
multi-level stress	204
mushrooms and tobaccos	787
MW drying	92
nanofluid	977
nanoparticles	595
nano-serpentine	948
nanotechnology	595
nano-TiO ₂	664
neuro-DEA	455
new rural sewage treatment	176
Newtonian heating	977
Ni-Co alloys	313
ninhydrin	331
nitrogenated heterocycles	690
<i>n</i> -octylaniline	914
non-uniform heat generation/absorption	977
numerical method	469
numerical solution	399
OAS gene	697
oil sorbent	335
oil-based drilling fluid	527
olefins	134
oleic acid	846
one-pot	478, 483
optimization	17
oscillatory stretching sheet	320
oxidative degradation	669
palm oil	127
paper	936
partial mass transfer coefficient	399
pathogens	264
PBX explosive	210, 217
pentaerythritol tetranitrate	735
peroxymonosulphate activation	761
pesticide residues	269
pharmaceutical preparations	339
phase structure	313
phenolic composition	879, 923
phenolic compounds	40
phenylhydrazine derivatives	87
pH-metric titrations	347
photocatalysts	652
photometric detection	269
phthalimide- <i>N</i> -sulfonic acid	562
physical	250
physicochemical properties	127
phytochemical composition	836
<i>Pichia Pastoris</i>	621
plant materials	399
plasma samples	994
PLS1 algorithms: NIPALS, SIMPLS, KERNEL, BIDIAGONALIZATION	410
PoF model	204
point cloud data (PCD)	288
polyelectrolytes	557
polymers	600
polysaccharids	282
polyvinyl alcohol	245
polyvinyl chloride (PVC)	360
potato peels	816
potentiodynamic polarisation curve	943
potentiometry	449
potentiostat	444
precipitated phases	943
precision	384
pressure	829
principal components analysis	890
PR-MPLC	658
propagation path	969
propanoic acid	87
proteins	557
Pt annealing	190
Pt-TiO ₂ sol gel film	190
PVC membrane	449
QSAR	768
QSPR	852
quality	928
quality grading of Jadeite-Jade green	961
quercetin	115
rapid detection	264
Reactive Black 5	652
real sample	729
reclaim characteristics	436

reduction	569
release of active substance	339
removing impurity by two step	678
resin	635
resistive	487
resorcinol	478
reverse flotation	678
rheology	527
<i>Rhinanthus angustifolius</i> subsp. <i>Grandiflorus</i>	923
Rhodamine B degradation	761
rock asphalt	520
rotating	487
RP HPLC	377
rubber crumb	436
<i>Russelia equisetiformis</i>	354
Ruthenium(III)	914
ryegrasses	697
safe assessment	157
SARIDON formulation	410
saturated fats	782
scalable synthesis	79
Schiff's base	890
scoring functions	768
sea silt	250
<i>Selaginella tamariscina</i> (Beauv) spring	658
self-repairing film	948
SEM	26
SEM image	46
sensitivity	955
sensitizing treatment	943
sensor	449
silver nanoparticles	569
sintering	250
slotted quartz tube	884
sodium malonate	914
sodium tripolyphosphate	390
sol-gel method	121
solid acid	331
solid mushroom fermentation	282
solid phase extraction	884
solid-liquid extraction	399
solvent-free	562
sorption capacity	335
soybean oil	493
spectral overlapping	410
spectrophotometry	787, 890
spectroscopy	621
square pyramidal	74
SRB	534
St3gal 1 gene	161
stability	228
stability constant	347
stabilization	30
stagnation point	977
starches	422
starch-fatty acid complex	936
storage	928
storage temperature	879
streaming	487
strength properties	936
stress intensity factor	210, 217
structure	199
substituted bis-arylchloromethanes	79
substrate pretreatment	430
sugar	629
sulphate radicals	761
sunflower oil	30, 493
surface and adsorption properties	742
surface fitting	768
surface free energies	742
surface morphology	948
synthesis	17, 145, 199
syringic acid	354
tailing micro structure	228
tailings dam	228
tar-application as a crosslinking agent of epoxy resin	34
tea samples	823
technical hydrolyzed lignin	139
TEM	569
terrestrial laser scanning (TLS)	288
test and evaluation	520
thermal decomposition	444
thermal properties	26
thermodynamic parameters	347
thermodynamics	115
thermogravimetric analysis	608
thermophoresis	977
thiazolidine-2,4-dione	643
thiazolidinone derivatives	742
thin film of oil	335
thiosemicarbazone	908
three-component reaction	562
TiO ₂	190, 595
topological indices	852
toxic gases	583
TPCK-trypsin	161
TPH	534
transmission	608
treatment plant	455
tree organ classification	288
tribological properties	948
<i>Trichoderma harzianum</i>	390
two-step preconcentration method	884
ultrasonic	483
ultrasonic treatment	859
ultrasound-assisted emulsification-microextraction	994
ultrasound-assisted hollow fibre liquid-phase microextraction	151
uncertainty	509
UV filter	608
UV radiation	360
UV spectrometry	629
UV/Vis spectrometry	823
UV-detection	377
vaccine	557
validation	852
VBF	176
velocity radial non-uniformity	706, 711, 720
vic-dioxime	908

wall shear	775	X-ray diffraction.....	366, 608
waste hydrolyzed lignocellulosic materials	40	zinc oxide	121
waste water treatment	685	zirconium (IV) chloride.....	483
water resistance performance.....	969	Zn(II) complex	901
working electrode	444	α -2,3 linked receptor	161
xanthenes	483	β -cyclodextrin	792
X-ray crystal structure	74		

SUBJECT INDEX

- | | |
|--|-------------------|
| 1-(2-хидроксифенил)-3-фенилпропен-1,3-дионаи .. | 309 |
| 1,4-дихидропиридини..... | 82 |
| 1-амидоалкил-2-нафтол..... | 562 |
| 2,3,4,6- <i>O</i> -тетраацетил- α -D-гликокопиранозил бромид .. | 17 |
| | |
| 2,4,6-тринитротолуен | 735 |
| 2 <i>H</i> -хромен..... | 643 |
| 2-амино-4 <i>H</i> -хромени | 478 |
| 2-нафтол..... | 483 |
| 3D електронно принтиране | 193 |
| 3 <i>H</i> -индол..... | 87 |
| 3-хлоро-2-фенил-4 <i>H</i> -хромен-4-они | 309 |
| 4-фенилфенол..... | 635 |
| 4-хидроксикумарин | 478 |
| 5-нитросалицилалдехид | 800 |
| Al-Si-Zr | 371 |
| <i>Aspergillus niger</i> | 390 |
| Au комплекси | 621 |
| B3LYP/6-31G..... | 134 |
| <i>Brassica rapa</i> | 493 |
| <i>Camellia sinensis</i> | 20 |
| <i>Cancer pagurus</i> hemocyanin | 11 |
| <i>Carica papaya</i> leaves | 20 |
| CASS | 176 |
| <i>Cladophora glomerata</i> | 504, 540 |
| CO ₂ | 509 |
| CO ₂ секвестриране | 509 |
| Co ₃ O ₄ /MgO | 761 |
| CoFe ₂ O ₄ /MgO | 791 |
| Cu(II) комплекс | 901, 908 |
| <i>Echium italicum L.</i> | 836 |
| <i>Jacaranda mimosifolia</i> | 171 |
| LiAlSiO ₄ | 366 |
| LNCaP | 664 |
| L-млечна киселина | 256 |
| <i>Mucor plumbeus</i> | 390 |
| Ni-Co сплави..... | 313 |
| <i>n</i> -октиланилин | 914 |
| pH-метрични титрувания | 347 |
| <i>Pichia Pastoris</i> | 621 |
| TiO ₂ | 190, 595 |
| <i>Trichoderma harzianum</i> | 390 |
| <i>vic</i> -диоксим..... | 908 |
| α -2,3 свързан рецептор | 161 |
| β -циклодекстрин | 792 |
| абиратеронов ацетат | 199 |
| абсорбционни и емисионни спектри | 366 |
| адсорбционни изотерми | 635 |
| адсорбция | 20, 509, 635, 868 |
| аеробни процеси | 896 |
| аерозоли..... | 589 |
| азо съединения | 46 |
| азотирани хетероцикли | 690 |
| аквакултурни патогени..... | 276 |
| акриламид..... | 449, 685 |
| активация на пероксимоносулфат | 761 |
| активен въглен | 139 |
| активираща енергия | 986 |

- | | |
|--|----------|
| алгоритми PLS1 | 410 |
| Алжир | 67 |
| алифатни алкохоли | 852 |
| алифатни кетони | 87 |
| алкална обработка | 40 |
| алкидна смола | 127 |
| алуминий, анодизиран | 371 |
| аментофлавон | 658 |
| анаеробно разлагане | 430 |
| анализ на обхватата на данните | 455 |
| анализ на основните компоненти | 890 |
| анти микробактериална активност | 643 |
| анти микробна активност | 923 |
| антиоксидант | 449, 669 |
| антиоксидантен потенциал | 30 |
| антиоксидантна активност | 493, 879 |
| антиоксидантни свойства | 11 |
| антипролиферативни / цитотоксични ефекти | 643 |
| антоцианини | 115 |
| арганово масло | 846 |
| ароилхидразони | 800 |
| асфалтови смеси | 520 |
| аустенит | 239 |
| багрило директно синьо-15 | 20 |
| багрило реактивно черно 5 | 652 |
| безопасно оценяване | 157 |
| бензофуран-2-карбоксамид | 145 |
| БЕТ изотерма | 139 |
| биогенен материал | 652 |
| биогориво | 504 |
| био-кинетични параметри | 896 |
| биологична активност | 836 |
| биологична стойност | 782 |
| биологично активни вещества | 79 |
| биологично изследване | 46 |
| биологично третиране | 896 |
| биологично увеличение | 735 |
| биометан - добив | 430 |
| биоразградими полимери | 859 |
| биосъвместимост | 371 |
| биполярна мембрana | 611 |
| блокови носители | 583 |
| Брауново движение | 977 |
| бърза пиролиза | 504 |
| ваксина | 557 |
| валидиране | 852 |
| взаимодействие | 908 |
| взривна капсула | 829 |
| висока степен на срязване | 527 |
| висока температура | 948 |
| висока тиксотропия | 527 |
| високоефективна течна хроматография | 339 |
| високочувствително третиране | 943 |
| ВНА | 30 |
| ВНТ | 30 |
| водно съпротивление | 969 |
| водорасли | 504 |
| вторични продукти | 157 |

въглен.....	504
въглеродни нанотръби.....	62
въглища.....	509, 600
въртящ се обръщац	775
газ	611
газова абсорбция	720
газова хроматография.....	377, 928
газови сензори.....	121
гама облучване.....	82
гелообразуване	422
ген OAS.....	697
ген <i>St3gal</i>	161
гъби и тютюни	787
гътит	652
двестъпален метод за преконцентрация	884
двоен дескриптор	690
двустепенно очистване на примеси	678
девулканизационни условия	436
декарбонизиране	669
декстран	792
делта опиоиден рецептор	768
десорбция	635
детергент.....	390
ди-(2-етилхексил)фталат (ДЕХФ)	360
диамантено зелено багрило	816
дизайн	469
динамичен мониторинг	617
динамична адсорбция	635
дихидропирано[с]хромени	478
ДНК.....	908
ДНК свързване	901
ДНК-зна активност	901
дънни слоеве	969
едностадиен	478, 483
екстракция	40, 658
електродиализа.....	611
електроокисление	729
електростатичен потенциал	800
електрохимична импедансна спектрометрия	943
елементи	874
емулгатор.....	256
емулясия	527
енергия.....	782
енолируеми системи	331
ЕПР дозиметрия	629
естрадиол	377
естрадиол хемихидрат	384
етерично масло.....	923
етилен-пропилен-диенов каучук	26
етокси-олеил-цетилов алкохол	390
ефект на сдвояване	617
ефективен дифузионен коефициент	399
ефективност.....	455
ефективност на улавяне.....	276
жадеит-нефритово зелено	961
железни хелатори.....	800
желязо, тежко	629
заготовка за инжектиране	534
закаляване	190
заливане на скална ядка	534
заместени бис-арилхлорометани	79
засичане, бързо	264
захар.....	629
зелена химия	331
зол гел филм Pt-TiO ₂	190
зол-гел метод	121
изотерма	819
изотерма на Лангмюир	20, 868
изотерма на Фреунлич	868
използвани растителни мазнини	67
изследване на оръжия	101
изсушаване	469
изчислително изследване.....	46
импеданс	264
импедансна спектроскопия	121
иммунизация	557
индоленин	87
индометацин	994
индустрия	583
иницииращ капацитет	829
интегриран микрофлуид	264
инхибиране на корозия	846
инхибиране на микроорганизъм	171
йонообмен на Cs ⁺	577
йон-селективен електрод	449
Иран	504, 540
ИЧ сущене	92
кадмий	697, 884
калциев диклофенак	994
калциев пектат	868
капацитет за съхранение на водород	109
картофени кори	816
катализатор	62, 583, 600, 914
катехин	354
кафеена киселина	354
качество	928
квадратно прирамидална геометрия	74
керцетин	115
кинематичен вискозитет	589
кинетика	399, 577
кинетика и механизъм	569
кинетика на отлагане	313
кинетични модели	816
кипящ слой	504
киселинни дисоционни константи	890
киселинно-основни константи за Люисови	742
класификация на дървесни органи	288
кленбутерол	955
клетъчни култури	371
клиноптиолит	577
кобалт	787
Коензим А	621
колоидни дисперсии	775
колонен апарат	706, 711, 720
комбинирани форми	377
комплекс кофеин-танини	339
компресирамо	487
компютърна динамична симулация	176
компютърно моделиране	768
конвекционно-дифузионен модел	706, 711, 720

константа на стабилност	347
ко-пигментация	115
корозионна устойчивост	943
корозия.....	204, 444, 669
кост, животинска	34
костни въглен и катран.....	34
кофеин.....	339, 823
криогел.....	792
криSTALLИЗАционно поведение	245
ксантени.....	483
куркумин	792
лазерно лъчево сканиране	589
лепидокрокит	652
линейност	384
линолова киселина.....	846
локална терапия на кожната форма на Т-клетъчен лимфом	792
Люисова киселина	483
магнезиев перхлорат.....	478
магнеситна руда	678
магнитна изолация.....	276
магнитно поле	977
магнитногравитационен	487
мазнини.....	928
макропорести гъби.....	792
малахитово зелено	652
малононитрил.....	331
малтоза.....	256
малтозен естер на млечната киселина.....	256
мас спектрометрия.....	621
масова плътност	589
масопренос	611
матрица	955
матрично-асистирана лазерна йонизация	955
мащабирам синтез.....	79
мед (II) комплекс	74
меден йон.....	685
медицински уреди	360
меркаптани	449
метални йони.....	151
метални хелати.....	347
метил протокатехат	354
метилов естер на мастни киселини	928
метод на Де Лука	410
механохимично активиране	600
микровълново сушене	92
микровълново сушене	986
микроструктура на хвостохранилище.....	228
микрофлуиден	269
микрофлуиден чип.....	276
минимална пластична зона	969
мицели	569
много-степенно напрежение	204
множествен източник	874
модел PoF	204
модел на Абашло	92
модел на средните концентрации.....	706, 711, 720
моделиране	399, 986
моделиране на локализирани елементи	193
модификация на монтморилонит	685
модифициран асфалт.....	520
модифициран диатомит	936
модифициран електрод	729
молекулна реактивоспособност	690
монтморилонит.....	245
морковена пулпа	816
морска сол	250
морфология	313
моторен транспорт	583
нагряване	928
наземно лазерно сканиране	288
налягане	829
нано-TiO ₂	664
нанокомпозити Mg-C	109
нано-серпентина	948
нанотехнология	595
нанофлуид	977
наночастици	595
напитки	823
наситени мазнини	782
настройка на размера на капките	193
натриев малонат	914
натриев триполифосфат	390
натриев хумат	685
невро-DEA	455
невронни мрежи, изкуствени	455
неравномерно генериране / абсорбция на топлина	977
несигурност	509
нечувствителен основен заряд	
нинхиридри.....	331
нисък вискозитет	527
нишестета	422
Нютоново загряване	977
обезсоляване	157, 469
обълчване	557, 629
обратна газова хроматография	742
обърната флотация	678
овлажняване	469
ограничен обем	589
окислително разпадане	669
околна среда	890
олеинова киселина	846
олефини	134
олово	868
определяне на материалната композиция	234
оптимизация	17
освобождаване	157
освобождаване на активно вещество	339
остатъци от изстрел	101
осцилиращо-разтяган лист	320
откриване	874
отпадни води от мандри	896
оценка на зеления цвят на жадеит-нефрита	961
оценявачи функции	768
оцетна киселина	87
палмово масло	127
патогени	264
ПВЦ мембрана	449
пентаеритритол тетранитрат	735
периодичен реактор	807, 896

пестицидни остатъци.....	269	ронливост на каучук.....	436
петрол-базирана сондажна течност.....	527	ротация	487
петролен сорбент	335	Рутений (III)	914
пивоварство	807	саламура	157
пиролиз на кости	34	саморегенериращ се филм	948
пламъкова атомна абсорбционна спектрометрия	151, 884	селскостопански отпадъци	986
планиран експеримент	436	СЕМ снимка.....	46
плодови екстракти	879	сензор	449
повърхностна енергия	742	силови свойства	936
повърхностна морфология	948	синтез	17, 145, 199
повърхностни и адсорбционни свойства	742	синтероване.....	250
подобрена биодеградация	735	сирингова киселина.....	354
поливинилов алкохол	245	скален асфалт.....	520
поливинилхлорид (ПВЦ).....	360	скорбялно-мастни киселинни комплекси	936
полиелектролити.....	557	скоростна радиална неравномерност.....	706, 711, 720
полизахариди.....	282	слънчогледово олио	30, 493
полимери	600	смес	127
потенциодинамични поляризационни криви	943	смесване	775
потенциометрия	449	смесени лиганди	74
потенциостат	444	смесени филми	859
потоци газ-течност.....	617	смилане, топково	109
поточен	487	смола.....	635
правотокови потоци.....	711	смола Амберлит CG-120	884
прах	874	снимков сегмент	234
предварителна обработка на субстрат	430	соево масло	493
прецизност	384	сорбционен капацитет.....	335
пречистване на отпадни води	685	спектрално застъпване	410
пречиствателна станция	455	спектроскопия.....	621
приложение	787	спектрофотометрия	787, 890
приложение на катран като омрежващ агент на епоксидна смола	34	сплав Инколой 028	943
проби от околната среда.....	151	сребърни наночастици	569
проби от плазма	994	стабилизация.....	30
проби от чай	823	стабилност.....	228
продухване с газ.....	617	стандартен светлинен източник	961
пропанолова киселина.....	87	стенно срязване	775
протеини	557	стомана с високо съдържание на никел	239
противо-растителна патогенна гъбична активност	145	стрес, фактор на интензивност	210, 217
противотокови потоци.....	720	строителни материали.....	239
пукнатина	210, 217	структура.....	199
пчелна колония, изкуствена.....	234	суlfатни радикали	761
път за разпространение	969	сущене, характеристики	127
работен електрод.....	444	схема с крайни разлики.....	320
равновесие	577	съдебни науки.....	101
равновесна константа	115	съпротивителен	487
разпадане на Романин В	761	Състав на Саридон	410
разпространение на пукнатините	969	съхранение	928
разтворител, без	562	съхранение на водород	62
райграс	697	твърда киселина	331
растеж от разтвор.....	608	твърдо-течна екстракция	399
растителни материали	399	твърдофазна екстракция	884
реални проби	729	твърдо-фазна ферментация на гъби	282
регенерационни характеристики	436	твърдофазно заваряване	239
регион Фараҳабад	504, 540	TEM	569
редукция	569	температура на съхранение	879
резорцинол	478	термични свойства	26
рентгенова дифракция	366, 608	термично разпадане	444
рентгено-кристална структура.....	74	термогравиметричен анализ	608
реология.....	527	термодинамика	115
		термодинамични параметри	347
		термофореза	977

тестване и оценяване	520	флуид на Ейринг-Пауъл	320
тестване на материали	859	форматиране	264
техника за смилане	309	фотокатализатор	652
технически хидролизиран лигнин	139	фотометрично засичане	269
течно-течна екстракция	914	фталимид- <i>N</i> -сулфонова киселина	562
течнофазна ултразвуково асистирана куховлакнеста микроекстракция	151	фумарова киселина	127
тиазолидин-2,4-дион	643	характеризиране	67
тиазолидинон производни	742	хартия	936
тиосемикарбазон	908	хвостохранилище	228
токсични газове	583	хелатираща активност на желязо	11
топлина на полимеризация	134	хибридно сущене	92
топлинна интеграция	807	хидантоин	643
топлинни резервоари	807	хидриране/дехидриране	109
топологични индекси	852	хидрогениране	600
точка на стагнация	977	хидроксилен радикал	185
точкови данни в облак	288	хидролизирани отпадни лигноцелулозни материали	40
традиционн български храни	782	хидротермален метод	444, 664
трансмисия	608	химичен	250
третиране на канализационни отпадъци	176	химичен състав	313
трибологични свойства	948	химична реакция	706
трикомпонентна реакция	562	химични ефекти	320
TPCH-трипсин	161	химични и биохимични параметри	540
тънък филм от петрол	335	химично задърстване	228
тясна кварцова кювета	884	химия на храните	782
УВ детекция	377	хлор	250
УВ радиация	360	хлор-дотирана стъклокерамика	366
УВ спектрометрия	629	хлориране	157, 309
УВ филтър	608	хомотопен анализ	320
УВ/Виз спектрометрия	823	храна	449
ултразвуков	483	царевична обвивка	986
ултразвукова обработка	859	цветно оценяване	961
ултразвуково-асистирана микроекстракция	994	цефексим	729
усвояване на кадмий	697	цинк (II) комплекс	901
утаени фази	943	цинков оксид	121
фазова структура	313	циркониев (IV) хлорид	483
фармацевтични препарати	339	цитотоксичност	901
фенилхидразинови производни	87	частичен масопреносен коефициент	399
фенолни съединения	40	черен пипер	30
фенолно съдържание	879, 923	числени методи	469
ферити	444	числени решения	399
физикохимични свойства	127	човешки serum	994
физичен	250	чувствителност	955
фитохимично съдържание	836	Шрифова база	890
флавоноиди	901	ядливи медицински гъби	185

BULGARIAN CHEMICAL COMMUNICATIONS

Instructions about Preparation of Manuscripts

General remarks: Manuscripts are submitted in English by e-mail or by mail (in duplicate). The text must be typed double-spaced, on A4 format paper using Times New Roman font size 12, normal character spacing. The manuscript should not exceed 15 pages (about 3500 words), including photographs, tables, drawings, formulae, etc. Authors are requested to use margins of 3 cm on all sides. For mail submission hard copies, made by a clearly legible duplication process, are requested. Manuscripts should be subdivided into labelled sections, e.g. **Introduction, Experimental, Results and Discussion, etc.**

The title page comprises headline, author's names and affiliations, abstract and key words.

Attention is drawn to the following:

a) **The title** of the manuscript should reflect concisely the purpose and findings of the work. Abbreviations, symbols, chemical formulas, references and footnotes should be avoided. If indispensable, abbreviations and formulas should be given in parentheses immediately after the respective full form.

b) **The author's** first and middle name initials, and family name in full should be given, followed by the address (or addresses) of the contributing laboratory (laboratories). **The affiliation** of the author(s) should be listed in detail (no abbreviations!). The author to whom correspondence and/or inquiries should be sent should be indicated by asterisk (*).

The abstract should be self-explanatory and intelligible without any references to the text and containing not more than 250 words. It should be followed by key words (not more than six).

References should be numbered sequentially in the order, in which they are cited in the text. The numbers in the text should be enclosed in brackets [2], [5, 6], [9–12], etc., set on the text line. References, typed with double spacing, are to be listed in numerical order on a separate sheet. All references are to be given in Latin letters. The names of the authors are given without inversion. Titles of journals must be abbreviated according to Chemical Abstracts and given in italics, the volume is typed in bold, the initial page is given and the year in parentheses. Attention is drawn to the following conventions:

a) The names of all authors of a certain publications should be given. The use of "et al." in

the list of references is not acceptable.

b) Only the initials of the first and middle names should be given.

In the manuscripts, the reference to author(s) of cited works should be made without giving initials, e.g. "Bush and Smith [7] pioneered...". If the reference carries the names of three or more authors it should be quoted as "Bush *et al.* [7]", if Bush is the first author, or as "Bush and co-workers [7]", if Bush is the senior author.

Footnotes should be reduced to a minimum. Each footnote should be typed double-spaced at the bottom of the page, on which its subject is first mentioned.

Tables are numbered with Arabic numerals on the left-hand top. Each table should be referred to in the text. Column headings should be as short as possible but they must define units unambiguously. The units are to be separated from the preceding symbols by a comma or brackets.

Note: The following format should be used when figures, equations, *etc.* are referred to the text (followed by the respective numbers): Fig., Eqns., Table, Scheme.

Schemes and figures. Each manuscript (hard copy) should contain or be accompanied by the respective illustrative material as well as by the respective figure captions in a separate file (sheet). As far as presentation of units is concerned, SI units are to be used. However, some non-SI units are also acceptable, such as °C, ml, l, etc.

The author(s) name(s), the title of the manuscript, the number of drawings, photographs, diagrams, etc., should be written in black pencil on the back of the illustrative material (hard copies) in accordance with the list enclosed. Avoid using more than 6 (12 for reviews, respectively) figures in the manuscript. Since most of the illustrative materials are to be presented as 8-cm wide pictures, attention should be paid that all axis titles, numerals, legend(s) and texts are legible.

The authors are asked to submit **the final text** (after the manuscript has been accepted for publication) in electronic form either by e-mail or mail on a 3.5" diskette (CD) using a PC Word-processor. The main text, list of references, tables and figure captions should be saved in separate files (as *.rtf or *.doc) with clearly identifiable file names. It is essential that the name and version of

the word-processing program and the format of the text files is clearly indicated. It is recommended that the pictures are presented in *.tif, *.jpg, *.cdr or *.bmp format, the equations are written using “Equation Editor” and chemical reaction schemes are written using ISIS Draw or ChemDraw programme.

The authors are required to submit the final text with a list of three individuals and their e-mail addresses that can be considered by the Editors as potential reviewers. Please, note that the reviewers should be outside the authors' own institution or organization. The Editorial Board of the journal is not obliged to accept these proposals.

EXAMPLES FOR PRESENTATION OF REFERENCES

REFERENCES

1. D. S. Newsome, *Catal. Rev.–Sci. Eng.*, **21**, 275 (1980).
2. C.-H. Lin, C.-Y. Hsu, *J. Chem. Soc. Chem. Commun.*, 1479 (1992).
3. R. G. Parr, W. Yang, Density Functional Theory of Atoms and Molecules, Oxford Univ. Press, New York, 1989.
4. V. Ponec, G. C. Bond, Catalysis by Metals and Alloys (Stud. Surf. Sci. Catal., vol. 95), Elsevier, Amsterdam, 1995.
5. G. Kadinov, S. Todorova, A. Palazov, in: New Frontiers in Catalysis (Proc. 10th Int. Congr. Catal., Budapest, 1992), L. Guczi, F. Solymosi, P. Tetenyi (eds.), Akademiai Kiado, Budapest, 1993, Part C, p. 2817.
6. G. L. C. Maire, F. Garin, in: Catalysis. Science and Technology, J. R. Anderson, M. Boudart (eds), vol. 6, Springer-Verlag, Berlin, 1984, p. 161.
7. D. Pocknell, *GB Patent* 2 207 355 (1949).
8. G. Angelov, PhD Thesis, UCTM, Sofia, 2001.
9. JCPDS International Center for Diffraction Data, Power Diffraction File, Swarthmore, PA, 1991.
10. CA **127**, 184 762q (1998).
11. P. Hou, H. Wise, *J. Catal.*, in press.
12. M. Sinev, private communication.
13. <http://www.chemweb.com/alchem/articles/1051611477211.html>.

CONTENTS

<i>I. A. Slavova, St. G. Christoskova, M. K. Stoyanova</i> , Catalytic oxidation of Rhodamine B in aqueous solutions with sulphate radicals over $\text{Co}_3\text{O}_4/\text{MgO}$ and $\text{CoFe}_2\text{O}_4/\text{MgO}$	761
<i>F.I. Sapundzhi, T.A. Dzimbova, N.S. Pencheva, P.B. Milanov</i> , Modeling of the relationship between biological activity of delta-selective enkephalin analogues and docking results by polynomials	768
<i>S.D. Vlaev, D. Georgiev</i> , Shear on particles exposed to backswept mixing flow with a view to stress-sensitive cell response	775
<i>D.S. Hristov, S.K. Velikov, V.E. Vodenicharov, S.P. Tsanova-Savov, F.T. Ribarova</i> , Evaluation of chemical composition, energy and biological value of typical Bulgarian traditional foods derivatives	782
<i>L. Dospatliev, M. Ivanova</i> , Spectrophotometric investigations on liquid-liquid extraction systems containing cobalt and tetrazolium salts. Application of the developed method for analysis of the cobalt content of biological samples (mushrooms and tobaccos)	787
<i>M. Iv. Slavkova, D. B. Momekova, B. D. Kostova, G. Tz. Momekov, P. D. Petrov</i> , Novel dextran/ β -cyclodextrin and dextran macroporous cryogels for topical delivery of curcumin in the treatment of cutaneous T-cell lymphoma	792
<i>B. I. Nikolova-Mladenova, S. E. Angelova</i> , Synthesis of 5-nitrosalicylaldehyde based hydrazones and DFT-calculations of their structure and reactivity	800
<i>D. S. Nikolova, B. B. Ivanov, D. G. Dobruzhaliiev</i> , Optimal energy management in brewing	807
<i>R. Rehman, S. Alam, L. Mitu</i> , Diamond green dye adsorptive removal from water by carrot pulpy waste and potato peels	816
<i>R. Rehman, S. Ashraf</i> , Analysis of caffeine contents in commercial beverages and tea samples of Pakistan using UV/Visible spectrometry	823
<i>L.-Sh Hu, B.-F. Sun</i> , Experimental studies on a horn-shaped booster pellet	829
<i>I. D. Bošković, D. A. Dukić, P. Z. Mašković, L. G. Mandić</i> , Phytochemical composition and biological activity of <i>Echium italicum</i> L. plant extracts	836
<i>G. Gece</i> , Theoretical basis for the corrosion inhibition feature of Argan oil	846
<i>F. Arjmand, F. Shafiei</i> , Modeling of the physicochemical properties of aliphatic alcohols using topological indices and quantitative structure-property relationship	852
<i>U. Vr. Brodnjak</i> , Improvement of physical and optical properties of chitosan-rice starch films pre-treated with ultrasound	859
<i>D. Paliulis, A. Krinickaitė</i> , Removal of lead (Pb^{2+}) from synthetic wastewater using calcium pectate	868
<i>H. R. Dehghan, A. Negarestani, M. R. Rezaie</i> , Study of the possibility of using IXRF technique to detect the elements present in dust using Monte Carlo N Particles	874
<i>B. Radovanović, A. Radovanović, V. Nikolić, N. Manojlović, J. Dimitrijević</i> , Storage effect on phenolic content and antioxidant activity in selected fruit extracts	879
<i>Y. Arslan, D. Trak, E. Kendüzler</i> , Preconcentration and determination of cadmium in some samples using solid phase extraction with slotted quartz tube flame atomic absorption spectrometry	884
<i>K. Alizadeh, H. Soltani-Afarani</i> , A comparative study on the ionization constants of a Schiff's base in different environments by multiwavelength UV-Vis spectroscopy	890
<i>T. T. Bayram, A. Nuhoglu, E. Aladağ</i> , Investigation of biodegradation and growth kinetics of dairy wastewater in a batch reactor	896
<i>B. Atabey-Ozdemir, O. Demirkiran, U. Yildiz, I. O.Tekin, B. Coban</i> , Cytotoxicity and DNA binding of copper (II) and zinc (II) complexes of flavonoids: querçitrin, myricitrin, rutin	901
<i>B. Coban, N. Eser, I. Babahan</i> , DNA binding by copper (II) complexes of semithiocarbazone containing ligands	908
<i>A. P. Gaikwad, V. J. Suryavanshi, M. A. Anuse</i> , Liquid-liquid extraction studies of ruthenium(III) from malonate medium using <i>n</i> -octylaniline as an ion-pairing reagent: study of catalyst and alloys	914
<i>A. A. Kaya, O. Üçüncü, S. M. İlter, C. Baltaci, S. Öztürk</i> , Chemical composition and bioactive properties of the essential oil of <i>Rhinanthus angustifolius</i> subsp. <i>grandiflorus</i>	923
<i>R. Kowalski, G. Kowalska, U. Pankiewicz, M. Sujka, K. Kalwa</i> , GC analysis in evaluation of changes in fatty acids content of selected fats during storage and heating	928
<i>W. Shang, X. Qian, H. Liang</i> , Preparation of modified diatomite filler via a starch-fatty acid complex coating method for improvement of paper strength properties	936
<i>Z.Q. Yu, G.S. Zhou, S.D. Zhu, J.M. Li, L.J. Li</i> , Influence of sensitizing treatment on the corrosion resistance of Incoloy 028 alloy	943
<i>Z. N. Jia, Y. Y. Yang, X. W. Qi, X. M. Song</i> , Influence of nano-serpentine mineral powder as a lubricating additive on the high-temperature tribological properties of metal friction pairs	948
<i>Q. Huo, T. Zhou, J. He, J. Q. Xue</i> , Identification of Clenbuterol by MALDI-TOF Mass Spectrometry	955
<i>GuoYing</i> , Quality grading system of Jadeite-Jade green based on three colorimetric parameters under CIE standard light sources D_{65} , CWF and A	961

<i>H.L. Yu, J.M. Zhu, Y.S. Zhang, W.Q. Zhang , Zh.Ch. Wang</i> , Study on the water resistance performance of floor rockmass under different fracture combinations	969
<i>B. K. Mahatha, R. Nandkeolyar, M. Das, P. Sibanda</i> , Stagnation point nanofluid flow along a stretching sheet with non-uniform heat generation/absorption and Newtonian heating	977
<i>A. Akdogan, G. Caliskan Koç, S. N. Dirim</i> , Mathematical modeling of thin-layer microwave drying of corn husk and investigation of powder properties	986
<i>N. Chamkouri, V. Zare-Shahabadi, A. Niazi</i> , Ultrasound-assisted dispersive liquid-liquid microextraction with HPLC-UV for the simultaneous determination of Diclofenac potassium and Indomethacin in serum and plasma samples: Experimental design and optimization	994
<i>AUTHOR INDEX</i>	1001
<i>AUTHORS INDEX (IN BULGARIAN)</i>	1009
<i>SUBJECT INDEX</i>	1018
<i>SUBJECT INDEX (IN BULGARIAN)</i>	1024
<i>INSTRUCTIONS TO THE AUTHORS</i>	1029

СЪДЪРЖАНИЕ

<i>И. А. Славова, Ст. Г. Христоскова, М. К. Стоянова</i> , Каталитично окисление на Родамин В във водни разтвори със сулфатни радикали върху $\text{Co}_3\text{O}_4/\text{MgO}$ и $\text{CoFe}_2\text{O}_4/\text{MgO}$	767
<i>Ф.И. Сапунджи, Т.А. Дзимбова, Н.С. Пенчева, П.Б. Миланов</i> , Моделиране на връзката между биологичната активност на делта-селективни енкефалинови аналоги и резултати от молекулен докинг с полиноми	774
<i>С.Д. Влаев, Д. Георгиев</i> , Скорости на срязване върху частици при разбъркване с дъгообразни лопатки със значение за физиологията на микроорганизми чувствителни към механично напрежение	781
<i>Д.С. Христов, С.К. Великов, В.Е. Воденичаров, С.П. Цанова-Савова, Ф.Т. Рибарова</i> , Оценка на химичния състав, енергията и биологичната стойност на типични традиционни български храни	786
<i>Л. Доспашлиев, М. Иванова</i> , Спектрофотометрично изследване на системи за течно-течна екстракция, съдържащи кобалт и тетразолиеви соли. Прилагане на разработения метод за определяне съдържанието на кобалт в биологични преби (гъби и тютюн)	781
<i>М. Ив. Славкова, Д. Б. Момекова, Б. Д. Костова, Г. Цв. Момеков, П. Д. Петров</i> , Нови макропорести криогелове от декстран/ β -циклодекстрин и декстран за дермално доставяне на куркумин при лечение на кожен Т-клетъчен лимфом	799
<i>Б. И. Николова-Младенова, С. Е. Ангелова</i> , Синтез на хидразони, получени от 5-нитросалицилалдехид и DFT-изчисления за тяхната структура и реакционна способност	806
<i>Д. Ст. Николова, Б. Б. Иванов, Д. Г. Добруджалиев</i> , Оптимално управление на енергията в пивоварството	815
<i>Р. Рехман, С. Алам, Л. Миту</i> , Отстраняване на багрилото диамантено зелено от води чрез адсорбция върху отпадъчна морковена пулпа и картофени обелки	822
<i>Р. Рехман, С. Ашраф</i> , Анализ на съдържанието на кофеин в търговски напитки и преби от чай с помошта на УВ-спектрометрия	828
<i>Л.Ш. Ху, Б.Ф. Сун</i> , Експериментално изследване на рого-образни взривни капсули	835
<i>И.Д. Бушкович, Др.А. Джусукич, П.З. машкович, Л.Г. Мандич</i> , Фито-химичен състав и биологична активност на екстракти от <i>Echium italicum L.</i>	845
<i>Г. Гедже</i> , Теоретична основа за характеристиката на инхибиране на корозията на арганово масло	851
<i>Ф. Арджисанд, Ф. Шафией</i> , Моделиране на физикохимичните свойства на алифатни алкохоли, използвайки топологични индекси и количествена връзка структура-свойства	858
<i>У. Бр. Бродняк</i> , Подобряване на физичните и оптичните свойства на филмите от хитозан-оризово нищесте, предварително третирани с ултразвук	867
<i>Д. Палиулис, А. Кринискайте</i> , Отстраняване на олово (Pb^{2+}) от синтетични отпадни води с използване на калциев пектат	873
<i>Х.Р. Деган, А. Негарестани, М.Р. Резаие</i> , Изследване на възможностите на IXRF-техника за откриването на елементи в прах по метода Монте-Карло N частици	878
<i>Б. Радованович, А. Радованович, В. Николич, Н. Манолович, И. Димитриевич</i> , Ефект на съхранението върху съдържанието и антиоксидантната активност на феноли в избрани плодови екстракти	883
<i>Я. Арслан, Д. Трак, Е. Кендюзлер</i> , Пре-концентриране и определяне на кадмий в някои преби чрез твърдо-фазна екстракция и пламъкова атомно-абсорбционна спектрофотометрия (FAAS)	889
<i>К. Ализаде, Х. Солтани-Афарани</i> , Сравнително изследване на ионизациянните константи на Шифова база в различни среди чрез UV-Vis спектроскопия с полихроматична дължина на вълната	895
<i>Т. Т. Байрам, А. Нуходгу, Е. Аладаг</i> , Изследване на биоразграждането и кинетиката на растежа на млечните отпадни води в стандартен реактор	900
<i>Б. Атабей-Оздемир, О. Демиркиран, У. Йилдиз, И.О. Текин, Б. Джобан</i> , Цитотоксичност и ДНК-свързване на медни (II) и цинкови (II) комплекси на flavonoidи: куерцитрин, мирицитрин, рутин	907
<i>Б. Джобан, Н. Есер, И. Бабахан</i> , Комплекси на ДНК с мед (II) и лиганди от семикарбазони	913
<i>А.П. Гаикуад, В.Дж. Сурияваниши, М.А. Анусе</i> , Течно-течна екстракция на рутений (III) в среда на малонат при използването на n-октиланилин като йон-свързващ агент: изследване на катализатора и сплави	922
<i>А.А. Каая, О. Ючюнчу, Ш.М. Илтер, К. Балтаджъ, С. Йозтюрк</i> , Химичен състав и биоактивни свойства на есенциално масло от <i>Rhinanthus angustifolius</i> subsp. <i>grandiflorus</i>	927
<i>Р. Ковалски, Г. Ковалска, У. Панкиевич, М. Суйка, К. Калва</i> , Газ-хроматографски анализ при определянето на измененията в съдържанието на мастни киселини в избрани мазнини по време на съхранение и нагряване	935
<i>У. Шанг, Кс. Куан, Х. Лианг</i> , Получаване на модифициран диатомитен пълнител чрез нанасяне на комплекс от нищесте и мастна киселина за подобряване на здравината на хартия	942
<i>З. Ю, Г. Жоу, С. Жу^{2*}, Дж. М. Ли, Л. Дж. Ли</i> , Влияние на сенсибилизиращата обработка върху корозионната устойчивост на сплавта Incoloy 028.....	947

Ж. Жиа, Ю.Ю. Янг, Кс.У. Ку, Кс.М. Сонг, Влияние на наносерпентинов минерален прах като смазочна добавка върху трибологичните свойства на триещи се двойки метали	954
К. Хюо, Т. Жоу, Ж. Хе, Ж. Ксуе, Идентифициране на кленбутерол с помощта на MALDI-TOF масспектрометрия	960
Гую Инг, Система за оценка на зеления цвят на Жадеит-нефрит на основата на три колориметрични параметра на CIE стандартни светлинни източници D ₆₅ , CWF и A	968
Х.Л. Ю, Ж.М. Жу, И.С. Джсан, У.К. Джсан, Ж.Ч. Уан, Изследвания върху водоустойчивостта на стратифицирани скални маси при различни условия на разрушаване	976
Б. К. Махата, Р. Нандкейолар, М. Дас, П. Сибанда, Нанофлуиден поток с точка на стагнация по протежение на разтегляща се пластина с нееднакво генериране / погълщане на топлина и Нютоново нагрявани	986
А. Акдоган, Г. Чальшкан Koch, С.Н. Дирим, Математично моделиране на микровълново сушене в тъньк слой на царевични обивки и изследване свойствата на праха	807
Н. Чамкури, В. Заре-Шахабади, А. Ниязи, ЕДНОВРЕМЕННО определяне на диклофенак-калий и индометацин с проби от serum и плазма с помощта на едновременни ултразвукова дисперсионна течно-течна микро-екстракция и HPLC-UV. Планиран експеримент и оптимизация	1000
АВТОРСКИ УКАЗАТЕЛ НА АНГЛИЙСКИ.....	1009
АВТОРСКИ УКАЗАТЕЛ НА БЪЛГАРСКИ.....	1009
ПРЕДМЕТЕН УКАЗАТЕЛ НА АНГЛИЙСКИ.....	1058
ПРЕДМЕТЕН УКАЗАТЕЛ НА БЪЛГАРСКИ.....	1024
ИНСТРУКЦИЯ ЗА АВТОРИТЕ	1009